INSIGHTS IN PLANT BIOPHYSICS AND MODELING: 2021

EDITED BY: Maciej Andrzej Zwieniecki
PUBLISHED IN: Frontiers in Plant Science

frontiers Research Topics

frontiers

ISSN 1664-8714
ISBN 978-2-83250-470-3
DOI 10.3389/978-2-83250-470-3

About Frontiers

Frontiers is more than just an open-access publisher of scholarly articles: it is a pioneering approach to the world of academia, radically improving the way scholarly research is managed. The grand vision of Frontiers is a world where all people have an equal opportunity to seek, share and generate knowledge. Frontiers provides immediate and permanent online open access to all its publications, but this alone is not enough to realize our grand goals.

Frontiers Journal Series

The Frontiers Journal Series is a multi-tier and interdisciplinary set of open-access, online journals, promising a paradigm shift from the current review, selection and dissemination processes in academic publishing. All Frontiers journals are driven by researchers for researchers; therefore, they constitute a service to the scholarly community. At the same time, the Frontiers Journal Series operates on a revolutionary invention, the tiered publishing system, initially addressing specific communities of scholars, and gradually climbing up to broader public understanding, thus serving the interests of the lay society, too.

Dedication to Quality

Each Frontiers article is a landmark of the highest quality, thanks to genuinely collaborative interactions between authors and review editors, who include some of the world's best academicians. Research must be certified by peers before entering a stream of knowledge that may eventually reach the public - and shape society; therefore, Frontiers only applies the most rigorous and unbiased reviews.
Frontiers revolutionizes research publishing by freely delivering the most outstanding research, evaluated with no bias from both the academic and social point of view. By applying the most advanced information technologies, Frontiers is catapulting scholarly publishing into a new generation.

What are Frontiers Research Topics?

Frontiers Research Topics are very popular trademarks of the Frontiers Journals Series: they are collections of at least ten articles, all centered on a particular subject. With their unique mix of varied contributions from Original Research to Review Articles, Frontiers Research Topics unify the most influential researchers, the latest key findings and historical advances in a hot research area! Find out more on how to host your own Frontiers Research Topic or contribute to one as an author by contacting the Frontiers Editorial Office: frontiersin.org/about/contact

INSIGHTS IN PLANT BIOPHYSICS AND MODELING: 2021

Topic Editor:
Maciej Andrzej Zwieniecki, University of California, Davis, United States

Citation: Zwieniecki, M. A., ed. (2022). Insights in Plant Biophysics and Modeling: 2021. Lausanne: Frontiers Media SA. doi: 10.3389/978-2-83250-470-3

Table of Contents

frontiers in Plant Science

ORIGINAL RESEARCH
published: 03 February 2022
doi: 10.3389/fpls.2022.829580

Simulation of Wheat Response to Future Climate Change Based on Coupled Model Inter-Comparison Project Phase 6 Multi-Model Ensemble Projections in the North China Plain

Huizi Bai[1], Dengpan Xiao[1,2,3], Bin Wang[4], De Li Liu[4,5] and Jianzhao Tang[1]*

[1]Engineering Technology Research Center, Geographic Information Development and Application of Hebei, Institute of Geographical Sciences, Hebei Academy of Sciences, Shijiazhuang, China, [2]College of Geography Science, Hebei Normal University, Shijiazhuang, China, [3]Hebei Laboratory of Environmental Evolution and Ecological Construction, Shijiazhuang, China, [4]NSW Department of Primary Industries, Wagga Wagga Agricultural Institute, Wagga Wagga, NSW, Australia, [5]Climate Change Research Centre and ARC Centre of Excellence for Climate Extremes, University of New South Wales, Sydney, NSW, Australia

OPEN ACCESS

Edited by:
Maciej Andrzej Zwieniecki, University of California, Davis, United States

Reviewed by:
Mohammad Nauman Khan, Huazhong Agricultural University, China
Hadi Pirasteh-Anosheh, Agricultural Research, Education and Extension Organization, Iran

***Correspondence:**
Dengpan Xiao
xiaodp@sjziam.ac.cn

Specialty section:
This article was submitted to Plant Biophysics and Modeling, a section of the journal Frontiers in Plant Science

Received: *06 December 2021*
Accepted: *06 January 2022*
Published: *03 February 2022*

Citation:
Bai H, Xiao D, Wang B, Liu DL and Tang J (2022) Simulation of Wheat Response to Future Climate Change Based on Coupled Model Inter-Comparison Project Phase 6 Multi-Model Ensemble Projections in the North China Plain. Front. Plant Sci. 13:829580. doi: 10.3389/fpls.2022.829580

Global climate change results in more extreme temperature events, which poses a serious threat to wheat production in the North China Plain (NCP). Assessing the potential impact of temperature extremes on crop growth and yield is an important prerequisite for exploring crop adaptation measures to deal with changing climate. In this study, we evaluated the effects of heat and frost stress during wheat sensitive period on grain yield at four representative sites over the NCP using Agricultural Production System Simulator (APSIM)-wheat model driven by the climate projections from 20 Global Climate Models (GCMs) in the Coupled Model Inter-comparison Project phase 6 (CMIP6) during two future periods of 2031–2060 (2040S) and 2071–2100 (2080S) under societal development pathway (SSP) 245 and SSP585 scenarios. We found that extreme temperature stress had significantly negative impacts on wheat yield. However, increased rainfall and the elevated atmospheric CO_2 concentration could partly compensate for the yield loss caused by extreme temperature events. Under future climate scenarios, the risk of exposure to heat stress around flowering had no great change but frost risk in spring increased slightly mainly due to warming climate accelerating wheat development and advancing the flowering time to a cooler period of growing season. Wheat yield loss caused by heat and frost stress increased by –0.6 to 4.2 and 1.9–12.8% under SSP585_2080S, respectively. We also found that late sowing and selecting cultivars with a long vegetative growth phase (VGP) could significantly compensate for the negative impact of extreme temperature on wheat yields in the south of NCP. However, selecting heat resistant cultivars in the north NCP and both heat and frost resistant cultivars in the central NCP may be a more effective way to alleviate the negative effect of extreme temperature on wheat yields. Our findings showed that not only heat risk should be concerned under climate warming, but also frost risk should not be ignored.

Keywords: climate change, heat stress, frost stress, CMIP6, wheat yield, APSIM

INTRODUCTION

Climate change, as one of the most important factors that determine crop yield, could explain 30–50% of global yield variability (Ray et al., 2015; Rezaei et al., 2018). Along with warming climate, the intensity, frequency, and duration of extreme climate events are also increasing, which can exacerbate the instability of agricultural production systems (Zheng et al., 2012; Chen et al., 2018). Predicting the potential impact of future climate change and climate extreme on agricultural production is crucial for developing adaptation strategies to reduce climate risks (Chen et al., 2018).

China is currently the largest wheat-producing country in the world, accounting for more than 17.6% of the global wheat production (FAO, 2013). The North China Plain (NCP) is one of the major winter wheat planting areas in China, accounting for over 50% of China's total wheat production (Xiao et al., 2020). Therefore, ensuring wheat production in the NCP is not only for food security in China but also for the stability and sustainability of the global food market. However, wheat production will be threatened by the increased extreme climate events. For example, short episodes of heat stress during flowering can lead to sterility and abortion of grains, resulting in a low grain number (Ferris et al., 1998). During the grain filling period, heat stress can accelerate leaf senescence and affect final grain weight by shortening the duration of grain filling (Zhao et al., 2007; Dias and Lidon, 2009). For every unit increase of the sum of daily heat degrees over 30°C during anthesis and grain filling, grain yield was reduced by 1.0–1.6% (Liu et al., 2016).

Along with climate warming, most previous studies have been well concerned with the effect of heat stress on crop production (Talukder et al., 2014; Liu et al., 2016; Chen et al., 2018). However, the advancement of crop phenological stages caused by increasing temperature has the potential to increase the risk of spring frost (Saeidi et al., 2012; Chen et al., 2014). Actual frost risk for crop does not decrease as expected and shows an increasing trend in the future in some regions (He et al., 2012; Crimp, 2014). Moreover, experiencing a warm winter for winter wheat is more vulnerable to low temperature stress in the spring because warm winter could affect the process of cold hardening and even cause dehardening (Bokhorst et al., 2010; Li et al., 2015a). In the NCP, frost injury usually occurs in March and April during jointing and booting stages (Wu et al., 2014; Li et al., 2015a). Generally, the frost stress-induced yield loss is attributed mainly to the reduction of tiller and spike number, which are associated with a decrease in photosynthetic rate, specific leaf area, and shoot biomass (Valluru et al., 2012; Thakur and Nayyar, 2013; Li et al., 2015b). For example, each additional day in low temperature duration at jointing and booting stages could reduce grain yield by 4.3–4.8 and 5.2–6.7% for two different wheat cultivars under the minimum temperature of −2°C, respectively (Ji et al., 2017).

Generally, proper adjustment of cultivars and sowing dates can reduce the impact of extreme climate stress on crop production (Bai et al., 2020). Gouache et al. (2012) showed that compared to the reference strategy, earlier sowing wheat by 30 days can decrease heat stress days by 0.9 days, and heat-tolerant cultivar can reduce heat stress days by 3.5 days during wheat grain filling in the future period 2070–2099. In addition, late sowing date and using long-season cultivars could be possible strategies to minimize frost damage for wheat (Zheng et al., 2012; Xiao et al., 2018a).

Process-based crop models are valuable tools for evaluating the impact of climate change on crop production (Challinor et al., 2014). Numerous studies have employed crop models to assess the effects of temperature changes on crop production (Lobell and Asner, 2003; Tao and Zhang, 2013; Asseng et al., 2015). However, these studies mainly consider the impact of mean temperature on crop development and yield and ignore the effect of extreme temperature on crop production, which could underestimate climate change impacts on crop yield (Tao et al., 2012; Wang et al., 2013). This is because most crop models cannot directly and effectively simulate the effects of heat or frost stress on crop development, growth, and yield (Xiao and Tao, 2014). Currently, several studies have tried to consider extreme climate stress by incorporating a series of stress functions that accelerate leaf senescence and reduce grain number and yield into present crop models (Stöckle et al., 2003; Barlow et al., 2015; Bell et al., 2015). Using these improved crop models, some studies evaluated the response and adaptation of crop to extreme temperature under future climate scenarios, but most studies only focused on a type of extreme temperature, that is, heat stress (Gouache et al., 2012; He et al., 2012; Chen et al., 2018). To more realistically assess crop yields and explore adaptation measures for future climate change, it is necessary to analyze the potential impact of the co-occurrence of frost and heat stress on crop yield.

In this study, we aim to assess the impacts of future climate change mainly including heat and frost stress on wheat yield in the NCP using the Agricultural Production System Simulator (APSIM) model forced by statistically downscaled daily climate data from 20 Global Climate Models (GCMs) in the Coupled Model Inter-comparison Project phase 6 (CMIP6). The objectives of this study were to (1) investigate the response of wheat phenology and yield to future climate change in the NCP; (2) separately and jointly evaluate the impacts of heat and frost stress on wheat production; and (3) identify the optimum cultivar and sowing time to minimize the risk of yield loss mainly caused by heat and frost stress under future climate scenarios.

MATERIALS AND METHODS

Study Sites

The NCP as shown in **Figure 1** is an important base for wheat production in China. The main soil type in the NCP is loam of Aeolian origin, a soil type deposited by rivers over geological periods. The NCP has a warm and semi-humid continental monsoon climate. Seasonal precipitation is not evenly distributed, 50–80% of which occurs in the period from July to September. The NCP has a reliance on irrigation to support the intensive double cropping system with rotation

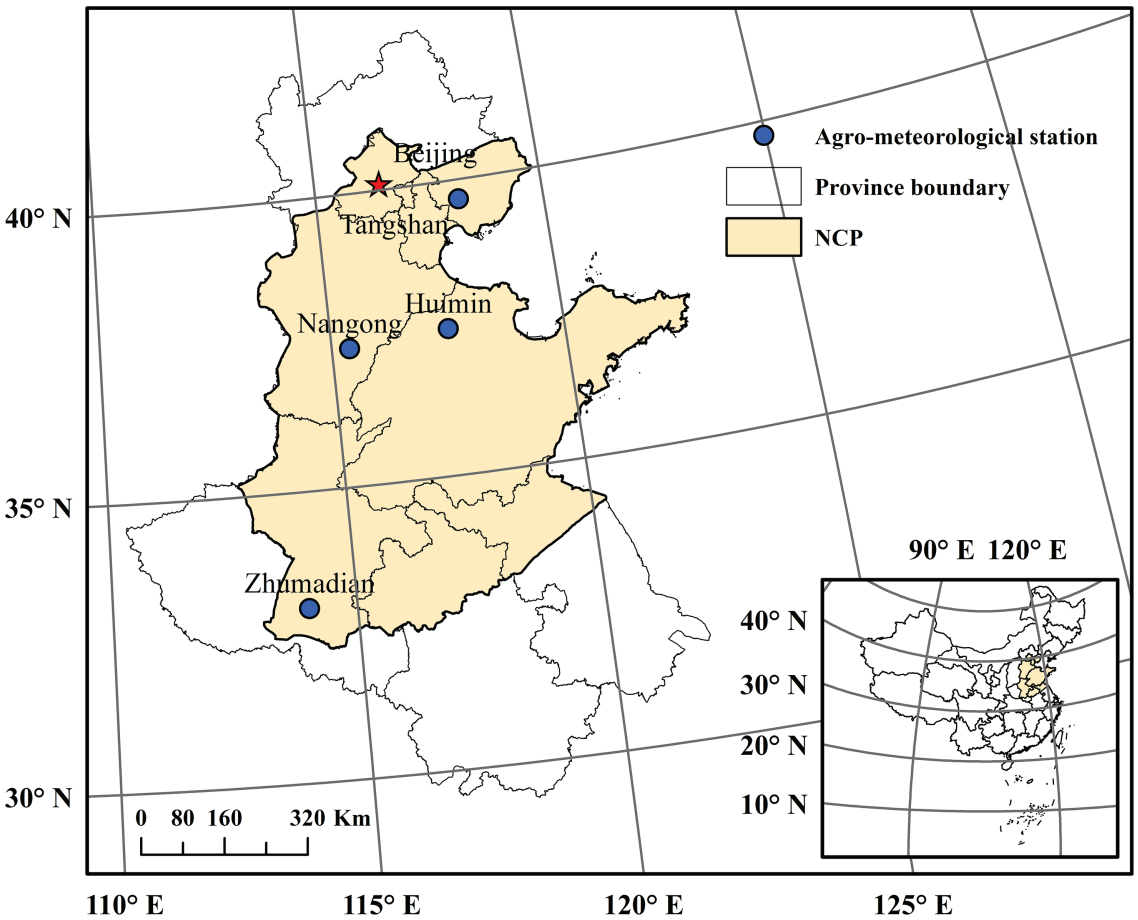

FIGURE 1 | Locations of the four investigated agro-meteorological stations in the North China Plain (NCP).

between winter wheat and summer maize. Winter wheat is grown from early October to June of the following year (the average growth period in the past 30 years) under irrigated conditions and intensive use of fertilizer, pesticides, and herbicides (Xiao et al., 2013; Xiao and Tao, 2014). After fully considering the completeness and quality of crop and climate data, we selected four representative sites in the northern, central, and southern parts of the North China Plain respectively, including Tangshan (TS) and Nangong (NG) stations in Hebei province, Huimin (HM) station in Shandong province and Zhumadian (ZMD) station in Henan province (**Figure 1**). All the selected sites are typical winter wheat production zones, representative of typical double cropping system in the NCP, which are geographically and climatologically different and have good records on weather/crop data. Detailed information about crop and climate for these four stations was given in **Table 1**.

Climate and Crop Data

Crop data for wheat at the four stations, including crop phenological stages, yield, and agronomic management practices, were also obtained from the CMA. Crop management practices at the stations were generally same as the local

TABLE 1 | General information about crop and climate data for the four investigated stations in the North China Plain (NCP).

Station	Tangshan (TS)	Nangong (NG)	Huimin (HM)	Zhumadian (ZMD)
Crop data				
Year	2005–2008	2006–2008	2005–2009	2006–2009
Cultivar	Jingdong8	Shimai12	Lumai23	Zhengmai9023
Mean sowing date (DOY)	277	285	281	295
Mean jointing date (DOY)	111	94	98	70
Mean flowering date (DOY)	132	122	126	104
Mean maturity date (DOY)	166	157	159	139
Mean yield (kg ha^{-1})	6415.4	6442.6	6833.2	5373.0
Climate data				
Mean daily temperature (°C)	12.8	14.0	13.5	15.7
Mean daily solar radiation (MJ m^{-2})	13.9	13.3	13.6	12.1
Total precipitation (mm)	587.7	454.4	538.9	999.7
Soil type	Loam	Loam	Loam	Silty loam

TABLE 2 | List of the 20 Global Climate Models (GCMs) for future climate projections used in this study.

Code	GCM name	Abbreviation	Institute ID	Country	Spatial resolution of atmospheric model
1	ACCESS-CM2	ACC1	CSIRO–ARCCSS	Australia	1.9° × 1.3°
2	ACCESS-ESM1-5	ACC2	CSIRO–ARCCSS	Australia	1.9° × 1.3°
3	BCC-CSM2-MR	BCC	BCC	China	1.1° × 1.1°
4	CanESM5	CAN1	CCCMA	Canada	2.8° × 2.8°
5	CanESM5-CanOE	CAN2	CCCMA	Canada	2.8° × 2.8°
6	CNRM-CM6-1	CNR1	CNRM	France	1.4° × 1.4°
7	CNRM-ESM2-1	CNR2	CNRM	France	1.4° × 1.4°
8	EC-Earth3-Veg	ECE1	EC–EARTH	Europe	0.7° × 0.7°
9	EC-Earth3	ECE2	EC–EARTH	Europe	0.7° × 0.7°
10	FGOALS-g3	FGO	FGOALS	China	2.0° × 2.3°
11	GFDL-ESM4	GFD	NOAA–GFDL	America	1.0° × 1.0°
12	GISS-E2-1-G	GIS	NASA–GISS	America	2.5° × 2.0°
13	INM-CM4-8	INM1	INM	Russia	2.0° × 1.5°
14	INM-CM5-0	INM2	INM	Russia	2.0° × 1.5°
15	IPSL-CM6A-LR	IPS	IPSL	France	2.5° × 1.3°
16	MPI-ESM1-2-HR	MPI1	MPI-M	Germany	0.9° × 0.9°
17	MPI-ESM1-2-LR	MPI2	MPI-M	Germany	1.9° × 1.9°
18	MIROC6	MIR1	MIROC	Japan	1.4° × 1.4°
19	MIROC-ES2L	MIR2	MIROC	Japan	2.8° × 2.8°
20	MRI-ESM2-0	MRI	MRI	Japan	1.9° × 1.9°

farmer's practices (Tao et al., 2014). Winter wheat at ZMD (high-rainfall site) was maintained under rainfed, while regular irrigation was applied to winter wheat at the other three stations. About 100 and 60 kg/ha nitrogen were applied at sowing and jointing, respectively.

Historical daily climate data from 1961 to 2014 at the four selected stations were obtained from the Chinese Meteorological Administration (CMA), including minimum (T_{min}) and maximum temperature (T_{max}), sunshine hours, and precipitation (Prec). Daily solar radiation (Rad) was calculated from daily sunshine hours using the Angstrom equation (Prescott, 1940).

Future climate projections were based on 20 GCMs from CMIP6 (**Table 2**).[1] These climate projections were driven by a new set of integrated assessment models (IAMs) based on the Shared Socioeconomic Pathways (SSPs) and the Representative Concentration Pathways (RCPs; O'Neill et al., 2016). In this study, we used future climate projections for two integrated scenarios (combining SSP2 with RCP4.5, defined by SSP245 and combining SSP5 with RCP8.5, defined by SSP585). SSP2 envisions a central pathway in which social, economic, and technological trends do not shift markedly from historical patterns. SSP5 envisions fossil-fueled development pathway with rapid technological progress and development of human capital (O'Neill et al., 2016). RCP4.5 is a medium radiative forcing pathway (4.5 W m^{-2} in 2100), and RCP8.5 is a high radiative forcing pathway (8.5 W m^{-2} in 2100).

Since the spatial resolution of different GCMs varied greatly and the crop data was site-based, we uniformly downscaled the grid data to sites. In addition, the APSIM model is driven by daily climate data. In this study, the monthly gridded data projected by the GCMs were downscaled to daily climate series for the four selected stations using a statistical downscaling method developed by Liu and Zuo (2012). This approach used monthly gridded GCM climate data and parameters derived from GCM projections and climate observations to generate a realistic time series of daily temperature, precipitation, and solar radiation. Firstly, monthly GCM simulations of the different climate variables were downscaled to specific stations using the inverse distance-weighted interpolation method (IDW). Secondly, quantile-quantile bias correction approach is applied to ensure that the model-derived monthly data matches well with the observed data for a historical training period (Liu and Zuo, 2012). Finally, daily climate data for each station were generated from the spatially downscaled monthly GCM projections using the modified stochastic weather generator (WGEN; Richardson and Wright, 1984). More detailed description of the method can be found in Liu and Zuo (2012). Bai et al. (2020) assessed the performance of the downscaled GCMs data from CMIP6 in reproducing historical changes of extreme climate indices using the multi-model arithmetic mean and found that the ensemble results could better reproduce historical changes of extreme climate than any individual GCM. In this study, we downscaled climate inputs for APSIM model for the 1961–2100 period at the four agro-meteorological stations under each of the 20 GCMs for SSP245 and SSP585.

APSIM-Wheat Model and Setting for Frost and Heat Stress

Agricultural Production System Simulator model is a biophysical model to simulate crop growth and development on a daily time step (Holzworth et al., 2014). It can be used to mimic the response of single crop or crop rotations to climate change with different management practices (Holzworth et al., 2014). In APSIM-wheat model, wheat phenological development is

[1]https://esgf-node.llnl.gov/search/cmip6/

defined by 11 crop stages and 10 crop phases (time between stages). The time of each phase is mainly determined by the accumulation of thermal time adjusted for other factors (e.g., vernalization and photoperiod) which vary with the phase considered. A more detailed description of the model is documented at http://www.apsim.info. In our study, APSIM-wheat version 7.10 was used to evaluate the responses of winter wheat yield to climate change, cultivar and sowing date adjusting.

In the NCP, wheat growth and development often suffer from heat and frost stress events. However, the APSIM-wheat model does not consider the effects of heat and frost stress on wheat yield (Bell et al., 2015). Under the background of global warming, it is very important to assess the impacts of heat and frost stress on wheat production. In the study area, frosts usually occur 3 or 4 weeks before head emergence when wheat is at the jointing stage (Zhong et al., 2008). In addition, cold stress during the period from booting to flowering can reduce the grain number per spike and decreased grain yield (Subedi et al., 1998). Based on previous studies and field trial data, spring frost damage generally occur when daily minimum temperature is below 0°C (Barlow et al., 2015; Zheng et al., 2015). Moreover, related studies indicated that wheat is more sensitive to heat stress that occurs at anthesis than it occurs during grain filling (Kang, 2015; Liu et al., 2016). The optimum temperature for wheat flowering and grain filling ranges from 19 to 22°C (Porter and Gawith, 1999). The threshold of 32°C is commonly regarded as the upper base temperature during the period of pre-anthesis (Porter and Gawith, 1999; Yang et al., 2017). For the grain filling period, the upper base temperature is between 33.4 and 37.4°C (Russell and Wilson, 1994; Porter and Gawith, 1999). We used the threshold of 35°C as the upper base temperature during the grain filling period in the NCP (Liu et al., 2016; Yang et al., 2017).

In this study, yield loss was calculated by multiplying influence coefficients depending on the frequency and intensity of heat and frost events during the critical phenological phase (**Table 3**). Since there are not sufficient data to test the impacts of frost or heat stress on winter yields for different cultivars at each site, yield reduction multipliers for heat and frost stress events are all the same in APSIM model for different sites based on the study of Bell et al. (2015). Although this approach in APSIM has not been fully calibrated, it provides some helpful information to capture the loss of crop yield due to heat and frost stress (Bell et al., 2015). This approach has been widely used to explore optimum flowering periods for wheat in Australia (Luo et al., 2018; Chen et al., 2020).

TABLE 3 | Temperature criteria and yield reductions caused by frost and heat stress during wheat growth stages (Zadoks growth stage).

Stress	Sensitive stage (corresponding phenological phase)	Temperatures condition for frost or heat stress	Yield loss (% per day)
Frost	Z31–60[a] (jointing to flowering)	$T_{min} \leq -2$°C	5%
	Z60–79 (flowering to grain filling)	$T_{min} \leq 0$°C	10%
Heat	Z55–65 (pre-flowering)	$T_{max} \geq 32$°C	10%
	Z65–79 (post-flowering to grain filling)	$T_{max} \geq 35$°C	10%

[a]*Note that Zadoks growth stage from Zadoks et al. (1974).*

Simulation Setting

The APSIM-wheat model at four investigated stations was calibrated and validated in Xiao et al. (2018b). The model was robust to simulate dates of flowering and maturity with the root-mean-square deviation (RMSD) less than 5 days and yield with RMSD less than 10% compared to the observed value (**Supplementary Figure S1**). Detailed information of field management practices (e.g., sowing density, fertilization, and irrigation) referred to Xiao et al. (2018b). Based on long-term historical phenology records, sowing dates of wheat at four investigated stations were shown in **Table 1**. In this study, we mainly focused on the analyses of the impact of climate change (including heat and frost stress), cultivar, and sowing dates on wheat yield for three different 30-year periods under SSP245 and SSP585 scenarios, including the historical period of 1981–2010 (referred to as the baseline period) and the two future periods, that is, 2031–2060 (referred to as the 2040S) and 2071–2100 (referred to as the 2080S).

Elevated atmosphere CO_2 concentration [(CO_2)] in the future can significantly affect crop yield. During the baseline period, we set the [CO_2] to 380 ppm. The yearly atmospheric [CO_2] for the two future periods were calculated using empirical equations that were obtained by non-linear least-squares regression, based on the concentration pathway given by The Scenario Model Inter-comparison Project (ScenarioMIP) for CMIP6 (O'Neill et al., 2016). The empirical equations for calculating [CO_2] for SSP245 and SSP585 are as follows:

$$CO_{2,\mathrm{SSP245}} = 62.044 + \frac{34.002 - 3.8702y}{0.24423 - 1.1542y^{2.4901}} + 0.028057(y-1900)^2 + 0.00026827(y-1960)^3 - 9.2751\times10^{-7}(y-1910)^4 - 2.2448(y-2030) \quad (1)$$

$$CO_{2,\mathrm{SSP585}} = 757.44 + \frac{84.938 - 1.537y}{2.2011 - 3.8289\mathrm{y}^{-0.45242}} + 2.4712\times10^{-4}(y+15)^2 + 1.9299\times10^{-5}(y-1937)^3 + 5.1137\times10^{-7}(y-1910)^4 \quad (2)$$

where y is the calendar year from 1900 to 2100 (i.e., $y = 1900, 1901, \ldots, 2100$).

Evaluating the Impacts of Heat and Frost Stress on Wheat Production

In this study, we evaluated the impacts of heat and frost stress on wheat yield at four study sites in the NCP with and without

TABLE 4 | Phenological parameters for historical cultivar (HC) and three virtual wheat cultivars (VC1, VC2, and VC3) in the Agricultural Production System Simulator (APSIM)-wheat model.

Station	Cultivar	tt_end_of_juvenile	tt_floral_initiation	startgf_to_mat	vern_sens	photop_sens
TS	HC	650	400	640	2.5	2.5
	VC1	715	440	640	2.5	2.5
	VC2	650	400	704	2.5	2.5
	VC3	715	440	704	2.5	2.5
NG	HC	590	460	590	2.4	2.5
	VC1	649	506	590	2.4	2.5
	VC2	590	460	650	2.4	2.5
	VC3	649	506	650	2.4	2.5
HM	HC	610	500	600	2.4	2.5
	VC1	671	550	600	2.4	2.5
	VC2	610	500	660	2.4	2.5
	VC3	671	550	660	2.4	2.5
ZMD	HC	505	460	620	2.3	2.5
	VC1	555	506	620	2.3	2.5
	VC2	505	460	682	2.3	2.5
	VC3	555	506	682	2.3	2.5

Note that vern_sens is sensitivity to vernalization; photop_sens is sensitivity to photoperiod; tt_end_of_juvenile is thermal time required from end of juvenile to floral initiation (°Cd); tt_floral_initiation is thermal time required from floral initiation to flowering (°Cd); and startgf_to_mat is thermal time required from flowering to grain filling (°Cd).

changing sowing time and cultivar. Impact of extreme stress on yield in the baseline period (Y_{bc}) at each station for each GCM was identified as

$$Y_{bc} = \frac{Y_B - Y_A}{Y_A} \times 100\% \quad (3)$$

where Y_A and Y_B were annual average of simulation results for baseline period without and with the effect of extreme stress, respectively.

The relative change of impacts of extreme stress on crop yield in the future period (Y_{fc}) compared to baseline at each station for each GCM was defined as:

$$Y_{fc} = \left(\frac{Y_D - Y_C}{Y_A} - Y_{bc} \right) \times 100\% \quad (4)$$

where Y_C and Y_D were average simulated yield for the future period without and with the effect of extreme stress, respectively.

Optimizing Cultivar and Sowing Time Under Future Climate Scenarios

Using agronomic adaptation options is an effective option to improve yield performance (Bai and Tao, 2017). In this study, we investigated the wheat yield performance of historical cultivar (HC) and three virtual cultivars [thermal time in the vegetative growth phase (VGP) of HC increased by 10%, VC1; thermal time in the reproductive growth phase (RGP) of HC increased by 10%, VC2; thermal time in both the vegetative and RGPs of HC increased by 10%, VC3] for each station under future climate scenarios without and with the effect of extreme stress. Phenological parameters for HCs and three created wheat cultivars in the APSIM-Wheat model were shown in **Table 4**.

To derive the optimum sowing date for wheat in the NCP under SSP245 and SSP585 scenarios, the yield performance for four investigated stations was evaluated with different sowing dates ranging from 20 days before historical sowing date (**Table 1**) to 30 days after historical sowing date with an interval of 5 days in the two future periods (2040S and 2080S).

RESULTS

Projected Future Climate Change

Changes in mean daily solar radiation and temperature (i.e., T_{max} and T_{min}) and total annual precipitation for the two future periods (2040S and 2080S) relative to the baseline period based on the downscaled data from the 20 GCMs under SSP245 and SSP585 scenarios were shown in **Supplementary Figure S2**. For T_{max} and T_{min}, four investigated stations showed significantly increasing trends in all the GCMs (**Supplementary Figures S2B,C**). For solar radiation, there were increasing trends at all the investigated stations for the two future periods under both SSP245 and SSP585 scenarios (**Supplementary Figure S2A**). Moreover, the increase in mean daily radiation during 2080S at four stations under SSP245 scenario was greater than that under SSP585 scenario (**Supplementary Figure S2A**). As for precipitation, the average change projected by 20 GCMs showed that precipitation increased at all the stations for two future periods under SSP245 and SSP585 scenarios (**Supplementary Figure S2D**). Moreover, precipitation variability projected by 20 GCMs was large.

Monthly heat (the number of days with $T_{max} \geq 32°C$) and frost (the number of days with $T_{min} < 0°C$) days for baseline period and two future periods under SSP245 and SSP585 scenarios are shown in **Figure 2**. Along with climate warming, heat days in each month increased significantly at all the

stations under future climate scenarios. Heat days were mainly concentrated from May to September (**Figures 2A,C,E,G**). In the baseline period, wheat bloomed in April at ZMD station and in May at other stations. Across the stations, the average number of heat days in May projected by 20 GCMs increased by 1.2–4.0 and 1.7–5.3 days under SSP245 and SSP585 scenarios during 2040S, respectively, and increased by 2.4–7.1 and 5.4–12.2 days under SSP245 and SSP585 scenarios during 2080S, respectively (**Figures 2A,C,E,G**). Heat days in April projected by 20 GCMs increased slightly. Frost days in each month decreased significantly at all the stations under future climate scenarios (**Figures 2B,D,F,H**). Frost days were mainly concentrated from December to February of the following year at ZMD station and concentrated from November to March of the following year at other stations. In the baseline period, wheat jointed in March at ZMD station and in April at other stations. There will be almost no frost days in March at ZMD station and no frost days in April at other stations under the future climate scenario (**Figures 2B,D,F,H**).

Shift in Wheat Phenology Under Future Climate Scenarios

Generally, warming climate could accelerate crop development rate and consequently reduce crop growth duration. In this study, the simulation results showed that there was a significant advancing trend in wheat phenology (e.g., jointing date, flowering date, and maturity date) under future climate scenarios (**Figure 3**). The advance in the days of wheat phenology during 2080S was greater than that during 2040S. Moreover, changes in wheat phenology under SSP585 scenario were greater than those under SSP245 scenario (**Figure 3**). As the sowing date remained unchanged for the two future periods, the advance in flowering and maturity dates significantly shortened the VGP (duration from sowing to flowering) and the whole growth phase (WGP, duration from sowing to maturity) of wheat. However, the RGP (duration from flowering to maturity) of wheat was prolonged by 0.2–1.3 and 0.4–1.7 days across the stations under SSP245 and SSP585 scenarios during 2040S, respectively, and prolonged by 0.5–2.5 and 2.1–5.3 days under

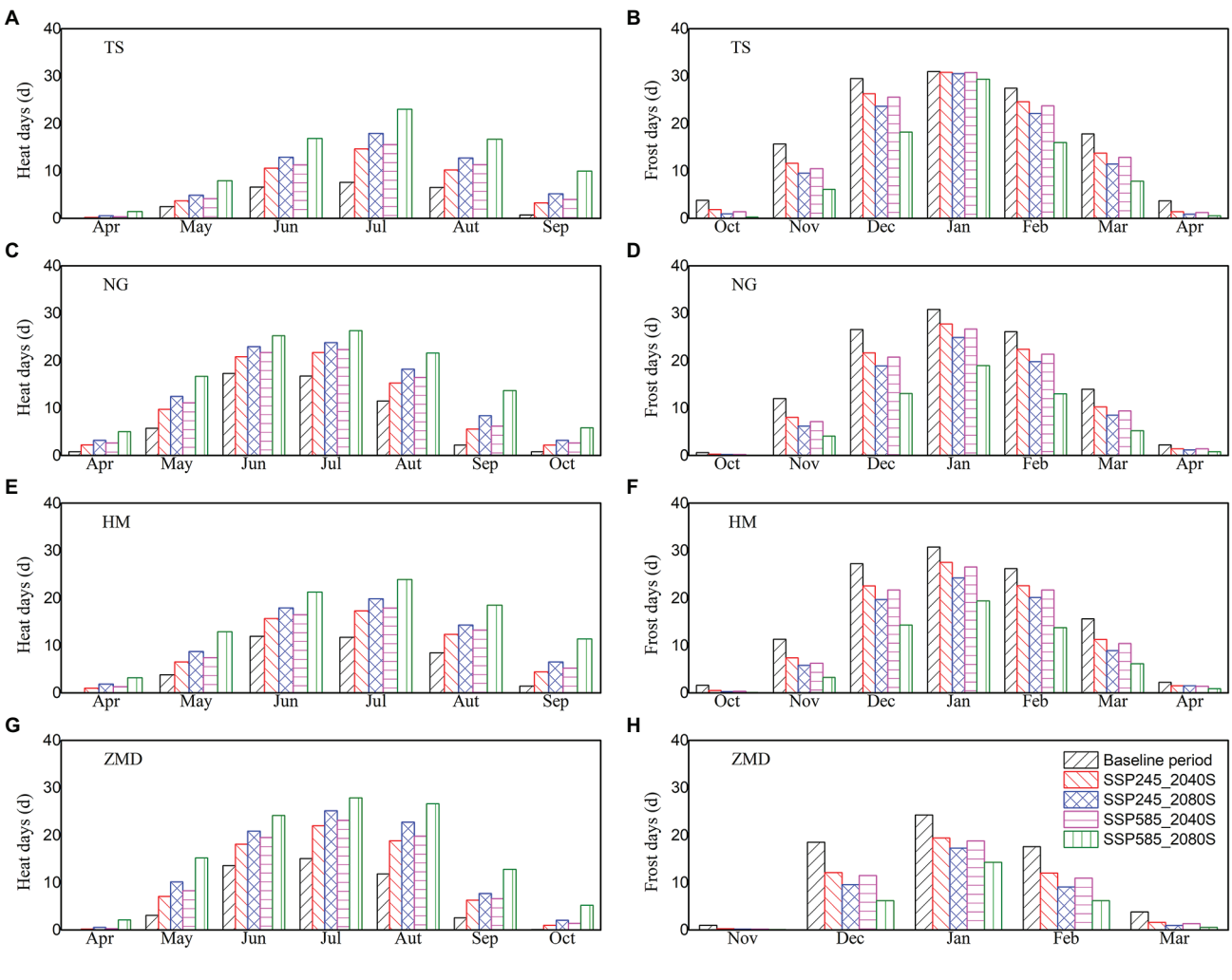

FIGURE 2 | Monthly heat **(A,C,E,G)** and frost **(B,D,F,H)** days for baseline period and two future periods under SSP245 and SSP585 scenarios.

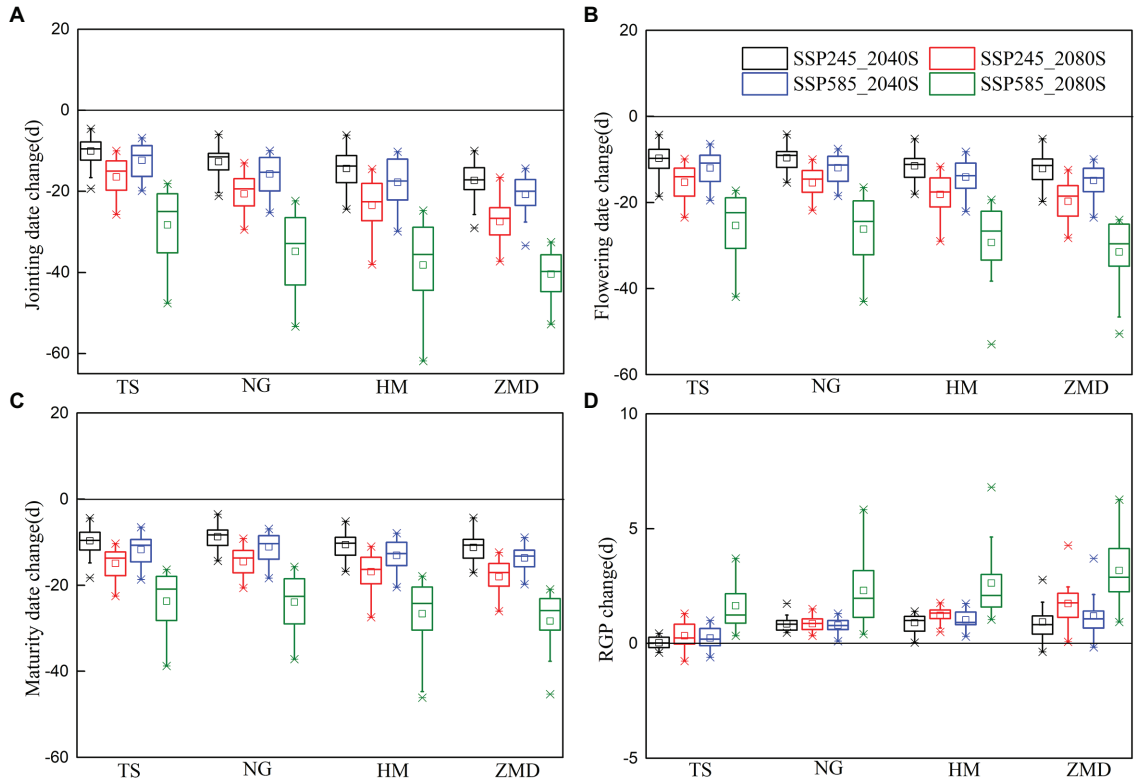

FIGURE 3 | Changes in jointing **(A)**, flowering **(B)**, and maturity **(C)** dates and the reproductive growth phase (RGP), **(D)** in the 2040S and 2080S under SSP245 and SSP585 scenarios relative to the baseline (1981–2010).

two scenarios during 2080S, respectively (**Figure 3D**). The main reason for the extension of the RGP was that the early trend in maturity date was less than that in the flowering date.

Impacts of Climate Change and Extreme Temperature on Wheat Yield

Winter wheat yields for the baseline and two future periods were investigated with and without considering the effect of extreme temperature (**Figure 4**). Without considering the effect of extreme temperature, wheat yield showed an increasing trend at all the stations under future climate scenarios. The yield increase was largest at ZMD station, increasing by averages of 7.2, 13.6, 9.7, and 13.9% across 20 GCMs under SSP245_2040S, SSP245_2080S, SSP585_2040S, and SSP585_2080S, respectively (**Figures 4G,H**).

The effects of extreme temperature events, including heat stress and frost stress, on yield have been accounted for in this study. In the baseline period, yield change caused by heat stress at NG and HM stations was large, but that at the other two stations was slight (**Figure 4**). The main reason was that the number of heat days during the high temperature sensitive stage of wheat at NG and HM stations was more than that at other stations in the baseline period (**Table 1**; **Figure 2**). Under future climate scenarios, heat days during flowering and grain filling period had a slight decrease at HM station but a slight increase at the other three stations (**Figure 5A**). As a result, wheat yield loss caused by heat stress at HM station decreased by 0.6–3.7% under future climate scenarios, but that at the other stations increased slightly (**Figure 6A**). With the combined effects of climate change and heat stress, wheat yield had an increasing trend under future climate scenarios at all the stations except for NG station (**Figure 4**).

Frost stress had no significant effect on yield at all the stations for the baseline period (**Figure 4**). However, due to the advancement of wheat phenology in the future climate scenarios, frost days from jointing to grain filling had a significant increase at all the stations except for TS station, especially for SSP585_2080S (**Figure 5B**). Wheat yield loss caused by frost stress increased by 3.7–12.8% at ZMD, but that at other stations increased slightly (except for NG and HM under SSP585_2080S; **Figure 6B**). Moreover, wheat yield loss caused by frost stress during 2080S was greater than that during 2040S. Wheat yield loss caused by frost stress under SSP585 scenario was larger than that under SSP245 scenario (**Figure 6B**). With the combined effects of climate change and frost stress, wheat yield had an increasing trend at TS station under future climate scenarios. However, wheat yield increased in 2040S and decreased in 2080S at NG, HM, and ZMD (except for 2040S) stations (**Figure 4**). Moreover, with the combined effects of climate change and heat and frost stress, wheat yield change was similar to that only considering the effect of climate change and frost stress under the future climate scenarios (**Figure 4**). Overall,

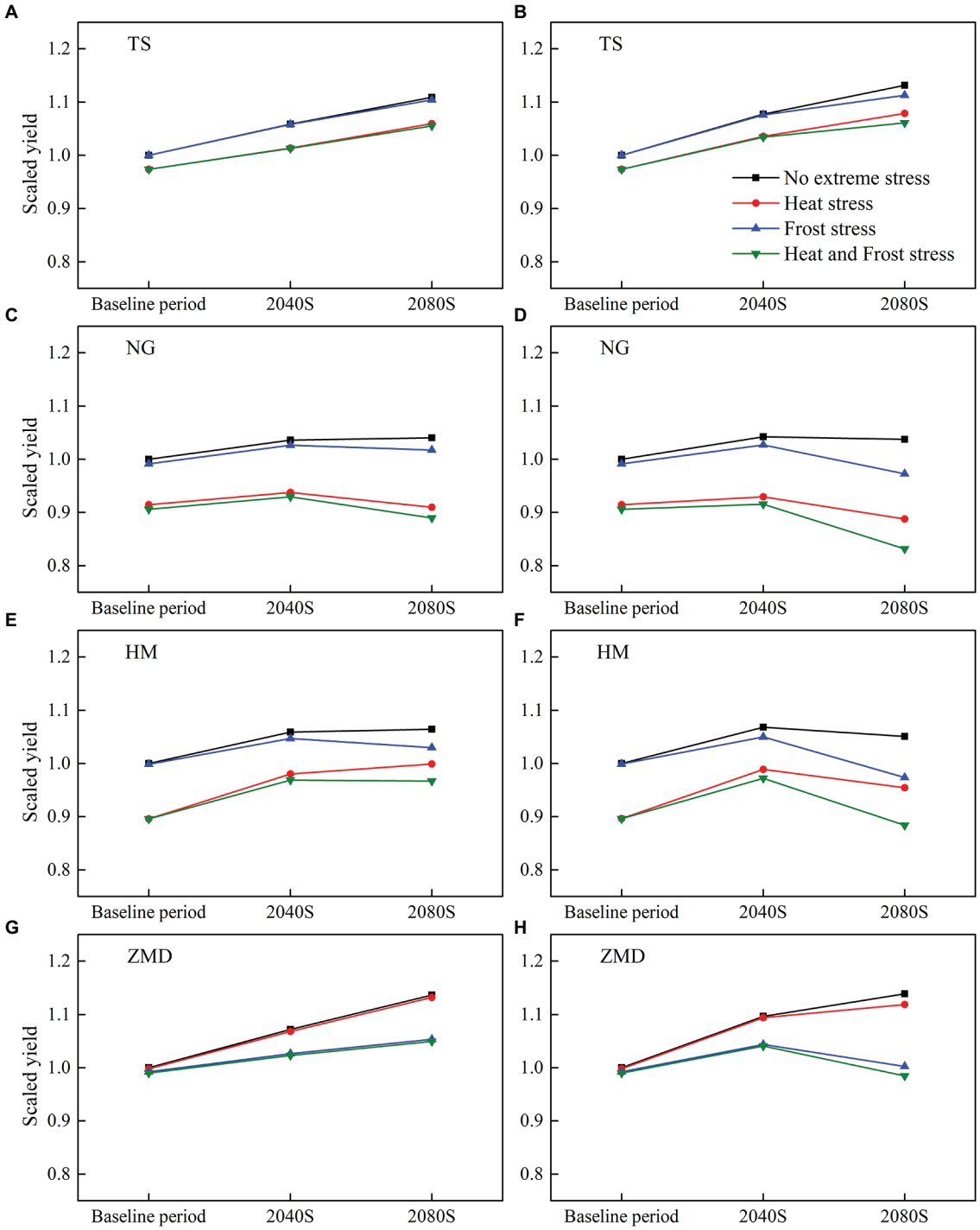

FIGURE 4 | Simulated multi-Global Climate Model (GCM) ensemble mean yield for the baseline and two future periods (2040S and 2080S) under SSP245 **(A,C,E,G)** and SSP585 **(B,D,F,H)** without and with the effect of extreme temperature stress (i.e., heat and frost stress). All the yields have been normalized by historical yield without the effect of extreme temperature events.

wheat yield loss caused by heat and frost stress increased by 3.9–14.4% at ZMD, but that had no significant change under all climate scenarios except for SSP585_2080S at other stations (**Figure 6C**).

Responses of Wheat Yield to Cultivar and Sowing Date Adjustment

Without considering the effects of extreme climate stress (e.g., heat and frost stress), wheat yield under VC2 cultivar

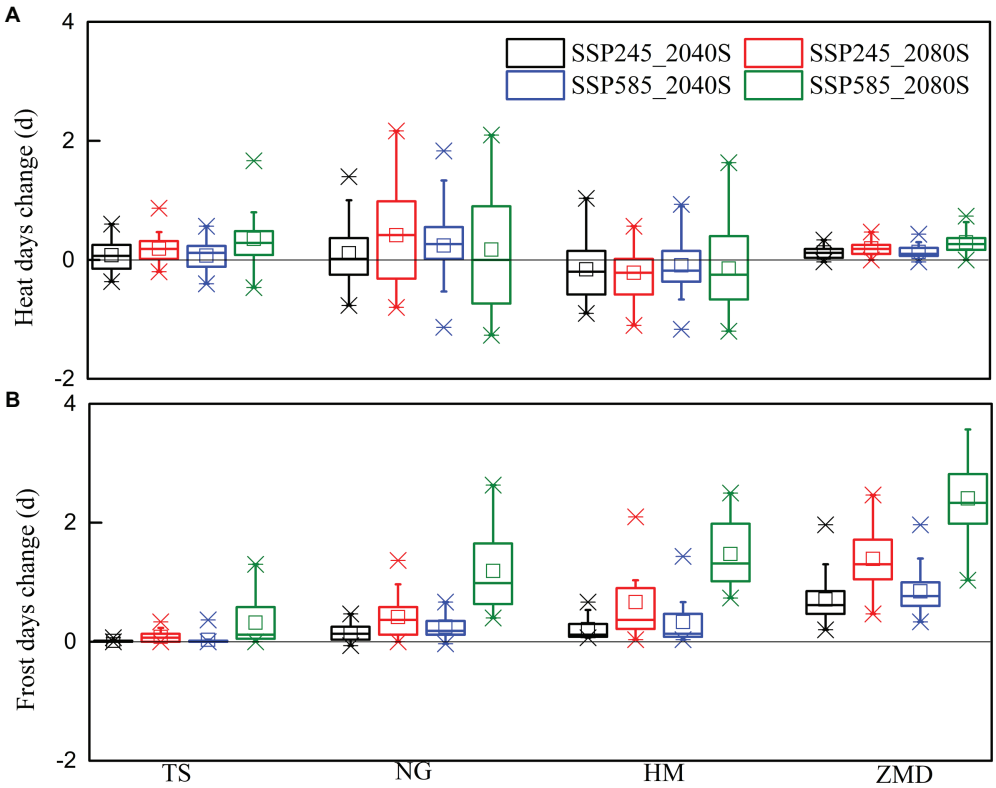

FIGURE 5 | Changes in heat **(A)** and frost days **(B)** during the temperature sensitive stage of wheat in the 2040S and 2080S under SSP245 and SSP585 scenarios compared to the baseline period (1981–2010).

showed the best performance at all the stations in two future periods under both SSP245 and SSP585 scenarios (**Supplementary Figure S3A**). Yield loss caused by heat stress using HC cultivar was smaller than using other virtual cultivars at all stations under future climate scenarios, and yield loss using VC3 cultivar was largest (**Figure 7A**). Moreover, cultivars changes had no significant effect on yield loss caused by heat stress at ZMD station. Yield loss caused by frost stress with VC1 and VC3 cultivars was less than with HC and VC2 at all stations for future climate scenarios (**Figure 7B**). Yield loss caused by heat and frost stress with VC1 cultivar was least at ZMD station, but yield loss with HC cultivar was least at other stations (**Figure 7C**). With the effect of extreme stress, wheat yield with VC1 cultivar showed the best performance at ZMD station for future climate scenarios, but wheat yield with HC cultivar showed the best performance at other stations (**Supplementary Figure S3B**). According to the simulated results, the optimum cultivar was HC cultivar at TS, NG, and HM stations, and the optimum cultivar was VC1 cultivar at ZMD station.

With the combined effect of heat and frost stress, responses of wheat yield to sowing dates in two future periods under SSP245 and SSP585 scenarios were shown in **Figure 8** and **Supplementary Figure S4**, respectively. With the advance of wheat sowing date from historical sowing date, the negative effect of heat stress on yield decreased at all stations except ZMD station under future climate scenarios. However, the negative effect of frost stress on yield significantly increased at all the stations under future climate scenarios (**Figure 8**; **Supplementary Figure S4**). However, with the delay of wheat sowing date from historical sowing date, the negative effect of heat stress on yield significantly increased at all the stations except for ZMD station under future climate scenarios, but the negative effect of frost stress on yield significantly decreased at all the stations except for TS station in 2040S (**Figure 8**; **Supplementary Figure S4**).

Under the combined effect of heat and frost stress, the fluctuation of yield change caused by shift in sowing date reached −42.8–2.0, −47.7–5.3, −45.8–2.8, and −43.0–9.8% under the four future climate scenarios, that is, SSP245_2040S, SSP245_2080S, SSP585_2040S, and SSP585_2080S, respectively, relative to the historical sowing date (**Figure 8**; **Supplementary Figure S4**). The optimum sowing window was to advance historical sowing date by 5–15 days for 2040S under SSP245 and SSP585 scenario at TS station, respectively. The optimum sowing window was to advance historical sowing date by 0–10 days at NG and HM stations during 2040S under the two climate scenarios, but the optimum sowing window was to delay historical sowing date by 5–15 days at ZMD station (**Figure 8**; **Supplementary Figure S4**). Moreover, for all the stations during 2080S under the two climate scenarios, the optimum sowing window was 5–10 days later than that during 2040S (**Figure 8**; **Supplementary Figure S4**).

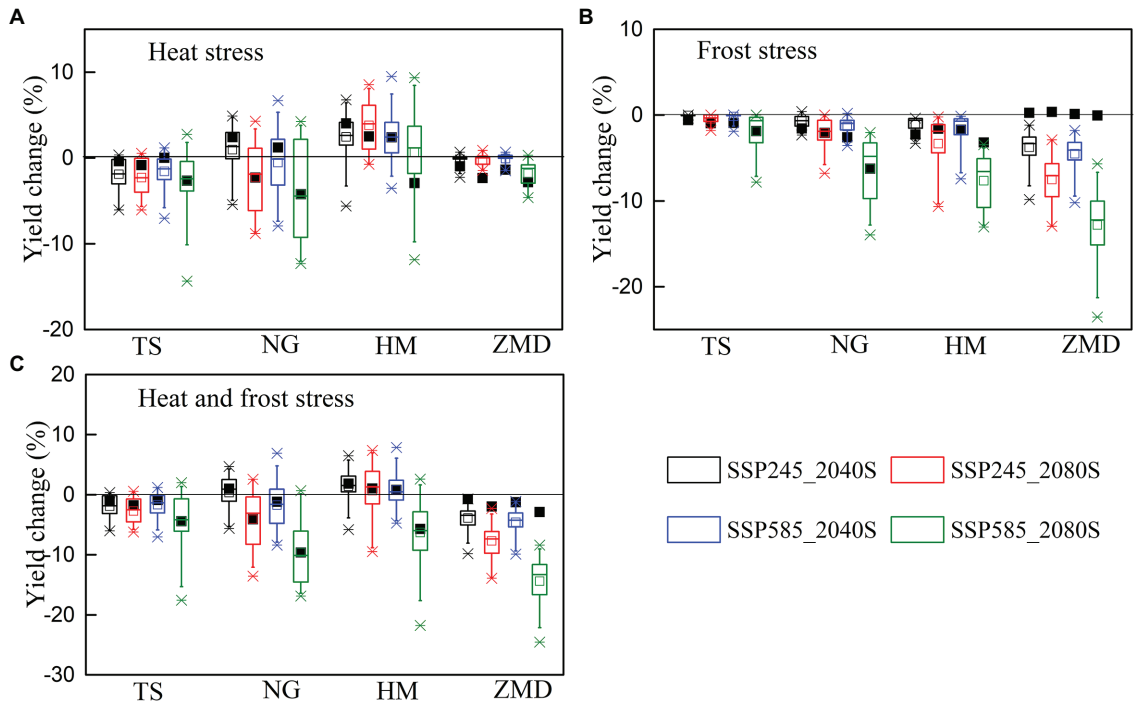

FIGURE 6 | Changes in impacts of heat **(A)**, frost **(B)**, heat and frost stress **(C)** on wheat yield in the 2040S and 2080S under SSP245 and SSP585 scenarios compared to the baseline period (1981–2010). Black rectangles represent multi-model mean values from simulations with optimum adaptation.

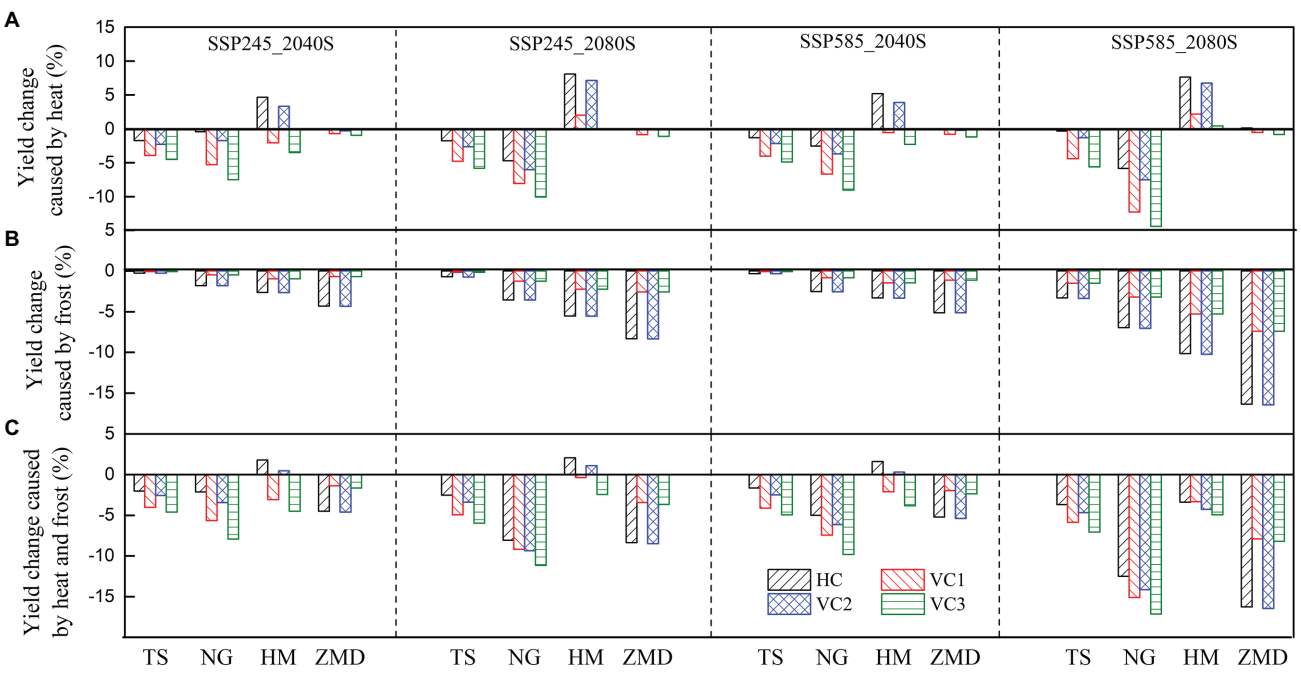

FIGURE 7 | The relative change of impact of heat **(A)**, frost **(B)**, heat and frost stress **(C)** for different cultivars on wheat yield in the 2040S and 2080S under SSP245 and SSP585 scenarios relative to historical cultivar in the baseline (1981–2010).

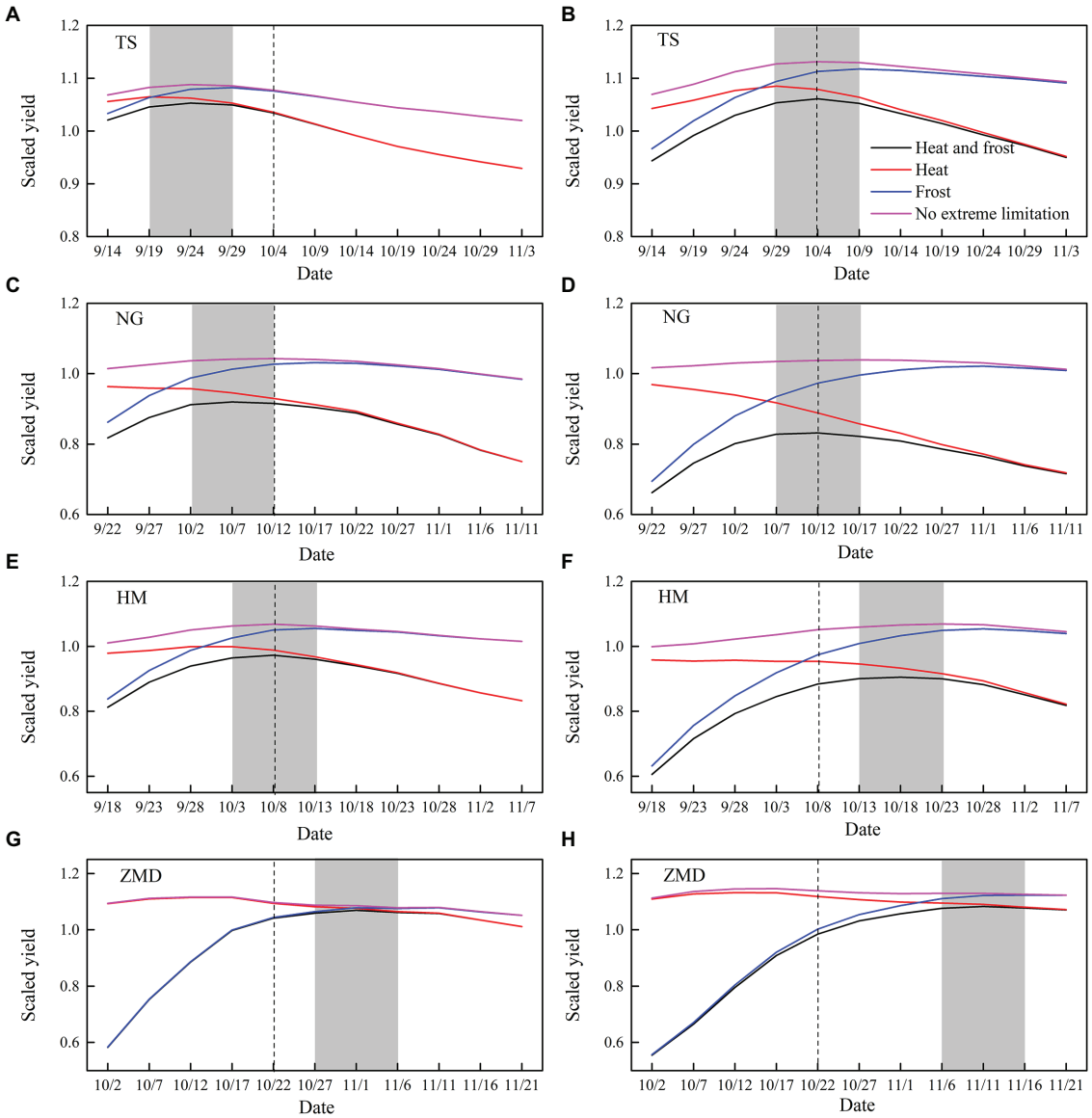

FIGURE 8 | Yield performance considering heat and frost stress in the different sowing dates during the 2040S **(A,C,E,G)** and 2080S **(B,D,F,H)** under SSP245 scenario. The black dotted line is the historical sowing date. The gray rectangle is the optimum sowing window. All the yields have been normalized by historical yield without the effect of extreme temperature events.

The relative changes of the impact of extreme temperature stress on wheat yield with optimum adaptation of sowing date and cultivar selection in the 2040S and 2080S under SSP245 and SSP585 scenarios relative to the baseline period were shown in **Figure 6**. The simulation results showed that there is a trade-off between the effects of heat and frost stress on yield with optimum adaptation. The optimum adaptation decreased the effect of heat stress on yield at TS and NG, but increased the effect of frost stress on yield (**Figures 6A,B**). The optimum adaptation significantly decreased the yield loss caused by the combined effect of heat and frost stress by 3.2–11.5% at ZMD under the future climate scenarios, but slightly reduced the yield loss at the other stations (**Figure 6C**).

DISCUSSION

Changes and variability of climate factors, such as temperature, solar radiation, precipitation, and [CO_2] during crop growing season, could strongly influence crop phenology and productivity (Lin et al., 2005; Tao et al., 2014; Zhang et al., 2016). Based on statistically downscaled daily climate data from 20 GCMs in CMIP6, we found that radiation, temperature (T_{min} and T_{max}), and precipitation have an increasing trend under future climate scenarios. Overall, the trends were consistent with the result of Xiao et al. (2018b) using 28 GCMs from CMIP5. Generally, warming climate could accelerate crop growth and development rate and thereby advance crop phenological stages

(Xiao et al., 2015; Hu et al., 2017). The length of VGP and WGP of wheat significantly shortened for the two future periods under SSP245 and SSP585 scenarios. The large decrease of crop VGP could cause insufficient biomass accumulation and lower leaf area index (LAI) in the early growth stage and has a negative impact on the accumulation of grain yield in the later growth stage (Juknys et al., 2017). However, the length of RGP was prolonged under future climate scenarios, which could provide the possibility of prolonging grain filling period and increasing grain yield (Wang and Yin, 2012). To some extent, increasing precipitation could improve soil moisture conditions during crop growing season (Rosenzweig et al., 2004). The increase in precipitation in the future could reduce irrigation water consumption and effectively alleviate the problems caused by overexploitation of groundwater in the area. However, Xiao et al. (2020) found that some areas in the northern NCP still had groundwater over-pumping in the future based on 33 GCMs from CMIP5. Irrigation is still an important guarantee for high yield of wheat in rainfed areas of the NCP. Solar radiation is an important climatic factor which influences photosynthesis rate and biomass accumulation of crop (Sheehy et al., 2006; Zhang et al., 2010). Increased radiation under future climate scenarios could benefit wheat production (Xiao et al., 2020). However, the shortening of growth period could result in less radiation interception (Xiao et al., 2018b). The elevated atmospheric CO_2 concentration under future climate scenarios has positive effects on crop yield, especially for the C3 plant wheat (Chen et al., 2018; Xiao et al., 2018b).

Without considering the effect of extreme climate, climate change increased winter wheat yield under both SSP245 and SSP585 scenarios in the NCP. However, due to warming climate, extreme climate events are anticipated to increase, which are likely to produce negative impacts on crop production (Porter and Semenov, 2005). When the crop phenology changes in the future are not considered, Bai et al. (2020) noted that the frequency and intensity of heat extremes during wheat growing season were projected to increase over the 21st century for SSP245 and SSP585 scenarios, but those of cold extremes will decrease. In this study, the results showed that heat days around flowering had no significant change or a slight decrease for wheat under SSP245 and SSP585 scenarios. Frost days from jointing to grain filling had a slight increase under future climate scenarios but significantly increased for SSP585_2080S scenario. The main reason for the differences was that our study considered the changes of wheat phenology caused by warming climate. Therefore, the actual changes of heat and frost stress are not only attributed to temperature change but also the variation of crop phenology (Gu et al., 2008). Increase in temperature accelerates wheat development and advances the temperature sensitive stage, which could reduce the risk of exposure to heat stress but increase the risk of frost (Zheng et al., 2012). Related studies also indicated that although rising temperature reduced spring frost significantly in most of wheat growing region, actual risk of spring frost during jointing to flowering had not decreased as expected and frost-related yield loss had an increasing trend (Zheng et al., 2015; Xiao et al., 2018b). Our simulation results also showed that wheat yield loss caused by frost stress significantly increased for 2080S under SSP585 scenario, especially for ZMD station. This is because the temperature sensitive stage of wheat was earlier at ZMD than that at the other three stations under future climate scenarios (the jointing date was advanced from March to February; **Figure 3**). Although frost days in each month decreased significantly due to the increase of temperature, the number of frost day in February under future climate scenarios were still significantly higher than those in March for the baseline period (**Figure 2H**).

The projected yield changes under future climate scenarios not only presented possible risks to crop production but also suggested potential opportunities for agricultural development. The negative impact of warming climate on crop generally resulted from the decrease in growth duration and the increase of extreme events (Chen et al., 2018). Although increasing temperature accelerated crop development rate, the variation of phenology was not completely consistent with the temperature variation (He et al., 2015; Li et al., 2016). Shift of crop phenology can be affected not only by climatic factors but also by cultivar changes and agronomic management (Tao et al., 2012; Wang et al., 2013). An optimum sowing window can reduce risks of frost and/or heat stress events during temperature sensitive stage (Zheng et al., 2012; Bell et al., 2015). In this study, we found that the fluctuation of yield change caused by shift in sowing dates under future climate scenarios was very large. Proper shift of sowing window could alleviate the negative effect of frost and heat stress events and maintain or even improve wheat yields. The optimum sowing window of wheat was different in different regions, which was controlled by climatic conditions and cultivar characteristics (Bai and Tao, 2017). Moreover, not all cultivars respond similarly to climate change, and cultivars renewal is the main mean of adaptation to climate change (Lobell et al., 2011). Several studies indicated that long-season cultivar could compensate for phenology acceleration induced by warming climate and stabilize wheat growth duration (Liu et al., 2010; Tao et al., 2012). Late sowing dates or using long-season cultivars could postpone the frost sensitive stage and decrease frost risk, but increase the risk of exposing wheat to more heat stress around flowering (Zheng et al., 2012). Therefore, the selection of adaptation measures needs to balance the risks associated with frost, heat, and other abiotic stresses (Barlow et al., 2015). In this study, we found late sowing and longer VGP cultivars could significantly compensate for the negative impact of extreme temperature on yields at ZMD in the south of NCP under future climate scenarios, but shift in sowing dates and growth period length of cultivars only slightly compensated for the negative impact at TS, NG, and HM in the north and central NCP. The results showed that changing the key growth period by management measures cannot effectively alleviate the combined effects of extreme temperature for wheat in the north and central NCP, and improving the tolerance to high temperature or low temperature of cultivars may be an effective measure to alleviate the negative effects of extreme temperature.

There are some uncertainties in future climate projections due to the differences between different climate models and

scenarios. We used a multiple model ensemble method to address the uncertainties from climate models and scenarios. To assess the impacts of extreme temperature on wheat production, we integrated yield reduction multipliers for heat and frost stress events during temperature sensitive stage into APSIM-wheat model based on relevant research reports. Due to limited data for model evaluation, our modeling results might over- or underestimate the magnitude of yield losses resulted from heat and frost stress. Nonetheless, capturing heat and frost losses to grain yield in some way could provide guidance for developing adaptation strategies to reduce climate risks (Bell et al., 2015). Further improvement of the definitions and physiological basis of this approach would enhance the accuracy of these predictions, but this is out of the scope of this study. Moreover, in the APSIM-wheat model, the increased photosynthesis due to elevated atmospheric [CO_2] was reported mainly from controlled, semi-controlled, and open-field experiments (Reyenga et al., 1999; Kimball et al., 2002). Therefore, the crop model might overestimate the positive effects of elevated atmospheric [CO_2] (Asseng et al., 2004). In order to more accurately evaluate the impact of climate change on crop production, the quality of the crop model and climate projection should be further elaborated.

CONCLUSION

Based on statistically downscaled data from 20 GCMs in CMIP6, we evaluated the potential changes in wheat phenology and yield across winter wheat cropping regions in the NCP using the APSIM-wheat model. Results showed that warming climate accelerated wheat development and significantly advanced the temperature sensitive stage. Without any adaptation methods under future climate scenarios, the risk of exposure to heat stress around flowering had no significant change or a slight decrease, but frost risk in spring season increased. Extreme temperature stress would have negative impacts on wheat production. However, agricultural climate resources, such as light, thermal, and CO_2 fertilization effects, could partly compensate for the yield decrease or even contribute to the yield increase. Moreover, we found that late sowing and longer VGP cultivar could significantly compensate for the negative impact of extreme temperature on wheat yields in the south of NCP under future climate scenarios. However, selecting heat resistant cultivars in the north NCP and both heat and frost resistant cultivars in the central NCP may be a more effective way to alleviate the negative effect of extreme temperature on wheat yields. Our analysis highlighted that not only heat risk should be concerned under climate warming, but also frost risk should not be ignored. Therefore, exploring agricultural management measures to balance the risks associated with frost, heat, and other abiotic stresses should be the priority to ensure wheat production in the NCP.

DATA AVAILABILITY STATEMENT

The raw data supporting the conclusions of this article will be made available by the authors, without undue reservation.

AUTHOR CONTRIBUTIONS

HB and DX carried out the study design and wrote the original draft. HB carried out the data collection and model simulation. BW, DL, and JT also gave critical revision of the manuscript. All authors contributed to the article and approved the submitted version.

FUNDING

This study was supported by the Natural Science Foundation of China (41901128) and the Natural Science Foundation of Hebei Province (D2018302012).

SUPPLEMENTARY MATERIAL

The Supplementary Material for this article can be found online at: https://www.frontiersin.org/articles/10.3389/fpls.2022.829580/full#supplementary-material

REFERENCES

Asseng, S., Ewert, F., Martre, P., Rötter, R. P., Lobell, D. B., Cammarano, D., et al. (2015). Rising temperatures reduce global wheat production. *Nat. Clim. Chang.* 5, 143–147. doi: 10.1038/nclimate2470

Asseng, S., Jamieson, P. D., Kimball, B., Pinter, P., Sayre, K., Bowden, J. W., et al. (2004). Simulated wheat growth affected by rising temperature, increased water deficit and elevated atmospheric CO_2. *Field Crop Res.* 85, 85–102. doi: 10.1016/S0378-4290(03)00154-0

Bai, H., and Tao, F. (2017). Sustainable intensification options to improve yield potential and eco-efficiency for rice-wheat rotation system in China. *Field Crop Res.* 211, 89–105. doi: 10.1016/j.fcr.2017.06.010

Bai, H., Xiao, D., Wang, B., Liu, D. L., Feng, P., and Tang, J. (2020). Multi-model ensemble of CMIP6 projections for future extreme climate stress on wheat in the North China plain. *Int. J. Climatol.* 41, 171–186. doi: 10.1002/joc.6674

Barlow, K. M., Christy, B. P., O'Leary, G. J., Riffkin, P. A., and Nuttall, J. G. (2015). Simulating the impact of extreme heat and frost events on wheat crop production: a review. *Field Crop Res.* 171, 109–119. doi: 10.1016/j.fcr.2014.11.010

Bell, L., Lilley, J., Hunt, J., and Kirkegaard, J. (2015). Optimising grain yield and grazing potential of crops across Australia's high-rainfall zone: a simulation analysis. 1. Wheat. *Crop Pasture Sci.* 66, 332–348. doi: 10.1071/CP14230

Bokhorst, S., Bjerke, J., Davey, M., Taulavuori, K., Taulavuori, E., Laine, K., et al. (2010). Impacts of extreme winter warming events on plant physiology in a sub-arctic heath community. *Physiol. Plant.* 140, 128–140. doi: 10.1111/j.1399-3054.2010.01386.x

Challinor, A. J., Watson, J., Lobell, D. B., Howden, S. M., Smith, D. R., and Chhetri, N. (2014). A meta-analysis of crop yield under climate change and adaptation. *Nat. Clim. Chang.* 4, 287–291. doi: 10.1038/nclimate2153

Chen, C., Wang, B., Feng, P., Xing, H., and Lawes, R. A. (2020). The shifting influence of future water and temperature stress on the optimal flowering

period for wheat in western Australia. *Sci. Total Environ.* 737:139707. doi: 10.1016/j.scitotenv.2020.139707

Chen, L., Xiang, H., Miao, Y., Zhang, L., Guo, Z., Zhao, X., et al. (2014). An overview of cold resistance in plants. *J. Agron. Crop Sci.* 200, 237–245. doi: 10.1111/jac.12082

Chen, Y., Zhang, Z., and Tao, F. (2018). Impacts of climate change and climate extremes on major crops productivity in China at a global warming of 1.5 and 2.0°C. *Earth Syst. Dynam.* 9, 543–562. doi: 10.5194/esd-9-543-2018

Crimp, S. (2014). Frost Risk on the Rise Despite Warmer Climate. Ground Cover Supplement. GRDC, Kingston, Australia.

Dias, A. S., and Lidon, F. C. (2009). Evaluation of grain filling rate and duration in bread and durum wheat, under heat stress after anthesis. *J. Agron. Crop Sci.* 195, 137–147. doi: 10.1111/j.1439-037X.2008.00347.x

FAO (2013). FAO Statistical Yearbook. http://www.fao.org/docrep/018/i3107e/i3107e.pdf (Accessed July 20, 2016).

Ferris, R., Ellis, R., Wheeler, T. R., and Hadley, P. (1998). Effect of high temperature stress at anthesis on grain yield and biomass of field-grown crops of wheat. *Ann. Bot.* 82, 631–639. doi: 10.1006/anbo.1998.0740

Gouache, D., Le Bris, X., Bogard, M., Deudon, O., Pagé, C., and Gate, P. (2012). Evaluating agronomic adaptation options to increasing heat stress under climate change during wheat grain filling in France. *Eur. J. Agron.* 39, 62–70. doi: 10.1016/j.eja.2012.01.009

Gu, L., Hanson, P., Post, W., Kaiser, D., Yang, B., Nemani, R., et al. (2008). The 2007 eastern US spring freeze: increased cold damage in a warming world. *BioScience* 58, 253–262. doi: 10.1641/B580311

He, L., Asseng, S., Zhao, G., Wu, D., Yang, X., Zhuang, W., et al. (2015). Impacts of recent climate warming, cultivar changes, and crop management on winter wheat phenology across the loess plateau of China. *Agric. For. Meteorol.* 200, 135–143. doi: 10.1016/j.agrformet.2014.09.011

He, Y., Wang, H., Qian, B., Mcconkey, B., and Hoogenboom, G. (2012). Effects of climate change on killing frost in the Canadian prairies. *Clim. Res.* 54, 221–231. doi: 10.3354/cr01114

Holzworth, D. P., Huth, N. I., deVoil, P. G., Zurcher, E., Herrmann, N. I., McLean, G., et al. (2014). APSIM—evolution towards a new generation of agricultural systems simulation. *Environ. Model. Softw.* 62, 327–350. doi: 10.1016/j.envsoft.2014.07.009

Hu, X., Huang, Y., Sun, W., and Yu, L. (2017). Shifts in cultivar and planting date have regulated rice growth duration under climate warming in China since the early 1980S. *Agric. For. Meteorol.* 247, 34–41. doi: 10.1016/j.agrformet.2017.07.014

Ji, H., Xiao, L., Xia, Y., Song, H., Liu, B., Tang, L., et al. (2017). Effects of jointing and booting low temperature stresses on grain yield and yield components in wheat. *Agric. For. Meteorol.* 243, 33–42. doi: 10.1016/j.agrformet.2017.04.016

Juknys, R., Velička, R., Kanapickas, A., Kriaučiūnienė, Z., Masilionytė, L., Vagusevičienė, I., et al. (2017). Projecting the impact of climate change on phenology of winter wheat in northern Lithuania. *Int. J. Biometeorol.* 61, 1765–1775. doi: 10.1007/s00484-017-1360-y

Kang, M. S. (2015). Plant genetic resources and climate change. *Crop Sci.* 55, 2390–2392. doi: 10.2135/cropsci2015.07.0002br

Kimball, B. A., Kobayashi, K., and Bindi, M. (2002). Responses of agricultural crops to free-air CO_2 enrichment. *Adv. Agron.* 77, 293–368. doi: 10.1016/S0065-2113(02)77017-X

Li, X., Cai, J., Liu, F., Li, X., Cao, W., and Jiang, D. (2015a). Spring freeze effect on wheat yield is modulated by winter temperature fluctuations: evidence from meta-analysis and simulating experiment. *J. Agron. Crop Sci.* 201, 288–300. doi: 10.1111/jac.12115

Li, X., Pu, H., Liu, F., Zhou, Q., Cai, J., Li, X., et al. (2015b). Winter wheat photosynthesis and grain yield responses to spring freeze. *Agron. J.* 107, 1002–1010. doi: 10.1016/j.fcr.2014.06.004

Li, K., Yang, X., Tian, H., Pan, S., Liu, Z., and Lu, S. (2016). Effects of changing climate and cultivar on the phenology and yield of winter wheat in the North China plain. *Int. J. Biometeorol.* 60, 21–32. doi: 10.1007/s00484-015-1002-1

Lin, E., Wei, X., Hui, J., Yinlong, X., Yue, L., Liping, B., et al. (2005). Climate change impacts on crop yield and quality with CO_2 fertilization in China. *Philos. Trans. R. Soc. Lond. B Biol. Sci.* 360, 2149–2154. doi: 10.1098/rstb.2005.1743

Liu, B., Asseng, S., Liu, L., Tang, L., Cao, W., and Zhu, Y. (2016). Testing the responses of four wheat crop models to heat stress at anthesis and grain filling. *Glob. Chang. Biol.* 22, 1890–1903. doi: 10.1111/gcb.13212

Liu, Y., Wang, E., Yang, X., and Wang, J. (2010). Contributions of climatic and crop varietal changes to crop production in the North China plain, since 1980S. *Glob. Chang. Biol.* 16, 2287–2299. doi: 10.1111/j.1365-2486.2009.02077.x

Liu, D. L., and Zuo, H. (2012). Statistical downscaling of daily climate variables for climate change impact assessment over New South Wales, Australia. *Clim. Chang.* 115, 629–666. doi: 10.1007/s10584-012-0464-y

Lobell, D. B., and Asner, G. P. (2003). Climate and management contributions to recent trends in U.S. agricultural yields. *Science* 299:1032. doi: 10.1126/science.1078475

Lobell, D. B., Banziger, M., Magorokosho, C., and Vaivek, B. (2011). Nonlinear heat effects on African maize as evidenced by historical yield trials. *Nat. Clim. Chang.* 1, 42–45. doi: 10.1038/nclimate1043

Luo, Q., Trethowan, R., and Tan, D. K. (2018). Managing the risk of extreme climate events in Australian major wheat production systems. *Int. J. Biometeorol.* 62, 1685–1694. doi: 10.1007/s00484-018-1568-5

O'Neill, B. C., Tebaldi, C., Vuuren, D., Eyring, V., Friedlingstein, P., Hurtt, G., et al. (2016). The scenario model intercomparison project (ScenarioMIP) for CMIP6. *Geosci. Model Dev.* 9, 3461–3482. doi: 10.5194/gmd-9-3461-2016

Porter, J. R., and Gawith, M. (1999). Temperatures and the growth and development of wheat: a review. *Eur. J. Agron.* 10, 23–36. doi: 10.1016/S1161-0301(98)00047-1

Porter, J. R., and Semenov, M. A. (2005). Crop responses to climatic variation. *Philos. Trans. R. Soc. Lond. B Biol. Sci.* 360, 2021–2035. doi: 10.1098/rstb.2005.1752

Prescott, J. A. (1940). Evaporation from a water surface in relation to solar radiation. *Trans. R. Soc. South Aust.* 64, 114–118.

Ray, D., Gerber, J., MacDonald, G., and West, P. (2015). Climate variation explains a third of global crop yield variability. *Nat. Commun.* 6:5989. doi: 10.1038/ncomms6989

Reyenga, P. J., Howden, S. M., Meinke, H., and McKeon, G. M. (1999). Modelling global change impacts on wheat cropping in south-east Queensland, Australia. *Environ. Model. Softw.* 14, 297–306. doi: 10.1016/S1364-8152(98)00081-4

Rezaei, E. E., Siebert, S., Manderscheid, R., Müller, J., Mahrookashani, A., Ehrenpfordt, B., et al. (2018). Quantifying the response of wheat yields to heat stress: the role of the experimental setup. *Field Crop Res.* 217, 93–103. doi: 10.1016/j.fcr.2017.12.015

Richardson, C. W., and Wright, D. A. (1984). *WGEN: A Model for Generating Daily Weather Variables* U. S. Department of Agriculture, Agricultural Research Service, Washington DC, ARS-8, 83 p.

Rosenzweig, C., Tubiello, F., Goldberg, R., Mills, E., and Bloomfield, J. (2004). Increased crop damage in the US from excess precipitation under climate change. *Glob. Environ. Chang.* 12, 197–202. doi: 10.1016/S0959-3780(02)00008-0

Russell, G., and Wilson, G.W. (1994). *An Agro-Pedo-Climatological Knowledge-Base of Wheat in Europe*. Luxembourg: Joint Research Centre, European Commission.

Saeidi, M., Eliasi, P., Abdoli, M., and Sasani, S. (2012). Freezing tolerance of wheat cultivars at the early growing season after winter. *Afr. J. Biotechnol.* 11, 4045–4052. doi: 10.5897/AJB11.3266

Sheehy, J. E., Mitchell, P. L., and Ferrer, A. B. (2006). Decline in rice grain yields with temperature: models and correlations can give different estimates. *Field Crop Res.* 98, 151–156. doi: 10.1016/j.fcr.2006.01.001

Stöckle, C. O., Donatelli, M., and Nelson, R. (2003). CropSyst, a cropping systems simulation model. *Eur. J. Agron.* 18, 289–307. doi: 10.1016/S1161-0301(02)00109-0

Subedi, K. D., Gregory, P. J., Summerfield, R. J., and Gooding, M. J. (1998). Cold temperatures and boron deficiency caused grain set failure in spring wheat (*Triticum aestivum* L.). *Field Crop Res.* 57, 277–288. doi: 10.1016/S0378-4290(97)00148-2

Talukder, A. S. M. H. M., McDonald, G. K., and Gill, G. S. (2014). Effect of short-term heat stress prior to flowering and early grain set on the grain yield of wheat. *Field Crop Res.* 160, 54–63. doi: 10.1016/j.fcr.2014.01.013

Tao, F., and Zhang, Z. (2013). Climate change, wheat productivity and water use in the North China plain: a new super-ensemble-based probabilistic projection. *Agric. For. Meteorol.* 170, 146–165. doi: 10.1016/j.agrformet.2011.10.003

Tao, F., Zhang, Z., Xiao, D., Zhang, S., Rötter, R. P., Shi, W., et al. (2014). Responses of wheat growth and yield to climate change in different climate

zones of China, 1981–2009. *Agric. For. Meteorol.* 189-190, 91–104. doi: 10.1016/j.agrformet.2014.01.013

Tao, F., Zhang, S., and Zhang, Z. (2012). Spatiotemporal changes of wheat phenology in China under the effects of temperature, day length and cultivar thermal characteristics. *Eur. J. Agron.* 43, 201–212. doi: 10.1016/j.eja.2012.07.005

Thakur, P., and Nayyar, H. (2013). "Facing the cold stress by plants in the changing environment: sensing, signaling, and defending mechanisms," in *Plant Acclimation to Environmental Stress*. eds. N. Tuteja and S. Singh Gill (New York, NY: Springer), 29–69.

Valluru, R., Link, J., and Claupein, W. (2012). Consequences of early chilling stress in two Triticum species: plastic responses and adaptive significance. *Plant Biol.* 14, 641–651. doi: 10.1111/j.1438-8677.2011.00540.x

Wang, J., Wang, E., Feng, L., Yin, H., and Yu, W. (2013). Phenological trends of winter wheat in response to varietal and temperature changes in the North China plain. *Field Crop Res.* 144, 135–144. doi: 10.1016/j.fcr.2012.12.020

Wang, J., and Yin, H. (2012). Increased yield potential of wheat-maize cropping system in the North China plain by climate change adaptation. *Clim. Chang.* 113, 825–840. doi: 10.1007/s10584-011-0385-1

Wu, Y., Zhong, X., Hu, X., Ren, D., Lv, G., Wei, C., et al. (2014). Frost affects grain yield components in winter wheat. *N. Z. J. Crop. Hortic. Sci.* 42, 194–204. doi: 10.1080/01140671.2014.887588

Xiao, D., Bai, H., and Liu, D. L. (2018b). Impact of future climate change on wheat production: a simulated case for China's wheat system. *Sustainability* 10:1277. doi: 10.3390/su10041277

Xiao, L., Liu, L., Asseng, S., Xia, Y., Tang, L., Liu, B., et al. (2018a). Estimating spring frost and its impact on yield across winter wheat in China. *Agric. For. Meteorol.* 260, 154–164. doi: 10.1016/j.agrformet.2018.06.006

Xiao, D., Moiwo, J. P., Tao, F., Yang, Y., Shen, Y., Xu, Q., et al. (2015). Spatiotemporal variability of winter wheat phenology in response to weather and climate variability in China. *Mitig. Adapt. Strateg. Glob. Chang.* 20, 1191–1202. doi: 10.1007/s11027-013-9531-6

Xiao, D., and Tao, F. (2014). Contributions of cultivars, management and climate change to winter wheat yield in the North China plain in the past three decades. *Eur. J. Agron.* 52, 112–122. doi: 10.1016/j.eja.2013.09.020

Xiao, D., Tao, F. L., Liu, Y. J., Shi, W. J., Wang, M., Liu, F. S., et al. (2013). Observed changes in winter wheat phenology in the North China plain for 1981–2009. *Int. J. Biometeorol.* 57, 275–285. doi: 10.1007/s00484-012-0552-8

Xiao, D., Wang, B., Feng, P., Bai, H., and Tang, J. (2020). Climate change impact on yields and water use of wheat and maize in the North China plain under future climate change scenarios. *Agric. Water Manag.* 238, 1–15. doi: 10.1016/j.agwat.2020.106238

Yang, X., Tian, Z., Sun, L., Chen, B., Tubiello, F. N., and Xu, Y. (2017). The impacts of increased heat stress events on wheat yield under climate change in China. *Clim. Chang.* 140, 605–620. doi: 10.1007/s10584-016-1866-z

Zadoks, J. C., Chang, T. T., and Konzak, C. F. (1974). A decimal code for the growth stages of cereals. *Weed Res.* 14, 415–421. doi: 10.1111/j.1365-3180.1974.tb01084.x

Zhang, T., Zhu, J., and Wassmann, R. (2010). Responses of rice yields to recent climate change in China: an empirical assessment based on long-term observations at different spatial scales (1981–2005). *Agric. For. Meteorol.* 150, 1128–1137. doi: 10.1016/j.agrformet.2010.04.013

Zhang, L., Zhu, L., Yu, M., and Zhong, M. (2016). Warming decreases photosynthates and yield of soybean [*Glycine max* (L.) Merrill] in the North China plain. *Crop J.* 4, 139–146. doi: 10.1016/j.cj.2015.12.003

Zhao, H., Dai, T., Jing, Q., Jiang, D., and Cao, W. (2007). Leaf senescence and grain filling affected by post-anthesis high temperatures in two different wheat cultivars. *Plant Growth Regul.* 51, 149–158. doi: 10.1007/s10725-006-9157-8

Zheng, B., Chapman, S., Christopher, J., Frederiks, T., and Chenu, K. (2015). Frost trends and their estimated impact on yield in the Australian wheatbelt. *Procedia Environ. Sci.* 29, 171–172. doi: 10.1016/j.proenv.2015.07.244

Zheng, B., Chenu, K., Dreccer, M., and Chapman, S. (2012). Breeding for the future: what are the potential impacts of future frost and heat events on sowing and flowering time requirements for Australian bread wheat (*Triticum aestivium*) varieties. *Glob. Chang. Biol.* 18, 2899–2914. doi: 10.1111/j.1365-2486.2012.02724.x

Zhong, X., Mei, X., Li, Y., Yoshida, H., Zhao, P., Wang, X., et al. (2008). Changes in frost resistance of wheat young ears with development during jointing stage. *J. Agron. Crop Sci.* 194, 343–349. doi: 10.1111/j.1439-037X.2008.00320.x

Conflict of Interest: The authors declare that the research was conducted in the absence of any commercial or financial relationships that could be construed as a potential conflict of interest.

Publisher's Note: All claims expressed in this article are solely those of the authors and do not necessarily represent those of their affiliated organizations, or those of the publisher, the editors and the reviewers. Any product that may be evaluated in this article, or claim that may be made by its manufacturer, is not guaranteed or endorsed by the publisher.

frontiers in Plant Science

ORIGINAL RESEARCH
published: 25 February 2022
doi: 10.3389/fpls.2022.809377

Agrometeorological and Agronomic Characterization of *Megathyrsus* Grasses Cultivated in Tropical Humid and Semi-Arid Conditions: A Multivariate Approach

Vitor Hugo Maués Macedo[1], Nauara Moura Lage Filho[2], Antônio Marcos Quadros Cunha[2], Marcos Neves Lopes[3], Rodrigo Gregório da Silva[4], José Antônio Alves Cutrim Junior[5], Cristian Faturi[1], Magno José Duarte Cândido[6] and Aníbal Coutinho do Rêgo[1]**

[1]Institute of Health and Animal Production, Federal Rural University of Amazon, Belém, Brazil, [2]Nucleus of Agricultural Sciences and Rural Development, Federal University of Pará, Castanhal, Brazil, [3]Federal Institute of Education, Science and Technology of Piauí, Valença, Brazil, [4]Federal Institute of Education, Science and Technology of Ceará, Limoeiro do Norte, Brazil, [5]Federal Institute of Education, Science and Technology of Maranhão, Maracanã, Brazil, [6]Department of Animal Science, Federal University of Ceará, Fortaleza, Brazil

OPEN ACCESS

Edited by:
Hartmut Stützel,
Leibniz University Hannover, Germany

Reviewed by:
Vijaya Gopal Kakani,
Oklahoma State University, United States
Juan De La Cruz Jiménez,
Nagoya University, Japan

***Correspondence:**
Vitor Hugo Maués Macedo
hmmvitor@gmail.com
Aníbal Coutinho do Rêgo
anibalcr@gmail.com

Specialty section:
This article was submitted to Plant Biophysics and Modeling, a section of the journal Frontiers in Plant Science

Received: 04 November 2021
Accepted: 03 February 2022
Published: 25 February 2022

Citation:
Macedo VHM, Lage Filho NM, Cunha AMQ, Lopes MN, da Silva RG, Cutrim Junior JAA, Faturi C, Cândido MJD and do Rêgo AC (2022) Agrometeorological and Agronomic Characterization of Megathyrsus Grasses Cultivated in Tropical Humid and Semi-Arid Conditions: A Multivariate Approach. Front. Plant Sci. 13:809377. doi: 10.3389/fpls.2022.809377

Variability in climatic conditions of low-latitude tropical grass cultivation can affect forage production dynamics. Pasture ecosystems are complex and preferably studied from a multifactorial point of view through multivariate approaches. Therefore, in this study, we characterized different growing conditions for grasses of the *Megathyrsus* genus through studies conducted in tropical humid and semi-arid conditions. We applied principal component, canonical correlation, and discriminant function analyses to the measurements of agronomic and agrometeorological variables in six studies with Guinea and Massai grasses. The principal component analysis, through the climatic characterization by the first principal component, reflects the contrast between water availability and nitrogen variables and energy supply. Agronomic characterization occurred through the distinction between the density of tillers, forage accumulation, and increase in height, versus the accumulation of stems and dead material. The canonical correlation analysis generated a correlation coefficient of 0.84 between the agronomic and agrometeorological variables. There was a contrast between the dead material accumulation and the other agronomic variables, while the agrometeorological variables showed characteristics similar to the first principal component. Discriminant function 1, with 70.36% separation power, distinguished the cultivation conditions based on the study locations. Grass cultivars were differentiated by discriminant function 2, with a 19.20% separation power. From a multivariate variability analysis, despite the similarities of radiation and temperature in the regions studied, the availability of water and nutrients and measurements of agronomic variables can aid in future modeling studies on forage production.

Keywords: agrometeorology, growing conditions, *Megathyrsus*, multivariate analysis, pasture ecosystems, semi-arid, tropical humid

INTRODUCTION

Pasture ecosystems at low latitudes (<10°) show little variation in photoperiod and temperature but exhibit important differences in other climatic factors, such as rainfall. In these areas, depending on the climate in which they are located, tropical forages have limited growth from a climatic point of view, usually due to water availability (Santos et al., 2013). Therefore, close to the equator, the water regime dictates plant growth both in a humid tropical climate and a semi-arid climate. Such weather types are present at lower latitudes on four of the seven continents. Humid tropical climates are observed in South American countries, such as those of the Amazon region, as well as in the central region of the Congo in Africa, and the Indonesian islands of Asia, all of which have humid tropical forests constituting the main biome. A semi-arid climate can be observed in northeastern Brazil, some African countries such as Ethiopia, Kenya, Somalia, and Tanzânia, and in northern Australia (Peel et al., 2007).

Forage plant growth and consequently, canopy productivity are the result of the genotype and its related environment (Durand et al., 1991; Simeão et al., 2021). Environmental factors refer to the edaphoclimatic conditions of plant cultivation, including aspects related to soil (texture, density, and fertility) and climate (temperature, humidity, and photoperiod). The water demand of plants depends mainly on their metabolic requirements, which are linked to characteristics such as stomatal conductance, transpiration rate, and leaf area. These characteristics vary according to the stage of development (Tardieu, 2013). Water demand is also determined by factors such as leaf surface evapotranspiration, which is dependent on radiation, temperature, air humidity, wind speed, and leaf surface properties (Rind et al., 1990). In tropical pastures, evapotranspiration, mean temperature, and solar radiation influence total forage accumulation, leaf accumulation, tiller population density, and nutritional value (Lage Filho et al., 2021; Macedo et al., 2021; Tapia et al., 2021). As for aspects related to the soil, nitrogen (N) is the most important nutrient in tissue flow, and its assimilation may be limited by a water deficit (Onillon et al., 1995). Therefore, when climate conditions are favorable and nitrogen supply is adequate, studies in the literature support that the growth of tropical grasses, especially of the genus *Megathyrsus*, will be rapid, as there will be an increase in regrowth vigor and a reduction in the interval between grazing (Oliveira et al., 2020).

Cultivated tropical pasture ecosystems represent the main food source for many herds worldwide (Silva et al., 2013). Understanding the relationship between the agronomic characteristics of the grasses that make up such systems, and the agrometeorological conditions of these regions would increase the knowledge of the interactions between these factors in pasture ecosystems. Therefore, multivariate analyses of the factors related to climatic influences exerted on plants and the dynamics of growth and biomass production can provide important information through a systemic view of the ecosystem (Yeater et al., 2014; Araújo Júnior et al., 2021). In addition, the exploration of data using multivariate analysis can contribute to research with direct modeling applied to plant growth (Qiu et al., 2016), although little research has been previously conducted on the prediction of forage accumulation in tropical conditions.

Regions located close to the equator, such as humid and semi-arid tropical regions, may have climatic factors that can distinguish them, such as variables related to humidity and the water regime (Alvares et al., 2013). Production systems in these drier places use technologies such as irrigation (Araújo Júnior et al., 2021), which is often not required in humid tropical regions. Thus, agrometeorological characterization and analysis of agronomic variables of forage plants grown in different regions can provide valuable information on how different growing conditions interact with their environment, and how these conditions can be distinguished. Conducting trials under different climates helps in understanding the climatic influences on the growth and development of forage crops, and contributes to modeling studies involving climate action in tropical forage grasses that are highly responsive to change, such as those of the genus *Megathyrsus*.

This study aimed to understand the growth dynamics of grasses of the genus *Megathyrsus* under different growing conditions in humid and semi-arid tropical regions, and to answer the following questions: How are the different growing conditions characterized in relation to the indices that group agronomic and agrometeorological variables? How do agrometeorological variables relate to the agronomic variables measured under these growing conditions?, and How can discriminant functions be described that can distinguish cultivation conditions regarding forage species evaluated in the humid and semi-arid tropical regions of Brazil?

MATERIALS AND METHODS

Experimental Sites

Data were retrieved from four experimental trials with Guinea grass (*Megathyrsus maximus* (syn. *Panicum maximum*; Jacq.) B.K. Simon & S.W.L. Jacobs "Guinea"). Two trials were conducted in the municipality of Igarapé-Açu (01°07′ S, 47°36′ W, 47 m altitude), state of Pará, and two in Pentecoste (03°48′ S, 49°19′ W, 71 m altitude), state of Ceará. Two other experiments with Massai grass (*Megathyrsus maximus* × *Megathyrsus infestus* (Peters) B.K. Simon & S.W.L. Jacobs "Massai") were performed in Igarapé-Açu and Fortaleza (03°44′ S, 38°34′ W, 20 m altitude) in the states of Pará and Ceará, respectively. The town of Igarapé-Açu is located in the eastern region of the Amazon biome, has a rainy climate with a short dry season, and is classified as type Am using the Köppen classification (Alvares et al., 2013) tropical humid monsoon. The Pentecoste experimental field is located in the Brazilian semi-arid region, with climate type "BSwh" according to the Köppen classification, indicating a dry climate with a short wet season. Fortaleza is a coastal city in northeastern Brazil located near the Brazilian semi-arid region. According to the Köppen classification, Fortaleza has a tropical savanna climate of the Aw' type with dry-winter characteristics. (**Figure 1**). The experiments were

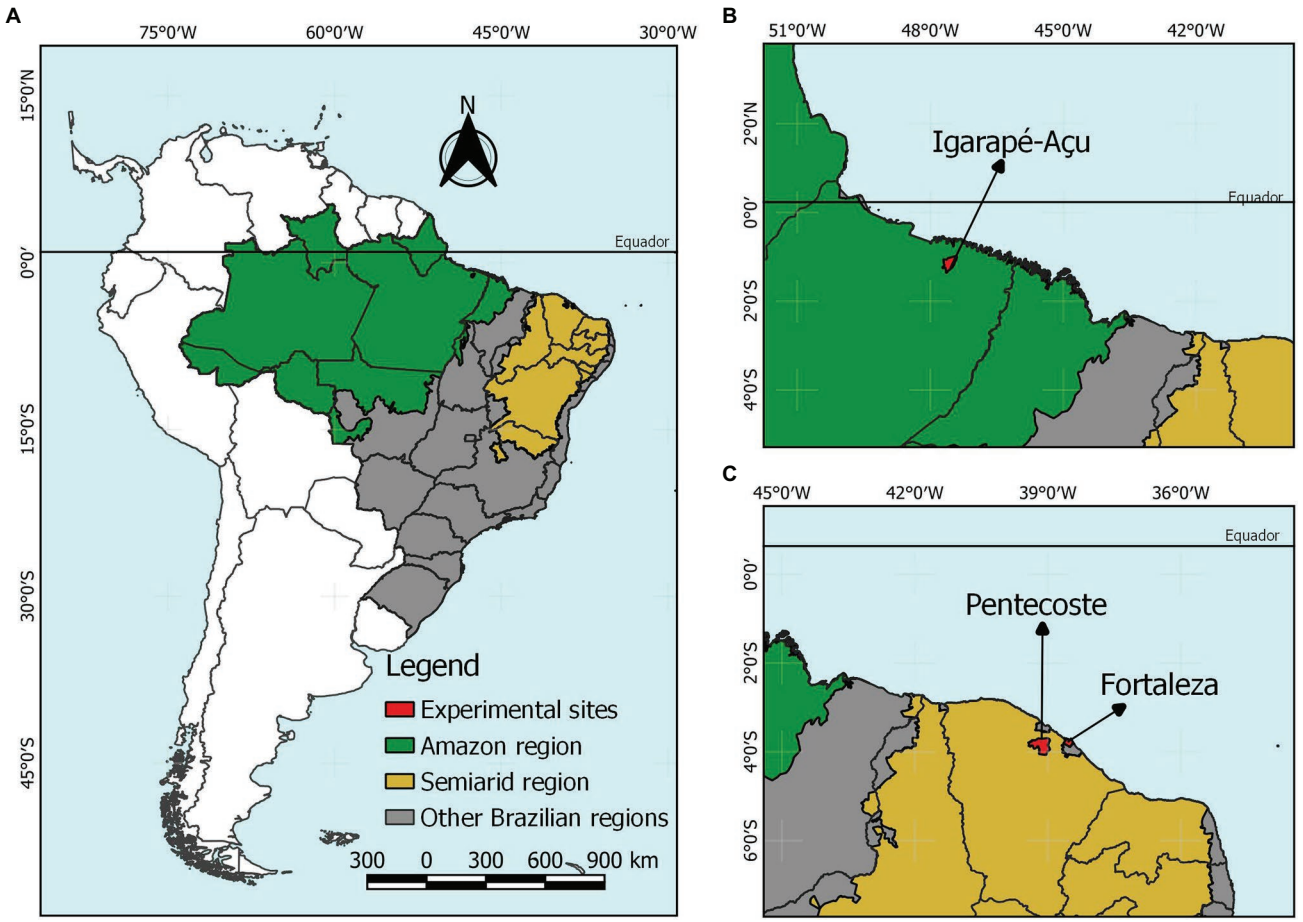

FIGURE 1 | Location map of experimental sites. **(A)** Representation of the delimitation of the humid tropical region of the Amazon and the semi-arid region in Brazil. **(B)** Location of the Igarapé-Açu experimental site. **(C)** Location of the experimental sites of Fortaleza and Pentecoste.

named GG.IGA.15 (Guinea grass in Igarapé-Açu during the year 2015), GG.IGA.17-18 (Guinea grass in Igarapé-Açu during 2017 and 2018), GG.PEN.03 (Guinea grass in Pentecost during the year 2003), GG.PEN.05-06 (Guinea grass in Pentecost during 2005 and 2006), MG.IGA.15 (Massai grass in Igarapé-Açu during the year 2015), and MG.FOR.09 (Massai grass in Fortaleza during the year 2009). The agrometeorological characteristics and the details of the growing conditions of grasses of the genus *Megathyrsus* are presented in **Table 1**.

Description of Experimental Trials and Growing Conditions

Experiments With Mechanized Forage Harvesting Without the Use of Irrigation

The GG.IGA.15 experimental trial was conducted at the Experimental Farm of Igarapé-Açu (FEIGA) of the Federal Rural University of Amazônia (UFRA). The grass was sown by hand on March 6, 2014, with a sowing rate equivalent to 40 pure seeds m^{-2} after tillage. In this trial, treatments with different harvest frequencies were tested in Guinea grass based on fixed days (14, 21, 28, 35, 42, and 49 days) of the rest period. Thus, the cuts and collection of biomass were carried out after each period of days established by the treatments. The forage was harvested using a hedge trimmer. The area was divided into 30 plots of 12 m^2 (3 m × 4 m), with corridors spaced 1 m apart. The experimental design was a randomized block with five replicates per treatment. We used data collected between March 14, 2015, and January 2, 2016, which covered collections in both the rainy and dry seasons of 2015. Irrigation was not used in this trial; therefore, during the rainy season, nitrogen fertilizers were applied at a rate of 200 kg N ha^{-1} $year^{-1}$ in the form of urea (45% N). The plots with 14, 21, 28, 35, 42, and 49 days of the rest period received doses equivalent to 17, 25, 34, 42, 51, and 59 kg N ha^{-1} $cycle^{-1}$, respectively. For more details on this study, see Macedo et al. (2021).

The GG.IGA.17-18 test used the same experimental units as the GG.IGA.15 test. This study evaluated the effect of different defoliation intensities based on the residue height (15, 25, 35, 45, and 55 cm) when the Guinea grass canopy reached 95% light interception, measured using an AccuPAR LP-80 canopy analyzer (Decagon®). The experimental design was a randomized

TABLE 1 | Means and standard deviations (SD) of agrometeorological and cultivation conditions during data collection for experimental trials.

ID[a]	Grass	Place	Weather condition	Soil[b]	Photo[c]	SR[d]	Tmean[e]	Eto[f]	Prec[g]	WA[h]	AWC[i]	ETa[j]
GG.IGA.15	Guinea Grass	Igarapé-Açu	Humid	Yellow Oxisol	12.00 ± 0.02	461.93 ± 76.08	27.21 ± 1.33	8.40 ± 1.37	4.95 ± 8.86	4.95 ± 8.86	100	3.78 ± 3.45
GG.IGA.17-18	Guinea Grass	Igarapé-Açu	Humid	Yellow Oxisol	12.00 ± 0.02	443.57 ± 90.32	26.56 ± 1.24	8.01 ± 1.59	6.40 ± 13.88	6.40 ± 13.88	100	4.26 ± 3.14
GG.PEN.03	Guinea Grass	Pentecoste	Semi-Arid	Fluvisol	12.00 ± 0.05	215.26 ± 25.60	26.78 ± 0.79	4.51 ± 0.53	0.04 ± 0.40	12.60 ± 20.46	56	4.18 ± 0.57
GG.PEN.05-06	Guinea Grass	Pentecoste	Semi-Arid	Fluvisol	12.08 ± 0.02	200.53 ± 34.04	30.30 ± 1.11	5.15 ± 0.98	0.93 ± 4.08	12.50 ± 20.80	56	4.69 ± 0.89
MG.IGA.15	Massai Grass	Igarapé-Açu	Humid	Yellow Oxisol	11.98 ± 0.01	433.61 ± 89.16	26.00 ± 0.85	7.79 ± 1.56	10.02 ± 11.76	10.02 ± 11.76	100	6.81 ± 1.53
MG.FOR.09	Massai Grass	Fortaleza	Semi-Arid	Yellow Ultisol	11.97 ± 0.04	284.60 ± 40.39	26.76 ± 0.82	5.82 ± 0.89	1.89 ± 7.26	8.82 ± 12.56	32	5.22 ± 0.88

[a]*Identification of the experimental trial.*
[b]*Soil classification according to IUSS Working Group WRB (2015).*
[c]*Average photoperiod (hours day^{-1}).*
[d]*Average of daily solar radiation (W m^{-2}).*
[e]*Mean daily temperature (°C).*
[f]*Average of reference evapotranspiration (mm day^{-1}).*
[g]*Precipitation (rainfall; mm day^{-1}).*
[h]*Water applied from rain and/or irrigation (mm day^{-1}).*
[i]*Available water capacity (mm).*
[j]*Average of actual evapotranspiration (mm).*

block with six replicates per treatment. The data from this study were collected from September 2, 2017 to September 12, 2018 and included collections during the dry and rainy seasons. For more details about this study, see Lage Filho et al. (2021). In both GG.IGA.15 and GG.IGA.17-18, nitrogen fertilizers were applied during the rainy season at a rate of 200 kg N ha^{-1} year^{-1} in the form of urea (45% N), and defoliations were performed using mechanical cutting.

In the experimental trial MG.IGA.15, the grass was sown by hand on May 20, 2014, with a sowing rate equivalent to 45 pure seeds m^{-2} after tillage. The Massai grass was subjected to six treatments: five doses of nitrogen fertilization (100, 200, 300, 400, and 500 kg ha^{-1} year^{-1}), in six fixed applications throughout the experimental period, and a control treatment (no nitrogen), with five replications in a completely randomized design. The area was divided into 30 plots of 12 m^2 (3 m × 4 m), with corridors spaced 1 m apart. Defoliation was performed using mechanized cutting when light interception reached 95%, as measured using an AccuPAR LP-80 canopy analyzer (Decagon®). The experiment was conducted at FEIGA from February 14, 2015, to August 5, 2015. For more details on this study, refer to Cunha et al. (in press).

Sheep Grazing Experiments Using Irrigation

The experimental trial GG.PEN.03 was conducted in the advanced Teaching and Research Unit in Forage (NEEF) in Pentecoste-CE. The grass was sown manually in January 2003. Guinea grass was subjected to three rest periods, defined as a function of the time needed for expansion of 1.5, 2.5, and 3.5 new sheets per tiller, with two repetitions per treatment. Therefore, the area was divided into six rotating stocking systems, two for each rest period, for evaluation. The data from this study included collections from August 3, 2003, to November 8, 2003 and covered the dry period in the region. Harvesting was performed by sheep in an area under sprinkler irrigation with a water depth of approximately 11.4 mm day^{-1} and a four-day watering shift. Nitrogen fertilizers were applied at a rate of 160 kg N ha^{-1} year^{-1} in the form of urea (45% N). The design was completely randomized. For more details on this study, see Silva et al. (2007).

The experimental trial GG.PEN.05–06 was performed at NEEF in Pentecoste-CE in the same area as the trial GG.PEN.03. Guinea grass was subjected to three rest periods based on the time required for the canopy to reach 85, 95, and 97% light interception, in combination with two post-grazing residues based on a residual leaf area index of 1.0 or 1.8 for a total of six treatments. Light interception and leaf area index were measured using an AccuPAR LP-80 canopy analyzer (Decagon®). The design was completely randomized with four replicates, totaling 24 experimental units divided into 24 paddocks. The data from this study were collected from October 25, 2005, to March 7, 2006. Harvesting was performed by sheep in an area under fixed sprinkler irrigation with a water depth of approximately 11.4 mm day^{-1} and a four-day watering shift. Nitrogen fertilizers were applied at a rate of 220 kg N ha^{-1} year^{-1} in the form of urea (45% N). For more details about this study, see Cutrim Junior et al. (2011).

TABLE 2 | Characterization of the experimental and management conditions of each experimental trial.

ID[a]	Planting date	Trial period	Experimental design	Treatments	Nitrogen fertilization	Type of harvest	Use of irrigation
GG.IGA.15	March 6, 2014	March 14, 2015 to January 2, 2016	Randomized block design	Harvest frequencies based on fixed days (14, 21, 28, 35, 42, and 49 days) of the rest period	200 kg of N ha^{-1} $year^{-1}$ in the form of urea (45% N)	Mechanical cutting	No
GG.IGA.17-18	March 6, 2014	September 2, 2017 to September 12, 2018	Randomized block design	Harvest intensities based on the residue height (15, 25, 35, 45, and 55 cm)	200 kg of N ha^{-1} $year^{-1}$ in the form of urea (45% N)	Mechanical cutting	No
GG.PEN.03	January 2003	August 3, 2003 to November 8, 2003	Completely randomized design	Harvest frequencies based on time needed for expansion of 1.5, 2.5, and 3.5 new sheets per tiller	160 kg of N ha^{-1} $year^{-1}$ in the form of urea (45% N)	Grazed by sheep	Yes
GG.PEN.05–06	January 2003	October 25, 2005 to March 7, 2006	Completely randomized design	Harvest frequencies in combination with post-grazing residues	220 kg of N ha^{-1} $year^{-1}$ in the form of urea (45% N).	Grazed by sheep	Yes
MG.IGA.15	May 20, 2014	February 14, 2015 to August 5, 2015	Completely randomized design	Nitrogen fertilization (control, 100, 200, 300, 400, and 500 kg ha^{-1} $year^{-1}$)	Same as treatments	Mechanical cutting	No
MG.FOR.09	September 2008	July 14, 2009 to October 18, 2009	Completely randomized design	Nitrogen fertilization (control, 400, 800, and 1,200 kg ha^{-1} $year^{-1}$)	Same as treatments	Grazed by sheep	Yes

[a]*Identification of the experimental trial.*

The experimental test MG.FOR.09 was performed in the experimental field of NEEF in Fortaleza, CE. The grass was sown by hand in September 2008, with a sowing rate equivalent to 2 kg of pure seeds ha^{-1} after tillage. Massai grass was subjected to increasing doses of nitrogen (0-control; 400, 800, and 1,200 kg ha^{-1} $year^{-1}$) under a fixed sprinkler irrigated area with a liquid depth of 7.0 mm day^{-1} and watering shift of 3 days, in an intermittent stocking system grazed by sheep. The experimental design was completely randomized with two repetitions and evaluations at each regrowth cycle lasting 22, 18, 16, and 13 days for the control treatments (without fertilization), and 400, 800, and 1,200 kg of nitrogen fertilization, respectively. The experiment was conducted at FEIGA from July 14, 2009, to October 18, 2009. For more details on this study, see Lopes et al. (2016).

A summary of the experimental and management conditions of each trial is presented in **Table 2**.

Measured Agronomic Variables

In all trials, the common variables measured prior to defoliation were biomass accumulation and its morphological components, tiller population density (TPD), and canopy height increment (CHI). The number of days of the rest period (RP) between pastures was also determined.

The accumulation of biomass was measured by destructive collections with the use of known area frames used in each experimental trial, which were converted to hectares, considering the forage above the height of a particular residue in each trial. In the GG.IGA.15, GG.IGA.17-18, and MG.IGA.15 trials, forage collection was performed using two samplings in a 0.5 m^2 frame (1.0 m 0.5 m). In the GG.PEN.03 and GG.PEN.05–06 trials, collection was performed using two samplings in a 1.0 m^2 frame (1.0 m × 1.0 m). In the MG.FOR.09 trial, the collection was performed using two samplings in a frame of 0.0625 m^2 (0.25 m × 0.25 m).

From biomass collection, the total forage accumulation (FA) and the morphological composition were determined through the separation of its plant components, obtaining the leaf blade accumulation (LBA), stem accumulation (stem + sheath; SA), and dead material accumulation (DMA). Each sample was placed in a forced ventilation oven (55°C to constant weight) to determine biomass accumulation in terms of dry matter. The CHI was obtained by the difference in canopy height before and after defoliation, measured with the aid of a ruler graduated in centimeters (Barthram, 1986). The TPD was estimated by counting the live tillers within a known area frame and converting to the number of tillers per square meter.

Agrometeorological Variables

The mean temperature (Tmean) and precipitation (Prec) data for the municipality of Igarapé-Açu were obtained through the conventional meteorological station of Brazilian Agricultural Research Corporation (Embrapa), 900 m from the experiments. The same meteorological data, along with air humidity and wind speed, were obtained by the UFC automatic meteorological station at 800 and 550 m from the experimental area in the municipalities of Pentecoste and Fortaleza, respectively. Due to the absence of radiation measurements at some stations, global solar radiation (SR) data for the three sites were retrieved from the National Solar Radiation Database (NSRDB).

The reference evapotranspiration (ETo) of the cities of Fortaleza and Pentecoste was provided by the Penman-Monteith FAO 56 (FAO, 1998), according to the following equation:

$$ETo = \frac{\mathbf{0.408}\Delta\left(R_n - G\right) + \gamma\frac{\mathbf{900}}{T_{\mathbf{mean}} + \mathbf{273}}u_2\left(e_s - e_a\right)}{\Delta + \gamma\left(\mathbf{1} + \mathbf{0.34}u_2\right)}$$

where Δ is the slope vapor pressure curve as a function of temperature (kPa°C^{-1}), and Rn is the net radiation at the crop surface (MJ.m^{-2} day^{-1}); G is the soil heat flux density (MJ m^{-2} day^{-1}); γ is the psychometric constant (kPa °C^{-1}); T_{mean} is the mean between maximum and minimum temperature (°C); u_2 is the wind speed (m s^{-1}); and (e_s-e_a) is the saturation vapor pressure deficit (kPa).

The absence of wind speed and humidity data at the Igarapé-Açu meteorological station required that the ETo be calculated according to the method of Turc (1961), which represents an adequate estimate of the ETo for the region (Silva Júnior et al., 2017; Farias et al., 2019):

$$ETo = \frac{\mathbf{0.013}T_{\mathbf{mean}}}{T_{\mathbf{mean}} + \mathbf{15}}\left(\mathbf{23.9}R_S + \mathbf{50}\right)$$

where T_{mean} is the mean between the maximum and minimum temperatures (°C) and R_s is the solar global radiation (MJ m^{-2} day^{-1}).

The water index (WI) was obtained from the relationship between the actual evapotranspiration (ETa) and reference (ETo):

$$WI = \frac{\textbf{actual evapotranspiration}}{\textbf{reference evapotranspiration}}$$

ETa was calculated from the preparation of the sequential water balance on a daily scale according to Thornthwaite and Mather (1955), based on the available water capacity (AWC), which was different for each location (**Table 1**). The AWC of the soil was calculated as the difference between the field capacity (FC) and the permanent wilting point (PWP). FC and PWP were obtained from undeformed soil samples saturated with water and subjected to tension of 10 and 1,500 kPA, respectively, in a Richards chamber.

Water from irrigation and/or precipitation was the applied water variable (WA). The supplied nitrogen (SN) was the agrometeorological variable for plant nitrogen availability in the form of fertilization.

Statistical Analysis

The mean and/or some of the values of the agrometeorological (Tmean, SR, ETo, ETa, WI, WA, and SN) and agronomic (TPD, CHI, RP, FA, LBA, SA, and DMA) variables related to the regrowth period of each forage production cycle were used to form two groups (the group of agrometeorological variables and the group of agronomic variables).

The characterization of the observations from each trial was verified using principal component analysis (PC) through the generation of indices summarizing the agrometeorological and agronomic variables and represented in biplot graphs. The eigenvalues and eigenvectors were calculated from the correlation matrix to ensure that the results were not biased by large numerical variables. The choice of the number of components was based on the PC that obtained eigenvalues greater than 1, according to the Kaiser criterion (Kaiser, 1958).

To analyze how agronomic and agrometeorological variables are related, the data were subjected to canonical correlation analysis, whereby the participation of each variable in the generation of canonical indices was determined by the correlation of the canonical and the original variable.

Agrometeorological and agronomic variables were used in a discriminant function analysis to verify the functions responsible for maximizing the difference between the trials, based on the grass cultivar and the location of the experiment. To determine which variables were responsible for the separation, the generated discriminant functions were correlated with the original variables, and the Pearson correlation coefficients were described in a biplot graph. To verify how the assays differed, the new variables (discriminating functions) generated were subjected to the F test for mean differences and Tukey's test for mean comparisons, both at a significance level of 0.05. The studentized residues of the model were subjected to the identification of outliers (values above 3.0 and below −3.0) and normality using the Shapiro–Wilk test. The homoscedasticity of variances test was performed, and the tests that showed heterogeneous variances were grouped to the model using the restricted maximum likelihood method.

The vectors that describe the variables in the biplot graphs generated in the principal component and discriminant analyses were multiplied by factors 10 and 20, respectively. Such adjustments were made to improve the scaling of vectors in the graph. In all the analyses described, R software (R Core Team, 2019) was used as a tool for data processing.

RESULTS

How Are the Different Cultivation Conditions Characterized in Relation to the Indices That Group Agronomic and Agrometeorological Variables?

Choosing the PC number using the Kaiser criterion allowed the selection of the first two components for characterization based on agrometeorological variables and the first three components based on agronomic variables, as observed in the scree plot graphs (**Figure 2**).

The characterization of the six trials, through the agrometeorological variables, was influenced by the first main component (PC1; **Figure 3**), which accounted for 65.33% of the data variation. PC1 (**Figure 3**) demonstrated a contrast between variables related to water availability (ETa, WA, and WI) and SN versus variables related to energy supply (SR and Tmean) that result in potential evapotranspiration (ETo). There was a greater variability in the tests that used Guinea grass in the municipality of Igarapé-Açu (GG.IGA.15 and GG.IGA.17-18) than the other tests (**Figure 3**).

Principal component 2 (PC2, **Figure 3**) explained 18.49% of the data variation and was related to a greater variability of the humid tropical climate tests of the Amazon region, both for Massai grass and Guinea grass in relation to those in the Northeast region. With the exception of WA, the other

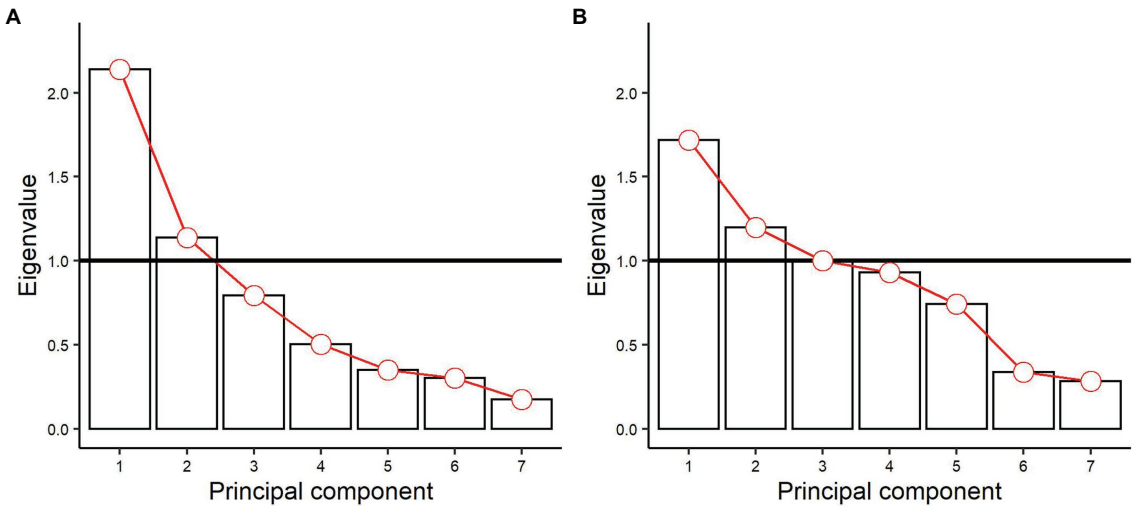

FIGURE 2 | Variance explained by each principal component, through their respective eigenvalues. **(A)** Eigenvalues of the principal components referring to agrometeorological variables. **(B)** Eigenvalues of the principal components referring to agronomic variables.

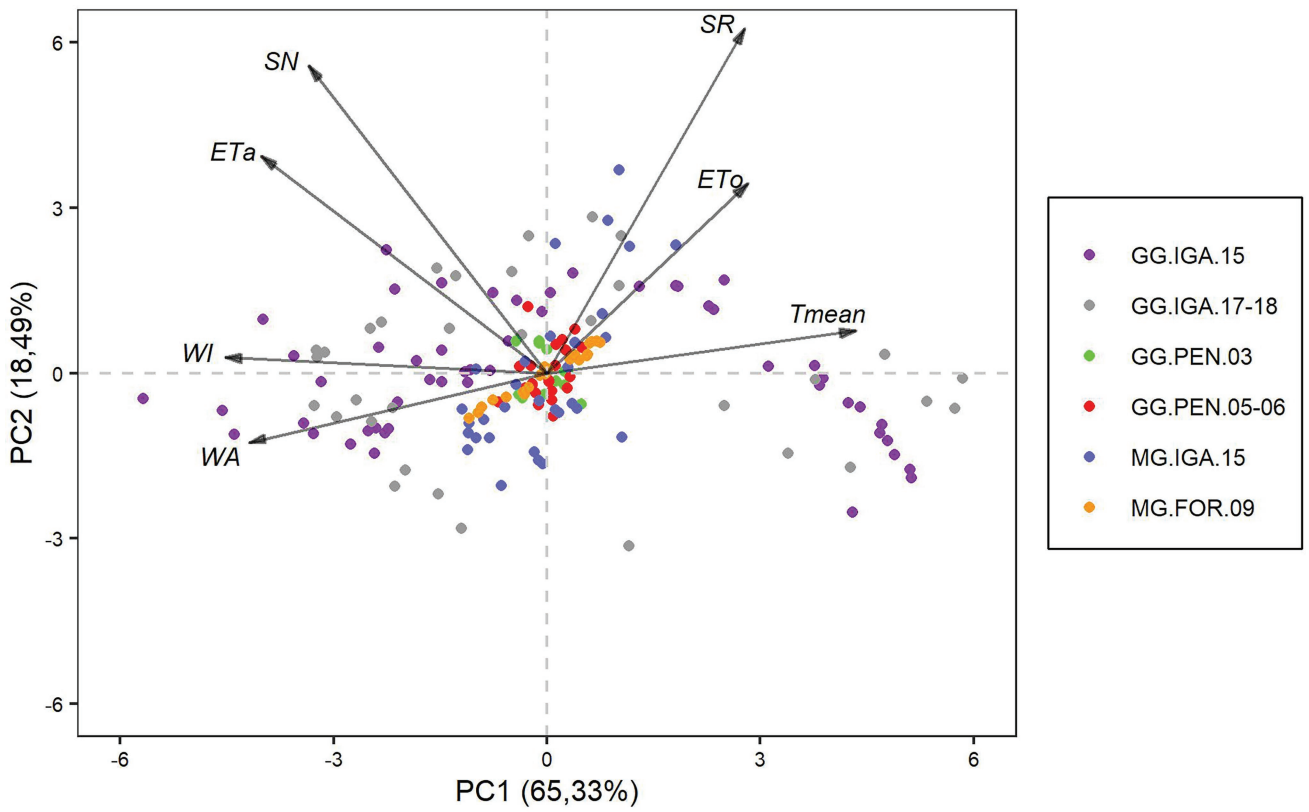

FIGURE 3 | Biplot representation of the first two main components obtained from the agrometeorological variables, with observations from the six types of trials with cultivars of the species *Megathyrsus maximus*. ETa, Actual Evapotranspiration; ETo, Reference Evapotranspiration; SN, Supplied nitrogen; SR, Solar radiation; Tmean, Mean temperature; WA, Water applied; and WI, Water index.

agrometeorological variables showed positive coefficients for this component. There was also high participation for SR, SN, ETo, and ETa (**Figure 3**).

The biplot graph provides information related to the correlation between variables, where arrows in the same direction but opposite senses represent strong negative

correlations between the variables. The ETo and Tmean showed strong negative correlations with WI and WA (**Figure 3**). In contrast, the arrows that show close directions, forming a small angle between them, are more positively correlated. This can be observed between the energy supply variables (SR, ETo, and Tmean) and the water availability variables (WI and WA) for ETa and SN.

The first three main components of the agronomic variables accounted for 76.92% of the data variability. Principal component 1 (PC1, **Figure 4**), responsible for 42.14% of the variation, represents the growth of grasses, through an index that considers all agronomic variables, with low participation of RP. All trials were characterized by alterations in the high and low agronomic variable values (**Figures 4A,B**).

The second principal component (PC2, **Figure 4**), which held 20.50% of the data variability, was related to a contrast mainly between SA and DMA versus CHI, FA, and TPD, with a low participation of LBA. In this component, there was greater variability in the data from the Guinea grass trial in 2015 (**Figures 4A,C**). Principal component 3 (PC3, **Figure 4**) highlighted the importance of grass regrowth days. It accounted for 14.29% of the data variability and showed that this variation in the regrowth period between trials did not change substantially, except for some observations in the Guinea grass study in Igarapé-Açu during 2017 and 2018 (**Figures 4B,C**).

How Do Agrometeorological Variables Relate to Agronomic Variables?

The correlation between the canonical agrometeorological variables and their original counterparts showed a contrast between variables related to water availability (WA, ETa, and WI) with SN versus the variables related to energy supply in terms of temperature and radiation (ETo, SR, and Tmean; **Figure 5**). Through the correlation between the canonical agronomic variable and their original counterparts, it appears that former represented a contrast between DMA and the other variables (FA, LBA, TPD, and CHI), mainly with respect to the increase in height (**Figure 5**). SA and days of regrowth showed little participation in this canonical variable. Based

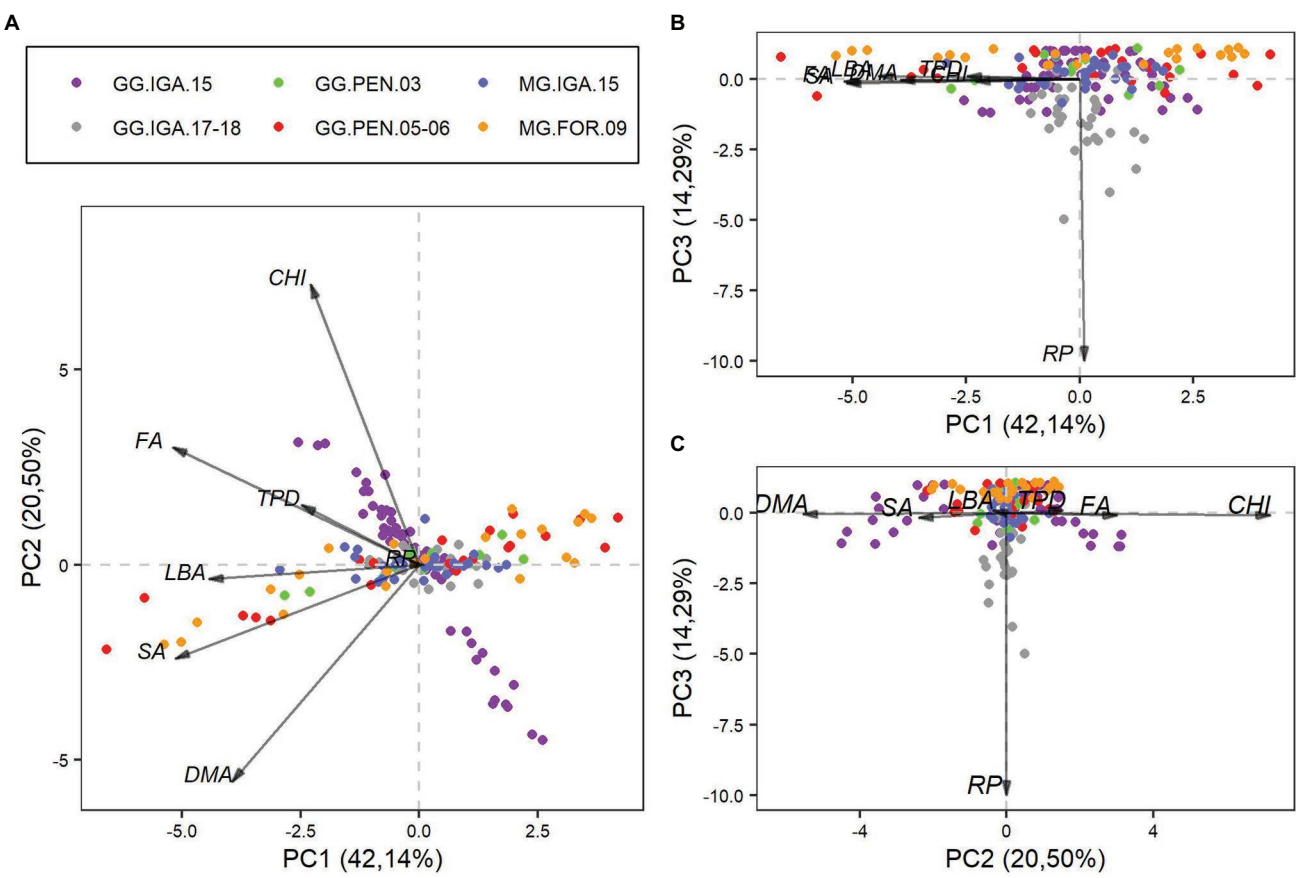

FIGURE 4 | Biplot representation of the first three main components obtained from the agrometeorological variables, with observations from the six types of trials with cultivars of the species *Megathyrsus maximus*. **(A)** Bidirectional relationship of principal component 1 with principal component 2. **(B)** Bidirectional relationship of principal component 1 with principal component 3. **(C)** Bidirectional relationship of principal component 2 with principal component 3. CHI, Canopy height increment; DMA, Dead material accumulation; FA, Forage accumulation; LBA, Leaf blade accumulation; SA, Stem accumulation; and TPD, Tiller population density.

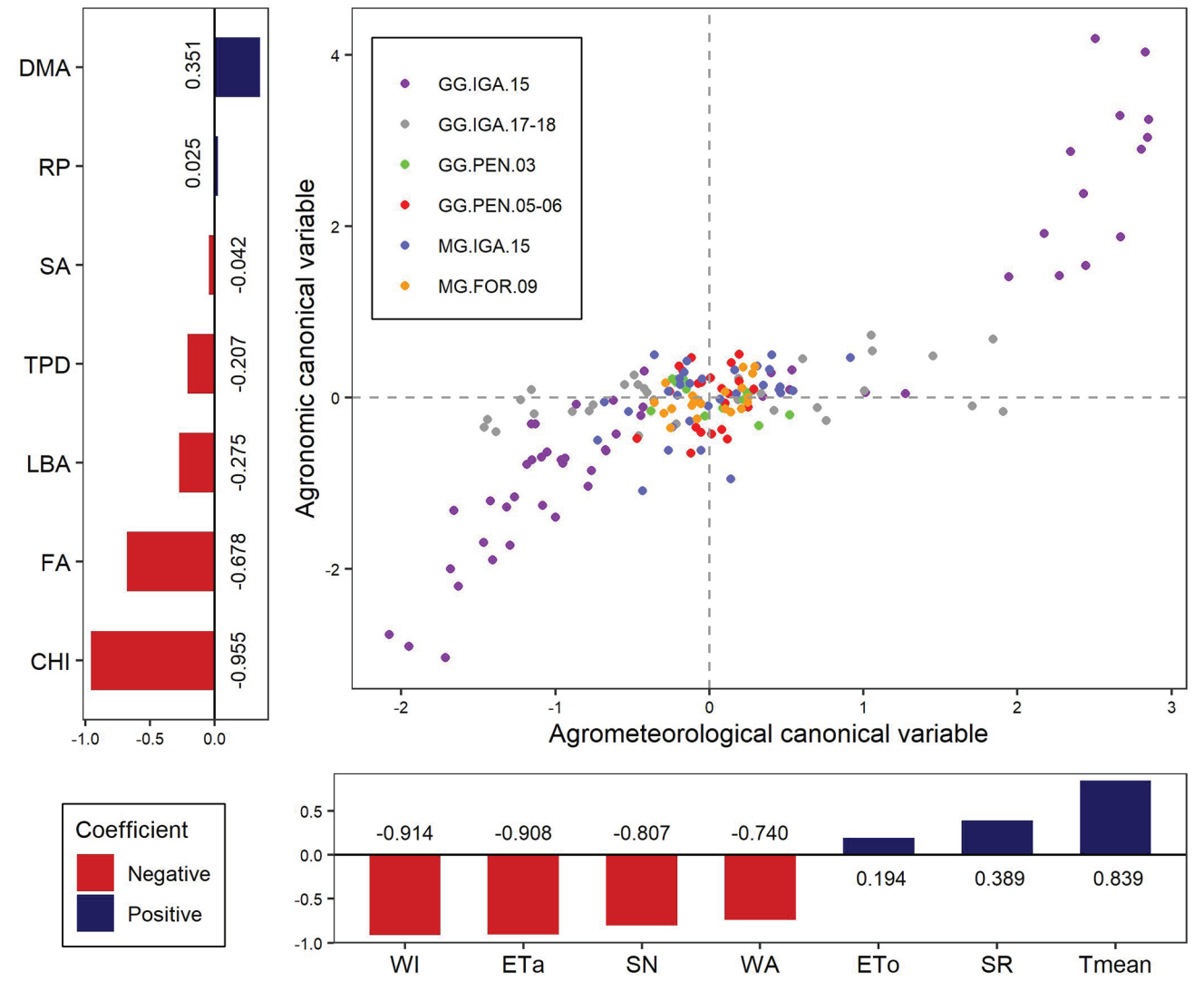

FIGURE 5 | Graphic representation of the canonical correlation between the group of agrometeorological variables (Agrometeorological canonical variable) with the agronomical variables (Agronomic canonical variable). The bar graphs to the left and below the agronomic and agrometeorological variables, respectively, represent the influence of each original variable in the generation of the canonical variable through the value of their correlation coefficient. ETa, Actual evapotranspiration; ETo, Reference evapotranspiration; SN, Supplied nitrogen; SR, Solar radiation; Tmean, Mean temperature; WA, Water applied; WI, Water index; CHI, Canopy height increment; DMA, Dead material accumulation; FA, Forage accumulation; LBA, Leaf blade accumulation; SA, Stem accumulation; and TPD, Tiller population density.

on this relationship, environments with high Tmean, low water availability, and low nitrogen supply promote low plant growth, mainly in terms of lower FA and CHI, while accelerating the death of plant material characterized by high DMA.

The correlation coefficient between the agrometeorological and agronomic canonical variables was 0.84, which represents 76.94% of the variation explained by the first pair of canonical variables. The data from the trial with Guinea grass in Igarapé-Açu during 2015 were the most heterogeneous of all trials in terms of both the canonical agrometeorological and agronomic variables. The trial with Guinea grass in Igarapé-Açu between 2017 and 2018 showed some variability in the canonical agrometeorological variable, but with more homogeneous results for the canonical agronomic variable (**Figure 5**).

How Can Discriminating Functions That Separate Experiments With Guinea and Massai Grasses Conducted in Distinct Regions, but at Similar Latitudes, Be Described?

The separation between the groups of experiments can be seen by the influence of two discriminant functions, which together represent 89.56% of the variation responsible for the maximum separation of the groups (**Figure 6**). Discriminant function 1

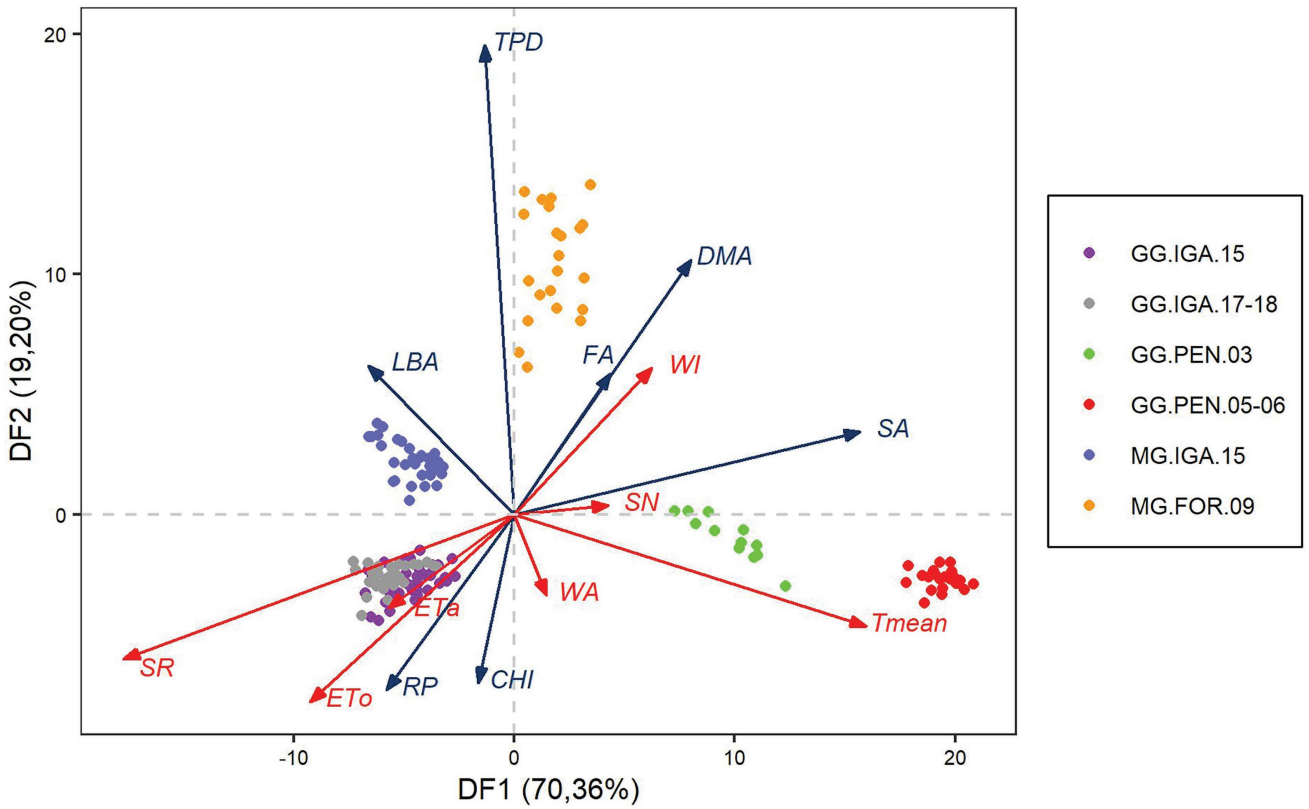

FIGURE 6 | Biplot representation of the first two discriminant functions with observations from six types of trials with cultivars of the species *Megathyrsus maximus*. The red and blue arrows show the participation of each agrometeorological and agronomic variable, respectively, in the formation of the discriminant function. ETa, Actual evapotranspiration; ETo, Reference evapotranspiration; SN, Supplied nitrogen; SR, Solar radiation; Tmean, Mean temperature; WA, Water applied; WI, Water index; CHI, Canopy height increment; DMA, Dead material accumulation; FA, Forage accumulation; LBA, Leaf blade accumulation; SA, Stem accumulation; and TPD, Tiller population density.

(DF1) revealed a contrast between the rest period and LBA versus FA, DMA, and SA. This discriminant function mainly separates the tests by region. The left side represents Igarapé-Açu, and the right denotes Fortaleza, and the extremes are the Pentecoste region. The data from semi-arid region were characterized by greater production of biomass and its components of the stalk and dead material, than those in the Amazon region, with emphasis on the tests with Guinea grass. For the agrometeorological variables, the separation of regions occurred through a contrast mainly between ETa, ETo, and SR on one side and between Tmean and WI on the other (**Figure 6**). DF1 had the highest mean for GG.PEN.05–06, followed by GG.PEN.03, and MG.FOR.09, for positive values on the axis. Regarding negative values, the MG.IGA.15 and GG.IGA.15 assays were equal, and the lowest values were found for the GG.IGA.17-18 study (**Table 3**).

Discriminant function 2 (DF2) separated the grass cultivars. This function separates the tests that used Massai grass, characterized by higher TPD, biomass accumulation, and its morphological components, from the tests that evaluated Guinea grass, which had a greater increase in height and regrowth days. The agrometeorological variables were influenced by Tmean, SR, and ETo, in contrast to WI (**Figure 6**). DF2 had the highest mean for the MG.FOR.09 study, followed by MG.IGA.15 with the positive values on the axis. The GG.PEN.03 assay had the highest mean negative value, followed by the GG.IGA.15, GG.IGA.17-18, and GG.PEN.05–06 studies, which were equal (**Table 3**).

DISCUSSION

The relationship between agrometeorological and agronomic variables in tropical grasses has been little explored using multivariate approaches. A correct understanding of these interactions will help identify the most efficient use for tropical grass management according to region as will direct-to-research studies on grazing management and tropical grass growth modeling. The importance of this knowledge was confirmed in our study by the formation of indices that summarize the variable information into two groups based on agrometeorological variables, both by principal component and canonical correlation analysis. One group included variables related to energy supply in terms of radiation and temperature, and the other by water and nitrogen availability factors. The *Megathyrsus* sp. in different climatic conditions

TABLE 3 | Difference between studies based on the comparison of the mean of the generated discriminant functions.

Studies	Discriminant functions	
	DF1[a]	DF2[b]
MG.IGA.15	–4.64 d	2.24 b
GG.IGA.15	–4.76 d	–2.82 d
GG.IGA.17-18	–5.67 e	–2.58 d
MG.FOR.09	1.78 c	10.50 a
GG.PEN.03	9.79 b	–0.96 c
GG.PEN.05-06	19.39 a	–2.69 d
value of *p*	<0.0001	<0.0001

[a]*Discriminant function 1.*
[b]*Discriminant function 2.*
Means followed by the same letter in the column do not differ by Tukey's test at 0.05.

was distinguished mainly by the availability of water. This corroborates our hypothesis that even in regions located close to the equator, such as the Amazon and semi-arid regions of Brazil, there are climatic factors capable of discriminating them in terms of productive potential (Silva et al., 2019a).

PC1 (**Figure 3**) shows that the cultivation conditions with Guinea grass in Igarapé-Açu (GG.IGA.15 and GG.IGA.17-18) had greater data dispersion than the other trials. Climatic variability during the trials may explain the main cause of this difference. The tests in the semi-arid region involved a greater control of climatic conditions through water supply irrigation. In this region, radiation and temperature variability were not as pronounced; water supply through irrigation ensures continuous water availability, and there is no significant variability in actual evapotranspiration (Graham et al., 2016).

Similar to the town of the semi-arid region, Igarapé-Açu is located close to the equator (**Figure 1**). Consequently, the photoperiod, solar radiation, and temperature data did not vary substantially over the experimental period (**Table 1**). However, the variability observed in ETa, particularly in the GG.IGA.15 and GG.IGA.17-18 studies (**Table 1**), can be attributed to the cultivation conditions that included evaluations in both the rainy and the dry periods (Lage Filho et al., 2021; Macedo et al., 2021). In the MG.IGA.15 trial, the evaluations covered only the rainy season and the rainy-dry transition period.

PC1 also considered supply nitrogen, along with the water variables (**Figure 3**). The SN in Guinea grass trials in Igarapé-Açu showed greater variability due to the absence of nitrogen fertilization during the dry period, which was not required because of the lack of soil moisture (Kunrathm et al., 2018). The contrast observed by PC1 (**Figure 3**) was related to a greater dispersion of the variables related to water availability and SN than the energy supply and potential water loss variables, mainly in Igarapé-Açu. Based on this, we consider that statistical methods, such as principal component regression, can be potential alternatives for modeling studies with agrometeorological variables and soil properties, as observed in other studies, such as those by Zhou et al. (2021). These authors used principal component regression to relate climatic variables, soil properties, and plant characteristics to the spatial variability of the net exchange of CO_2 between land and atmosphere, using data from croplands, pastures, and forests in different regions. Dispersion of observations in the Amazon region was observed in the second principal component (PC2, **Figure 3**), in which there was greater participation of the Massai grass trial (MG.IGA.15). In this trial, no evaluations were conducted during the dry season; therefore, the component was generated with most of the variables from only the positive side of the axis (**Figure 3**). For empirical modeling purposes, the variability in growing conditions of the GG.IGA.15 and GG.IGA.17-18 trials are important for obtaining models that can be generalized in prediction processes (Andrade et al., 2015).

We obtained three main components for the agronomic variables. All experimental tests showed some variability in the first principal component (PC1; **Figures 4A,B**). This is because the variation in observations is due to the treatments adopted in the trials, whether using different doses of nitrogen fertilization (trials with Massai grass) or different management techniques (trials with Guinea grass). In pasture production systems, it is common to adopt different management techniques based on grazing goals, which will depend on the technological level, production system, and possible edaphoclimatic variation in the region (Silva et al., 2019b,c; Macedo et al., 2021). These factors are indispensable when considering the changeability of response variables that are relevant for monitoring the structure and productivity of pastures.

Not only agrometeorological conditions are important in understanding and predicting productive variables in pastures. Other factors such as management of mechanistic models that estimate biomass production, such as CROPGRO (Bosi et al., 2020b; Brunetti et al., 2021) and APSIM (Bosi et al., 2020a; Gomes et al., 2020), are also relevant.

The second principal component (PC2; **Figures 4A,C**) mainly showed the larger variability in relation to the GG.IGA.15 trial, because the data from this trial reflected canopies with high and low values of agronomic variables due to use of rest days ranging from 14 to 49 (Macedo et al., 2021). The low participation of LBA in this study is linked to the small variability of this factor in the observed data. It is likely that the accumulation of leaf blades between canopies with different intervals between defoliations did not vary substantially because of TPD and the number of leaves per tiller. Canopies with higher RP had more leaves per tiller and wider and larger leaves, but lower TPD. Canopies with lower RP had fewer leaves per tiller and thinner leaves, but higher TPD. In general, compensation for the number of tillers did not modify the LBA (Sbrissia et al., 2010).

The third principal component (PC3; **Figures 4B,C**) highlighted the effect of regrowth days. Except for some data for the GG.IGA.17-18 trial, the trials presented a similar distribution of observations for this component. Fixed regrowth periods were not considered, and evaluations occurred during the dry period; therefore, the time for the canopy to reach 95% light interception (experiment goal) was high in some cycles of the GG.IGA.17-18 trial (Lage Filho et al., 2021). This may be related to the increased variability of observations

in this trial for this component. Using management goals based on light interception in periods in which there are no favorable conditions for plant growth can be challenging, which has been described in other studies (Carnevalli et al., 2006).

The existing linear relationships between the set of agronomic and agrometeorological variables can be represented by canonical variables, whereby the maximum possible canonical correlation is desired (Araújo Júnior et al., 2021). Therefore, the high canonical correlation (0.84) between the agrometeorological and agronomic variables demonstrates the close interaction between these two groups. This influence is related to the fact that water availability and SN contrast with factors related to potential water loss (ETo, SR, and Tmean). Thus, this directly affects the set of agronomic variables linked to forage canopy growth (FA, LBA, TPD, and CHI), which are important factors in herbivore production systems. These important factors contrast with DMA (**Figure 5**), which is the result of plant tissue death and is viewed negatively in intensive production systems (Carnevalli et al., 2006).

Multiple regression analysis is a particular case of canonical correlation that can be used to understand which agrometeorological variables are important in the composition of empirical models for estimating productive variables, such as biomass production and tiller density (Qiu et al., 2016; Mathieu and Aires, 2018). In this case, these productive variables would be more related to data on water availability, particularly ETo, WI, and SN. High temperature is an important growth factor for C4 cycle grasses that is related to the increased metabolic activity of plants; however, water stress can be a harmful factor for plant development (Prasad et al., 2011; Mathieu and Aires, 2018). In forage plants, this may be linked to increased plant material death in contrast to biomass accumulation, as observed in the canonical agronomic variable. This was mainly due to the greater variability of the data in the environmental conditions during the conduct of the tests, reflecting the lack of control of the water supply of the crop in the GG.IGA.15 and GG.IGA.17-18 tests (**Figure 5**). The aspects related to the management of the GG.IGA.15 study, considering regrowth periods that ranged from 14 to 49 days, caused this cultivation condition to present high variability in the canonical agronomic variable which leads to the high variability of forage canopy structural conditions (Macedo et al., 2021).

The variability of observations from these assays, both by principal component and canonical correlation analysis, is related to the response characteristics of grasses to environmental conditions. Unlike many other species, such as those of the genus *Urochloa* (syn. *Brachiaria*), grasses of the genus *Megathyrsus* are more responsive to edaphoclimatic conditions and highly productive when these conditions are favorable, so they are used in intensive production systems under grazing (Pontes et al., 2016). Discriminant function 1, which had the greatest power to separate the studies, discriminated the trials mainly by location (**Figure 6**). In other words, the difference between the climatic regions (humid tropical and semi-arid) promotes a greater power of distinction than the studied cultivars (Guinea and Massai grass).

It is possible to visualize the difference between experiments GG.PEN.03 and GG.PEN.05–06 (**Table 3**) despite having the same locations. This was likely due to climatic differences between the times the tests were conducted, mainly with regard to temperature, which was 3.52°C higher in the period from 2005 to 2006 compared to the experimental period in 2003 (**Table 1**). Regarding the tests in Igarapé-Açu, the temperature difference was only 0.65°C between GG.IGA.15 and GG.IGA.17-18. There was a difference between these two studies regarding DF1, which did not occur between GG.IGA.15 and MG.IGA.15 (**Table 3**), which that took place in the same year. Thus, the importance of climate-related variables in the composition of DF1 is evident. As both Pentecoste trials were adequately supplied with water through irrigation, the effect of temperature change may have been the main factor in discriminating these trials (**Table 2**). Temperature influences the acceleration of the physiological processes of the plant, resulting in greater forage accumulation, stem elongation, and dead material (Ivory and Whiteman, 1978). DF1 was more clearly observed by the greater effect of Tmean and SA, since the effect of temperature on stem elongation is well evidenced in grasses (Liu et al., 1998; Pierre et al., 2011; Yang et al., 2014).

The discrimination of the trials regarding the forage cultivar was based on the discriminant function 2. This function accounted for only 19.20% of the variation in the separation power of the studies. It is possible to observe the strong influence of agronomic variables on this discriminant function, mainly regarding the effects of TPD, FA, DMA, and LBA. Massai grass dominated for these variables because it presented higher TPD and biomass production compared to Guinea grass (Veras et al., 2020). In contrast, Guinea grass presented greater values in height increment, as this cultivar is larger than Massai grass. It is possible to see here the negative relationship between canopy height and TPD for tropical grasses observed in recent studies (Macedo et al., 2021; Xiliang et al., 2021), in which canopies with greater height tend to have lower TPD. Unlike DF1, DF2 did not differ in the Guinea grass trials in Igarapé-Açu at different times (**Table 3**). The highest values for the MG.FOR.09 study showed the strong production capacity of the Massai grass cultivated under conditions of high temperature and radiation in low-latitude regions (**Table 1**). Associated with this, the high availability of water explained the stronger positive correlation of WI with DF2 than the other variables (**Figure 6**).

Through a multivariate approach with experimental test data, we show that in production systems based on the cultivation of grasses of the genus *Megathyrsus* in regions located near the equator, despite the similarities in energy supply in terms of radiation and temperature, water availability, and nutrient supply are the determining factors for biomass accumulation. Therefore, these factors should be prioritized in future studies modeling forage biomass accumulation. However, in tropical pastoral ecosystems, forage plant management also had a determining effect on the accumulation of total biomass and its components, which should be considered in studies of

relationships between productive variables and pasture characterization.

DATA AVAILABILITY STATEMENT

The data analyzed in this study is subject to the following licenses/restrictions: Dataset will be used in future modeling research by the team. Requests to access these datasets should be directed to anibal.cr@ufra.edu.br

AUTHOR CONTRIBUTIONS

VM: conceptualization, methodology, formal analysis, investigation, data curation, and writing—original draft. NL, AC, ML, RS, and JC: investigation, resources, data curation, and writing—review and editing. CF, MC, and AR: conceptualization, resources, writing—review and editing, supervision, and project administration. All authors contributed to the article and approved the submitted version.

FUNDING

This study was financed in part by the Coordenação de Aperfeiçoamento de Pessoal de Nível Superior—Brazil (CAPES; Finance Code 001).

ACKNOWLEDGMENTS

We would like to thank the Study Group on Ruminants and Forage Production of the Amazon (GERFAM—www.gerfam.com.br) and Teaching and Research Unit in Forage (NEEF—www.neef.ufc.br) for their support in conducting the experiments.

REFERENCES

Alvares, C. A., Stape, J. L., Sentelhas, P. C., Gonçalves, J. L. M., and Sparovek, G. (2013). Köppen's climate classification map for Brazil. *Meteorol. Z.* 22, 711–728. doi: 10.1127/0941-2948/2013/0507

Andrade, A. S., Santos, P. M., Pezzopane, J. R. M., Araújo, L. C., Pedreira, B. C., Pedreira, C. G. S., et al. (2015). Simulating tropical forage growth and biomassaccumulation: an overview of model developmentand application. *Grass Forage Sci.* 71, 54–65. doi: 10.1111/gfs.12177

Araújo Júnior, G. N., Jardim, A. M. R. F., Silva, M. J., Alves, C. P., Souza, C. A. A., Costa, S. A. T., et al. (2021). Growth dynamics and accumulation of forage mass of forage cactus clones as affected by meteorological variables and water regime. *Eur. J. Agrom.* 131:126375. doi: 10.1016/j.eja.2021.126375

Barthram, G. T. (1986). *Experimental Techniques: the HFRO Sward Stick*. In: Alcock, M.M. (Ed.), The Hill Farming Research Organisation – Biennial Report (1984–1985), Midlothian, 29–30.

Bosi, C., Sentelhas, P. C., Huth, N. I., Pezzopane, J. R. M., Andreucci, M. P., and Santos, P. M. (2020a). APSIM-tropical pasture: a model for simulating perennial tropical grass growth and its parameterisation for palisade grass (*Brachiaria brizantha*). *Agric. Syst.* 184:102917. doi: 10.1016/j.agsy.2020.102917

Bosi, C., Sentelhas, P. C., Pezzopane, J. R. M., and Santos, P. M. (2020b). CROPGRO-perennial forage model parameterization for simulating Piatã palisade grass growth in monoculture and in a silvopastoral system. *Agric. Syst.* 177:102724. doi: 10.1016/j.agsy.2019.102724

Brunetti, H. B., Boote, K. J., Santos, P. M., Pezzopane, J. R. M., Pedreira, C. G. S., Lara, M. A. S., et al. (2021). Improving the CROPGRO perennial forage model for simulating growth and biomass partitioning of guineagrass. *Agron. J.* 113, 3299–3314. doi: 10.1002/agj2.20766

Carnevalli, R. A., Silva, S. C., Bueno, A. A. O., Uebele, M. C., Bueno, F. O., Hodgson, J., et al. (2006). Herbage production and grazing losses in Panicum maximum cv. Mombaça under four grazing managements. *Trop. Grassl.* 40, 165–176.

Cutrim Junior, J. A. A., Cândido, M. J. D., Valente, B. S. M., Carneiro, M. S. D., and Carneiro, H. A. V. (2011). Características estruturais do dossel de capim-tanzânia submetido a três frequências de desfolhação e dois resíduos pós-pastejo. *R. Bras. de Zootec.* 40, 489–497. doi: 10.1590/S1516-35982011000300005

Durand, J. L., Grancher, C. V., Lemaire, G., Gastal, F., and Moulia, B. (1991). Carbon partitioning in forage crops. *Acta Biotheor.* 39, 213–224. doi: 10.1007/BF00114177

FAO (1998). Crop evapotranspiration-Guidelines for computing crop water requirements-FAO Irrigation and Drainage Paper 56, Rome, Italy.

Farias, V. D. S., Costa, D. L. P., Pinto, J. V. N., Souza, P. J. O. P., Souzs, E. B., and Farias, S. O. (2019). Calibration of reference evapotranspiration models in Pará. *Acta Sci. Agron.* 42:e42475. doi: 10.4025/actasciagron.v42i1.42475

Gomes, F. J., Bosi, C., Pedreira, B. C., Santos, P. M., and Pedreira, C. G. S. (2020). Parameterization of the APSIM model for simulating palisadegrass growth under continuous stocking in monoculture and in a silvopastoral system. *Agric. Syst.* 184:102876. doi: 10.1016/j.agsy.2020.102876

Graham, S. L., Kochendorfer, J., Mcmillan, A. M. S., Duncan, M. J., Srinivasan, M. S., and Hertzog, G. (2016). Effects of agricultural management on measurements, prediction, and partitioning of evapotranspiration in irrigated grasslands. *Agric. Water Manag.* 177, 340–347. doi: 10.1016/j.agwat.2016.08.015

Ivory, D., and Whiteman, P. (1978). Effect of temperature on growth of five subtropical grasses. I. Effect of day and night temperature on growth and morphological development. *Aust. J. Plant Physiol.* 5, 131–148. doi: 10.1071/PP9780131

Kaiser, H. F. (1958). The varimax criteria for analytical rotation in factor analysis. *Psychom. Theory* 23, 187–200. doi: 10.1007/BF02289233

Kunrathm, T. R., Lemaire, G., Sadras, V. O., and Gastal, F. (2018). Water use efficiency in perennial forage species: interactions betweennitrogen nutrition and water déficit. *Field Crop Res.* 222:31. doi: 10.1016/j.fcr.2018.02.031

Lage Filho, N. M., Lopes, A. R., Rêgo, A. C., Domingues, F. N., Faturi, C., Silva, T. C., et al. (2021). Effects of stubble height and season of the year on morphogenetic, structural and quantitative traits of Guinea grass. *Trop. Grassl. - Forrajes Trop.* 9, 256–267. doi: 10.17138/tgft(9)256-267

Liu, D. L., Kingston, G., and Bull, T. A. (1998). A new technique for determining the thermal parameters of phenological development in sugarcane, including suboptimum and supra-optimum temperature regimes. *Agric. For. Meteorol.* 90, 119–139. doi: 10.1016/S0168-1923(97)00087-7

Lopes, M. N., Cândido, M. J. D., Pompeu, R. C. F. F., Silva, R. G., Morais Neto, L. B., Carneiro, M. D. S., et al. (2016). Tillering dynamics in massai grass fertilized with nitrogen and grazed by sheep. *Biosci. J.* 32, 446–454. doi: 10.14393/BJ-v32n2a2016-26106

Macedo, V. H. M., Cunha, A. M. Q., Cândido, E. P., Domingues, F. N., Silva, W. L., Lara, M. A. S., et al. (2021). Canopy structural variations affect the relationship between height and light interception in Guinea grass. *Field Crop Res.* 271:108249. doi: 10.1016/j.fcr.2021.108249

Mathieu, J. A., and Aires, F. (2018). Assessment of the agro-climatic indices to improve crop yield forecasting. *Agric. For. Meteorol.* 253, 15–30. doi: 10.1016/j.agrformet.2018.01.031

Oliveira, J. K. S., Corrêa, D. C. C., Cunha, A. M. Q., Rêgo, A. C., Faturi, C., Silva, W. L., et al. (2020). Effect of nitrogen fertilization on production, chemical composition and morphogenesis of Guinea grass in the humid tropics. *Agronomy* 10:1840. doi: 10.3390/agronomy10111840

Onillon, B., Durand, J. L., Gastal, F., and Tournebize, R. (1995). Drought effects on growth and carbon partitioning in a tall fescue sward grown at different rates of nitrogen fertilization. *Eur. J, Agrom.* 4, 91–99. doi: 10.1016/S1161-0301(14)80020-8

Peel, M. C., Finlayson, B. L., and Mcmahon, T. A. (2007). Updated world map of the Köppen-Geiger climate classification. *Hydrol. Earth Syst. Sci.* 11, 1633–1644. doi: 10.5194/hess-11-1633-2007

Pierre, K. J., Yuan, S., Chang, C. C., Avolio, M. L., Hallett, L. M., Schreck, T., et al. (2011). Explaining temporal variation in above-ground productivity in a Mesic grassland: the role of climate and flowering. *J. Ecol.* 99, 1250–1262. doi: 10.2307/23027534

Pontes, L. S., Baldissera, T. C., Giostri, A. F., Stafin, G., Santos, B. R. C., and Carvalho, P. C. F. (2016). Effects of nitrogen fertilization and cutting intensityon the agronomic performance of warm-seasongrasses. *Grass Forage. Sci.* 72, 663–675. doi: 10.1111/gfs.12267

Prasad, P. V. V., Pisipati, S. R., Momcilovic, I., and Ristic, Z. (2011). Independent and combined effects of high temperature and drought stress during grain filling on plant yield and chloroplast EF-Tu expression in spring wheat. *J. Agron. Crop Sci.* 197, 430–441. doi: 10.1111/j.1439-037X.2011.00477.x

Qiu, Q., Shi, K., Qiao, X. J., and Jiang, K. (2016). Determining the dominant environmental parameters for greenhouse tomato seedling growth modeling using canonical correlation analysis. *IFAC* 49, 387–391. doi: 10.1016/j.ifacol.2016.10.071

R Core Team (2019). R: A Language and Environment for Statistical Computing. R Foundation for Statistical Computing. Available at: https://www.R-project.org (Acessed July 15, 2021).

Rind, D., Goldberg, R., Hansen, J., Rosenzweig, C., and Ruedt, R. (1990). Potential evapotrnspration and the likelihook of future drough. *J. Geophys. Res.* 95, 9983–10004. doi: 10.1029/JD095iD07p09983

Santos, P. M., Cruz, P. G., Araújo, L. C., Pezzopane, J. R. M., Valle, C. B., and Pezzopane, C. G. (2013). Response mechanisms of Brachiaria cultivars to water déficit stress. *R. Bras. Zootec.* 42, 767–773. doi: 10.1590/S1516-35982013001100001

Sbrissia, A. F., Silva, S. C., Sarmento, D. O. L., Molan, L. K., Andrade, F. M. E., Gonçalves, A. C., et al. (2010). Tillering dynamics in palisadegrass swards continuously stocked by cattle. *Plant Ecol.* 206, 349–359. doi: 10.1007/s11258-009-9647-7

Silva, S. C., Bueno, A. A. O., Carnevalli, R. A., Silva, G. P., and Chiavegato, M. B. (2019b). Nutritive value and morphological characteristics of Mombaça grass managed with different rotational grazing strategies. *J. Agric. Sci.* 157, 592–598. doi: 10.1017/S0021859620000052

Silva, R. G., Cândido, M. J. D., Neiva, J. N. M., Lôbo, R. N., and Silva, D. S. (2007). Características estruturais do dossel de pastagens de capim-tanzânia mantidas sob três períodos de descanso com ovinos. *R. Bras. Zootec.* 36, 1255–1265. doi: 10.1590/S1516-35982007000600006

Silva, W. L., Costa, J. P. R., Caputti, G. P., Lage Filho, N. M., Ruggieri, A. C., and Reis, R. A. (2019c). Effects of grazing intensity and supplemantation strategies on Tifton 85 procuction and on sheep performace. *Small Rumin. Res.* 174, 118–124. doi: 10.1016/j.smallrumres.2019.03.015

Silva, S. C., Gimenes, F. M. A., Sarmento, D. O. L., Sbrissia, A. F., Oliveira, D. E., Garat, A. H., et al. (2013). Grazing behaviour, herbage intake and animal performance of beef cattle heifers on marandu palisade grass subjected to intensities of continuous stocking management. *J. Agric. Sci.* 151, 727–739. doi: 10.1017/S0021859612000858

Silva Júnior, R. O., Souza, E. B., Tavares, A. L., Mota, J. A., Ferreira, D. B. S., Souza Filho, P. W. M., et al. (2017). Three decades of reference evapotranspiration estimates for a tropical watershed in the eastern Amazon. *An. Acad. Bras. Cienc.* 89, 1985–2002. doi: 10.1590/0001-3765201720170147

Silva, P. E., Silva, C. M. S., Spyrides, M. H. C., and Andrade, L. M. B. (2019a). Precipitation and air temperature extremes in the Amazon and northeast Brazil. *Int. J. Climatol.* 39, 579–595. doi: 10.1002/joc.5829

Simeão, R. M., Resende, M. D., Alves, R. S., Pessoa-Filho, M., Azevedo, A. L. S., Jones, C. S., et al. (2021). Genomic selecion in tropical forage grasses: current status and future applications. *Flont. Plant Sci.* 12:665195. doi: 10.3389/fpls.2021.665195

Tapia, J. I. C., Mazabel, J., and Quila, N. J. V. (2021). Classification of *Megathyrsus* maximus acessions grown in the Colombian dry tropical forest by nutritional assessment during contrasting seasons. *Front. Sustain. Food Syst.* 5:684747. doi: 10.3389/fsufs.2021.684747

Tardieu, F. (2013). Plant response to environmental conditions: assessing potential production, water demand, and negative effects of water deficit. *Front. Physiol.* 4:17. doi: 10.3389/fphys.2013.00017

Thornthwaite, C. W., and Mather, J. R. (1955). *The Water Balance.* New Jersey: Publications in Climatology.

Turc, L. (1961). Water requirements assessment of irrigation, potential evapotranspiration: simplified and updated climatic formula. *Ann. Agron.* 12, 13–49.

Veras, E. L. L., Difante, G. S., Gurgel, A. L. C., Costa, A. B. G., Rodrigues, J. G., Costa, C. M., et al. (2020). Tillering and structural characteristics of Panicum cultivars in the Brazilian semiarid region. *Susteinability.* 12:3849. doi: 10.3390/su12093849

Xiliang, L., Png, G. K., Li, Y., Jimoh, S. O., Ding, Y., Li, F., et al. (2021). Leaf plasticity contributes to plant anti-herbivore defenses and indicates selective foraging: implications for sustainable grazing. *Ecol. Indic.* 122:107273. doi: 10.1016/j.ecolind.2020.107273

Yang, Y., Massa, G. D., and Mitchell, C. A. (2014). Temperature DIP at the beginning of the photoperiod reduces plant height but not seed yield of maize grown in controlled environments. *Ind. Crop. Prod.* 53, 120–127. doi: 10.1016/j.indcrop.2013.12.002

Yeater, K. M., Duke, S. E., and Riedell, W. E. (2014). Multivariate analysis: greater insights into complex systems. *Agron. J.* 107, 799–810. doi: 10.2134/agronj14.0017

Zhou, H., Shao, J., Liu, H., Du, Z., Zhou, L., Liu, R., et al. (2021). Relative importance of climatic variables, soil properties and plant traits to spatial variability in net CO_2 exchange across global forests and grasslands. *Agric. For. Meteorol.* 307:108506. doi: 10.1016/j.agrformet.2021.108506

Conflict of Interest: The authors declare that the research was conducted in the absence of any commercial or financial relationships that could be construed as a potential conflict of interest.

Publisher's Note: All claims expressed in this article are solely those of the authors and do not necessarily represent those of their affiliated organizations, or those of the publisher, the editors and the reviewers. Any product that may be evaluated in this article, or claim that may be made by its manufacturer, is not guaranteed or endorsed by the publisher.

frontiers in Plant Science

SYSTEMATIC REVIEW
published: 23 March 2022
doi: 10.3389/fpls.2022.837648

Wood Formation Modeling – A Research Review and Future Perspectives

Annemarie H. Eckes-Shephard[1†], Fredrik Charpentier Ljungqvist[2,3,4*], David M. Drew[5], Cyrille B. K. Rathgeber[6,7] and Andrew D. Friend[1]*

[1] Department of Geography, University of Cambridge, Cambridge, United Kingdom, [2] Department of History, Stockholm University, Stockholm, Sweden, [3] Bolin Centre for Climate Research, Stockholm University, Stockholm, Sweden, [4] Swedish Collegium for Advanced Study, Uppsala, Sweden, [5] Department of Forest and Wood Science, Stellenbosch University, Stellenbosch, South Africa, [6] Université de Lorraine, AgroParisTech, INRAE, SILVA, Nancy, France, [7] Swiss Federal Research Institute for Forest, Snow and Landscape Research WSL, Birmensdorf, Switzerland

OPEN ACCESS

Edited by:
Maciej Andrzej Zwieniecki, University of California, Davis, United States

Reviewed by:
Sebastian Pfautsch, Western Sydney University, Australia
Cristina Nabais, University of Coimbra, Portugal

***Correspondence:**
Annemarie H. Eckes-Shephard annemarie.eckes-shephard@nateko.lu.se
Fredrik Charpentier Ljungqvist fredrik.c.l@historia.su.se

†Present address:
Annemarie H. Eckes-Shephard, Department of Physical Geography and Ecosystem Science, Lund University, Lund, Sweden

Specialty section:
This article was submitted to Plant Biophysics and Modeling, a section of the journal Frontiers in Plant Science

Received: *16 December 2021*
Accepted: *24 January 2022*
Published: *23 March 2022*

Citation:
Eckes-Shephard AH, Ljungqvist FC, Drew DM, Rathgeber CBK and Friend AD (2022) Wood Formation Modeling – A Research Review and Future Perspectives. Front. Plant Sci. 13:837648. doi: 10.3389/fpls.2022.837648

Wood formation has received considerable attention across various research fields as a key process to model. Historical and contemporary models of wood formation from various disciplines have encapsulated hypotheses such as the influence of external (e.g., climatic) or internal (e.g., hormonal) factors on the successive stages of wood cell differentiation. This review covers 17 wood formation models from three different disciplines, the earliest from 1968 and the latest from 2020. The described processes, as well as their external and internal drivers and their level of complexity, are discussed. This work is the first systematic cataloging, characterization, and process-focused review of wood formation models. Remaining open questions concerning wood formation processes are identified, and relate to: (1) the extent of hormonal influence on the final tree ring structure; (2) the mechanism underlying the transition from earlywood to latewood in extratropical regions; and (3) the extent to which carbon plays a role as "active" driver or "passive" substrate for growth. We conclude by arguing that wood formation models remain to be fully exploited, with the potential to contribute to studies concerning individual tree carbon sequestration-storage dynamics and regional to global carbon sequestration dynamics in terrestrial vegetation models.

Keywords: wood formation models, tree growth, terrestrial carbon cycle, dendroclimatology, forestry, growth–climate interactions, xylogenesis

1. INTRODUCTION

Wood formation and its interaction with the environment are of great relevance for a multitude of disciplines. For example, the value of wood as a raw material is of key interest for forestry as well as increasingly as bioenergy fuel (Downes and Drew, 2008; Séguin, 2011). Furthermore, wood has become an important topic in carbon sequestration offsetting (Frank et al., 2010; van der Gaast et al., 2018; Anderegg et al., 2020). Tree ring features are also used to reconstruct past climate (see, e.g., Fritts, 1976; Speer, 2010; Esper et al., 2016, 2018; Ljungqvist et al., 2020a) and for archaeological dating (e.g., Schweingruber, 1988; Baillie, 1995; Ljungqvist et al., 2018). Recently, there is increasing recognition that tree growth, in particular wood formation, is a crucial process for biomass allocation that needs to be explicitly considered in dynamic global vegetation models as part of climate change projections (Fatichi et al., 2014, 2019; Körner, 2015; Friend et al., 2019). As

a result of the central importance of wood for forestry, dendroclimatology, dendrochronology, and in fundamental biological research, many models have been constructed to simulate its formation. Nevertheless, there is scope for improving existing wood formation models and to develop new models.

Fritts et al. (1991, p. 114) describe the use of wood formation models as "a beginning effort to serve as an unambiguous medium of communication, which represent the state of knowledge at the present moment as we perceive it." In this spirit, the history of knowledge increase, hypotheses, and modeling approaches are well-summarized in wood formation models since the 1960s. These have been applied in forestry, dendroclimatology, and the study of wood formation itself. Different mechanisms, environmental or internal drivers of growth, have received attention at various levels of detail. They are a mix of hypotheses on what internally regulates an organism and what physically limits it. Besides a limited, and now outdated, review by Downes et al. (2009), a systematic and process-focused research review on wood formation models has hitherto been lacking. The aim of this review is to summarize the knowledge of growth processes collected in wood formation models, especially with regards to growth–climate relationships and with a focus on carbon. It will highlight some unresolved mechanisms, discipline-specific findings, and the utility and requirements of more data for model-development.

In order to better understand the models reviewed here, we briefly introduce the biological fundamentals of wood formation (i.e., xylogenesis). Xylogenesis involves the production and differentiation of new xylem cells, which eventually mature into functional wood cells (Plomion et al., 2001; Fromm, 2013). Wood formation is a form of plant growth, which can be defined as irreversible expansive and structural growth (Hilty et al., 2021). It follows the same principles as growth in all plants: (1) the production of new cells by stem cells and mother cells in the region called the cambium; (2) the subsequent further radial enlargement of these cells in the enlargement zone; followed by (3) wall thickening, involving the deposition of a secondary cell wall, which in the case of woody plants can be very thick and in addition to cellulose is also lignified to provide extra rigidity and hydrophobic properties; (4) the programmed cell death which transforms mature xylem cells into functional tracheary elements. The wood formation processes are pictured in **Figure 1**; the biological basis for wood formation is also well-summarized in Rathgeber et al. (2016).

This review covers 17 wood formation models (see **Table 1**) from the first in 1968 to the most recent in 2020. A brief history is followed by analysis of specific topics such as different mechanistic hypotheses, discipline-specific findings, and data needs. All 17 wood formation models are contrasted based on their levels of complexity and environmental vs. internal drivers/regulators. The baseline for this comparison is the first computer model of wood formation, viz. Wilson and Howard (1968). This model is chosen as the baseline because of its sole focus on cell type-specific processes and its lack of any environmental influences. Thus, any model containing all cell types *and* environmental/tree-internal factors is usually more complex than the baseline model. Models located below or at the same level as the baseline model usually only contain a subset of cell types and processes relevant for wood formation. Exceptions to the latter exist however, and will be described as such.

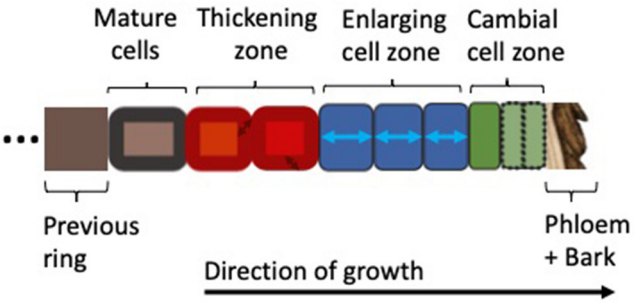

FIGURE 1 | Xylogenesis along a single radial file of developing cells, showing the zones of cell division, enlargement, wall thickening, and mature (dead) cells (Plomion et al., 2001; Fromm, 2013; Rathgeber et al., 2016). Depending on their different stages of development, the cells are assumed to be under varying environmental constraints and tree-internal regulation. Wood formation models covered in this review follow this schema and resolve one or more cell types with their associated processes.

Selection criteria for models included in this review are that they simulate one or more xylogenesis processes such as cell division, enlargement or thickening, and the respective cell types at the scale of a radial file (**Figure 1**). The dynamics should be resolved in a sufficiently mechanistic manner that process-hypotheses can be compared across models. Not considered in this review were models which do not follow the wood formation model framework introduced in **Figure 1**. These models are most commonly whole-tree models that produce intra-ring features of growth dynamics, often along the whole stem, instead of a single radial file. For example, hormonal flow from the crown received attention by Kramer (2001) in a whole-tree auxin-only model of cambial growth and orientation, where the cambium is approximated as a cylindrical surface along the modeled tree. Modeling of auxin flow along the stem of a tree also plays a large role to determine wood orientation (Kramer, 2002). Other models were developed to simulate timber quality characteristics and do not explicitly consider wood formation, but rather volume and mass increment leading to intra-ring features. These are mostly driven by carbon allocation and water-transport based on the Pipe Theory (Mäkelä and Mäkinen, 2003; Deckmyn et al., 2006). Other models not considered in-depth here can be categorized as radial growth or stem increment models, which do not disentangle increment dynamics into enlarging and cell production components (Steppe et al., 2006; Chan et al., 2016; Mencuccini et al., 2017; Eckes-Shephard et al., 2021; Peters et al., 2021) Overall, most of these models either do not consider the cambium as the driving feature of cell production, or explicit cell enlargement and thickening as the underlying processes for intra-ring patterning and are therefore not considered further in this review.

TABLE 1 | Wood formation models covered in this review.

Reference	Discipline	Inputs	Cell types simulated	Aims of the model	Species
Wilson and Howard (1968)	Fundamental research	–	CAM, ENL, THK, MAT	Test a cell developmental framework for secondary growth	*Pinus resinosa, Pinus strobus*
Howard and Wilson (1972)	Fundamental research	–	CAM, ENL, THK, MAT	Test influence of stochasticity on (above model's) rates and transition thresholds	*Pinus resinosa*
Wilson (1973)	Fundamental research	Signalling compound concentration	CAM, ENL, THK, MAT	"Provide new insights into cambial activity"	*Pinus resinosa*
Fritts et al. (1991)	Dendro-climatology	soil moisture, daylength, temperature	ENL	Contribute to understanding of tree ring-climate relationships	*Pinus sylvestris, Pinus ponderosa*
Deleuze and Houllier (1998)	Forestry	temperature, soil moisture, carbohydrates, +)	CAM, ENL, THK	Use a simple model to "understand or simulate the effects of changing environmental conditions [..] on forest production"	*Pinus sylvestris*
Fritts et al. (1999), TreeRing 3	Dendro-climatology	water stress (function of stomatal resistance), carbohydrates, temperature, hormones	CAM, ENL, THK, MAT	"Exactly how do trees record environmental information in the structure of their growth rings in both temperate and tropical environments?"	*Pinus ponderosa*
Vaganov et al. (2006), VS-model	Dendro-climatology	soil moisture, temperature, daylength,	CAM, (ENL, THK)	Construct a model "to achieve wide application to the study of tree ring dynamcis in dendrochronology"	
Drew et al. (2010), CAMBIUM	Forestry	xylem water potential, temperature, carbohydrates, hormones	CAM, ENL, THK, MAT	"[P]rovide a physiologically plausible and testable platform to assist in the understanding of the causes of wood property variation."	*Eucalyptus spp.*
Hölttä et al. (2010)	Fundamental research, forestry	xylem water potential, carbohydrates, temperature, *)	CAM, ENL, THK, MAT	Link cambial growth with tree-level processes such as transpiration and photosynthesis	*Pinus sylvestris*
Drew and Downes (2015)	Forestry, Fundamental research	xylem water potential, temperature, carbohydrates	CAM, ENL, THK, MAT	Provide framework for testing wood formation concepts and highlight areas of research	*Pinus radiata*
Schiestl-Aalto et al. (2015)	Fundamental research	temperature, carbohydrates, prescribed growth curve	CAM, (ENL, THK)	"[P]rovide a framework for [whole-tree] carbon consumption related to cambial growth"	*Pinus sylvestris*
Hartmann et al. (2017), XyDyS	Fundamental research	signalling compound concentration	CAM, ENL	"[Assess] the predictions of the morphogenetic gradient theory."	*Pinus sylvestris*
Cartenì et al. (2018)	Fundamental research	carbohydrates	ENL, THK	Understand the impact of (assumed to be) seasonally increasing carbohydrate availability to the radial file on the "general anatomical pattern of tracheids across the tree ring and the rate and duration of cell enlargement and cell-wall formation"	*Pinus cembra, Picea abies, Larix decidua, Picea mariana*
Hartmann et al. (2021), XyDyS2	Fundamental research	two signaling compounds' concentration	CAM, ENL	"[I]nvestigate the potential of the crosstalk between two biochemical signals in controlling tree radial growth, wood formation, and tree-ring structure"	*Pinus sylvestris*
Friend (2020), RINGS	Carbon studies	temperature, carbohydrates	CAM, ENL, THK, MAT	Investigate 1) "mechanisms for the observed high sensitivity of cell-mass density to temperature within the latewood," 2) "the influence of carbohydrates on the density profile" 3) "the effect of changing zone widths"	*Pinus sylvestris*
Cabon et al. (2020)	Fundamental research	temperature, water	CAM	"[assess] the biophysical effect of [temperature] and [water potential] on cambial cell enlargement and division"	*Picea abies Larix decidua*

*CAM, cambial cells; ENL, enlarging cells; THK, thickening cells; MAT, mature cells. The author's aim of the model is, where explicitly stated, quoted from the publication. All models are run at daily time-steping, unless otherwise highlighted in the "Inputs" column: *) = subdaily, +) = weekly.*

2. A REVIEW OF WOOD FORMATION MODELS

This section introduces the models covered by this review (**Table 1**) in a chronological fashion. It describes and contrasts models in their complexity and environmental drivers (**Figure 2**), their applications and the evolution of ideas therein, to provide background to the subsequent sections.

2.1. The First Models

The first computer model of wood formation was developed to summarize current knowledge of wood formation processes (Wilson and Howard, 1968). It did not consider environmental impacts on wood formation, shown by the empty circles in **Figure 2**. Instead, it was concerned with verifying the concept of the wood formation framework (**Figure 1**). With prescribed rates as input, and very rigid rules for transition between cell types, the model remained of a rather descriptive nature. The first hypotheses which were tested with such models were the impact of stochastic influences on growth parameters (Howard and Wilson, 1972). Howard and Wilson (1972) simulated 16 radial files to study the impact of stochasticity on production, expansion and thickening rates along with zone widths during wood formation on the resulting anatomy of the cells. They find that stochasticity adds too much variability between the files, which makes them conclude that some exogenously imposed signal is necessary for between-file coordination in trees, later to be explained by a hormonal gradient (e.g., Uggla et al., 1996). The then still hypothetical gradients of hormones in the developing radial file were achieved in a model by Wilson (1973) which stimulated hormones that can diffuse across the developing file. Besides slight changes in seasonal hormone input concentration, a "growth sensitivity" parameter was also required to change throughout the growing season in order to obtain a good model–data fit for red pine (*Pinus resinosa*). Wilson (1973) hypothesized that this changing of the parameter could be mechanistically attributed to water availability.

2.2. Dendroclimatology Gets Involved

None of these early models explicitly resolved specific environmental influences until dendroclimatology turned to wood formation modeling (Fritts et al., 1991). Dendroclimatology is a discipline primarily concerned with extracting climate information from tree rings (Fritts, 1976; Esper et al., 2018). It follows that their models would naturally resolve what dendroclimatology perceives as the main environmental drivers (or limiters) of growth. Until then, the discipline had exclusively relied on statistical methods to reconstruct climate from tree-growth patterns (Fritts, 1976; Schweingruber, 1988). In using mechanistic modeling of tree growth, dendroclimatologists were attempting to obviate the need to assume linearity and stationarity when studying climate–growth relationships (Tolwinski-Ward et al., 2011; Støve et al., 2012; Ljungqvist et al., 2020b; Wilmking et al., 2020). To address stationarity, it was required that models could vary in the strength of the relationship between growth and an environmental factor. To address linearity, it was required that models accommodate the more biologically realistic non-linear response of growth to environmental factors, for example the decrease in growth activity at very high temperatures (Wilson et al., 2007; D'Arrigo et al., 2008; Ljungqvist et al., 2020b).

TRACH (Fritts et al., 1991) was the first published wood formation model that considers environmental influences, such as temperature, soil moisture, and daylength, to calculate a growth response to the environment. This model is a direct forerunner of the VS-model, now widely used in dendroclimatology. For example, relative growth responses (between 0 and 1) to temperature, water, and daylength are combined to calculate a "common growth response" (in later publications called an "integral growth response"). In TRACH this common growth response can be modeled in two ways, by multiplying all environmental factors (multiplicative model of growth), or as a limited model of growth, where the common growth response reflects the effect of the most limiting factor only (Fritts et al., 1991). The latter approach is adopted in subsequent dendroclimatology models such as the VS-model. The common growth response drives daily changes in cell size from a user-prescribed input of number of cells, combined with either information on mean cell diameter or ring with. As wall thickening is not mechanistically represented, it is derived using an empirical relationship. A degree-day approach is used to initiate cambial activity in the spring in temperate climates. To obtain individual cell sizes within the ring, the integral of the common growth response over the growing season is discretised and an algorithm deployed to transform small intervals of this integral into cell size increment of the prescribed number of cells. The ideological beginnings for this approach are based on the TRACHeidogram technique by Vaganov (1990). Cell-wall thickness in TRACH is then calculated based on the two empirical relationships between cell size and wall thickness as observed by Vaganov (1990). A single radial file is modeled and at the end of the year holds information on cell size, wall thickness, and therefore wood density. The model output was compared with the performance of a statistical model and both were equally capable of reconstructing past ring width (Fritts et al., 1991).

TreeRing (Fritts and Shashkin, 1995), largely developed by Alexander Shashkin, superseded TRACH a few years later. Its representation of the delineation of the cambial zone—first through linear functions (Fritts and Shashkin, 1995), and in a later version through exponential functions (Fritts et al., 1999)—form the basis of the representation of cambial activity in the VS-model (in which this part of the model is called "cambial block"). Besides zone delineation, the two models are conceptually similar in the treatment of cambial activity response to the environment and cell position. This new cambial block enables TreeRing and the VS-model to ultimately simulate tree ring width in response to the environment, not only by enlarging a predefined number of cells (as done in TRACH), but by simulating the cells themselves. In combination with additional inputs such as mean and minimum cell size, a tree ring could be simulated.

The complexity differences between TRACH, the latest version of Treering3, and the VS-model are large (**Figure 2**). Nevertheless, these models share many concepts related to how environmental influences are evaluated and how these drive

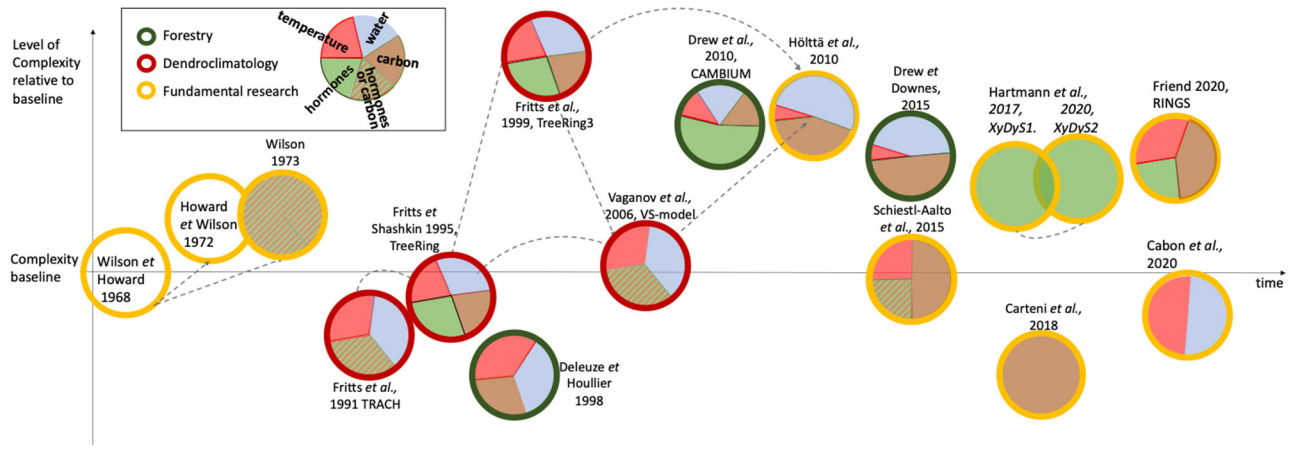

FIGURE 2 | Schematic view of wood formation models over time, their level of complexity, and the environmental/tree-internal influences used within them. Differently colored circles represent the principle focus of the model. Where appropriate, gray dashed arrows highlight structural similarity between models (discussed in more detail in the text). The pie chart proportions represent relative approximate levels of comprehensiveness by which an environmental- or tree-internal- factor (e.g., hormone, carbon) influences model outcome. Striped pie chart components represent a daylength signal, that according to the authors can either be interpreted as carbohydrate availability for growth or a daylength-dependent hormonal signal. Model position on the vertical axis reflects relative complexity. Wilson and Howard (1968) is used as the standard baseline complexity level as, while it considers all cell phases and includes simple transition rules, it does not resolve any environmental or tree-internal regulatory factors. Models below this baseline either contain fewer processes of wood formation e.g., only resolve enlargement and thickening, as in Cartenì et al. (2018), or do not resolve other aspects on wood formation e.g., Deleuze and Houllier (1998) do not resolve a cell undergoing all developmental stages, but assume that it matures within one time step (= 1 week). Some models are integrated into single-tree models (e.g., Fritts et al., 1999; Hölttä et al., 2010; Schiestl-Aalto et al., 2015), but this is not considered in the complexity ranking. Models considered of high complexity either regard all cellular processes and transitions, as well as environmental influences with significant detail (e.g., Fritts et al., 1999), resolve more than one cell type (e.g., Drew et al., 2010), or resolve some processes at such levels of detail that for stability reasons they must run on a very small time step (i.e., 1 s, e.g., Hölttä et al., 2010).

cell differentiation (where applicable). For example, all three models combine relative growth responses (between 0 and 1) to temperature, water, and daylength (or carbon availability for TreeRing) to calculate the "common growth response" based on the principle of a limiting factor. This common growth rate, in the case of TRACH, is applied to cell size only. In the VS-model it drives cell production (and separately cell size), and in TreeRing3 impacts cambial, enlargement, and thickening activities in different ways. More specifically, TreeRing3 simulates the rates of all three growth processes based on complicated interactions between regulating factors, such as hormones, a cell's position within the cell development zone, and the integrated growth rate as a function of water, temperature, and carbohydrates. The VS-model is less complex but inherits aspects of the above two models (see also gray arrows in **Figure 2**).

The VS-model (Vaganov et al., 2006, 2011) and its various derivatives (Tolwinski-Ward et al., 2011; Shishov et al., 2016, 2021; Popkova et al., 2018) have so far been the most applied and published wood formation models in the discipline of dendroclimatology. Not all derivatives (e.g., Tolwinski-Ward et al., 2011; Tychkov et al., 2018) cover the definition of a wood formation model used in this paper. For example, Tychkov et al. (2018) do not resolve any cellular processes, and Tolwinski-Ward et al. (2011) resolve them at a monthly time step. The VS-model's success especially in reconstructing standardized ring width indices in response to the environment has resulted in simpler model spin-offs based on monthly environmental growth rate reconstruction only (VS-lite) (Tolwinski-Ward et al., 2011). The VS-model, along with the cambial block (developed by Alexander Shashkin), is able to simulate cell proliferation in a sophisticated manner. It combines the influence of environmental factors such as water, temperature and daylength as either a proxy for hormones or carbon, in a common relative growth rate similar to Fritts et al. (1991), which modifies cambial growth rates and zone width. The VS-model's most recent cambial zone framework (Vaganov et al., 2011) is based on Treering3, Fritts et al. (1999), which was also used in Hölttä et al. (2010) (**Figure 2**). As example of application, using the VS-model, Anchukaitis et al. (2006) simulated TRW chronologies in the southeastern United States. First, they calibrate the VS-model to generate the best fit between synthetic TRW and standardised observed TRW. The pattern of the simulated TRW can then be attributed to the environmental impacts which generated the TRW. They discovered that the pattern in the soil moisture-driven environmental growth rate modifier had changed over time. They suggest that the decreased summer precipitation and resulting soil moisture has developed as a new constraint on TRW in that area in the last 60 years. Anchukaitis et al. (2006) predict this constraint to become stronger with projected decreases in summer precipitation.

A new concept of what drives wood growth is implemented in TreeRing (Fritts and Shashkin, 1995) and Treering3 (Fritts et al., 1999). Besides water and temperature, carbon and hormones (in TreeRing3) were important regulating factors for wood formation (the gray literature also contains a manual for TreeRing2000 (Fritts et al., 2000), which is not considered here). Any of these four factors (water, temperature, carbon and

hormones) remained as the building block of regulating factors (either as a normalized scalar or explicitly and mechanistically modeled) for all subsequent models (see **Figure 2**), usually along with the structure of developing and transitioning cells as proposed by Wilson and Howard (1968). Overall, with dendroclimatology becoming involved in wood formation modeling, the link between growth and the environment started to be explored more thoroughly, through the consideration of environmental factors.

2.3. Forestry Models

In the 1990s, researchers from a third discipline, forestry, started to publish research output on wood formation modeling, with the view to simulate wood quantity and quality, such as density (Deleuze and Houllier, 1998), vessel frequency (Drew et al., 2010) or later microfibril angle (Drew and Downes, 2015). While dendroclimatology was then mostly concerned with the modeling of simple conifer wood formation processes, forestry also explored the modeling of new species as well as new growth–hypotheses.

The first forestry model by Deleuze and Houllier (1998) is very parsimonious and considers a collection of simple two-parametric equations that transform temperature into a number of cells, soil moisture into volume and carbon availability into mass increase, respectively. So far dendrochronology models such as TRACH, TreeRing3 or the VS-model, had combined all environmental factors to act upon a cellular process e.g., enlargement. This new model differentiates between cell types and their assumed distinct environmental sensitivities to different growth processes (temperature on cell production, soil moisture on cell enlargement and carbohydrate availability on wall thickening). However, another assumption makes the model less biologically realistic: it assumes that a cohort of cells goes through all developmental phases within 1 week. Thus, environmental influences and carbon availability of a single week impact upon volume and mass increase within that batch only. In contrast, when studying observations of xylogenesis, the following picture of cellular dynamics throughout the season is apparent: What is generally observed (Plomion et al., 2001; Fromm, 2013; Rathgeber et al., 2016) is that initial dynamics of xylogenesis during the growing season see the increase of cambial cells first. After a few weeks, some of these cells transition into enlarging cells. Their numbers quickly increase and then slowly decrease throughout the rest of the season. The decrease is accompanied with an increase in thickening cells. Often thickening cells can still be visible while the cambium is thought to be no longer active. This description of the empirical observations shows that the model assumption of all three processes (division, enlarging and thickening) concluding for cell cohorts in only 1 week may lead to the integration of climate and growth factors at the wrong time of the year, potentially affecting the models' predictive skills. Nevertheless, two publications applying the model have been able to show good overlap with observations both qualitatively (Deleuze and Houllier, 1998) and quantitatively (Wilkinson et al., 2015).

Forestry also produced other models which are in their complexity similar to TreeRing3 (see **Figure 2**). CAMBIUM (Drew et al., 2010) explores hormonal diffusion as a function of crown control and its impact on cell growth rate, developmental phases and differentiation into multiple cell types in *Eucalyptus* xylogenesis. Until CAMBIUM, all previous models had been developed on softwoods, which have simple cell types (thus easier to model), and of which some grow close to the climatic limits of their distribution (relevant for dendroclimatologists). As CAMBIUM focuses on conceptual morphogenic gradients, environmental factors are represented in less detail, through an environmental modifier which includes the influence of water and temperature, in a manner similar to dendroclimatology models, based on the principle of a limiting-factor. Carbohydrate availability also influences cambial, enlargement and thickening activity. The CAMBIUM model heavily invoked an interpretation of the canalization hypothesis (Sachs and Cohen, 1982) and radial auxin distribution findings of Uggla et al. (1996) for its cell fate determination algorithm.

An example demonstrated on two forestry models is some models' structure-dependent, intrinsic reliance on specific environmental factors to obtain a desired feature in the tree ring. Annual tree rings are common to trees in temperate zones, as is a distinct increase in wood density within the ring toward the end of the season. The different regions of low and high density are called earlywood and latewood, respectively. In middle and high latitudes early and latewood commonly form early or later, respectively, during the growing season. Drew and Downes (2015) as well as Deleuze and Houllier (1998) developed forestry models to simulate and study wood property variations, especially wood density. Both models use very different modeling approaches, but both simulate density reasonably well, with Deleuze and Houllier (1998) being able to recreate the relative patterns, and the more complex model by Drew and Downes (2015) being able to replicate up to 80% of the variation within the mean sample wood density observations in tree rings. However, for density to sufficiently increase toward the end of the year, Deleuze and Houllier (1998) rely on climatic conditions to be dry. At mesic sites, the model will not decrease its volume increment, as this process is directly and uniquely dependent on water availability. Similarly in Drew and Downes (2015) latewood is induced by soil moisture stress, but in addition, latewood is induced by a switch in the model, which is related to the day of the year. In the Australian context in which it was developed and applied, the model was used to explore potential wood density shifts in pine plantations under future scenarios in which water availability varied and temperature increased (Drew et al., 2017).

2.3.1. Physiological Models of Wood Formation in Forestry and Fundamental Research

Until the 2000s, most wood formation models were not of a physiological nature. What this means is that growth or wall thickening rates were largely determined based on a combination of scaled relative growth rates. These follow general response-function type relationships. Physiological models of wood formation are concerned with biophysical and biochemical mechanisms that result in growth dynamics within and between cells in response to environmental conditions. Specifically, these models consider the mechanisms that underlie cell proliferation,

enlargement or wall thickening processes. For example, they may resolve the interaction between hormonal concentrations on a given day and their hypothesized influences on cell wall elasticity, from which an enlargement rate emerges (Drew et al., 2010). Likewise, the thickening rate may emerge out of a combination of carbon availability, based on the position of the cell in the developing radial file of the tree ring, and temperature (Friend, 2020). Increased computational efficiency made it possible for processes to be resolved and studied at such levels of detail. This trend is also shown in **Figure 2**, where models become increasingly complex. Yet some models stand out from this trend. These models either only mechanistically resolve a subset of cell types and processes (e.g., Fritts et al., 1991; Vaganov et al., 2006; Cartenì et al., 2018; Cabon et al., 2020) or do not consider transition between cell types (Deleuze and Houllier, 1998). The lower complexity may be the result of various reasons. For example, these models may not require a higher level of detail for their research questions, e.g., Vaganov et al. (2006) simulate only tree-ring width (TRW) for climate reconstruction purposes.

Physiological models are able to explore hypotheses on certain drivers (e.g., water or carbon), regulators (e.g., hormones) or processes (e.g., thickening) at high levels of physiological detail. For example, Hölttä et al. (2010) published a complex model calibrated to Scots pine (*Pinus sylvestris*) that explicitly treated water diffusion through the stem and individually modeled cells. Sugar transport was modeled based on diffusion; a cell's water potential was based on water and sugar content, of which both entities diffuse through the developing xylem. Growth in cambial and enlarging cells was turgor-driven, cell division based on a size-threshold value, and cell wall synthesis rate based on sugar content. Diffusion of water across the developing cells in the file required very small (<1 s) time-stepping to remain stable. Another forestry model by Drew and Downes (2015) explores water and sugar interactions on enlargement, this time in Monterey pine (*Pinus radiata*) using a different, optimisation-based approach, where sugar is considered the primary driver of osmotic potential and therefore turgor. This places the model marginally below (Hölttä et al., 2010) in terms of its complexity (**Figure 2**). The influence of hormonal control was handled differently compared to CAMBIUM (Drew et al., 2010), with a focus in the 2015 model on the influence of turgor on cell expansion. Specifically, Drew and Downes (2015) assume a 3D (rectangular prism) cell and use an optimization routine to determine how many cells were able to expand given each cell's volume and the amount of available sugar and estimated water deficit. Drew and Downes (2015) also explore a novel approach with regards to cell wall thickening, which besides carbon availability is dependent on the dynamically-changing cell lumen surface area.

2.4. From Direct Applications to Fundamental Research and Hypothesis Testing

While many of the forestry models discussed above also had fundamental research in mind, their dominant aim can be considered to be practical applicability in forestry. Recently, numerous models intended for fundamental research have been built with the exclusive aim to test different hypotheses, increase our knowledge on wood formation processes, explain open questions or challenge existing ideas. The latest models have largely taken up the idea of hormonal regulation at various levels of detail. A morphogen-only model (XyDyS) was developed by Hartmann et al. (2017) and extended (XyDyS2) in 2020. Hartmann et al. (2017) and Hartmann et al. (2021) simulate the explicit diffusion of a morphogen (such as auxin), and an additional compound (Hartmann et al., 2021) and found that two interacting compounds, acting as morphogen and process rate-determinants, are needed to explain the seasonal kinetics of cell differentiation and final tree-ring structure. The two models are in aim and approach very similar to the first ever hormonal model (Wilson, 1973), but include much more reference to recent molecular knowledge such as protein-channel mediated diffusion of auxin.

All models have, until recently, considered cell enlargement and wall thickening as two separate processes. Cartenì et al. (2018) challenged this idea and could indeed replicate the patterns observed in tree-ring density profiles when combining these two processes. In order to focus on the enlargement-thickening processes, they omit cell production (in a similar manner to TRACH). The consequence, and one of their core model assumptions, is the need for an increase in carbon supply to wood formation toward the end of the season to replicate an increase in density in the latewood sections. In contrast, a constant amount of carbon allocated to the developing cells, but with decreased cell production toward the end of the season reproduces realistic tree ring density profiles in RINGS (Friend, 2020): RINGS incrementally decreases the zone widths of the developing cell types toward the end of the season. This increases the amount of carbon available to late forming cells. With this zone-width approach the model avoids the explicit modeling of e.g., a hormonal signal across the radial file. RINGS is able to reproduce both intra-seasonal cellular dynamics and final ring density patterns well. Friend (2020) could also use the zone-width patterning to explain compensating effects of growth dynamics in response to environmental factors observed by Cuny et al. (2019). Other hypothesized mechanisms related to wall thickening that result in latewood formation will be discussed in another section below.

The timings and significance of individual environmental and internal drivers on tree growth continue to be unresolved and therefore recent models still work on addressing these seemingly fundamental questions. Cabon et al. (2020) describe a cell production model, where a constant number of cambial cells grow in size dependent on water (turgor) and temperature. Division at a threshold value leads to one cell immediately leaving the cambial zone. The model is tested against the final number of cells at the end of the year and within-season cell production dynamics. Keeping some environmental drivers constant in different simulation scenarios, they find that the model required variable temperatures to explain tracheid production onset, and that water potential, probably even trunk water potential, may be necessary to better simulate production cessation and number of cells produced. To investigate other

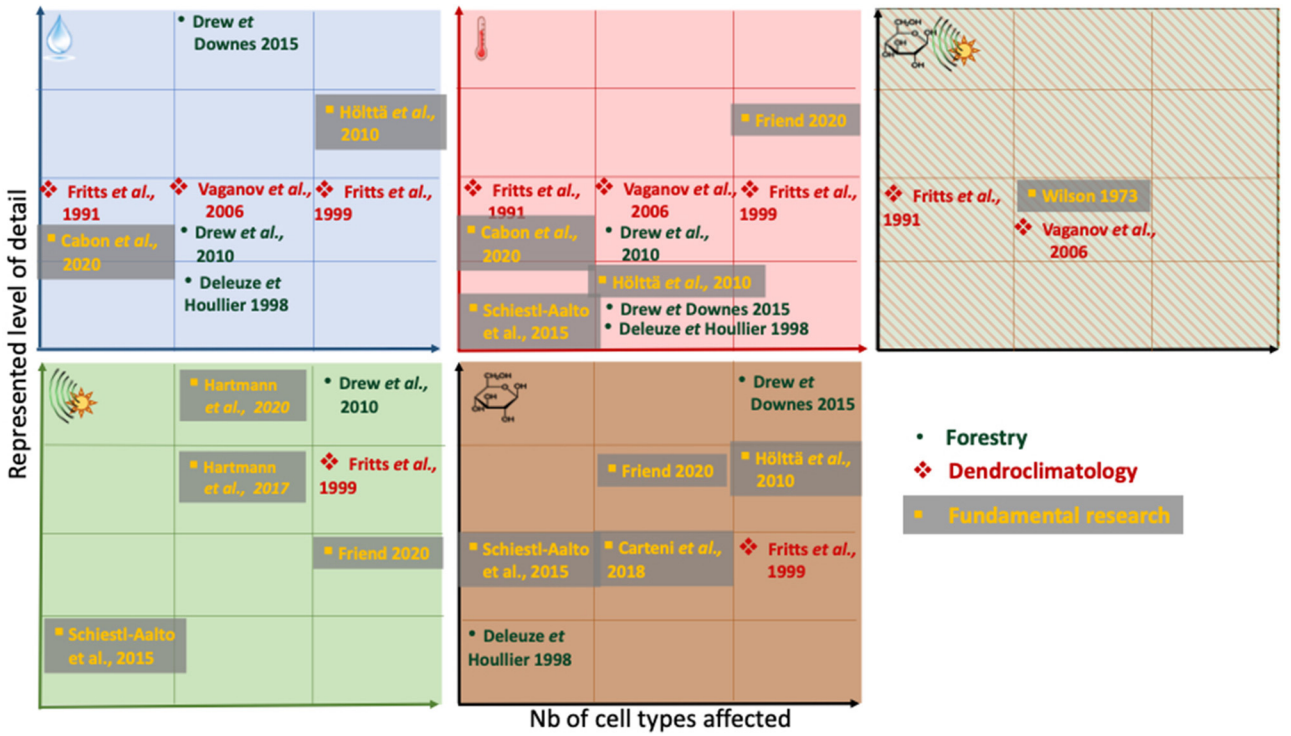

FIGURE 3 | Schematic of environmental and tree-internal drivers and regulators represented in the wood formation models discussed in this paper. Drivers reported are (top-left to bottom-right) water, temperature, either daylength (phenological) signal or carbon, hormonal/daylength (phenological) signal, carbon (note the absence of nutrients as growth rate modifiers in all models). The positioning along the axes within each box reflects (1) the number of cell types affected by an external/internal driver and (2) the level of detail driver-cell interactions are resolved. Left to right: First square: one cell type is affected only (this could be e.g., cambial cells or wall thickening cells only), last square: all three cell types are affected. Bottom to top: low level of complexity with which an environmental driver influences the model e.g., as single part of a physical equation (e.g., through a threshold parameter to promote an on-off switch environmental switch (e.g., assume metabolic activity occurs only above 5°C (Deleuze and Houllier, 1998))) next square: as part of a response-function e.g., increasing enlargement rate with temperature (Fritts et al., 1991; Friend, 2020). Complexity can increase even further to a detailed physiological level, for example through spatial interactions e.g., diffusion of carbon across the developing radial file, followed by arriving carbon being included into the thickening cell wall, as sort of done in Friend (2020). Note that for Schiestl-Aalto et al. (2015), we interpret the "ontogenetic development" used as one the modifiers of cell proliferation dynamics by the authors, as an internal signal, and therefore place it in the bottom-left square, as a hormonal/daylength (phenological) signal. If a model is absent from an environmental factor matrix, it does not resolve this particular environmental factor. Within the squares, no ranking is attempted. Note that the relative position along the y-axis is not comparable between the environmental /internal factors. Note that this is a rough scheme, derived from text-descriptions and equations in the publications, which sometimes may not represent the entirety or complexity of an operation in the model itself. Only the latest version of Treerings (Treerings3) is shown here.

fundamental but unresolved questions related to intra-tree carbon source-sink dynamics and the environment, Schiestl-Aalto et al. (2015) use a wood formation component in the whole-tree carbon-balance model CASSIA. Therein, when growth is active, cambial cell numbers are determined by 1) temperature, 2) an empirical term reflecting commonly-observed patterns of intra-seasonal cambial activity levels (referred to as "ontogenetic development"), 3) carbon availability from storage, and 4) photosynthetic activity (**Figure 3**). Enlarging and thickening cell numbers on a given day depend on the duration spent in their respective stage of development, which is 1) driven by cambial cell production and 2) earlywood and latewood fraction of the calibration year. The model-focus is not on physiological details and individual cells and their dynamics are not explicitly considered. Therefore, it is in its structure one of the more parsimonious models covered here. However, due to the environmental and internal drivers on cell production, it is placed at a similar level of complexity as the baseline-model (**Figure 2**). The authors use this framework within a whole-tree model to determine the impact of environmental factors on growth (sink) activities in cold environments. They found that stored carbon did not limit intra-annual growth, whereas temperature did.

Knowledge increase through fundamental research was also the aim of the very first wood formation models. We have gone full circle across more than half a century of wood formation modeling since the 1960s. The discipline-specific wood formation models have already helped answer a wide-ranging suite of questions, from improving our knowledge on fundamental growth hypotheses, to wood quality prediction and attributing large-scale climatic impacts to observed growth patterns. The next section will summarize and discuss old and new model hypotheses for various selected mechanisms, in context with new and old observations. This includes open questions about growth

mechanisms. Furthermore, data needs, new software and new areas for wood formation modeling are discussed.

2.5. Current Knowledge, Open Questions and Future Opportunities

The historic overview of wood formation models contrasted the models in terms of their level of complexity relative to the baseline model by Wilson and Howard (1968) (**Figure 2**). It further highlighted the diversity in modeling approaches over time, and pointed out the breadth in wood formation model applications and findings (from the cellular to the regional). This section will examine how unresolved process are modeled (specifically: hormones, earlywood–latewood transition and the involvement and representation of sugars in different cell developmental phases), discusses existing and novel data useful for model parameterisation and testing, and finally turns to additional disciplines where wood formation modeling is useful but still in its infancy, such as in carbon storage modeling and global vegetation modeling.

2.5.1. Wood Formation Process Hypotheses: Resolving Hormones

Hormones have been hypothesized to play a key role in determining aspects of wood formation since at least Larson (1960). While many hormones are thought to be involved (reviewed by Buttò et al., 2020a), most wood formation models today explicitly treat one (Fritts et al., 1999; Drew et al., 2010), at most two hormones (Hartmann et al., 2021), with good model–data fit (but see Hartmann et al., 2017). This section reviews the different model strategies to represent auxin, the hormone that is most commonly referenced within the wood formation frameworks.

New observations have both enabled the testing of new hypotheses, as well as acted as additional source to compare models against. Models have also suggested hypotheses before the emergence of data in support of it. For example, Wilson (1973) assumed in his hormonal diffusion model that regulatory compounds (hormones) must be entering the developing radial file from the phloem, then diffusing radially inward, thus creating a concentration gradient across the developing file. While evidence from tissue culture (Wetmore and Rier, 1963) at this time was already strongly suggestive of such hypothesized gradients (Wilson and Wilson, 1961), methods were still insufficient to directly measure a concentration gradient across the first 2 mm of the phloem or developing xylem. In simulating a compound diffusing through the developing file and interacting with a second potential compound, Wilson could reproduce the cell radial diameters of a red pine (*Pinus resinosa*) annual ring grown during a year with summer drought. This modeling exercise added to the emerging evidence of compound-diffusion across the tissue. A "steep radial concentration gradient" of auxin was indeed found 23 years later in Scots pine (*Pinus sylvestris*) by Uggla et al. (1996), followed by hybrid aspen (*Populus tremula L. x Populus tremuloides Michx*) (Tuominen et al., 1997), and was hypothesized to be involved in regulating cell identity (Uggla et al., 1996) and growth-differentiation rate (Aloni and Zimmermann, 1983; Tuominen et al., 1997).

According to observations, a hormone such as auxin seems to be actively involved in regulating cell enlargement rate under non-limiting conditions (Du et al., 2020) as modeled in Wilson (1973), Fritts et al. (1999), Drew et al. (2010), and Hartmann et al. (2021), but not in Hartmann et al. (2017). It is observed to act as a positional signal for cell identity (Uggla et al., 1996; Bhalerao and Fischer, 2014), as modeled in Wilson (1973), Fritts et al. (1999), Drew et al. (2010), Hartmann et al. (2017), Hartmann et al. (2021), Friend (2020), and Vaganov et al. (2006) for cambial cells. Vaganov et al. (2006) is presently the only model in which cambial zone width can change with environmental conditions. The above seems to suggest that models contain robust hypotheses when it comes to auxin-related processes. However, while these models assume that auxin works in a dose-dependent manner, no specific concentration threshold has yet been identified that can delineate zone widths, or no auxin-concentration dependent growth-rates have been measured, two fundamental assumptions of most of these models.

Moreover, the existing observations and models are inconclusive as to whether the morphogen (auxin) is also directly required for growth rate regulation (e.g., Friend (2020), Hartmann et al. (2021) assume no influence on growth rate by auxin whereas Wilson (1973), Fritts et al. (1999), Drew et al. (2010) do assume auxin modification on the growth rate). Some models and observations seem to suggest that spatial (length of the developing zones) interactions with tree-internal factors (morphogens) go hand in hand (Uggla et al., 1996; Tuominen et al., 1997; Friend, 2020; Hartmann et al., 2021). On top of that, environmental (e.g., end of season drought or lower temperatures) factors influence either (1) the size of the zone (Vaganov et al., 2006) or (2) growth rates directly (Wilson, 1973; Drew et al., 2010; Friend, 2020).

All hypotheses used in the models rely on empirical evidence upon which to base their assumptions. The plethora of model approaches with which anatomic (sometimes together with dynamic) patterns can be replicated, shows that this complex system has many tree-internal and external components, which can regulate the outcome. Wood formation models have helped to formalize hypotheses on hormonal influence and hormonal-environmental interactions in various ways. No approaches can be dismissed outright, as they all replicate observations within the context of their studies. To clarify the current incompatible hypotheses among models, more observations on the interactions between hormones, the environment and wood formation at the molecular level are urgently needed (e.g., Uggla et al., 1996).

2.5.2. Wood Formation Process Hypotheses: Earlywood to Latewood Transition

A currently-relevant and contested question is the mechanism behind the earlywood–latewood transition in temperate forest conifers. The subject remains open to the extent that it is even unclear whether the change in density across the ring is (H1) an emergent property caused by physical limitations to growth, (H2) caused by seasonal changes in carbon availability to the developing tree ring or, or (H3) is caused by the temperate tree's strategy to anticipate future environmental limitations (i.e., winter). The number of hypotheses raised here reflect the number

of ways this mechanism is represented in wood formation models.

2.5.2.1. H1: Environmental Limitation Leads to EW–LW Transition

An earlywood–latewood pattern is altogether absent in some low and mid-latitude regions or in diffuse porous angiosperms. For example, conifers growing at low latitudes, where temperature, water availability and daylength are relatively stable, such as in tropical rainforests, do not show an annual distinction between large thin-walled cells and narrow thick-walled cells. Hence seasonal tree rings are hard to discern under these non-limiting conditions since the cambium remains active throughout the year. For example, de Mil (2018) found that many tropical forest trees did not have easily detectable, and only "non-periodic" rings. However, in areas where drought periods frequently occur, such the Bolivian Amazon region, narrow wood cells are formed periodically, and these resulting tree rings can be attributed to precipitation (Brienen and Zuidema, 2005). Similar responses to rain and dry seasons have been observed in teak (*Tectona grandis*) wood in Ivory Coast of West Africa (Dié et al., 2012). Tree rings in the tropics also form under conditions of flooding, when the roots do not receive enough oxygen, temporarily arresting growth (Worbes, 1985, 1995). These empirical evidences indicate that environmental limitations such as drought and wet seasons can at least cause patterns similar to high and mid-latitude earlywood and latewood.

That earlywood–latewood transitioning is a consequence of environmental (water) limitation (Hypothesis 1) is covered by the DH-model (Deleuze and Houllier, 1998). In their model they assume that cell enlargement decreases under water stress. Similarly, water-related mechanisms, modeled at higher physiological detail, would decrease cell diameter in Hölttä et al. (2010) and Drew and Downes (2015). The latter two models could also be to some degree influenced by an increase in carbon availability (Hypothesis 2). However, in both models carbon increase will not be able to rescue cell enlargement indefinitely. Therefore, Drew and Downes (2015) additionally assume a daylength signal (Hypothesis 3)—dependent decrease in cell size and increase in carbohydrates allocated to individual secondary wall thickening cells. Thus even if no water stress occurs, the desired earlywood—latewood pattern will emerge.

2.5.2.2. H2: Carbon Availability Influences EW–LW Transition

One model exclusively relying on a change in carbon availability to the developing cells toward the end of the growing season is Cartenì et al. (2018). They assume that the thin-walled earlywood cells, followed by thick-walled latewood cells, result from the carbon allocation pattern during the growing season. Specifically, they assume that allocation of carbohydrates to wood formation processes increases when primary growth ends (Cartenì et al., 2018). Additionally, they suggest an alternative approach for the succession between the phase of enlargement to thickening: Until Cartenì et al. (2018), all frameworks had assumed that cell enlargement and wall thickening are two separate processes following Wilson and Howard (1968). The model by Cartenì et al. (2018) tested the hypothesis that these two processes could occur simultaneously and that thickening is the mechanism by which the end of enlargement is determined. In contrast, in their alternative approach, Cartenì et al. (2018) simulate cell enlargement and secondary wall deposition occurring simultaneously within a cell. Enlargement stops once a cell wall grows too thick to further expand. This process-representation is dependent on carbon influx increasing toward the end of the growing season, in order to reach a critical wall thickness sooner and thus obtain smaller cells later during the season.

Defoliation and daylength experiments are cited as the basis for separating these two processes. Particularly, Larson (1964a) finds that modification of hormones through partial crown coverage leads to cells remaining large but having thick walls. Additional direct evidence comes from Larson (1960), who applied auxin to decapitated seedlings within the latewood formation season and induced larger earlywood-type cells. That auxin levels regulate xylem cell size and differentiation is also found in Tuominen et al. (1997). Molecular mechanisms ("acid-growth theory") for auxin-mediated cell enlargement have been suggested decades ago but had not been validated. According to the acid-growth theory auxin influences ATP-ase activity and thus cell vacuole (and thus cell) enlargement. In recent years strong genetic and biochemical evidence in support of this theory have emerged (reviewed in Du et al., 2020, see also Perrot-Rechenmann, 2010).

Nevertheless, some overlap between cell enlargement and thickening processes has been observed, at least in European aspen (*Populus tremula*). Sundell et al. (2017) found that tissue that was visually determined to be the beginning of the thickening zone had a stronger molecular signature of still being enlarging cells. This means that early thickening cells were either still enlarging or had not yet stopped expressing the genes necessary for cell enlargement. If the former is true, to bring this in context with the hypothesis by Cartenì et al. (2018), there seems to be a small spatial overlap where thickening and enlarging is ongoing simultaneously. However, this area of shared activity within the radial file is relatively narrow and does not indicate that these processes compete to determine cell radial diameter. Instead, with the early indirect evidence of hormonal influences, as well as the increased evidence on auxin-mediated acid-growth theory on cell enlargement, one can tentatively conclude that what regulates cell size under non-limiting conditions is not wall thickening (= carbon), but hormonal signals. Carbon and hormonal manipulation studies will be useful to solidify this evidence.

Many other models also assume the earlywood–latewood pattern to be carbon-related. While some models directly impose carbon-related mechanisms for the transition, other models find that the pattern, though carbon related, does not have to be imposed, but is an emergent property of the late season growth dynamics. The increase in carbon availability, by prioritizing carbon allocation to thickening cells, is a mechanism to ultimately obtain thicker cell walls in Drew and Downes (2015). This is mediated through a daylength-induced hormonal signal, as stated above. Increases in carbon availability to thickening cells emerge naturally through a shorter radial file, where fewer

cells are closer to the phloem and share the incoming amount of carbon in RINGS (Friend, 2020). When it comes to spatial representation of carbon across the radial file, interestingly, both Friend (2020) and Drew and Downes (2015) use carbohydrate gradient observations to justify their carbohydrate allocation schemes, with very different effects. Uggla (2001) observe high levels of carbohydrates at the phloem, which then gradually decreases across the developing radial file. Drew and Downes (2015) treat the gradient as an emerging property which is only observable because thickening cells (1) take precedent when it comes to carbon allocation to the cells and these thickening cells then (2) take out more carbon than enlarging cells, thus there are lower nonstructural carbon levels observed in the thickening zone of the radial file. In contrast, RINGS (Friend, 2020) is based on the assumption of equilibrium between diffusion and consumption. In practice this means that RINGS calculates the carbohydrate diffusion profile into the radial file as an outcome of (1) the carbohydrate input into the radial file, (2) each cell's individual demand, and (3) the diffusion itself. More studies exploring not only the seasonal carbon dynamics, but also their gradient across the developing tree ring (as done in Uggla, 2001), would be useful to better deduce the relationship between carbon dynamics and latewood formation.

2.5.2.3. H3: EW–LW Transition as Strategy to Anticipate Future Environmental Limitations

Other models assume that a hormonal signal induces latewood-formation in temperate regions, in line with Hypothesis 3. For example, toward the end of the growing season, a signal from the crown helps to create narrow latewood cells by decreasing enlargement rate in TreeRing3 (Fritts et al., 1999), decreasing zone width and enlargement rates in CAMBIUM (Drew et al., 2010), or by decreasing zone widths and hence enlargement duration in RINGS (Friend, 2020). Empirical studies support these model assumptions by finding that the seasonal growth and development of foliar organs release (auxin) signals, which decline in strength toward the end of the season (e.g., Larson, 1964b). Xylogenesis studies have also correlated the highest cellular activity with daylength (Rossi et al., 2006b; Cuny et al., 2014). In temperate regions, one could expect a daylength-driven signal for trees to anticipate temperature changes, that make growth unfavorable (Petterle et al., 2013). This may be needed in order for the tree not to be surprised by cold temperatures, which may damage immature cells (Rathgeber et al., 2016). Specifically, some processes have to be concluded before unfavorable conditions emerge. For example, lignification is strongly constrained by temperature (Gindl et al., 2000; Körner et al., 2019), and it has been shown that the last xylem cells need up to 2 months until reaching maturity (Cuny and Rathgeber, 2016). In order for these processes to fall into the growing season, the tree can most reliably use daylength as a measure of time progression.

All in all, there seem to be multiple mechanisms which could lead to "earlywood–latewood" patterns and thus tree rings. Some mechanisms are of a physical nature such as water stress in areas not constrained by temperature and daylength, such as tropical regions. Nevertheless, in the temperate regions all maturation processes must be concluded before too low temperatures occur in order to avoid damage. Thus trees might use daylength-perceiving hormones to 'look ahead'. Both such mechanisms are implemented in different models. For example, RINGS (Friend, 2020) functions on the hypothesis of daylength-induced zone-width decreases (which are possibly hormone induced). However, RINGS does not contain any water-driven enlargement or stress-function and therefore may not be able to replicate large and small cells at low-latitude sites with water stress. On the other hand, models which rely on water stress only for this pattern to emerge may not work at high-latitude mesic sites (e.g., Deleuze and Houllier, 1998). Fritts et al. (1999) and Drew and Downes (2015) can accommodate for both these conditions in their models. A universally applicable wood formation framework would have to accommodate both physical and tree-internal regulatory mechanisms to replicate intra-annual changes in cell diameters across all latitudes and environmental gradients.

2.5.3. Carbon Availability and Growth Dynamics in Wood Formation Models

Whether growth is actively demanding carbohydrates or passively receiving carbon as a function of photosynthesis is a point of contention (Sala et al., 2012; Dietze et al., 2014), with potential implications on modeling tree growth behavior and ecosystem carbon storage (Leuzinger et al., 2013). Specifically, an open question remains to what degree growth is limited by carbon supply rate (and hence the carbon source) or by its own environmentally and internally-determined activity (and hence itself as the carbon sink). While carbon is necessary for structural and metabolic purposes during xylogenesis, an experimental study by Sundberg et al. (1991) suggests that it is cambial activity, and not carbohydrate availability that determines wood production. Observed NSC concentrations in the cambial region (xylem and phloem) (Giovannelli et al., 2011) can be statistically or qualitatively related to the number of total living (cambial, enlarging and thickening) cells (Deslauriers et al., 2016), and wall thickening or predominantly radial growth periods (Simard et al., 2013). Nevertheless, the direct mechanism by which carbon influences each cell type remains unclear. Therefore, the question remains whether carbohydrate gradients observed across the developing xylem (Uggla, 2001) are, similar to co-occuring auxin gradients, "instructive or incidental" (Bhalerao and Fischer, 2014). While there is some molecular evidence for different sugars acting as signaling molecules for different cellular stages (Riou-Khamlichi et al., 2000), the nature of this relationship has not yet been described usefully for wood formation modeling. How do wood formation models resolve carbon–growth interactions?

The first model that considered carbon explicitly was Deleuze and Houllier (1998), where wall thickening is assumed to be carbohydrate-dependent. This means that in their model, all mass gain of the radial file (through cell wall thickening) is directly related to carbon availability. The first model that considered the influence of carbon on wood growth rates was TreeRings (Fritts and Shashkin, 1995). There, the cell production rate is a function of three limiting factors $F(s, W, T)$, with water availability W, temperature T and carbohydrate availability

s. In a subsequent version, TreeRings3 (Fritts et al., 1999), $F(s, W, T)$ is involved in deriving the rates of all processes for all cell types. If there was little carbon available, *s* would dominate the equation, if *W* and *T* were not limiting at the time. However, if it was particularly cold or dry, the other factors were able to override this "source dependent" behavior of the model. Indirect growth-rate dependent representation of carbohydrate influence as above is represented in a similar manner in Fritts et al. (1991) and Vaganov et al. (2006). They use a daylength growth-modifier ($F(D, W, T)$, width *D* as daylength) to influence cell enlargement (or optionally also wall thickening in Vaganov et al., 2006). Both articles say that daylength can either represent a phenological signal from the crown or an indirect representation of photosynthesis and thus carbohydrate availability. In summary, early models already assumed a carbon-dependency of one or more processes, either explicitly as substrate or as rate modifier.

Carbohydrate influences are represented in more complex, physiological ways in recent models. Related to cell production, a cell in CAMBIUM Drew et al. (2010) and Drew and Downes (2015) can only divide if a minimum quantity of carbohydrate is available for this process, giving the model a source-centric behavior. Nevertheless, Drew et al. (2010) and Drew and Downes (2015) also enable storage of surplus carbon in the radial file, which decouples cambial and mass growth, and photosynthesis to some degree, should the environment be favorable to growth again (see also Drew et al., 2009). Secondary wall thickening in CAMBIUM (Drew et al., 2010) is dependent on carbohydrate as substrate, similarly to Deleuze and Houllier (1998).

Besides as substrate, carbon has also been assumed to be a driver in processes such as cell enlargement. For example, Hölttä et al. (2010) and Drew and Downes (2015) explore the influence of carbohydrates together with water availability to represent turgor-driven cell enlargement, making these models also subject to carbohydrate control. As cell enlargement also occurs in cambial cells before division, cell production rates are also carbon-dependent in these models, but due to the small size threshold after which they divide, a carbon-dependent "rescue" of cell production dynamics are probably most prevalent under water-limiting conditions. Both models subsequently use the carbon that contributed to cell expansion as substrate for cell wall synthesis. A constant carbohydrate influx in RINGS Friend (2020) is in contrast with Cartenì et al. (2018), who must assume an increase in carbohydrate supply toward the end of a season in order to obtain an increase in wood density, making the model strongly dependent on 1) carbon availability itself but also, 2) the hypothesized timings of carbon availability to growth. In Drew and Downes (2015), allocation to thickening cells is actively prioritized toward the end of the season, equivalent to an enforced sink demand by wall thickening-cells. In RINGS the density increase toward the end of the ring is governed by increased proximity of the thickening cells to the phloem, the source of carbohydrates. Thus, under normal conditions, according to this model, the only conditions under which carbohydrates are limiting are at the periphery of the developing radial file early during the growing season. This carbon limitation is not however directly caused by the carbon input into the file, but by the physical position of a cell and the diffusibility of carbohydrates across the file. Nevertheless, carbon (source) limitation could influence wall thickening in RINGS, if carbon levels in the phloem are low. Overall, carbon in the above wood formation models is not only assumed to be required as structural component in cell walls of newly formed or wall thickening cells, but also regulates cell enlargement activity by contributing to cell turgor. Some models are more sensitive to intra-annual fluctuations in carbon availability than others. It becomes clear that there are many models which could be subject to source-limitation in one or more of their processes if carbohydrates became limiting and thus the question remains, whether carbohydrates are ever limiting to any of these processes in reality.

Carbon storage regulates cell proliferation in CASSIA (Schiestl-Aalto et al., 2015) by asymptotically declining growth rates dependent on carbohydrate availability after carbohydrate availability falls below a threshold. Using a threshold-only evaluation, Drew and Downes (2015) also have such a safety-mechanism where cell proliferation stops immediately if insufficient carbon is available to build new cell wall plates between dividing cells. Cell cycle studies confirm the plausibility of this mechanism. For example, Riou-Khamlichi et al. (2000) found that carbohydrates act directly as signaling molecules in the cell cycle regulation of *Arabidopsis*. From a tree's perspective, regulating growth at its first process (cambial activity) makes sense as carbon used in wood formation is irretrievable and must be closely regulated to avoid wastage (McCahill and Hazen, 2019). Some evidence suggests that in cases such as under strongly carbon-limited condition, storage is prioritized over growth (Hartmann et al., 2015; Weber et al., 2018), a behavior which may however also strongly be linked to ecological strategy (Mitchell et al., 2016). The concept of a carbon storage threshold limiting growth activity is also a useful framework to connect storage to growth dynamics in models, while still allowing for assumptions on the sink dynamics to remain relatively autonomous from the source otherwise. However, large difficulties will remain to parameterise such a threshold as, if it exists, it may be tissue-, species-, age/size and/or growth environment dependent.

This section has examined the cell developmental processes at which current wood formation models require carbon in order to execute growth dynamics (i.e., irreversible volume or mass growth). With many processes requiring carbon for structural or procedural purposes (metabolism has not been mentioned here), on the wood formation model level, carbon limitation on growth cannot be excluded. Under a low tree carbon status, the source *vs*. sink balance may shift to a sink *vs*. storage story. Under high tree carbon status, wood formation may be limited by environmental factors, while processes requiring carbon are not limited by it. For example, through observations in oak (*Quercus*) (Lempereur et al., 2015) and modeling of larch (*Larix*) and pine (*Pinus*) (Eckes-Shephard et al., 2021), it has been shown that under water-limiting conditions tree growth stops earlier than photosynthesis. Further, modeling of an individual pine (*Pinus*) (Schiestl-Aalto et al., 2019) showed that wood growth variations could be explained by temperature-driven sink activity

on a daily basis and that carbon does not seem to be the ultimate driver or limiter of the growth dynamics on a daily timescale. Wood formation models will not in themselves be able to answer the source-sink controversy, especially with the added complexity of storage competing with growth under some conditions. Nevertheless, wood formation modeling can play a useful role to better study the interplay between photosynthesis, storage and biomass increase. With the exception of Schiestl-Aalto et al. (2019), there seem to be no modeling studies explicitly resolving wood formation to interrogate how source-sink-storage relations interact on an intra-annual scale.

2.6. Model–Data Comparison

Together with established types of observations, new sources of data have emerged against which models can be directly compared. These are not fully exploited today. The following section reviews two categories of data that have been used for model validation. We make a case that these and novel observations, as well as the combined use of observations, could be more commonly applied for model parameterisation and verification in order to increase our understanding of the mechanisms that drive xylogenesis. Observations related to wood formation (**Figure 4**) can be divided into 1) static data, which are end-of season observations of anatomical properties of mature cells or the ring itself (e.g., TRW, cell wall thickness, density profile) and 2) dynamic data, such as xylogenesis monitoring data from which we obtain snapshots on the number of cells in a given phase at the time of sampling. Both types of observations have deficits, but when used in tandem can supplement each other: Anatomical data originate through the process of xylogenesis, but the timing of individual processes cannot be reliably retraced from the data. In contrast, dynamic data can tell us about the kinetics of cell differentiation, but cell anatomy such as cell sizes or wall thicknesses cannot be inferred, as often the sampling distorts the true cell dimensions (e.g., the pressure applied to the still delicate cambial and enlarging cells during microcoring using a Trephor (Rossi et al., 2006a; but see Uggla et al., 1996). Observations can also be divided into data-sparse (e.g., the date of the start or the end of the enlargement process, the tree-ring width) and data-dense (e.g., weekly xylogenesis data, dendrometer data or intra-ring profiles of cell dimensions) observations. Wood formation models have been able to generate one or multiple types of output against which they can be compared with observations, depending on their aim and structure (see **Table 2**). Importantly, one must distinguish between using data for model development, parameterisation, and validation: the same data should not be used in all three instances.

2.6.1. Static Observations

Some of the most common static variables which wood formation models try to replicate are end of the year observations of ring width (e.g., Friend, 2020) or ring width index, (e.g., Vaganov et al., 2006) cell numbers (e.g., Vaganov et al., 2006; Friend, 2020) or wood intra-ring density profiles (e.g., Deleuze and Houllier, 1998; Drew and Downes, 2015; Friend, 2020). A hitherto unused type of static observations for wood formation model parameterisation or validation are isotope ratios (but see Tolwinski-Ward et al., 2015, which we however do not count as a wood formation model in this review).

Static observations differ in the extent to which they can validate a wood formation model or its individual processes. Firstly, models can be validated against data-sparse, single-point tree-ring parameters e.g., width, wood density, isotope ratio. While the former two observations are very abundant, the downside of only relying on this type of observation is that this involves the fitting of complex models to a single annual data point (e.g., TRW). This means for wood formation models that many different hypotheses will be able to replicate this type of observation through overfitting. Secondly, more data-rich static observations offer a higher spatial resolution for model validation. For example the final structure within the tree ring, such as its density profile can resolve intra-annual dynamics to some degree. Some wood formation models (Deleuze and Houllier, 1998; Fritts et al., 1999; Drew and Downes, 2015; Friend, 2020) simulate wood density profiles and compare their output against density profile observations. Treering3 (Fritts et al., 1999) can even automatically interface (code written by Geoffrey M. Downes) with the SilviScan digital output for model verification. SilviScan is a semi-automated device to rapidly obtain wood density observations (amongst others) using X-ray technology and image analysis. It was originally developed in 1992 for commercial forestry (Evans et al., 1994) and, after several upgrades, is still widely used in the scientific community. Nevertheless, while at a higher resolution, these static observations do not allow for the exact inference on the timing of the inception of these high and low-density features. Therefore, care is needed when applying a distance-to-time conversion approach across tree ring anatomical features (i.e., equally-sized sections of the ring have not emerged during an equally-long period (Pérez-de-Lis et al., 2021). This makes the attribution to environmental events from anatomical features alone difficult (but see Drew and Downes (2009) for how the additional use of dendrometers can address this issue to some degree). An exception is a specific type of data-rich static observations of cell anatomy, so-called intra-annual density fluctuations (IADFs). IADFs are unusual variations in cell size and wall thickness along a tree ring (Battipaglia et al., 2016). These density fluctuations can either be caused by earlywood-like cells in the latewood section of a tree ring or latewood-like cells in the earlywood section of a tree ring. Age or width of the rings can also play a role in the absence/presence of IADFS under IADF-conducive environmental conditions (Rigling et al., 2011). Both phenomena have been associated with precipitation after a summer drought (earlywood-like IADFS) (Campelo et al., 2007; Rigling et al., 2011), or the absence of precipitation during early spring (latewood-like IADFS) (Wimmer et al., 2000). Thus, the resulting signal in the cell anatomy can be related back to a specific period during the growing season. However, there are many open questions as to the mechanisms that cause IADFs (see Battipaglia et al., 2016 for a good overview), and it is still unclear what cell developmental phase is affected to cause these deviations from the common anatomy. Therefore, these observations are especially valuable for the validation of wood

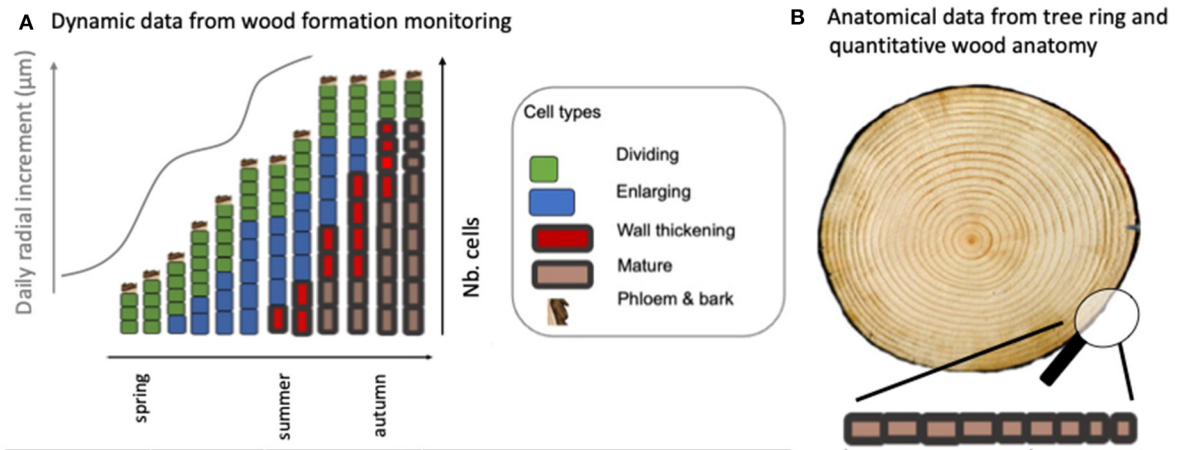

(sub) daily measure-ments	Weekly classify-cation (c)	Weekly measurements (m)	Derived data from weekly c and m
Stem - (band dendrometer) or radial increment (point dendrometer)	Number of cells in each phase	Developing xylem radial increment, optical density, biomass, zone-width	**Phenology parameters:** Onset, cessation, duration of development periods at tissue level (e.g. enlargement) or at aggregated variable level (e.g. volume and mass); **Kinetics parameters:** residence time of each cell in each zone, volume and mass dynamics

Annual data	Seasonal data	Profiles
TRW, tree ring density, total cell numbers, ...	EW/LW widths, maximum density, IADFs, ...	Cell diameter, cell lumen diameter, cell wall thickness, cell wall area ...

FIGURE 4 | (A) Dynamic **(B)** static observations useful for wood formation model interrogation. **(A)**: (sub)-daily radial increment measurements are taken using dendrometers. Weekly classification requires staining methods, light microscopy and a human to identify and count cells of a given type. Weekly measurements can be semi-automated and do not necessarily involve the identification of specific cell phases. Weekly cell counts and measurements can be used to derive observations such as a period of presence/absence of a cell type (at the xylem tissue level) or the residence time of each cell in each phase (at the cell level, but also possible to derive at the tissue level). Tree disk image from Cuny et al. (2014).

formation model hypotheses. Similarly, wood formation models can help explore which cell processes are the most likely to be affected. IADFs comparison with model-simulated IADFs has far only been done by Wilkinson et al. (2015) who applied the model from Deleuze and Houllier (1998) and could indeed replicate IADFs at a water-limited site. Overall, static observations, with some exceptions through IADFs, cannot be fully be used to reconstruct the timing and thus environmental conditions of wood formation processes occurring intra-annually.

2.6.2. Dynamic Observations

This issue of static observations can be overcome when using dynamic xylogenesis observations. Generating dynamic observations typically involves the weekly sampling of the growing ring, to derive weekly cell counts of each cell type within a differentiation phase, or (more common for angiosperms) the width of each developing zone. Models which have used xylogenesis observations to some degree are Cabon et al. (2020) for cell production, Hartmann et al. (2017) and Hartmann et al. (2021) for cambial and enlarging cells and Schiestl-Aalto et al. (2015) for all cell types. While some models are able to produce xylogenesis output (e.g., Fritts et al., 1999, see **Table 2**), they do not compare it against data (but see Schiestl-Aalto et al., 2015). Instead, they discuss qualitatively the shape of the observed cell numbers. Xylogenesis observations can be data-rich, if sampled frequently, across many trees, throughout the growing season. One issue with xylogenesis data is the between-tree variability in the dynamics, which so far have been addressed through normalization approaches, e.g., by standardizing against the total number of cells of the previous year Rossi et al. (2003) to fit gomperts or general additive models Cuny et al. (2013) to cell production observations. Besides for phenological purposes, such as determining onset or cessation of wood formation (critical dates), these observations can be directly related to co-occuring environmental conditions, which is useful for increased process-understanding related to environmental factors acting upon different cell types. Other data-rich observations of stem radius variations are dendrometer-data, which, while temporally very fine-grained (i.e., tens of minutes), are however impossible to interpret when it comes to disentangling which cell phase (cambial or enlarging) contributes to the observed growth increment and are therefore more useful to verify wood formation models' overall increment dynamics. Nevertheless, dendrometers are essential tools to determine the critical sub-daily time periods during which growth variations actually occur and which environmental factors matter. For example, Zweifel et al. (2021) determine that wood radial growth is most likely to occur during the night or at dawn, when vpd is low. Their findings make clear that daily aggregation of environmental variables to drive wood formation models must

TABLE 2 | ⊕ model output compared against observations, ⌀ (possible) output but not compared against observations. † Possible output but not reported. () model output, but created using an empirical relationship with previously modeled outputs. *Microdensity profile derived from wall thickness. Wilkinson et al. (2015) used the model by Deleuze and Houllier (1998), to simulate wall thickness rather than mass increase and could therefore resolve and compare against microdensity (see second ⊕*). CAM, cambial cells; ENL, enlarging cells. Note that being able to resolve xylogenesis, enables phenological events (e.g., start of CAM, Start /end of ENL, etc). Note that some models display output, which are not listed here, eg. maximum density, mean density, microfibril angle. Anatomical output related to wall thickness can be expressed in cell position (Hölttä et al., 2010) or as proportion of annual ring (%) (Drew and Downes, 2015), which is not distinguished in this table. Radial diameter can refer to either cell or lumen radial diameter. Tree ring width is equivalent to the end-of season value of cumulative radial growth, measured as cumulative cell anatomy properties or directly as ring width. Cell numbers is equivalent to end of season cumulative tracheid production. Xylogenesis refers to cell numbers or cell production rates derived from xylogenesis observations. TRWi, Tree ring width index.

Model	TRW	Cell numbers	Density profile	Wall thickness	Radial diameter	Xylogenesis
Wilson and Howard (1968)	⌀	⊕	⌀	⊕	⊕	
Howard and Wilson (1972)	⌀	⊕	⌀*	⊕	⊕	⊕
Wilson (1973)	⌀	⌀			⊕	⊕
Fritts et al. (1991)				()	⊕	
Deleuze and Houllier (1998), Wilkinson et al. (2015)	⌀	⌀	⊕ ⊕*	⌀	⊕	
Fritts et al. (1999)						
Vaganov et al. (2006)	TRWi	⊕				⌀ (CAM)
Drew et al. (2010)		⌀	⌀	⌀	⌀	⌀
Hölttä et al. (2010)	⌀	⌀		⌀	⌀	⌀
Drew and Downes (2015)	⌀	⌀	⊕	⊕ (mean) ⊕	⊕ (mean) ⊕	†
Schiestl-Aalto et al. (2015)	⊕	⊕				⊕
Hartmann et al. (2017)	†	†			⌀	⊕ (CAM, ENL)
Cartenì et al. (2018)	†	†		⊕	⊕	
Hartmann et al. (2021)	⊕	†	⊕		⊕	⊕
Friend (2020)	⌀	⌀	⊕		⌀	
Cabon et al. (2020)		⌀				⊕ (CAM)

be done with care. To our knowledge, dendrometer data has so far not been used for wood formation model validation, rather for radial growth or stem increment models. Therefore, we see scope for involvement of this type of observation to help fill the gap between cell counts at weekly time-scales with daily-resolved "anatomical" information on radial increment. Nevertheless, challenges remain to attribute observed increments to irreversible growth due to diurnal shrinking and swelling of the stem (but see Mencuccini et al. (2017) and Zweifel et al. (2016)) and to account also for phloem growth dynamics.

New types of observations continue to be developed which are able to enhance inter-species comparison and monitoring of variables emerging from xylogenesis dynamics such as volume and mass variables, also relevant for wood formation model validation. For example, zone width information from weekly microcores, rather than cell count, is less time-consuming and may enhance comparison across species (e.g., angiosperms vs. gymnosperms): instead of counting cells week^{-1}, one only measures the weekly zone width of a certain type of cells (e.g., see Prislan et al., 2019) (e.g., enlarging and thickening, mature cells). While the latter zone-width approach is more coarse, it is common practice in angiosperms, which have to overcome increased complexity by more cell types developing, such as large vessels, that can make it hard to objectively count a single radial file (as depicted in **Figure 1**). An angiosperm-gymnosperm comparison of xylogenesis dynamics using zone-width observations has so far only been done by Martinez del Castillo et al. (2016). Another study has used Norway spruce *(Picea abies (L.) Karst)* to investigate a novel histological approach that only monitors the dynamics of volume or mass increase (Andrianantenaina et al., 2019) as opposed to the conventional cellular-based approach which monitors cell developmental stages separately. The monitoring of volume and mass variables only are potentially useful for parameterizing and verifying parsimonious wood formation models useful for regional-scale to global modeling, for example in new generations of DGVMs. Recently a new method called high-resolution X-ray computed tomography (HRXCT) is also capable of monitoring intraannual stem radial width (called "size growth" by the authors), and biomass dynamics and promises to create further such observations relevant to modeling wood formation (Lehnebach et al., 2021). However, whether or not all information content necessary for model validation can be retained by all these new types of observations remains unclear, as neither zone-width nor volume and mass- only data have so far been used to validate any wood formation models. While cell numbers have been used for model validation, neither zone-widths, nor volume and mass-based approaches have hitherto been exploited in wood formation modeling.

Overall, the use of intra-ring (especially cell anatomical) and xylogenesis data in tandem will likely provide the best way to challenge individual model process hypotheses around each cell developmental phase, its drivers, and the resulting anatomical features. The only model which to our knowledge has formally compared output against both dynamic (xylogenesis) and static (cell anatomical) data is XyDys1 and 2 (Hartmann et al., 2017,

2021). The challenge remains to integrate dynamic and static data in the light of a lot of sample variability. While significant progress has been made in this from the data analysis side (e.g., Cuny et al., 2013), wood formation models will be a useful bridge between the datasets.

Not discussed in any detail in this review are molecular-level and gene expression observations, which remain unused in wood formation model verification or hypothesis construction, with the exception of auxin and sugar. Whether statistical association of small genetic mutation with observed traits, currently mostly used for molecular breeding (e.g., reviewed by Du et al., 2018), gene expression level analysis across the developing wood and in response to hormonal changes (e.g., Schrader et al., 2004; Immanen et al., 2016), or the construction of knockout tree variants to obtain functional understanding through the artificial absence of a protein in a crucial process within wood formation (e.g., Xu et al., 2021), all knowledge and data generated from these methods are additional powerful resources that can be harnessed for wood formation model development and verification in the future.

2.6.3. Model-Data Interoperability Through Data Standards and Analysis Tools

Data standards help both modelers and experimentalists make their research output interoperable among each other. Recently developed data-analysis tools such as CaviaR (Rathgeber et al., 2018) can help clarify concepts such as critical dates (of when enlargement or wall thickening begin and end) and provide a standard format in which to handle wood formation observations. These data analysis tools offer opportunities for modelers to develop similar-looking "virtual tree" output, thus facilitating model-data comparison. Whereas, Fritts and Shashkin (1995) were impeded by the lack of image analysis tools and therefore slow sample processing, today, image analysis tools such as WinCELL (Regent Instruments, 2012), ROXAS (von Arx and Carrer, 2014), or ImageJ (cf. Schuldt et al., 2013 for user-example) can be used to study tree ring anatomical structure including cell diameter, lumen area, or wall thickness amongst others. These tools provide valuable smaller-scale data which can be used to confront models. Their semi-automated nature can provide large datasets to verify models against. When used together with dynamic xylogenesis observations they have great potential to constrain wood formation models and shed more light onto their plausible structures.

Overall, the use of data should help verify wood formation models further. The utility of the data depends on the model, the processes it resolves and the purposes it serves. However, in general the most useful combination of datasets for model validation are a combination of both dynamic (xylogenesis) and static (anatomical) data. Observations can both be used for model hypothesis validation, but there is unused potential to also apply it to model calibration. An enhanced integration between data and model output through shared formats will facilitate direct model–data comparison. Ultimately, model development and gathering of observations and their standardized analysis should go hand-in-hand to generate new knowledge.

2.7. Wood Formation Under Climate Change

That wood growth will be impacted by climate change is already evident (e.g., Briffa et al., 1998; Pretzsch et al., 2018; Babst et al., 2019). However, only few wood formation models have been originally built to investigate climate change impacts on tree growth as principle motivation. Indeed, few wood formation modeling studies even mention the importance of wood formation modeling to predict growth responses in a climate change context. The exception is Drew and Downes (2015), who point out the suitability of their model to better predict future forest productivity. In the preface to their book, Vaganov et al. (2006) mention a potential for global carbon cycle modeling, but the ultimate model focus of the VS-model is extracting historical climate patterns. Nevertheless, the VS-model has been used to reconstruct and forecast growth phenology from climate forcings and TRW data at the Tibetan Plateau and it was found that growth start has shifted forward by 6 days (Yang et al., 2017), and that growing season length will continue to increase with climate change (He et al., 2018a,b). However, it is important to note that while these authors found a prolonged period of potential growth which could be associated with increased TRW and thus carbon sequestration, climate change-induced changes in phenology cannot be universally seen as cause for increased tree growth (Körner and Basler, 2010). Therefore, not only the growing season length but within-season processes must be addressed using wood formation models. Nevertheless, there is potential in improving the mechanisms related to wood formation phenology in the models: A chilling-influenced heat sum model performed best in an intercomparison of approaches for simulating the onset of enlargement in developing wood (Delpierre et al., 2018), an interesting mechanism to test in wood formation models. Predicting the end of wood formation processes, e.g., cessation of cambial activity (Buttò et al., 2020b) or until full maturation (Cuny et al., 2019) has hitherto been difficult and more research is needed in this area. Since wood is a large and long-term carbon store, and wood formation dynamics can help predict carbon allocation in trees (Buttò et al., 2021), wood formation models should be integrated to study global carbon cycle dynamics. However, due to the lack of wood formation models suitable for global use, their application in global carbon cycle and vegetation modeling are currently lacking (Friend et al., 2019).

The tree ring and wood formation community has started to encourage the use of wood formation and tree ring observations for the global modeling of wood formation (Babst et al., 2014, 2018; Zuidema et al., 2018). Some vegetation modelers have also started work to this end (Friend et al., 2019; Friend, 2020; Eckes-Shephard et al., 2021). This new area of modeling offers a new application of wood formation models, namely to help improve predictions on global vegetation carbon responses to climate change.

Hitherto unexplored areas in wood formation modeling is the growth response to wind sway and nutrient availability. Nutrients were not important in previous study contexts and there is large uncertainty in how to represent these additional processes. For a global wood formation model, this is an important area for further research, as global productivity, especially in forests, has commonly been found to be nutrient limited (LeBauer and Treseder, 2008; Fernández-Martínez et al., 2014). It has also been shown that macro nutrients may impact wood density and timber stiffness in fast grown pines (see e.g., Wessels et al., 2015). Especially for new areas of applications of wood formation models, e.g., global modeling, nutrients may need to be considered to some extent. It is important that the coverage of observations of wood formation dynamics, anatomy, and tree rings increases in low-latitude areas in order to inform the development of globally-applicable wood formation models.

3. CONCLUSION AND OUTLOOK

This review has shown how wood formation modeling, from the pioneering efforts in the 1960s to today, has greatly improved our mechanistic understanding of wood formation. We have highlighted areas where existing wood formation hypotheses may need to be challenged. There is significant scope for exploring new hypotheses and to better integrate them within the models. There is great potential for collaboration between researchers performing long-term field monitoring (e.g., Integrated Carbon Observation System (ICOS)), experimentalists (e.g., Free Air Carbon Enrichment (FACE) and greenhouse experiments) and modelers to address outstanding questions. We envision that wood formation modeling can help to address key challenges related to global change and carbon cycle modeling.

We have summarized the current knowledge of growth process representation in wood formation models. Researchers from three disciplines have developed 17 wood formation models at various levels of detail and with different assumptions on environmental drivers and applications in mind. While dendroclimatologists are interested in the growth–climate relationships in order to reconstruct past climate from tree rings, foresters aim to predict wood quantity and quality. Finally, more fundamental researchers have built many models with the aim to better understand variability, hormonal influences, or growth-carbon interactions. Underlying all these models are a wide range of different hypotheses, supported by multiple lines of empirical evidence on what processes are necessary to resolve when modeling tree growth. The questions posed with the models very much determine their focus and level of complexity. It is therefore not surprising that the models differ substantially from each other. However, the fact that there is rather little agreement on some basic processes (e.g., the influence of hormones on wood formation; what causes the transition between earlywood and latewood; the influence of carbon supply), and their drivers (see **Figure 3**) shows that there is still a lot to be studied about wood formation, which manifests itself in uncertain wood formation models.

Wood formation models have already been successfully applied to answer many different scientific questions. Besides their current remit, they have the potential to be useful in many other areas. For example, simple wood formation models may be useful for global application to better project vegetation carbon responses to the environment and hence climate change (Friend et al., 2019). For this, understanding the role of carbohydrates on wood formation (regulatory or as substrate and at what developmental process is it restricting) will need to increase for example through manipulation experiments (e.g., Rademacher et al., 2019). Additionally, simulating future tree rings could help forecast tree mortality in conjunction with tree ring-based mortality algorithms (Cailleret et al., 2017). Finally, resolving growth processes as a carbon sink within the tree may help to answer questions on active vs. passive storage and can in the same context also help address the source-sink controversy (Schiestl-Aalto et al., 2015).

Data sources to verify growth hypotheses within the models are far from fully exploited. Most models compare their output against end-of-the-year observations such as density, ring width, number of cells, or mean tracheid diameter. Dynamic data such as xylogenesis data can help verify whether the intra-annual dynamics are indeed captured well in those models. While many different model hypotheses may be able to replicate a final-year result well, this finer-grained data is important for challenging model hypotheses on a shorter time-scale, and hence addressing mechanisms more precisely. Additional end-of-season output that may also be more challenging for wood formation models to replicate are IADFs, which in tandem with xylogenesis data deserve more attention from wood formation modelers. Future efforts should also make use of molecular studies for hypothesis building or model verification.

This review identified three main areas (carbon, hormones, and more broadly, or as a result earlywood-latewood transition) where model hypotheses diverge and therefore on which additional research should be done. However, while wood formation seems to be subject to multiple internal and external controls simultaneously, observations *in natura* may not always provide conclusive evidence toward one mechanistic hypothesis for a model. Therefore, we call for a move toward manipulation experiments (e.g., Baba et al., 2018; Rademacher et al., 2019) and combinations of anatomical data, IADFs, and weekly xylogenesis monitoring. From our summary of the current state of wood formation modeling research, we identified the following (inter-related) areas in which open questions remain:

(1) hormonal influences on growth
(2) carbon influences on growth.
    Addressing these two areas of research will already contribute to the outstanding mechanisms on
(3) earlywood–latewood transitions.

Global change will affect wood formation in all forested regions of the world and challenge the plausibility of existing hypotheses encapsulated in wood formation models. The modeling and wood formation observations are currently biased toward the northern hemisphere. Therefore, there is great potential in the wood formation modeling and observation community to increase their area of research into other low-latitude ecosystems. This, together with an increased use of diverse observations from multiple disciplines, will be crucial in verifying the

hypotheses behind wood formation's mechanisms and drivers. Getting these right will be critical for all applications of wood formation hypotheses, for the single tree or global vegetation model.

DATA AVAILABILITY STATEMENT

The original contributions presented in the study are included in the article/supplementary material, further inquiries can be directed to the corresponding authors.

AUTHOR CONTRIBUTIONS

AE-S conceived the content of the review and drafted the manuscript with input from all authors. AF supervised the project. All authors commented on the final manuscript.

FUNDING

AE-S acknowledges support from the European Research Council under the European Union Horizon 2020 Programme (grant no. 758873, TreeMort). FCL was supported by the Swedish Research Council (Vetenskapsrådet, grant no. 2018-01272) and conducted the work with this article as a Pro Futura Scientia XIII Fellow funded by the Swedish Collegium for Advanced Study through Riksbankens Jubileumsfond. This study contributes to the Strategic Research Areas BECC and MERGE. CR was supported by a grant overseen by the French National Research Agency (ANR) as part of the Investissements d'Avenir program (ANR-11-LABX-0002-01, Lab of Excellence ARBRE).

ACKNOWLEDGMENTS

We thank Christine Eckes for proofreading the manuscript.

REFERENCES

Aloni, R., and Zimmermann, M. H. (1983). The control of vessel size and density along the plant axis. *Differentiation* 24, 203–208. doi: 10.1111/j.1432-0436.1983.tb01320.x

Anchukaitis, K. J., Evans, M. N., Kaplan, A., Vaganov, E. A., Hughes, M. K., Grissino-Mayer, H. D., et al. (2006). Forward modeling of regional scale tree-ring patterns in the southeastern United States and the recent influence of summer drought. *Geophys. Res. Lett*. 33, L04705. doi: 10.1029/2005GL025050

Anderegg, W. R., Trugman, A. T., Badgley, G., Anderson, C. M., Bartuska, A., Ciais, P., et al. (2020). Climate-driven risks to the climate mitigation potential of forests. *Science* 368, eaaz7005. doi: 10.1126/science.aaz7005

Andrianantenaina, A. N., Rathgeber, C. B. K., Pérez-de Lis, G., Cuny, H., and Ruelle, J. (2019). Quantifying intra-annual dynamics of carbon sequestration in the forming wood: a novel histologic approach. *Ann. For. Sci*. 76, 62. doi: 10.1007/s13595-019-0846-7

Baba, K., Kurita, Y., and Mimura, T. (2018). Wood structure of *Populus alba* formed in a shortened annual cycle system. *J. Wood Sci*. 64, 1–5. doi: 10.1007/s10086-017-1664-x

Babst, F., Alexander, M. R., Szejner, P., Bouriaud, O., Klesse, S., Roden, J., et al. (2014). A tree-ring perspective on the terrestrial carbon cycle. *Oecologia* 176, 307–322. doi: 10.1007/s00442-014-3031-6

Babst, F., Bodesheim, P., Charney, N., Friend, A. D., Girardin, M. P., Klesse, S., et al. (2018). When tree rings go global: Challenges and opportunities for retro- and prospective insight. *Quat. Sci. Rev*. 197, 1–20. doi: 10.1016/j.quascirev.2018.07.009

Babst, F., Bouriaud, O., Poulter, B., Trouet, V., Girardin, M. P., and Frank, D. C. (2019). Twentieth century redistribution in climatic drivers of global tree growth. *Sci. Adv*. 5, eaat4313. doi: 10.1126/sciadv.aat4313

Baillie, M. G. (1995). *A Slice Through Time: Dendrochronology and Precision Dating*. London: Routledge.

Battipaglia, G., Campelo, F., Vieira, J., Grabner, M., De Micco, V., Nabais, C., et al. (2016). Structure and function of intra-annual density fluctuations: mind the gaps. *Front. Plant Sci*. 7, 595. doi: 10.3389/fpls.2016.00595

Bhalerao, R. P., and Fischer, U. (2014). Auxin gradients across wood – instructive or incidental? *Physiol. Plant* 151, 43–51. doi: 10.1111/ppl.12134

Brienen, R. J. W., and Zuidema, P. A. (2005). Relating tree growth to rainfall in Bolivian rain forests: a test for six species using tree ring analysis. *Oecologia* 146, 1–12. doi: 10.1007/s00442-005-0160-y

Briffa, K. R., Schweingruber, F. H., Jones, P. D., Osborn, T. J., Shiyatov, S. G., and Vaganov, E. A. (1998). Reduced sensitivity of recent tree-growth to temperature at high northern latitudes. *Nature* 391, 678–682. doi: 10.1038/35596

Buttò, V., Deslauriers, A., Rossi, S., Rozenberg, P., Shishov, V., and Morin, H. (2020a). The role of plant hormones in tree-ring formation. *Trees* 34, 315–335. doi: 10.1007/s00468-019-01940-4

Buttò, V., Rozenberg, P., Deslauriers, A., Rossi, S., and Morin, H. (2021). Environmental and developmental factors driving xylem anatomy and micro-density in black spruce. *New Phytol*. 230, 957–971. doi: 10.1111/nph.17223

Buttò, V., Shishov, V., Tychkov, I., Popkova, M., He, M., Rossi, S., et al. (2020b). Comparing the cell dynamics of tree-ring formation observed in microcores and as predicted by the Vaganov–Shashkin model. *Front. Plant Sci*. 11, 1268. doi: 10.3389/fpls.2020.01268

Cabon, A., Peters, R. L., Fonti, P., Martínez-Vilalta, J., and Cáceres, M. D. (2020). Temperature and water potential co-limit stem cambial activity along a steep elevational gradient. *New Phytol*. 226, 1325–1340. doi: 10.1111/nph.16456

Cailleret, M., Jansen, S., Robert, E. M. R., Desoto, L., Aakala, T., Antos, J. A., et al. (2017). A synthesis of radial growth patterns preceding tree mortality. *Glob. Chang Biol*. 23, 1675–1690. doi: 10.1111/gcb.13535

Campelo, F., Nabais, C., Freitas, H., and Gutiérrez, E. (2007). Climatic significance of tree-ring width and intra-annual density fluctuations in *Pinus pinea* from a dry Mediterranean area in Portugal. *Ann. For. Sci*. 64, 229–238. doi: 10.1051/forest:2006107

Cartenì, F., Deslauriers, A., Rossi, S., Morin, H., De Micco, V., Mazzoleni, S., et al. (2018). The physiological mechanisms behind the earlywood-to-latewood transition: a process-based modeling approach. *Front. Plant Sci*. 9, 1053. doi: 10.3389/fpls.2018.01053

Chan, T., Hölttä, T., Berninger, F., Mäkinen, H., Nöjd, P., Mencuccini, M., et al. (2016). Separating water-potential induced swelling and shrinking from measured radial stem variations reveals a cambial growth and osmotic concentration signal. *Plant Cell Environ*. 39, 233–244. doi: 10.1111/pce.12541

Cuny, H. E., Fonti, P., Rathgeber, C. B. K., Arx, G., v., Peters, R. L., et al. (2019). Couplings in cell differentiation kinetics mitigate air temperature influence on conifer wood anatomy. *Plant Cell Environ*. 42, 1222–1232. doi: 10.1111/pce.13464

Cuny, H. E., and Rathgeber, C. B. (2016). Xylogenesis: coniferous trees of temperate forests are listening to the climate tale during the growing season but only remember the last words! *Plant Physiol*. 171, 306–317. doi: 10.1104/pp.16.00037

Cuny, H. E., Rathgeber, C. B., Kiessé, T. S., Hartmann, F. P., Barbeito, I., and Fournier, M. (2013). Generalized additive models reveal the intrinsic complexity of wood formation dynamics. *J. Exp. Bot*. 64, 1983–1994. doi: 10.1093/jxb/ert057

Cuny, H. E., Rathgeber, C. B. K., Frank, D., Fonti, P., and Fournier, M. (2014). Kinetics of tracheid development explain conifer tree-ring structure. *New Phytol*. 203, 1231–1241. doi: 10.1111/nph.12871

D'Arrigo, R., Wilson, R., Liepert, B., and Cherubini, P. (2008). On the 'divergence problem' in northern forests: a review of the tree-ring evidence and possible causes. *Glob. Planet. Change* 60, 289–305. doi: 10.1016/j.gloplacha.2007.03.004

de Mil, T. (2018). Non-periodical growth in a tropical moist semi-deciduous forest of Central Africa. *Afrika Focus* 30:137–41. doi: 10.21825/af.v30i1.4987

Deckmyn, G., Evans, S. P., and Randle, T. J. (2006). Refined pipe theory for mechanistic modeling of wood development. *Tree Physiol.* 26, 703–717. doi: 10.1093/treephys/26.6.703

Deleuze, C., and Houllier, F. (1998). A simple process-based xylem growth model for describing wood microdensitometric profiles. *J. Theor. Biol.* 193, 99–113. doi: 10.1006/jtbi.1998.0689

Delpierre, N., Lireux, S., Hartig, F., Camarero, J., Cheaib, A., Cufar, K., et al. (2018). Chilling and forcing temperatures interact to predict the onset of wood formation in Northern Hemisphere conifers. *Glob. Change Biol.* 25, 1089–1105. doi: 10.1111/gcb.14539

Deslauriers, A., Huang, J.-G., Balducci, L., Beaulieu, M., and Rossi, S. (2016). The contribution of carbon and water in modulating wood formation in black spruce saplings. *Plant Physiol.* 170, 2072–2084. doi: 10.1104/pp.15.01525

Dié, A., Kitin, P., Kouamé, F. N., Van den Bulcke, J., Van Acker, J., and Beeckman, H. (2012). Fluctuations of cambial activity in relation to precipitation result in annual rings and intra-annual growth zones of xylem and phloem in teak (*Tectona grandis*) in Ivory Coast. *Ann. Bot.* 110, 861–873. doi: 10.1093/aob/mcs145

Dietze, M. C., Sala, A., Carbone, M. S., Czimczik, C. I., Mantooth, J. A., Richardson, A. D., et al. (2014). Nonstructural carbon in woody plants. *Annu. Rev. Plant Biol.* 65, 667–687. doi: 10.1146/annurev-arplant-050213-040054

Downes, G., and Drew, D. M. (2008). Climate and growth influences on wood formation and utilisation. *South For.* 70, 155–167. doi: 10.2989/SOUTH.FOR.2008.70.2.11.539

Downes, G. M., Drew, D., Battaglia, M., and Schulze, D. (2009). Measuring and modelling stem growth and wood formation: an overview. *Dendrochronologia* 27, 147–157. doi: 10.1016/j.dendro.2009.06.006

Drew, D. M., Bruce, J., and Downes, G. M. (2017). Future wood properties in Australian forests: effects of temperature, rainfall and elevated CO_2. *Austr. For.* 80, 242–254. doi: 10.1080/00049158.2017.1362937

Drew, D. M., and Downes, G. (2015). A model of stem growth and wood formation in *Pinus radiata*. *Trees* 29, 1395–1413. doi: 10.1007/s00468-015-1216-1

Drew, D. M., and Downes, G. M. (2009). The use of precision dendrometers in research on daily stem size and wood property variation: a review. *Dendrochronologia* 27, 159–172. doi: 10.1016/j.dendro.2009.06.008

Drew, D. M., Downes, G. M., and Battaglia, M. (2010). CAMBIUM, a process-based model of daily xylem development in Eucalyptus. *J. Theor. Biol.* 264, 395–406. doi: 10.1016/j.jtbi.2010.02.013

Drew, D. M., Schulze, E. D., and Downes, G. M. (2009). Temporal variation in $\delta^{13}C$, wood density and microfibril angle in variously irrigated Eucalyptus nitens. *Funct. Plant Biol.* 36, 1–10. doi: 10.1071/FP08180

Du, M., Spalding, E. P., and Gray, W. M. (2020). Rapid auxin-mediated cell expansion. *Annu. Rev. Plant Biol.* 71, 379–402. doi: 10.1146/annurev-arplant-073019-025907

Du, Q., Lu, W., Quan, M., Xiao, L., Song, F., Li, P., et al. (2018). Genome-wide association studies to improve wood properties: challenges and prospects. *Front. Plant Sci.* 9, 1912. doi: 10.3389/fpls.2018.01912

Eckes-Shephard, A. H., Tiavlovsky, E., Chen, Y., Fonti, P., and Friend, A. D. (2021). Direct response of tree growth to soil water and its implications for terrestrial carbon cycle modelling. *Glob. Chang Biol.* 27, 121–135. doi: 10.1111/gcb.15397

Esper, J., Krusic, P. J., Ljungqvist, F. C., Luterbacher, J., Carrer, M., Cook, E., et al. (2016). Ranking of tree-ring based temperature reconstructions of the past millennium. *Quat. Sci. Rev.*, 145, 134–151. doi: 10.1016/j.quascirev.2016.05.009

Esper, J., St. George, S., Anchukaitis, K., D'Arrigo, R., Ljungqvist, F. C., Luterbacher, J., et al. (2018). Large-scale, millennial-length temperature reconstructions from tree-rings. *Dendrochronologia* 50, 81–90. doi: 10.1016/j.dendro.2018.06.001

Evans, M. L., Ishikawa, H., and Estelle, M. A. (1994). Responses of *Arabidopsis* roots to auxin studied with high temporal resolution: Comparison of wild type and auxin-response mutants. *Planta* 194, 215–222. doi: 10.1007/BF01101680

Fatichi, S., Leuzinger, S., and Körner, C. (2014). Moving beyond photosynthesis: from carbon source to sink-driven vegetation modeling. *New Phytol.* 201, 1086–1095. doi: 10.1111/nph.12614

Fatichi, S., Pappas, C., Zscheischler, J., and Leuzinger, S. (2019). Modelling carbon sources and sinks in terrestrial vegetation. *New Phytol.* 221, 652–668. doi: 10.1111/nph.15451

Fernández-Martínez, M., Vicca, S., Janssens, I. A., Sardans, J., Luyssaert, S., Campioli, M., et al. (2014). Nutrient availability as the key regulator of global forest carbon balance. *Nat. Clim. Chang* 4, 471–476. doi: 10.1038/nclimate 2177

Frank, D. C., Esper, J., Raible, C. C., Büntgen, U., Trouet, V., Stocker, B., et al. (2010). Ensemble reconstruction constraints on the global carbon cycle sensitivity to climate. *Nature* 463, 527–530. doi: 10.1038/nature08769

Friend, A. D. (2020). Wood structure explained by complex spatial source-sink interactions. *bioRxiv*. doi: 10.1101/2020.05.02.073643

Friend, A. D., Eckes-Shephard, A. H., Fonti, P., Rademacher, T. T., Rathgeber, C. B. K., Richardson, A. D., et al. (2019). On the need to consider wood formation processes in global vegetation models and a suggested approach. *Ann. For. Sci.* 76, 49. doi: 10.1007/s13595-019-0819-x

Fritts, H. (1976). *Tree Rings and Climate*. New York, NY: Academic Press.

Fritts, H., and Shashkin, A. (1995). "Modeling tree-ring structure as related to temperature, precipitation, and day length (Chapter 2)," in *Tree Rings as Indicators of Ecosystem Health*, ed T. Lewis (Ann Arbor, MI: CRC Press), 17–57.

Fritts, H., Shashkin, A., and Downes, G. (1999). "A simulation model of conifer ring growth and cell structure," in *Tree Ring Analysis: Biological, Methodological and Environmental Aspects*, eds R. Wimmer and R. Vetter (Wallingford, UK: CABI Publishing), 3–32.

Fritts, H., Vaganov, E., Sviderskaya, I., and Shashkion, A. (1991). Climatic variation and tree-ring structure in conifers: empirical and mechanistic models of tree-ring width, number of cells, cell size, cell-wall thickness and wood density. *Climate Res.* 1, 97–116. doi: 10.3354/cr001097

Fritts, H. C., Shashkin, A. V., Hemming, D. L., Leavitt, S. W., Wright, W. E. and Downs, G. M. (2000). *Preliminary Draft: User Manual for Treering 2000*. Tucson: Laboratory of Tree Ring Research Arizona.

Fromm, J. (Ed.). (2013). *Cellular Aspects of Wood Formation. Number v. 20 in Plant Cell Monographs*. Berlin; New York, Ny: Springer; OCLC: ocn825736984.

Gindl, W., Grabner, M., and Wimmer, R. (2000). The influence of temperature on latewood lignin content in treeline Norway spruce compared with maximum density and ring width. *Trees* 14, 409–414. doi: 10.1007/s004680000057

Giovannelli, A., Emiliani, G., Traversi, M. L., Deslauriers, A., and Rossi, S. (2011). Sampling cambial region and mature xylem for non structural carbohydrates and starch analyses. *Dendrochronologia* 29, 177–182. doi: 10.1016/j.dendro.2011.01.001

Hartmann, F. P., Rathgeber, C. B. K., Badel, E., Fournier, M., and Moulia, B. (2021). Modelling the spatial crosstalk between two biochemical signals explains wood formation dynamics and tree-ring structure. *J. Exp. Bot.* 72, 1727–1737. doi: 10.1093/jxb/eraa558

Hartmann, F. P. K., Rathgeber, C. B., Fournier, M., and Moulia, B. (2017). Modelling wood formation and structure: power and limits of a morphogenetic gradient in controlling xylem cell proliferation and growth. *Ann. For. Sci.* 74, 14. doi: 10.1007/s13595-016-0613-y

Hartmann, H., McDowell, N. G., and Trumbore, S. (2015). Allocation to carbon storage pools in Norway spruce saplings under drought and low CO_2. *Tree Physiol.* 35, 243–252. doi: 10.1093/treephys/tpv019

He, M., Yang, B., Shishov, V., Rossi, S., Bräuning, A., Ljungqvist, F. C., et al. (2018a). Projections for the changes in growing season length of tree-ring formation on the Tibetan Plateau based on CMIP5 model simulations. *Int. J. Biometeorol.* 62, 631–641. doi: 10.1007/s00484-017-1472-4

He, M., Yang, B., Shishov, V., Rossi, S., Bräuning, A., Ljungqvist, F. C., et al. (2018b). Relationships between wood formation and cambium phenology on the Tibetan Plateau during 1960–2014. *Forests* 9, 86. doi: 10.3390/f9020086

Hilty, J., Muller, B., Pantin, F., and Leuzinger, S. (2021). Plant growth: the what, the how, and the why. *New Phytol.* 232, 25–41. doi: 10.1111/nph.17610

Hölttä, T., Makinen, H., Nøjd, P., Makela, A., and Nikinmaa, E. (2010). A physiological model of softwood cambial growth. *Tree Physiol.* 30, 1235–1252. doi: 10.1093/treephys/tpq068

Howard, R. A., and Wilson, B. F. (1972). A stochastic model for cambial activity. *Bot. Gazette* 133, 410–414. doi: 10.1086/336665

Immanen, J., Nieminen, K., Smolander, O.-P., Kojima, M., Alonso Serra, J., Koskinen, P., et al. (2016). Cytokinin and auxin display distinct but interconnected distribution and signaling profiles to stimulate cambial activity. *Curr. Biol.* 26, 1990–1997. doi: 10.1016/j.cub.2016.05.053

Körner, C. (2015). Paradigm shift in plant growth control. *Curr. Opin. Plant Biol.* 25, 107–114. doi: 10.1016/j.pbi.2015.05.003

Körner, C., and Basler, D. (2010). Phenology under global warming. *Science* 327, 1461–1462. doi: 10.1126/science.1186473

Körner, C., Riedl, S., Keplinger, T., Richter, A., Wiesenbauer, J., Schweingruber, F., et al. (2019). Life at 0°C: the biology of the alpine snowbed plant *Soldanella pusilla*. *Alpine Bot*. 129, 63–80. doi: 10.1007/s00035-019-00220-8

Kramer, E. M. (2001). A Mathematical Model of Auxin-mediated Radial Growth in Trees. *J. Theor. Biol.* 208, 387–397. doi: 10.1006/jtbi.2000.2220

Kramer, E. M. (2002). A mathematical model of pattern formation in the vascular cambium of trees. *J. Theor. Biol.* 216, 147–158. doi: 10.1006/jtbi.2002.2551

Larson, P. R. (1960). A physiological consideration of the springwood summerwood transition in Red Pine [*Pinus resinosa*]. *For. Sci*. 6, 110–122.

Larson, P. R. (1964a). Contribution of different-aged needles to growth and wood formation of young red pines. *For. Sci*. 10, 224–238.

Larson, P. R. (1964b). "Some indirect effects of environment on wood formation," in *The Formation of Wood in Forest Trees*, ed M. H. Zimmermann (Cambridge, MA: Academic Press), 345–365.

LeBauer, D. S., and Treseder, K. K. (2008). Nitrogen limitation of net primary productivity in terrestrial ecosystems is globally distributed. *Ecology* 89, 371–379. doi: 10.1890/06-2057.1

Lehnebach, R., Campioli, M., Gričar, J., Prislan, P., Mariën, B., Beeckman, H., et al. (2021). High-resolution X-ray computed tomography: a new workflow for the analysis of xylogenesis and intra-seasonal wood biomass production. *Front. Plant Sci.* 12, 1495. doi: 10.3389/fpls.2021.698640

Lempereur, M., Martin-StPaul, N. K., Damesin, C., Joffre, R., Ourcival, J.-M., Rocheteau, A., et al. (2015). Growth duration is a better predictor of stem increment than carbon supply in a Mediterranean oak forest: implications for assessing forest productivity under climate change. *New Phytol.* 207, 579–590. doi: 10.1111/nph.13400

Leuzinger, S., Manusch, C., Bugmann, H., and Wolf, A. (2013). A sink-limited growth model improves biomass estimation along boreal and alpine tree lines. *Glob. Ecol. Biogeogr.* 22, 924–932. doi: 10.1111/geb.12047

Ljungqvist, F. C., Piermattei, A., Seim, A., Krusic, P. J., Büntgen, U., He, M., et al. (2020a). Ranking of tree-ring based hydroclimate reconstructions of the past millennium. *Quat. Sci. Rev.* 230, 106074. doi: 10.1016/j.quascirev.2019.106074

Ljungqvist, F. C., Tegel, W., Krusic, P. J., Seim, A., Gschwind, F. M., Haneca, K., et al. (2018). Linking European building activity with plague history. *J. Archaeol. Sci.* 98, 81–92. doi: 10.1016/j.jas.2018.08.006

Ljungqvist, F. C., Thejll, P., Björklund, J., Gunnarson, B. E., Piermattei, A., Rydval, M., et al. (2020b). Assessing non-linearity in European temperature-sensitive tree-ring data. *Dendrochronologia* 59, 125652. doi: 10.1016/j.dendro.2019.125652

Mäkelä, A., and Mäkinen, H. (2003). Generating 3D sawlogs with a process-based growth model. *For. Ecol. Manage.* 184, 337–354. doi: 10.1016/S0378-1127(03)00152-X

Martinez del Castillo, E., Longares, L. A., Gricar, J., Prislan, P., Gil-Pelegrín, E., Cufar, K., et al. (2016). Living on the edge: contrasted wood-formation dynamics in *Fagus sylvatica* and *Pinus sylvestris* under Mediterranean conditions. *Front. Plant Sci.* 7, 370. doi: 10.3389/fpls.2016.00370

McCahill, I. W., and Hazen, S. P. (2019). Regulation of cell wall thickening by a medley of mechanisms. *Trends Plant Sci.* 24, 853–866. doi: 10.1016/j.tplants.2019.05.012

Mencuccini, M., Salmon, Y., Mitchell, P., Hölttä, T., Choat, B., Meir, P., et al. (2017). An empirical method that separates irreversible stem radial growth from bark water content changes in trees: theory and case studies: separating irreversible stem radial growth. *Plant Cell Environ.* 40, 290–303. doi: 10.1111/pce.12863

Mitchell, P. J., McAdam, S. A. M., Pinkard, E. A., and Brodribb, T. J. (2016). Significant contribution from foliage-derived ABA in regulating gas exchange in *Pinus radiata*. *Tree Physiol.* 37, 236–245. doi: 10.1093/treephys/tpw092

Pérez-de-Lis, G., Rathgeber, C. B. K., Fernández-de-Uña, L., and Ponton, S. (2021). Cutting tree rings into time slices: how intra-annual dynamics of wood formation help decipher the space-for-time conversion. *New Phytol.* 233, 1520–1584. doi: 10.5194/egusphere-egu2020-22286

Perrot-Rechenmann, C. (2010). Cellular responses to auxin: division versus expansion. *Cold Spring Harb. Perspect. Biol.* 2, a001446–a001446. doi: 10.1101/cshperspect.a001446

Peters, R. L., Steppe, K., Cuny, H. E., De Pauw, D. J., Frank, D. C., Schaub, M., et al. (2021). Turgor – a limiting factor for radial growth in mature conifers along an elevational gradient. *New Phytol.* 229, 213–229. doi: 10.1111/nph.16872

Petterle, A., Karlberg, A., and Bhalerao, R. P. (2013). Daylength mediated control of seasonal growth patterns in perennial trees. *Curr. Opin. Plant Biol.* 16, 301–306. doi: 10.1016/j.pbi.2013.02.006

Plomion, C., Leprovost, G., and Stokes, A. (2001). Wood formation in trees. *Plant Physiol.* 127, 1513–1523. doi: 10.1104/pp.010816

Popkova, M. I., Vaganov, E. A., Shishov, V. V., Babushkina, E. A., Rossi, S., Fonti, M. V., et al. (2018). Modeled tracheidograms disclose drought influence on *Pinus sylvestris* tree-rings structure from Siberian forest-steppe. *Front. Plant Sci.* 9, 1144. doi: 10.3389/fpls.2018.01144

Pretzsch, H., Biber, P., Schütze, G., Kemmerer, J., and Uhl, E. (2018). Wood density reduced while wood volume growth accelerated in Central European forests since 1870. *For. Ecol. Manage.* 429, 589–616. doi: 10.1016/j.foreco.2018.07.045

Prislan, P., Gricar, J., Cufar, K., de Luis, M., Merela, M., and Rossi, S. (2019). Growing season and radial growth predicted for *Fagus sylvatica* under climate change. *Clim. Change* 153, 181–197. doi: 10.1007/s10584-019-02374-0

Rademacher, T. T., Basler, D., Eckes-Shephard, A. H., Fonti, P., Friend, A. D., Le Moine, J., et al. (2019). Using direct phloem transport manipulation to advance understanding of carbon dynamics in forest trees. *Front. For. Glob. Change* 2, 11. doi: 10.3389/ffgc.2019.00011

Rathgeber, C. B. K., Cuny, H. E., and Fonti, P. (2016). Biological basis of tree-ring formation: a crash course. *Front. Plant Sci.* 7, 734. doi: 10.3389/fpls.2016.00734

Rathgeber, C. B. K., Santenoise, P., Cuny, H. E., and Tognetti, R. (2018). CAVIAR: an R package for checking, displaying and processing wood-formation-monitoring data. *Tree Physiol.* 38, 1246–1260. doi: 10.1093/treephys/tpy054

Regent Instruments. (2012). *Manual for WinCELL for Wood Cell Analysis (Version 2012a)*. Regent Instruments Canada Inc.

Rigling, A., Waldner, P. O., Forster, T., Bräker, O. U., and Pouttu, A. (2011). Ecological interpretation of tree-ring width and intraannual density fluctuations in Pinus sylvestris on dry sites in the central Alps and Siberia. *Can. J. For. Res.* doi: 10.1139/x00-126

Riou-Khamlichi, C., Menges, M., Healy, J. M. S., and Murray, J. A. H. (2000). Sugar control of the plant cell cycle: differential regulation of arabidopsis D-type cyclin gene expression. *Mol. Cell. Biol.* 20, 4513–4521. doi: 10.1128/MCB.20.13.4513-4521.2000

Rossi, S., Anfodillo, T., and Deslauriers, A. (2006a). Assessment of cambial activity and xylogenesis by microsampling tree species: an example at the alpine timberline. *IAWA J.* 27, 383–394. doi: 10.1163/22941932-90000161

Rossi, S., Deslauriers, A., Anfodillo, T., Morin, H., Saracino, A., Motta, R., et al. (2006b). Conifers in cold environments synchronize maximum growth rate of tree-ring formation with day length. *New Phytol.* 170, 301–310. doi: 10.1111/j.1469-8137.2006.01660.x

Rossi, S., Deslauriers, A., and Morin, H. (2003). Application of the Gompertz equation for the study of xylem cell development. *Dendrochronologia* 21, 33–39. doi: 10.1078/1125-7865-00034

Sachs, T., and Cohen, D. (1982). Circular vessels and the control of vascular differentiation in plants. *Differentiation* 21, 22–26. doi: 10.1111/j.1432-0436.1982.tb01189.x

Sala, A., Woodruff, D. R., and Meinzer, F. C. (2012). Carbon dynamics in trees: feast or famine? *Tree Physiol.* 32, 764–775. doi: 10.1093/treephys/tpr143

Schiestl-Aalto, P., Kulmala, L., Mäkinen, H., Nikinmaa, E., and Mäkelä, A. (2015). CASSIA – a dynamic model for predicting intra-annual sink demand and interannual growth variation in Scots pine. *New Phytol.* 206, 647–659. doi: 10.1111/nph.13275

Schiestl-Aalto, P., Ryhti, K., Mäkelä, A., Peltoniemi, M., Bäck, J., and Kulmala, L. (2019). Analysis of the NSC storage dynamics in tree organs reveals the allocation to belowground symbionts in the framework of whole tree carbon balance. *Front. For. Glob. Change* 2, 17. doi: 10.3389/ffgc.2019.00017

Schrader, J., Moyle, R., Bhalerao, R., Hertzberg, M., Lundeberg, J., Nilsson, P., et al. (2004). Cambial meristem dormancy in trees involves extensive remodelling of the transcriptome: cambial meristem dormancy. *Plant J.* 40, 173–187. doi: 10.1111/j.1365-313X.2004.02199.x

Schuldt, B., Leuschner, C., Brock, N., and Horna, V. (2013). Changes in wood density, wood anatomy and hydraulic properties of the xylem along the root-to-shoot flow path in tropical rainforest trees. *Tree Physiol.* 33, 161–174. doi: 10.1093/treephys/tps122

Schweingruber, F. (1988). *Tree Rings: Basics and Applications of Dendrochronology*. Dodrecht: Kluwer Academic Publishers.

Séguin, A. (2011). How could forest trees play an important role as feedstock for bioenergy production? *Curr. Opin. Environ. Sustain.* 3, 90–94. doi: 10.1016/j.cosust.2010.12.006

Shishov, V. V., Tychkov, I. I., Anchukaitis, K. J., Zelenov, G. K., and Vaganov, E. A. (2021). A band model of cambium development: opportunities and prospects. *Forests* 12, 1361. doi: 10.3390/f12101361

Shishov, V. V., Tychkov, I. I., Popkova, M. I., Ilyin, V. A., Bryukhanova, M. V., and Kirdyanov, A. V. (2016). VS-oscilloscope: a new tool to parameterize tree radial growth based on climate conditions. *Dendrochronologia* 39, 42–50. doi: 10.1016/j.dendro.2015.10.001

Simard, S., Giovannelli, A., Treydte, K., Traversi, M. L., King, G. M., Frank, D., et al. (2013). Intra-annual dynamics of non-structural carbohydrates in the cambium of mature conifer trees reflects radial growth demands. *Tree Physiol.* 33, 913–923. doi: 10.1093/treephys/tpt075

Speer, J. H. (2010). *Fundamentals of Tree-Ring Research*. Tucson: University of Arizona Press.

Steppe, K., De Pauw, D. J. W., Lemeur, R., and Vanrolleghem, P. A. (2006). A mathematical model linking tree sap flow dynamics to daily stem diameter fluctuations and radial stem growth. *Tree Physiol.* 26, 257–273. doi: 10.1093/treephys/26.3.257

Støve, B., Ljungqvist, F. C., and Thejll, P. (2012). A test for nonlinearity in temperature proxy records. *J. Clim.* 25, 7173–7186. doi: 10.1175/JCLI-D-11-00632.1

Sundberg, B., Little, C. H. A., Cui, K., and Sandberg, G. (1991). Level of endogenous indole-3-acetic acid in the stem of *Pinus sylvestris* in relation to the seasonal variation of cambial activity. *Plant Cell Environ.* 14, 241–246. doi: 10.1111/j.1365-3040.1991.tb01342.x

Sundell, D., Street, N. R., Kumar, M., Mellerowicz, E. J., Kucukoglu, M., Johnsson, C., et al. (2017). AspWood: high-spatial-resolution transcriptome profiles reveal uncharacterized modularity of wood formation in *Populus tremula*. *Plant Cell* 29, 1585–1604. doi: 10.1105/tpc.17.00153

Tolwinski-Ward, S. E., Evans, M. N., Hughes, M. K., and Anchukaitis, K. J. (2011). An efficient forward model of the climate controls on interannual variation in tree-ring width. *Clim. Dyn.* 36, 2419–2439. doi: 10.1007/s00382-010-0945-5

Tolwinski-Ward, S. E., Tingley, M. P., Evans, M. N., Hughes, M. K., and Nychka, D. W. (2015). Probabilistic reconstructions of local temperature and soil moisture from tree-ring data with potentially time-varying climatic response. *Clim. Dyn.* 44, 791–806. doi: 10.1007/s00382-014-2139-z

Tuominen, H., Puech, L., Fink, S., and Sundberg, B. (1997). A radial concentration gradient of indole-3-acetic acid is related to secondary xylem development in hybrid aspen. *Plant Physiol.* 115, 577–585. doi: 10.1104/pp.115.2.577

Tychkov, I. I., Sviderskaya, I. V., Babushkina, E. A., Popkova, M. I., Vaganov, E. A., and Shishov, V. V. (2018). How can the parameterization of a process-based model help us understand real tree-ring growth? *Trees.* 33, 345–357. doi: 10.1007/s00468-018-1780-2

Uggla, C. (2001). Function and dynamics of auxin and carbohydrates during earlywood/latewood transition in Scots pine. *Plant Physiol.* 125, 2029–2039. doi: 10.1104/pp.125.4.2029

Uggla, C., Moritz, T., Sandberg, G., and Sundberg, B. (1996). Auxin as a positional signal in pattern formation in plants. *Proc. Natl. Acad. Sci. U.S.A.* 93, 9282–9286. doi: 10.1073/pnas.93.17.9282

Vaganov, E. A. (1990). "The tracheidogram method in tree-ring analysis and its application," in *Methods of Dendrochronology: Applications in the Environmental Sciences, Vol. 16*, eds E. R. Cook and L. A. Kairiukstis (Dordrecht: Kluwer Academic Publishers; Elsevier Ltd.), 63–76.

Vaganov, E. A., Anchukaitis, K. J., and Evans, M. N. (2011). "How well understood are the processes that create dendroclimatic records? A mechanistic model of the climatic control on conifer tree-ring growth dynamics," in *Dendroclimatology, Vol. 11*, eds M. K. Hughes, T. W. Swetnam, and H. F. Diaz (Dordrecht: Springer Netherlands), 37–75.

Vaganov, E. A., Hughes, M. K., and Shashkin, A. V. (2006). *Growth Dynamics of Conifer Tree Rings: Images of Past and Future Environments*. Berlin; Heidelberg: Ecological Studies; Springer-Verlag.

van der Gaast, W., Sikkema, R., and Vohrer, M. (2018). The contribution of forest carbon credit projects to addressing the climate change challenge. *Clim. Policy* 18, 42–48. doi: 10.1080/14693062.2016.1242056

von Arx, G., and Carrer, M. (2014). ROXAS – A new tool to build centuries-long tracheid-lumen chronologies in conifers. *Dendrochronologia* 32, 290–293. doi: 10.1016/j.dendro.2013.12.001

Weber, R., Schwendener, A., Schmid, S., Lambert, S., Wiley, E., Landhäusser, S. M., et al. (2018). Living on next to nothing: tree seedlings can survive weeks with very low carbohydrate concentrations. *New Phytol.* 218, 107–118. doi: 10.1111/nph.14987

Wessels, C. B., Malan, F. S., Seifert, T., Louw, J., and Rypstra, T. (2015). The prediction of the flexural lumber properties from standing South African-grown *Pinus patula* trees. *Eur. J. For. Res.* 134, 1–18. doi: 10.1007/s10342-014-0829-z

Wetmore, R. H., and Rier, J. P. (1963). Experimental induction of vascular tissues in callus of angiosperms. *Am. J. Bot.* 50, 418–430. doi: 10.1002/j.1537-2197.1963.tb07210.x

Wilkinson, S., Ogee, J., Domec, J.-C., Rayment, M., and Wingate, L. (2015). Biophysical modelling of intra-ring variations in tracheid features and wood density of *Pinus pinaster* trees exposed to seasonal droughts. *Tree Physiol.* 35, 305–318. doi: 10.1093/treephys/tpv010

Wilmking, M., van der Maaten-Theunissen, M., van der Maaten, E., Scharnweber, T., Buras, A., Biermann, C., et al. (2020). Global assessment of relationships between climate and tree growth. *Glob. Chang Biol.* 26, 3212–3220. doi: 10.1111/gcb.15057

Wilson, B. F. (1973). A diffusion model for tracheid production and enlargement in conifers. *Bot. Gazette* 134, 189–196. doi: 10.1086/336703

Wilson, B. F., and Howard, R. A. (1968). A computer model for cambial activity. *For. Sci.* 14, 77–90.

Wilson, J. W., and Wilson, P. M. W. (1961). The position of regenerating cambia-a new hypothesis. *New Phytol.* 60, 63–73. doi: 10.1111/j.1469-8137.1961.tb06240.x

Wilson, R., D'Arrigo, R., Buckley, B., Büntgen, U., Esper, J., Frank, D., et al. (2007). A matter of divergence: tracking recent warming at hemispheric scales using tree ring data. *J. Geophys. Res.* 112, D17103. doi: 10.1029/2006JD008318

Wimmer, R., Strumia, G., and Holawe, F. (2000). Use of false rings in Austrian pine to reconstruct early growing season precipitation. *Can. J. For. Res.* 30, 1691–1697. doi: 10.1139/x00-095

Worbes, M. (1985). Structural and other adaptation to long-term flooding by trees in Central Amazonia. *Amazoniana* 9, 459–484.

Worbes, M. (1995). How to Measure Growth Dynamics in Tropical Trees a Review. *IAWA J.* 16, 337–351. doi: 10.1163/22941932-90001424

Xu, W., Cheng, H., Zhu, S., Cheng, J., Ji, H., Zhang, B., et al. (2021). Functional understanding of secondary cell wall cellulose synthases in *Populus trichocarpa* via the Cas9/gRNA-induced gene knockouts. *New Phytol.* 231, 1478–1495. doi: 10.1111/nph.17338

Yang, B., He, M., Shishov, V., Tychkov, I., Vaganov, E., Rossi, S., et al. (2017). New perspective on spring vegetation phenology and global climate change based on Tibetan Plateau tree-ring data. *Proc. Natl. Acad. Sci. U.S.A.* 114, 6966–6971. doi: 10.1073/pnas.1616608114

Zuidema, P. A., Poulter, B., and Frank, D. C. (2018). A wood biology agenda to support global vegetation modelling. *Trends Plant Sci.* 23, 1006–1015. doi: 10.1016/j.tplants.2018.08.003

Zweifel, R., Haeni, M., Buchmann, N., and Eugster, W. (2016). Are trees able to grow in periods of stem shrinkage? *New Phytol.* 211, 839–849. doi: 10.1111/nph.13995

Zweifel, R., Sterck, F., Braun, S., Buchmann, N., Eugster, W., Gessler, A., et al. (2021). Why trees grow at night. *New Phytol.* 231, 2174–2185. doi: 10.1111/nph.17552

Conflict of Interest: The authors declare that the research was conducted in the absence of any commercial or financial relationships that could be construed as a potential conflict of interest.

Publisher's Note: All claims expressed in this article are solely those of the authors and do not necessarily represent those of their affiliated organizations, or those of the publisher, the editors and the reviewers. Any product that may be evaluated in this article, or claim that may be made by its manufacturer, is not guaranteed or endorsed by the publisher.

frontiers | Frontiers in Plant Science

ORIGINAL RESEARCH
published: 05 April 2022
doi: 10.3389/fpls.2022.872738

Maize Leaf Appearance Rates: A Synthesis From the United States Corn Belt

*Caio L. dos Santos[1], Lori J. Abendroth[2], Jeffrey A. Coulter[3], Emerson D. Nafziger[4], Andy Suyker[5], Jianming Yu[1], Patrick S. Schnable[1] and Sotirios V. Archontoulis[1]**

[1]Department of Agronomy, Iowa State University, Ames, IA, United States, [2]Cropping Systems and Water Quality Research Unit, USDA-ARS, Columbia, MO, United States, [3]Department of Agronomy and Plant Genetics, University of Minnesota, St. Paul, MN, United States, [4]Department of Crop Sciences, College of Agricultural, Consumer and Environmental Sciences, University of Illinois at Urbana–Champaign, Urbana, IL, United States, [5]School of Natural Resources, University of Nebraska-Lincoln, Lincoln, NE, United States

OPEN ACCESS

Edited by:
Zhong-Hua Chen, Western Sydney University, Australia

Reviewed by:
Mukhtar Ahmed, Pir Mehr Ali Shah Arid Agriculture University, Pakistan
Yong He, Institute of Environment and Sustainable Development in Agriculture (CAAS), China

***Correspondence:**
Sotirios V. Archontoulis
sarchont@iastate.edu

Specialty section:
This article was submitted to Plant Biophysics and Modeling, a section of the journal Frontiers in Plant Science

Received: *09 February 2022*
Accepted: *21 March 2022*
Published: *05 April 2022*

Citation:
dos Santos CL, Abendroth LJ, Coulter JA, Nafziger ED, Suyker A, Yu J, Schnable PS and Archontoulis SV (2022) Maize Leaf Appearance Rates: A Synthesis From the United States Corn Belt. Front. Plant Sci. 13:872738. doi: 10.3389/fpls.2022.872738

The relationship between collared leaf number and growing degree days (GDD) is crucial for predicting maize phenology. Biophysical crop models convert GDD accumulation to leaf numbers by using a constant parameter termed phyllochron (°C-day leaf^{-1}) or leaf appearance rate (LAR; leaf °C-day^{-1}). However, such important parameter values are rarely estimated for modern maize hybrids. To fill this gap, we sourced and analyzed experimental datasets from the United States Corn Belt with the objective to (i) determine phyllochron values for two types of models: linear (1-parameter) and bilinear (3-parameters; phase I and II phyllochron, and transition point) and (ii) explore whether environmental factors such as photoperiod and radiation, and physiological variables such as plant growth rate can explain variability in phyllochron and improve predictability of maize phenology. The datasets included different locations (latitudes between 48° N and 41° N), years (2009–2019), hybrids, and management settings. Results indicated that the bilinear model represented the leaf number vs. GDD relationship more accurately than the linear model ($R^2 = 0.99$ vs. 0.95, $n = 4{,}694$). Across datasets, first phase phyllochron, transition leaf number, and second phase phyllochron averaged 57.9 ± 7.5°C-day, 9.8 ± 1.2 leaves, and 30.9 ± 5.7°C-day, respectively. Correlation analysis revealed that radiation from the V3 to the V9 developmental stages had a positive relationship with phyllochron ($r = 0.69$), while photoperiod was positively related to days to flowering or total leaf number ($r = 0.89$). Additionally, a positive nonlinear relationship between maize LAR and plant growth rate was found. Present findings provide important parameter values for calibration and optimization of maize crop models in the United States Corn Belt, as well as new insights to enhance mechanisms in crop models.

Keywords: phenology, phyllochron, leaf appearance rate, maize, crop models

INTRODUCTION

The phenological scale for maize (*Zea mays*) development between emergence and the beginning of the reproductive phase is based on successive appearance and collaring of new leaves (Ritchie et al., 1986; Abendroth et al., 2011). Beginning at the first visible collar, developmental stages are defined by the letter V followed by the number of visible collars. For example, the first visible collar would denote the developmental stage V1, while the fifteenth collar would denote the developmental stage V15 (Ritchie et al., 1986; Abendroth et al., 2011). Phenological stages are an important part of managing cropping systems as several crop management decisions depend upon phenology, such as split nitrogen (N) applications (Slaton et al., 2013). Thus, predicting the number of collared leaves accurately in empirical models or complex crop models is decisive (Tollenaar et al., 2018).

The environmental variable influencing phenological development the most is the temperature (Vinocur and Ritchie, 2001). Consequently, crop development is often expressed as a function of cumulative thermal units, specifically growing degree days (GDD; Soltani and Sinclair, 2012). Many different models have been proposed for the accumulation of GDD, including empirical linear, nonlinear, and process-based functions (Kumudini et al., 2014). These functions differ in number and meaning of parameters, and complexity. Process-based models, such as the one developed by Wilson et al. (1995) and used in the APSIM model (Holzworth et al., 2014), offer a level of precision second only to nonlinear empirical models (Kumudini et al., 2014). Process-based functions have the advantage of maintaining their precision when temperatures are greater than the optimum temperature for maize development, demonstrating its usefulness in future scenarios.

Biophysical crop models convert GDD accumulation to leaf numbers by using parameter values termed phyllochron or leaf appearance rate (LAR). While phyllochron is the cumulative thermal time between the appearance of successive leaves in units of °C-day leaf^{-1} (Wilheim and McMaster, 1995), LAR is the reciprocal of phyllochron in units of leaf °C-day^{-1} (Birch et al., 1998). Phyllochron parameter values are crucial for accurately simulating crop growth and development in models such as APSIM (Holzworth et al., 2014) and DSSAT (Hoogenboom et al., 2019). In maize simulation models, once the number of developed leaves reaches its maximum number, crop models trigger flowering, which is a pivotal phenological stage, as stresses during the flowering period can strongly influence maize yield (Bruce et al., 2002; Wang et al., 2019).

In field conditions and with no nutrient or water limitations, phyllochron has been reported as a constant rate from emergence to flowering (Birch et al., 1998), indicating a linear relationship between leaf number and GDD. However, exponential and bilinear relationships have also been utilized in previous research to describe the relationship between leaf number and GDD (Muchow and Carberry, 1989; Abendroth et al., 2011). The bilinear relationship typically has a high phyllochron value at the beginning of the crop's lifecycle (phase I: slow appearance of leaves) followed by low phyllochron values (phase II: fast appearance of leaves). Common maize phyllochron values for phases I and II are 52 and 36°C-day leaf^{-1} at a base temperature of 8°C (Birch et al., 1998; Van Esbroeck et al., 2008).

Environment, genetics, and management can alter phyllochron values, which can cause inaccuracy in crop model predictions when a constant value is used. For instance, a decrease in radiation has been reported to increase phyllochron (slower appearance of leaves; Birch et al., 1998; Tollenaar, 1999; Tollenaar et al., 2018), while long photoperiods can decrease phyllochron (faster appearance of leaves; Warrington and Kanemasu, 1983). Padilla and Otegui (2005) reported up to 10% variability in phyllochron among 16 maize hybrids and strong coupling between leaf appearance and leaf initiation rate. Van Esbroeck et al. (2008) confirmed the genetic variability in phyllochron in another set of maize hybrids. Muchow and Carberry (1989) and McCullough et al. (1994) reported that water and nitrogen stress can decrease leaf appearance rate. However, the effect of nitrogen stress on leaf appearance is inconsistent across experiments (Vos et al., 2005).

Despite the importance of accurately predicting leaf number and time to flowering, research on maize phyllochron is limited. As a result, most simulation models use phyllochron values developed decades ago. The current literature lacks data for modern maize hybrids and currently we do not know the range of variability that exists in phyllochron to inform crop model parameterization and optimization as well to enable scenarios toward developing future ideotypes (Rötter et al., 2015). For instance, in a comprehensive review of the CERES-Maize model (Jones and Kiniry, 1986) worldwide, Basso et al. (2016) reported a single study that investigated the relationship between leaf number and GDD (Hodges and Evans, 1992). The default phyllochron values in the APSIM classic maize model are 65 (phase I) and 35°C-day leaf $^{-1}$ (phase II). Extensive APSIM model testing in the United States Corn Belt found that leaf appearance occurs at faster rates of 57 (phase I) and 32°C-day leaf $^{-1}$ (phase II; Archontoulis et al., 2014a). Contrastingly, DSSAT works with leaf tips, as opposed to leaf collars, and assumes a constant phyllochron value (Lizaso et al., 2011). The leaf tip method is generally 2.5–5.5 developmental stages ahead of the leaf collar method (Abendroth et al., 2011). The need for research on maize phyllochron is further substantiated by the high turnover rate of maize hybrids in the seed market (Edgerton, 2009).

The current study aims to enhance our knowledge on maize leaf number relative to GDD accumulation by combining and analyzing experimental data from a range of environmental conditions, genotypes, and management settings in the United States Corn Belt. Our first objective is to derive phyllochron parameter values for modern maize hybrids and estimate the range of existing variation in phyllochron values. To do this, we used two frequent used models, simple linear and bilinear. Additionally, we explored environmental and physiological factors that can explain variability in phyllochron. For instance, Tollenaar et al. (2018) proposed adjustments in LAR based on changes in solar radiation. Baumont et al. (2019) identified carbon limitations in wheat LAR, but such a limitation has not been explored in maize. Therefore, our second objective

is to explore whether environmental factors such as photoperiod or radiation can explain variability in LAR and improve predictability of maize phenology, and lastly to investigate whether a direct coupling between development and growth exists in maize.

MATERIALS AND METHODS

We combined 98 datasets with in-season observations of collared leaves from maize experiments in Iowa, Illinois, Nebraska, and North Dakota (**Figure 1**; **Supplementary Table S1**). The experiments were replicated, and each dataset had at least five in-season observations during the leaf production phase. In each experiment, leaf numbers were determined based on the V/R system (Ritchie et al., 1986; Abendroth et al., 2011) from emergence until plants reached their maximum leaf number on intervals ranging from 3 to 7 days. Each of the 98 datasets corresponds to a unique combination of location, year (2005–2015), genotype (relative maturity 73–115-day; seed from companies Pioneer, DeKalb, Stine, and Ex-PVP hybrids), and management practices such as previous crop, planting date, irrigation, and nitrogen rate (**Supplementary Table S1**). The management factors and the hybrids were seldom replicated at different locations and years, limiting our capability to compare the causal effects of genotype, and management practices on LAR. Thus, we analyzed each dataset separately.

Daily weather data including minimum and maximum air temperature, precipitation, and solar radiation per site-year were obtained from local weather stations. Daily photoperiod was calculated using the method described by Pereira et al. (2003). The compiled dataset reflected a wide range of environmental conditions (**Figure 2**). From emergence to flowering, the average minimum air temperature ranged from 12.3 to 20.2°C, the average maximum air temperature from 22.6 to 30.8°C, the average photoperiod from 14.7 to 15.9 h, the cumulative solar radiation from 892.9 to 1485.8 MJm^{-2}, and the cumulative precipitation from 95 to 433 mm (**Figure 1**). The North Dakota sites had the lowest average maximum and minimum air temperatures, while the Iowa sites had the highest.

Beginning at emergence, GDD was calculated as a function of daily average air temperature (Eq. 1; Wilson et al., 1995). We followed the APSIM model approach (Holzworth et al., 2014) in which T_{ave} is the average daily air temperature from

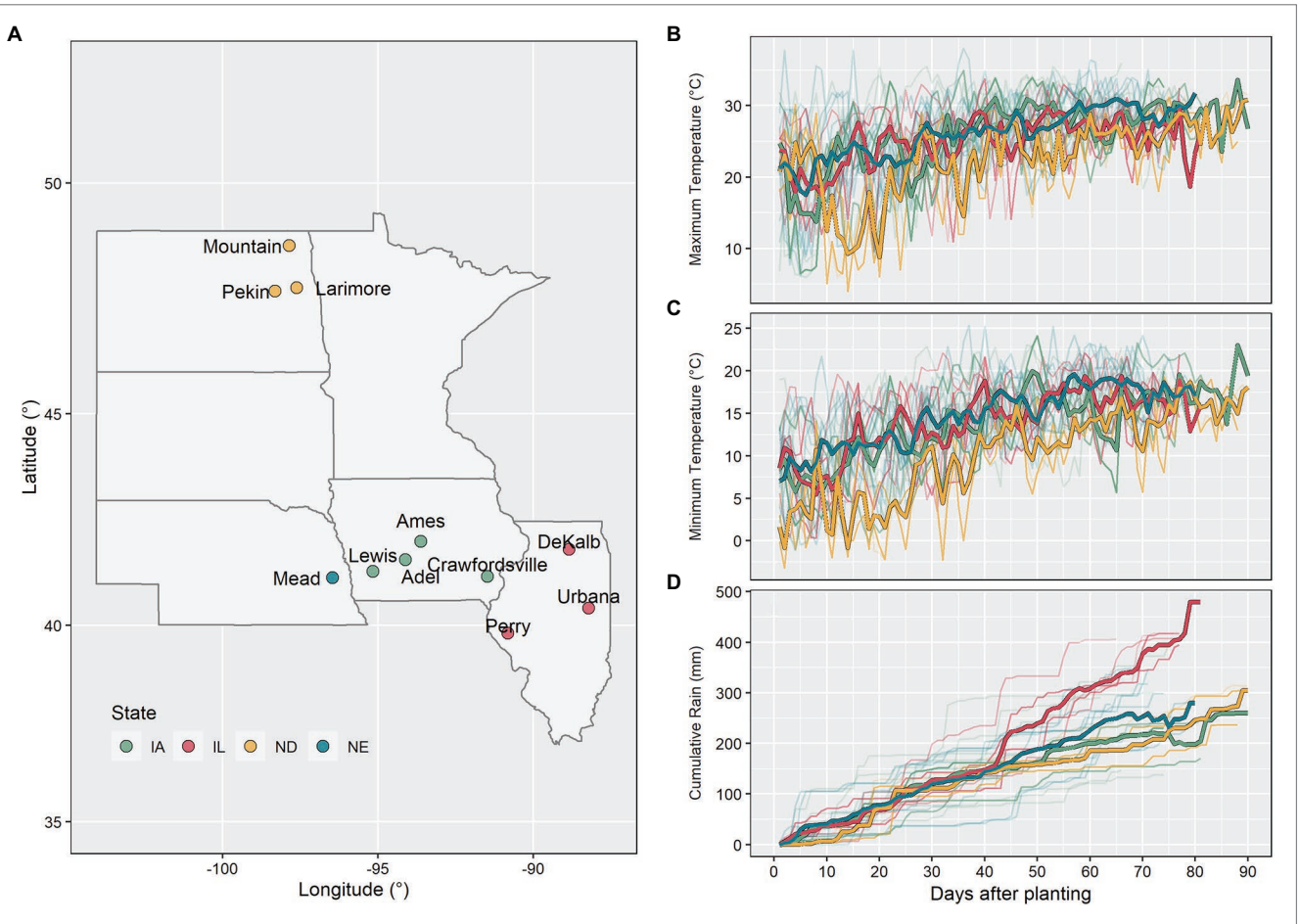

FIGURE 1 | Map with the experimental locations used in this study **(A)**. Maximum temperature **(B)**, minimum temperature **(C)**, and cumulative rain **(D)** between planting and beginning of the reproductive phase for all 98 datasets (thin lines represent individual datasets and thick lines represent the average by state).

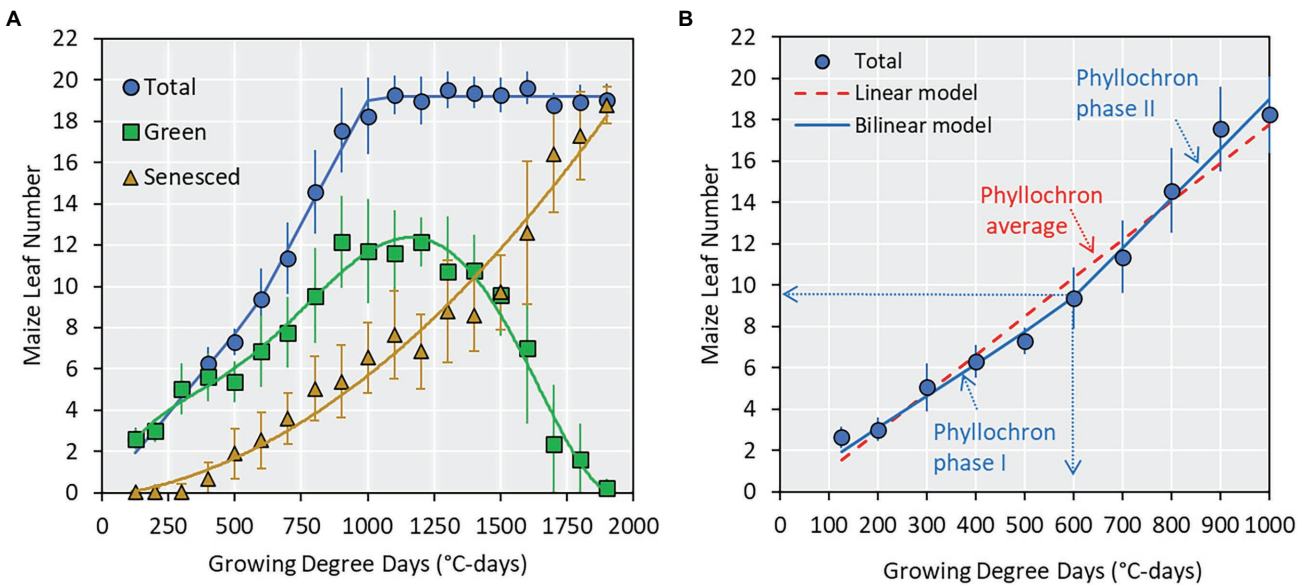

FIGURE 2 | (A) Relationship between collared maize leaf number and growing degree days (GDD; base of 8°C). Points indicate average values ± SE from all datasets and lines are best regression fits (not shown). **(B)** A subset of **(A)** showing total leaf number from emergence to silking and the two prediction models used in this study and the associated parameters. The vertical and horizontal dotted arrows indicate the transition point (e.g., 9 leaf number or 600 GDD) at which phyllochron transitions from phase I to phase II.

eight 3-h interpolations from a third-order polynomial using as inputs minimum and maximum daily temperature.

$$GDD\left(T_{ave},°C\right)=\begin{cases}0,\ T_{ave}\le 0\\ \dfrac{T_{ave}}{1.8},\ 0<T_{ave}\le 18\\ T_{ave}-8,\ 18<T_{ave}\le 34\\ 26-\left[\left(T_{ave}-34\right)\times 2.6\right],\ 34<T_{ave}\le 44\\ 0,\ 44<T_{ave}\end{cases}\quad(1)$$

Data were analyzed in R 4.1 (R Core Team, 2021), and the relationship between GDD and leaf number was investigated by fitting linear and bilinear models. The slope of the linear model represented a single phyllochron value for the entire vegetative period. Conversely, the bilinear model contained a phase I phyllochron value, a transition point, and a phase II phyllochron value (**Figure 2**). Model fit was assessed by three statistical indices: R-squared, modeling efficiency, and relative root mean square error (equations in Archontoulis and Miguez, 2015).

The relationships between model coefficients and environmental variables were investigated in a correlation analysis at different windows after emergence. Average air temperature, photoperiod, radiation, and cumulative precipitation were calculated at different windows between emergence and flowering for each dataset. The examined window began at emergence and increased in 26°C-day intervals (equivalent to 1 biological day) until flowering. For instance, the environmental variables were calculated between 0 and 26°C-day, 0 and 52°C-day, and so on. Then, the beginning of the window was advanced to 26°C-day and the same process was applied. This process was repeated for all subsequent combinations of the beginning and end of the window. A similar search approach was followed by Li et al. (2018) and Guo et al. (2020).

In five out of the 98 total datasets (dataset ID from 6 to 10 in **Supplementary Table S1**), we had detailed information on in-season biomass accumulation, and leaf number (Archontoulis et al., 2020). Each of these random variables were fit to regression exponential models (see Supplementary Materials for the goodness of fit) and the predicted values of these models were resampled every 100°C-day to obtain point values of plant growth rate and LAR. The relationship between instant LAR and instant plant growth rate was investigated using nonlinear Michaelis–Menten models (Archontoulis and Miguez, 2015).

RESULTS

Across all datasets, the average maximum leaf number was 20 leaves (**Figure 2**, range 16–23, **Supplementary Table S1**). The appearance of collared leaves followed a bilinear pattern between emergence and flowering. The maize plant was able to maintain a maximum of 14 green leaves during the vegetative period, with loss of lower canopy leaves beginning at approximately the V6 stage (**Figure 2**). The leaf senescence followed an exponential pattern until physiological maturity. In this study, we use the total leaf number from emergence to flowering (commensurate with the V-stage) and fit two types of models (linear and bilinear; **Figure 2**) to derive phyllochron parameters.

Phyllochron determined by linear models ranged from 36.1 to 54.8°C-day leaf^{-1}, averaging 51.5°C-day leaf^{-1} (**Figure 3**). The coefficient of variation was 9.4%. The first and second phase phyllochron values in the bilinear models ranged from 42.5 to 77.9°C-day leaf^{-1} and from 16.2 to 49.5°C-day leaf^{-1}, averaging 57.9°C-day leaf^{-1} and 30.9°C-day leaf^{-1}, respectively (**Figure 3**). The transition point between the two phases of the bilinear model ranged from 7.4 to 13.4 leaves, averaging 9.8 leaves (**Figure 3**). The phyllochron values and the obtained variability in phyllochron were consistent among locations even though each location included a different set of management factors and hybrids (**Supplementary Table S1**). The coefficient of variation for the phyllochron I, phyllochron II, and the transition point observed across 98 datasets was 13, 19, and 12%, respectively.

The bilinear model estimated V-stages (GDD accumulation) more accurately than the linear model (**Figure 4**). The bilinear model had a 3% higher modeling efficiency, a 40% lower relative root mean square error, and a lower bias compared to the linear model. The residual plots showed that the linear model overpredicted GDD at the beginning and the end of the vegetative period. The model residuals ranged from −2 to 2 leaves (**Figure 4**).

The search for correlation between model coefficients (phyllochron values and transition point) and environmental variables produced inconsistent results (**Figure 5**; **Supplementary Figures S1–S4**). The average radiation calculated between 208 and 520°C-day had a positive correlation with the phase I phyllochron of the bilinear model ($r = 0.69$; **Figure 5**), suggesting that high radiation will slow initial leaf appearance. Further, the average radiation from 182 to 546°C-day had a significant negative relationship with the transition leaf in the bilinear model ($r = -0.52$; **Supplementary Figure S1**) suggesting that high radiation will accelerate the transition from phase I to II phyllochron. Weak correlations were found between radiation and the phyllochron of the linear model or phase II phyllochron of the bilinear model (**Supplementary Figure S1**). Photoperiod had a weak correlation with phyllochron but a strong positive correlation with time to flowering (**Supplementary Figure S2**). The average temperature calculated between the windows 156–208°C-day and 130–234°C-day presented an inverse relationship with phyllochron values of the linear model ($r = -0.5$) and the phase I phyllochron of the bilinear model ($r = -0.66$; **Supplementary Figure S3**). The cumulative precipitation calculated in the window 234–338°C-day presented an inverse relationship with the phase I phyllochron of the bilinear model ($r = -0.54$; **Supplementary Figure S4**), suggesting that water-limited conditions (reduced prediction) slow leaf appearance.

In a subset of the experimental datasets with the detailed in-season biomass observations, the relationship between instant LAR and instant plant growth rate was positive and characterized by a rectangular hyperbola relationship (**Figure 6**). As the instant plant growth rate increased, the instant LAR increased, but as the instant plant growth rate continued to increase beyond 0.3 g plant^{-1} GDD^{-1}, the instant LAR did not increase at the same rate (**Figure 6**).

DISCUSSION

The present study analyzed 98 recent experimental datasets to advance our predictive capabilities and knowledge pertaining to the maize leaf number-GDD relationship. This is important

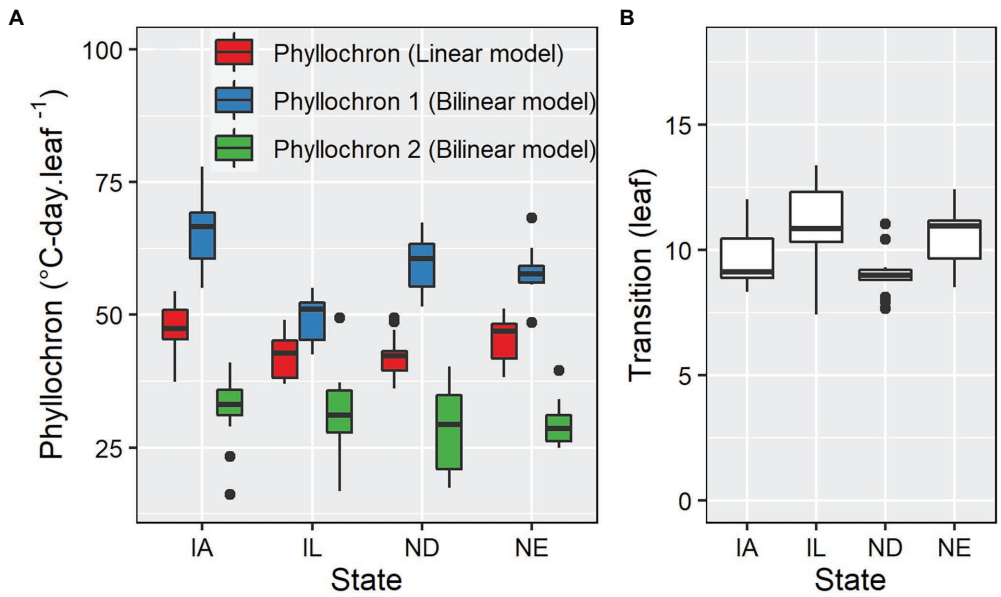

FIGURE 3 | Phyllochron parameter values for linear and bilinear models **(A)** and transition leaf number for the bilinear model **(B)** for datasets in IA ($n = 64$), IL ($n = 13$), ND ($n = 13$), and NE ($n = 8$).

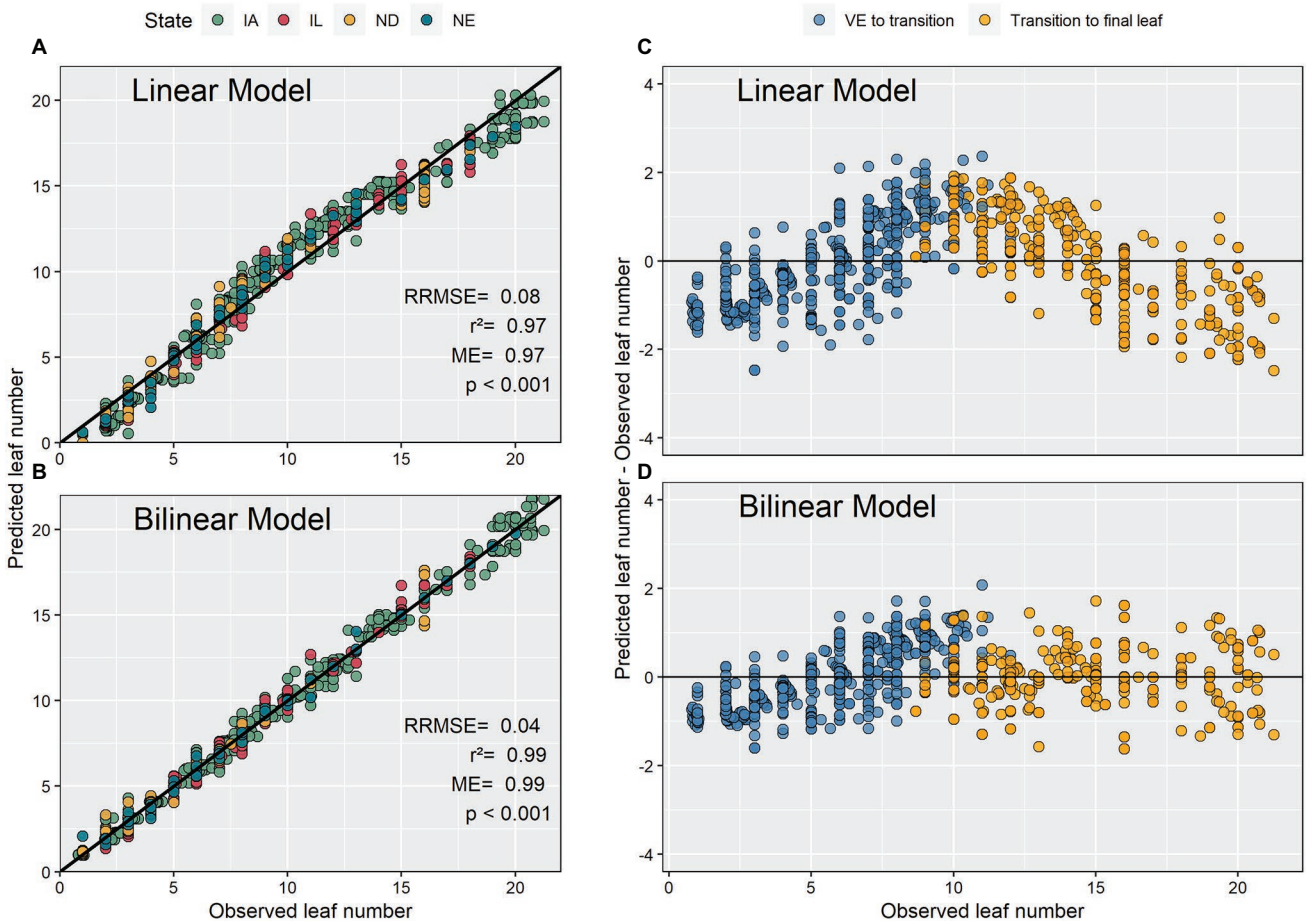

FIGURE 4 | Predicted and observed maize leaf numbers using linear and bilinear models **(A,B)** and their associated residual plots **(C,D)**.

as many crop management decisions are phenology dependent. Between differing methodologies of leaf tips and collared leaves, we focused on collared leaves because leaf collars are most frequently used to determine maize phenology (Ritchie et al., 1986; Abendroth et al., 2011). Our findings indicated that the use of a linear model to describe the leaf number-GDD relationship suffers from systemic over and underestimations, especially around the middle of the V phase (**Figure 4**) and should be used with caution. The bilinear model described the relationship between leaf number and GDD with greater accuracy. These results are consistent with previous research that reported an acceleration in leaf collaring after the V8 to V11 developmental stages (Warrington and Kanemasu, 1983; Zhu et al., 2014). Furthermore, Ritchie and NeSmith (1991) argued that leaf collaring in plants with large leaves occurs more rapidly for the last few leaves as a function of an accelerated expansion of the internodes, when compared to the beginning to the developmental cycle. Similarly, Warrington and Kanemasu (1983) observed an acceleration in leaf appearance rate after the V12 developmental stage and associated this to rapid stem elongation. We theorize that the bilinear model represents the relationship between leaf number and GDD more accurately than linear models by capturing the acceleration in leaf collaring expansion resulting from rapid internode expansion. The use of bilinear models is advised in future studies.

Limitations of our datasets did not allow us to delineate the effect of genotypes or management practices on maize phyllochron. However, our summary analysis provided valuable insights, especially on the range of phyllochron values in modern maize hybrids and correlations with environmental and physiological factors. The range of phyllochron values is pivotal for crop model calibration, and the development of parameter values within physiological limits for optimization (Jones et al., 2011; Archontoulis et al., 2014b). This range of parameter values is also needed for scenario studies and ideotype design. The present study has identified a range of values for phyllochron I (36.1–54.77°C-day leaf^{-1}), phyllochron II (16.2–49.5°C-day leaf^{-1}), and transition point (7.4–13.4 leaves). The values agree well with previous estimates using the same base temperature for GDD accumulation (Birch et al., 1998; Van Esbroeck et al., 2008; Archontoulis et al., 2014a). Caution should be exercised when interpreting literature values as the base temperature and model used affect the magnitude of phyllochron estimates (Padilla and Otegui, 2005).

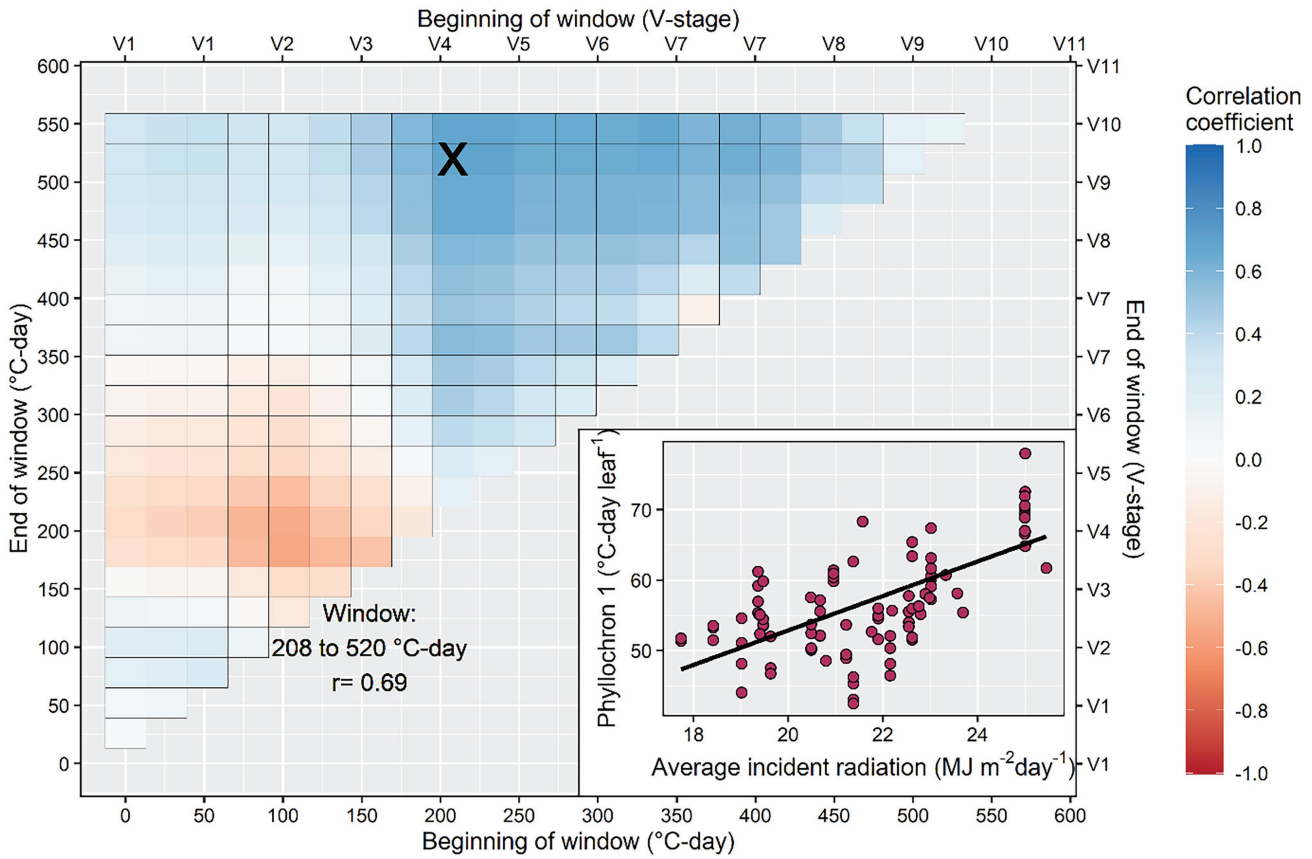

FIGURE 5 | Search process to identify the critical window during the growing season in which average incident radiation determines the rate of leaf appearance. The inset figure shows in detail the strongest relationship between phyllochron and average incident radiation calculated in the interval between 208 and 520°C-day. This interval corresponds to the period between the 4th and the 10th collared leaf, approximately.

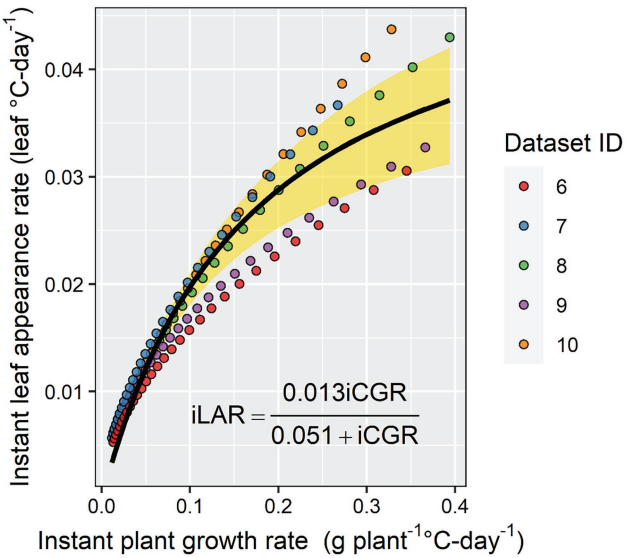

FIGURE 6 | The relationship between instant leaf appearance rate and instant crop growth rate. The yellow shaded area represents the 95% CI.

Across a range of different locations, hybrids, and management practices, we estimated a 13% variability in phyllochron I, a 19% variability in phyllochron II and a 12% variability in the transition point. The observed variability in our study is higher than the 10% variability observed by Padilla and Otegui (2005) in a study exploring 16 maize hybrids. To put that in perspective, a 10% change in phyllochron I and II values can change flowering time by 5 days in central Iowa, United States. Therefore, the observed 13–19% coefficient of variation in phyllochron can alter flowering time by over a week. This can have large consequences in crop models because phyllochron affects plant processes such as leaf area index, biomass partitioning, N uptake, and therefore grain yield. This reinforces the need for accurate estimation of phyllochron to accurately predict leaf number and therefore maize phenology.

Our results indicate the average solar incident radiation between 208 and 520°C-day (roughly, between the V3 and V9 developmental stages) had a positive correlation with the phase I phyllochron (**Figure 5**). This suggests leaf appearance decelerates as radiation increases, contrasting previous research that indicated a faster leaf appearance as radiation increased (Birch et al., 1998; Tollenaar et al., 2018). Part of this discrepancy may be due to our experimental dataset, which contained a range of genotypes and management

settings across temperate environments as opposed to a single factor-location controlled experiment. Another reason may be the period considered for the correlation analysis and the type of model used (linear vs. bilinear). More research is needed in this area. We explored all possible combinations of periods, similarly to Guo et al. (2020) for rice and Li et al. (2018) for sorghum, with the result of V3–V9 developmental stages as the most important. Tollenaar et al. (2018) used the previous week's radiation to adjust phyllochron.

Although previous studies have shown an influence of photoperiods greater than 13 h in leaf appearance rate (Warrington and Kanemasu, 1983), photoperiod did not explain the variability in phyllochron in our analysis. Warrington and Kanemasu (1983) investigated the effect of photoperiod in leaf appearance rate at 18 and 28°C in a controlled environment room and found the effect of photoperiod was present only in the lower temperature regime. In our study, we rarely encountered consecutive days with low temperatures and long days. Additionally, we found that photoperiod was positively correlated with total leaf number (time to flowering) which agrees with previous findings (Tollenaar et al., 2018). Similarly, the average temperature between 0 and 338°C-day presented a strong ($r = -089$; **Supplementary Figure S3**) negative relationship with the number of days to reach flowering which agrees with research by Guo et al. (2020). However, we were not able to confirm the correlation between phyllochron and average temperature reported by Birch et al. (1998).

Baumont et al. (2019) have shown that phyllochron can be limited by carbon availability in wheat. In the present study, we provided evidence that the carbon limitation theory also holds for maize (**Figure 6**). However, our findings are based on in-season estimates and not on whole season estimates as done by Baumont et al. (2019). This topic deserves further research as direct linkages between plant development and growth can stimulate further enhancements in mechanistic crop modeling, i.e., reduce the number of input parameters and empiricism in models. Currently, in crop modeling, development has a substantial influence on growth, but growth has very little influence on development.

CONCLUSION

Our research advanced the leaf number-GDD mathematical relationship and for the first time developed a range of phyllochron values for modern maize hybrids growing across a range of management settings in the United States Corn Belt (98 datasets). The present results can improve the predictability of leaf number, an important attribute for timely crop management, and can assist crop model optimization and scenario tasks. We also identified correlations between phyllochron and radiation, and plant growth rate that can stimulate model improvements. As maize hybrids continue to rapidly change in the market, research on the leaf number–GDD relationship should be regularly updated given the importance of accurately predicting phenology.

DATA AVAILABILITY STATEMENT

The raw data supporting the conclusions of this article will be made available by the authors, without undue reservation.

AUTHOR CONTRIBUTIONS

CdS and SA designed the study. SA, JC, LA, AS, and EN contributed datasets. CdS performed data analysis. All authors contributed to the article and approved the submitted version.

FUNDING

This work was sponsored by NSF (#1830478, #1842097), USDA Hatch project (IOW10480), the Iowa State University Plant Sciences Institute, Stine Seed, and Pioneer Crop Management research award.

ACKNOWLEDGMENTS

The authors thank Zach Fore, Emily Wright, Raziel Ordonez, and Patrick Edmonds, for help with data collection.

SUPPLEMENTARY MATERIAL

The Supplementary Material for this article can be found online at: https://www.frontiersin.org/articles/10.3389/fpls.2022.872738/full#supplementary-material

REFERENCES

Abendroth, L. J., Elmore, R. W., Boyer, M. J., and Marlay, S. K. (2011). *Corn Growth and Development (PMR 1009)*. Ames: Iowa State University.

Archontoulis, S. V., Castellano, M. J., Licht, M. A., Nichols, V., Baum, M., Huber, I., et al. (2020). Predicting crop yields and soil-plant nitrogen dynamics in the US corn belt. *Crop Sci.* 60, 721–738. doi: 10.1002/csc2.20039

Archontoulis, S. V., and Miguez, F. A. (2015). Nonlinear regression models and applications in agricultural research. *Agron. J.* 107, 786–798. doi: 10.2134/agronj2012.0506

Archontoulis, S. V., Miguez, F. E., and Moore, K. J. (2014a). Evaluating APSIM maize, soil water, soil nitrogen, manure, and soil temperature modules in the Midwestern United States. *Agron. J.* 106, 1025–1040. doi: 10.2134/agronj2013.0421

Archontoulis, S. V., Miguez, F. E., and Moore, K. J. (2014b). A methodology and an optimization tool to calibrate phenology of short-day species included in the APSIM PLANT model: application to soybean. *Environ. Model. Softw.* 62, 465–477. doi: 10.1016/j.envsoft.2014.04.009

Basso, B., Liu, L., and Rictchie, J. T. (2016). A comprehensive review of the CERES-Wheat, -Maize and -Rice models' performances. *Adv. Agron.* 136, 27–132. doi: 10.1016/bs.agron.2015.11.004

Baumont, M., Parent, B., Manceau, L., Brown, H. E., Driever, S. M., Muller, B., et al. (2019). Experimental and modeling evidence of carbon limitation of

leaf appearance rate for spring and winter wheat. *J. Exp. Bot.* 70, 2449–2462. doi: 10.1093/jxb/erz012

Birch, C. J., Vos, J., Kiniry, H. J., Bos, H. J., and Elings, A. (1998). Phyllochron responds to acclimation to temperature and irradiance in maize. *Field Crop Res.* 59, 187–200. doi: 10.1016/S0378-4290(98)00120-8

Bruce, W. B., Edmeades, G. O., and Barker, T. (2002). Molecular and physiological approaches to maize improvement for drought tolerance. *J. Exp. Bot.* 53, 13–25. doi: 10.1093/jexbot/53.366.13

Edgerton, M. D. (2009). Increasing crop productivity to meet global needs for feed, food, and fuel. *Plant Physiol.* 149, 7–13. doi: 10.1104/pp.108.130195

Guo, T., Mu, Q., Wang, J., Vanous, A., Onogi, A., Iwata, H., et al. (2020). Dynamic effects of interacting genes underlying rice flowering-time phenotypic plasticity and global adaptation. *Genome Res.* 30, 673–683. doi: 10.1101/gr.255703.119

Hodges, T., and Evans, D. W. (1992). Leaf emergence and leaf duration related to thermal time calculations in ceres-maize. *Agron. J.* 84, 724–730. doi: 10.2134/agronj1992.00021962008400040034x

Holzworth, D. P., Huth, N. I., Zurcher, E. J., Herrmann, N. I., McLean, G., Chenu, K., et al. (2014). APSIM-evolution towards a new generation of agricultural systems simulation. *Environ. Model. Softw.* 62, 327–350. doi: 10.1016/j.envsoft.2014.07.009

Hoogenboom, G., Porter, C. H., Shelia, V., Boote, K. J., Singh, U., White, J. W., et al. (2019). Decision Support System for Agrotechnology Transfer (DSSAT), version 4.7.5. DSSAT Foundation, Gainesville, FL. Available at: https://DSSAT.net (Accessed November 06, 2021).

Jones, J. W., He, J., Boote, K. J., Wilkens, P., Porter, C. H., and Hu, Z. (2011). "Estimating DSSAT cropping system cultivar-specific parameters using Bayesian techniques," in *Methods of Introducing System Models Into Agricultural Research, SSSA Book Series*. eds. L. R. Ahuja and L. Ma (Madison: ASA, CSSA, and SSSA), 365–393.

Jones, C. A., and Kiniry, J. R. (1986). *CERES Maize: A Simulation Model of Maize Growth and Development*. College Station: Texas A&M University Press.

Kumudini, S., Andrade, F. H., Boote, K. J., Brown, G. A., Dzotsi, K. A., Edmeades, G. O., et al. (2014). Predicting maize phenology: intercomparison of functions for developmental response to temperature. *Agron. J.* 106, 2087–2097. doi: 10.2134/agronj14.0200

Li, X., Guo, T., Mu, Q., Li, X., and Yu, J. (2018). Genomic and environmental determinants and their interplay underlying phenotypic plasticity. *Proc. Natl. Acad. Sci. U. S. A.* 115, 6679–6684. doi: 10.1073/pnas.1718326115

Lizaso, J. I., Boote, K. J., Jones, J. W., Porter, C. H., Echarte, L., Westgate, M. E., et al. (2011). CSM-IXIM: A new maize simulation model for DSSAT version 4.5. *Agron. J.* 103, 766–779. doi: 10.2134/agronj2010.0423

McCullough, D. E., Mihajlovic, M., Aguilera, A., Tollenaar, M., and Girardin, P. H. (1994). Influence of N supply on development and dry matter accumulation of an old and a new maize hybrid. *Can. J. Plant Sci.* 74, 471–477.

Muchow, R. C., and Carberry, P. S. (1989). Environmental control of phenology and leaf growth in a tropically-adapted maize. *Field Crop Res.* 20, 221–236. doi: 10.1016/0378-4290(89)90081-6

Padilla, J. M., and Otegui, M. E. (2005). Co-ordination between leaf initiation and leaf appearance in field-grown maize (*Zea mays*): genotypic differences in response of rates to temperature. *Ann. Bot.* 96, 997–1007. doi: 10.1093/aob/mci251

Pereira, A. B., Villa Nova, N. A., and Galvani, E. (2003). Estimation of global solar radiation flux density in Brazil from a single measurement at solar noon. *Biosyst. Eng.* 86, 27–34. doi: 10.1016/S1537-5110(03)00081-3

R Core Team (2021). *R: A Language and Environment for Statistical Computing*. Vienna, Austria: R Foundation for Statistical Computing.

Ritchie, S. W., Hanway, J. J., and Benson, G. O. (1986). How a Corn Plant Develops. Special Report No. 48. Ames, IA: Iowa State University.

Ritchie, J. T., and NeSmith, D. S. (1991). "Temperature and crop development," in *Modeling Plant and Soil Systems, Agronomy Monograph No. 31*. eds. J. Hanks and J. T. Ritchie (Madison, WI: ASA, CSSA, and SSSA), 5–29.

Rötter, R. P., Tao, F., Höhn, J. G., and Palosuo, T. (2015). Use of crop simulation modelling to aid ideotype design of future cereal cultivars. *J. Exp. Bot.* 66, 3463–3476. doi: 10.1093/jxb/erv098

Slaton, N. A., Mozaffari, M., Espinoza, L., Roberts, T. L., Norman, R. J., and Kelley, J. P. (2013). "Nitrogen rate recommendations for corn grown on clayey and loamy soils," in *Wayne E. Sabbe Arkansas Soil Fertility Studies 2013 (Research Series 616)*. ed. N. A. Slaton (Fayetteville: University of Arkansas), 60–67.

Soltani, A., and Sinclair, T. R. (2012). *Modeling Physiology of Crop Development, Growth, and Yield*. Cambridge, MA: CABI.

Tollenaar, M. (1999). Duration of the grain-filling period in maize is not affected by photoperiod and incident PPFD during the vegetative phase. *Field Crop Res.* 62, 15–21. doi: 10.1016/S0378-4290(98)00170-1

Tollenaar, M., Dzotsi, K., Kumudini, S., Boote, K., Chen, K., Hatfield, J., et al. (2018). "Modeling the effects of genotypic and environmental variation on maize phenology: the phenology subroutine of the AgMaize crop model," in *Agroclimatology*. eds. J. L. Hatfield, M. V. Sivakumar and J. H. Prueger (Madison, WI: ASA, CSSA, and SSSA), 173–200.

Van Esbroeck, G. A., Ruiz Corral, J. A., Sanchez Gonzalez, J. J., and Holland, J. B. (2008). A comparison of leaf appearance rates among teosinte, maize landraces and modern maize. *Maydica* 53, 117–123.

Vinocur, M. G., and Ritchie, J. T. (2001). Maize leaf development biases caused by air–apex temperature differences. *Agron. J.* 93, 767–772. doi: 10.2134/agronj2001.934767x

Vos, J., van der Putten, P. E. L., and Birch, C. J. (2005). Effect of nitrogen supply on leaf appearance, leaf growth, leaf nitrogen economy and photosynthetic capacity in maize (*Zea mays* L.). *Field Crop Res.* 93, 64–73. doi: 10.1016/j.fcr.2004.09.013

Wang, Y., Tao, H., Tian, B., Sheng, D., Xu, C., Zhou, H., et al. (2019). Flowering dynamics, pollen, and pistil contribution to grain yield in response to high temperature during maize flowering. *Environ. Exp. Bot.* 158, 80–88. doi: 10.1016/j.envexpbot.2018.11.007

Warrington, I. J., and Kanemasu, E. T. (1983). Corn growth response to temperature and photoperiod II. Leaf-initiation and leaf-appearance Rates1. *Agron. J.* 75, 755–761. doi: 10.2134/agronj1983.00021962007500050009x

Wilheim, W. W., and McMaster, G. S. (1995). Importance of the phyllochron in studying development and growth in grasses. *Crop Sci.* 35, 1–3. doi: 10.2135/cropsci1995.0011183X003500010001x

Wilson, D. R., Muchow, R. C., and Murgatroyd, C. J. (1995). Model analysis of temperature and solar radiation limitations to maize potential productivity in a cool climate. *Field Crop Res.* 43, 1–18. doi: 10.1016/0378-4290(95)00037-Q

Zhu, J., Vos, J., van der Werf, W., van der Putten, P. E. L., and Evers, J. B. (2014). Early competition shapes maize whole-plant development in mixed stands. *J. Exp. Bot.* 65, 641–653. doi: 10.1093/jxb/ert408

Conflict of Interest: PS is a co-lead of the Genomes to Fields Initiative and PI of the USDA-NIFA funded Agricultural Genome to Phenome Initiative. He is co-founder of Data2Bio, LLC; Dryland Genetics, Inc.; EnGeniousAg, LLC; and LookAhead Breeding, LLC. He is a member of the scientific advisory board and a shareholder of Hi-Fidelity Genetics, Inc., and a member of the scientific advisory boards of Kemin Industries and Centro de Tecnologia Canavieira. He is a recipient of research funding from Iowa Corn and Bayer Crop Science.

The remaining authors declare that the research was conducted in the absence of any commercial or financial relationships that could be construed as a potential conflict of interest.

Publisher's Note: All claims expressed in this article are solely those of the authors and do not necessarily represent those of their affiliated organizations, or those of the publisher, the editors and the reviewers. Any product that may be evaluated in this article, or claim that may be made by its manufacturer, is not guaranteed or endorsed by the publisher.

frontiers | Frontiers in Plant Science

ORIGINAL RESEARCH
published: 15 April 2022
doi: 10.3389/fpls.2022.827497

Ecological Niche Shifts Affect the Potential Invasive Risk of *Rapistrum rugosum* (L.) All. in China

Xiaoqing Xian[1†], Haoxiang Zhao[1†], Rui Wang[1], Huijie Qiao[2], Jianyang Guo[1], Guifen Zhang[1], Wanxue Liu[1] and Fanghao Wan[1]*

[1] State Key Laboratory for Biology of Plant Diseases and Insect Pests, Institute of Plant Protection, Chinese Academy of Agricultural Sciences, Beijing, China, [2] Institute of Zoology, Chinese Academy of Sciences, Beijing, China

Ecological niche is a key concept that links species distributions. Ecological niche shifts are expected to affect the potential invasive risk of alien species. *Rapistrum rugosum* is an invasive agricultural weed in many countries. Wild populations of *R. rugosum* have been recorded in China, representing a great threat to the regional crops. Based on distribution records from different regions and relevant environmental variables, the present study predicted the potential distribution and estimated the invasive risk of *R. rugosum* in China. Ecological niche shifts strongly affected the potential invasive risk of *R. rugosum* in China. The two most important variables were annual temperature range (Bio7) and mean temperature of the coldest quarter (Bio11). The total suitable habitat for the species covered an area of 287.53×10^4 km^2 and was mainly distributed in Southwest, Southeast, and Central China. Australia, Canada, Brazil, the United States, and Argentina accounted for over 90% of the inspection records of *R. rugosum* from Chinese entry ports during 2015–2018. The intercepted *R. rugosum* was frequently mixed in *Glycine max* (L.) Merr., *Hordeum vulgare* L., linseed, *Triticum aestivum* L., and *Sorghum bicolor* (L.) Moench. Moreover, 80% interceptions were recorded from Tianjin, Guangdong, Nanjing, and Chengdu customs. Climatic conditions do not limit the establishment capability of *R. rugosum* in China. Our results provide a theoretical reference for the development of monitoring and control measures for this invasive weed.

Keywords: ***Rapistrum rugosum*, ecological niche, suitable habitat, MaxEnt model, invasive risk**

OPEN ACCESS

Edited by:
Lars Hendrik Wegner, Foshan University, China

Reviewed by:
Enrico Vito Perrino, International Centre for Advanced Mediterranean Agronomic Studies, Italy
Lefort François, University of Applied Sciences and Arts of Western Switzerland, Switzerland

***Correspondence:**
Wanxue Liu
liuwanxue@caas.cn

† These authors have contributed equally to this work

Specialty section:
This article was submitted to Plant Biophysics and Modeling, a section of the journal Frontiers in Plant Science

Received: *02 December 2021*
Accepted: *17 March 2022*
Published: *15 April 2022*

Citation:
Xian X, Zhao H, Wang R, Qiao H, Guo J, Zhang G, Liu W and Wan F (2022) Ecological Niche Shifts Affect the Potential Invasive Risk of Rapistrum rugosum (L.) All. in China. Front. Plant Sci. 13:827497. doi: 10.3389/fpls.2022.827497

INTRODUCTION

Biological invasions, as part of global change, are considered to be one of the important factors contributing to the decline in global biodiversity as well as high economic losses to the society (Mačić et al., 2018; Essl et al., 2020; Pyšek et al., 2020; Diagne et al., 2021; Pisani et al., 2021; Stinca et al., 2021). In recent years, China has become one of the countries that are most seriously affected by biological invasions worldwide (Yan et al., 2017). To date, more than 600 Invasive Alien Species (IAS) have been identified in China, of which more than 45% were invasive alien plants (Wan et al., 2017). *Rapistrum rugosum* (L.) All., a new reported invasive alien plant in China, belongs to the Brassicaceae family, and it is a relatively common weed in agricultural fields in

wheat- and corn-growing regions (Pardo et al., 2019; Ali et al., 2020). *R. rugosum* is profusely branched and possesses a well-developed root system. In plots where wheat was mixed with *R. rugosum*, the former was at a competitive disadvantage, and its growth and yield were severely affected. In Australia, competition from *R. rugosum* led to 72–78% yield reduction in wheat (Manalil and Chauhan, 2019). *R. rugosum* can grow up to 1–5-feet-tall and bears a taproot that can become rather large (Lemke and Worthington, 1991). It can successfully outcompete native plant species, forming a vegetative cover of a single species (Manalil et al., 2018). *R. rugosum* originated in Central Europe, the Mediterranean, northern Africa, and western and temperate Asia (Brown, 1878), from where it has dispersed to the Americas, Oceania, and East Asia (Global Biodiversity Information Facility, 2021). The oval, dark brown, smooth, and minute seeds of *R. rugosum* can be dispersed over long distances aboard logs, other seeds, and contaminated materials. China has 306 international ports of entry (Cao, 2020). Information from different plant quarantine Customs revealed that over 100 interceptions of *R. rugosum* have been made each year since 2016. *R. rugosum* has been detected in the containers and seeds of incoming shipments to China.

Recently, wild populations of *R. rugosum* were discovered in China, representing a great potential threat to the regional crops. On Chinese mainland, *R. rugosum* was recorded for the first time in the Xi'an City (Shaanxi Province, northwestern China); it was found growing in patches and showed the tendency to disperse rapidly (Xun et al., 2020). Majority of the recent studies on *R. rugosum* mainly focused on its biological characteristics (Hichri et al., 2019), herbicide resistance (Hatami et al., 2016), and control measures (Simmons, 2005); however, only a few studies have assessed its global invasive risk in habitats through species distribution modeling. Risk assessment and early warning are the most effective strategies to prevent the introduction and dispersal of IAS (Greenberg et al., 2012). For IAS, a stable ecological niche is an invasive area that is identical to the region of origin (Liu et al., 2020). Meanwhile, a shifted ecological niche is different from the region of origin. However, it is impossible to accurately predict the distribution of IAS in the invasive area based on habitat information of its origin (Fernández and Hamilton, 2015). Although predictions of species distribution modeling are reliable in the model-fitted area, the model simulation capacity must be interpreted cautiously when switching to a new prediction area (Broennimann and Guisan, 2008; Beaumont et al., 2009; Tang et al., 2021). When IAS invade new habitats, they gradually adapt to the given conditions, expand their ecological niche, and adversely affect agroecosystems and biodiversity (Hejda et al., 2015). Thus, ecological niche models cannot predict ecological niches based solely on the information of species origin.

Species distribution models (SDMs) have been playing an increasingly important role in predicting the potential geographic distribution of species, particularly IAS (Srivastava et al., 2019; Thomas et al., 2021). The MaxEnt model uses species distribution records and the corresponding environmental variables in a given habitat, and this model is suitable for predicting the potential geographic distribution of species (Elith et al., 2011; Liu et al., 2017; Adhikari et al., 2019). In recent years, the application of the MaxEnt model has expanded not only to the examination of ecological degradation processes, such as biological invasions (Yeh et al., 2021) and ecological damage (Venne and Currie, 2021), but also to the potential risk assessment of IAS (Simpson and Prots, 2013). "kuenm," an R package in the ecological niche model (ENM), uses MaxEnt as the modeling algorithm to automate the calibration of models, creation of optimized models and their transfer and evaluations, as well as assessment of extrapolation risks (Cobos et al., 2019). The MaxEnt model, combined with ArcGIS, has been widely used to identify areas at a high risk of IAS invasion (Kariyawasam et al., 2019) and to predict the impacts of climate change on IAS, enabling scientists and policymakers to establish effective and early warning strategies.

To this end, based on the optimized MaxEnt model, related environmental variables, and distribution records of *R. rugosum* in native, invasive, and native + invasive regions, the present study simulated the invasion risk habitats of *R. rugosum* in China. For the simulated risk area in China, we speculated that the ecological niche of *R. rugosum* would shift based on the distribution records of native, invasive, or native + invasive. Therefore, the risk area identified based on the native and invasive distribution records of *R. rugosum* was integrated as the final result of the invasion risk habitat in China. Further, the environmental variables that significantly affect the invasion risk habitats of *R. rugosum* in China were clarified. Finally, the specific distribution range in the invasion risk habitats of *R. rugosum* in China was explored to predict its dispersal risk and propose early warning measures.

MATERIALS AND METHODS

Distribution Records of *Rapistrum rugosum*

The distribution records of *R. rugosum* were collected from the Global Biodiversity Information Facility (GBIF[1]) and Invasive Species Compendium (ISC) of the Center for Agriculture and Bioscience International (CABI[2]). A total of 31.585 distribution records were obtained. Duplicate records and distribution points without detailed geographic information were removed using ENMtools (Warren et al., 2010). Regarding the resolution of the environmental variables, only one distribution point was retained within each 5 km × 5 km raster. Finally, a total of 8.938 valid distribution records of *R. rugosum* were retained. Among these, respectively, 6.259 and 2.679 distribution records were in native and invasive areas (**Figure 1**).

Environmental Variables, Mapping, and Modeling

Raster files for 19 bioclimatic variables and elevation at a resolution of 2.5′ were downloaded from the World

[1]https://www.gbif.org/

[2]https://www.cabi.org/isc

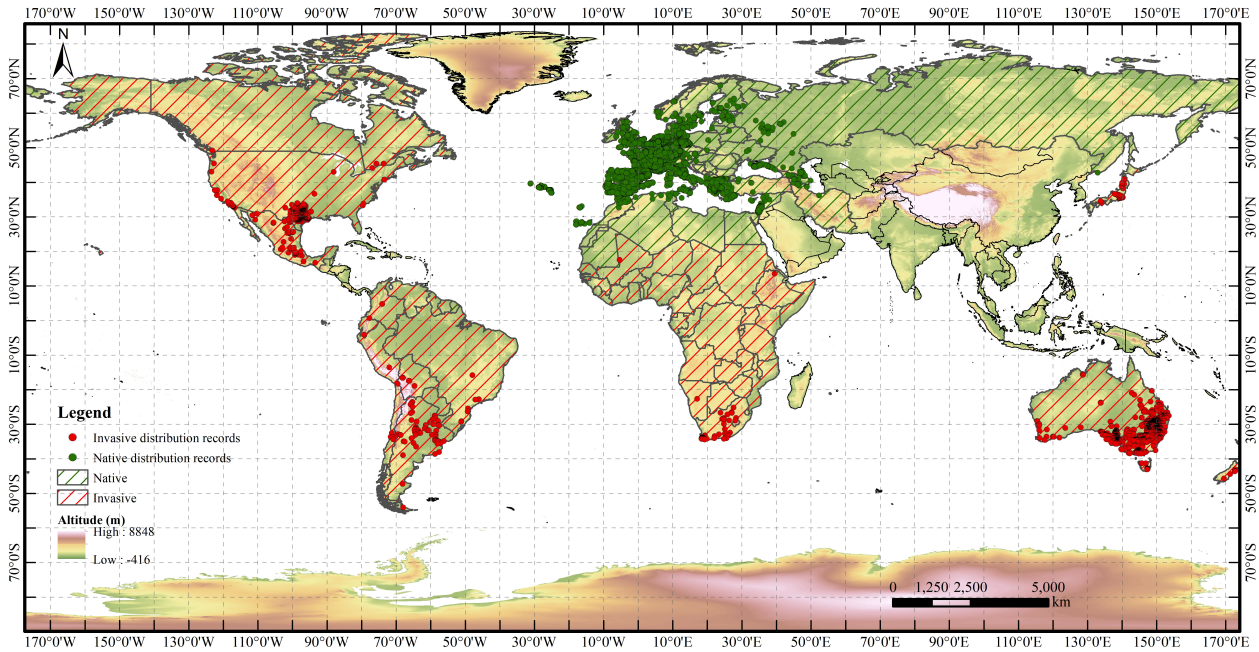

FIGURE 1 | World distribution records of *Rapistrum rugosum*. Red and green points indicate invasive and native distribution records, respectively.

Climate Database Version 2.1[3]. This database includes detailed meteorological information from meteorological stations around the world during 1970–2000. Soil data were obtained from the Harmonized World Soil Database v1.2 (Fischer et al., 2008). Land use data for China in 2020 were downloaded from the Resource and Environment Science and Data Center[4]. All the data were converted to a resolution of 2.5′ (the same as that of the bioclimatic variables; **Supplementary Table 1**). The world administrative map was downloaded from the National Earth System Science Data Center, National Science and Technology Infrastructure of China[5]. MaxEnt 3.4.4 is freely available online[6].

Correlation analysis of the 19 bioclimatic variables was performed using ENMtools to eliminate multivariate collinearity (Yang et al., 2013). The bioclimatic variables were selected through two steps: (1) the bioclimatic variables were imported into the MaxEnt model three times, and the bioclimatic variables with zero contribution were removed; and (2) all bioclimatic variables with contribution rates greater than zero were selected for correlation analysis using ENMtools. When the correlation coefficient of two bioclimatic variables was greater than or equal to 0.8 (**Supplementary Figure 1**), the one with the highest contribution rate was retained. The final environmental variables were retained for MaxEnt modeling (**Supplementary Tables 2–4**).

MaxEnt Model Calibration

MaxEnt is an ecological niche model based on the theory of maximum entropy based on the Java platform (Phillips et al., 2006). The most important parameters of the MaxEnt model are the feature classes (FCs) and regularization multiplier (RM). FC and RM calibration can significantly improve the prediction accuracy of the MaxEnt model. In the present study, the MaxEnt model calibrated by setting different combinations of FCs and incremental RMs. FCs include five basic parameters, namely linear (L), quadratic (Q), product (P), threshold (T), and hinge (H), and there are 31 different combinations of FCs (Radosavljevic and Anderson, 2014). Generally, RM is set from 0.1 to 4 with an interval of 0.1. A total of 40 RM values were used in the present study. The "kuenm" package in R was used to create 1.240 candidate models. Finally, using R, significant models with the omission rate of > 5% and delta Akaike Information Criterion (AICc) value of <2 (Cobos et al., 2019) were selected. The candidate model with the smallest delta AICc was selected for the final analysis.

Model Settings and Evaluation

Following model calibration, 25% of the distribution records were used to test the MaxEnt model, and the remaining 75% were used to train the optimized MaxEnt model. In total, maximum 500 iterations and 10.000 background points were used. The importance of the environmental variables limiting *R. rugosum* distribution was assessed using the contribution rates and the Jackknife method. The receiver operating characteristic (ROC) curve and area under the curve (AUC) were used to test the accuracy of the model results. The ROC curve is an acceptance curve with the horizontal coordinate indicating the false positive

[3]http://www.worldclim.org

[4]https://www.resdc.cn/

[5]http://www.geodata.cn

[6]https://biodiversityinformatics.amnh.org/open_source/maxent/

rate (1 - specificity) and the vertical coordinate indicating the true positive rate (1 - omission rate) (Fan et al., 2006). Because the AUC values are not affected by the thresholds, it is an objective assessment of the model. An AUC value closer to 1 indicates that the model results are better. The evaluation criteria of model simulation accuracy were classified into three levels: poor (AUC $\leq$ 0.50), acceptable (0.5 $<$ AUC $\leq$ 0.80), and excellent (0.80 $<$ AUC $\leq$ 1.00) (Swets, 1988).

The maximum value of 10 replications was selected as the final MaxEnt model result in the present study. The ASCII raster layers were generated based on the logical value (P) of the presence probability of *R. rugosum*, ranging from 0 to 1. A higher *P* values indicates a higher probability of the presence of *R. rugosum*. The results were converted to a raster file and extracted using the administrative division map of China in ArcGIS. Then, the suitable habitats were ranked and visualized. The suitable areas were classified into four classes: highly suitable habitat ($0.5 < P \leq 1.0$), moderately suitable habitat ($0.3 < P \leq 0.5$), slightly suitable habitat ($0.1 < P \leq 0.3$), and unsuitable habitat ($0.0 \leq P \leq 0.1$). Grids in each class were counted, and the proportion of suitable habitats in each class was calculated. Next, the precise invasion risk area of *R. rugosum* was determined by removing the suitable habitats of *R. rugosum* in water and unused land as the final result. The ecological niche overlap of *R. rugosum* was expressed in terms of the Schoener's *D* (*D*) value in ENMtools. A higher Schoener's *D* indicates a greater overlap of the ecological niches (Warren et al., 2010).

RESULTS

Feature Classes and Regularization Multiplier of the Optimized Model

The results of R analysis revealed that 1.160 of the 1.240 selected candidate models were statistically significant. The optimized model was selected based on the smallest delta AICc value. Based on the native distribution records of *R. rugosum*, the FCs were L and Q and the RM was 0.7 in the optimized model. Based on the invasive distribution records of *R. rugosum*, the FCs were L, P, T, and H and the RM was 0.4 in the optimized model. Based on the native + invasive distribution records of *R. rugosum*, the FCs were L, P, T, and H and the RM was 1.3 in the optimized model (**Figure 2**). Based on the native, invasive, and native + invasive distribution records of *R. rugosum*, the suitable habitats of *R. rugosum* were simulated using the MaxEnt model under current climatic conditions and the mean AUC values of, respectively, 0.813, 0.910, and 0.789 were obtained for the MaxEnt models **Supplementary Figure 2**). Model fitting based on the native or invasive distribution records of *R. rugosum* was excellent and that based on both native and invasive distribution records was acceptable.

Significant Environmental Variables

Regularized training gain was used to determine the significant environmental variables, which were modeled in MaxEnt based on native and invasive distribution records of *R. rugosum*. Jackknife analysis revealed that the two most significant influencing factors for regularized training gain with a single variable were annual temperature range (Bio7) and mean temperature of the coldest quarter (Bio11). These two environmental variables provided information that the other environmental variables did not (**Figure 3**).

In the present study, the relationship between the presence probability of *R. rugosum* and environmental variables was determined based on the response curves of environmental variables to the presence probability (**Figure 4**). When the presence probability of *R. rugosum* was greater than the threshold of highly suitable habitat classification (0.5), the corresponding interval was suitable for the growth of *R. rugosum*. The annual temperature range suitable for the growth of *R. rugosum* was 1.2–29.5°C, and the mean temperature of the coldest quarter suitable for the growth of *R. rugosum* was 8.1–13.4°C.

Ecological Niche Shifts of *Rapistrum rugosum*

The suitable habitats and ecological niches of *R. rugosum* differed based on invasive, native, and native + invasive distribution records (**Figure 5**; **Table 1** and **Supplementary Table 5**). Based on the invasive distribution records (**Figure 5A**), the area of the highly suitable habitat was 80.55×10^4 km^2, accounting for 8.39% of Chinese mainland, and these habitats were mainly distributed in southern and southeastern China. The area of the moderately suitable habitat was 60.35×10^4 km^2, accounting for 8.39% of Chinese mainland, and these habitats were mainly distributed around highly suitable habitats.

Based on the native distribution records (**Figure 5B**), the area of the highly suitable habitat was 21.56×10^4 km^2, accounting for 2.25% of Chinese mainland, and these habitats were mainly distributed in Zhejiang, Fujian, and Hainan provinces. The area of the moderately suitable habitat was 153.69×10^4 km^2, accounting for 16.01% of Chinese mainland, and these habitats were mainly distributed in Southwest, Southeast, and Central China.

Based on the native + invasive distribution records (**Figure 5C**), the area of the highly suitable habitat was 0.02×10^4 km^2, and these habitats were only distributed in Shanghai City. The area of the moderately suitable habitat was 31.33×10^4 km^2, accounting for 3.26% of Chinese mainland, and these habitats were mainly distributed in Jiangsu, Anhui, Hubei, Hunan, Guizhou, and Yunnan provinces.

The ecological niche centroid of *R. rugosum* was located in Hunan Province (**Figure 5D**). The highest ecological niche overlap (Schoener's $D = 0.92$) was observed in the simulation results based on the invasive and native + invasive distribution records of *R. rugosum*, while the lowest overlap (Schoener's $D = 0.25$) was between the native distribution records of *R. rugosum* (**Table 1**).

In summary, the results based on the invasive and native distribution records were consistent with the invasion risk habitats of *R. rugosum* in China, while the results based on the native + invasive distribution records were less consistent. Overall, the prediction of the risk habitats based on different

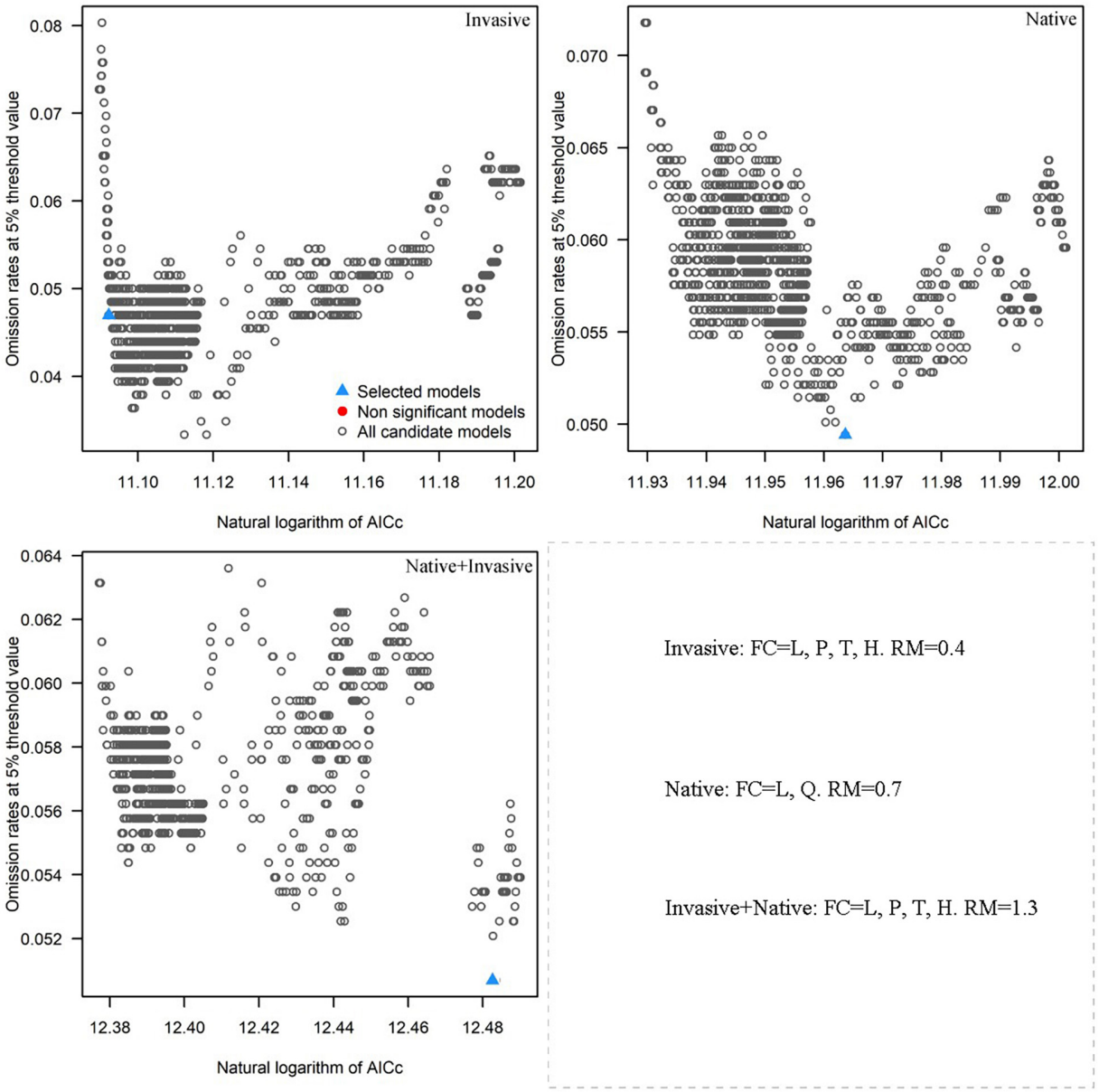

FIGURE 2 | Omission rates and AICc values for all, non-significant, and selected "best" candidate models based on the invasive, native, and native + invasive records of *Rapistrum rugosum*.

distribution records revealed that the ecological niches of *R. rugosum* have shifted.

Interception Records of *Rapistrum rugosum* at Chinese Ports

There have been 1.061 inspection records of *R. rugosum* from Chinese entry ports during 2015–2018 (**Figure 6**). The top five countries of origin associated with over 50 interceptions were Australia, Canada, Brazil, the United States, and Argentina, together accounting for >90% of all records. Of the *R. rugosum* interceptions recorded from imported commodities, 37.5% were from *Glycine max* (L.) Merr., 20.9% from *Hordeum vulgare* L., 17.3% from linseed, 9.5% from *Triticum aestivum* L., 7.2% from *Sorghum bicolor* (L.) Moench, and the remaining 7.6% from other goods. The frequent *R. rugosum* interceptions were recorded from 17 of 42 customs directly under the General Administration of Customs, China. Overall, 80% interception records were primarily from Tianjin, Guangdong, Nanjing, and Chengdu customs (more than 50 records each). Given the diversity of the countries of origin and commodities of *R. rugosum* interceptions at Chinese customs, the risk areas of this IAS in China must be first identified based on the invasive or native distribution records and then subjected to overlap analysis.

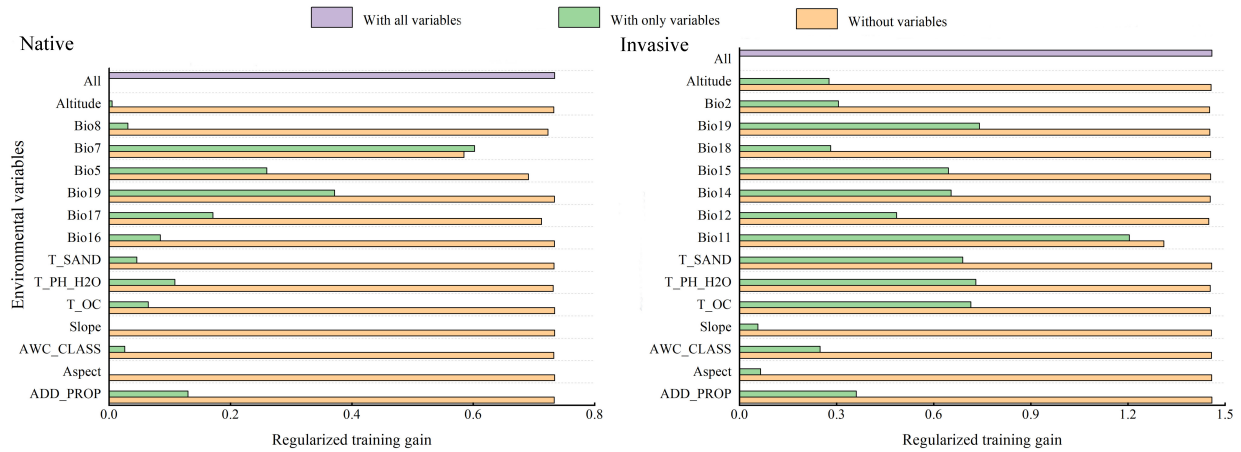

FIGURE 3 | Regularized training gains of environmental variables using the Jackknife method in MaxEnt based on the native and invasive distribution records of *Rapistrum rugosum*.

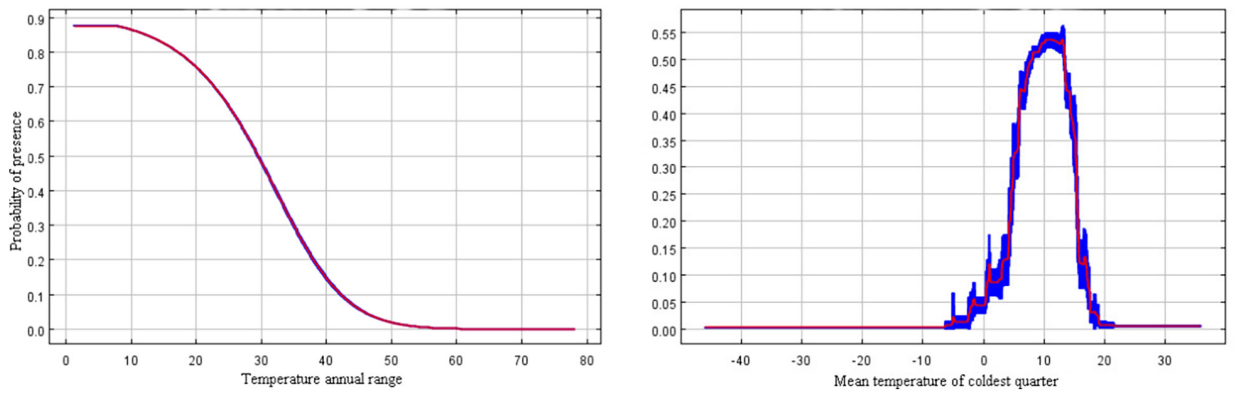

FIGURE 4 | Response curves of the presence probability of *Rapistrum rugosum*.

Potential Invasive Risk Areas of *Rapistrum rugosum* in China

The area of the highly suitable habitat of *R. rugosum* in China was 91.09×10^4 km^2, accounting for 9.49% of Chinese mainland, and these habitats were mainly distributed in Anhui, Zhejiang, Fujian, Jiangxi, Hunan, Guangdong, Hainan, Sichuan, Yunnan, Guizhou, Guangxi, Xizang, Shanghai, Chongqing, and Taiwan (**Figure 7**). The area of the moderately suitable habitat was 101.79×10^4 km^2, accounting for 10.6% of Chinese mainland, and these habitat was mainly distributed around the highly suitable habitat. The area of the total suitable habitat was 287.53×10^4 km^2, accounting for 29.95% of Chinese mainland.

DISCUSSION

MaxEnt Model Development Using "kuenm"

Model calibration determines the combination of parameters that best represents the result by finding the best fit with the distribution records and environmental variables. In the present study, the R package "kuenm" was used to create optimized models based on model significance, performance, and simplicity. This approach helps prevent the overinterpretation of model outcomes (Cobos et al., 2019). "kuenm" has been previously used to optimize the MaxEnt model and predict the distribution of *Zanthoxylum bungeanum* in China; the optimized model reduced the overfitting degree, and the MaxEnt model fit was excellent (Zhuo et al., 2020). In the present study, the mean AUC values of the optimized MaxEnt models based on native, invasive, and native + invasive distribution records of *R. rugosum* were 0.813, 0.910, and 0.789, respectively, and the MaxEnt model fit was acceptable to excellent. Model optimization significantly improved the accuracy of the results.

Ecological Niche Shifts for the Native and Invasive Populations of *Rapistrum rugosum*

Ecological niches play pivotal roles in understanding the patterns of species distribution (Liu et al., 2020). The native ecological

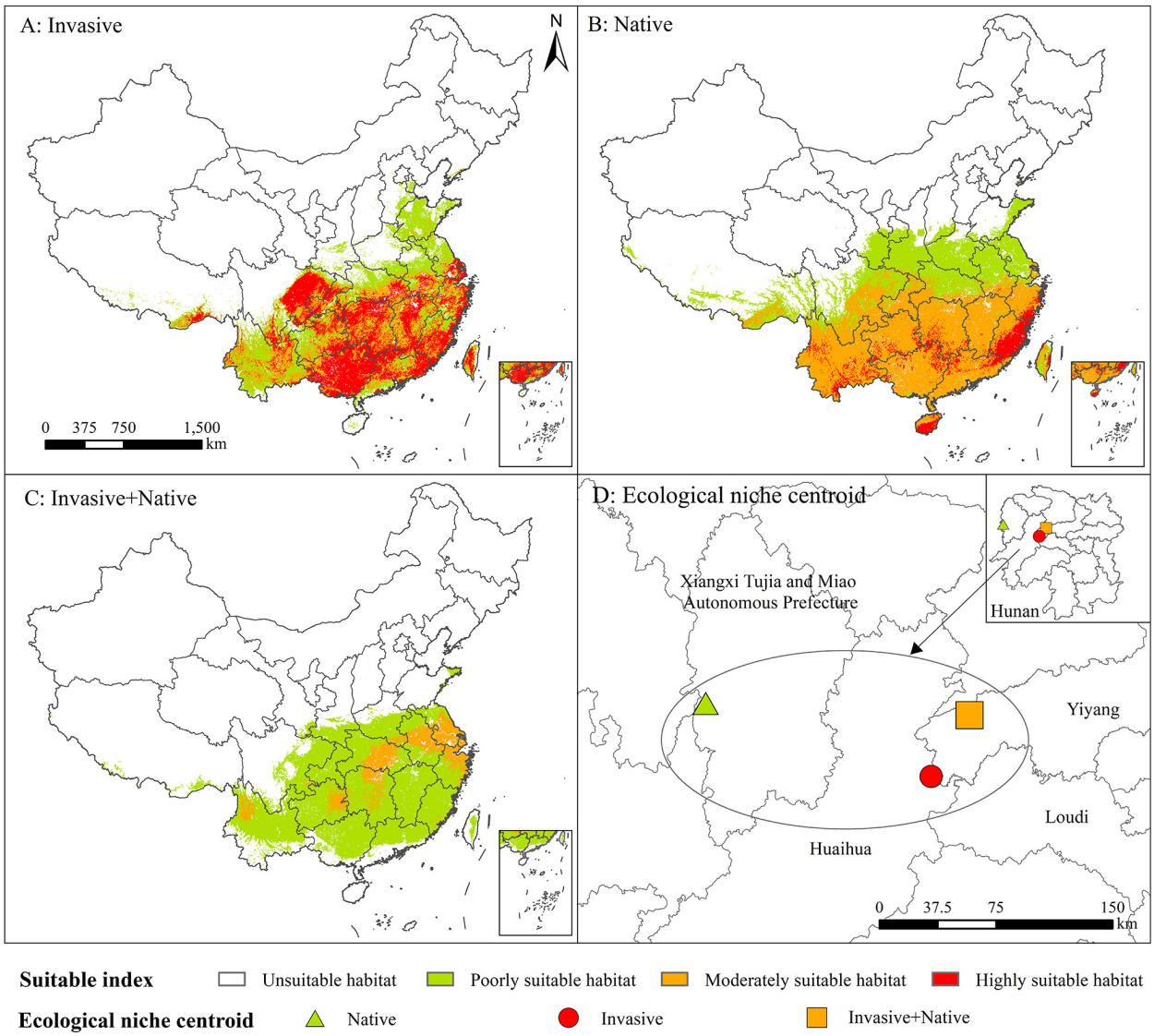

FIGURE 5 | Potential geographic distribution of *Rapistrum rugosum* based on the native **(A)**, invasive **(B)**, and native + invasive **(C)** distribution records and the ecological niche centroid of *R. rugosum* **(D)**.

TABLE 1 | Ecological niche overlap of *Rapistrum rugosum*.

Ecological niche overlap	Native + Invasive	Invasive	Native
Native + Invasive	1	0.92	0.25
Invasive	0.92	1	0.49
Native	0.25	0.49	1

niche of a species does not encompass all suitable habitats for its growth. The ecological niche of a species, particularly an IAS, is expected to shift if it is allowed to disperse freely (David and Menges, 2011). In 1785, *R. rugosum* was first reported in France, and thereafter, it rapidly spread over Europe and the Mediterranean region (Bruno and Solène, 2016). *R. rugosum* invaded the United States in 1883 and rapidly expanded throughout the Americas. Thus, it is considered a problematic agricultural weed worldwide. In the 2000s, *R. rugosum* was recorded from North and South America, southern Africa, East Asia, and Oceania (Staten Island Museum, 2021). In 2019, *R. rugosum* newly invaded northwestern China, without any information on its origin. The interception records indicated that the source countries of *R. rugosum* were home to both native and invasive populations of this weed. Invasive species can adapt to new environments in various ways and expand their ecological niches spatially, leading to inconsistencies between the ecological niches of the invasive and native populations (Zenni et al., 2014). The differences in phenology between the invasive and native populations of plants lead to a shift in the ecological niche of IAS (Wolkovich and Cleland, 2011). *R. rugosum* occupies widely variable climatic and ecological niches. The MaxEnt model

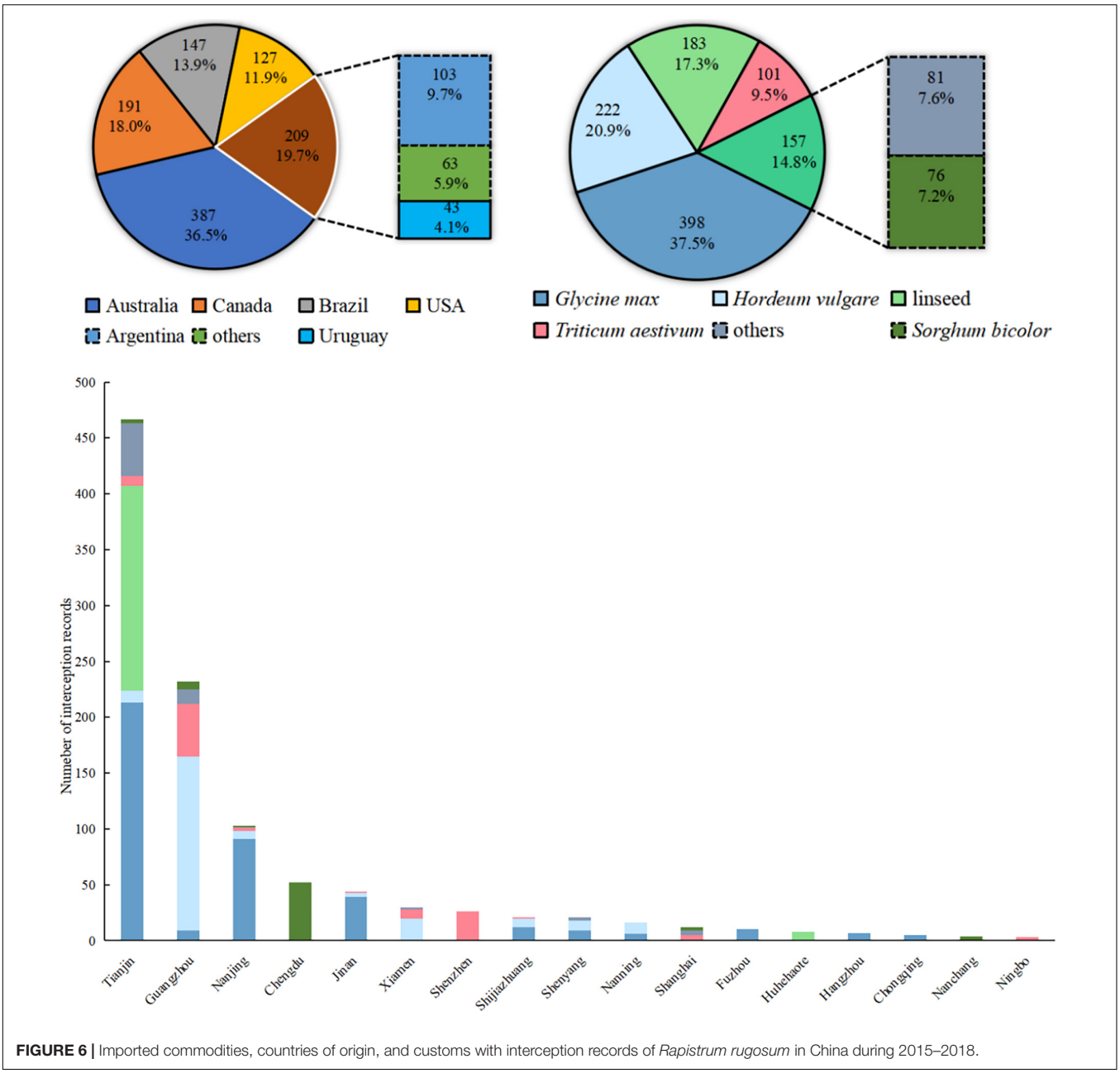

FIGURE 6 | Imported commodities, countries of origin, and customs with interception records of *Rapistrum rugosum* in China during 2015–2018.

cannot predict the potential invasive risk of IAS if they disperse beyond their native range (Sillero et al., 2021). Thus, ecological niche shifting should be considered when predicting the invasive risk habitats of IAS based on species distribution modeling.

Comprehensive multi-angle considerations are fundamental to predict the invasion risk areas of *R. rugosum* in China. Based on native, invasive, native + invasive distribution records of *R. rugosum*, our results showed that when modeled with the distribution records of native or invasive, the ecological niche had shifted. Ecological niche shifts during biological invasion have been proven in many case studies of IAS (Broennimann and Guisan, 2008; Manzoor et al., 2020). MaxEnt models consistently provided qualitatively different predictions based on native and invasive distribution records, mainly because SDMs fit on native range data poorly predict introduced range occupancy or because ecological niche shifts significantly reduce the transferability of MaxEnt SDMs (Atwater and Barney, 2021). Meanwhile, SDMs can only predict the initial spread of the introduced population but cannot accurately predict its future spread trend. When an IAS first invades a new habitat, the ecological niche does not change. However, the phenology, thermal tolerance, and life history of invasive plants may change after they gradually adapt to the new habitats and expand their ecological niche (Colautti et al., 2017; Atwater et al., 2018). Shifts in the realized niche are common during plant bioinvasion. Ecological niche shifts are practically important, as they alter the predicted geographical

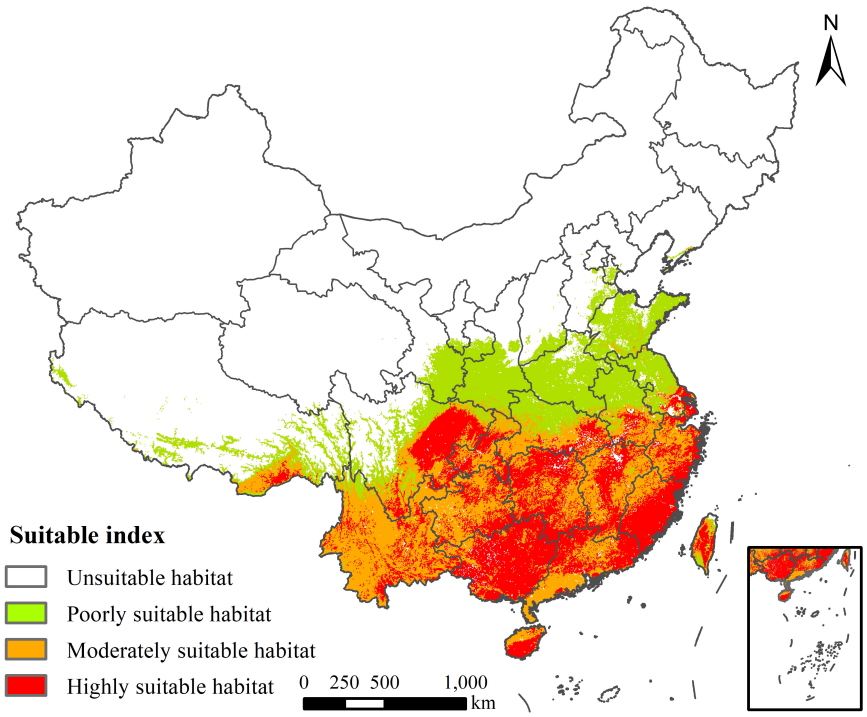

FIGURE 7 | Potential invasive risk areas of *Rapistrum rugosum* in China.

distribution of IAS (Pearman et al., 2008). Therefore, ecological niche shifts play a key role in predicting the spread of IAS. Studies on the identification of the invasive risk areas of IAS have mainly focused on a combination of native and invasive data, regardless of whether the species has spread to a broad ecological niche (Qin et al., 2015; Saranya et al., 2021). Our predictions of the invasive risk areas of *R. rugosum* based on specific climate variables together with a combination of native and invasive records may be less or more one-sided than predictions based on native and invasive records considered separately, which may have affected model accuracy. *R. rugosum* is a new IAS in China that has been intercepted from many countries (including native and invasive ranges). Therefore, multiple invasions of mixed populations are expected to contribute to the further spread of *R. rugosum* in China. Therefore, in the present study, the native and invasive records of *R. rugosum* were separately used to model the potential invasive risk areas of this IAS in China. Overall, the ecological niche of *R. rugosum* has shifted, affecting its potential invasion risk in China.

Colonization and Dispersal Risk of *Rapistrum rugosum* in China and Significant Environmental Variables

Rapistrum rugosum is a globally important IAS. All customs in China should implement strict plant quarantine regulations on imported grain from Australia, Canada, Brazil, the United States, and Argentina to prevent the introduction of this species to new areas in the country. *R. rugosum* poses a great risk of invasion in China. The number of interception records from Tianjin Customs was the highest. Even though Tianjin customs is located in a slightly suitable habitat, it was also associated with the greatest risk of potential introduction. Moreover, Guangzhou Customs is associated with a high risk of potential introduction, because it is located in a highly suitable habitat and recorded many interceptions. Thus, Tianjin and Guangzhou customs should be closely monitored in terms of the quarantine of imported grain to prevent the introduction of *R. rugosum* mixed in imported grain. A wild population of *R. rugosum* has been discovered in Xi'an, and this population continues to spread in the surrounding areas. American countries accounted for over 50% of the total interception records of *R. rugosum*. In general, China, Europe, and North America have comparable climatic conditions. North America, Europe, and China have climate zones located south of the 40th parallel; therefore, most North American species can readily adapt to new habitats following their introduction into China and can effectively colonize in a relatively short time (Peel et al., 2007). According to the China Environment Report 2019, presented by the Ministry of Ecology and Environment, there are over 660 IAS in China; plants account for a majority of them, and over 50% originated from the United States. Therefore, climatic conditions cannot limit the ability of *R. rugosum* to establish populations in China.

Many Brassicaceae weeds germinate in a similar manner under different temperature conditions (Long et al., 2011). Temperature is an important variable affecting the germination of *R. rugosum* seeds (Ohadi et al., 2011; Hasanfard et al., 2021). Our analysis revealed that the most significant variables shaping *R. rugosum*

distribution were annual temperature range (Bio7) and mean temperature of the coldest quarter (Bio11). These results further proved that temperature was an important factor limiting the survival of this weed. *R. rugosum* is a fast-growing weed, and its invasiveness is facilitated by its ability to germinate under a wide range of temperatures. In Australia, the seeds of *R. rugosum* could germinate at most temperatures ranging from 5 to 30°C (Ali et al., 2020). Our results showed that the annual temperature range and the mean temperature of the coldest quarter suitable for the growth of *R. rugosum* were 1.2–29.5°C and 8.1–13.4°C, respectively. We found that when the mean temperature of the coldest quarter was between 0 and 20°C, the survival probability of *R. rugosum* showed a fluctuating increase, followed by a fluctuating decrease. Our results are consistent with previous reports. Moreover, the mean annual temperature of suitable habitats for *R. rugosum* in China was >10°C, and the mean annual temperature of highly suitable habitats was >15°C. Overall, the mean annual temperature and mean temperature of the coldest quarter in southern China are suitable for the germination of *R. rugosum* seeds; thus, this region faces a risk of colonization and dispersal of *R. rugosum*.

In recent years, *R. rugosum* was frequently detected in the commodities and containers of importing grains and seeds, indicating that this weed can spread over long distances aboard other seeds, logs, and other contaminated materials. Early warning and control measures are essential to prevent and reduce *R. rugosum* invasion in China. Tianjin, Guangdong, Nanjing, and Chengdu customs have reported frequent interceptions of *R. rugosum*, underscoring the need for strict quarantine measures to prevent and reduce the introduction and survival of this IAS in the surrounding areas of entry ports and imported grain processing factories. Specific attention should be paid to the imported grains, including *Glycine max*, *Hordeum vulgare*, and linseed, from Australia, Canada, and Brazil. For wild populations of *R. rugosum*, chemical control tends to be problematic because of the potential risk of development of resistance to a number of specific herbicides (Hatami et al., 2016; Ntoanidou et al., 2019). Manual removal of the plant and its taproot and seed disposal are successful but time-consuming.

CONCLUSION

The present study used the R package "kuenm" to develop comprehensive MaxEnt models. The overall model fit was excellent. Through the simulation of risk areas based on distribution records from different regions in China, we predicted that the ecological niche of *R. rugosum* would shift, and our model results confirmed this assumption. The two most significant variables shaping *R. rugosum* distribution were annual temperature range and mean temperature of the coldest quarter. Invasion risk assessment revealed that the area of the total suitable habitat for *R. rugosum* in China is 287.53×10^4 km^2, and these habitats are mainly distributed in Southwest, Southeast, and Central China. The potential habitats of *R. rugosum* accounted for a large proportion of Chinese mainland. Furthermore, climatic conditions will not limit the ability of *R. rugosum* to establish populations in China, and it has already successfully colonized specific regions within the country. Australia, Canada, Brazil, the United States, and Argentina are the five major source countries of *R. rugosum* in China. Meanwhile, *Glycine max*, *Hordeum vulgare*, linseed, *Triticum aestivum*, and *Sorghum bicolor* are the major grain sources of *R. rugosum*. Tianjin, Guangzhou, Nanjing, and Chengdu customs are the high-risk regions for the introduction of *R. rugosum* into China. Our results can serve as the reference to develop effective control measures against this IAS. Information about latitudinal clines in defense and joint clinical evolution of growth and defense in *R. rugosum* is essential for its adaptive evolution. Our further investigations will primarily focus on the re-establishment of heritable latitudinal clines in growth-related traits of *R. rugosum*.

DATA AVAILABILITY STATEMENT

The original contributions presented in the study are included in the article/**Supplementary Material**, further inquiries can be directed to the corresponding author.

AUTHOR CONTRIBUTIONS

XX, HZ, and WL: conception and design of the research. XX and HZ: acquisition of data, analysis and interpretation of data, statistical analysis, and drafting the manuscript. RW, HQ, JG, GZ, and FW: manuscript revision. All authors contributed to the article and approved the submitted version.

FUNDING

This project was funded by the National Key R&D Program of China (grant no. 2021YFC2600400) and Technology Innovation Program of Chinese Academy of Agricultural Sciences (grant no. caascx-2017-2022-IAS).

SUPPLEMENTARY MATERIAL

The Supplementary Material for this article can be found online at: https://www.frontiersin.org/articles/10.3389/fpls.2022.827497/full#supplementary-material

REFERENCES

Adhikari, P., Jeon, J.-Y., Kim, H. W., Shin, M.-S., Adhikari, P., and Seo, C. (2019). Potential impact of climate change on plant invasion in the Republic of Korea. *J. Ecol. Environ.* 43:36. doi: 10.1186/s41610-019-0134-3

Ali, H. H., Kebaso, L., Manalil, S., and Chauhan, B. S. (2020). Emergence and germination response of *Sonchus oleraceus* and *Rapistrum rugosum* to different temperatures and moisture stress regimes. *Plant Species Biol.* 35, 16–23. doi: 10.1111/1442-1984.12254

Atwater, D. Z., and Barney, J. N. (2021). Climatic niche shifts in 815 introduced plant species affect their predicted distributions. *Glob. Ecol. Biogeogr.* 30, 1671–1684. doi: 10.1111/geb.13342

Atwater, D. Z., Ervine, C., and Barney, J. N. (2018). Climatic niche shifts are common in introduced plants. *Nat. Ecol. Evol.* 2, 34–43. doi: 10.1038/s41559-017-0396-z

Beaumont, L. J., Gallagher, R. V., Thuiller, W., Downey, P. O., Leishman, M. R., and Hughes, L. (2009). Different climatic envelopes among invasive populations may lead to underestimations of current and future biological invasions. *Divers. Distrib.* 15, 409–420. doi: 10.1111/j.1472-4642.2008.00547.x

Broennimann, O., and Guisan, A. (2008). Predicting current and future biological invasions: both native and invaded ranges matter. *Biol. Lett.* 4, 585–589. doi: 10.1098/rsbl.2008.0254

Brown, A. (1878). Plants introduced with ballast and on made land. *Bull. Torrey Bot. Club* 6, 255–258. doi: 10.2307/2476788

Bruno, D., and Solène, R. (2016). *INPN - Données Flore Des CBN Agrégées Par La FCBN. Version 1.2. PatriNat, U. (OFB-CNRS-MNHN), Paris*. Paris: UMS PatriNat (OFB-CNRS-MNHN). doi: 10.15468/omae84

Cao, Z. D. (2020). *China's Ports-Of-Entry 2019 Yearbook*. Beijing: China Customs Press.

Cobos, M. E., Peterson, A. T., Barve, N., and Osorio-Olvera, L. (2019). Kuenm: an R package for detailed development of ecological niche models using Maxent. *PeerJ.* 7:e6281. doi: 10.7717/peerj.6281

Colautti, R. I., Ågren, J., and Anderson, J. T. (2017). Phenological shifts of native and invasive species under climate change: insights from the *Boechera–Lythrum* model. *Philos. Trans. R. Soc. Lond. B Biol. Sci.* 372:20160032. doi: 10.1098/rstb.2016.0032

David, A. S., and Menges, E. S. (2011). Microhabitat preference constrains invasive spread of non-native natal grass (*Melinis repens*). *Biol. Invas.* 13, 2309–2322. doi: 10.1007/s10530-011-0044-5

Diagne, C., Leroy, B., Vaissière, A. C., Gozlan, R. E., Roiz, D., Jarić, I., et al. (2021). High and rising economic costs of biological invasions worldwide. *Nature* 592, 571–576. doi: 10.1038/s41586-021-03405-6

Elith, J., Phillips, S. J., Hastie, T., Dudík, M., Chee, Y. E., and Yates, C. J. (2011). A statistical explanation of MaxEnt for ecologists. *Divers. Distrib.* 17, 43–57. doi: 10.1111/j.1472-4642.2010.00725.x

Essl, F., Lenzner, B., Bacher, S., Bailey, S., Capinha, C., Daehler, C., et al. (2020). Drivers of future alien species impacts: an expert-based assessment. *Glob. Change Biol.* 26, 4880–4893. doi: 10.1111/gcb.15199

Fan, J., Upadhye, S., and Worster, A. (2006). Understanding receiver operating characteristic (ROC) curves. *Can. J. Emerg. Med.* 8, 19–20. doi: 10.1017/s1481803500013336

Fernández, M., and Hamilton, H. (2015). Ecological niche transferability using invasive species as a case study. *PLoS One* 10:e0119891. doi: 10.1371/journal.pone.0119891

Fischer, G., Nachtergaele, F., Prieler, S., Teixeira, E., Tóth, G., Velthuizen, H., et al. (2008). *Global Agro-ecological Zones Assessment for Agriculture (GAEZ 2008*. Laxenburg: FAO.

Global Biodiversity Information Facility (2021). *Rapistrum Rugosum* (L.) All. Available online at: https://www.gbif.org/species/5373368 (accessed December 22, 2021).

Greenberg, M., Haas, C., Cox, A. Jr., Lowrie, K., McComas, K., and North, W. (2012). Ten most important accomplishments in risk analysis, 1980–2010. *Risk Anal.* 32, 771–781. doi: 10.1111/j.1539-6924.2012.01817.x

Hasanfard, A., Rastgoo, M., Izadi Darbandi, E., Nezami, A., and Chauhan, B. S. (2021). Regeneration capacity after exposure to freezing in wild oat (*Avena ludoviciana* Durieu.) and turnipweed (*Rapistrum rugosum* (L.) All. in comparison with winter wheat. *Environ. Exp. Bot.* 181:104271. doi: 10.1016/j.envexpbot.2020.104271

Hatami, Z. M., Gherekhloo, J., Rojano-Delgado, A. M., Osuna, M. D., Alcántara, R., Fernández, P., et al. (2016). Multiple mechanisms increase levels of resistance in *Rapistrum rugosum* to ALS herbicides. *Front. Plant Sci.* 7:169. doi: 10.3389/fpls.2016.00169

Hejda, M., Chytrý, M., Pergl, J., and Pyšek, P. (2015). Native-range habitats of invasive plants: are they similar to invaded-range habitats and do they differ according to the geographical direction of invasion? *Divers. Distrib.* 21, 312–321. doi: 10.1111/ddi.12269

Hichri, A. O., Hichri, F., Mastouri, M., Brahmia, A., Flamini, G., and Selmi, B. (2019). Study of chemical composition, antibacterial and antioxidant activities of *Rapistrum rugosum* L. essential oils from flowers, leaves, and stems. *J. Essent. Oil Bear. Plants* 22, 1416–1426. doi: 10.1080/0972060X.2019.1682682

Kariyawasam, C. S., Kumar, L., and Ratnayake, S. S. (2019). Invasive plant species establishment and range dynamics in Sri Lanka under climate change. *Entropy* 21:571. doi: 10.3390/e21060571

Lemke, D. E., and Worthington, R. D. (1991). *Brassica* and *Rapistrum* (Brassicaceae) in Texas. *Southwest. Nat.* 36, 194–197. doi: 10.2307/3671920

Liu, C., Wolter, C., Xian, W., and Jeschke, J. M. (2020). Most invasive species largely conserve their climatic niche. *Proc. Natl Acad. Sci. U.S.A.* 117, 23643–23651. doi: 10.1073/pnas.2004289117

Liu, X., Liu, H., Gong, H., Lin, Z., and Lv, S. (2017). Appling the one-class classification method of Maxent to detect an invasive plant *Spartina alterniflora* with time-series analysis. *Remote Sens.* 9:1120. doi: 10.3390/rs9111120

Long, R. L., Stevens, J. C., Griffiths, E. M., Adamek, M., Gorecki, M. J., Powles, S. B., et al. (2011). Seeds of *Brassicaceae* weeds have an inherent or inducible response to the germination stimulant karrikinolide. *Ann. Bot.* 108, 933–944. doi: 10.1093/aob/mcr198

Mačić, V., Albano, P. G., Almpanidou, V., Claudet, J., Corrales, X., Essl, F., et al. (2018). Biological invasions in conservation planning: a global systematic review. *Front. Mar. Sci.* 5:178. doi: 10.3389/fmars.2018.00178

Manalil, S., and Chauhan, B. S. (2019). Interference of turnipweed (*Rapistrum rugosum*) and Mexican pricklepoppy (*Argemone mexicana*) in wheat. *Weed Sci.* 67, 666–672. doi: 10.1017/wsc.2019.42

Manalil, S., Haider Ali, H., and Chauhan, B. S. (2018). Germination ecology of turnip weed (*Rapistrum rugosum* (L.) All.) in the northern regions of Australia. *PLoS One* 13:e0201023. doi:10.1371/journal.pone.0201023

Manzoor, S. A., Griffiths, G., Obiakara, M. C., Esparza-Estrada, C. E., and Lukac, M. (2020). Evidence of ecological niche shift in *Rhododendron ponticum* (L.) in Britain: hybridization as a possible cause of rapid niche expansion. *Ecol. Evol.* 10, 2040–2050. doi: 10.1002/ece3.6036

Ntoanidou, S., Madesis, P., and Eleftherohorinos, I. (2019). Resistance of *Rapistrum rugosum* to tribenuron and imazamox due to Trp574 or Pro197 substitution in the acetolactate synthase. *Pestic. Biochem. Physiol.* 154, 1–6. doi: 10.1016/j.pestbp.2018.12.001

Ohadi, S., Mashhadi, H. R., and Tavakol-Afshari, R. (2011). Effects of storage and burial on germination responses of encapsulated and naked seeds of turnipweed (*Rapistrum rugosum*) to light. *Weed Sci.* 59, 483–488. doi: 10.1614/WS-D-10-00153.1

Pardo, G., Marí, A. I., Aibar, J., Vilaplana, L., and Cirujeda, A. (2019). Bastard cabbage (*Rapistrum rugosum* L.) resistance to Tribenuron-methyl and Iodosulfuron-methyl-sodium in Spain and alternative herbicides for its control. *Agronomy* 9:492. doi: 10.3390/agronomy9090492

Pearman, P. B., Guisan, A., Broennimann, O., and Randin, C. F. (2008). Niche dynamics in space and time. *Trends Ecol. Evol.* 23, 149–158. doi: 10.1016/j.tree.2007.11.005

Peel, M. C., Finlayson, B. L., and McMahon, T. A. (2007). Updated world map of the Köppen-Geiger climate classification. *Hydrol. Earth Syst. Sci.* 11, 1633–1644. doi: 10.5194/hess-11-1633-2007

Phillips, S. J., Anderson, R. P., and Schapire, R. E. (2006). Maximum entropy modeling of species geographic distributions. *Ecol. Modell.* 190, 231–259. doi: 10.1016/j.ecolmodel.2005.03.026

Pisani, D., Pazienza, P., Perrino, E. V., Caporale, D., and De Lucia, C. (2021). The economic valuation of ecosystem services of biodiversity components in protected areas: a review for a framework of analysis for the gargano national park. *Sustainability* 13:11726. doi: 10.3390/su132111726

Pyšek, P., Hulme, P. E., Simberloff, D., Bacher, S., Blackburn, T. M., Carlton, J. T., et al. (2020). Scientists' warning on invasive alien species. *Biol. Rev. Camb. Philos. Soc.* 95, 1511–1534. doi: 10.1111/brv.12627

Qin, Z., Zhang, J. E., DiTommaso, A., Wang, R. L., and Wu, R. S. (2015). Predicting invasions of *Wedelia trilobata* (L.) Hitchc. with Maxent and GARP models. *J. Plant Res.* 128, 763–775. doi:10.1007/s10265-015-0738-3

Radosavljevic, A., and Anderson, R. P. (2014). Making better Maxent models of species distributions: complexity, overfitting and evaluation. *J. Biogeogr.* 41, 629–643. doi: 10.1111/jbi.12227

Saranya, K. R. L., Lakshmi, T. V., and Reddy, C. S. (2021). Predicting the potential sites of *Chromolaena odorata* and *Lantana camara* in forest landscape of Eastern Ghats using habitat suitability models. *Ecol. Inform* 66:101455. doi: 10.1016/j.ecoinf.2021.101455

Sillero, N., Arenas-Castro, S., Enriquez-Urzelai, U., Vale, C. G., Sousa-Guedes, D., Martínez-Freiría, F., et al. (2021). Want to model a species niche? A step-by-step guideline on correlative ecological niche modelling. *Ecol. Modell.* 456:109671. doi: 10.1016/j.ecolmodel.2021.109671

Simmons, M. T. (2005). Bullying the bullies: the selective control of an exotic, invasive annual (*Rapistrum rugosum*) by oversowing with a competitive native species (*Gaillardia pulchella*). *Restor. Ecol.* 13, 609–615. doi: 10.1111/j.1526-100X.2005.00078.x

Simpson, M., and Prots, B. (2013). Predicting the distribution of invasive plants in the Ukrainian Carpathians under climatic change and intensification of anthropogenic disturbances: implications for biodiversity conservation. *Environ. Conserv.* 40, 167–181. doi: 10.1017/S037689291200032X

Srivastava, V., Lafond, V., and Griess, V. C. (2019). Species distribution models (SDM): applications, benefits and challenges in invasive species management. *CAB Rev.* 14, 1–13. doi: 10.1079/PAVSNNR201914020

Staten Island Museum (2021). *Staten Island museum. Occurrence Dataset*. Staten Island, NY: Staten Island Museum. doi: 10.15468/ctqpb5

Stinca, A., Musarella, C. M., Rosati, L., Laface, V. L. A., Licht, W., Fanfarillo, E., et al. (2021). Italian vascular flora: new findings, updates and exploration of floristic similarities between regions. *Diversity* 13:600. doi: 10.3390/d13110600

Swets, J. A. (1988). Measuring the accuracy of diagnostic systems. *Science* 240, 1285–1293. doi: 10.1126/science.3287615

Tang, X., Yuan, Y., Liu, X., and Zhang, J. (2021). Potential range expansion and niche shift of the invasive *Hyphantria cunea* between native and invasive countries. *Ecol. Entomol.* 46, 910–925. doi: 10.1111/een.13028

Thomas, S. M., Verhoeven, M. R., Walsh, J. R., Larkin, D. J., and Hansen, G. J. A. (2021). Species distribution models for invasive *Eurasian watermilfoil* highlight the importance of data quality and limitations of discrimination accuracy metrics. *Ecol. Evol.* 11, 12567–12582. doi: 10.1002/ece3.8002

Venne, S., and Currie, D. J. (2021). Can habitat suitability estimated from MaxEnt predict colonizations and extinctions? *Divers. Distrib.* 27, 873–886. doi: 10.1111/ddi.13238

Wan, F., Jiang, M., and Zhan, A. (2017). "Biological invasions and its management in China," in *Biological Invasion and Its Research in China: An Overview*, Vol. 1, eds Y. Yan, X. Xian, M. Jiang, and F. Wang (Dordrecht: Springer), 3–20. doi: 10.1007/978-94-024-0948-2

Warren, D. L., Glor, R. E., and Turelli, M. (2010). ENMTools: a toolbox for comparative studies of environmental niche models. *Ecography* 33, 607–611. doi: 10.1111/j.1600-0587.2009.06142.x

Wolkovich, E. M., and Cleland, E. E. (2011). The phenology of plant invasions: a community ecology perspective. *Front. Ecol. Environ.* 9, 287–294. doi: 10.1890/100033

Xun, L., Li, S., Li, W., Zhou, Y., Lu, Y., Mao, S., et al. (2020). Newly recorded plants of Brassicaceae from Shaanxi Province. *Acta Bot. Boreali Occidentalia Sin.* 40, 1425–1435. doi: 10.7606/.j.issn.100-4025.2020.05.1428

Yan, Y., Xian, X., Jiang, M., and Wan, F. (2017). "Biological invasion and its research in China: an overview," in *Biological Invasions And Its Management In China: 2*, eds F. Wan, M. Jiang, and A. Zhan (Dordrecht: Springer Netherlands), 3–19. doi: 10.1371/journal.pone.0001208

Yang, X., Kushwaha, S. P. S., Saran, S., Xu, J., and Roy, P. S. (2013). Maxent modeling for predicting the potential distribution of medicinal plant. *Justicia adhatoda L.* in lesser himalayan foothills. *Ecol. Eng.* 51, 83–87. doi: 10.1016/j.ecoleng.2012.12.004

Yeh, H. T., Cheah, H. Y., Chiu, M. C., Liao, J. R., and Ko, C. C. (2021). Assessment of potential invasion for six phytophagous quarantine pests in Taiwan. *Sci. Rep.* 11:10666. doi: 10.1038/s41598-021-89914-w

Zenni, R. D., Bailey, J. K., and Simberloff, D. (2014). Rapid evolution and range expansion of an invasive plant are driven by provenance–environment interactions. *Ecol. Lett.* 17, 727–735. doi: 10.1111/ele.12278

Zhuo, Z., Xu, D., Pu, B., Wang, R., and Ye, M. (2020). Predicting distribution of *Zanthoxylum bungeanum* Maxim. in China. *BMC Ecol.* 20:46. doi: 10.1186/s12898-020-00314-6

Conflict of Interest: The authors declare that the research was conducted in the absence of any commercial or financial relationships that could be construed as a potential conflict of interest.

Publisher's Note: All claims expressed in this article are solely those of the authors and do not necessarily represent those of their affiliated organizations, or those of the publisher, the editors and the reviewers. Any product that may be evaluated in this article, or claim that may be made by its manufacturer, is not guaranteed or endorsed by the publisher.

frontiers | Frontiers in Plant Science

ORIGINAL RESEARCH
published: 27 April 2022
doi: 10.3389/fpls.2022.849896

Climate Change and Management Impacts on Soybean N Fixation, Soil N Mineralization, N_2O Emissions, and Seed Yield

Elvis F. Elli[1], Ignacio A. Ciampitti[2], Michael J. Castellano[1], Larry C. Purcell[3], Seth Naeve[4], Patricio Grassini[5], Nicolas C. La Menza[5], Luiz Moro Rosso[2], André F. de Borja Reis[6], Péter Kovács[7] and Sotirios V. Archontoulis[1]**

[1] Department of Agronomy, Iowa State University, Ames, IA, United States, [2] Department of Agronomy, Kansas State University, Manhattan, KS, United States, [3] Department of Crop, Soil, and Environmental Sciences, University of Arkansas, Fayetteville, AR, United States, [4] Department of Agronomy and Plant Genetics, University of Minnesota, Saint Paul, MN, United States, [5] Department of Agronomy and Horticulture, University of Nebraska-Lincoln, Lincoln, NE, United States, [6] Agricultural Center, Louisiana State University, Alexandria, LA, United States, [7] Department of Agronomy, Horticulture, and Plant Science, South Dakota State University, Brookings, SD, United States

OPEN ACCESS

Edited by:
Peter Thorburn,
Commonwealth Scientific and Industrial Research Organisation (CSIRO), Australia

Reviewed by:
Caitlin Peterson,
University of California, Davis, United States
Zvi Hochman,
Commonwealth Scientific and Industrial Research Organisation (CSIRO), Australia

***Correspondence:**
Elvis F. Elli
efelli@iastate.edu
Sotirios V. Archontoulis
sarchont@iastate.edu

Specialty section:
This article was submitted to Plant Biophysics and Modeling, a section of the journal Frontiers in Plant Science

Received: 06 January 2022
Accepted: 25 March 2022
Published: 27 April 2022

Citation:
Elli EF, Ciampitti IA, Castellano MJ, Purcell LC, Naeve S, Grassini P, La Menza NC, Moro Rosso L, de Borja Reis AF, Kovács P and Archontoulis SV (2022) Climate Change and Management Impacts on Soybean N Fixation, Soil N Mineralization, N_2O Emissions, and Seed Yield. Front. Plant Sci. 13:849896. doi: 10.3389/fpls.2022.849896

Limited knowledge about how nitrogen (N) dynamics are affected by climate change, weather variability, and crop management is a major barrier to improving the productivity and environmental performance of soybean-based cropping systems. To fill this knowledge gap, we created a systems understanding of agroecosystem N dynamics and quantified the impact of controllable (management) and uncontrollable (weather, climate) factors on N fluxes and soybean yields. We performed a simulation experiment across 10 soybean production environments in the United States using the Agricultural Production Systems sIMulator (APSIM) model and future climate projections from five global circulation models. Climate change (2020–2080) increased N mineralization (24%) and N_2O emissions (19%) but decreased N fixation (32%), seed N (20%), and yields (19%). Soil and crop management practices altered N fluxes at a similar magnitude as climate change but in many different directions, revealing opportunities to improve soybean systems' performance. Among many practices explored, we identified two solutions with great potential: improved residue management (short-term) and water management (long-term). Inter-annual weather variability and management practices affected soybean yield less than N fluxes, which creates opportunities to manage N fluxes without compromising yields, especially in regions with adequate to excess soil moisture. This work provides actionable results (tradeoffs, synergies, directions) to inform decision-making for adapting crop management in a changing climate to improve soybean production systems.

Keywords: biological N fixation, soil N mineralization, APSIM, N_2O emissions, N balance, climate change, weather variability, soybean yield

INTRODUCTION

Nitrogen (N) is among the largest factors influencing crop productivity and environmental performance (Cassman and Dobermann, 2022). The cycling of N in the soil–plant-atmosphere continuum is complex and involves many processes including biological N fixation (BNF), plant N uptake, soil N mineralization, and N loss. These processes interact with each other creating tradeoffs

and synergies, varying in magnitude and temporal patterns, and are also affected by interactions among genotype, environment, and management—GxExM (e.g., Assefa et al., 2019; de Borja Reis et al., 2021). Environmental sustainability challenges are highly associated with N processes (e.g., N leaching, low BNF). Profitable and environmentally sustainable cropping systems will require alterations in the magnitude of some N processes in certain ways to achieve desired outcomes. Our knowledge of how and in which direction N processes are affected by climate change, weather variability, and management settings are limited. This is because most research work focuses on a single aspect of the system, making it difficult to understand how alterations to part of the system we control—genetics and management—will function in the context of a changing environment including both weather variability and climate change. This knowledge gap needs to be addressed in the context of sustainable intensification of existing cropping systems in changing environments (Hunter et al., 2017).

High seed yields require a high amount of N uptake by the crops and/or partitioning of greater amounts of N to the seeds (Sinclair and de Wit, 1976; Salvagiotti et al., 2008; Cafaro La Menza et al., 2017; Gaspar et al., 2017; Balboa et al., 2018). For example, a soybean seed yield of 2.7 Mg ha^{-1} (global average; FAOSTAT, 2021) requires 208 Kg N uptake ha^{-1}, while a high yielding soybean of 5.5 Mg/ha (Cafaro La Menza et al., 2019) requires 423 kg N uptake ha^{-1}. The N required by the soybean crop can derive from four sources: BNF, soil organic matter mineralization, residual soil nitrate from previous cropping years, and least commonly N fertilization. The contribution of each source is highly variable across GxExM conditions. Previous research indicated that BNF contributes on average between 50 and 60% of the total N uptake (Ciampitti and Salvagiotti, 2018) while the remaining N is supplied by soil indigenous ammonium and nitrate.

Several agricultural practices have been explored in field experiments to increase crop N uptake and close yield gaps. Examples include changes in sowing dates, cultivars, irrigation, N fertilization, plant arrangements, and results are highly variable depending on the environment (Bender et al., 2015; Moreira et al., 2015; Wegerer et al., 2015; Ortel et al., 2020; Zhao et al., 2020; de Borja Reis et al., 2021; Radzka et al., 2021). Projected soybean yield responses to climate change are highly variable depending on model assumptions and baseline climates (Kothari et al., 2022). Some model-based climate change studies indicate soybean seed yields will decline in future climates scenarios (Jin et al., 2017; Schauberger et al., 2017; Zabel et al., 2021) due to a 1.5°C temperature increase by 2050 (Intergovernmental Panel on Climate Change [IPCC], 2018) and changes in precipitation patterns. Rising temperature negatively impacts seed yield by accelerating crop development, but it can also increase soil N mineralization (De Valpine and Harte, 2001; Turner and Henry, 2010). An increase in drought and flooding events can potentially affect BNF more than soil N supply (Purcell et al., 2004; Pasley et al., 2020). The net impact of climate change on sustainability metrics such as N balance (aboveground N derived from BNF minus seed N removal, Collino et al., 2015; Santachiara et al., 2017) remains unknown.

Climate change, crop improvement, and agronomic advances are not incremental but continuous. In the context of these changes, interannual weather variability is large and management interventions must be dynamic to maximize sustainability for specific weather conditions and regions (Iqbal et al., 2018). A simultaneous evaluation of soil–plant N processes and how they are affected by GxExM alterations would improve our understanding of the complex agronomic system while will facilitate systems thinking and conceptualization of solutions to enhance productivity and environmental performance in soybean-based cropping systems. Therefore, we performed a GxExM simulation experiment across 10 soybean production regions in the United States using the Agricultural Production Systems sIMulator–APSIM (Holzworth et al., 2014). The use of cropping systems modeling is necessary because system-level assessments are limited by experimental data. Key N processes such as BNF and mineralization are impossible to measure at high temporal and spatial resolution or estimated for future climate scenarios. Furthermore, past work has demonstrated that the APSIM model can simulate well several processes of the system (soil N dynamics, BNF, crop N uptake, and yields) in a range of conditions and management settings in the United States (Archontoulis et al., 2014, 2020; Puntel et al., 2016; Ebrahimi-Mollabashi et al., 2019; Martinez-Feria et al., 2019; Pasley et al., 2020, 2021). Our objectives were to:

1. Create a systems understanding of how ecosystem N dynamics, including soil N mineralization, BNF, crop N uptake, soil nitrate pool size, and N_2O emissions, vary across United States soybean production as a function of GxExM interactions.
2. Separate the contribution of weather variability (uncontrollable factors) from crop and soil management practices (controllable factors) to understand potential interventions needed to increase productivity and environmental performance.
3. Quantify the impact of climate change on productivity and key sustainability metrics including N balance (BNF–seed N removal), N_2O emissions, and seed yield.

MATERIALS AND METHODS

Study Locations and Weather

We performed a simulation experiment across 10 locations in the United States (**Figure 1A**). The locations were selected to capture different production situations (i.e., soybean maturity groups, water management, and soil and weather conditions, **Figures 1**, **2**). Three locations were rainfed with a water table depth below 3.5 m (Kansas and South Dakota locations), four locations were irrigated with water tables below 3.5 m (Nebraska and Arkansas), one location was rainfed with a shallow water table at about 1.2 m (Ames, IA, United States), and two locations were rainfed with the shallow water table at about 1.2 m and subsurface drainage systems at 1.1 m (Nashua and Crawfordsville, IA, United States). Water table

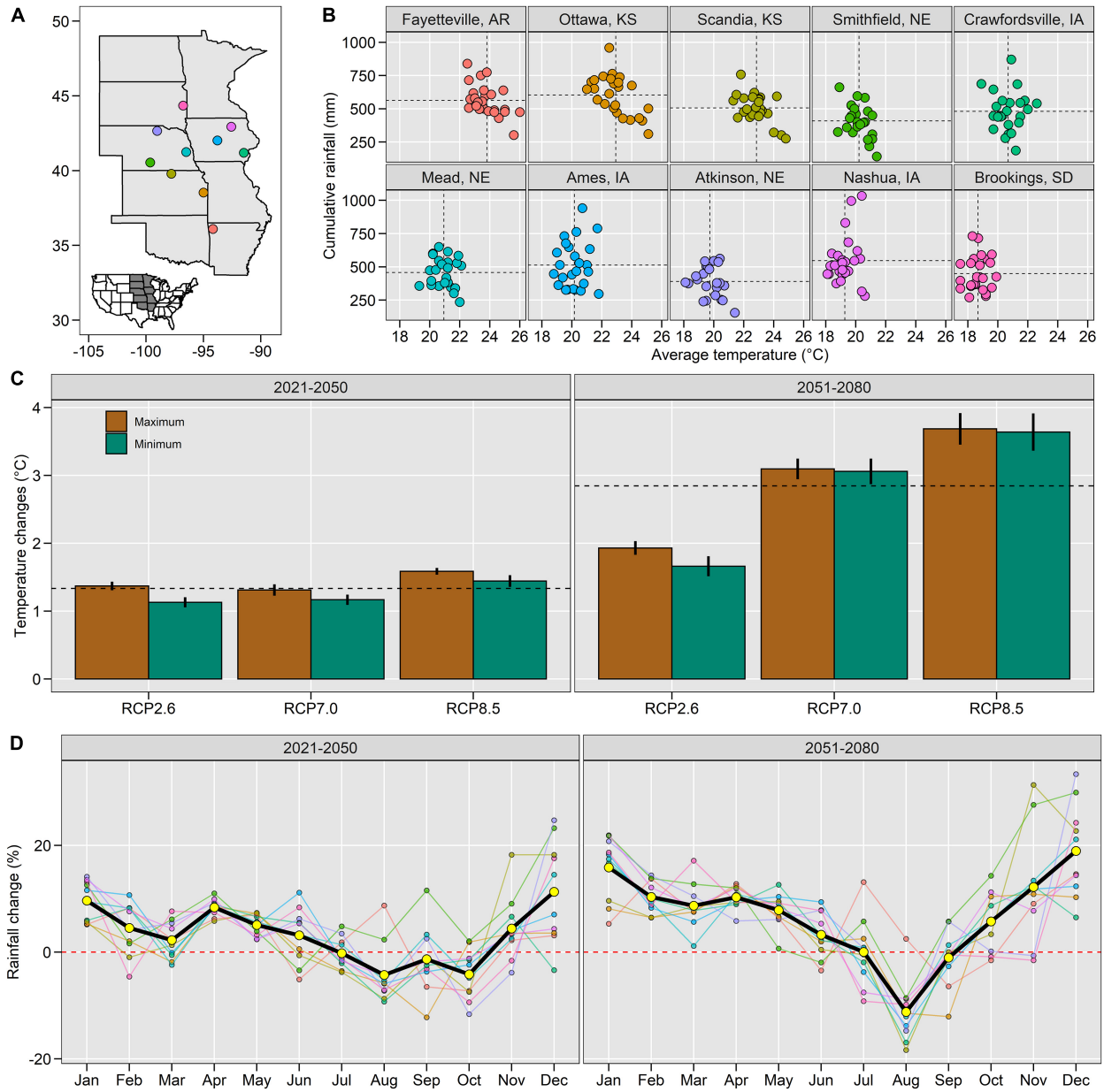

FIGURE 1 | Spatial distribution of experimental locations **(A)**, year-to-year (1995–2020) variability of average temperatures and cumulative rainfall from May to September (horizontal and vertical dashed lines indicate the average values) **(B)**, average temperature changes in relation to the baseline for 2021–2050 and 2051–2080 under RCP2.6, RCP7.0, and RCP8.5 (vertical bars represent the standard deviation from the 10 locations and horizontal dashed lines represent the average change) **(C)**, monthly rainfall changes in relation to the baseline (black lines indicate averages from five global circulation models, three RPCs and 10 locations, while colored lines represent the variability across the 10 locations) **(D)**.

depth data were derived from field measurements and SSURGO (Soil Survey Staff, 2019).

Historical weather data (1995–2020) were retrieved from local weather stations. From May to September, the average temperatures ranged from 18.7 to 23.8°C and rainfall from 390 to 604 mm (**Figure 1B**). Bias-corrected future climate projections were retrieved from five global circulation models: UKESM1-0-LL, MRI-ESM2-0, MPI-ESM1-2-HR, IPSL-CM6A-LR, and GFDL-ESM4 (Müller et al., 2021; Zabel et al., 2021) and included three representative concentration pathway combinations (RCP2 0.6, RCP 7.0, and RCP 8.5). Bias correction was implemented by using the linear scaling method (Teutschbein and Seibert, 2012), which consists of applying a monthly "delta" correction factor based on the differences between observed and simulated present-day values. On average across all 15 climate scenarios, these projections estimated a 1.3 and 2.8°C increase in the average temperature for the 2020–2050 and 2050–2080 periods, respectively (**Figure 1C**), and about a 6%

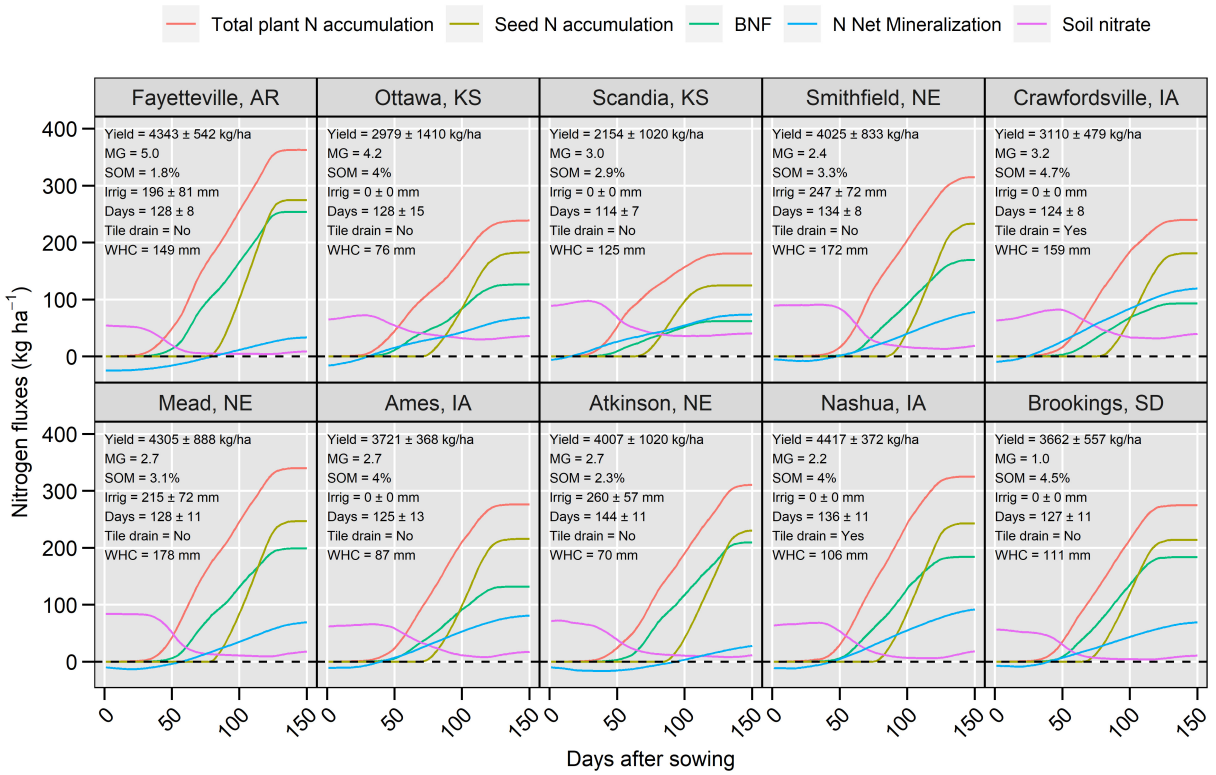

FIGURE 2 | Soil-plant N dynamics including plant and seed N accumulation, biological N fixation (BNF), soil N net mineralization and soil nitrate (0–120 cm) for all locations. The values are averages over 25-year simulations. Inset top-left panels indicate soybean 25-year average seed yield (Yield), maturity group (MG), soil organic matter (SOM, 0–30 cm), irrigation applied during the crop season (Irrig), number of days to physiological maturity (Days), existence of subsurface tile drainage (Tile drain) and soil water holding capacity to 120 cm (WHC). The N balance is illustrated in **Supplementary Figure 2**. The N_2O emissions fluxes are illustrated in **Supplementary Figure 4**.

increase in spring rainfall and nearly 3% decrease in summer rainfall (**Figure 1D**).

APSIM Model Set Up, Calibration, and Evaluation

The APSIM software is an advanced simulator of farming systems (Holzworth et al., 2014). The model simulates crop growth and development of several crops (including rotations), soil water balance, nitrogen, and carbon cycling and contains various management rules such as tillage and subsurface drainage. The soybean crop model simulates biomass production based on a combined radiation and water use efficiency concept and BNF as a function of crop growth rate (crop stage-specific value), which is mediated by drought and excess moisture stresses (Robertson et al., 2002; Pasley et al., 2021). The soil N model simulates soil carbon mineralization, immobilization, nitrification, denitrification, nitrous oxide emissions, and N leaching. The model simulates N mineralization as a function of soil carbon, soil C:N ratio, temperature, and moisture by layer (Probert et al., 1998). The decomposition of crop residue can increase or decrease net mineralization depending on the amount and the CN ratio of the stover (Probert et al., 2005; Archontoulis et al., 2016). The denitrification (and N_2O emissions) in the model is favored by high soil moisture, temperature, inorganic N, and carbon availability (Huth et al., 2010; Thorburn et al., 2010). The model assumes that crop N uptake can derive from soil inorganic N or BNF, with the soil nitrate being the first priority due to the lower energetic cost (Herridge et al., 2001; Robertson et al., 2002; Chen et al., 2016). For additional information, refer to www.apsim.info.

The APSIM model has been extensively validated in many agroecosystems around the world for the simulation of crop growth, soil water, and soil nitrogen and carbon fluxes (Mohanty et al., 2012; Chen et al., 2016; Battisti et al., 2017; Gaydon et al., 2017; Wu et al., 2019; Archontoulis et al., 2020). Here we used a well-calibrated APSIM version 7.9 (Archontoulis et al., 2020), which has been tested across many high-temporal resolutions, multifaceted, and multi-location datasets in the US Midwest, United States. This version includes algorithms to simulate excess moisture stress on root depth (Ebrahimi-Mollabashi et al., 2019), and on plant growth, development, and BNF (Pasley et al., 2020). Additional studies have verified APSIM capacity in simulating N loss (Malone et al., 2007; Dietzel et al., 2016; Martinez-Feria et al., 2016, 2019; Pasley et al., 2021) and soil N mineralization in the United States Corn Belt (Archontoulis et al., 2014; Puntel et al., 2016). For the simulation of soil water, we used the

SWIM3 module available in APSIM (Huth et al., 2012) which uses Richard's equation and enables the simulation of shallow water tables (Ebrahimi-Mollabashi et al., 2019).

In this study, we further tested the capacity of the model to simulate soil–plant N dynamics before its application to explore climate and management impacts. Experimental data covering high and low soybean yielding environments and maturity groups from 1 to 6 (**Supplementary Table 1**) were used to develop cultivar coefficients (**Supplementary Table 2**) with no further changes to the crop or soil models. Soil profile input values were derived from SSURGO (Soil Survey Staff, 2019) or measured data when available and are provided in **Supplementary Table 3**. Overall, the model proved robust and accurate in simultaneously simulating crop–soil N dynamics across the 10 study locations (**Supplementary Figure 1** and **Supplementary Table 4**).

Baseline Simulation Conditions

For the baseline simulation, we ran the model for 25 years (1995–2020). Model initial conditions were reset every year on January 1 and were similar among locations to facilitate comparison. Initial conditions included total inorganic N in the profile (75 kg N ha^{-1}), maize stover on the surface (4,500 kg ha^{-1} with a C:N ratio of 70), and soil water at field capacity. At each location, we included a moderate tillage event on April 1, with 20% of the surface residue being incorporated to a 20 cm depth. The sowing date was variable per year and per location following USDA-NASS 50% sowing progress (NASS, 2020). Cultivars were site-specific and ranged from maturity group 1 (South Dakota) to 5 (Arkansas, **Supplementary Table 2**). Plant density ranged from 25 to 32 plants m^{-2} (depending on the location) and row spacing was 0.76 m for all locations except Nashua, IA, United States, which was 0.46 m.

GxExM Scenarios

Using the well-tested APSIM model for each location, we simulated 22 scenarios (each with 25 weather-years) to create different GxExM conditions (**Table 1**). The scenarios accounted for climate change (see # 1–3; **Table 1**), N management strategies (4–7), residue management and quality (8–12), plant management (13–16), cultivar seed protein (17–18), soil organic carbon (19–20), and water management (21–22).

For climate change scenarios, we updated the baseline weather per location with the projected changes in monthly maximum and minimum temperature and rainfall (**Figure 1**). Monthly changes were site-specific (**Supplementary Table 5**). N management scenarios included two fertilization strategies, in the early spring or pod development stage (Mourtzinis et al., 2018), and a high/low initial soil inorganic N to reflect different amounts of leftover N from the previous maize crop, within the ranges

TABLE 1 | GxExM scenarios assessed using APSIM.

No	Scenario	Acronym	Changes compared to the baseline
1	Rainfall change	Rain change	Relative changes in rainfall (%) based on future climate projections (**Figure 1** and **Supplementary Table 5**)
2	Temperature change	Temp change	Changes in maximum and minimum temperatures (°C) based on future climate projections (**Figure 1** and **Supplementary Table 5**)
3	Rainfall and temperature changes	Rain*Temp	Scenario 1 + Scenario 2
4	Early spring N fertilization	Fer spring	Application of 30 kg N ha^{-1} (DAP or MAP fertilizer)[1]
5	R3-stage N fertilization	FerR3	Application of 60 kg N ha^{-1} (urea fertilizer)
6	More soil leftover N	+ LeftoverN	150 instead of 75 kg N/ha initial N
7	Less soil leftover N	−LeftoverN	38 instead of 75 kg N/ha initial N
8	High residue CN ratio	+ ResCN	150 instead 70 residue CN ratio
9	Low residue CN ratio	−ResCN	35 instead of 70 residue CN ratio
10	More crop residue	+ Residue	9,000 instead of 4,500 kg ha^{-1} residue
11	Less crop residue	−Residue	1,000 instead of 4,500 kg ha^{-1} residue
12	Full tillage	Full tillage	90% instead of 20% residue incorporation to 20 cm depth
13	High sowing density	+ Density	10 plants/m^2 increase from baseline
14	Low sowing density	−Density	10 plants/m^2 decrease from baseline
15	Early sowing date	Early sow	12 days earlier sowing than baseline
16	Late sowing date	Late sow	12 days later sowing than baseline
17	High seed protein	+ Seed protein	39.6% instead of 37.1% critical seed protein[2]
18	Low seed protein	−Seed protein	34.6% instead of 37.1% critical seed protein[2]
19	More initial soil organic carbon	+ SOC	15% increase in soil organic carbon
20	Less initial soil organic carbon	−SOC	15% decrease in soil organic carbon
21	Irrigation	Irrig	Irrigation between R1 and R7 when soil water falls below 50% PAW[3]
22	Tile drainage	Tile drainage	Model subsurface drainage function enabled

[1] *DAP, diammonium phosphate; MAP, monoammonium phosphate.*
[2] *Seed protein = 6.25 *N concentration (APSIM model uses N concentration).*
[3] *PAW, plant available water is defined as the difference between field capacity and wilting point at 0–45 cm depth.*

reported by Martinez-Feria et al. (2019). Residue management scenarios included alterations in the residue amount (Nunes et al., 2021) and CN ratio (Burgess et al., 2011). We also considered a scenario with a full tillage event before sowing (Daigh et al., 2018). Plant management scenarios included different sowing densities and dates. Sowing densities consisted of 10 plants/m^2 increase and decrease from baseline, consistent with the ranges reported by Carciochi et al. (2019). We varied the sowing date by ± 12 days from the baseline (50% NASS planting progress) to reflect early and late sowing date, which corresponds to approximately 20 and 80% NASS planting progress by year.

To represent high and low seed protein cultivars we changed the critical seed N concentration thresholds in the APSIM model. Demand for grain N attempts to maintain N at the critical (non-stressed) level (Robertson and Lilley, 2016). For the soil-related scenarios, we altered soil organic carbon (SOC) values across the profile by ± 15%, consistent with the ranges found by Nunes et al. (2020). The changes in SOC were not accompanied by changes in soil water properties (drained upper limit, lower limit, and saturated volumetric water contents). This is justified by the small effect that this level of change in SOC would have on soil water properties and systems outcomes (Palmer et al., 2017). For water management scenarios, we included irrigation and subsurface drainage (Helmers et al., 2012). In the irrigated locations, we added a rainfed scenario (e.g., Mead, NE, United States), while in the rainfed locations we added an irrigation scenario. Similarly, in locations with subsurface drainage (e.g., Nashua, IA, United States), we considered a no subsurface drainage scenario and vice versa. For the irrigation, we used an auto-irrigation rule (see #21 in **Table 1**) and considered a 5-day interval between irrigations to better represent reality.

Data Analysis

Data analysis and visualization were conducted in R version 4.1.1 (R Development Core Team, 2010). Data included daily soybean BNF, plant and seed N uptake, net N mineralization, soil nitrate, and N_2O across a range of scenarios. The coefficient of variation (CV) was calculated across weather years and management scenarios to quantify the contribution of weather and management to the variation of crop and N variables. N balance was calculated as the difference between fixed N in above ground biomass and seed N removal. For the scenarios with N fertilization, this input was accounted in the N balance (BNF + N fertilization–seed N removal). A relative sensitivity index was calculated (Hamby, 1994) to assess the influence of GxExM scenarios on N dynamics.

RESULTS

Nitrogen Fluxes Followed Similar Temporal Patterns Across Locations but of Different Magnitude

The temporal patterns in simulated BNF, seed and total aboveground plant N accumulation, soil N mineralization, and nitrate pools were similar among locations, but of different magnitude (**Figure 2**). Soil nitrate decreased during the growing period, with a sharp evident decline 50 days after sowing (**Figure 2**). During the seed filling period, soil nitrate was nearly zero with values at crop harvest ranging from 9 to 40 kg N ha^{-1}. Cumulative net N mineralization had negative values in the spring reflecting immobilization of inorganic N caused by the maize stover decomposition followed by positive values that were associated with high N mineralization rates during summer. The positive values of mineralization did not increase soil nitrate pool size during the seed filling period because the mineralized N was immediately taken up by the crop. At the end of the season, net N mineralization averaged 73 kg N ha^{-1} with values ranging from 31 kg ha^{-1} (Atkinson, NE, United States) to 121 kg ha^{-1} (Crawfordsville, IA, United States). These two locations had the lowest and highest soil organic matter values (**Figure 2**).

Biological N fixation accounted on average for 53% of the total aboveground N, with values ranging from 30 to 70% across locations (**Figure 2**). BNF initiated a week after plant N uptake and ceased at physiological maturity. While BNF was variable across locations, in all cases the cumulative BNF was lower than the seed N accumulation. The seed N accumulation initiated on average 49 days after BNF and followed a much steeper rate of increase (4.8 ± 0.8 kg N ha^{-1} day^{-1}) compared to BNF (2.4 ± 0.5 kg N ha^{-1} day^{-1}). As a result, the N balance (BNF + N fertilization–seed N removal) had positive values from sowing to about 1/3 of the seed filling period and then declined to negative values at physiological maturity (−21 to −88 kg ha^{-1}; **Supplementary Figure 2**). Even when N balance was calculated by considering more N fluxes such as N loss and N mineralization, the trends were similar (**Supplementary Figure 3**). Across locations, the simulated 25-year average soybean yield (0% moisture) ranged from 2.1 to 4.3 Mg ha^{-1} (**Figure 2**).

Cumulative N_2O fluxes exhibited an east to the west spatial gradient in terms of magnitude with average values ranging from 3.7 kg ha^{-1} $year^{-1}$ in Crawfordsville, IA to 0.2 kg ha^{-1} $year^{-1}$ in Atkinson, NE (**Supplementary Figure 4A**). Environments with shallow water tables (e.g., Iowa locations) had the highest N_2O emissions and variance across years. The majority of N_2O fluxes occurred in the spring (**Supplementary Figure 4B**).

Grouping the 25-year baseline weather as warm-wet, cool-wet, warm-dry, and cool-dry revealed that the N_2O emissions had the largest sensitivity to weather patterns when compared to the other N fluxes (**Supplementary Figure 5**). In general, wet years increased BNF, seed N accumulation, N net mineralization, and N_2O emissions. Residual soil nitrate at crop maturity was more associated with temperature than rainfall shifts, with lower values under cooler conditions. Site-specific responses were observed (**Supplementary Figure 5**).

Equal Contribution of Weather Variability and Management Settings on Nitrogen Fluxes

The year-to-year weather variability accounted for 31% of the variation in N fluxes while management accounted for 32% (average across all locations, **Figure 3**). The N_2O flux was

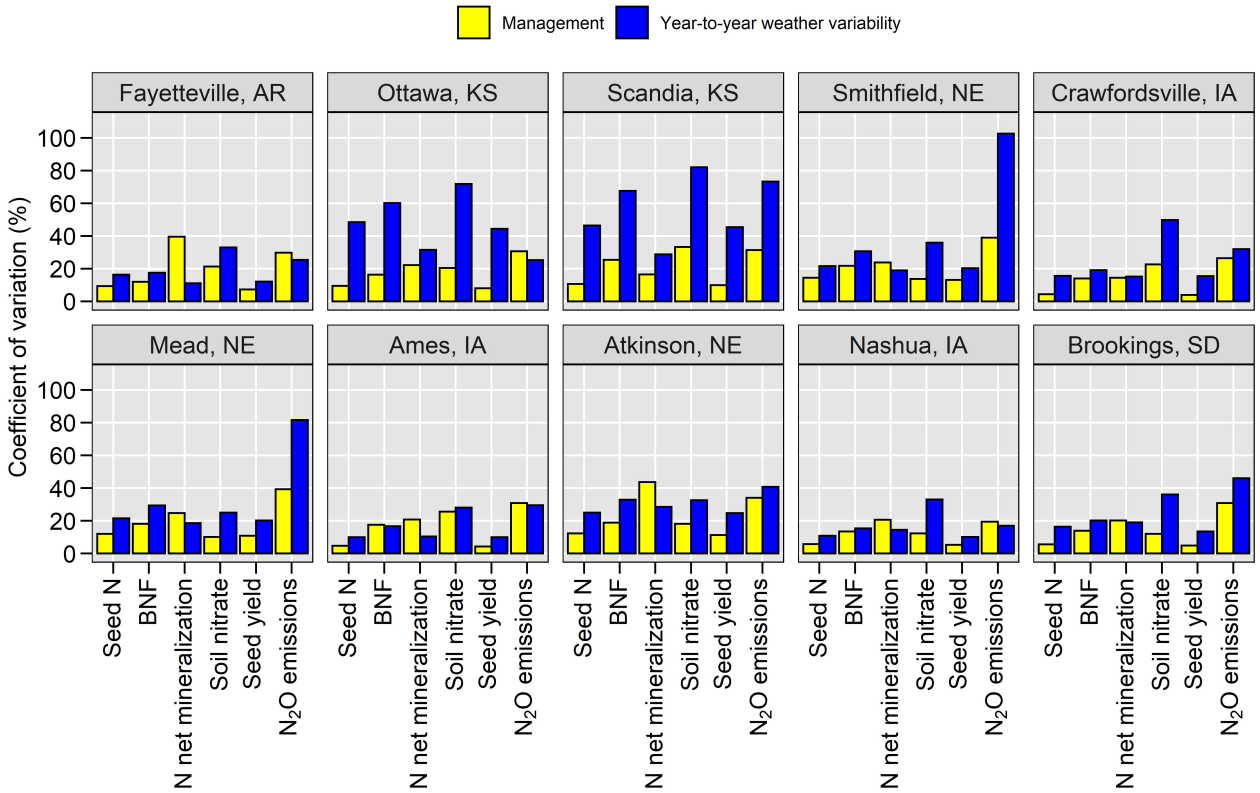

FIGURE 3 | Coefficient of variation for seed N, biological N fixation (BNF), N net mineralization, soil nitrate at harvest, seed yield and N_2O emissions from different weather years and management scenarios across contrasting environments in the United States Corn Belt.

influenced the most by weather variability and management (**Figure 3**). However, N_2O is also the smallest N flux in terms of magnitude (**Supplementary Figure 4**). Soil N mineralization and BNF were the next most influenced N fluxes while seed N and yields were the least affected. Hence, soybean yield buffered part of the variability created by management and weather on N fluxes.

Our analysis revealed a strong east to west (wet to dry) spatial gradient on the importance of weather and management (**Figure 3**). In environments with sufficient-to-excess moisture, management caused more variability in N fluxes than the inter-annual weather variability (e.g., Iowa), while in environments with insufficient moisture, management caused less variability in N fluxes than weather (e.g., Kansas). In irrigated environments (Nebraska and Arkansas), the contribution of weather on N flux variability was slightly lower than management practices. As a result, in environments with water limitations, management-induced changes in N_2O, BNF, and mineralization fluxes are less likely to be realized.

GxExM Scenarios Affect Nitrogen Fluxes in Different Ways

Although specific environments differed in the magnitude of responses to climate and management changes, the general responses were similar and were averaged over all locations to simplify the presentation (**Figures 4–6**).

Climate Change

The 2°C temperature increase under future climate scenarios (**Figure 1**) decreased BNF by 32% (**Figures 4A**, **5A**), seed N accumulation by 20% (**Figure 4A** and **Supplementary Figure 6A**), and N balance by 20% (**Figure 4A** and **Supplementary Figure 7A**), while increased N net mineralization by 24% (**Figures 4A**, **6A**), soil nitrate by 34% (**Figures 4A**, **6G**), and N_2O emissions by 19% (**Figure 4A** and **Supplementary Figure 8A**). Changes in rainfall patterns alone had a small effect on N fluxes (up to 3%). The combination of rainfall and temperature changes showed similar responses to single changes in temperature (**Figure 4**). Seed yield decreased under climate change scenarios, similar to seed N (**Supplementary Figure 9A**).

Nitrogen Management

High soil inorganic N levels created by the application of N fertilizers or carryover nitrate from the previous maize crop (**Table 1**) decreased BNF up to 23% (**Figures 4A**, **5B**) but increased soil nitrate at crop harvest up to 42% (**Figures 4A**, **6H**) and N_2O emissions up to 93% (**Figure 4A** and **Supplementary Figure 8B**). Seed N accumulation and N net mineralization were minimally affected by N management scenarios (**Figures 4**, **6B** and **Supplementary Figure 6B**). The application of fertilizers

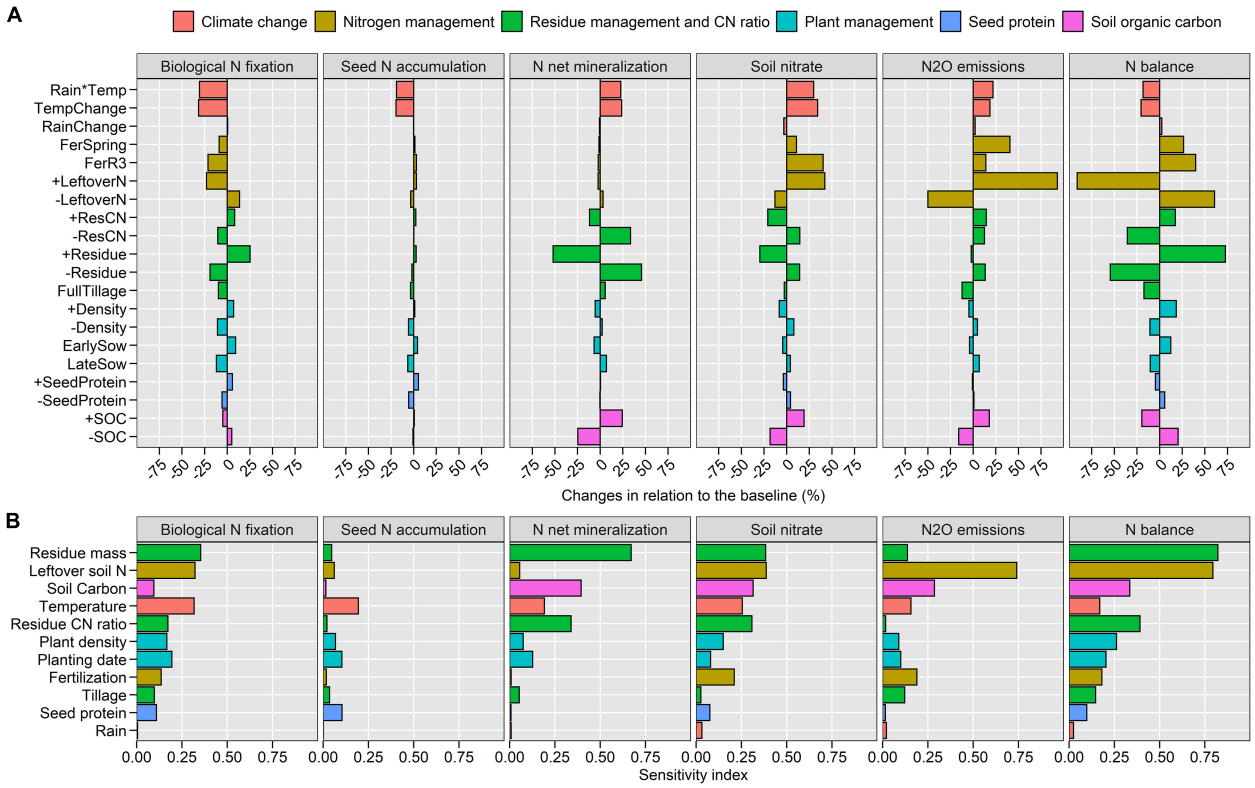

FIGURE 4 | Relative effects of climate change and management scenarios on soil-plant N dynamics compared to the baseline **(A)** and ranking of the importance of different GxExM variables with respect to N fluxes based on a sensitivity analysis **(B)**. Values were averaged over all locations and years. A summary table is also presented in **Supplementary Table 6**.

increased the N balance while the high carryover nitrate from the previous cropping years decreased the N balance (**Figure 4A** and **Supplementary Figure 7B**).

Residue Management and CN Ratio

Crop residue management influenced N fluxes the most (**Figure 4B**). Large amounts of stover increased BNF by 25% (**Figures 4A**, **5C**), decreased net mineralization by 52%, and soil nitrate at harvest by 30% (**Figures 4A**, **6C,I**). The high CN ratio scenario altered N fluxes similar to the stover scenario but at a threefold lower magnitude. Both large stover amount and high CN ratio increased N balance by 73 and 14%, respectively, because of the increase in BNF. Stover incorporation by tillage decreased 10% BNF, 17% N balance, and 12% N_2O emissions (**Figure 4**).

Plant Management and Seed Protein

Changes in plant management and seed protein influenced N fluxes considerably less than stover and N management (**Figure 4**). High plant density, early sowing date, and soybean variety with high seed protein increased BNF by 7, 9, and 6%, respectively (**Figures 4**, **5**). Plant management had little impact on mineralization, seed N, and yield. As a result, the N balance increased (**Figure 4**).

Soil Organic Carbon

A 15% increase in soil organic carbon increased net N mineralization by 25%, soil nitrate by 19%, and N_2O emissions by 20% (**Figures 4A**, **6F,L**). On the other hand, it decreased BNF by 5% and N balance by 20% (**Figures 4A**, **5F** and **Supplementary Figure 7F**). Seed N and yield were minimally influenced by increasing soil carbon (<1%; **Figure 4** and **Supplementary Figures 6F, 9F**). After stover and leftover soil N management practices, soil organic carbon showed the greatest influence on N fluxes (**Figure 4B**).

Water Management

To investigate the impact of water source and management (irrigation: water comes from surface vs. shallow water table: water comes from the subsoil) we performed region-specific simulations (**Table 2**). In the irrigated Nebraska and Arkansas locations, a simulation with no-irrigation revealed that irrigation increased BNF by 58%, seed N by 50%, net mineralization by 66%, and N_2O emission by 21% while decreasing N balance by 4%. In rainfed Kansas locations, the application of irrigation altered N fluxes similarly to Nebraska and Arkansas (**Table 2**). However, in rainfed Iowa locations with shallow water tables, irrigation had a substantially lower impact on N fluxes (up to 10%) compared to the impact of irrigation at the eastern locations. In contrast, the presence of shallow water tables in the Iowa locations increased

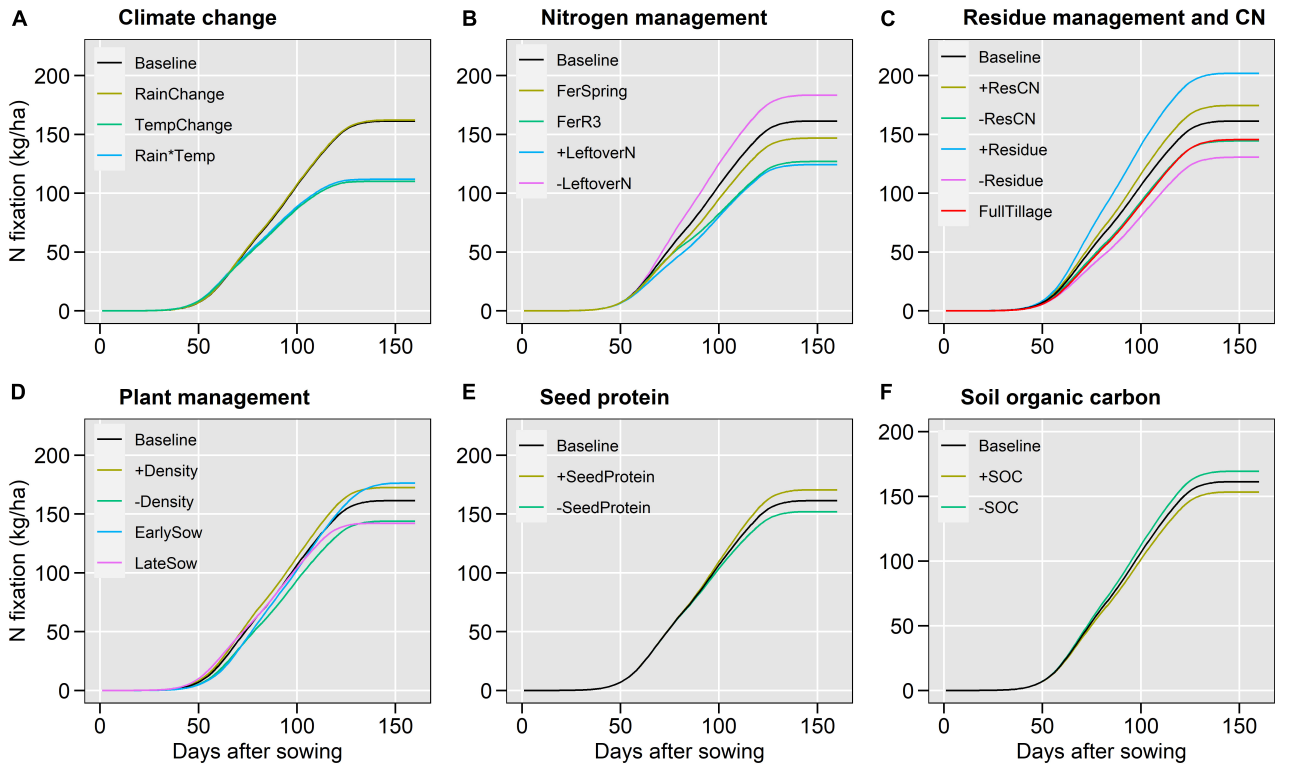

FIGURE 5 | GxExM effects on cumulative aboveground N fixation during the soybean growing season for different scenarios including climate change **(A)**, nitrogen management **(B)**, residue management and quality **(C)**, plant management **(D)**, seed protein **(E)** and soil organic carbon **(F)**. Values were averaged over 10 locations and 25-years per locations.

BNF by 21%, seed N by 16%, net mineralization by 10%, and N_2O emission by 68% while decreasing the N balance by 9%. The subsurface drainage that is used to regulate the water table depth in the Iowa locations had a low impact on BNF and seed N (less than 3%), increased N net mineralization by 9%, and decreased N_2O emissions and N balance by 24 and 8%, respectively. There were specific years and locations where subsurface drainage was more influential (**Supplementary Figure 10**).

DISCUSSION

Climate Change Impacts on Nitrogen Fluxes and Soybean Yields

Typically, climate change scenarios combined with uncertain assumptions for the future sowing date, sowing density, and varieties are used to drive crop model simulations to predict seed yield impacts, which generates inherent uncertainties in model predictions (Challinor et al., 2013; Folberth et al., 2016; Corbeels et al., 2018). Here we took a different approach. We performed a sensitivity analysis of both climate change and management settings on whole system processes across 10 soybean production environments to deeper understand and quantify the temporal dynamics of key N fluxes influencing productivity and environmental performance. Therefore, this study provides actionable data for improved management and adaptation to climate change (Thornton et al., 2014; Tui et al., 2021).

Our study revealed three important results: (1) climate change without management adaptation will decrease seed yields and N balance. This is mostly driven by temperature increases rather than shifts in rainfall patterns; (2) climate change will increase mineralization (and thus the soil N pool) and will decrease BNF, therefore, altering the source of N available for plant uptake; and (3) climate change will increase N_2O emissions because of the larger available mineral N during crop growth.

The decrease in BNF, seed N, and yields were mostly caused by the shortening of the crop growth duration due to increased temperatures (average reduction of 14 days, **Supplementary Figure 11**), which agrees with other studies (Purcell et al., 2004; Schlenker and Roberts, 2009; Zhang and Cai, 2013; Zipper et al., 2016; Jin et al., 2017; Schauberger et al., 2017; Zhao et al., 2017; Ciampitti et al., 2021). A portion of the anticipated future decline can be offset by adjusting the cultivar maturity group (Kucharik and Serbin, 2008; Zabel et al., 2021). Plant N uptake and BNF are highly coupled with dry matter accumulation (Herridge et al., 2001; Salvagiotti et al., 2008; Santachiara et al., 2017; Córdova et al., 2019), which explains why both N fluxes are decreasing. However, BNF is more sensitive to drought and excess water stress than photosynthesis or mineralization, another aspect that decreases BNF more than other plant–soil processes (Herridge et al., 2001; Purcell et al., 2004; Pasley et al., 2020). This leads to

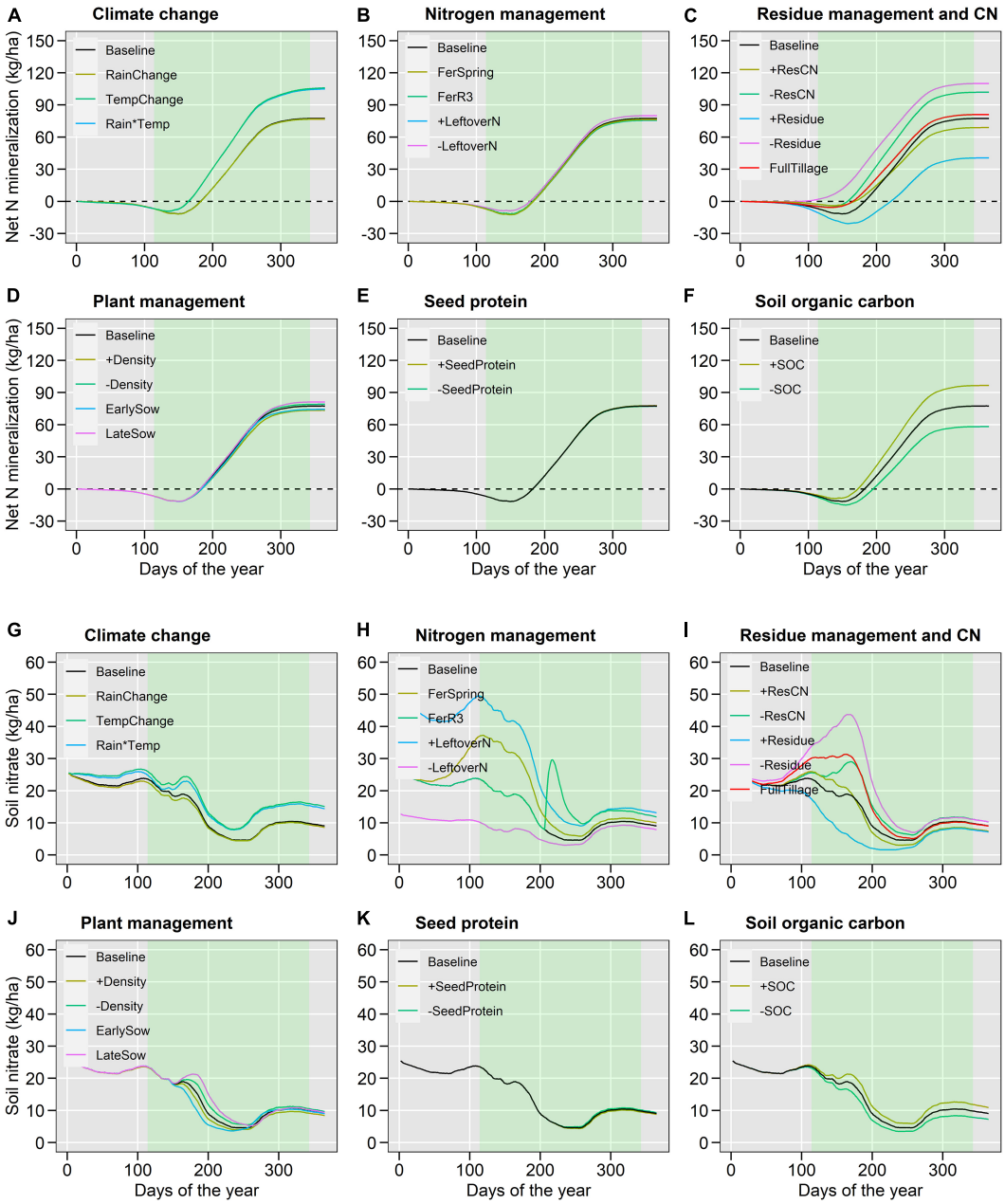

FIGURE 6 | GxExM effects on cumulative net N mineralization **(A–F)** and soil nitrate at 0–30 cm **(G–L)** for different scenarios including climate change **(A,G)**, nitrogen management **(B,H)**, residue management and quality **(C,I)**, plant management **(D,J)**, seed protein **(E,K)** and soil organic carbon **(F,L)**. The shaded area represents the average soybean growing period. Values were averaged over 10 locations and 25-years per locations.

further diminished N balance values at crop harvest (**Figure 4** and **Supplementary Figure 7**). N balance at harvest time had negative values across all assessed scenarios. Santachiara et al. (2017) found that a neutral N balance can be attained when BNF represents 80% of total soybean N uptake. The values found in the present study ranged from 30 to 70% (baseline conditions), which is consistent with the findings of Ciampitti and Salvagiotti (2018).

The increasing N mineralization and topsoil nitrate (**Figures 4–6**) with the simultaneous decrease in seed N uptake and soybean yields under climate change are of concern. Actions should be taken to manage the unused N after crop harvest, such as using cover crops (Udvardi et al., 2021). Our results revealed a 19% average increase in N_2O with climate change, which is probably an underestimate because we initialized the model at the start of every year. In the sensitivity analysis, we found that increased amounts of leftover N can increase N_2O by 93% (**Figure 4**). These results are supported by Iqbal et al. (2018) who observed increases in

TABLE 2 | Simulated impacts of water management on N fluxes (% changes in relation to baseline conditions).

Water management baseline	Scenarios	BNF	Seed N accumulation	N Net Mineralization	Soil nitrate	N_2O emissions	N balance
Irrigated (Nebraska and Arkansas)	Rainfed	−58	−50	−66	−24	−21	4
Rainfed (Kansas)	Irrigated	43	34	30	−11	7	−27
Rainfed with shallow WT (Ames, Iowa)	Irrigated	−1.5	0.6	8	6	1.1	−4
	No-WT	−25	−20	−12	−11	−72	15
	Tile	−0.5	0.7	3	1.1	−8	−3
Rainfed with shallow WT and tile drainage (Crawfordsville and Nashua, Iowa)	Irrigated	0.7	2	10	9	4	−6
	No-WT	−17	−12	−7	−11	−65	2
	No-Tile	−0.7	−4	−14	−6	41	14

BNF, biological N fixation; WT, water table.

N_2O losses in seasons following dry years (and thus high residual N values).

Management and Weather Variability Effects on Nitrogen Fluxes

Management practices altered N fluxes at a similar (or larger) magnitude than climate change (**Figure 4**). This suggests that there are opportunities to improve the productivity and environmental performance of soybean-based systems in the context of a changing climate. We found that N fluxes were affected the most by water management, then by soil management, and finally by plant management (**Table 2** and **Figure 4**). Water management requires long term investment in irrigation infrastructure and is dependent on water availability, while soil and plant management are more feasible and easier to adopt in the short term. Our results suggest that the management of stover (amount and quality) and of the carryover N from the previous year is very important for improving soybean performance in the short term (**Figure 4**). Large amounts of stover can enhance BNF (in accordance with Xie et al., 2021), decrease soil N pools (as inorganic N is used to break down stover) and reduce N_2O emissions, which is beneficial. To a smaller extent, plant management such as early sowing date and high plant density could also increase BNF (**Figure 4**), which is explained by the greater biomass production and yield (**Supplementary Figure 9**). These findings are consistent with Seneviratne et al. (2000) and de Borja Reis et al. (2021). While not explored in this study, we believe that stacked soil and plant management practices (e.g., Martinez-Feria et al., 2019) can reveal either a higher potential role of management practices to improve soybean-based systems performance and compensate, or even reverse, the negative impacts of climate change on soybean productivity. Future studies could explore this.

Our study revealed the key role of water source (irrigation, water table) and management (subsurface drainage) on N fluxes, which is not surprising given its control over key microbiological processes governing N dynamics. Irrigation had a large influence on N fluxes, increasing BNF, seed N, and mineralization by 50, 42, and 48%, respectively (**Table 2**). This practice has contributed to high and stable yield levels in the western Corn Belt and is standard practice (Grassini et al., 2014, 2015; Gibson et al., 2018). In the central-east part of the Corn Belt with rainfed crops, the existence of a shallow water table enhanced seed N by 16%, BNF by 21%, and mineralization by 10% compared to a non-water table scenario (**Table 2**). This result highlights the importance of considering the subsoil moisture on N fluxes, something that has been overlooked in previous studies. The subsurface drainage practice further increased seed N up to 4% (**Table 2**), which is similar to the findings of Mourtzinis et al. (2021) using experimental data. The small differences in the average results (drained vs. undrained) can be partially explained by the year-to-year weather variability. In dry years, the impact of subsurface drainage on yields and N fluxes was negligible, but in wet years (11 of 25 years; **Figure 1**) the impact was more pronounced, consistent with Castellano et al. (2019) and Mourtzinis et al. (2021). Subsurface drainage also reduced N_2O emissions by 24% (**Table 2**) due to increased soil aeration, which is consistent with Kumar et al. (2014) and Castellano et al. (2019).

Changes in management practices should be evaluated in the context of inter-annual weather variability (**Figure 3**). We found opportunities to alter N fluxes through management toward decreasing N_2O and increasing BNF but it is also concerning that an improvement in management can be overwhelmed by weather. An east-to-west gradient on the importance of management vs. weather variability was observed. When water limits crop production, changes in management practices are less likely to alter N fluxes in the desired way (e.g., increase BNF, decrease N_2O emissions). The CV in N fluxes arising from weather variability was twofold larger than that of management in Kansas (**Figure 3**). Therefore, management strategies are expected to increase BNF and productivity in regions and years with moderate to no water limitations. These results are supported by Battisti et al. (2018) who found that under favorable climate conditions in Brazil, soybean crop responses to improved management can be maximized. Current findings reinforce the concept that GxExM interactions preclude a single management recommendation for all environments (Serraj et al., 1999; Salvagiotti et al., 2008; Ciampitti and Salvagiotti, 2018). Simulation modeling and machine learning approaches can help in that respect. Future studies could leverage machine

learning (e.g., Shahhosseini et al., 2021) to create meta-models using results from process-based models for the identification of relationships between easily measured variables in the field and complex but important processes, such as BNF and N mineralization that are difficult to measure. This could lead to fast assessments and informed decisions.

The Value of the Systems Approach to Understanding Nitrogen Fluxes in the Context of Climate Change

Our study provides the first systems-level evaluation of soybean N dynamics across a wide range of environments, management practices, and climate change scenarios. This is important for understanding the complex agronomic system and conceptualizing metrics for environmental assessments in soybean-based systems as reported for maize in the United States Corn Belt (Tenorio et al., 2019). The high temporal resolution of generated results aided understanding of when soil N pools and N fluxes -the main determinants of seed N uptake- decrease or increase during the growing season. For example, we learned that seed N accumulation exceeds cumulative BNF around 110 days after sowing, leading to a negative N balance thereafter. If the target is a positive N balance, research should be directed on how to keep seed N below BNF in the last month of soybean growth. The soil nitrate pools declined to near-zero values approximately 50 days after sowing across locations, in accordance with Córdova et al. (2019), which explains the very low N_2O loss during soybean growth (**Supplementary Figure 4**). High soil inorganic N levels created by the application of N fertilizers or carryover nitrate from the previous maize crop were the main driver of increased N_2O emissions, which is consistent with Lu et al. (2021). We found the majority of N_2O fluxes to occur in the spring, while the magnitude of N_2O loss followed east to west spatial gradient (from 0.2 to 3.7 kg ha^{-1} $year^{-1}$). We attributed this gradient to higher cumulative rainfall (**Figure 1**) associated with the existence of shallow water tables in the eastern locations (**Table 2**).

The process-based systems analysis revealed tradeoffs and synergies among N fluxes (**Figures 4–6**, e.g., stover effects on BNF and mineralization). We found that the inter-annual weather variability in soybean yield and seed N uptake was less than the variability in other N fluxes (**Figure 3**). This suggests that soybean buffers are part of the variability caused by management and weather and that there are opportunities to alter N fluxes without compromising yields. Future climate change impact studies should expand the focus from seed yield impacts to whole system evaluation to further understand trade-offs and synergies in different environments.

We acknowledge that the representation of the agronomic system through simulation modeling is a big challenge. No biotic factors were considered in the simulations, which may preclude some identified solutions. While we believe that our modeling approach captures the most important abiotic factors for this study, we recognize that a model will never capture all bio-physical-chemical processes. We also recognize that model structure can bias results (Tao et al., 2018), and using a multi-model approach could increase confidence in the results (Li et al., 2015; Martre et al., 2015; Battisti et al., 2017). In our case, we ensured through extensive testing (**Supplementary Figure 1**) that the model used here could represent reality well. In fact, very few prior studies have tested a model against so many high-resolution and multi-faceted datasets before its application to answer scientific questions. While the approach we used to evaluate climate change impacts is relatively simple, it gives similar trends compared to more complex approaches such as using daily bias-corrected future climate outputs from RCPs-GCMs combinations (**Supplementary Figure 12**). Our study also captures important signals of future climate extremes (**Supplementary Figure 13**). Future studies could explore the impact of a maize-soybean rotation without a yearly reset to quantify potential synergies, negative impacts, and interactions. We also encourage exploring uncertainties in more detail by using daily future climate projections as well as a thorough assessment of climate extremes impacts.

CONCLUSION

This study enhances our understanding of the temporal and spatial dynamics of soil-plant N dynamics under current and future climate conditions in the United States. Climate change is expected to increase N mineralization and N_2O emissions and decrease BNF, seed N, and yields. Management practices altered N fluxes at about the same magnitude as climate change but in many different directions suggesting large opportunities to improve productivity and environmental performance in soybean-based cropping systems. Among many practices explored, we conclude that the management of maize stover (amount and quality) is very important in the short term, and water management (irrigation, subsurface drainage) is critical in the long term. Soybean yield buffered much of the variability caused by management and weather on N fluxes, which creates opportunities to manage N fluxes without compromising yields. This is more likely to be realized in regions with adequate to excess soil moisture.

DATA AVAILABILITY STATEMENT

The original contributions presented in the study are included in the article/**Supplementary Material**, further inquiries can be directed to the corresponding author/s.

AUTHOR CONTRIBUTIONS

EE contributed to methodology, software, data curation, formal analysis, visualization, and writing – original draft, review, and editing. IC, MC, LP, SN, PG, and PK contributed to fund

acquisition, investigation, and writing – review, and editing. NL, LM, and AB contributed to the investigation, writing – review, and editing. SA contributed to the conceptualization, supervision, funding acquisition, methodology, software, and writing – original draft, review, and editing. All authors contributed to the article and approved the submitted version.

FUNDING

This work was mainly funded by the United Soybean Board (2020-152-0104), Environmental Defense Fund, FFAR (#534264; improving the simulation of soil moisture and crop yields in the United States Corn Belt), the Plant Sciences Institute of Iowa State University, Iowa Soybean Association and USDA Hatch project (IOW10480), the South Dakota Soybean Research and Promotional Council.

ACKNOWLEDGMENTS

We thank Isaiah Huber for his assistance in retrieving the future climate projections for modeling, and C. Cordova, K. Togliatti, A. Mastrodomenico, A. King and L. F. Antunes de Almeida for assistance with data collection from field experiments. Lastly, we thank the APSIM Initiative for quality assurance and a structured innovation program for APSIM's modeling software, which is provided free for research and development use.

SUPPLEMENTARY MATERIAL

The Supplementary Material for this article can be found online at: https://www.frontiersin.org/articles/10.3389/fpls.2022.849896/full#supplementary-material

REFERENCES

Archontoulis, S. V., Castellano, M. J., Licht, M. A., Nichols, V., Baum, M., Huber, I., et al. (2020). Predicting crop yields and soil-plant nitrogen dynamics in the US Corn Belt. *Crop Sci.* 60, 721–738. doi: 10.1002/csc2.20039

Archontoulis, S. V., Huber, I., Miguez, F. E., Thorburn, P. J., Rogovska, N., and Laird, D. A. (2016). A model for mechanistic and system assessments of biochar effects on soils and crops and trade-offs. *GCB Bioenergy* 8, 1028–1045. doi: 10.1111/GCBB.12314

Archontoulis, S. V., Miguez, F. E., and Moore, K. J. (2014). Evaluating APSIM maize, soil water, soil nitrogen, manure, and soil temperature modules in the Midwestern United States. *Agron. J.* 106, 1025–1040. doi: 10.2134/agronj2013.0421

Assefa, Y., Purcell, L. C., Salmeron, M., Naeve, S., Casteel, S. N., Kovács, P., et al. (2019). Assessing variation in us soybean seed composition (protein and oil). *Front. Plant Sci.* 10:298. doi: 10.3389/FPLS.2019.00298

Balboa, G. R., Sadras, V. O., and Ciampitti, I. A. (2018). Shifts in soybean yield, nutrient uptake, and nutrient stoichiometry: a historical synthesis-analysis. *Crop Sci.* 58, 43–54. doi: 10.2135/CROPSCI2017.06.0349

Battisti, R., Sentelhas, P. C., and Boote, K. J. (2017). Inter-comparison of performance of soybean crop simulation models and their ensemble in southern Brazil. *F. Crop. Res.* 200, 28–37. doi: 10.1016/j.fcr.2016.10.004

Battisti, R., Sentelhas, P. C., Pascoalino, J. A. L., Sako, H., de Sá Dantas, J. P., and Moraes, M. F. (2018). Soybean yield gap in the areas of yield contest in Brazil. *Int. J. Plant Prod.* 12, 159–168. doi: 10.1007/s42106-018-0016-0

Bender, R. R., Haegele, J. W., and Below, F. E. (2015). Nutrient uptake, partitioning, and remobilization in modern soybean varieties. *Agron. J.* 107, 563–573. doi: 10.2134/AGRONJ14.0435

Burgess, M. S., Mehuys, G. R., and Madramootoo, C. A. (2011). Decomposition of grain-corn residues (Zea mays L.): a litterbag study under three tillage systems. *Can. J. Soil Sci.* 82, 127–138. doi: 10.4141/S01-013

Cafaro La Menza, N., Monzon, J. P., Specht, J. E., and Grassini, P. (2017). Is soybean yield limited by nitrogen supply? *F. Crop. Res.* 213, 204–212. doi: 10.1016/J.FCR.2017.08.009

Cafaro La Menza, N., Monzon, J. P., Specht, J. E., Lindquist, J. L., Arkebauer, T. J., Graef, G., et al. (2019). Nitrogen limitation in high-yield soybean: seed yield, N accumulation, and N-use efficiency. *F. Crop. Res.* 237, 74–81. doi: 10.1016/J.FCR.2019.04.009

Carciochi, W. D., Schwalbert, R., Andrade, F. H., Corassa, G. M., Carter, P., Gaspar, A. P., et al. (2019). Soybean seed yield response to plant density by yield environment in North America. *Agron. J.* 111, 1923–1932. doi: 10.2134/agronj2018.10.0635

Cassman, K. G., and Dobermann, A. (2022). Nitrogen and the future of agriculture: 20 years on: this article belongs to Ambio's 50th anniversary collection. theme: solutions-oriented research. *Ambio* 51, 17–24. doi: 10.1007/S13280-021-01526-W

Castellano, M. J., Archontoulis, S. V., Helmers, M. J., Poffenbarger, H. J., and Six, J. (2019). Sustainable intensification of agricultural drainage. *Nat. Sustain.* 2, 914–921. doi: 10.1038/s41893-019-0393-0

Challinor, A. J., Smith, M. S., and Thornton, P. (2013). Use of agro-climate ensembles for quantifying uncertainty and informing adaptation. *Agric. For. Meteorol.* 170, 2–7. doi: 10.1016/J.AGRFORMET.2012.09.007

Chen, C., Lawes, R., Fletcher, A., Oliver, Y., Robertson, M., Bell, M., et al. (2016). How well can APSIM simulate nitrogen uptake and nitrogen fixation of legume crops? *F. Crop. Res.* 187, 35–48. doi: 10.1016/J.FCR.2015.12.007

Ciampitti, I. A., and Salvagiotti, F. (2018). New insights into soybean biological nitrogen fixation. *Agron. J.* 110, 1185–1196. doi: 10.2134/agronj2017.06.0348

Ciampitti, I. A., de Borja Reis, A. F., Córdova, S. C., Castellano, M. J., Archontoulis, S. V., Correndo, A. A., et al. (2021). Revisiting biological nitrogen fixation dynamics in soybeans. *Front. Plant Sci.* 12:2011. doi: 10.3389/FPLS.2021.727021

Collino, D. J., Salvagiotti, F., Perticari, A., Piccinetti, C., Ovando, G., Urquiaga, S., et al. (2015). Biological nitrogen fixation in soybean in Argentina: relationships with crop, soil, and meteorological factors. *Plant Soil* 392, 239–252. doi: 10.1007/s11104-015-2459-8

Corbeels, M., Berre, D., Rusinamhodzi, L., and Lopez-Ridaura, S. (2018). Can we use crop modelling for identifying climate change adaptation options? *Agric. For. Meteorol.* 256–257, 46–52. doi: 10.1016/J.AGRFORMET.2018.02.026

Córdova, S. C., Castellano, M. J., Dietzel, R., Licht, M. A., Togliatti, K., Martinez-Feria, R., et al. (2019). Soybean nitrogen fixation dynamics in Iowa, USA. *F. Crop. Res.* 236, 165–176. doi: 10.1016/j.fcr.2019.03.018

Daigh, A. L. M., Dick, W. A., Helmers, M. J., Lal, R., Lauer, J. G., Nafziger, E., et al. (2018). Yields and yield stability of no-till and chisel-plow fields in the Midwestern US Corn Belt. *F. Crop. Res.* 218, 243–253. doi: 10.1016/J.FCR.2017.04.002

de Borja Reis, A. F., Moro Rosso, L., Purcell, L. C., Naeve, S., Casteel, S. N., Kovács, P., et al. (2021). Environmental factors associated with nitrogen fixation prediction in soybean. *Front. Plant Sci.* 12:675410. doi: 10.3389/FPLS.2021.675410

De Valpine, P., and Harte, J. (2001). Plant responses to experimental warming in a Montane Meadow. *Ecology* 82, 637–648. doi: 10.2307/2680185

Dietzel, R., Liebman, M., Ewing, R., Helmers, M., Horton, R., Jarchow, M., et al. (2016). How efficiently do corn- and soybean-based cropping systems use water? A systems modeling analysis. *Glob. Chang. Biol.* 22, 666–681. doi: 10.1111/gcb.13101

Ebrahimi-Mollabashi, E., Huth, N. I., Holzwoth, D. P., Ordóñez, R. A., Hatfield, J. L., Huber, I., et al. (2019). Enhancing APSIM to simulate excessive moisture effects on root growth. *F. Crop. Res.* 236, 58–67. doi: 10.1016/j.fcr.2019.03.014

FAOSTAT (2021). *Food and Agriculture Organization of the United Nations Statistics Division*. Available online at: http://www.fao.org/faostat/en/#data/TP (accessed on July 27, 2021)

Folberth, C., Skalský, R., Moltchanova, E., Balkovič, J., Azevedo, L. B., Obersteiner, M., et al. (2016). Uncertainty in soil data can outweigh climate impact

signals in global crop yield simulations. *Nat. Commun.* 7:11872. doi: 10.1038/ncomms11872

Gaspar, A. P., Laboski, C. A. M., Naeve, S. L., and Conley, S. P. (2017). Dry matter and nitrogen uptake, partitioning, and removal across a wide range of soybean seed yield levels. *Crop Sci.* 57, 2170–2182. doi: 10.2135/CROPSCI2016.05.0322

Gaydon, D. S., Balwinder-Singh, Wang, E., Poulton, P. L., Ahmad, B., Ahmed, F., et al. (2017). Evaluation of the APSIM model in cropping systems of Asia. *F. Crop. Res.* 204, 52–75. doi: 10.1016/J.FCR.2016.12.015

Gibson, K. E. B., Yang, H. S., Franz, T., Eisenhauer, D., Gates, J. B., Nasta, P., et al. (2018). Assessing explanatory factors for variation in on-farm irrigation in US maize-soybean systems. *Agric. Water Manag.* 197, 34–40. doi: 10.1016/J.AGWAT.2017.11.008

Grassini, P., Specht, J. E., Tollenaar, M., Ciampitti, I., and Cassman, K. G. (2015). "High-yield maize-soybean cropping systems in the US Corn Belt," in *Crop Physiology: Applications for Genetic Improvement and Agronomy: Second Edition*, eds V. O. Sadras and D. F. Calderini (Amsterdam: Elsevier Inc), 17–41. doi: 10.1016/B978-0-12-417104-6.00002-9

Grassini, P., Torrion, J. A., Cassman, K. G., Yang, H. S., and Specht, J. E. (2014). Drivers of spatial and temporal variation in soybean yield and irrigation requirements in the western US Corn Belt. *F. Crop. Res.* 163, 32–46. doi: 10.1016/J.FCR.2014.04.005

Hamby, D. M. (1994). A review of techniques for parameter sensitivity analysis of environmental models. *Environ. Monit. Assess.* 32, 135–154. doi: 10.1007/BF00547132

Helmers, M., Christianson, R., Brenneman, G., Lockett, D., and Pederson, C. (2012). Water table, drainage, and yield response to drainage water management in southeast Iowa. *J. Soil Water Conserv.* 67, 495–501. doi: 10.2489/JSWC.67.6.495

Herridge, D. F., Turpin, J. E., and Robertson, M. J. (2001). Improving nitrogen fixation of crop legumes through breeding and agronomic management: analysis with simulation modelling. *Aust. J. Exp. Agric.* 41, 391–401. doi: 10.1071/EA00041

Holzworth, D. P., Huth, N. I., deVoil, P. G., Zurcher, E. J., Herrmann, N. I., McLean, G., et al. (2014). APSIM – evolution towards a new generation of agricultural systems simulation. *Environ. Model. Softw.* 62, 327–350. doi: 10.1016/J.ENVSOFT.2014.07.009

Hunter, M. C., Smith, R. G., Schipanski, M. E., Atwood, L. W., and Mortensen, D. A. (2017). Agriculture in 2050: recalibrating targets for sustainable intensification. *Bioscience* 67, 386–391. doi: 10.1093/biosci/bix010

Huth, N. I., Bristow, K. L., and Verburg, K. (2012). SWIM3: model use, calibration, and validation. *Trans. ASABE* 55, 1303–1313. doi: 10.13031/2013.42243

Huth, N. I., Thorburn, P. J., Radford, B. J., and Thornton, C. M. (2010). Impacts of fertilisers and legumes on N2O and CO2 emissions from soils in subtropical agricultural systems: a simulation study. *Agric. Ecosyst. Environ.* 136, 351–357. doi: 10.1016/j.agee.2009.12.016

Intergovernmental Panel on Climate Change [IPCC] (2018). "Summary for policymakers," in *Global Warming of 1.5°C. An IPCC Special Report on the Impacts of Global Warming of 1.5°C Above Pre-industrial Levels and Related Global Greenhouse Gas Emission Pathways, in the Context of Strengthening the Global Response to the Threat of Climate Change, Sustainable Development, and Efforts to Eradicate Poverty*, eds V. Masson-Delmotte, P. Zhai, H.-O. Pörtner, D. Roberts, J. Skea, P. R. Shukla, et al. (Geneva: World Meteorological Organization), 32.

Iqbal, J., Necpalova, M., Archontoulis, S. V., Anex, R. P., Bourguignon, M., Herzmann, D., et al. (2018). Extreme weather-year sequences have nonadditive effects on environmental nitrogen losses. *Glob. Chang. Biol.* 24, e303–e317. doi: 10.1111/GCB.13866

Jin, Z., Zhuang, Q., Wang, J., Archontoulis, S. V., Zobel, Z., and Kotamarthi, V. R. (2017). The combined and separate impacts of climate extremes on the current and future US rainfed maize and soybean production under elevated CO2. *Glob. Chang. Biol.* 23, 2687–2704. doi: 10.1111/gcb.13617

Kothari, K., Battisti, R., Boote, K. J., Archontoulis, S. V., Confalone, A., Constantin, J., et al. (2022). Are soybean models ready for climate change food impact assessments? *Eur. J. Agron.* 135:126482. doi: 10.1016/J.EJA.2022.126482

Kucharik, C. J., and Serbin, S. P. (2008). Impacts of recent climate change on Wisconsin corn and soybean yield trends. *Environ. Res. Lett.* 3:034003. doi: 10.1088/1748-9326/3/3/034003

Kumar, S., Nakajima, T., Kadono, A., Lal, R., and Fausey, N. (2014). Long-term tillage and drainage influences on greenhouse gas fluxes from a poorly drained soil of central Ohio. *J. Soil Water Conserv.* 69, 553–563. doi: 10.2489/JSWC.69.6.553

Li, T., Hasegawa, T., Yin, X., Zhu, Y., Boote, K., Adam, M., et al. (2015). Uncertainties in predicting rice yield by current crop models under a wide range of climatic conditions. *Glob. Chang. Biol.* 21, 1328–1341. doi: 10.1111/gcb.12758

Lu, C., Yu, Z., Zhang, J., Cao, P., Tian, H., and Nevison, C. (2021). Century-long changes and drivers of soil nitrous oxide (N2O) emissions across the contiguous United States. *Glob. Chang. Biol.* 28, 2505–2524. doi: 10.1111/GCB.16061

Malone, R. W., Huth, N., Carberry, P. S., Ma, L., Kaspar, T. C., Karlen, D. L., et al. (2007). Evaluating and predicting agricultural management effects under tile drainage using modified APSIM. *Geoderma* 140, 310–322. doi: 10.1016/j.geoderma.2007.04.014

Martinez-Feria, R. A., Dietzel, R., Liebman, M., Helmers, M. J., and Archontoulis, S. V. (2016). Rye cover crop effects on maize: a system-level analysis. *F. Crop. Res.* 196, 145–159. doi: 10.1016/J.FCR.2016.06.016

Martinez-Feria, R., Nichols, V., Basso, B., and Archontoulis, S. (2019). Can multi-strategy management stabilize nitrate leaching under increasing rainfall? *Environ. Res. Lett.* 14:124079. doi: 10.1088/1748-9326/AB5CA8

Martre, P., Wallach, D., Asseng, S., Ewert, F., Jones, J. W., Rötter, R. P., et al. (2015). Multimodel ensembles of wheat growth: many models are better than one. *Glob. Chang. Biol.* 21, 911–925. doi: 10.1111/gcb.12768

Mohanty, M., Probert, M. E., Reddy, K. S., Dalal, R. C., Mishra, A. K., Subba Rao, A., et al. (2012). Simulating soybean-wheat cropping system: APSIM model parameterization and validation. *Agric. Ecosyst. Environ.* 152, 68–78. doi: 10.1016/j.agee.2012.02.013

Moreira, A., Moraes, L. A. C., Schroth, G., and Mandarino, J. M. G. (2015). Effect of Nitrogen, Row Spacing, and Plant Density on Yield, Yield Components, and Plant Physiology in Soybean–Wheat Intercropping. *Agron. J.* 107, 2162–2170. doi: 10.2134/AGRONJ15.0121

Mourtzinis, S., Andrade, J. F., Grassini, P., Edreira, J. I. R., Kandel, H., Naeve, S., et al. (2021). Assessing benefits of artificial drainage on soybean yield in the North Central US region. *Agric. Water Manag.* 243:106425. doi: 10.1016/J.AGWAT.2020.106425

Mourtzinis, S., Kaur, G., Orlowski, J. M., Shapiro, C. A., Lee, C. D., Wortmann, C., et al. (2018). Soybean response to nitrogen application across the United States: a synthesis-analysis. *F. Crop. Res.* 215, 74–82. doi: 10.1016/J.FCR.2017.09.035

Müller, C., Franke, J., Jägermeyr, J., Ruane, A. C., Elliott, J., Moyer, E., et al. (2021). Exploring uncertainties in global crop yield projections in a large ensemble of crop models and CMIP5 and CMIP6 climate scenarios. *Environ. Res. Lett.* 16:34040. doi: 10.1088/1748-9326/abd8fc

NASS (2020). *Surveys. National Agricultural Statistics Service*. San Antonio, TX: USDA.

Nunes, M. R., De, M., McDaniel, M. D., Kovar, J. L., Birrell, S., and Karlen, D. L. (2021). Science-based maize stover removal can be sustainable. *Agron. J.* 113, 3178–3192. doi: 10.1002/AGJ2.20724

Nunes, M. R., van Es, H. M., Veum, K. S., Amsili, J. P., and Karlen, D. L. (2020). Anthropogenic and Inherent Effects on Soil Organic Carbon across the U.S. *Sustainability* 12:5695. doi: 10.3390/su12145695

Ortel, C. C., Roberts, T. L., Hoegenauer, K. A., Purcell, L. C., Slaton, N. A., and Gbur, E. E. (2020). Soybean maturity group and planting date influence grain yield and nitrogen dynamics. *Agrosystems Geosci. Environ.* 3:e20077. doi: 10.1002/AGG2.20077

Palmer, J., Thorburn, P. J., Biggs, J. S., Dominati, E. J., Probert, M. E., Meier, E. A., et al. (2017). Nitrogen cycling from increased soil organic carbon contributes both positively and negatively to ecosystem services in wheat agro-ecosystems. *Front. Plant Sci.* 8:731. doi: 10.3389/FPLS.2017.00731/BIBTEX

Pasley, H. R., Huber, I., Castellano, M. J., and Archontoulis, S. V. (2020). Modeling Flood-Induced Stress in Soybeans. *Front. Plant Sci.* 11:62. doi: 10.3389/fpls.2020.00062

Pasley, H., Nichols, V., Castellano, M., Baum, M., Kladivko, E., Helmers, M., et al. (2021). Rotating maize reduces the risk and rate of nitrate leaching. *Environ. Res. Lett.* 16:064063. doi: 10.1088/1748-9326/ABEF8F

Probert, M. E., Delve, R. J., Kimani, S. K., and Dimes, J. P. (2005). Modelling nitrogen mineralization from manures: representing quality aspects by varying C:N ratio of sub-pools. *Soil Biol. Biochem.* 37, 279–287. doi: 10.1016/J.SOILBIO.2004.07.040

Probert, M. E., Dimes, J. P., Keating, B. A., Dalal, R. C., and Strong, W. M. (1998). APSIM's water and nitrogen modules and simulation of the dynamics of water and nitrogen in fallow systems. *Agric. Syst.* 56, 1–28. doi: 10.1016/S0308-521X(97)00028-0

Puntel, L. A., Sawyer, J. E., Barker, D. W., Dietzel, R., Poffenbarger, H., Castellano, M. J., et al. (2016). Modeling long-term corn yield response to nitrogen rate and crop rotation. *Front. Plant Sci.* 7:1630. doi: 10.3389/FPLS.2016.01630

Purcell, L. C., Serraj, R., Sinclair, T. R., and De, A. (2004). Soybean N2 fixation estimates, ureide concentration, and yield responses to drought. *Crop Sci.* 44, 484–492. doi: 10.2135/CROPSCI2004.4840

R Development Core Team (2010). *R: A Language and Environment for Statistical Computing*. Vienna: R Foundation for Statistical Computing.

Radzka, E., Rymuza, K., and Wysokinski, A. (2021). Nitrogen uptake from different sources by soybean grown at different sowing densities. *Agronomy* 11:720. doi: 10.3390/AGRONOMY11040720

Robertson, M. J., and Lilley, J. M. (2016). Simulation of growth, development and yield of canola (Brassica napus) in APSIM. *Crop Pasture Sci.* 67, 332–344. doi: 10.1071/CP15267

Robertson, M. J., Carberry, P. S., Huth, N. I., Turpin, J. E., Probert, M. E., Poulton, P. L., et al. (2002). Simulation of growth and development of diverse legume species in APSIM. *Aust. J. Agric. Res.* 53, 429–446. doi: 10.1071/AR01106

Salvagiotti, F., Cassman, K. G., Specht, J. E., Walters, D. T., Weiss, A., and Dobermann, A. (2008). Nitrogen uptake, fixation and response to fertilizer N in soybeans: a review. *F. Crop. Res.* 108, 1–13. doi: 10.1016/j.fcr.2008.03.001

Santachiara, G., Borrás, L., Salvagiotti, F., Gerde, J. A., and Rotundo, J. L. (2017). Relative importance of biological nitrogen fixation and mineral uptake in high yielding soybean cultivars. *Plant Soil* 418, 191–203. doi: 10.1007/S11104-017-3279-9

Schauberger, B., Archontoulis, S., Arneth, A., Balkovic, J., Ciais, P., Deryng, D., et al. (2017). Consistent negative response of US crops to high temperatures in observations and crop models. *Nat. Commun.* 8:13931. doi: 10.1038/ncomms13931

Schlenker, W., and Roberts, M. J. (2009). Nonlinear temperature effects indicate severe damages to U.S. crop yields under climate change. *Proc. Natl. Acad. Sci. U.S.A.* 106, 15594–15598. doi: 10.1073/pnas.0906865106

Seneviratne, G., Van Holm, L. H. J., and Ekanayake, E. M. H. G. S. (2000). Agronomic benefits of rhizobial inoculant use over nitrogen fertilizer application in tropical soybean. *F. Crop. Res.* 68, 199–203. doi: 10.1016/S0378-4290(00)00123-4

Serraj, R., Sinclair, T. R., and Purcell, L. C. (1999). Symbiotic N2 fixation response to drought. *J. Exp. Bot.* 50, 143–155. doi: 10.1093/jxb/50.331.143

Shahhosseini, M., Hu, G., Huber, I., and Archontoulis, S. V. (2021). Coupling machine learning and crop modeling improves crop yield prediction in the US Corn Belt. *Sci. Rep.* 11:1606. doi: 10.1038/s41598-020-80820-1

Sinclair, T. R., and de Wit, C. T. (1976). Analysis of the Carbon and Nitrogen limitations to soybean yield. *Agron. J.* 68, 319–324. doi: 10.2134/AGRONJ1976.00021962006800020021X

Soil Survey Staff (2019). *Soil Survey Geographic (SSURGO) Database*. Washington, DC: USDA Natural Resources Conservation Service.

Tao, F., Rötter, R. P., Palosuo, T., Gregorio Hernández Díaz-Ambrona, C., Mínguez, M. I, Semenov, M. A., et al. (2018). Contribution of crop model structure, parameters and climate projections to uncertainty in climate change impact assessments. *Glob. Chang. Biol.* 24, 1291–1307. doi: 10.1111/GCB.14019

Tenorio, F. A. M., Eagle, A. J., McLellan, E. L., Cassman, K. G., Howard, R., Below, F. E., et al. (2019). Assessing variation in maize grain nitrogen concentration and its implications for estimating nitrogen balance in the US North Central region. *F. Crop. Res.* 240, 185–193. doi: 10.1016/j.fcr.2018.10.017

Teutschbein, C., and Seibert, J. (2012). Bias correction of regional climate model simulations for hydrological climate-change impact studies: review and evaluation of different methods. *J. Hydrol.* 456–457, 12–29. doi: 10.1016/J.JHYDROL.2012.05.052

Thorburn, P. J., Biggs, J. S., Collins, K., and Probert, M. E. (2010). Using the APSIM model to estimate nitrous oxide emissions from diverse Australian sugarcane production systems. *Agric. Ecosyst. Environ.* 136, 343–350. doi: 10.1016/j.agee.2009.12.014

Thornton, P. K., Ericksen, P. J., Herrero, M., and Challinor, A. J. (2014). Climate variability and vulnerability to climate change: a review. *Glob. Chang. Biol.* 20, 3313–3328. doi: 10.1111/GCB.12581

Tui, S. H.-K., Descheemaeker, K., Valdivia, R. O., Masikati, P., Sisito, G., Moyo, E. N., et al. (2021). Climate change impacts and adaptation for dryland farming systems in Zimbabwe: a stakeholder-driven integrated multi-model assessment. *Clim. Chang.* 168:10. doi: 10.1007/S10584-021-03151-8

Turner, M. M., and Henry, H. A. L. (2010). Net nitrogen mineralization and leaching in response to warming and nitrogen deposition in a temperate old field: the importance of winter temperature. *Oecologia* 162, 227–236. doi: 10.1007/S00442-009-1435-5

Udvardi, M., Below, F. E., Castellano, M. J., Eagle, A. J., Giller, K. E., Ladha, J. K., et al. (2021). A research road map for responsible use of agricultural Nitrogen. *Front. Sustain. Food Syst.* 5:660155. doi: 10.3389/FSUFS.2021.660155

Wegerer, R., Popp, M., Hu, X., and Purcell, L. (2015). Soybean maturity group selection: irrigation and nitrogen fixation effects on returns. *F. Crop. Res.* 180, 1–9. doi: 10.1016/J.FCR.2015.05.002

Wu, Y., Wang, E., He, D., Liu, X., Archontoulis, S. V., Huth, N. I., et al. (2019). Combine observational data and modelling to quantify cultivar differences of soybean. *Eur. J. Agron.* 111:125940. doi: 10.1016/J.EJA.2019.125940

Xie, Z., Li, Y., Yu, Z., Wang, G., Tang, C., Mathesius, U., et al. (2021). Incorporation of maize crop residue maintains soybean yield through the stimulation of nitrogen fixation rather than residue-derived nitrogen in Mollisols. *F. Crop. Res.* 272:108269. doi: 10.1016/J.FCR.2021.108269

Zabel, F., Müller, C., Elliott, J., Minoli, S., Jägermeyr, J., Schneider, J. M., et al. (2021). Large potential for crop production adaptation depends on available future varieties. *Glob. Chang. Biol.* 27, 3870–3882. doi: 10.1111/GCB.15649

Zhang, X., and Cai, X. (2013). Climate change impacts on global agricultural water deficit. *Geophys. Res. Lett.* 40, 1111–1117. doi: 10.1002/GRL.50279

Zhao, C., Liu, B., Piao, S., Wang, X., Lobell, D. B., Huang, Y., et al. (2017). Temperature increase reduces global yields of major crops in four independent estimates. *Proc. Natl. Acad. Sci. U.S.A.* 114, 9326–9331. doi: 10.1073/pnas.1701762114

Zhao, S., Xu, X., Wei, D., Lin, X., Qiu, S., Ciampitti, I., et al. (2020). Soybean yield, nutrient uptake and stoichiometry under different climate regions of northeast China. *Sci. Rep.* 10:8431. doi: 10.1038/s41598-020-65447-6

Zipper, S. C., Qiu, J., and Kucharik, C. J. (2016). Drought effects on US maize and soybean production: spatiotemporal patterns and historical changes. *Environ. Res. Lett.* 11:094021. doi: 10.1088/1748-9326/11/9/094021

Conflict of Interest: The authors declare that the research was conducted in the absence of any commercial or financial relationships that could be construed as a potential conflict of interest.

Publisher's Note: All claims expressed in this article are solely those of the authors and do not necessarily represent those of their affiliated organizations, or those of the publisher, the editors and the reviewers. Any product that may be evaluated in this article, or claim that may be made by its manufacturer, is not guaranteed or endorsed by the publisher.

frontiers | Frontiers in Plant Science

ORIGINAL RESEARCH
published: 09 May 2022
doi: 10.3389/fpls.2022.817909

Undirected Sucrose Efflux Mitigation by the FT-Like SP6A Preferentially Enhances Tuber Resource Partitioning

*Bas van den Herik and Kirsten ten Tusscher**

Computational Developmental Biology, Utrecht University, Utrecht, Netherlands

The yield of harvestable plant organs depends on overall photosynthetic output and the subsequent distribution of the produced assimilates from source leaves across different sink organs. In this study, we aimed to obtain, using a two-sink transport model, mechanistic understanding of how the interplay between sink and pathway properties together determines sink resource partitioning. As a working example, we analyzed the partitioning of resources within potato plants, investigating the determinants of tuber sink yield. Our results indicated that, contrary to earlier studies, with a spatially explicit biophysically detailed model, transport pathway properties significantly affect sink resource partitioning within the physiologically relevant domain. Additionally, we uncovered that xylem flow, through its hydraulic coupling to the phloem, and sucrose efflux along the phloem, also significantly affected resource partitioning. For tubers, it is the cumulative disadvantage compared to sink leaves (distance, xylem flow, and sucrose efflux) that enable an undirected SP6A-mediated reduction of sucrose efflux to preferentially benefit tuber resource partitioning. Combined with the SP6A-mediated sink strength increase, undirected SP6A introduction significantly enhances tuber resource partitioning.

Keywords: resource partitioning, sucrose, phloem, xylem, SP6A, potato, biophysical model, SWEET

OPEN ACCESS

Edited by:
Maciej Andrzej Zwieniecki, University of California, Davis, United States

Reviewed by:
Robert D. Hancock, The James Hutton Institute, United Kingdom
Teemu Hölttä, University of Helsinki, Finland

***Correspondence:**
Kirsten ten Tusscher
K.H.W.J.tenTusscher@uu.nl

Specialty section:
This article was submitted to Plant Biophysics and Modeling, a section of the journal Frontiers in Plant Science

Received: *18 November 2021*
Accepted: *18 March 2022*
Published: *09 May 2022*

Citation:
van den Herik B and ten Tusscher K (2022) Undirected Sucrose Efflux Mitigation by the FT-Like SP6A Preferentially Enhances Tuber Resource Partitioning. Front. Plant Sci. 13:817909. doi: 10.3389/fpls.2022.817909

INTRODUCTION

Photosynthesis and the subsequent distribution of produced assimilates across different sink organs together determine the yield of harvestable plant organs. Most study efforts have focused on optimization of photosynthesis (Nölke et al., 2014; Driever et al., 2017). However, competition for sucrose between sink organs also has a major impact on final crop yield. An important question is, thus, which factors affect sucrose partitioning between sinks, how the impact of these factors depends on sucrose availability and environmental conditions, and how these different factors interact. As an example, in potato, upon tuber formation, sucrose delivery to tubers is substantially increased at the cost of other plant organs (Fernie et al., 2020). It is generally accepted that this enhanced tuber sucrose partitioning is achieved through a switch from symplastic to apoplastic unloading, increasing the sucrose unloading rate at tubers (Viola et al., 2001). However, this enhanced unloading operates against a background in which tuber organs may have a different affinity for sucrose than, e.g., plant roots, reside at a larger distance from source leaves than young

developing sink leaves, and differ physiologically from sink leaves, which evaporate rather than take up water. To fully understand how much tuber unloading must increase for efficient tuber filling to occur and how this may be enhanced through targeted breeding, the importance of, and interplay with, other sink and transport pathway properties must be investigated.

Mathematical models have developed as an invaluable tool in investigating plant yield. However, to gain insight into factors determining resource partitioning, appropriate models considering all the relevant aspects are needed. Currently, in large-scale agronomic models aimed at predicting field level yields as a function of plant type and environmental conditions, sucrose partitioning between sinks is based on experimentally measured, developmental stage specific, partitioning tables (de Wit et al., 2019). As such, these models provide no insight in the mechanistic basis of sucrose partitioning between plant organs. More detailed models describing individual plant performance as a function of plant physiology and architecture, such as the frequently used functional–structural plant (FSP) models, typically assume that relative sink strength determines sucrose partitioning (Lescourret et al., 2011; Da Silva et al., 2014; de Vries et al., 2021). These latter models, thus, implicitly assume that properties of the transport pathway such as resistance, length, or relative nearness of different sinks to the source organs do not significantly impact sink resource allocation, which at least under certain conditions have been shown to be incorrect (Pallas et al., 2010).

In contrast, based on the generally accepted Münch hypothesis, biophysically detailed transport models describe sucrose and water transport as a convective flow resulting from an osmotically driven pressure gradient (Thompson and Holbrook, 2003; Hölttä et al., 2006; Lacointe and Minchin, 2008). Besides automatically integrating pathway resistance and length, more detailed biophysical models can also include the effects of xylem water flow (Hölttä et al., 2006, 2009) and radial sucrose efflux (Minchin and Lacointe, 2017; van den Herik et al., 2021). In a single-sink context, these biophysical transport models have highlighted the importance of pathway properties on transport dynamics, efficiency, and, thus, eventually sucrose delivery to sinks. However, currently available two-sink models have produced conflicting outcomes on the relevance of pathway properties for sucrose partitioning. Minchin et al. (1993) demonstrated that, due to pathway resistance effects, for two sinks differing in sink strength (v_{max}), the sink with the lowest v_{max} obtained a larger fraction of available sucrose than expected based on the v_{max} ratios alone. In other words, the weaker sink receives more sugar relative to its v_{max} than the stronger sink, while in absolute numbers, the stronger sink is still dominant. This suggested that sink characteristics are not the sole determinants of resource competition. Paradoxically, results of a later study slightly extending the model of Minchin et al. (1993) by Bancal and Soltani (2002) suggested that for physiologically relevant source concentrations, this phenomenon is negligible. This would imply that within the relevant range, sink characteristics fully dictate resource partitioning. Importantly, both the models used a simplified phenomenological description of pathway resistance and its effect on transport, rather than explicitly modeling the osmotically driven pressure gradient driving transport. A recent study, integrating biophysically detailed transport dynamics in a multisink FSP model, instead indicated that both the distance and sink strength determine sugar partitioning in grape (Zhu et al., 2021). Thus, it remains unclear what the exact relevance of pathway properties is on resource partitioning and how this may depend on sink properties. A first goal of this study is, therefore, to investigate the impact of modeling choices for the relevance of pathway properties on resource partitioning.

While most often only the length and/or resistance of the pathway between source and sink is considered relevant for resource partitioning, *in planta* extensive radial water and sucrose transport occurs along this pathway as well, also potentially affecting resource distribution. In addition to their roles in source and sink loading and unloading (Braun et al., 2014), SWEET transporters also facilitate bidirectional, gradient-dependent sucrose transport between the phloem and the apoplast in the long-distance phloem, with sucrose export from the phloem dominating (Chen et al., 2012). Similarly, SUC/SUTs localized in the source region facilitate active, proton-coupled, sucrose loading into the phloem, while along the long-distance phloem, these SUC/SUTs facilitate retrieval of sucrose from the apoplastic space (Hafke et al., 2005). Apart from these transporters' dependence on local sucrose levels, additional regulation of transport capacity takes place. As an example, in potato, it was recently shown that the phloem mobile peptide StSP6A, or so-called tuberigen, inducing the transition from stolon to tuber under short-day conditions, binds to and thereby reduces StSWEET11 transport capacity by approximately 40% (Abelenda et al., 2019). The relevance of sucrose efflux from the long-distance transport phloem on resource partitioning has, thusfar not been investigated. Additionally, while sink strength and affinity have been generally considered as important properties for resource partitioning, so far physiological sink properties, particularly the direction and rate of water exchange with the environment and, hence, xylem flow, have not been considered. A second goal of this study is, thus, to obtain a mechanistic understanding of how the interplay between sink and pathway properties (length, xylem flow, and sucrose efflux) together determines sink resource partitioning. As a working example, we will analyze the partitioning of resources within potato plants, investigating the determinants of tuber sink yield. The differences in sink strengths, locations, and physiological properties between developing leaves, roots, and tubers provide an interesting context for studying sink resource partitioning. To this end, we used our previously developed biophysical transport model parameterized for potato (van den Herik et al., 2021), which we here extended from a single sink to a two-sink model.

MATERIALS AND METHODS

According to the Münch hypothesis, plant sucrose transport in the phloem occurs through convective flow generated by an osmotically driven pressure gradient that needs to overcome pathway resistance. Depending on the study, researchers have

made different assumptions on the relevance of pathway resistance, the significance of feedback effects of sucrose concentration (*via* sap viscosity) thereon and the importance of explicitly modeling water transport, and the associated radial and xylem water transport. Later, we briefly introduce three models for sucrose transport differing in these assumptions. To resolve whether the previously obtained paradoxical result that pathway resistance does not significantly impacts sink resource competition depends on modeling details, these models were compared with regard to their results on sucrose partitioning between two sinks:

$$PC_1 = \frac{v_1}{v_1 + v_2} \tag{1}$$

where PC_1 is the partitioning coefficient for sink 1, v_1 and v_2 are the respective unloading rates in the two sinks. For a system without radial solute flux, $v_1 + v_2$ is equal to the loading rate (v_0).

Model Overview and Underlying Assumptions

Model 1: No Resistance

The no resistance or VK model (sink strength, v_{max}; sink affinity, k_m) is the simplest model we introduce (**Figure 1A**). It assumes that there is no resistance in the phloem and, thus, no pressure gradient is required. Source concentration (c_0) is equal to sink concentration (c_1, c_2) as a result. Sink unloading rates are modeled using the Michaelis–Menten equation, implying an active unloading mode. Differences in partitioning between the two sinks, thus, solely depend on differences in sink v_{max} and K_m, enabling a simple analytical solution:

$$v1 = v_{max,1}\frac{c_1}{c_1 + k_1} \tag{2a}$$

$$v2 = v_{max,2}\frac{c_2}{c_2 + k_2} \tag{2b}$$

$$v_0 = v_1 + v_2 \tag{2c}$$

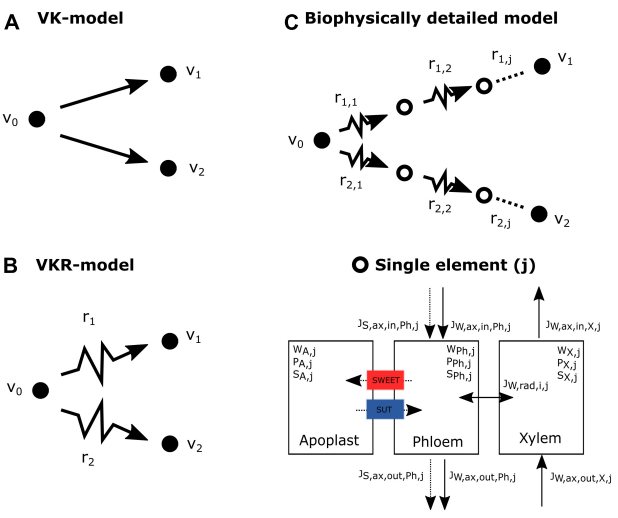

FIGURE 1 | Model overview of the three compared models. **(A)** Resource partitioning in the VK model solely depends on the sink properties, as visualized by the straight lines leading from source (v_0) to sinks. **(B)** Partitioning in the VKR model does not only depend on sink properties, but also depend on pathway resistance (r). **(C)** In the biophysically detailed model, pathway resistance depends on local conditions (open circles representing a single element). In a single element, water and sucrose flows are calculated based on local resistance, pressure, and sucrose concentration. Furthermore, a single element consists not only of a phloem compartment, but also contains a xylem and apoplastic compartment with which water, respectively, sucrose exchange occur.

Model 2: Sucrose-Dependent Resistance

In the resistance or VKR model (**Figure 1B**), transport resistance is included by introducing a total pathway resistance term (r_i) (Minchin et al., 1993). Consequently, source and sink concentrations are different ($c_0 \neq c_1 \neq c_2$) and resistance can impact resource partitioning. Bancal and Soltani (2002) further extended this model by including the influence of sucrose concentration on pathway resistance *via* sap viscosity. Specifically, sucrose concentrations halfway the pathway ($S_{1/2}$) are taken to calculate overall pathway resistance. The equation used to calculate sucrose-dependent resistance used by Bancal and Soltani (2002), valid for sucrose concentration between 0 and 1.5 M, is:

$$R_s = R_3\Big(\ 0.685S_{\frac{1}{2}}^4 - 1.0411S_{\frac{1}{2}}^3 + 0.9512S_{\frac{1}{2}}^2 + 0.1364S_{\frac{1}{2}} + 0.3396\Big) \tag{3}$$

where R_3 is the reference viscosity at a sucrose concentration of 1 M. The equation above directly gives a relationship between sucrose concentration and pathway resistance. The equation is based on the viscosity effects on resistance, thus by replacing the reference resistance (R_3) for a reference viscosity, the effect of sucrose concentration on viscosity is obtained.

For steady-state conditions, the unloading rates in the sinks can be found by numerically solving the system of equations below (i = 1, 2 for a 2-sink system):

$$v_0 - v_i = \frac{c0\,(c0 - c_i)}{r_i} - \frac{v_{max,i}c_i}{k_i + c_i} = 0 \tag{4}$$

In the comparison here, we use this extended model of Bancal and Soltani (2002), including the sucrose-dependent pathway resistance.

Model 3: Spatially Explicit Sucrose and Water Flows

This biophysically detailed model explicitly describes water and solute flow in the phloem resulting from an osmotically driven pressure gradient as described by the Münch hypothesis (van den Herik et al., 2021; **Figure 1C**). Local pathway resistance depends on local phloem characteristics and sap viscosity (and, hence, sucrose concentrations), rather than a global pathway resistance being superimposed from calculated average pathway characteristics and sucrose concentrations. We initially only incorporated water ($J_{W,ax,Ph/X}$) and sucrose phloem flow ($J_{S,ax,Ph}$) as well as radial water flow ($J_{W,rad,Ph/X}$) to ensure

conservation of water mass (W) and sucrose (S). These radial fluxes were modeled using the following equation:

$$J_{W,rad,Ph,j} = L_r A_{rad,j}\left(0 - \Psi_{Ph,j}\right), with \Psi_{Ph,j} = P_{Ph,j} + \Pi_{Ph,j} \quad (5a)$$

where L_r is the radial hydraulic membrane permeability, $A_{rad,j}$ is the radial area between phloem and xylem, Ψ_{Ph} is the phloem water potential, P_{Ph} is the phloem turgor pressure, and Π_{Ph} is the phloem osmotic potential. For later simulations, we also incorporated water flow in the xylem, which we described following the cohesion-tension theory. In these simulations, radial water exchange occurs between phloem and xylem, following similar approaches by Hölttä et al. (2006) and applied earlier by van den Herik et al. (2021):

$$J_{W,rad,Ph,j} = L_r A_{rad,j}\left(\Psi_{X,j} - \Psi_{Ph,j}\right), with \Psi_{Ph,j} = P_{Ph,j} + \Pi_{Ph,j} \quad (5b)$$

Because of the complexity, the biophysically detailed model is solved numerically in an explicit geometry consisting of interconnected elements. For this study, we extended our previously developed model (van den Herik et al., 2021) to multiple sinks by endowing individual elements with the possibility for multiple inflow and outflow terms. Radial inflow and outflow can still be described by a single term within an element. Combined, this results in the reformulated water and sucrose mass balances below:

$$\frac{\partial W_{Ph/X,j}}{\partial t} = \left(\sum_{i=1}^{n} J_{W,ax,in,Ph/X,j,i} - \sum_{i=1}^{m} J_{W,ax,out,Ph/X,j,i} + J_{W,rad,Ph/X,j}\right)\rho \quad (6a)$$

$$\frac{\partial S_{Ph,j}}{\partial t} = \sum_{i=1}^{n} J_{S,ax,in,Ph,j,i} - \sum_{i=1}^{m} J_{S,ax,out,Ph,j,i} + J_{S,Rad,Ph,j} \quad (6b)$$

where *n* is the amount of upward oriented elements connected to element j and m is the amount of downward oriented elements connected to element j. Descriptions of the variables and parameters are given in **Tables 1**, **2**. A more detailed description of the model, its underlying assumptions, and potato-specific parameterization can be found in a study by van den Herik et al. (2021). While the original single-sink model incorporated a passive unloading mechanism, in this study, we included active unloading through incorporating the Michaelis–Menten equation to enable a one-to-one comparison with the VK and VKR model. Importantly, when comparing different types of sink organs—roots, leaves, and tubers—we maintain for all the sinks an active unloading mode. We do this despite stolon ends upon tuberization switching from an active to passive unloading mode (Viola et al., 2001). The reason for not incorporating a passive unloading-specific equation for tuber sinks is that this would introduce an additional dependence on the sucrose concentration assumed for tubers, complicating a comparison of how differences in sink properties such as xylem water transport and distance from source leaves affects resource partitioning.

In this more detailed model, there is no single parameter (r) for total pathway resistance. Instead, local pathway resistance depends on local viscosity and pressure differences. To see this more clearly, we rewrote the phloem-specific water flow rate:

$$J_{w,ax,in,Ph} = A_{Ph}\frac{k_{Ph}}{\mu_{Ph}}\frac{\Delta P_{Ph}}{L} = N_{Ph}\pi a_{Ph}^2\frac{k_{Ph}}{\mu_{Ph}}\frac{\Delta P_{Ph}}{L} \quad (7a)$$

in terms of pressure differential and resistance (r):

$$J_{w,ax,in,Ph} = \frac{\Delta P_{Ph}}{r_{Ph}}, where\ r_{Ph} = \frac{\mu_{Ph}L}{k_{Ph}N_{Ph}\pi a_{Ph}^2} \quad (7b)$$

This yielded an expression for pathway resistance, which is proportional to viscosity (μ) and pathway length ($_L$) and inversely proportional to phloem axial permeability (k), number of phloem conduits (N), and individual phloem conduit radius (a). To study the effect of resistance on sucrose transport in

TABLE 1 | Symbols and units for the used variables/equations in the biophysically detailed model.

Variable	Symbol	Units
Water mass	$W_{Ph/X,j}$	g
Sucrose	$S_{Ph,j}$	mol
Pressure	$P_{Ph/X,j}$	MPa
Sucrose concentration	$c_{Ph,j}$	mol/m^3
Axial water flow	$J_{W,ax,in/out,Ph/X,j}$	g/s
Axial sucrose flow	$J_{S,ax,in/out,Ph/X,j}$	mol/s
Radial water flow	$J_{W,rad,Ph/X,j}$	g/s
Radial sucrose flow	$J_{S,rad,Ph,j}$	mol/s
Water potential	$_{Ph/X,j}$	MPa
Axial area	$A_{Ph/X,j}$	m^2
Radial area	$A_{rad,j}$	m^2
Osmotic potential phloem	$_{\Pi,j}$	MPa
Dynamic viscosity phloem	$_{\mu,j}$	MPa s

TABLE 2 | Relevant parameters for the biophysically detailed model used in this study, for a full description of the model, parameters, and parameter estimation (see van den Herik et al. (2021)).

Parameter	Symbol	Value	Units
Density of water	ρ	0.998e6	g/m^3
Radial hydraulic membrane permeability	L_r	5e-8	m/MPa/s
Dynamic viscosity water/xylem	μ_x	1.0019e-9	MPa s
Phloem sieve element radius	a_{Ph}	8.4e-6 at t = 0	m
Xylem conduit radius	a_x	30e-6	m
Axial permeability phloem	k_p	3.82e-12	m^2
Elastic modulus phloem	ε_p	30	MPa
Elastic modulus xylem	ε_x	750	MPa
Transpiration rate	J_{trans}	0.02	g/s
Water potential soil	ψ_{soil}	0	MPa

this model and compare its effects to that in other models, we varied pathway length, as this parameter is directly proportional to resistance. While for the between-model comparison, we could have varied other resistance parameters from Eq. 7b instead, we decided to vary length as this also enabled us to investigate the effect of different source-sink distances on resource partitioning, assuming all other pathway properties are equal. Importantly, *in planta*, hydraulic architecture/axial permeability of phloem may vary over the length of the plant and/or between plant organs (Clerx et al., 2020), making the linear scaling of pathway length with resistance a simplifying assumption.

In the biophysical model, we used the equation for sucrose-dependent viscosity as described by Morison (2002), i.e., using the volume fraction of sucrose (Φ) to calculate the viscosity:

$$\mu_{Ph,j} = \mu_X exp\left(\frac{4.68*0.956\ \phi_{Ph,j}}{1 - 0.956\ \phi_{Ph,j}}\right) with\ \phi_{Ph,j} = \frac{V_{suc}S_{Ph,j}}{V_{suc}S_{Ph,j} + V_{Ph,j}} \quad (8)$$

Given that the VKR and biophysical model use different equations to calculate viscosity, we checked to what extent that this result in different sucrose concentrations to viscosity mapping, as this could potentially underlie differences in outcomes between the two models. **Supplementary Figure 1** illustrates that despite the different applied equations, a highly similar mapping occurs, indicating that this cannot be the cause of differences in model results.

Simulation Details and Model Implementation

Standard sink strength was set at v_{max} = 12.5 nmol/s, sink affinity was set at K_m = 75 mM, and pathway resistance was set at r = 7.5e12 Tmol s/m^6 (for the VKR model) or pathway length was set at l = 0.25 m (for the biophysically detailed model). The pathway length of 0.25 m corresponds to an equal resistance, as the VKR model for a sugar concentration of 0 mM. That is, the resistances are equal for conditions in which viscosity effects of solutes are ignored. To investigate differences in resource partitioning between the three models, we considered three different scenarios in a single-source, two-sink system, with the two sinks differing in either sink strength (v_{max}), sink affinity (K_m), or pathway resistance (r). For the v_{max} scenario, we used 22.5 nmol/s for sink 1 and 2.5 nmol/s for sink 2; for the K_m scenario, we used 75 mM for sink 1 and 750 mM for sink 2; and for the resistance scenario, we used 7.5 and 150 Tmol s m^{-6} for the VKR model and 0.25 and 5 m for the biophysically detailed model. To compare the three models, steady-state solutions for a range of loading rates (0.025–25 nmol/s) were calculated and phloem-only conditions were used (Eq. 5a). Aforementioned values were taken from a study by Bancal and Soltani (2002), to enable comparison between their earlier results and our model outcomes. To validate the robustness of the analysis, we compared our results for a default zero resistance shared pathway to a non-zero resistance shared pathway from source to sink. This did not significantly affect the results (**Supplementary Figure 2**).

The impact of xylem flow on resource partitioning was investigated using a constant water uptake of sink 2 (2e–8 m^3/s, equal to total uptake in a study by van den Herik et al., 2021) representing a root organ, while varying water flow in sink 1 between -1e-8 m^3/s (water evaporation equal to source) and 2e–8 m^3/s (water uptake equal to sink 2), representing organs on the continuum from leaf to tuber to root. Evaporation in the source region was set equal to the net sum of the water flow in both the sinks and simulations were performed for three different source loading rates. We also investigated 3 biologically realistic 2 sink scenarios (root-root, tuber-root, and young sink leaf-root), where we imposed a soil water potential of 0 MPa (Perämäki et al., 2001), simulating tubers by decreasing water uptake permeability by 90% relative to roots and young leaves through an evaporation rate of 10% of that of mature leaves.

Radial sucrose transport between phloem and apoplast and sucrose removal from the apoplast were modeled as done in a study by van den Herik et al. (2021). In summary, bidirectional SWEET transport facilitates efflux from the phloem (v_{max} = 0.148 mol/m^3/s, K_m = 70 mM, Chen et al., 2012) and retrieval from the apoplast (v_{max} = 0.148 mol/m^3/s, K_m = 10 mM, Chen et al., 2012), while SUT transporters (v_{max} = 0.117 mol/m^3/s, K_m = 1 mM, Schulze et al., 2000) also facilitate retrieval from the apoplast to the phloem. Efflux and retrieval rates were implemented as mol per m^3 per s and were, therefore, constant on a per length basis during the steady-state conditions at which we evaluate model outcomes. SP6A-mediated efflux mitigation was modeled by decreasing the v_{max} of SWEETs by 40%, as reported in a study by Abelenda et al. (2019).

The VK model was analytically solved. The system of equations describing the VKR model was solved in MATLAB R2020b using the build in function "fsolve" with a function threshold of 1e–13. Residual function values were checked to ensure the correctness of the solution and various initial values were used to search for alternative solutions of the system. We only considered biologically valid solutions, i.e., positive solute concentrations. The system of differential equations describing the biophysically detailed model was implemented in MATLAB R2020b and was solved using the build-in solver "ode15s," using an integration time step of Δt = 1 s using a non-homogeneous mesh for loading (20 elements, 0.005 m/element), long-distance pathway (30 elements, 0.0083 m/element), and unloading zones (20 elements, 0.005 m/element), as described in detail by van den Herik et al. (2021). The source code for the biophysically detailed model and implementation of the VKR and VK models are available on https://tbb.bio.uu.nl/khwjtuss/TwoSinkSucroseTransport/.

RESULTS

To investigate whether the previously found limited importance of pathway resistance on sink resource partitioning depends on modeling details, we compared the previously used, simpler VKR model with the more detailed biophysical model, with the VK

model serving as a baseline. First, we started with investigating model differences in a single-sink setting.

Structural Underestimation of Sucrose Concentration and Resistance in the VKR Model

A major difference between the VKR and biophysical model is the manner in which sucrose phloem concentrations are used to calculate resistance. In the biophysical model, sucrose gradients are calculated in a spatially resolved manner with explicit source loading zones, sink unloading zones, and lateral water transport resulting in non-linear gradients (**Figures 2A–C**, blue lines). In contrast, the VKR model assumes a linear source-sink concentration gradient (**Figures 2A–C**, green lines indicate the linear gradient for the biophysical model). In the biophysical model, local pathway resistance is subsequently calculated from local sucrose concentration, while in the VKR model, an average, overall pathway resistance is calculated from mean pathway sucrose concentration. This results in an underestimation of pathway sucrose concentration (**Figures 2D,F**) and resistance (**Figures 2E,G**) when using a linear VKR-type gradient. The level of underestimation increases with concentration gradient steepness, i.e., increasing loading (**Figure 2A** vs. **2B** and **Figures 2D,E**) and unloading rates (**Figure 2B** vs. **2C** and **Figures 2F,G**).

Instead of extracting a VKR-type gradient from the biophysical model, we next explicitly simulate the VKR model using equal parameterization as for the biophysical model. Due to the dynamic feedback between resistance and concentration, the general tendency for lower resistances in the VKR model results in significantly less steep source-sink concentration gradients and lower source concentrations (**Figures 2A–C**, orange lines). Importantly, these lower source concentrations in the VKR model result in an overestimation of the minimum loading rates necessary to obtain physiologically relevant source concentrations (0.1–2 M).

Effects of Resistance and Biophysical Detail on Resource Allocation

Next, we investigated the impact of using either a baseline VK, simple VKR, or the biophysical model on resource partitioning between two sinks. We hypothesized that the structural underestimation of pathway resistance in the VKR compared with the biophysically detailed model impacts resource partitioning.

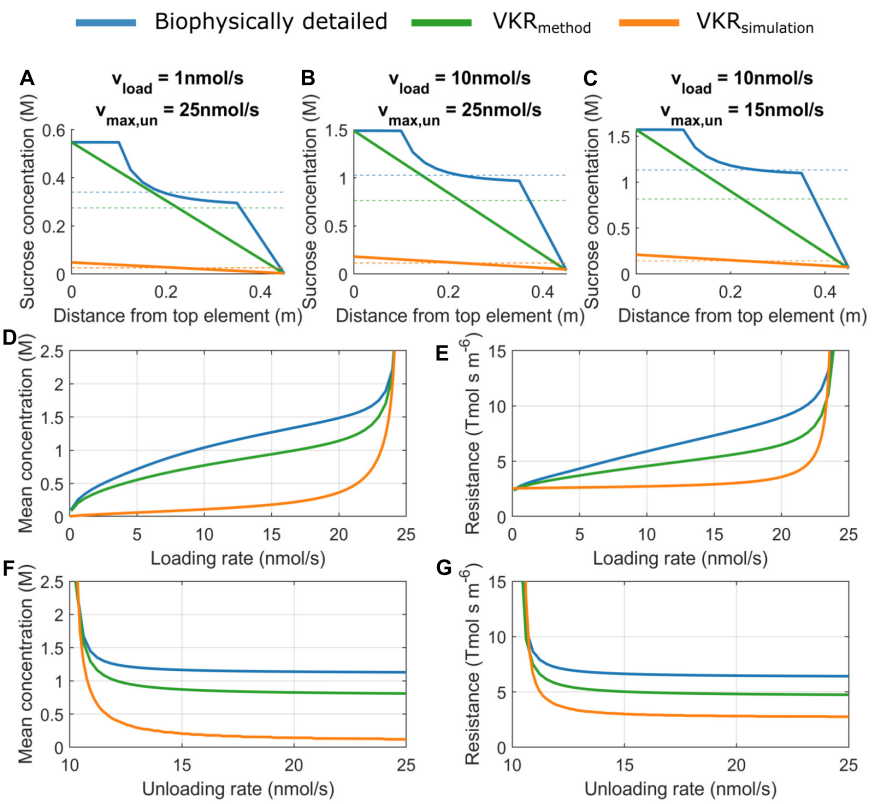

FIGURE 2 | Sucrose concentration and resistance are underestimated when not including a spatial sucrose gradient. Concentration gradients for **(A)** v_{load} = 1 nmol/s, $v_{max,un}$ = 25 nmol/s, **(B)** v_{load} = 10 nmol/s, $v_{max,un}$ = 25 nmol/s **(C)**, v_{load} = 10 nmol/s, $v_{max,un}$ = 15 nmol/s. Dotted lines indicate mean pathway sucrose concentration. **(D)** Mean concentration as a function of source loading rate for a constant unloading rate of 25 nmol/s and **(E)** mean pathway resistance as a function of source loading rate. **(F)** Mean concentration as a function of sink unloading rate for constant loading rate of 10 nmol/s and **(G)** mean pathway resistance as a function of sink unloading rate.

Sink Strength (V_{max})

At the onset of tuberization, a switch from symplastic to apoplastic unloading mode increases tuber sucrose unloading rate. As a logical first scenario, we, thus, investigated the effect of differences in sink strength on resource partitioning. For $v_{max,1}$ = 22.5 nmol/s and $v_{max,2}$ = 2.5 nmol/s, the simple VK model predicts the partitioning coefficient to equal the v_{max} ratio ($v_{max,1}/v_{max,2}$ = 90%) (**Figure 3A**, dotted line). In absence of resistance, source concentration equals sink concentration, resulting in equal sink concentrations. This causes the sinks to be equally saturated, resulting in v_{max} values being the sole source of differences in sink uptake. In contrast, the VKR model predicts the partitioning coefficient to start at 50% and increase in a saturating manner toward the v_{max} ratio defined 90% (**Figure 3A**, dashed line). In the presence of resistance, differences between source and sink concentrations arise, allowing for between sink concentration differences. The higher unloading rate at sink 1 results in a lower local sink concentration (**Figure 3B**, dashed blue vs. dashed orange lines) and reduced saturation (**Figure 3C**, compare position of blue vs. orange squares on the saturation curves). This causes sink 1 resource partitioning to be lower than expected based on v_{max} ratio alone. Partitioning reaches the expected v_{max} defined value when both the sinks approach saturation at high loading rates (approximately 20 nmol/s).

The biophysically detailed model predicts a slower, sigmoidal increase to 90% partitioning (**Figure 3A**, solid line). In both the VKR and biophysical model, the higher $v_{max,1}$ resulted in a lower c_1, lower mean pathway concentration, and resistance, causing $r_1/r_2 < 1$ (**Figure 3D**). However, a lower c_1 also results in a steeper concentration gradient c_0-c_1 that is more underestimated in the VKR model than the c_0-c_2 gradient. As a consequence, the VKR model overestimates r_1-r_2 differences, resulting in a r_1/r_2 ratio closer to 1 in the biophysical model (**Figure 3D**). Thus, while absolute resistance levels are higher in both the pathways, relative resistance differences between the two pathways are smaller in the biophysical model. Since the resistance difference acts against the v_{max} driven concentration gradient difference (lower resistance causes higher sink concentrations), the reduced relative resistance difference in the biophysical model allows for larger difference between sink concentration (**Figure 3B**) and saturation differences (**Figure 3C**, compare location of the dots representing the biophysical model with the squares representing the VKR model). This further diminishes the advantage of sink 1 from its higher v_{max}. Summarizing, over a large range of loading rates, an increased unloading at the tubers (with higher v_{max}) has less effect than expected based on unloading rates only.

Sink Affinity (k_m)

In addition to sink strength, plant sink organs may also differ in sucrose affinity. For higher sink 1 affinity (k_1 = 75 mM, k_2 = 750 mM), at equal sink concentrations, the effective uptake rate of sink 1 (v_1) is significantly higher than that of sink 2 (v_2). In the VK model, with its equal sink concentrations, this causes the partitioning coefficient to heavily favor sink 1 at low loading rates and, hence, sink concentrations (**Figure 4A**, dotted line). At higher loading rates, both the sinks saturate, causing the partitioning to converge to the 50% defined by the equal v_{max} values. In the VKR model, the higher affinity of sink 1 and, hence, higher uptake at low loading rates result in lower local concentration at sink 1 (**Figure 4B**). Consequently, even though $k_2 >> k_1$, sink 2 is more saturated than sink 1 (**Figure 4C**). As a result, partitioning to sink 1 is lower than expected based on K_m differences for low loading rates. As loading rate increases first, sink 1 approaches saturation, enabling it to profit from its higher affinity. As loading rates increase further (beyond 10 nmol/s), sink 2 also approaches saturation, removing sink 1's higher affinity benefit and causing partitioning to approach the 50% defined by the equal v_{max} values (**Figure 4A**, dashed line).

As above for the different unloading rates, source concentrations, source-sink concentration gradients, resistance ratio (**Figure 4D**), and between sink concentration, differences are larger in the biophysical model, explaining again the decreased advantage of sink 1 in the biophysical model (**Figure 4A**, solid line).

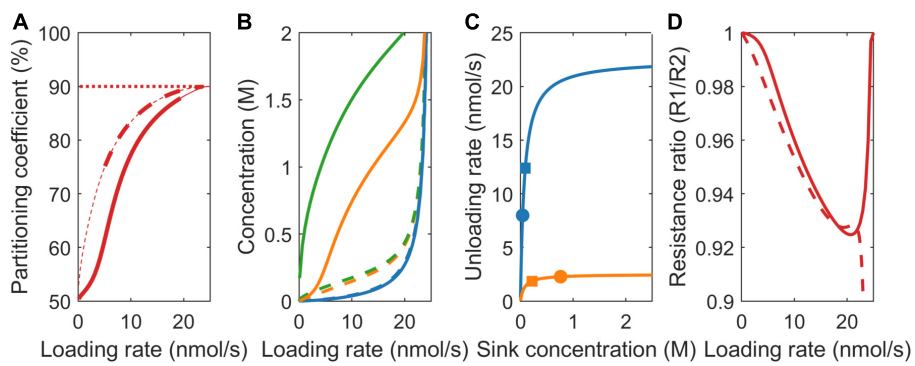

FIGURE 3 | Impact of model choice on partitioning coefficients and the underlying mechanisms for different sink strengths (v_{max}). **(A)** Partitioning coefficient for the VK (dotted), VKR (dashed), and biophysical (solid) models. The bold lines in **(A)** represent physiologically relevant conditions ($0.1 < c_0 < 2$ M) showing that the biophysical model has a much broader physiologically relevant range. **(B)** Sink 1 (blue), sink 2 (orange), and source (green) sucrose concentrations. **(C)** The Michaelis–Menten curves for unloading rates, with dots representing the biophysical model and squares representing the VKR model. **(D)** Resistance ratios for the VKR (dashed) and biophysical (solid) models.

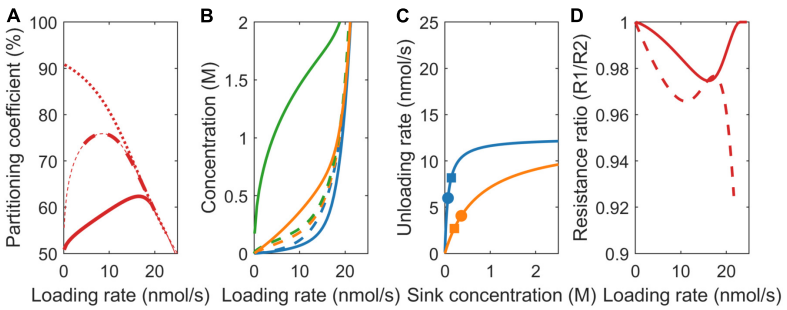

FIGURE 4 | Impact of model choice on partitioning coefficients and the underlying mechanisms for different sink affinities (K_m). **(A)** Partitioning coefficient for the VK (dotted), VKR (dashed), and biophysical (solid) models. The bold lines in **(A)** represent physiologically relevant conditions ($0.1 < c_0 < 2$ M), showing that the biophysical model has a much broader physiologically relevant range. **(B)** Sink 1 (blue), sink 2 (orange), and source (green) sucrose concentrations. **(C)** The Michaelis–Menten curves for unloading rates, with dots representing the biophysical model and squares representing the VKR model. **(D)** Resistance ratios for the VKR (dashed) and biophysical (solid) models.

Pathway Resistance

Sink organs are formed at different positions in the plant, with different transport pathway lengths from source to sink resulting in different pathway resistances, e.g., tubers form at a larger distance from the sucrose providing source leaves than young developing sink leaves. Importantly, resistance both affects and is dependent on concentration differences. For comparison purposes, we use equal baseline resistance values at zero sucrose concentrations for the two models, while allowing net, sucrose-dependent resistance values to differ. In the VK model, partitioning equals the v_{max} defined value of 50% (**Figure 5A**, dotted line), as all the sink parameters are equal and resistance is not incorporated.

For the VKR model, $r_1 << r_2$ (r_1 = 7.5e12 Tmol s/m^6 and r_2 = 150 Tmol s/m^6) implies that $c_1 >> c_2$ (Eq. 3), causing a reversal in the sink 1 and 2 concentration differences compared to the earlier two scenarios (**Figure 5B**, dashed lines). Additionally, between sink concentration, differences are significantly larger. The higher r_2 now leads to lower sink 2 concentrations and, thus, a lower unloading rate in sink 2 when sinks are not yet saturated (**Figure 5C**, compare the position of blue vs. orange squares on the saturation curves), resulting in a higher partitioning toward sink 1 (**Figure 5A**, dashed line). When sink 1 becomes saturated (∼10 nmol/s), a further increase in loading rate increases unloading at sink 2, increasing c_2, and decreasing sink 1 favored partitioning. As loading rate further increases, sink 2 also saturates and the v_{max} defined ratio of 50% partitioning is reached.

Again, in the biophysical model, source concentrations are higher, source-sink gradients are steeper (**Figure 5B**), and relative resistance differences are smaller (**Figure 5D**, r_1/r_2 slightly closer to 1 for unsaturated sinks). In the v_{max} and K_m scenarios, resistance differences oppose the v_{max} and K_m driven sink concentration differences, which, in turn, limit v_{max} and K_m driven resource partitioning advantages. Here, it is solely the resistance difference that drives concentration differences instead, with these concentration differences causing rather than reducing resource partitioning advantages. Reduced relative resistance differences in the biophysical model now reduce rather than enhance between sink concentration (**Figure 5B**) and saturation differences (**Figure 5C**, compare location of the dots representing the biophysical model with the squares representing the VKR model) and, thereby, limit the advantage of a lower resistance for sink 1 relative to the VKR model. Thus, for a broad range of loading rates, the disadvantage that a tuber experiences from its larger transport pathway length and resistance is significantly less than expected based on resistance differences alone.

Xylem Water Flow Differences Affect Sucrose Partitioning

As phloem and xylem are hydraulically connected, changes in xylem water potential affect phloem water and solute transport (Sevanto et al., 2011; Savage et al., 2016; Konrad et al., 2019). An interesting question, thus, is whether, in addition to differences in sink characteristics and pathway resistance/length, differences between sink organs in terms of xylem water flow affect resource partitioning. Note that to investigate this only, the biophysically detailed model is suitable. To investigate the impact of xylem flow on resource partitioning, we used constant, equal VKR characteristics, a constant water uptake of sink 2 representing a root organ, while varying water flow in sink 1. When sink 1 xylem water uptake rate equals that of sink 2 (2e-8 m^3/s), sucrose partitioning equals 50% (**Figure 6A**). A linear increase in sink 1 resource allocation occurred when moving from gradually decreasing water uptake to gradually increasing water evaporation in sink 1. This increased allocation to sink 1 is stronger for lower loading rates, when sinks are less saturated (**Figure 6A**). These results indicate that a smaller xylem counterflow and even more so a xylem co-flow increased partitioning toward a sink.

Increased Turgor Gradient and Sucrose Concentration Causes Increased Sucrose Partitioning

To understand this phenomenon, we investigated scenarios in which sink 1 takes up water at a lower rate than sink 2 (**Figure 6B**)

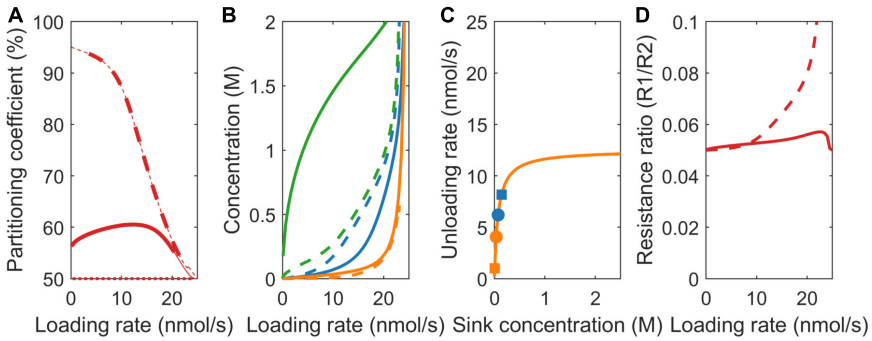

FIGURE 5 | Impact of model choice on partitioning coefficients and the underlying mechanisms for different pathway resistance/length (r). **(A)** Partitioning coefficient for the VK (dotted), VKR (dashed), and biophysical (solid) models. The bold lines in **(A)** represent physiologically relevant conditions ($0.1 < c_0 < 2$ M), showing that the biophysical model has a much broader physiologically relevant range. **(B)** Sink 1 (blue), sink 2 (orange), and source (green) sucrose concentrations. **(C)** The Michaelis–Menten curves for unloading rates, with dots representing the biophysical model and squares representing the VKR model. **(D)** Resistance ratios for the VKR (dashed) and biophysical (solid) models.

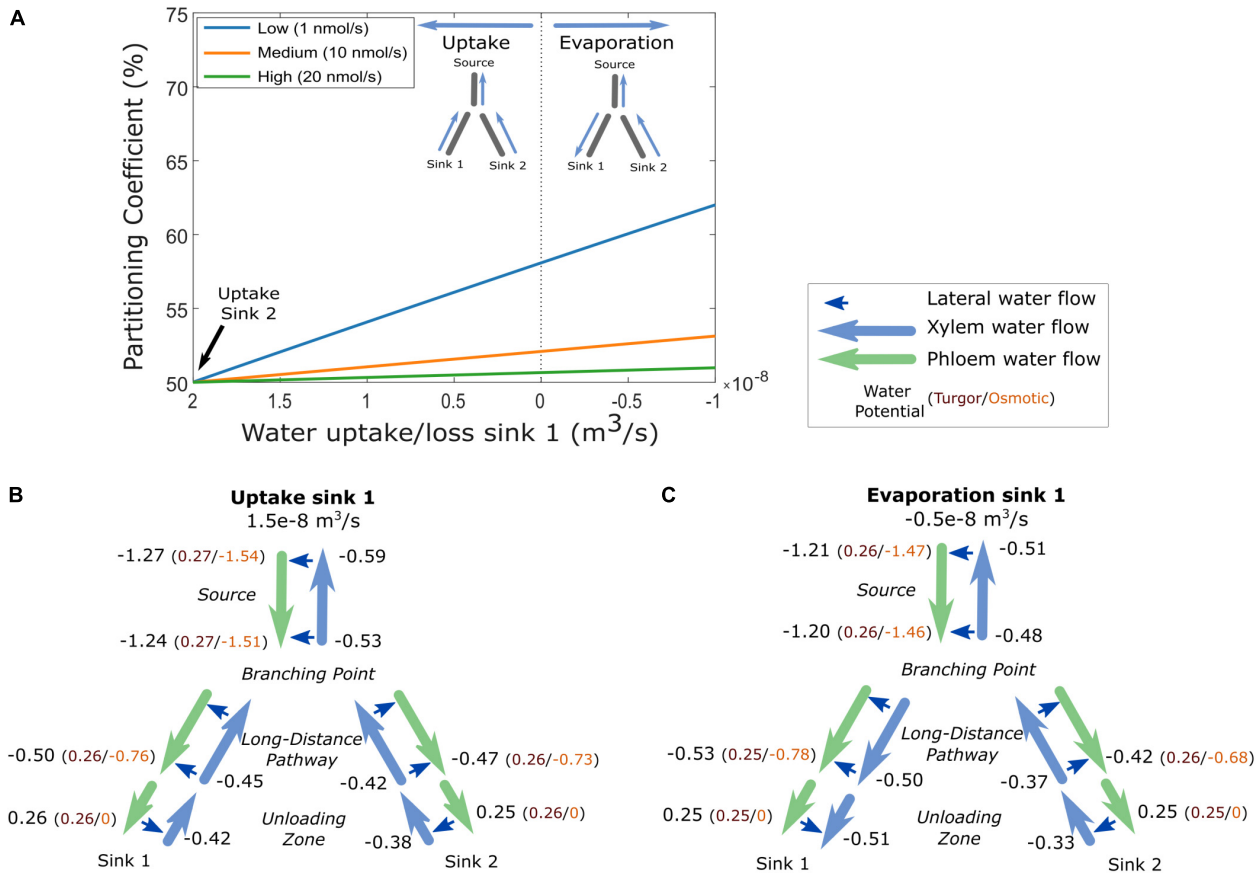

FIGURE 6 | The effect of xylem boundaries on carbon partitioning between two sinks. **(A)** Partitioning coefficient for three loading rates as a function of xylem water boundary conditions in sink 1, for a constant sink 2 water uptake of 2e–8 m^3/s. Water potentials of phloem and xylem (in MPa) at various locations in the model for a situation in which sink 1 evaporates at a rate of 0.5e–8 m^3/s **(B)** or takes up water at a rate of 1.5e–8 m^3/s **(C)** The scenarios in B and C are taken from the low-loading rate conditions of A. For the phloem water potential, the separate contributions of turgor and osmotic potential are given in brackets.

or evaporates water (**Figure 6C**). Both the lower water uptake and evaporation resulted in a more negative xylem potential in the pathway. Additionally, for an evaporating sink 1, a reversal in the xylem potential gradient occurs. As radial water flow is directed from high (least negative) to low (most negative) water potentials (Eq. 5b), differences in xylem potential impact lateral

water flow and, thereby, phloem water potential. For phloem to deliver solutes to the sinks, water potentials in phloem and xylem must fulfill the constraint that lateral waterflow is directed toward the phloem in the source and long-distance pathway and toward the xylem in the sinks (Hölttä et al., 2006, 2009; Windt et al., 2006). The decreased (more negative) xylem water potential in the pathway toward sink 1, thus, dictates an accompanying decrease in phloem water potential that is largest in the scenario where sink 1 evaporates water. Phloem water potential consists of a turgor pressure (P) and osmotic potential (Π) component. Our simulations show that the decreased (more negative) phloem potential in the pathway toward sink 1 arises from a combination of lower turgor pressure and more negative osmotic potential in both the scenarios. A lower turgor pressure toward sink 1, combined with an equal turgor pressure at the branching point, results in a larger turgor pressure gradient and, hence, water flow toward sink 1 relative to sink 2. Additionally, the decreased osmotic potential arises from increased sucrose concentration in the pathway toward sink 1. The combined larger flow and higher sucrose concentration explain the increased sucrose partitioning toward sink 1, with a larger effect in the evaporation scenario where xylem and phloem potential become more negative.

Resource Allocation Differences Between Roots, Tubers, and Developing Leaves

In the simulations earlier, we imposed water flow boundaries (influx or efflux rate) to systematically investigate the influence of xylem water flow rate and direction on resource partitioning. However, in most model applications, xylem water flow rate and direction are not a control parameter, but rather an emergent property from soil and atmosphere water potential or organ evaporation rates. We, therefore, also investigated 3 biologically realistic 2 sink scenarios (root-root, tuber-root, and young sink leaf-root), where we imposed a soil water potential of 0 MPa, simulating tubers by decreasing water uptake permeability by 90%, and young leaves through an evaporation rate of 10% of that of mature leaves. While this results in different, biologically more realistic, xylem water potentials (**Figure 7A**; Bland and Tanner, 1986), we again observe enhanced resource allocation to sinks with a reduced xylem counterflow (tuber vs. root) and even more so for xylem co-flow (leaf vs. root) (**Figure 7B**). Summarizing, we demonstrate that not only sink VK or pathway resistance properties affect resource partitioning, but that also differences in xylem water flow influence partitioning *via* the hydraulic connection with the phloem. Differences in xylem water flow cause tubers to have a resource partitioning advantage relative to the roots yet a disadvantage relative to sink leaves.

Sucrose Efflux Further Aggravates Disadvantage of Roots and Tubers

Besides simulating the effect of xylem flow and radial water exchange between phloem and xylem, the biophysically detailed model is also capable of simulating the effects of radial sucrose exchange between phloem and the apoplast. This exchange is

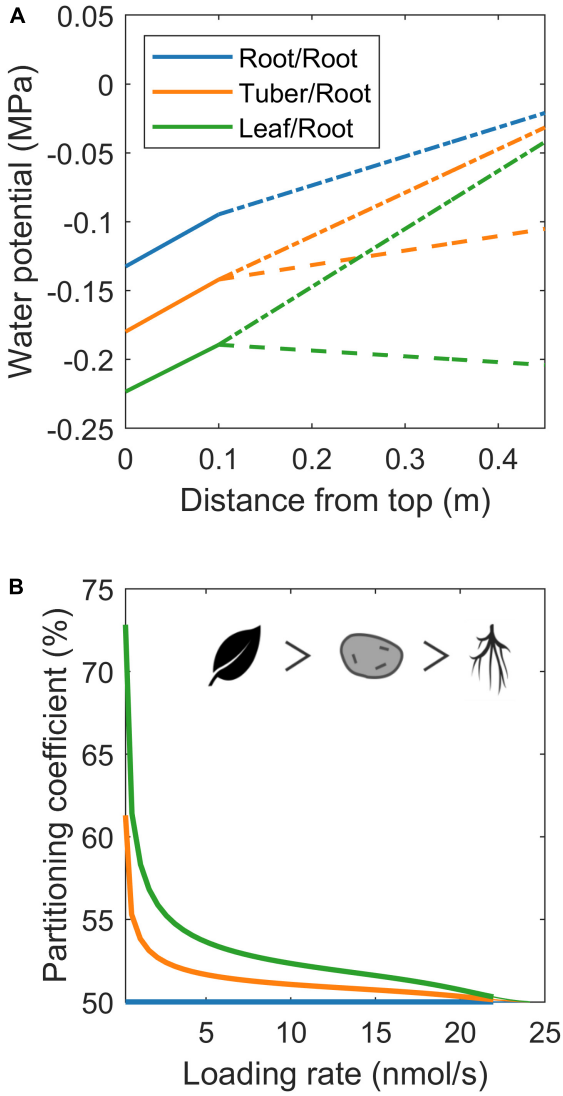

FIGURE 7 | Resource allocation differences between roots, tubers, and developing leaves. **(A)** Xylem water potential along the plant for the three specific organ scenarios. Solid lines represent the water potential in the part of the plant stem containing source leaves, dashed lines represent the water potential along the long-distance pathway leading toward sink 1 (root/tuber/leaf), and dash-dotted lines represent the water potential along the long-distance pathway ending at sink 2 (root). **(B)** Partitioning coefficient as a function of loading rate for the same three organ type cases as shown in **(A)**. The symbols show the organ priority.

mediated by bidirectional SWEET transporters (Chen et al., 2012) and active SUC/SUT importers (Hafke et al., 2005). It was previously shown that sucrose efflux, retrieval, and efflux mitigation can strongly affect phloem transport characteristics and sucrose delivery to sinks (Minchin and Lacointe, 2017; van den Herik et al., 2021).

To investigate the impact of long-distance sucrose efflux, we simulate a young leaf and root/tuber, with initially equal sink and pathway properties (v_{max} = 5 nmol/s, K_m = 75 mM, l = 0.25 m), incrementally adding different properties affecting

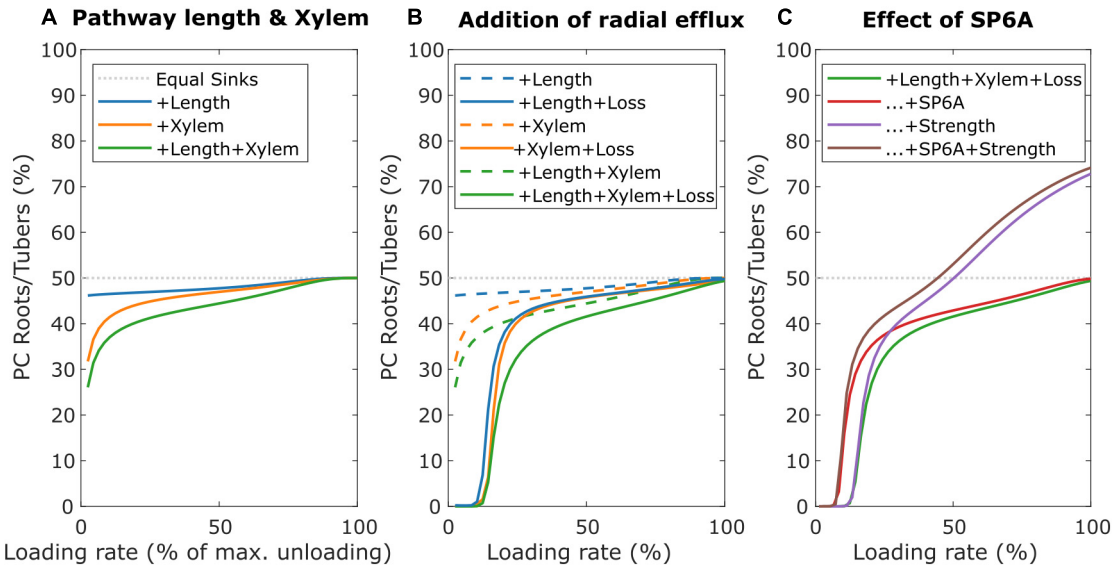

FIGURE 8 | Individual and combined effects of pathway properties and SP6A on sucrose partitioning toward roots/tubers. **(A)** Individual and combined effect of pathway length and xylem water flow for further equal sink leaves and roots/tubers sink and pathway characteristics. **(B)** The effect of radial efflux on resource partitioning toward roots/tubers. **(C)** The dual effect of SP6A, mitigating efflux and increasing roots/tubers sink strength.

resource partitioning. First, we incorporated differences in source-sink distance, with the leaf sink located at 0.1 m and sink roots/tubers located at 0.3 m from the source, replicating a potato plant architecture. Like before, the sink with smaller pathway length, and, thus, resistance, experiences higher resource partitioning (**Figure 8A**, blue line). Second, we incorporated differences in xylem flow, setting leaf sink evaporation at 10% of that of mature leaves, and water potential in the soil at 0 MPa. Differences in xylem flow strongly benefit leaves sucrose partitioning (**Figure 8A**, orange line). Combining length and xylem flow differences demonstrate that these effects are largely additive (**Figure 8A**, green line).

Next, we incorporated SWEET-mediated sucrose efflux along the long-distance pathway, following a study by van den Herik et al. (2021), with radial efflux amounting to up to 23% of total sucrose loading rate. Trivially, sucrose export along the long-distance phloem aggravates the resource partitioning disadvantage due to an increased pathway length (**Figure 8B**, blue lines). However, also the disadvantage due to different xylem flow conditions (**Figure 8B**, orange lines) and their combination (**Figure 8B**, Green lines) are aggravated, indicating that xylem flow differences also impact radial sucrose transport. Note that, for low loading rates (below 15% of maximum unloading rate), partitioning toward tubers is close to 0%. For these low loading rates, while the phloem localized SWEET still experiences sufficient sucrose, the resulting efflux of sucrose along the pathway causes almost no sucrose to arrive at sinks. The longer pathway length and different xylem flow conditions result in larger sucrose efflux toward tubers, resulting in a near zero partitioning coefficient despite leaf sucrose yield also being very low (**Supplementary Figure 3**). Smaller length differences or lower leaf evaporation rate decreased the regime in which partitioning toward roots/tubers is 0% (**Supplementary Figure 4**).

Efflux Mitigation and Increased Sink Strength Mediated by SP6A Work in Different Saturation Regimes

SWEET-mediated sucrose efflux is reduced by 40% upon the introduction of the FT-like protein SP6A in the phloem (Abelenda et al., 2019). However, there is currently no mechanism known that would restrict the loading and transport of SP6A specifically to tuber-directed phloem. We hypothesized that instead, the cumulative disadvantage tubers experience from their longer source-sink distance, xylem flow and sucrose export may enable undirected SP6A (i.e., present in all long-distance phloem) to preferentially increase tuber sucrose partitioning. Based on the experimental data, the undirected SP6A effect on sucrose transport was incorporated into our model by reducing for all the long-distance pathways, independent of the sink organ they are directed toward, the v_{max} parameter to 60% of its original value. Indeed, undirected SP6A introduction preferentially enhanced sucrose delivery toward roots/tubers (**Figure 8C**, red line) mostly through decreasing the regime of loading rates for which no sucrose reaches the roots/tubers due to radial efflux. Still, this SP6A effect does not enable tubers to become the dominant sucrose sinks. Besides its role in sucrose efflux mitigation, SP6A has been previously identified as important factor initiating tuberization (Navarro et al., 2011). During tuberization, the switch in unloading mode together with sink expansion increases sink strength. We, therefore, investigated the effect of an increased sink strength and the interplay with SP6A-mediated efflux mitigation. Experimental

observations suggest sink-source feedback, with sink-strength affecting loading rates, likely through phloem sucrose levels (Chiou and Bush, 1998). We, therefore, assumed the tuber sink strength increase to be accompanied by an equal sized source strength increase. An increased tuber sink strength (5–15 nmol/s) enhanced tuber partitioning particularly at higher loading rates (**Figure 8C**, purple line). For very low loading rates, no sucrose arrived at the roots/tubers, rendering enhanced sink strength irrelevant. Beyond these loading rates, the effect of tuber sink strength increased with loading rate due to enhanced sink saturation (**Supplementary Figure 5**). As a result, for high-loading rates, tubers can now become the dominant sink organ. When combining SP6A-mediated efflux mitigation and sink strength increase (**Figure 8C**, brown line), we observe mostly additive effects, with efflux mitigation effects dominating at low and an increased sink strength effects dominating at high-loading rates. Combined, these results indicate that undirected SP6A sucrose efflux reduction broadens the range of loading rates over which tubers obtain significant amounts of sugars.

DISCUSSION

Yield of harvestable plant organs critically depends on sucrose partitioning between competing sinks. Understanding the mechanisms determining resource partitioning is, thus, of great agroeconomic relevance and modeling studies play an important role in unraveling the complex underlying processes. In this modeling study, we performed a systematic investigation into the individual and combined effects of sink characteristics (unloading strength, sucrose affinity, and water uptake or evaporation) and pathway properties (length, resistance, and radial sucrose efflux) on sucrose partitioning, taking potato tuber sucrose delivery as an example case.

We demonstrated that in our biophysically detailed model, the effects of sink strength and affinity, as well as pathway resistance/length, are significantly enhanced compared to earlier studies using simplified sucrose transport models (Minchin et al., 1993; Bancal and Soltani, 2002). These differences could be attributed to the underestimation of sucrose concentration and pathway resistance in the simplified models. We further show that these effects are relevant in a much broader loading rate range compared to a study by Bancal and Soltani (2002) due to higher source concentrations. Our findings on the importance of pathway properties are supported by recent findings that source-sink distance differences drive divergence in yield between grapes (Pallas et al., 2010; Zhu et al., 2021). Additionally, we observed that the previously reported phenomenon of weakest sink prioritization—the larger than expected sucrose allocation to the weaker sink for non-saturating sucrose loading—occurs not only for sinks differing in sink strength, but also for differences in sucrose affinity or pathway length.

Interestingly, we found that in addition to phloem pathway length, the rate and direction of the coupled, parallel xylem flow also impacted sink partitioning. For equal sink characteristics, sucrose partitioning to a sink linearly increased with xylem flow and potential. This effect could be explained from the hydraulic coupling between phloem and xylem and the concomitant changes in both the phloem osmotic and turgor pressure. Thus, while previous study focused on the impact of xylem flow *via* leaf water potential and photosynthetic activity on plant organ growth (Solari et al., 2006), we show that even for constant photosynthesis and, hence, loading rates, the hydraulic coupling between xylem and phloem causes xylem flow to impact sucrose transport and growth.

In the case of potato tubers, we showed that their limited water uptake causes them to be at an advantage in terms of resource partitioning relative to roots that take-up considerably more water, yet at a disadvantage to young leaves that evaporate limited amounts of water. An additional disadvantage arises from the larger distance tubers and roots that have compared to young leaves from source leaves. Both the disadvantages are increased when including SWEET-mediated radial sucrose export. This exacerbated disadvantage enables undirected SP6A-mediated export mitigation to preferentially benefit root/tuber resource allocation. This export mitigating effect of SP6A that dominates at lower loading rates for which phloem transport resistance and xylem water flow differences are relevant complements the effect of SP6A on tuber sink strength that becomes fully effective for high, saturating loading rates. Overall, the undirected SP6A signal significantly broadens the range of loading rates over which tubers obtain significant amounts of sugars.

A major point of discussion is the *in-planta* relevance of the reported results. In essence, this issue revolves around the question whether sinks under most physiological conditions operate at/near saturation or rather operate under non-saturating conditions. As our, and previous results (Minchin et al., 1993; Bancal and Soltani, 2002) show, under saturating conditions, the ratio between sink strength (v_{max}) dictates resource partitioning. It is only under non-saturating conditions that other factors such as sink affinity, pathway resistance/length, xylem flow rate and direction, and radial sucrose efflux significantly affect resource partitioning, weakest sink prioritization occurs, and SP6A efflux mitigation effects weigh in. Classical experiments have demonstrated that upon chemically (Farrar and Minchin, 1991) or cooling induced sink strength reduction (Minchin et al., 1997), sucrose import in unaffected sinks adjusts to the new conditions on a timescale of hours. This slow adaptation has been taken as evidence for sink saturation, reasoning that enhanced uptake requires upregulation of sink uptake capacity (Minchin and Lacointe, 2005). Here, we challenge this view. First, only if remaining sinks are unable to import *any* additional sucrose would this support prior sink saturation, while if remaining sinks are unable to import *all* the extra sucrose immediately this merely implies that maximum sink uptake capacity is now exceeded. Second, upon enhanced sucrose availability, sucrose metabolism requires upregulation. This delayed increase in utilization could lead to sucrose accumulation with negative feedback on sink uptake limiting the initial increase in uptake (Farrar and Minchin, 1991). Similarly, feedback regulation between sink demand and source supply may result in reduced source loading upon sink removal due to sugar accumulation in phloem or leaves, limiting actual extra sucrose availability. Finally, our model generates a 1–2 h timescale for partitioning to adapt to instant changes

in one sink, without any changes occurring in the second sink (**Supplementary Figure 6**). This demonstrates that delayed adaptation of partitioning can at least partly be explained by slow adaptation of the long-distance transport and does not necessarily imply sink upregulation and prior saturation.

In further support of the relevance of pathway properties and incomplete sink saturation for resource partitioning, many stress conditions such as water shortage, salt stress, and infections will reduce harvestable organ sucrose availability through either reducing photosynthesis efficiency or affecting energy budget allocation. We, thus, stress that while simple partitioning models, such as relative growth rate approaches, may serve as a first-order approximation for predicting harvestable organ yields, they do not take into account all the relevant factors. Therefore, in case, substantial deviations with experimental observations occur or more detailed predictions are need, more biophysically detailed and biologically realistic models are essential. These are particularly relevant when studying regulatory mechanisms impinging on sucrose transport, such as the SP6A-SWEET interaction studied here. For future study, it would be of great interest to study resource partitioning in a dynamic, growing architecture. Here, we used a static architecture to study the effects of sink and pathway properties, as inclusion of a growing, more complex, architecture would generate complex feedbacks, further complicating interpretation of the results. Similarly, this model does not include variations in sieve element architecture or vascular bundle numbers along the long-distance phloem or between different organ types. Including such details in the hydraulic architecture of the model are expected to further improve our understanding and capability to predict resource partitioning. Nonetheless, with the insights and modeling from this article, it should now already be possible to interpret resource partitioning in more complex scenarios, which can give insights in important agroeconomic factors such as tuber size distribution.

DATA AVAILABILITY STATEMENT

The original contributions presented in the study are included in the article/**Supplementary Material**, further inquiries can be directed to the corresponding author/s.

AUTHOR CONTRIBUTIONS

BH developed, implemented, analyzed the model, and wrote the manuscript. KT conceived the project, analyzed the model, and wrote the manuscript. Both authors contributed to the article and approved the submitted version.

FUNDING

This study was done in the framework of the MAMY project, with BH funded by the TTW (Grant No. 16889.2019C00026), jointly funded by the MinLNV and the HIP consortium of companies.

ACKNOWLEDGMENTS

We thank Christian Bachem and Sara Bergonzi for the valuable discussions and input on this study.

SUPPLEMENTARY MATERIAL

The Supplementary Material for this article can be found online at: https://www.frontiersin.org/articles/10.3389/fpls.2022.817909/full#supplementary-material

REFERENCES

Abelenda, J. A., Bergonzi, S., Oortwijn, M., Sonnewald, S., Du, M., Visser, R. G. F., et al. (2019). Source-Sink Regulation Is Mediated by Interaction of an FT Homolog with a SWEET Protein in Potato. *Curr. Biol.* 29, 1178–1186. doi: 10.1016/j.cub.2019.02.018

Bancal, P., and Soltani, F. (2002). Source–sink partitioning. Do we need Münch? *J. Exp. Bot.* 53, 1919–1928. doi: 10.1093/jxb/erf037

Bland, W. L., and Tanner, C. B. (1986). Potato tuber water potential components during storage. *Am. Potato J.* 63, 649–653. doi: 10.1007/BF02852927

Braun, D. M., Wang, L., and Ruan, Y.-L. (2014). Understanding and manipulating sucrose phloem loading, unloading, metabolism, and signalling to enhance crop yield and food security. *J. Exp. Bot.* 65, 1713–1735. doi: 10.1093/jxb/ert416

Chen, L.-Q., Qu, X.-Q., Hou, B.-H., Sosso, D., Osorio, S., Fernie, A. R., et al. (2012). Sucrose Efflux Mediated by SWEET Proteins as a Key Step for Phloem Transport. *Science* 335, 207–211. doi: 10.1126/science.1213351

Chiou, T.-J., and Bush, D. R. (1998). Sucrose is a signal molecule in assimilate partitioning. *Proc. Natl. Acad. Sci. U. S. A.* 95, 4784–4788. doi: 10.1073/pnas.95.8.4784

Clerx, L. E., Rockwell, F. E., Savage, J. A., and Holbrook, N. M. (2020). Ontogenetic scaling of phloem sieve tube anatomy and hydraulic resistance with tree height in Quercus rubra. *Am. J. Bot.* 107, 852–863. doi: 10.1002/ajb2.1481

Da Silva, D., Qin, L., DeBuse, C., and DeJong, T. M. (2014). Measuring and modelling seasonal patterns of carbohydrate storage and mobilization in the trunks and root crowns of peach trees. *Ann. Bot.* 114, 643–652. doi: 10.1093/aob/mcu033

de Vries, J., Evers, J. B., Kuyper, T. W., Ruijven, J., and Mommer, L. (2021). Mycorrhizal associations change root functionality: a 3D modelling study on competitive interactions between plants for light and nutrients. *New Phytol.* 231, 1171–1182. doi: 10.1111/nph.17435

de Wit, A., Boogaard, H., Fumagalli, D., Janssen, S., Knapen, R., van Kraalingen, D., et al. (2019). 25 years of the WOFOST cropping systems model. *Agric. Syst.* 168, 154–167. doi: 10.1016/j.agsy.2018.06.018

Driever, S. M., Simkin, A. J., Alotaibi, S., Fisk, S. J., Madgwick, P. J., Sparks, C. A., et al. (2017). Increased SBPase activity improves photosynthesis and grain yield in wheat grown in greenhouse conditions. *Philos. Trans. R. Soc. Lond. B Biol. Sci.* 372, 1–10. doi: 10.1098/rstb.2016.0384

Farrar, J. F., and Minchin, P. E. H. (1991). Carbon Partitioning in Split Root Systems of Barley: relation to Metabolism. *J. Exp. Bot.* 42, 1261–1269. doi: 10.1093/jxb/42.10.1261

Fernie, A. R., Bachem, C. W. B., Helariutta, Y., Neuhaus, H. E., Prat, S., Ruan, Y.-L., et al. (2020). Synchronization of developmental, molecular and metabolic aspects of source–sink interactions. *Nat. Plants* 6, 55–66. doi: 10.1038/s41477-020-0590-x

Hafke, J. B., Amerongen, J. K., van, Kelling, F., Furch, A. C. U., Gaupels, F., et al. (2005). Thermodynamic Battle for Photosynthate Acquisition between Sieve Tubes and Adjoining Parenchyma in Transport Phloem. *Plant Physiol.* 138, 1527–1537. doi: 10.1104/pp.104.058511

Hölttä, T., Mencuccini, M., and Nikinmaa, E. (2009). Linking phloem function to structure: analysis with a coupled xylem–phloem transport model. *J. Theor. Biol.* 259, 325–337. doi: 10.1016/j.jtbi.2009.03.039

Hölttä, T., Vesala, T., Sevanto, S., Perämäki, M., and Nikinmaa, E. (2006). Modeling xylem and phloem water flows in trees according to cohesion theory and Münch hypothesis. *Trees* 20, 67–78. doi: 10.1007/s00468-005-0014-6

Konrad, W., Katul, G., Roth-Nebelsick, A., and Jensen, K. H. (2019). Xylem functioning, dysfunction and repair: a physical perspective and implications for phloem transport. *Tree Physiol.* 39, 243–261. doi: 10.1093/treephys/tpy097

Lacointe, A., and Minchin, P. E. H. (2008). Modelling phloem and xylem transport within a complex architecture. *Funct. Plant Biol.* 35:772. doi: 10.1071/FP08085

Lescourret, F., Moitrier, N., Valsesia, P., and Génard, M. (2011). QualiTree, a virtual fruit tree to study the management of fruit quality. I. Model development. *Trees* 25, 519–530. doi: 10.1007/s00468-010-0531-9

Minchin, P. E. H., and Lacointe, A. (2005). New understanding on phloem physiology and possible consequences for modelling long-distance carbon transport. *New Phytol.* 166, 771–779. doi: 10.1111/j.1469-8137.2005.01323.x

Minchin, P. E. H., and Lacointe, A. (2017). Consequences of phloem pathway unloading/reloading on equilibrium flows between source and sink: a modelling approach. *Funct. Plant Biol.* 44:507. doi: 10.1071/FP16354

Minchin, P. E. H., Thorpe, M. R., and Farrar, J. F. (1993). A Simple Mechanistic Model of Phloem Transport which Explains Sink Priority. *J. Exp. Bot.* 44, 947–955. doi: 10.1093/jxb/44.5.947

Minchin, P. E. H., Thorpe, M. R., Wünsche, J. N., Palmer, J. W., and Picton, R. F. (1997). Carbon partitioning between apple fruits: short- and long-term response to availability of photosynthate. *J. Exp. Bot.* 48, 1401–1406. doi: 10.1093/jxb/48.7.1401

Morison, K. R. (2002). "Viscosity equations for sucrose solutions: old and new 2002," *Proceedings of the 9th APCChE Congress and CHEMECA*.

Navarro, C., Abelenda, J. A., Cruz-Oró, E., Cuéllar, C. A., Tamaki, S., Silva, J., et al. (2011). Control of flowering and storage organ formation in potato by FLOWERING LOCUS T. *Nature* 478, 119–122. doi: 10.1038/nature10431

Nölke, G., Houdelet, M., Kreuzaler, F., Peterhänsel, C., and Schillberg, S. (2014). The expression of a recombinant glycolate dehydrogenase polyprotein in potato (*Solanum tuberosum*) plastids strongly enhances photosynthesis and tuber yield. *Plant Biotechnol. J.* 12, 734–742. doi: 10.1111/pbi.12178

Pallas, B., Christophe, A., and Lecoeur, J. (2010). Are the common assimilate pool and trophic relationships appropriate for dealing with the observed plasticity of grapevine development? *Ann. Bot.* 105, 233–247. doi: 10.1093/aob/mcp278

Perämäki, M., Nikinmaa, E., Sevanto, S., Ilvesniemi, H., Siivola, E., Hari, P., et al. (2001). Tree stem diameter variations and transpiration in Scots pine: an analysis using a dynamic sap flow model. *Tree Physiol.* 21, 889–897. doi: 10.1093/treephys/21.12-13.889

Savage, J. A., Clearwater, M. J., Haines, D. F., Klein, T., Mencuccini, M., Sevanto, S., et al. (2016). Allocation, stress tolerance and carbon transport in plants: how does phloem physiology affect plant ecology? *Plant Cell Environ.* 39, 709–725. doi: 10.1111/pce.12602

Schulze, W., Weise, A., Frommer, W. B., and Ward, J. M. (2000). Function of the cytosolic N-terminus of sucrose transporter AtSUT2 in substrate affnity. *FEBS Lett.* 485, 189–194. doi: 10.1016/s0014-5793(00)02180-3

Sevanto, S., Hölttä, T., and Holbrook, N. M. (2011). Effects of the hydraulic coupling between xylem and phloem on diurnal phloem diameter variation. *Plant Cell Environ.* 34, 690–703. doi: 10.1111/j.1365-3040.2011.02275.x

Solari, L. I., Johnson, S., and DeJong, T. M. (2006). Relationship of water status to vegetative growth and leaf gas exchange of peach (Prunus persica) trees on different rootstocks. *Tree Physiol.* 26, 1333–1341. doi: 10.1093/treephys/26.10.1333

Thompson, M. V., and Holbrook, N. M. (2003). Application of a Single-solute Non-steady-state Phloem Model to the Study of Long-distance Assimilate Transport. *J. Theor. Biol.* 220, 419–455. doi: 10.1006/jtbi.2003.3115

van den Herik, B., Bergonzi, S., Bachem, C. W. B., and Tusscher, K. (2021). Modelling the physiological relevance of sucrose export repression by an Flowering Time homolog in the long-distance phloem of potato. *Plant Cell Environ.* 44, 792–806. doi: 10.1111/pce.13977

Viola, R., Roberts, A. G., Haupt, S., Gazzani, S., Hancock, R. D., Marmiroli, N., et al. (2001). Tuberization in Potato Involves a Switch from Apoplastic to Symplastic Phloem Unloading. *Plant Cell* 13, 385–398. doi: 10.1105/tpc.13.2.385

Windt, C. W., Vergeldt, F. J., Jager, P. A. D., and As, H. V. (2006). MRI of long-distance water transport: a comparison of the phloem and xylem flow characteristics and dynamics in poplar, castor bean, tomato and tobacco. *Plant Cell Environ.* 29, 1715–1729. doi: 10.1111/j.1365-3040.2006.01544.x

Zhu, J., Gou, F., Rossouw, G., Begum, F., Henke, M., and Johnson, E. (2021). Simulating organ biomass variability and carbohydrate distribution in perennial fruit crops: a comparison between the common assimilate pool and phloem carbohydrate transport models. *In Silico Plants* 3:diab024. doi: 10.1093/insilicoplants/diab024

Conflict of Interest: The authors declare that the research was conducted in the absence of any commercial or financial relationships that could be construed as a potential conflict of interest.

Publisher's Note: All claims expressed in this article are solely those of the authors and do not necessarily represent those of their affiliated organizations, or those of the publisher, the editors and the reviewers. Any product that may be evaluated in this article, or claim that may be made by its manufacturer, is not guaranteed or endorsed by the publisher.

frontiers | Frontiers in Plant Science

TYPE Review
PUBLISHED 28 July 2022
DOI 10.3389/fpls.2022.921469

OPEN ACCESS

EDITED BY
Shahin S. Ali,
American Type Culture Collection (ATCC), United States

REVIEWED BY
Muthusamy Ramakrishnan,
Nanjing Forestry University, China
Indrani Kakati Baruah,
United States Department of Agriculture (USDA), United States

*CORRESPONDENCE
Yeirme Y. Jaimes-Suárez
yjaimes@agrosavia.co

SPECIALTY SECTION
This article was submitted to Plant Biophysics and Modeling, a section of the journal Frontiers in Plant Science

RECEIVED 15 April 2022
ACCEPTED 06 July 2022
PUBLISHED 28 July 2022

CITATION
Jaimes-Suárez YY, Carvajal-Rivera AS, Galvis-Neira DA, Carvalho FEL and Rojas-Molina J (2022) Cacao agroforestry systems beyond the stigmas: Biotic and abiotic stress incidence impact. *Front. Plant Sci.* 13:921469. doi: 10.3389/fpls.2022.921469

Cacao agroforestry systems beyond the stigmas: Biotic and abiotic stress incidence impact

Yeirme Y. Jaimes-Suárez*, Albert S. Carvajal-Rivera, Donald A. Galvis-Neira, Fabricio E. L. Carvalho and Jairo Rojas-Molina

Centro de Investigación La Suiza, Corporación Colombiana de Investigación Agropecuaria—AGROSAVIA, Rionegro, Colombia

Low technological knowledge in production chains, global climate change, and misinformation are concrete threats to food security. In addition, these combined threats also trigger ecological instability in megadiverse areas of the world, especially in some cacao-producing countries in South America, where this crop plays an important socio-economic role, even being used to replace illicit crops. Accordingly, the use of agroforestry systems approaches has emerged as a good alternative to maintain productivity, add high-value commodities to producers, and provide important ecosystem services for sustainable agriculture. However, limitations associated with the competition for resources between the species composing the system, and the higher incidence of some diseases, have led many producers to abandon this strategy, opting for monoculture. In this review, we seek to gather the main information available in the literature, aiming to answer the question: what is the real scientific evidence that supports the benefits and harms of adopting agroforestry systems in cacao production? We seek to make critical scrutiny of the possible negative effects of certain associations of the agroforestry system with biotic and abiotic stress in cacao. Here, we review the possible competition for light and nutrients and discuss the main characteristics to be sought in cacao genotypes to optimize these inter-specific relationships. In addition, we review the research advances that show the behavior of the main cacao diseases (Witch's broom disease, frosty pod rot, black pod rot) in models of agroforestry systems contrasted with monoculture, as well as the optimization of agronomic practices to reduce some of these stresses. This compendium, therefore, sheds light on a major gap in establishing truly sustainable agriculture, which has been treated much more from the perspective of negative stigma than from the real technological advantages that can be combined to the benefit of a balanced ecosystem with generating income for farmers.

KEYWORDS

AFS, black pod rot, frosty pod rot, light use efficiency, water use efficiency, witch's broom disease

Introduction

Cacao (*Theobroma cacao L.*) is a native plant from the northern Amazon, currently cultivated in tropical regions of the world, especially in African countries (Motamayor et al., 2008). In America, the main producer countries are Ecuador, Brazil, Peru, and Colombia (FAOStat, 2021). Although this species comes from the undergrowth and has a wide variety of adaptations to grow under conditions of low light availability (Salazar et al., 2018), due to its phenotypic plasticity, some countries have found success in adopting monoculture cacao cultivation systems with full sun exposure (Lennon et al., 2021). Accordingly, cacao is grown in the world in both monoculture and agroforestry systems, and the two are considered to have different approaches to production and sustainability.

The cacao agroforestry systems (CAFS) can be classified as traditional or associated with planting arrangements. The traditional CAFS have intervened forests composed of different species in multi strata, where the cacao enters to replace one of the strata and the upper strata are kept as a shade. The CAFS with planting arrangements have a design with a homogeneous planting pattern involving cacao and one or more accompanying tree species to provide the shade. In these systems, the species selected for shading also represents a good part of the financial income of the plantation, as in the case of timber trees, which may be used to add high-value products to the system (Álvarez-Carrillo et al., 2012; Sambuichi et al., 2012). In the CAFS, the canopies of the forest trees may buffer environmental conditions, reducing air temperature, helping to retain moisture, and contributing to the improvement of physicochemical properties in the soil, as well as impacting the maintenance of biodiversity (Rojas-Molina et al., 2017; Marconi and Armengot, 2020). However, inadequate management of these canopies limits the entry of light and consequently limits photosynthesis, thus negatively affecting cacao production (Salazar et al., 2018).

The inadequate management of CAFS has generated a growing need to increase cacao productivity, and cacao monoculture has become an alternative to achieve this (Zuidema et al., 2005; de Almeida and Valle, 2010). However, this alternative also has disadvantages, such as the possibility of photooxidative stress, associated with excess light (Bassi and Dall'Osto, 2021), and the pressure for the use of water and fertilizers, which can also represent a negative factor for cacao sustainability if not properly managed. On the other hand, some authors positively correlate cacao diseases with CAFS (Andres et al., 2016). Although plant diseases can cause up to 100% yield losses in cacao, their severity depends on the level of management of the cacao plantation. The three main cacao diseases of particular interest are: (1) *Moniliophthora perniciosa*, the causal agent of the witch broom disease (WBD), (2) *Moniliophthora roreri*, which causes the frosty pod rot (FPR), and (3) *Phytophthora* spp. which causes the black pod rot (BPR). Notwithstanding, environmental conditions are strongly linked to pathogenesis processes in agricultural systems (Cooke, 2006). There is still controversy over the use of shade trees in cacao crops and their contribution to the incidence of diseases, which is complex and requires a comprehensive understanding of the factors that favor their development. CAFS said to have microenvironments with high relative humidity and reduced light input, which favors the incidence of these diseases. This pre-conception has encouraged many producers to remove or reduce the number of shade trees from plantations (Marconi and Armengot, 2020). However, the life cycle of each of these pathogens differs from the others. In addition, the plant–pathogen interactions are non-linear and extremely complex systemic processes, which are highly affected by the environment, including the incidence of other ecosystemic factors such as the presence of natural biocontrollers.

Unfortunately, few studies compare CAFS and cacao monocultures regarding the advantages and disadvantages that may occur. This information would make it possible to resolve multiple aspects associated with the cost–benefit of cacao production, the socio-economic reality of cacao farmers, and the long-term sustainability of the production system. Hence there is a growing need to document these advantages and disadvantages, with agroforestry systems (AFS) being of special interest. In this current review, we explore how the AFS influences the physiology of cacao plants based on the use of light, water, and nutrients and highlight the possible correlations between cacao diseases and the agronomic model employed. Moreover, in this document, we attempted to scrutinize how forest tree management can favor or limit the development of cacao crop diseases. This information will contribute to the implementation of best practices and planting designs for the CAFS management, as well as help to select the best strategies for integrated management of cacao diseases.

Cacao agroforestry systems vs. monoculture: Use of light, water, and nutrients

Shading and light use efficiency in agroforestry systems

Light is one of the most crucial resources for the growth and development of plant, and consequently, this is a determining factor for crop productivity. Plants can absorb light in the photosystem complexes of thylakoids and employ this energy as the primary source for all assimilatory reactions, including nitrogen, sulfur, and carbon assimilation (Brestic et al., 2021). Consequently, these reactions are the primordial event for biomass formation that defines plant growth and productivity (Foyer et al., 2017; Lima Neto et al., 2021). Although all plants depend on light, the excess of this resource can be potentially harmful to plants. Accumulation of electrons in the thylakoid transport chain can promote the formation of reactive oxygen species that, can cause cell death, chlorosis, leaf abscission, and even plant death (Foyer, 2018). On the other hand, low light

seriously limits the energy available for chemical reactions, crucial for plant growth and productivity (Lawlor and Tezara, 2009). Indeed, of the total light that falls on leaves, about 85% is absorbed by chlorophylls, and only about 5% of this energy is stored as organic matter (Pinnola and Bassi, 2018). Therefore, to survive in contrasting conditions of light fluctuation, as found in different agronomical designs, plants need to develop several molecular and biochemical strategies related to improving light use efficiency (LUE) in the shadow (AFS) or dissipate the excess of light to avoid oxidative stress (monoculture).

Cacao originated in understory regions of Amazon and is relatively adapted to tolerate shade conditions (González-Orozco et al., 2020). In shade conditions caused by the other plant leaves, as occurs in the understory, the taller plants absorb most of the light energy available, especially in the blue and red range. This absorbance contrasts with the light transmission of the longer wavelengths, with less available energy, mainly composed of the far-red range (Lorrain et al., 2008). The relative proportions between red and far-red are also important environmental signals capable of modulating processes in plants related to the best use of light and, consequently, signaling greater efficiency in the use of this resource (Puthiyaveetil et al., 2012; Goldschmidt-Clermont and Bassi, 2015). Among the strategies triggered by plants under these conditions are: (1) a relative increase in the proportion between antennas and reaction centers; (2) downregulation of dissipation processes such as non-photochemical quenching (NPQ); (3) anatomical changes related to leaf area and density; and (4) adjustments in the proportion between photosystems I and II (Coopman et al., 2010; Hughes et al., 2014; Ruban, 2015). Therefore, cacao plants need to exhibit one or more of these acclimatory characteristics to survive and produce in shade conditions.

However, despite its adaptation to shaded environments, cacao also has remarkable phenotypic plasticity that allows it to grow and develop in conditions of full-sun exposition (Salazar et al., 2018; Baligar et al., 2021). This plasticity probably raises from the ability to modulate the expression of genes and regulate morpho-anatomic features that enable the plant to increase its photosynthesis capacity while promoting defense mechanisms against the excess of light, as expected for the full-sun conditions (Scheibe, 2019). Following the increased photosynthesis, cacao plants grown in full sun have higher productivity than plants grown in shaded environments (Mortimer et al., 2018). Nevertheless, studies have also shown that although productivity is increased under full-sun conditions, the productive life cycle is shortened by many years (Rajab et al., 2016). In addition, the incidence of some biotic stresses can become more frequent under full sun conditions than in shading, such as WBD. These responses in the life cycle and plant–disease interactions may also be possibly associated with increased competition in the energetic balance flow (Figure 1). Moreover, the ecosystemic services provided by AFS timber trees must be considered because of their environmental sustainability. Therefore, to maximize the long-term productivity of cacao, planting plots associated with AFS have been recommended and widely used in South America.

The average saturation light for cacao is about 400–500 $\mu mol\, m^{-2}\, s^{-1}$ (Salazar et al., 2018). This intensity is relatively low, as it can reach 1,000 in beans and up to 1,500 $\mu mol\, m^{-2}\, s^{-1}$ in some monocot crop species such as rice and wheat (Carvalho et al., 2014; Lobo et al., 2019). This data indicates that for most cacao varieties, luminous intensities above 500 $\mu mol\, m^{-2}\, s^{-1}$ do not have positive effects on photosynthesis, otherwise may consist of excess energy. Considering that cacao cultivation may take place in tropical regions (Rodriguez-Medina et al., 2019), excess energy can indeed raise a problem for cacao farmers, therefore justifying its use in shaded AFS conditions.

The use of approximately 30–40% shading is strongly recommended for the proper management of cacao (Beer et al., 1998; Álvarez-Carrillo et al., 2012). However, light conditions below 400–500 $\mu mol\, m^{-2}\, s^{-1}$ can potentially limit the availability of energy processed by the photosystem's antennas, demanding a greater LUE to ensure growth and productivity. In addition, other factors such as the altitude, cartesian orientation, and the frequent incidence of clouds in the region must be considered to maximize light availability in AFS (Salazar et al., 2018). Therefore, cacao plants presenting higher LUE may be more productive under shader AFS conditions. In this way, the arrangement of the CAFS is of fundamental importance to ensure that the appropriate luminous intensity will be available for cacao growth and productivity (Mortimer et al., 2018). Exploiting the great phenotypic plasticity and genetic diversity presented by cacao plants may also allow further selection of genotypes with higher LUE. This approach could lead to a new, more dynamic, and efficient CAFS design.

The LUE, however, cannot be taken as a static process since it is extremely dynamic. For example, recent studies in coffee AFS have reported that even when irradiance was reduced by 60%, coffee light-use efficiency was increased by 50%, leaving net primary productivity stable across all shade levels (Charbonnier et al., 2017). In these plants, the endogenous features and other environmental conditions have more effect on productivity than the light intensity *per sea*. The authors concluded that the age of plants and the interspecific competition for water and soil nutrients among coffee and the tree species were more relevant for crop productivity (Charbonnier et al., 2017). In cacao, there are no studies regarding the LUE plasticity as a response to different microclimate conditions and interspecific interactions inside the different CAFS plots. However, some studies approached photosynthetic responses under contrasting CAFS designs (Gómez-Yarce et al., 2020) and evaluated contrasting cacao varieties (Agudelo-Castañeda et al., 2018). These studies also reinforce the great plasticity of cacao genotypes and the importance of interspecific interactions in CAFS designs.

The mechanisms underlying the LUE adjustment in plants as a response to different light intensities are still not completely elucidated to date. Source–sink relationships, which are strongly associated with carbon allocation during the reproductive phase,

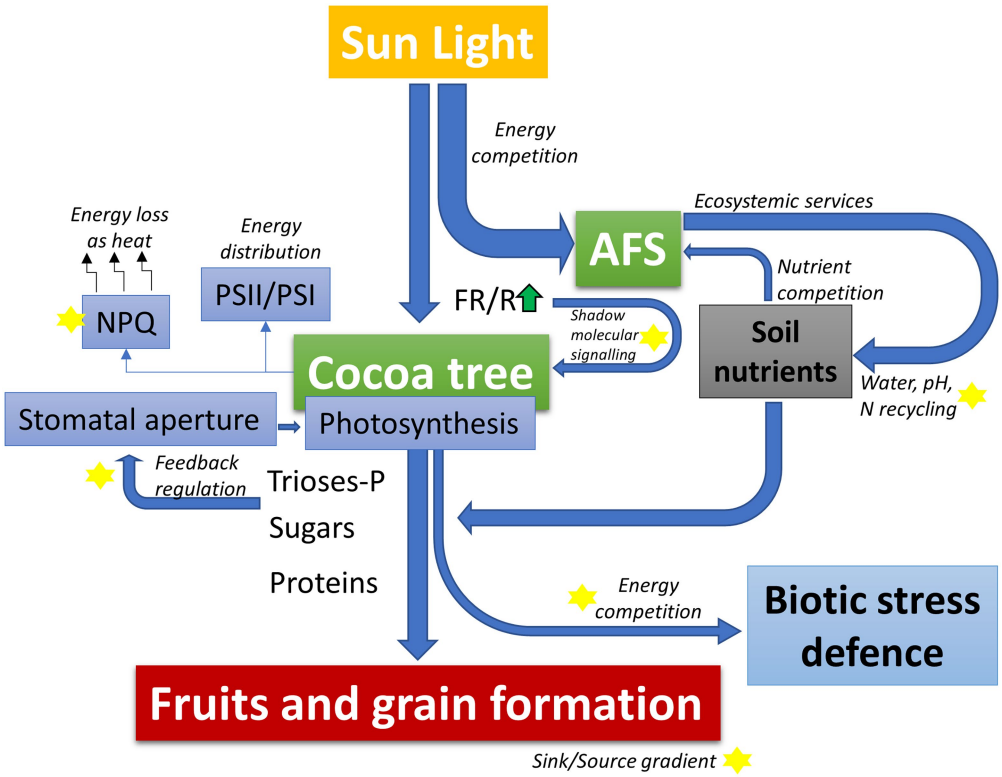

FIGURE 1
Schematic model highlighting the balance of light energy, carbon skeletons, and nutrients use distributed between activation of protection mechanisms against biotic stresses and productivity within the context of an agroforestry systems (AFS). In AFS, cocoa competes for light energy and soil nutrients with the shading tree species. This competition is directly counterbalanced by the ecosystem services provided by the shading trees that can favor water use efficiency and chemical soil properties (better availability of nutrients). Furthermore, differences in light quality (red/far-red light composition – FR/R) and contrasting balance in the levels of trioses-phosphate and other signaling molecules may activate physiological compensation pathways to optimize the energy balance of cocoa plants depending on the genetic background. These physiological compensatory responses may include adjustments in stomatal regulation, induction/relaxation of excess energy dissipation mechanisms (non-photochemical quenching, NPQ), and stoichiometric adjustments in the photosystem complexes (PSII/PSI). Finally, the resulting dynamic energetic and metabolic balance of the AFS-cacao model may directly compete with the energetic/metabolic demand of biotic stress defense mechanisms, thus determining the degree of limitation on the potential productivity of each genotype specifically. Yellow stars in the figure represent central processes for deeper investigation in AFS-cocoa models.

could represent a decisive factor in determining the LUE in shaded plant species (Cannell, 1971). According to this hypothesis, the light use efficiency is adjusted in response to the activation of sink-source gradients. In this case, the energy demand, mainly related to fruit production, would be ultimately the limiting factor for determining the LUE. This response, in turn, would be highly determined by other environmental conditions, besides light, which in fact would be the driving force behind the regulation of the LUE (Charbonnier et al., 2017). Many molecular mechanisms are known to directly compete for the energetic flow driven to the sugar biosynthesis, consequently affecting indirectly the allocation of carbon to fruits (Figure 1). For example, the non-photochemical quenching (Murchie and Ruban, 2020) and the photorespiratory activity (Guilherme et al., 2019) may drastically affect the energy balance in the leaves. Studies aiming to understand the physiological, molecular, and genetic components associated with these processes in cacao, especially within an integrative and multidisciplinary context associating the possible interactions of pathogens within the CAFS competitive model are still needed.

Cacao agroforestry systems ecosystemic services: Water and nutrient availability

In the CAFS, the interspecific competition for water and nutrients also must be considered (Niether et al., 2019). Different species of timber trees are capable of interfering in many ways with the fertility and microbiology of soils, consequently affecting the availability of nutritional resources for cacao to complete its biological cycle of growth and development. However, several advantages of CAFS have been documented. These can decrease air and soil temperatures compared to monoculture, reducing evapotranspiration (Mortimer et al., 2018). Thus, CAFS can play ecosystemic services that contribute to increasing the resilience of cacao plants to climate variability (Green et al., 2021).

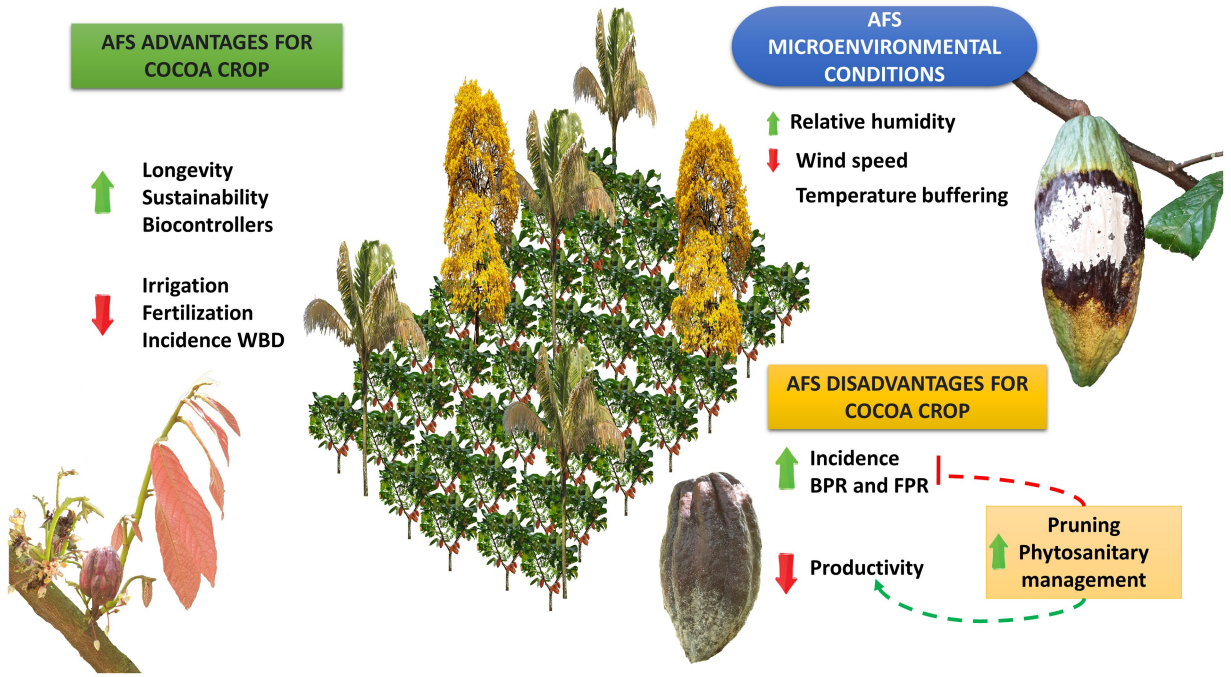

FIGURE 2
Impact on the development of diseases and cacao productivity in agroforestry systems as compared to monoculture. Green arrows mean a favored process and red arrows mean an unfavorable process. AFS promotes specific changes in the cocoa microenvironment, especially related to higher humidity and potentially a greater buffering of temperature changes, despite it may reduce the wind speed inside the system. These changes have the potential to induce an increase in the longevity of cocoa plants, better use of pest and disease biocontrollers, and ultimately promote environmental sustainability. In addition, it may promote a lower need for irrigation and fertilization, as well as a lower incidence of witch's broom disease (WBD), impacting positively the producers' costs. However, in parallel AFS models have a great potential to negatively impact cocoa productivity due to higher susceptibility to black pod rot (BPR) and frosty pod rot (FPR) if pruning and phytosanitary management are not carried out properly.

Likewise, different tree species have distinct requirements for water resources, which can be an extremely important factor in conditions in which this resource becomes scarce. In a CAFS, cacao productivity will be determined by the intersection of four main factors: (1) the specific genotype genetic background of cacao, which determines the degree of plasticity of the phenotypic response under environmental oscillations; (2) the specificity of the habit of the accompanying trees; (3) the biophysical characteristics of the environment where the system is developing, including temperature, altitude, and rainfall; and (4) the possibility of the occurrence or not of biotic stress; which are all subject to human factor interference (Figure 2).

According to the AFS hypothesis, timber trees can interfere (allelopathy + competition) with the crop and generate complementary effects (Hierro and Callaway, 2021). Through allelopathy and competition, timber trees can deplete some nutrients or release potentially phytotoxic substances, with negative effects on the growth and productivity of some crops (Scavo et al., 2018). On the other hand, favorable interspecific interactions can also make some mineral resources more available by altering the chemical properties of soils, for example (Hosseini Bai et al., 2017). It has even been reported that some AFS models can affect the pH and increase the availability of organic carbon, inducing the microbiological quality of soils and thus favoring the associated crops (Bai et al., 2016). Likewise, the AFS can contribute to several processes to improve the water use efficiency of AFS crops, reducing the need for irrigation complementation (Hatfield and Dold, 2019). Therefore, the potential ecosystem services related to better use of water resources performed by the AFS model should be considered as an extremely positive factor in the balance that includes disease incidence, management cost, and productivity, when compared with the monoculture system, especially under the projected scenario of global climate changing.

In cacao, Zuidema et al. (2005) found that the annual radiation and the accumulated precipitation of the dry seasons explain 70% of the variation in production concerning the simulated potential, in more than 30 localities around the tropics, with a strong correlation between the precipitation of the driest months and the annual dry cacao beans yield. These data confirm the importance of water availability for cacao productivity. However, despite the high importance of the water resource in cacao, there are few publications of practical value on the responses of the crop to drought or irrigation (Jegadeeswari and Kumar, 2019; Hebbar et al., 2020), especially under agroforestry arrangements. Niether et al. (2019) reported that the AFS modifies the hydric relations of cacao through changes in the percentage of transmitted light, effective precipitation, and microclimate, where evapotranspiration reaches values of 5.12 mm day^{-1} in the monoculture and 4.51 mm day^{-1} in an AFS. Experimental evidence has shown that fully exposed cacao trees have shorter production cycles, leading

to progressive plant deterioration, loss of vigor (proliferation of some diseases and insect attacks), and finally death (Alpízar et al., 1986).

In addition, at full exposure, factors such as high radiation and air temperature can have negative effects on cacao plants (Salazar et al., 2018). When the cacao leaves are exposed directly to the sun, there is a 40% increase in the temperature of the leaf, about the leaves under shady (28°C). This results in a high increase in photorespiration from leaves exposed to full sun (Huang et al., 2016), increasing the possibility of water stress. In addition, if the water requirements are not met, the imbalance between the contribution of incident light energy in the leaves and the consumption by metabolic processes can generate photoinhibition, photodamage, and irreversible effects on plant growth and development (Cunha et al., 2019). This problem is of particular importance for Colombia, which can present variations of more than 1,000% of daily light intensity (Salazar et al., 2018), reaching peaks of 2,500 $\mu E\, m^{-2}\, s^{-1}$ in some regions. In fact, in stressed cacao plants, at least a 25% reduction in CO_2 assimilation rates may occur, while transpiration rates can decrease by 40% due to stomatal closure (Agudelo-Castañeda et al., 2018), which can be aggravated by the occurrence of parallel biotic stress and nutritional deficiencies. Moreover, CAFS are completely dynamic systems. The time and intensity of pruning are essential to balance light and water availability in environmental conditions that varies seasonally to conserve microenvironments for cacao production with less exposure to unfavorable climates (Niether et al., 2019).

Therefore, despite possible productivity reductions, which may be also compensated by more appropriate management procedures, AFS can benefit the long-term durability and stability of the associated crops. In addition, AFS strategies can bring cost-saving benefits in the use of fertilizers and irrigation (Wartenberg et al., 2020). Nevertheless, the possible correlation between the use of AFS and the incidence of biotic stress would still be by far the most controversial point for its widespread use in cacao production systems. In the next sections, this review will scrutinize facts and myths about the disease susceptibility of AFS associated with cacao.

Cacao agroforestry systems vs. monoculture: Development of cacao diseases

Witch's broom disease

The WBD, caused by the fungus *M. perniciosa*, may generate losses of up to 100% of production, even causing the abandonment of the crop (Pereira et al., 1996; Meinhardt et al., 2008; Andres et al., 2016; Sousa Filho et al., 2021). Four biotypes (C, H, L, and S) are reported for *M. perniciosa*, which are classified by their reproductive biology and host specificity. Biotype C infects plants of the Malvaceae family, including the genus *Theobroma* (*T. cacao*, *T. grandiflorum*, *T. bicolor*, *T. obovatum*, *T. microcarpum*, *T. speciosum*, *T. subincana*, *T. sylvestris*; Meinhardt et al., 2008). Two pathotypes have been reported within biotype C identified as pathotypes A and B, where pathotype A is the most virulent and is found distributed in Colombia, Bolivia, and Ecuador. On the other hand, pathotype B is found in Brazil and Venezuela and presents less virulence (Gramacho et al., 2016).

Moniliophthora perniciosa is a hemibiotrophic pathogen, characterized by having two different phases in its life cycle (Evans, 2016). Remarkably, the pathogen is an obligate parasite whose mycelium is not infective and only spores are capable of inducing infection (Kilaru and Hasenstein, 2005). After infection, *M. perniciosa* colonizes the host as a biotrophic pathogen, affecting new shoots, flower cushions, and fruits, presenting various symptoms. Vegetative brooms develop on the stem and branches, where the axillary and lateral buds suffer hyperplasia, producing elongated and swollen stems with flaccid leaves and long petioles (Silva et al., 2002). After 3–4 months, the leaves fall off, leaving only the withered branches that resemble a broom. In the flower buds, multiple parthenocarpic flowers and fruits can form, shaped like carrots or custard apples that quickly necrotize, becoming woody, hard, and "mummified." In developing fruits, irregular dark brown lesions are formed that, unlike *M. roreri*, harden and remain free of mycelium (Aime and Phillips-Mora, 2005; Evans, 2016). Finally, the pathogen begins its necrotrophic or saprophytic phase in the infected dead tissues, producing the fungus fruiting bodies, called basidiocarps. If favorable environmental conditions are present, the pathogen releases the basidiospores, which are dispersed with the help of the wind to start a new cycle of infection (Evans, 2016).

Some studies report on the incidence of WBD in cacao plantations grown on CAFS, coinciding that agroforestry plantations with cacao have a lower incidence of WBD (Table 1; Evans, 1998). Consequently, it is possible to assume that as cacao crops gradually become monocultures, the incidence of WBD may increase significantly (Jacobi et al., 2013). When cacao plantations are exposed to the full sun without shade trees, this leads to an increase in bud and flower formation and, associated with this, an increase in susceptibility of meristematic tissues (Milz, 2006). The ideal conditions for this pathogen to progress in monocultures are based on the change in the environment of the pathosystem, which also implies a low activity of biocontrollers (Figure 2). In this sense, CAFS harbor native plant species that contribute to the formation of multiple antagonistic microorganisms and saprophytes, which have evolved together with *M. perniciosa*. Generally, these microorganisms grow under the canopy of the trees, in the phylloplane, and in the soil (organic matter), which under CAFS environmental conditions are protected from direct sunlight, temperature, and desiccation (Schroth et al., 2000; Vaast and Somarriba, 2014; Armengot et al., 2020). At the same time, intensive technical management of crops at full exposure promotes overproduction of flowers and branches, in turn increasing potential sites of infection. This situation, combined with the adverse factor caused by overexposure to light and the increase in wind speed, may facilitate the conditions for the development of

TABLE 1 Literature review on the use of agroforestry systems (AFS) in cocoa production, evidencing its effects on the incidence of diseases and potential impact on productivity.

Pathogen	Impact on disease development	AFS impact on cocoa crop productivity	Country	Reference
Phythpthora spp.	There are no significant differences compared to monocultures if cultural practices are applied opportunely	Positive-conditioned	Bolivia	Armengot et al. (2020)
Phythpthora spp.	There are no significant differences compared to monocultures if cultural practices are applied opportunely	Positive-conditioned	Ghana	Leitão (2020)
Phythpthora spp.	The incidence and severity of black pod disease increases proportionally with increasing shade level.	Negative	Cameron	Ambang et al. (2019)
Phythpthora megakarya	Companion species of AFS are hosts and spread the disease.	Negative	Cameron	Holmes et al. (2003)
Phythpthora megakarya	Companion species of AFS are hosts and spread the disease.	Negative	West Africa	Opoku et al. (2002)
Phythpthora palmivora, Phythpthora megakarya	Companion species of AFS are hosts and spread the disease.	Negative	Ghana	Akrofi (2015)
Moniliophthora roreri	There are no significant differences compared to monocultures if cultural practices are applied opportunely	Positive-conditioned	México	Torres de la Cruz et al. (2011)
Moniliophthora roreri	There are no significant differences compared to monocultures if cultural practices are applied opportunely	Positive-conditioned	Perú	Krauss and Soberanis (2001)
Moniliophthora roreri	There are no significant differences compared to monocultures if cultural practices are applied opportunely	Positive-conditioned	Bolivia	Armengot et al. (2020)
Moniliophthora perniciosa	The incidence and severity of witch's broom disease decrease proportionally with increasing shade level.	Positive	Ecuador	Evans (1998)
Moniliophthora perniciosa	The incidence and severity of witch's broom disease decrease proportionally with increasing shade level.	Positive	Perú	Krauss and Soberanis (2001)
Moniliophthora perniciosa	The incidence and severity of witch's broom disease decrease proportionally with increasing shade level.	Positive	Bolivia	Jacobi et al. (2013)
Moniliophthora perniciosa	The incidence and severity of witch's broom disease decrease proportionally with increasing shade level.	Positive	Venezuela	Hernández-Villegas (2016)
Moniliophthora perniciosa	The incidence and severity of witch's broom disease decrease proportionally with increasing shade level.	Positive	Bolivia	Andres et al. (2016)
Moniliophthora perniciosa	The incidence and severity of witch's broom disease decrease proportionally with increasing shade level.	Positive	Bolivia	Armengot et al. (2020)

A positive impact means that there was no significant difference concerning the incidence of a given disease, while a negative impact indicates that there is a higher incidence of the disease, in both cases comparing the AFS model with the monoculture. A positive-conditioned impact means that there are no differences in the disease progression comparing AFS and monoculture systems if adequate cultural practices are opportunely adopted.

M. perniciosa infection (Evans, 1998; Schroth et al., 2000). Relative humidity also plays an important role in the formation of brooms. If this climatic variable is stable and does not suffer strong alterations, it has been shown that the occurrence of brooms is favored (Nunes et al., 2002).

The higher constant humidity allows the basidiospores to germinate and penetrate the germ tube. Studies have reported that at least 4–6 h of high humidity (100% RH) is required for the germination of basidiospores, but after 14 h of exposure to 100% RH, the successful infection reaches the maximum percentage (Frias et al., 1995). This condition is favored in the cultivation of cacao under shade or in seasons of high rainfall. At the end of the necrotrophic phase, brooms require a particular condition to generate their basidiocarps, which requires alternation between wet and dry periods to stimulate the generation of basidiocarps and develop the infection. The environmental conditions related to monoculture promote rapid drying of the brooms, increasing the sporulation period and inoculum potential (Schroth et al., 2000; Meinhardt et al., 2008; Evans, 2016). In this sense, CAFS is presented as a viable alternative for mitigating the economic effects produced by the WBD. The CAFS promotes adverse environmental conditions for the spores to spread and the development of the disease, damping the temperature and ventilation on the cacao plantations (Milz, 2006; Niether et al., 2020).

Frosty pod rot

The FPR or moniliasis, caused by the hemibiotrophic pathogen *Moniliophthora roreri*, is classified as the most important cacao disease in America and the Caribbean. This disease is

considered more destructive and difficult to control than the BPR and the WBD and may cause up to 90% of economic losses, leading to the abandonment of important grain-producing regions such as Ecuador, Peru, Colombia, and Costa Rica (Krauss and Soberanis, 2001; Phillips-Mora and Wilkinson, 2007; Bailey et al., 2018). Its high dispersal capacity (more than seven billion spores in a diseased fruit) and its ability to adapt to a wide range of environmental conditions (Phillips-Mora and Wilkinson, 2007), make it an aggressive pathogen that has had a fast distribution over the south and central America. After penetration, the spores generate oily spots, hyperplasia, manifesting as swellings (humps), premature ripening of the fruits, and brown spots, after 4–5 days on the spot a layer of white mycelium develops that becomes darker as spores mature. Finally, the fruits dry and mummify, remaining attached to the tree (Jaimes and Aranzazu, 2010; Bailey et al., 2018).

The response of moniliasis to the shading conditions provided by the CAFS is positive for the disease, finding that the incidence of the disease grows proportionally to the increase in the level of shade. The shady environment provided by the AFS implies damping of temperature, a reduction in the availability of light and wind speed, and consequently an increase in relative humidity (Niether et al., 2020). These microclimatic conditions provided by the CAFS positively respect the intensity and development of the disease, since the FPR is favored by an increase in relative humidity (> 90%) and by lower temperatures (20–26, 9°C; Torres de la Cruz et al., 2011). In Mexico, it is reported that a 50% reduction in the shade, independent of the management used, can lower the incidence of FPR by up to 20%, and it is also found that if integrated management is applied, the incidence could be reduced by up to 68% (Torres de la Cruz et al., 2011). Similarly, in Peru, it was found that the incidence of FPR is 25% higher in the treatment with dense shade than with crops with full sun exposure (Krauss and Soberanis, 2001). In Bolivia, they reveal that the successional agroforestry system developed a higher incidence of FPR than monoculture (Armengot et al., 2020). However, both studies also reveal no significant differences in the incidence of FPR when integrated disease management is applied, regardless of the shade level of the crop (Table 1).

On the other hand, the organization and selection of the plant community that integrates the CAFS is an important criterion in the development of the disease, where there are species that generate a drier microclimate that favors the dispersal of spores, such as the case of *Erythrina poeppigiana*, which carries a greater quantity of spores in the air concerning *Inga edulis* and *Gliricidia sepium*. This condition is probably due to the physiological properties of the species since *E. poeppigiana* supports a greater intervention of the tree through pruning (Meléndez and Somarriba, 1999). Nevertheless, this companion species should not be disqualified, since by generating drier conditions, infection with *M. roreri* is also unfavorable. It can be said that the incidence and severity of the FPR also depend on the cacao genotype, also referred to as "clone" (Jaimes et al., 2019), and the diversity and aggressiveness of the *M. roreri* isolate (Jaimes et al., 2016), which will determine the level of intervention required for the cacao plants. Also, it has been found that the shade tree density and cacao tree density have a negative correlation with the intensity of the FPR. To establish CAFS that are not conducive to FPR, the architecture of the shade tree should be considered and its distribution should be moderate and uniform within the plantation (Gidoin et al., 2014). Therefore, the CAFS and monoculture strategies present both positive and negative characteristics related to the progression of the disease, its success will depend on its management, the cacao genotype, and the planting design. Low or high incidence of FPR may also depend on the microclimate conditions generated since the pathogen requires different climatic conditions (humidity and temperature) to complete each phase of its cycle (Evans, 1981).

Black pod rot

Black pod rot caused by *Phytophthora* spp. is the disease with the greatest economic importance in the cultivation of cacao in the world, causing losses of 30% of the production, in addition to causing the mortality of up to 10% of the trees annually. Producing cankers on the stems (Guest, 2007). So far, seven species of *Phytophthora* have been reported related to the etiology of BPR disease in cacao cultivation, being *P. palmivora* the cosmopolitan species of the group (Akrofi, 2015), with pantropical distribution (Perrine-walker, 2020). The other species have only been found in specific countries or geographic regions such as South and Central America: *P. capsici, P. citropthora,* and *P. tropicalis* (Barreto et al., 2015; de Bahia et al., 2015; Fernández Maura et al., 2018), Brazil: *P. theobromicola* (Decloquement et al., 2021), Venezuela: *P. megasperma* (Molina et al., 2016), West Africa: *P. megakarya,* and *P. katsurae* (Guest, 2007; Liyanage and Wheeler, 2007). Among these species, *P. megakarya* is the most important economically in the world, since it is reported in the African countries with the highest cacao production (FAOStat, 2021). The disease may cause losses of 60–100% of production in countries such as Cameroon, Gabon, and Ghana (Deberdt et al., 2008; Akrofi et al., 2015; COCOBOD, 2019). In turn, *P. megakarya* produces significant effects on production costs concerning other species since requires the application of fungicides (Opoku et al., 2002), costing up to 21 million fungicides packages per year in Ghana (COCOBOD, 2019).

Phytophthora infection in nursery seedlings causes leaf necrosis and root rot, while stems and branch infections in the field cause cankers. Every stage of fruit development, from flowering to ripening, is susceptible to infection and produces necrosis, but immature fruits are the most susceptible (Akrofi, 2015). The first symptoms appear 2–3 days after the infection, consisting of a translucent chlorotic spot, then the spot turns brown, and spread rapidly to cover the entire fruit after 10–14 days (Luz and Silva, 2001). Infected fruits in an advanced stage develop

a characteristic fishy odor 3–5 days after the appearance of the first symptom, which is associated with the mycelium spot with whitish spores (Barreto et al., 2015).

Black pod rot is positively influenced by humid and cold conditions (Akrofi, 2015), especially when the temperature is below 20°C and the relative humidity is greater than 85% (De Oliveira and Luz, 2005). These are conditions that can occur under CAFS, and based on this data, we could assume a negative influence of CAFS on the control of this disease. It has been reported that CAFS, which include fruit trees, palms, and forests, have a microclimate that differs from the monocultures conditions with a full solar exposure (Niether et al., 2020). Most farmers relate the microclimatic conditions generated in CAFS as one of the causes of a higher incidence of fungal diseases, compared to monocultures with full sun exposure (Armengot et al., 2020).

Diverse theories have been reported on the influence of CAFS in the development of *Phytophthora* spp. in cacao plants, which include investigations on the proportion of shade provided by various AFS and its impact on the development of the BPR disease (Table 1). These studies reveal the influence that some companion species of AFS may have on the dissemination and inoculum potential of *Phytophthora* spp. in cacao cultivation, some of these species may even work as hosts of the pathogen. Indeed, from the root of nine species often used in the CAFS in Ghana was isolated *P. megakarya* (Akrofi et al., 2015). These species are reported in the floristic composition of AFS with cacao from Africa (Sonwa et al., 2007) and are widely used in agroforestry systems in American countries, such as *Musa paradisiaca, Persea americana, Mangifera indica* and *Carica papaya* (Ramírez-Meneses et al., 2013; Guiracocha et al., 2016; Peña et al., 2019; Mercedes Ordoñez and Rangel-Ch, 2020; Jaimes et al., 2021). Other species frequently used in this system in Africa are also reported as hosts of *P. megakarya* and *P. palmivora*, among which we can find forest and palm species such as *Irvingia gabonensis*, *Funtumia elastica*, *Sterculia tragacanta, Ricinodendron heudelotii,* and *Elaeis guinnensis*; shrubs and short plants such as *Dracaena mannii, Xanthosoma saggitifolium, Colocasia esculenta, Athyrium nipponicum* and *Ananas comosus* (Opoku et al., 2002; Holmes et al., 2003; Akrofi et al., 2015). These reports suggest that the influence of the inoculum potential of *Phytophthora* spp., which is harbored by the companion species of cacao, could explain the inefficiency in the control of the disease (Akrofi et al., 2015). In addition, to adjust disease management strategies, it is necessary to propose control methods that not only contemplate the management of the disease in cacao but also in the accompanying species, especially in those that can be a primary inoculum reservoir since these plants are asymptomatic.

On the other hand, there is little information on the levels of shade that favor the FPR disease. However, in one of these studies, it was found that a diverse floristic composition in CAFS can cause problems with spatial structure when its distribution in the plantation is heterogeneous. The heterogeneous distribution of trees can project dense shade in most cases, and thus generates predisposing microclimate conditions for the development of pathogens (Figure 2). With this, it can be concluded that the incidence and severity of *Phytophthora* spp. in CAFS increase proportionally to the shade level (Ambang et al., 2019). Additionally, the incidence of the FPR is not always related to high shade density, in crops with few but diseased trees the incidence of this disease is increased as well as the number of diseased mature pods (Armengot et al., 2020; Leitão, 2020). Not always, the development of FPR is related to the high level of shade, it is also necessary to consider an adequate distribution of shade trees to regulate the level of shade in the plantation. Inadequate distribution can generate microclimates with high relative humidity and low wind speed (Niether et al., 2020), predisposing conditions to the FPR development. Nonetheless, some authors report that there is no difference between disease incidence in PBS and incidence in a monoculture, as long as proper management practices are implemented on the plantation (Armengot et al., 2020; Leitão, 2020).

Biotic and abiotic stress interactions in cacao

In their natural environment, plant exposure to combined biotic and abiotic stress conditions is a rule rather than an exception. Indeed, this is a hot topic in literature (Suzuki et al., 2014; Kissoudis et al., 2016; Fichman and Mittler, 2020) and the complex responses triggered by these combined events are still very poorly understood. Interestingly, the combination of conditions potentially causing stress in plants does not promote solely additive responses, that is, the sum of two events that alone have the potential to induce stress in plants does not necessarily generate a more severe stress response. Yes, in fact, on many occasions additive responses have been observed, for example in cowpea, where pre-exposure to saline stress can generate susceptibility to diseases caused by viruses in known resistant genotypes (Varela et al., 2019).

However, the combination of stress has also been shown to be interactive, that is, when changing a specific potentially stressful environmental condition, systemic plasticity responses at different levels in plant agents can trigger mechanisms such as assays that promote a pre-acclimatization of the organism to others. Types of future stressful conditions. This phenomenon is known as plant stress memory (Nikiforou and Manetas, 2017; Pintó-Marijuan et al., 2017; Auler et al., 2021) and is directly related to the cross-tolerance processes that have been observed in plants (Carvalho and Silveira, 2020). For example, recently Chávez-Arias et al. (2021) highlighted that the combination of some abiotic stresses and arthropod herbivory in maize may increase the production of volatile and non-volatile compounds resulting in improved response to pest infestations.

In cocoa, however, in-depth studies on the combination of biotic and abiotic stresses are still rare. On the one hand, yes, we have very instigating studies as reported in the present

review (Beer et al., 1998; Schroth et al., 2000; Niether et al., 2019, 2020) which compare, for example, the influence of the environment associated with CAFS with that of the environment associated with monoculture in terms of incidence or not of the typical cacao tree diseases. These approaches allow us to discern with a high degree of clarity that yes, in some situations, especially when associated with inadequate management of CAFS, it is possible to observe a higher incidence of diseases in cacao plants. However, when comparing the CAFS environment with the monoculture environment, several abiotic factors can vary simultaneously, such as light, humidity, temperature, and wind intensity, thus making it impossible to distinguish the interactive factors between each of the components of the environmental system. Therefore, this information still presents a very important gap in the understanding of the effects of combined stresses in cacao and deserves future investigation.

We are currently facing a global crisis associated with the imminence of the irreversible effects of global climate change, which should be further exacerbated by the collateral consequences triggered by the global pandemic of COVID-19. In this context, more drastic climatic events such as rains and dry seasons (Lahive et al., 2019), increase in fertilizer costs, and high prices of agricultural products stand out, threatening global food security (Roubík et al., 2022). Therefore, understanding the processes of interaction between combined biotic and abiotic stresses in species where these processes are still poorly understood, such as cocoa, may anticipate early strategic actions that may be of great importance.

Economic return: CAFS vs. monoculture

In terms of economic return, there is a negative perception of CAFS vs. monocultures. This is because the comparison is made based only on cocoa bean production in the short term. Clearly, in this period there is a higher production in monoculture. However, in the long term, cocoa production under agroforestry trees shade will be compensated because the productive life of a tree is extended. This is because the leaves of the cocoa tree under shade are longer-lived since their exposure to solar radiation is reduced (Niether et al., 2020).

On the other hand, to maintain adequate productivity of monocultures, chemical fertilization is required, since with organic fertilization there are no differences with the production of a CAFS. In the CAFS, there are no differences in production between the use of organic and inorganic fertilizers. This can be associated to the fact that fertilization does not have the same relevant effect as the availability of light in agroforestry systems. Therefore, it is believed that to improve cocoa productivity in agroforestry systems, shade tolerant varieties should be selected, as well as adequate conditions to increase the size of the pollinator population (Armengot et al., 2016).

Economic point of view, agroforestry is less profitable than monoculture, but the economic benefit is given in the longer term and at the level of society in general by establishing agroforestry systems with an adequate level of shade, since the environmental services offered are greater and sustainable in the long term (Owusu et al., 2021). In addition, agroforestry systems provide additional income from shade trees (timber, fruit, medicinal, etc.) and reduce the use of external inputs (herbicides and large amounts of fertilizers) and, for many small producers, hired labor, which in the long term makes agroforestry more profitable.

To promote the implementation of CAFS and compensate for lower yields that have led to lower adoption, incentives have been proposed for the benefits that this system provides, from an ecological point of view, such as alternative markets, environmental certificates, fair trade, or as a strategy to reduce the problem of climate change. Although cocoa yields are 25% lower in CAFS compared to monoculture, the additional benefits of product diversification make the two systems comparable (Niether et al., 2020).

Conclusion and perspectives

The works gathered in this review reject the hypothesis that CAFS are always related to biotic and abiotic stresses. Monocultures would be favored in terms of productivity and incidence of diseases compared to CAFS, excluding WBD, since some characteristics such as increased flowering and buds can favor the incidence of this disease in crops with full sun exposure. Therefore, this cultivation condition requires a greater demand for water and nutrients, related to CAFS, representing a concrete threat to productive sustainability, especially considering the projected scenarios of global climate change.

On the other hand, even though some studies report that the incidence of BPR and FPR can be favored in CAFS designs, it is also reported that the correct selection of the model agroforestry and the inclusion of opportune agronomic practices, including biological and cultural control, would mitigate the incidence of these diseases, as well as increase productivity, equaling monocultures. In addition, it is important to emphasize that the CAFS provides ecosystemic services such as the maintenance of pollinators, greater efficiency in the use of water, nutrient demand that may generate a more sustainable production. In the same way, the selection of genotypes with better performance in low light conditions (higher efficiency in the use of light) and better energy balance, can contribute to the mitigation of abiotic stresses normally attributed to CAFS. Therefore, it is necessary to explore the technological and scientific resources that are already available and apply them to production models based on AFS. In addition, it is still necessary to deepen our understanding of the mechanisms

triggered by cacao in the face of these complex interactions. Knowing and understanding how these processes work is the key to improving agricultural practices and guaranteeing food security in a future of global climate change.

Author contributions

JR-M and YJ-S: idea behind this literature review. AC-R, DG-N, and FELC: literature search and the preparation of the draft manuscript. FELC: critical review and exhaustive editing. YJ-S and FELC: revised the final version of the manuscript prior to its submission. All authors contributed to the article and approved the submitted version.

Funding

The project was financed by the Sistema General de Regalias through the project "Investigación, desarrollo e innovación en cacaos especiales bajo sistemas agroforestales" (BPIN 2013000100255).

Acknowledgments

We thank Corporación Colombiana de Investigacion Agropecuaria (AGROSAVIA) for providing the infrastructure and the support for the development of this research.

Conflict of interest

The authors declare that the research was conducted in the absence of any commercial or financial relationships that could be construed as a potential conflict of interest.

Publisher's note

All claims expressed in this article are solely those of the authors and do not necessarily represent those of their affiliated organizations, or those of the publisher, the editors and the reviewers. Any product that may be evaluated in this article, or claim that may be made by its manufacturer, is not guaranteed or endorsed by the publisher.

References

Agudelo-Castañeda, G. A., Cadena-Torres, J., Almanza-Merchán, P. J., and Pinzón-Sandoval, E. H. (2018). Desempeño fisiológico de nueve genotipos de cacao (*T. cacao* L.) bajo la sombra de tres especies forestales en Santander. *Colombia. Rev. Colomb. Ciencias Hortícolas* 12, 223–232. doi: 10.17584/rcch.2018v12i1.7341

Aime, M. C., and Phillips-Mora, W. (2005). The causal agents of witches' broom and frosty pod rot of cacao (chocolate, *T. cacao*) form a new lineage of Marasmiaceae. *Mycologia* 97, 1012–1022. doi: 10.1080/15572536.2006.11832751

Akrofi, A. (2015). Phytophthora Megakarya: a review on its status as a pathogen on cacao in West Africa five major diseases of cocoa (*T. cacao* Lss.), Phytophthora pod rot (black pod), witches broom, swollen shoot virus, vascular streak dieback, and monilia pod. *African Crop Sci. J.* 23, 67–87. Available at: https://www.ajol.info/index.php/acsj/article/view/113716/103435

Akrofi, A., Amoako-Atta, I., Assuah, M., and Asare, E. K. (2015). Black pod disease on cacao (*T. cacao*, L) in Ghana: spread of Phytophthora megakarya and role of economic plants in the disease epidemiology. *Crop Prot.* 72, 66–75. doi: 10.1016/j.cropro.2015.01.015

Alpízar, L., Fassbender, H. W., Heuveldop, J., Fölster, H., and Enríquez, G. (1986). Modelling agroforestry systems of cacao (*T. cacao*) with laurel (*Cordia alliodora*) and poro (*E. poeppigiana*) in Costa Rica. *Agrofor. Syst.* 4, 175–189. doi: 10.1007/BF02028353

Álvarez-Carrillo, F., Rojas-Molina, J., and Suarez-Salazar, J. C. (2012). Simulación de arreglos agroforestales de cacao como una estrategia de diagnóstico y planificación para productores. *Cienc. Tec. Agrop.* 13, 145–150. Available at: http://www.scielo.org.co/pdf/ccta/v13n2/v13n2a04.pdf

Ambang, Z., Dida-Lontsi, S. L., and Bertrand-Mboussi, S. (2019). Influence of the structure of cocoa agroforestry systems on the development of black pod disease in central region of influence of the structure of cocoa agroforestry systems on the development of black pod disease in central region. *Am. J. Innov. Res. Appl. Sci.* 9, 338–342. Available at: http://www.american-jiras.com/Zachee-Ref.1-ajira260819.pdf

Andres, C., Comoé, H., Beerli, A., Schneider, M., Rist, S., and Jacobi, J. (2016). "Cocoa in monoculture and dynamic agroforestry," in *Sustainable Agriculture Reviews. 19th Edn.* ed E. Lichtfouse (Cham, Switzerland: Springer,) 121–153.

Armengot, L., Barbieri, P., Andres, C., Milz, J., and Schneider, M. (2016). Cacao agroforestry systems have higher return on labor compared to full-sun monocultures. *Agron. Sustain. Dev.* 36, 1–10. doi: 10.1007/s13593-016-0406-6

Armengot, L., Ferrari, L., Milz, J., Velásquez, F., Hohmann, P., and Schneider, M. (2020). Cacao agroforestry systems do not increase pest and disease incidence compared with monocultures under good cultural management practices. *Crop Prot.* 130:105047. doi: 10.1016/j.cropro.2019.105047

Auler, P. A., Souza, G. M., da Silva Engela, M. R. G., Do Amaral, M. N., Rossatto, T., Da Silva, M. G. Z., et al. (2021). Stress memory of physiological, biochemical and metabolomic responses in two different rice genotypes under drought stress: The scale matters. *Plant Sci.* 311, 110994–110910. doi: 10.1016/j.plantsci.2021.110994

Bai, W., Sun, Z., Zheng, J., Du, G., Feng, L., Cai, Q., et al. (2016). Mixing trees and crops increases land and water use efficiencies in a semi-arid area. *Agric. Water Manag.* 178, 281–290. doi: 10.1016/j.agwat.2016.10.007

Bailey, B. A., Evans, H. C., Phillips-Mora, W., Ali, S. S., and Meinhardt, L. W. (2018). Moniliophthora roreri, causal agent of cacao frosty pod rot. *Mol. Plant Pathol.* 19, 1580–1594. doi: 10.1111/mpp.12648

Baligar, V. C., Elson, M. K., Almeida, A.-A. F., de Araujo, Q. R., Ahnert, D., and He, Z. (2021). The impact of carbon dioxide concentrations and low to adequate photosynthetic photon flux density on growth, physiology and nutrient use efficiency of juvenile cacao genotypes. *Agronomy* 11:397. doi: 10.3390/agronomy11020397

Barreto, M. A., Santos, J. C. S., Corrêa, R. X., Luz, E. D. M. N., Marelli, J., and Souza, A. P. (2015). Detection of genetic resistance to cocoa black pod disease caused by three Phytophthora species. *Euphytica* 206, 677–687. doi: 10.1007/s10681-015-1490-4

Bassi, R., and Dall'Osto, L. (2021). Dissipation of light energy absorbed in excess: the molecular mechanisms. *Annu. Rev. Plant Biol.* 72, 47–76. doi: 10.1146/annurev-arplant-071720-015522

Beer, J., Muschler, R., Kass, D., and Somarriba, E. (1998). Shade management in coffee and cacao plantations. *Agrofor. Syst.* 38, 139–164. doi: 10.1007/978-94-015-9008-2_6

Brestic, M., Yang, X., Li, X., and Allakhverdiev, S. I. (2021). Crop photosynthesis for the twenty-first century. *Photosynth. Res.* 150, 1–3. doi: 10.1007/s11120-021-00869-5

Cannell, M. G. R. (1971). Production and distribution of dry matter in trees of *Coffea arabica* L. in Kenya as affected by seasonal climatic differences and the presence of fruits. *Ann. Appl. Biol.* 67, 99–120. doi: 10.1111/j.1744-7348.1971.tb02910.x

Carvalho, F. E. L., Ribeiro, C. W., Martins, M. O., Bonifacio, A., Staats, C. C., Andrade, C. M. B., et al. (2014). Cytosolic APX knockdown rice plants sustain photosynthesis by regulation of protein expression related to photochemistry, Calvin cycle and photorespiration. *Physiol. Plant.* 150, 632–645. doi: 10.1111/ppl.12143

Carvalho, F. E. L., and Silveira, J. A. G. (2020). "H2O2-retrograde signaling as a pivotal mechanism to understand priming and cross stress tolerance in plants," in

Priming-Mediated Stress and Cross-Stress Tolerance in Crop Plants. eds. M. A. Hossain, F. Liu and D. J. Burritt (Cambridge, MA: Academic Press), 57–78.

Charbonnier, F., Roupsard, O., le Maire, G., Guillemot, J., Casanoves, F., Lacointe, A., et al. (2017). Increased light-use efficiency sustains net primary productivity of shaded coffee plants in agroforestry system. *Plant Cell Environ.* 40, 1592–1608. doi: 10.1111/pce.12964

Chávez-Arias, C. C., Ligarreto-Moreno, G. A., Ramírez-Godoy, A., and Restrepo-Díaz, H. (2021). Maize responses challenged by drought, elevated daytime temperature and arthropod Herbivory stresses: A physiological, biochemical and molecular view. *Front. Plant Sci.* 12:702841. doi: 10.3389/fpls.2021.702841

COCOBOD (2019). Annual reports and Consolitated financial statements-GHANA-COCOA BOARD. Available at: https://cocobod.gh/

Cooke, B. M. (2006). "Disease assessment and yield loss," in *The Epidemiology of Plant Diseases*. eds. B. M. Cooke, D. G. Jones and B. Kaye (Netherlands: Springer), 43–80.

Coopman, R. E., Fuentes-Neira, F. P., Briceño, V. F., Cabrera, H. M., Corcuera, L. J., and Bravo, L. A. (2010). Light energy partitioning in photosystems I and II during development of *Nothofagus nitida* growing under different light environments in the Chilean evergreen temperate rain forest. *Trees Struct. Funct.* 24, 247–259. doi: 10.1007/s00468-009-0395-z

Cunha, J. R., Carvalho, F. E. L., Lima-Neto, M. C., Jardim-Messeder, D., Cerqueira, J. V. A., Martins, M. O., et al. (2019). Proteomic and physiological approaches reveal new insights for uncover the role of rice thylakoidal APX in response to drought stress. *J. Proteome* 192, 125–136. doi: 10.1016/j.jprot.2018.08.014

de Almeida, A.-A. F., and Valle, R. R. (2010). "Cacao: ecophysiology of growth and production," in *Ecophysiology of Tropical Tree Crops, Chapter 3*. ed. F. M. DaMatta (Hauppauge, NY: Nova Science Publishers).

de Bahia, R. C., Aguilar-Vildoso, C. I., Luz, E. D. M. N., Lopes, U. V., Machado, R. C. R., and Corrêa, R. X. (2015). Resistance to black pod disease in a segregating cacao tree population. *Trop. Plant Pathol.* 40, 13–18. doi: 10.1007/s40858-014-0003-7

De Oliveira, M. L., and Luz, E. D. M. N. (2005). Identificação e Manejo das Principais Doenças do Cacaueiro no Brasil. Ilhéus: CEPLAC/CEPEC/SEFIT.

Deberdt, P., Mfegue, C. V., Tondje, P. R., Bon, M. C., and Ducamp, M. (2008). Impact of environmental factors, chemical fungicide and biological control on cacao pod production dynamics and black pod disease (Phytophthora megakarya) in Cameroon. *Biol. Control* 44, 149–159. doi: 10.1016/j.biocontrol.2007.10.026

Decloquement, J., Ramos-Sobrinho, R., Elias, S. G., Britto, D. S., Puig, A. S., Reis, A., et al. (2021). Phytophthora theobromicola sp. nov.: A new species causing black pod disease on cacao in Brazil. *Front. Microbiol.* 12:537399. doi: 10.3389/fmicb.2021.537399

Evans, H. C. (1981). Pod rot of cacao caused by Moniliophthora (Monilia) Roreri. *Phytopathol. Pap.* 24, 1–44. Available at: https://www.cabdirect.org/cabdirect/abstract/19811373782

Evans, H. C. (1998). Disease and sustainability in the cocoa agroecosystem. in *sustainable cocoa Workshop30 Mar-3 Abr 1998 (Panamá)*.

Evans, H. C. (2016). "Witches' Broom Disease (Moniliophthora perniciosa): History and Biology," in *Cacao Diseases*. eds. B. Bailey and L. Meinhardt (Dordrecht: Springer), 137–177.

FAOStat (2021). FAOSTAT. *Food Agric. Organ.* Available at: http://www.fao.org/faostat/en/#data%0D (Accessed August 4, 2021).

Fernández Maura, Y., Lachenaud, P., Decock, C., Díaz Rodríguez, A., and Abreu Romero, N. (2018). Caracterización de Phytophthora, agente etiológico de la pudrición negra de la mazorca del cacao en Cuba y Guyana Francesa. *Cent. Agrícola* 45, 17–26. Available at: http://scielo.sld.cu/pdf/cag/v45n3/0253-5785-cag-45-03-17.pdf

Fichman, Y., and Mittler, R. (2020). Rapid systemic signaling during abiotic and biotic stresses: is the ROS wave master of all trades? *Plant J.* 102, 887–896. doi: 10.1111/tpj.14685

Foyer, C. H. (2018). Reactive oxygen species, oxidative signaling and the regulation of photosynthesis. *Environ. Exp. Bot.* 154, 134–142. doi: 10.1016/j.envexpbot.2018.05.003

Foyer, C. H., Ruban, A. V., and Nixon, P. J. (2017). Photosynthesis solutions to enhance productivity. *Philos. Trans. R Soc. Lond B Biol. Sci.* 372:20160374. doi: 10.1098/rstb.2016.0374

Frias, G. A., Purdy, L. H., and Schmidt, R. A. (1995). An inoculation method for evaluating resistance of cacao to Crinipellis perniciosa. *Plant Dis.* 79:787. doi: 10.1094/PD-79-0787

Gidoin, C., Avelino, J., Deheuvels, O., Cilas, C., and Bieng, M. A. N. (2014). Shade tree spatial structure and pod production explain frosty pod rot intensity in cacao agroforests, Costa Rica. *Phytopathology* 104, 275–281. doi: 10.1094/PHYTO-07-13-0216-R

Goldschmidt-Clermont, M., and Bassi, R. (2015). Sharing light between two photosystems: mechanism of state transitions. *Curr. Opin. Plant Biol.* 25, 71–78. doi: 10.1016/j.pbi.2015.04.009

Gómez-Yarce, J. P., Mompotes-Largo, E. R., López-Castro, A., Hernández-Arredondo, J. D., and Córdoba-Gaona, O. D. J. (2020). Gas exchange efficiency in cocoa – spanish elm agroforestry system in the Northwest Antioquia, Colombia. *Rev. Fac. Nac. Agron. Medellin* 73, 9283–9291. doi: 10.15446/rfnam.v73n3.85278

González-Orozco, C. E., Galán, A. A. S., Ramos, P. E., and Yockteng, R. (2020). Exploring the diversity and distribution of crop wild relatives of cacao (*T. cacao* L.) in Colombia. *Genet. Resour. Crop. Evol.* 67, 2071–2085. doi: 10.1007/s10722-020-00960-1

Gramacho, K. P., Newman Luz, E. D. M., Da Silva, F. S., Lopes, U. V., Pires, J. L., and Pereira, L. (2016). Pathogenic variability of Moniliophthora perniciosa in three agroecological zones of the cacao region of Bahia, Brazil. *Crop Breed. Appl. Biotechnol.* 16, 7–13. doi: 10.1590/1984-70332016v16n1a2

Green, A. G., Abdulai, A.-R., Duncan, E., Glaros, A., Campbell, M., Newell, R., et al. (2021). A scoping review of the digital agricultural revolution and ecosystem services: implications for Canadian policy and research agendas. *Facets* 6, 1955–1985. doi: 10.1139/facets-2021-0017

Guest, D. (2007). Black pod: diverse pathogens with a global impact on cocoa yield. *Phytopathology* 97, 1650–1653. doi: 10.1094/PHYTO-97-12-1650

Guilherme, E. A., Carvalho, F. E. L., Daloso, D. M., and Silveira, J. A. G. (2019). Increase in assimilatory nitrate reduction and photorespiration enhances CO2 assimilation under high light-induced photoinhibition in cotssston. *Environ. Exp. Bot.* 159, 66–74. doi: 10.1016/j.envexpbot.2018.12.012

Guiracocha, G., Harvey, C., Somarriba, E., Krauss, U., and Carrillo, E. (2016). Conservación de la biodiversidad en sistemas agroforestales con cacao y banano en Talamanca, Costa Rica. *Agroforestería en las américas* 8, 77–86. Available at: http://45.32.134.17/bitstream/handle/11554/5948/Conservacion_de_la_biodiversidad.pdf?sequence=1&isAllowed=y

Hatfield, J. L., and Dold, C. (2019). Water-use efficiency: advances and challenges in a changing climate. *Front. Plant Sci.* 10:103. doi: 10.3389/fpls.2019.00103

Hebbar, K. B., Apshara, E., Chandran, K. P., and Prasad, P. V. V. (2020). Effect of elevated CO2, high temperature, and water deficit on growth, photosynthesis, and whole plant water use efficiency of cocoa (*T. cacao* L.). *Int. J. Biometeorol.* 64, 47–57. doi: 10.1007/s00484-019-01792-0

Hernández-Villegas, J. (2016). Incidencia de la escoba de bruja (Crinipellis perniciosa) sobre el rendimiento de dos agroecosistemas de cacao con diferentes condiciones de manejo. *Bioagro.* 28, 59–64. Available at: http://ve.scielo.org/scielo.php?script=sci_arttext&pid=S1316-33612016000100008&lng=es&tlng=es

Hierro, J. L., and Callaway, R. M. (2021). The ecological importance of Allelopathy. *Annu. Rev. Ecol. Evol. Syst.* 52, 25–45. doi: 10.1146/annurev-ecolsys-051120-030619

Holmes, K. A., Evans, H. C., Wayne, S., and Smith, J. (2003). Irvingia, a forest host of the cocoa black-pod pathogen, Phytophthora megakarya, in Cameroon. *Plant Pathol.* 52, 486–490. doi: 10.1046/j.1365-3059.2003.00869.x

Hosseini Bai, S., Trueman, S. J., Nevenimo, T., Hannet, G., Bapiwai, P., Poienou, M., et al. (2017). Effects of shade-tree species and spacing on soil and leaf nutrient concentrations in cocoa plantations at 8 years after establishment. *Agric. Ecosyst. Environ.* 246, 134–143. doi: 10.1016/j.agee.2017.06.003

Huang, W., Yang, Y., Hu, H., and Zhang, S. (2016). Biology response of the water – water cycle to the change in photorespiration in tobacco. *J. Photochem. Photobiol. B Biol.* 157, 97–104. doi: 10.1016/j.jphotobiol.2016.02.006

Hughes, N. M., Carpenter, K. L., Keidel, T. S., Miller, C. N., Waters, M. N., and Smith, W. K. (2014). Photosynthetic costs and benefits of abaxial versus adaxial anthocyanins in *C. esculenta* 'mojito'. *Planta* 240, 971–981. doi: 10.1007/s00425-014-2090-6

Jacobi, J., Schneider, M., Bottazzi, P., Pillco, M., Calizaya, P., and Rist, S. (2013). Agroecosystem resilience and farmers' perceptions of climate change impacts on cocoa farms in alto Beni, Bolivia. *Renew. Agric. Food Syst.* 30, 170–183. doi: 10.1017/S174217051300029X

Jaimes, Y. Y., Agudelo-Castañeda, G. A., Báez, E., Rengifo, G., and Rojas, J. (2021). *Modelo productivo para el cultivo de cacao (T. cacao L) en el departamento de Santander*. Colombia: Editorial AGROSAVIA Santander.

Jaimes, Y. Y., and Aranzazu, F. (2010). *Manejo de las enfermedades del cacao (T. cacao L) en Colombia, con énfasis en monilia (Moniliophthora roreri)* (Bucaramanga, Colombia: Corpoica), 90 Available at: http://catalogobac.hosted.exlibrisgroup.com/F?func=direct&local_base=BAC01&doc_number=000056560

Jaimes, Y. Y., Gonzalez, C., Rojas, J., Cornejo, O. E., Mideros, M. F., Restrepo, S., et al. (2016). Geographic differentiation and population genetic structure of Moniliophthora roreri in the principal cocoa production areas in Colombia. *Plant Dis.* 100, 1548–1558. doi: 10.1094/PDIS-12-15-1498-RE

Jaimes, Y. Y., Ribeyre, F., Gonzalez, C., Rojas, J., Furtado, E. L., and Cilas, C. (2019). Factors affecting the dynamics of frosty pod rot in the main cocoa areas of Santander state, Colombia. *Plant Dis.* 103, 1665–1673. doi: 10.1094/PDIS-10-18-1761-RE

Jegadeeswari, V., and Kumar, N. (2019). Effect of water deficit on physiological and biochemical responses in cocoa (*T. cacao* L.) clones. *J. Pharmacogn. Phytochem.*

8, 1820–1824. Available at: https://www.phytojournal.com/archives/2019/vol8issue3/PartW/8-2-426-874.pdf

Kilaru, A., and Hasenstein, K. H. (2005). Development and pathogenicity of the fungus Crinipellis perniciosa on interaction with cacao leaves development and pathogenicity of the fungus Crinipellis perniciosa on interaction with cacao leaves. *Phytopathology* 95, 101–107. doi: 10.1094/PHYTO-95-0101

Kissoudis, C., Sunarti, S., Van De Wiel, C., Visser, R. G. F., van der Linden, C. G., and Bai, Y. (2016). Responses to combined abiotic and biotic stress in tomato are governed by stress intensity and resistance mechanism. *J. Exp. Bot.* 67, 5119–5132. doi: 10.1093/jxb/erw285

Krauss, U., and Soberanis, W. (2001). Rehabilitation of diseased cacao fields in Peru through shade regulation and timing of biocontrol measures. *Agrofor. Syst.* 53, 179–184. doi: 10.1023/A:1013376504268

Lahive, F., Hadley, P., and Daymond, A. J. (2019). The physiological responses of cacao to the environment and the implications for climate change resilience. A review. *Agron. Sustain. Dev.* 39, 1–22. doi: 10.1007/s13593-018-0552-0

Lawlor, D. W., and Tezara, W. (2009). Causes of decreased photosynthetic rate and metabolic capacity in water-deficient leaf cells: A critical evaluation of mechanisms and integration of processes. *Ann. Bot.* 103, 561–579. doi: 10.1093/aob/mcn244

Leitão, M. C. C. (2020). Shade trees, disease and cocoa production in Western Ghana: a case study. Dissertation. Wageningen University, Wageningen, The Netherlands. Available at: https://bscmsc.pps.wur.nl/shade-trees-disease-and-cocoa-production-western-ghana-case-study

Lennon, A. M., Lewis, V. R., Farrell, A. D., and Umaharan, P. (2021). Photochemical responses to light in sun and shade leaves of *T. cacao* L. (West African Amelonado). *Sci. Hortic. (Amsterdam)* 276:109747. doi: 10.1016/j.scienta.2020.109747

Lima Neto, M. C., Carvalho, F. E. L., Souza, G. M., and Silveira, J. A. G. (2021). Understanding photosynthesis in a spatial–temporal multiscale: the need for a systemic view. *Theor. Exp. Plant Physiol.* 33, 113–124. doi: 10.1007/s40626-021-00199-w

Liyanage, N., and Wheeler, B. (2007). Phytophthora katsurae from cocoa. *Plant Pathol.* 38, 627–629. doi: 10.1111/j.1365-3059.1989.tb01463.x

Lobo, A. K. M., Orr, D. J., Gutierrez, O., Andralojc, P. J., Sparks, C., Parry, M. A. J., et al. (2019). Overexpression of ca1pase decreases Rubisco abundance and grain yield in wheat 1 [CC-BY]. *Plant Physiol.* 181, 471–479. doi: 10.1104/pp.19.00693

Lorrain, S., Allen, T., Duek, P. D., Whitelam, G. C., and Fankhauser, C. (2008). Phytochrome-mediated inhibition of shade avoidance involves degradation of growth-promoting bHLH transcription factors. *Plant J.* 53, 312–323. doi: 10.1111/j.1365-313X.2007.03341.x

Luz, E. D. M. N., and Silva, S. D. V. M. (2001). "Podridão-parda dos frutos, cancro e outras doenças causadas por Phytophthora no cacaueiro," in *Doenças causadas por Phytophthora no Brasil*. eds. E. D. M. N. Luz, A. F. Santos, K. Matsuoka and J. L. Bezerra (Campinas, Brasil: Livraria Editora Rural), 175–265.

Marconi, L., and Armengot, L. (2020). Complex agroforestry systems against biotic homogenization: The case of plants in the herbaceous stratum of cocoa production systems. *Agric. Ecosyst. Environ.* 287, 3–5. doi: 10.1016/j.agee.2019.106664

Meinhardt, L. W., Rincones, J., Bailey, B. A., Aime, M. C., Griffith, G. W., Zhang, D., et al. (2008). Moniliophthora perniciosa, the causal agent of witches' broom disease of cacao: what's new from this old foe? *Mol. Plant Pathol.* 9, 577–588. doi: 10.1111/j.1364-3703.2008.00496.x

Meléndez, L., and Somarriba, E. (1999). Microambiente y cantidad de sporas de Moniliophthora roreri en el aire bajo tres sistemas de sombra leguminosa en cacao. *Agroforestería en las Américas* 6, 39–41.

Mercedes Ordoñez, C., and Rangel-Ch, J. O. (2020). Composición florística y aspectos de la estructura de la vegetación en sistemas agroforestales con cacao (*T. cacao* L. - Malvaceae) en el departamento del Huila, Colombia. *Rev. la Acad. Colomb. Ciencias Exactas, Físicas y Nat.* 44, 1033–1046. doi: 10.18257/raccefyn.1183

Milz, J. (2006). Einfluss von Anbau-und Pflegemaßnahmen auf die Hexenbesenkrankheit (Crinipellis perniciosa (Stahel) Singer) bei Kakaoklonen im Siedlungsgebiet Alto Beni – Bolivien. dissertation.

Molina, S., Pérez-Martínez, S., Demey, J., Isturiz Zapata, M., and Sosa, D. (2016). Diversidad genética de Phytophthora spp. en plantaciones venezolanas de cacao mediante marcadores ISSR. *Rev. Protección Veg.* 31, 1–8. Available at: http://scielo.sld.cu/pdf/rpv/v31n1/rpv01116.pdf

Mortimer, R., Saj, S., and David, C. (2018). Supporting and regulating ecosystem services in cacao agroforestry systems. *Agrofor. Syst.* 92, 1639–1657. doi: 10.1007/s10457-017-0113-6

Motamayor, J. C., Lachenaud, P., Da Silva, W., Loor, R., Kuhn, D. N., Brown, J. S., et al. (2008). Geographic and genetic population differentiation of the Amazonian chocolate tree (*T. cacao* L). *PLoS One* 3:e3311. doi: 10.1371/journal.pone.0003311

Murchie, E. H., and Ruban, A. V. (2020). Dynamic non-photochemical quenching in plants: from molecular mechanism to productivity. *Plant J.* 101, 885–896. doi: 10.1111/tpj.14601

Niether, W., Jacobi, J., Blaser, W. J., Andres, C., and Armengot, L. (2020). Cocoa agroforestry systems versus monocultures: a multi-dimensional meta-analysis. *Environ. Res. Lett.* 15, 1–13. doi: 10.1088/1748-9326/abb053

Niether, W., Schneidewind, U., Fuchs, M., Schneider, M., and Armengot, L. (2019). Below-and aboveground production in cocoa monocultures and agroforestry systems. *Sci. Total Environ.* 657, 558–567. doi: 10.1016/j.scitotenv.2018.12.050

Nikiforou, C., and Manetas, Y. (2017). Ecological stress memory: evidence in two out of seven species through the examination of the relationship between leaf fluctuating asymmetry and photosynthesis. *Ecol. Indic.* 74, 530–534. doi: 10.1016/j.ecolind.2016.11.004

Nunes, A. M. L., Dias, C. T., Dos, S., and Nunes, M. A. L. (2002). *Estudos Epidemiológicos da Vassoura-de-bruxa do Cupuaçuzeiro (Crinipellis perniciosa) Utilizando Análise Canônica*. Portuguese: Embrapa.

Opoku, I. Y., Akrofi, A. Y., and Appiah, A. A. (2002). Shade trees are alternative hosts of the cocoa pathogen Phytophthora megakarya. *Crop Prot.* 21, 629–634. doi: 10.1016/S0261-2194(02)00013-3

Owusu, V., Akoto-Adjepong, V., Acheampong, E., and Barnes, V. R. (2021). Farmer perceptions and economic performance of cocoa agroforestry shade levels in Ghana. *J. Sustain. For.* 1–19. doi: 10.1080/10549811.2021.1883444

Peña, J., Velarde, N., and Sánchez, G. (2019). Composición florística, riqueza, diversidad y sscarbono secuestrado por diferentes tipos de sistemas agroforestales en la Provincia de Tambopata-Madre de Dios. Monograph. Universidad Nacional Amazónica de Madre de Dios, Puerto Maldonado, Perú. Available at: http://hdl.handle.net/20.500.14070/472

Pereira, J. L., De Almeida, L. C. C., and Santos, S. M. (1996). Witches' broom disease of cocoa in Bahia: attempts at eradication and containment. *Crop Prot.* 15, 743–752. doi: 10.1016/s0261-2194(96)00049-x

Perrine-walker, F. (2020). Phytophthora palmivora–cocoa interaction. *J. Fungi* 6, 1–20. doi: 10.3390/jof6030167

Phillips-Mora, W., and Wilkinson, M. (2007). Frosty pod of cacao: A disease with a limited geographic range but unlimited potential for damage. *Phytopathology* 97, 1644–1647. doi: 10.1094/PHYTO-97-12-1644

Pinnola, A., and Bassi, R. (2018). Molecular mechanisms involved in plant photoprotection. *Biochem. Soc. Trans.* 46, 467–482. doi: 10.1042/BST20170307

Pintó-Marijuan, M., Cotado, A., Fleta-Soriano, E., and Munné-Bosch, S. (2017). Drought stress memory in the photosynthetic mechanisms of an invasive CAM species, *Aptenia cordifolia*. *Photosynth. Res.* 131, 241–253. doi: 10.1007/s11120-016-0313-3

Puthiyaveetil, S., Ibrahim, I. M., and Allen, J. F. (2012). Oxidation–reduction signalling components in regulatory pathways of state transitions and photosystem stoichiometry adjustment in chloroplasts. *Plant Cell Environ.* 35, 347–359. doi: 10.1111/j.1365-3040.2011.02349.x

Rajab, Y. A., Leuschner, C., Barus, H., Tjoa, A., and Hertel, D. (2016). Cacao cultivation under diverse shade tree cover allows high carbon storage and sequestration without yield losses. *PLoS One* 11:e149949. doi: 10.1371/journal.pone.0149949

Ramírez-Meneses, A., García-López, E., Obrador-Olán, J. J., Ruiz-Rosado, O., and Camacho-Chiu, W. (2013). Diversidad florística en plantaciones agroforestales de cacao en Cárdenas, Tabasco, México. *Univ. y Cienc.* 29, 215–230. doi: 10.19136/era.a29n3.55

Rodriguez-Medina, C., Arana, A. C., Sounigo, O., Argout, X., Alvarado, G. A., and Yockteng, R. (2019). Cacao breeding in Colombia, past, present and future. *Breed. Sci.* 69, 373–382. doi: 10.1270/jsbbs.19011

Rojas-Molina, J., Caicedo, V., and Jaimes, Y. Y. (2017). Dinámica de descomposición de la biomasa en sistemas agroforestales con *T. cacao* L., Rionegro, Santander (Colombia). *Agron. Colomb.* 35, 182–189. doi: 10.15446/agron.colomb.v35n2.60981

Roubík, H., Lošťák, M., Ketuama, C. T., Procházka, P., Soukupová, J., Hakl, J., et al. (2022). Current coronavirus crisis and past pandemics - what can happen in post-COVID-19 agriculture? *Sustain. Prod. Consum.* 30, 752–760. doi: 10.1016/j.spc.2022.01.007

Ruban, A. V. (2015). Evolution under the sun: optimizing light harvesting in photosynthesis. *J. Exp. Bot.* 66, 7–23. doi: 10.1093/jxb/eru400

Salazar, J. C. S., Melgarejo, L. M., Casanoves, F., Di Rienzo, J. A., DaMatta, F. M., and Armas, C. (2018). Photosynthesis limitations in cacao leaves under different agroforestry systems in the Colombian Amazon. *PLoS One* 13:e206149. doi: 10.1371/journal.pone.0206149

Sambuichi, R. H. R., Vidal, D. B., Piasentin, F. B., Jardim, J. G., Viana, T. G., Menezes, A. A., et al. (2012). Cabruca agroforests in southern Bahia, Brazil: tree component, management practices and tree species conservation. *Biodivers. Conserv.* 21, 1055–1077. doi: 10.1007/s10531-012-0240-3

Scavo, A., Restuccia, A., and Mauromicale, G. (2018). "Allelopathy: principles and basic aspects for Agroecosystem control," in *Sustainable Agriculture Reviews*. ed. S. Gaba (Berlin: Springer-Nature), 47–101.

Scheibe, R. (2019). Maintaining homeostasis by controlled alternatives for energy distribution in plant cells under changing conditions of supply and demand. *Photosynth. Res.* 139, 81–91. doi: 10.1007/s11120-018-0583-z

Schroth, G., Gasparotto, L., Krauss, U., and Vohland, K. (2000). Pests and diseases in agroforestry systems of the humid tropics. *Agrofor. Syst.* 97, 131–141. doi: 10.1023/A1006468103914

Silva, S., Luz, E., Almeida, O. C., Gramacho, K., and Bezerra, J. (2002). Redescrição da sintomatologia causada por Crinipellis perniciosa em cacaueiro. *Agrotropica* 1, 1–23. Available at: https://biblat.unam.mx/es/revista/agrotropica/articulo/redescricao-da-sintomatologia-causada-por-crinipellis-perniciosa-em-cacaueiro

Sonwa, D. J., Nkongmeneck, B. A., Weise, S. F., Tchatat, M., Adesina, A. A., and Janssens, M. J. J. (2007). Diversity of plants in cocoa agroforests in the humid forest zone of southern Cameroon. *Biodivers. Conserv.* 16, 2385–2400. doi: 10.1007/s10531-007-9187-1

Sousa Filho, H. R., de Jesus, R. M., Bezerra, M. A., Santana, G. M., and de Santana, R. O. (2021). History, dissemination, and field control strategies of cocoa witches' broom. *Plant Pathol.* 70, 1971–1978. doi: 10.1111/ppa.13457

Suzuki, N., Rivero, R. M., Shulaev, V., Blumwald, E., and Mittler, R. (2014). Abiotic and biotic stress combinations. *New Phytol.* 203, 32–43. doi: 10.1111/nph.12797

Torres de la Cruz, M., Ortiz Garcia, C., Téliz Ortiz, D., Mora Aguilera, A., and Nava Díaz, C. (2011). Temporal progress and integrated management of frosty pod rot (Moniliophthora roreri) OF COCOA IN TABASCO, MEXICO. *J. Plant Pathol.* 93, 31–36. Available at: https://www.torrossa.com/en/resources/an/2466173

Vaast, P., and Somarriba, E. (2014). Trade-offs between crop intensification and ecosystem services: the role of agroforestry in cocoa cultivation. *Agrofor. Syst.* 88, 947–956. doi: 10.1007/s10457-014-9762-x

Varela, A. L. N., Oliveira, J. T. A., Komatsu, S., Silva, R. G. G., Martins, T. F., Souza, P. F. N., et al. (2019). A resistant cowpea (*Vigna unguiculata* [L.] Walp.) genotype became susceptible to cowpea severe mosaic virus (CPSMV) after exposure to salt stress. *J. Proteome* 194, 200–217. doi: 10.1016/j.jprot.2018.11.015

Wartenberg, A. C., Blaser, W. J., Roshetko, J. M., Van Noordwijk, M., and Six, J. (2020). Soil fertility and *T. cacao* growth and productivity under commonly intercropped shade-tree species in Sulawesi, Indonesia. *Plant Soil* 453, 87–104. doi: 10.1007/s11104-018-03921-x

Zuidema, P. A., Leffelaar, P. A., Gerritsma, W., Mommer, L., and Anten, N. P. R. (2005). A physiological production model for cocoa (*T. cacao*): model presentation, validation and application. *Agric. Syst.* 84, 195–225. doi: 10.1016/j.agsy.2004.06.015

frontiers | Frontiers in Plant Science

TYPE Review
PUBLISHED 16 August 2022
DOI 10.3389/fpls.2022.853309

OPEN ACCESS

EDITED BY
Sanna Sevanto,
Los Alamos National Laboratory (DOE), United States

REVIEWED BY
Vadim Volkov,
London Metropolitan University, United Kingdom
Sabine Dagmar Zimmermann,
Délégation Languedoc Roussillon (CNRS), France

*CORRESPONDENCE
Lars H. Wegner
lars.wegner@fosu.edu.cn

SPECIALTY SECTION
This article was submitted to Plant Biophysics and Modeling, a section of the journal Frontiers in Plant Science

RECEIVED 12 January 2022
ACCEPTED 15 July 2022
PUBLISHED 16 August 2022

CITATION
Wegner LH (2022) Empowering roots—Some current aspects of root bioenergetics.
Front. Plant Sci. 13:853309.
doi: 10.3389/fpls.2022.853309

Empowering roots—Some current aspects of root bioenergetics

Lars H. Wegner*

International Research Center for Environmental Membrane Biology, Foshan University, Foshan, China

Roots of higher plants provide the shoot with nutrients and water. In exchange, they receive photosynthates, which serve both as energy source and building blocks for maintenance and growth. While studies in plant bioenergetics used to focus on photosynthesis, several more recent findings also aroused or renewed interest in energy conversion and allocation in roots. Root building costs were identified as a long-undervalued trait, which turned out to be highly relevant for stress tolerance and nutrient use efficiency. Reduced building costs per root length (e.g., by aerenchyma formation or by increasing the cell size) are beneficial for exploring the soil for nutrient-rich patches, especially in low-input agrosystems. Also, an apparent mismatch was frequently found between the root energy budget in the form of the ATP pool on the one side and the apparent costs on the other side, particularly the costs of membrane transport under stress conditions, e.g., the Na^+ detoxification costs resulting from Na^+ sequestration at the plasma membrane. Ion transport across the plasma membrane (and also endomembranes) is coupled to the proton motive force usually believed to be exclusively generated by H^+ ATPases. Recently, an alternative mechanism, the biochemical pH clamp, was identified which relies on H^+ formation and binding in the apoplast and the cytosol, respectively, driven by metabolism (so-called active buffering). On this background, several aspects of root bioenergetics are discussed. These are (1) root respiration in soil, with a critical view on calorimetric vs. gas exchange measurements; (2) processes of energy conversion in mitochondria with a special focus on the role of the alternative oxidases, which allow adjusting carbon flow through metabolic pathways to membrane transport processes; and (3) energy allocation, in particular to transport across the plasma membrane forming the interface to soil solution. A concluding remark is dedicated to modeling root bioenergetics for optimizing further breeding strategies. Apparent "energy spoilers" may bestow the plant with a yet unidentified advantage only unfolding their beneficial effect under certain environmental conditions.

KEYWORDS

bioenergetics, mitochondria, alternative oxidase, biochemical pH clamp, root architecture, aerenchyma, salinity

Introduction

Life persists by a constant flow of free energy—when this energy flow and its tightly regulated partitioning comes to an end, this is, in fact, a hallmark of death. So, life ceases as soon as the process of energy conversion is irreversibly disrupted. By contrast, biological *matter* and structures remain intact and in place for a short while, varying from a few seconds up to days, before degradation sets in. Consistently, Dupré and Nicholson (2018), proponents of a process philosophy in the life sciences, agued "that the living world is a hierarchy of processes stabilized and actively maintained at different timescales," rather than one of "things" (i.e., matter). For a less drastic variation of this topic, we may refer to a situation of perfect homeostasis of a cell or an organism implying a living, but invariant state, (which should be considered a thought experiment and will hardly be encountered in reality). Life is operating far from equilibrium, and maintaining homeostasis is necessarily associated with constant energy dissipation and, often inseparably connected, also a flow of matter. A compelling case study was recently communicated by Dreyer (2021): Using a simple modeling approach, he showed that K^+ homeostasis in individual plant cells is necessarily associated with a free energy-consuming circular flow of K^+ across the plasma membrane. These considerations imply that it is bioenergetics, which is concerned with the very key processes of life, namely studying and analyzing the life-preserving energy flow and energy conversion. This is, in fact, the most concise definition of bioenergetics—for more details see Demirel and Sandler (2002) and Nicholls (2013). The significance of energy conversion is most obvious for plants which have (with few exceptions) monopolized the conversion of solar photon radiation into chemical energy, making the primary energy source on earth available to all forms of life. Therefore, plant bioenergetics is often exclusively associated with processes directly related to photosynthesis, while subsequent processes of energy conversion in the plant body such as respiration (oxidative phosphorylation) receive much less interest and tend to be undervalued. In this short review, the focus will be on the bioenergetics of roots.

Raising the issue of root bioenergetics provokes the initial inquiry "what is a root?" Not uncommon in the biological sciences, basic morphological/functional categories such as "root" become the fuzzier the closer you look at them, due to the diversity of life forms and the evolutionary radiation of morphological and anatomical adaptations in the plant kingdom (Graham et al., 2000). Luckily, we can refer to an excellent treatise of this issue by Raven and Edwards, who raised the same question some 20 years ago (Raven and Edwards, 2001). The most straightforward answer we can give to this question is related to function: Roots (i) anchor a plant in soil, providing mechanical stability (used in an allegorical sense in common language), (ii) provide an interface for exchange with soil, allowing the plant to extract water and nutrients, subsequently translocated to the shoot by long-distance transport *via* xylem vessels. As pointed out by Raven and Edwards (2001), these functions can also partly or fully by taken over, e.g., by rhizomes (if it comes to stability) or mycorrhiza (with respect to nutrient acquisition; Salvioli di Fossalunga and Novero, 2019). On the other hand, roots are not necessarily only below-ground organs. In contrast to shoots, their extension growth is strictly apical and in all vascular plants the meristematic tissue is protected by a root cap. Segmentation by nodes is never observed, in contrast to shoots (Raven and Edwards, 2001).

For our purpose, we can leave aside "exceptions" (even though it can be argued what is considered as "exceptional"; Groff and Kaplan, 1988) and address higher plants as typically possessing above-and below-ground organs which operate in a more or less strict "division of labor": Large parts of the aboveground parts perform photosynthesis making use of solar radiation and transforming this energy into energy-rich organic chemical bounds. Below-ground organs are excluded from this energy source and rely on a transfer of photo-assimilates from the shoot, usually in the form of sucrose transported *via* the phloem. In exchange, below-ground organs scavenge water and nutrients from the soil (in cooperation with mycorrhiza and microorganisms). Below-ground organs with this function will in the following be addressed as "roots" irrespective of exact morphological categories.

In the framework of this division of labor, roots, like all non-photosynthetic plant organs, are generally considered as an "investment" of the plant relying on constant feeding with products of photosynthesis, predominantly in the form of sucrose, both as building blocks, and as a source of energy. Revenues are expected in the form of new sources of water and nutrients made accessible by root growth, leading to a continuous expansion of the root system. According to a common heuristic principle widely used in (plant) ecophysiology for more than 4 decades (Bloom et al., 1985), life is thought to follow economic paradigms expressed by an adequate nomenclature. Lynch (Lynch and Ho, 2005; Lynch, 2007a) even introduced a new research field he coined "rhizoeconomics." The analogy is grounded on all life forms being continuously exposed to a selection pressure, "forcing" them to allocate limited resources in an economical way, and to reduce costs. "Benefits" and "trade-offs" are interpreted with respect to reproductive success and viability of the individual or the species. Species can follow different "strategies" for optimizing these parameters. Although this line of thinking has proven very successful in the past, it also tends to convey an anthropomorphic and teleonomic bias (see also the last section of this review).

Interest in the bioenergetics of plants, and particularly of root systems, has been revived recently on several grounds two of which will be treated here in more depth:

1. A new quest for energy-and nutrient-efficient crops has directed attention to hitherto undervalued anatomical features of the root. The search opted for more robust crops allowing to minimize the use of fertilizers, which is important both from an ecological and an economical viewpoint. This work was pioneered by JP Lynch and

coworkers (Lynch, 1995, 2007b, 2013). They highlighted the metabolic costs of soil exploration for water and nutrients and identified them as key traits for a resource-efficient agriculture, which is of particular importance in developing countries (Lynch, 2015). In particular, building costs per root length, a parameter that had been largely ignored hitherto, were addressed. A large cell volume was found to be beneficial (Colombi et al., 2019) since it tends to minimize, e.g., cell wall material required per root volume, whereas mechanical stability of root tissue is hardly compromised because it predominantly relies on the turgor pressure which is largely independent of cell size. Interestingly, formation of aerenchyma, e.g., in maize, which was hitherto only discussed in the context of oxygen supply to root tissue under waterlogging conditions (Wegner, 2010), also reduces metabolic costs of root expansion considerably (Lynch, 2015; Lynch et al., 2021) without compromising root mechanical properties too much unless soil compaction imposes special requirements on root stability (Colombi et al., 2019). Cost reduction is also obtained by root cortical senescence leading to a complete degradation of the root cortex in some Poaceae, or as a consequence of secondary growth in dicots (Lynch et al., 2021). It could be shown that this effect is indeed harnessed under natural conditions to minimize metabolic costs of soil exploration for nutrient-rich plaques—this had been identified as conveying considerable evolutionary benefits, since a large share of the daily assimilated C is invested into root growth. In the slow-growing grass *Festuca ovina*, e.g., it is about 40%. Some 25% of photosynthates is allocated to structural material used for root growth, and another 15% is spent on root growth-related respiration (including ion uptake; calculation based on data of Atkinson and Farrar, 1983 and Lambers et al., 2002).

In a study on the bioenergetics of salinity, Munns et al. (2020a) calculated the energetical benefit associated with reducing the thickness of the root cortex from two cell layers (as, e.g., in wheat branch roots) to a single layer (corresponding to the situation in *Arabidopsis* roots) when roots were exposed to salinity. They found a 20% lower ATP consumption due to the reduction in plasma membrane surface which, in turn, led to a reduction in the costs of Na^+ exclusion per root surface. A reduction in membrane surface reduces Na^+ influx and, hence, costs of Na^+ detoxifications. A re-organization of root morphology under saline conditions, favoring the development of branch roots while seminal root growth was hampered, is in accordance with this rationale. Arsova et al. (2020) observed a 70% lower energy requirement for branch roots per unit root length in wheat compared to seminal roots. These energy savings were associated with a severe reduction of transpiration-driven water uptake during daytime, though. This reminds us of the fact that energy savings usually come with a cost due to adverse side effects (see also the last section, further below). Energetic implications of root architecture and development will certainly receive continued interest in the near future, with a focus on modeling approaches like those of Munns et al. (2020a) and Arsova et al. (2020). When discussing root morphology and its adaptation to nutrient demand we should also be aware that most plant species (four out of five) rely on symbiosis with mycorrhiza for efficient nutrient foraging (Salvioli di Fossalunga and Novero, 2019), and root branching, apical growth, and root/shoot ratio are strongly affected by fungal colonization (Hughes et al., 2008). Among the three common types, i.e., arbuscular, ericoid, and ectomycorrhiza, the first is the most widespread and best studied one. Particularly the hyphae of arbuscular mycorrhiza operates as an extension of the root system, allowing to mine the soil for nutrients with low mobility, particularly P and K, but also facilitating the uptake of N. In return, the fungus is provided with monosaccharides and fatty acids by its host, thus providing building blocks and a source of energy. Specific building costs for fast hyphal growth are much lower compared to fine roots which are about 10 times thicker and possess a complex multicellular anatomy (Fitter, 1991). Hence, extending the root system with these symbionts is likely to be beneficial for the plant from an energetic point of view, even though for a cost-and-benefit evaluation it has to be taken into account that long-distance transport in hyphae is less effective than in the xylem conduits of roots.

2. Particularly under stress conditions such as salinity, an apparent mismatch between energy demand (being higher than in the absence of these stresses), and the root energy budget in terms of ATP production by oxidative phosphorylation was frequently observed. An instructive case study was provided by Foster and Miklavcic (2020) modeling costs of nutrient and water transport as well as Na^+ detoxification under saline conditions in *Arabidopsis* roots. In their model calculations based on the available experimental data, the apparent energy demand for membrane transport at the plasma membrane of cortical and stelar cells, and the root tonoplast exceeded the available ATP pool by a factor of at least 2. By varying the abundance of membrane transporters, costs could be lowered to somewhat more realistic values for the cortical plasma membrane only, whereas no cost reduction was attained for the other membranes. Experimental data obtained for circular Na^+ transport under saline conditions had also previously provided evidence for a high energy demand exceeding the free energy available in the form of the root ATP pool (Malagoli et al., 2008). This brought some authors to the conclusion that data on circular Na^+ transport across the plasma membrane of root cortical cells (obtained with radioactive tracers) are fallacious and represent ion exchange processes in the apoplast instead

(e.g., Munns et al., 2020b). Foster and Miklavcic (2020) also stated that "since our model is based on currently understood and accepted ion transport mechanisms, our predictions suggest there is a need to re-assess these mechanisms." When ATP production does not keep up with energy dissipation by membrane transport processes, transport could be fueled instead by processes which do not involve proton pump activity, i.e., do not rely on ATP hydrolysis. Na^+ secretion from cortical cells back into the root apoplast operates against a more or less steep Na^+ concentration gradient and is fueled by antiport with H^+ *via* SOS1 or another type of antiporter, taking advantage of the pH gradient across the membrane which favors H^+ influx. Recently Wegner and Shabala (2020) suggested that this antiport could be energized by an alternative mechanism denoted as the "biochemical pH clamp" (Figure 1). By a process called active buffering, a stable pH gradient across the membrane (with apoplastic and cytosolic pH values around 5.5 and 7.2, respectively) could be maintained despite continuous H^+ influx required, e.g., for Na^+ export from the cytosol even if this influx is not balanced by pump-driven H^+ extrusion. The biochemical pH clamp involves continuous H^+ release in the apoplast and H^+ scavenging in the cytosol *via* biochemical reactions. In the apoplast, H^+ is formed by conversion of CO_2 (previously released by oxidative phosphorylation) to HCO_3^-. H^+ then serves as a substrate for SOS1 (or another type of antiporter) and is channeled into the cytosol by exchange with Na^+. In the cytosol, H^+ is subsequently bound again by a biochemical reaction involving a decarboxylation reaction, which is the case with those catalyzed by malic enzyme and glutamate decarboxylase. A more detailed account will be given in the section. "The energetics of membrane transport" further below. Note that in contrast to the limited buffer capacity of apoplast and cytosolic matrix, active buffering is, in principle, inexhaustible because substrates are continuously replenished by metabolism.

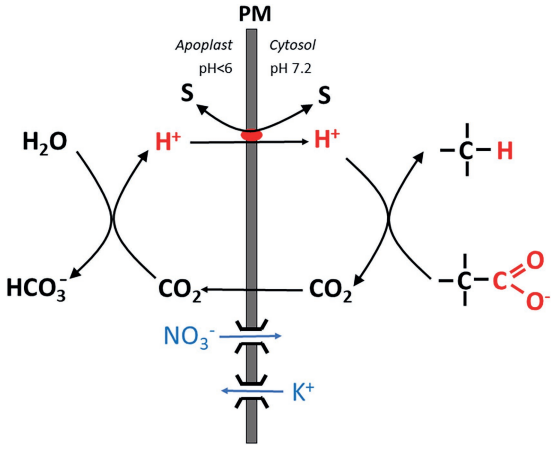

FIGURE 1
Simplified scheme showing the basic mechanism of the "biochemical pH clamp" in a root cell. H^+ is generated in the apoplast when bicarbonate is formed from CO_2. Upon translocation into the cytosol, H^+ is resorbed by a biochemical reaction which involves decarboxylation of an organic acid. CO_2 is released by this reaction and passes through the membrane into the apoplast. Thus, a pH gradient is maintained across the membrane by active buffering, which can be harnessed to drive a solute "S" across the membrane, either in symport or antiport with H^+. Charge balance is maintained by nitrate influx or K^+ efflux *via* ion channels. PM, plasma membrane.

In the following, recent work related to root bioenergetics will be discussed in light of more than 60 years of research on this issue. The journey will start with whole-plant physiology, and with ecophysiological work on roots in their natural environment (i.e., in soil), including respiration measurements. Subsequently, energy metabolism will be treated with a focus on more recent work on mitochondria and oxidative phosphorylation. Then, the bioenergetics of plasma membrane transport will be treated in some depth. Finally a prospect on possible directions of future research will be given.

Observations on the whole plant level

As a starting point for a more comprehensive treatise of root bioenergetics, we may choose energy export from source tissues in the shoot, mainly leaves, to the root. Photosynthetic products, predominantly sucrose, are shuttled to the root *via* mass flow in the phloem. Simple equations can be used to estimate the related transfer of free energy (which has to be attained by photosynthesis). From the phloem flow velocity, the virtual cross sectional area of the phloem and sucrose concentration in the xylem sap, the rate of sucrose transfer from shoot to root, is accessible. From these data, the free energy transfer rate can be estimated by inserting the energy that can potentially be harvested from one sucrose molecule by energy metabolism.

$$J_{suc} = v_{ph} * A_{Ph} * c_{suc,Ph} \quad (1)$$

$$J_E = J_{suc} * G_{suc} \quad (2)$$

With J_{suc} = sucrose flux from shoot to root; v_{Ph} = phloem flow velocity; A_{Ph} = conductive phloem cross section at the shoot base; $c_{suc,Ph}$ = sucrose concentration in phloem sap; J_E = free energy flux from root to shoot; G_{suc} = free energy of sucrose. The most exact and reliable data on phloem flow velocity can be obtained by MRI imaging allowing non-invasive flow monitoring. For *Ricinus communis*, Peuke et al. (2006) obtained a flow velocity of ~0.3 mm s^{-1}. Similar values for flow velocity ranging from 0.25 to 0.4 mm s^{-1} were reported for *Ricinus* and three other species [poplar, tomato, and tobacco;

Windt et al. (2006)]. Volume flow was in the range of 0.1 $mm^3\ s^{-1}$ for tomato and tobacco and 0.2 $mm^3\ s^{-1}$ for *Ricinus*; only in poplar, values were somewhat higher (around 0.9 $mm^3\ s^{-1}$). At a sucrose concentration of phloem sap around 0.44 M in *Ricinus* (Peuke et al., 2006), we obtain a sucrose transport velocity of ~80 nmol s^{-1} for this species. A Gibbs free energy of 5,795 kJ/mol for sucrose renders an energy transport rate of 0.46 J s^{-1}. The above approach provides us with something like an upper limit of the true energy transfer rate from shoot to root, since sucrose is not fully oxidized to CO_2. It has to be kept in mind that sugars also play an important role as building blocks/precursors, e.g., for amino acids, lipids, and ribonucleotides (see also further below). Even if the material required for growth can be quantified, residual sucrose is not fully available for energy metabolism due to root exudation of organic acids (Wegner et al., 2021), and the rapid turnover of enzymes and other molecules. A fraction of 15–67% of total carbohydrates allocated to the root is invested into energy metabolism, i.e., root respiration (Table 1 in Lambers et al., 2002).

A more promising approach to quantify root energy metabolism is provided by directly monitoring root respiration which is usually quantified by measuring CO_2 release and/or O_2 consumption. Both parameters can be assessed by gas exchange measurements in soil. They are related by the respiratory quotient (RQ), which is supposed to be close to 1 when sucrose is the exclusive substrate of energy metabolism (Lambers and Oliveira, 2019). RQ can exceed this value, e.g., when malate synthesized in the shoot is transported to the root and decarboxylated there (see also further below), and with nitrate assimilation occurring in the root. The last two decades have seen some technical advance in this field, including chamber techniques for measuring soil respiration with more efficient CO_2 detectors (Rochette and Hutchinson, 2005). Numerous studies have been published focusing on measuring respiratory activity in soil samples, mostly by assessing CO_2 release. The contribution of roots to soil respiration was shown to vary considerably, ranging from 8 to 64% (Wang and Fang, 2009). Separating root respiration from other biological activity, microbial and fungal respiration, is a major challenge in ecological research (Ruehr and Buchmann, 2010). Root respiration can be "subtracted" from total soil respiration by making use of root exclusion chambers surrounded by meshes of µm pore size which cannot be invaded by root growth. Additionally, the contribution of fine roots can be estimated by separately determining respiration on root samples and calculating their overall contribution on the basis of fine root biomass. In a mixed forest close to Zurich (Switzerland) with beech, ash, fir, spruce, lime, maple, oak, and elm trees, these measurements revealed a strong dependence of root respiration on plant phenology and photosynthetic activity (Ruehr and Buchmann, 2010). Temperature dependence of root respiration in tree stands reported previously may at least partly depend on such phenological effects. In recent years, this technique has been refined to assess mycorrhizal CO_2 release separately from the contribution of roots (both usually being summarized as autotrophic respiration) and from heterotrophic bacterial activity by using meshes of a pore size of ~50 µm which allow penetration of hyphae and exclude roots, in addition to fully closed and fully accessible root collars. Mycorrhizal CO_2 emission was shown to be relevant for overall soil respiration, but its share varied strongly. It depended, among other things, on the type of mycorrhiza and the ecosystem that was investigated. For example, in a larch forest (*Larix kaempferi*) about 6% of total soil respiration was ascribed to mycorrhiza (roots 42%; Makita et al., 2021) and in a barley field it was 4.8% [roots 25%; Moyano et al. (2007)]. Larger shares were found, e.g., for an apple orchard (mycorrhiza 11%, roots 12%; Tomè et al., 2016) in a lodgepole pine forest (mycorrhiza 25%, roots 15%; Heinemeyer et al., 2007), and in a stand of Norway spruce (mycorrhiza 18–44%, roots did not contribute significant under most conditions; Neumann and Matzner, 2014). In the latter two studies, ectomycorrhiza were dominant. An average value of 15% mycorrhizal contribution to total soil CO_2 emission was recently reported in a metastudy by Han et al. (2021). A detailed record on all aspects of soil respiration, including its relevance for global change modeling approaches, can be obtained from Luo and Zhou (2006). Soil emission is the largest CO_2 source on earth, and its management is considered highly relevant for limiting global temperature increase.

Recently, calorimetric techniques have been advocated as an alternative approach to monitoring CO_2 release for a broader and more precise quantitative assessment of root energy metabolism (Colombi et al., 2019; Herrmann and Colombi, 2019). Model calculations generally rely on the assumption of CO_2 release being driven by oxidative phosphorylation, implying that O_2 supply is not a limiting factor. However, soil O_2 partial pressures can be highly inhomogeneous and, hence, root tissue may locally be in a hypoxic state, undetected by bulk measurements. Indeed, heat dissipation can be measured with a high precision and comparatively little effort and provides an interesting alternative to gas exchange measurements for assessing root respiration. However, the underlying concept needs to be considered with some care. Calculations based on calorimetric measurements rely on the assumption of zero net energy input in a biological system residing in a "steady state" (which *de facto* comes down to the absence of growth). Free energy input *via* the phloem under these conditions is hypothesized to be eventually fully transduced to heat. This is definitely an oversimplification, since sugars are still needed as building blocks, e.g., for the synthesis of root exudates which are secreted into the soil (Wegner et al., 2021). Moreover, free energy required for maintaining steep concentration gradients with the environment remains unconsidered (see the Introduction). This energy does not contribute to heat release, but rather counteracts the entropy-driven free energy loss by (electro) diffusion (Wegner, 2015). According to the theoretical framework used by proponents of the calorimetric method, in a growing tissue catabolic (=dissipative) processes leading to heat production are complemented by an anabolic component which is equal to the energy stored in biomass surplus, as, e.g., determined by combustion. For relating heat dissipation to CO_2 release (and, in turn, to glucose consumption) a calorespirometric ratio is defined; under aerobic conditions a value of 30 kJ per g CO_2-C is assumed,

but under hypoxic conditions this value is thought to double. Even though these values are based on empirical measurements, it is at least questionable if they can be treated as constants. Heat dissipation by metabolism will depend, e.g., on the role of the alternative oxidase in respiratory processes in mitochondria (see further below). Moreover, the local differences in oxygen supply in soil emphasized by the proponents of the calorimetric method are hard to quantify and hamper the interpretation of calorimetric data in terms of glucose consumption.

Despite methodological difficulties and limitations, a combination of field ecological studies and whole plant physiology lab experiments has considerably extended our understanding of autotrophic soil respiration in recent decades (Hopkins et al., 2013). Generally, the rate of CO_2 release from roots follows photo-assimilation in aboveground organs, as expected for a source limitation and blockage of assimilate transport by stem girdling in trees impairs it. Consistently, leaf pruning, e.g., in wheat (Bingham and Stevenson, 1993), significantly reduces specific root respiration while in bean, removal of pods increases it (Fanello et al., 2020), as root pruning does in the roots that remain attached (Bingham and Stevenson, 1993; Fanello et al., 2020). This provides evidence for a competition between sinks. Cellular adenylate levels provide for a fine regulation by both regulating glycolysis and the mitochondrial electron transport chain [Lambers et al. (2002); see also the following section]. A large fraction of root maintenance costs is invested into nitrate uptake and assimilation (Bouma and De Visser, 1993; Bouma et al., 1994; Scheurwater et al., 1998; Hopkins et al., 2013), and root N has even been employed as a proxy for fine root respiration in some ecological studies (Jia et al., 2011).

Processes of energy conversion in mitochondria

Ecophysiological work on root bioenergetics, highlighting, among other things, the relevance of anatomical and morphological traits for the bioenergetics of nutrient acquisition, has renewed attention to this field, which received only marginal interest by plant physiologists for quite a while. For a quantitative approach, a profound knowledge of energy metabolism down to the molecular scale is certainly required to understand its fine-tuning in response to a plethora of individual physiological conditions. This includes nutrient availability, photosynthetic activity in source tissues, and challenges by biotic and abiotic stressors, which may act in various intensities and combinations. Indeed, tremendous progress has also been made in this field, particularly with respect to research on plant mitochondria which play a key role in energy conversion. Basic principles of the chemiosmotic theory for ATP synthesis relying on a proton motive force (pmf) across the inner mitochondrial membrane date back to the 60s of the last century, and the organization of the electron transport chain with four redox complexes, three of which (I, III, and IV) translocating H^+ from the mitochondrial matrix into the intermembrane space, and with an intermediate ubichinone pool was unraveled in the 70 and 80s (Figure 2A). This basic knowledge will not be covered here, and the reader is referred to excellent description in textbooks (e.g., Nicholls, 2013; Lambers and Oliveira, 2019). In more recent work, the focus shifted to the genetic basis and molecular structure of these complexes and, most prominently, to their regulation. Interest in the latter was stimulated by the growing awareness for challenges to the stability of energy transduction processes in mitochondria, e.g., by the generation of reactive oxygen species (ROS) when the proton motive force and/or the membrane potential at the inner mitochondrial membrane shift into a critical range (Wagner and Moore, 1997). Research into the regulation of electron transport in mitochondria was initiated some 50 years ago when an alternative oxidase (AOX) was identified shown to be insensitive to the inhibitor cyanide and transferring electrons from the ubichinone pool to O_2 (Figure 2A) without contributing to the trans-membrane pH gradient (Bendall and Bonner, 1971). The small family of AOX proteins consists of two subfamilies, AOX1 and AOX2, both of which are encoded by nuclear genes. Monocots usually only possess AOX1 and lack the AOX2 subfamily. AOX proteins include a four-helix bundle coordinating binuclear di-iron center which is able to bind and activate oxygen (Moore et al., 2013; May et al., 2017). Current evidence indicates that AOX exists as a homodimer. Reduction of disulfide bounds induce a transition from an inactive state to a "dormant" state of low activity readily mobilized by other factors like intermediates of the tricarboxylic acid (TCA) cycle (Vanlerberghe et al., 2020). The inner mitochondrial membrane also contains (alternative) NAD(P)H dehydrogenases (NDs), which are insensitive to the inhibitor rotenone. Alternative NDs accept electrons from NAD(P)H and feed them into the ubichinone pool in the same way as the complex I (the "ordinary" NAD(P)H dehydrogenase; Figure 2A), but without translocating H^+. Two dehydrogenases, NDA and NDC, are associated with the inner surface of the mitochondrial membrane, whereas NDB is located at the outer surface (Sweetman et al., 2019). Acting sequentially, NDs and AOXs transfer electrons from NAD(P)H to O_2 without converting the energy into a chemiosmotic gradient; rather it is dissipated as heat. Thus the "standard" electron transport chain is completely short-circuited, as demonstrated for *Arabidopsis* (Clifton et al., 2005, 2006). A bypass also exists for the F0F1 ATP synthase: The uncoupling proteins (UCPs) found, e.g., in potato tubers channel H^+ and dissipate the pmf, but do not contribute to ATP synthesis (Hourton-Cabassa et al., 2004). The role of these enzymes apparently just "spoiling" the redox equivalents provided by metabolism has puzzled researchers for decades. Numerous studies devoted to unraveling their function (usually focusing on the AOX) have been published since then (Moore and Rich, 1980; Wagner and Krab, 1995; Millenaar and Lambers, 2003; Vanlerberghe, 2013; Vanlerberghe et al., 2020). From these publications, we can distill several non-exclusive explanations: (i) Experimentally well founded is a role of the alternative oxidase for heat generation, e.g., in spade leaves of the Araceae, which employ

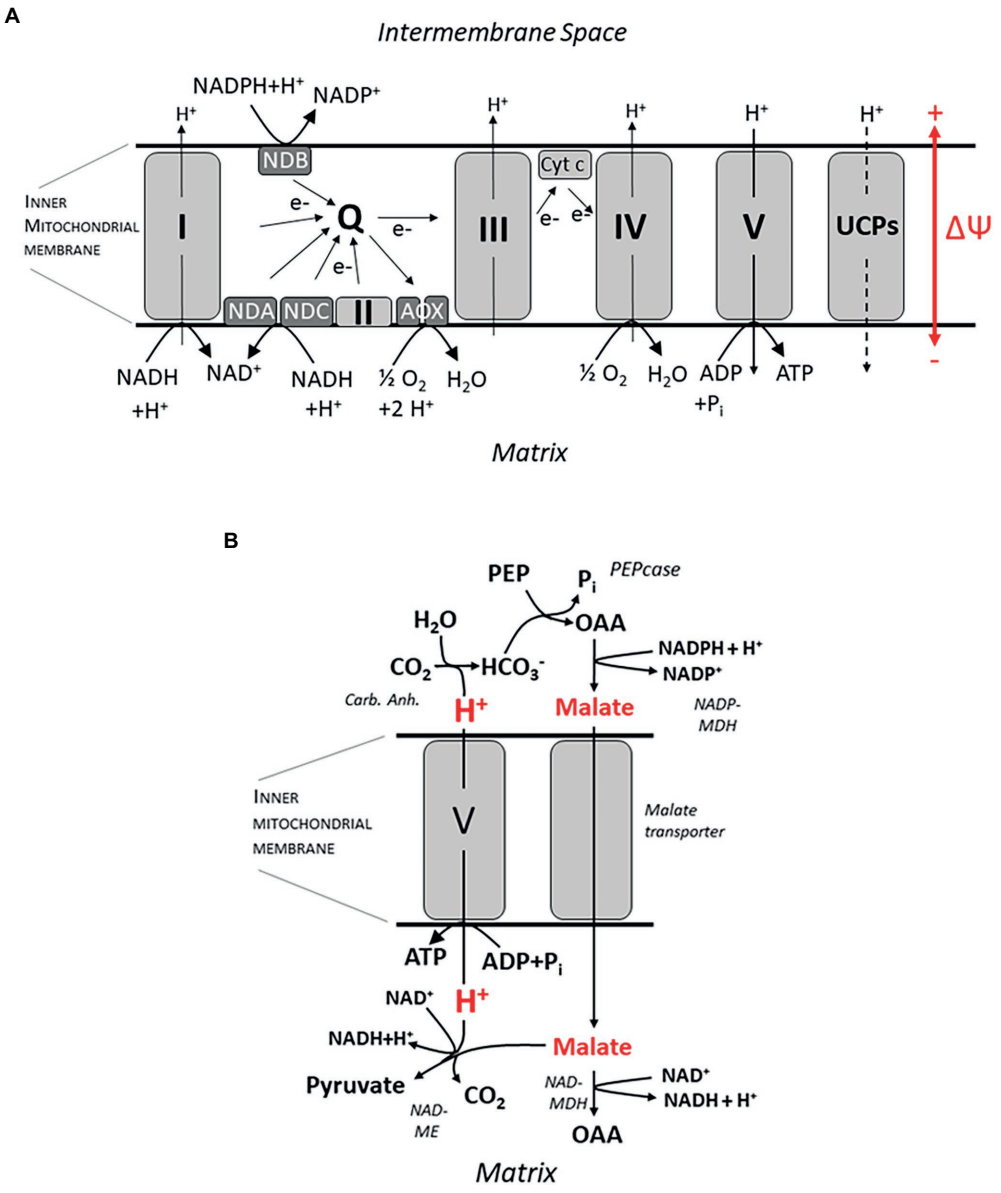

FIGURE 2
ATP synthesis at the inner mitochondrial membrane. In **(A)** an overview on the electron transport chain is given, including complexes I–V, NAD(P)H dehydrogenases (ND) A, B and C and the alternative oxidases (AOX). Q, ubichinone pool; UCPs, uncoupling proteins; and ΔΨ, membrane potential. A putative mechanism for ATP synthesis which does not involve circular H^+ flow is shown in **(B)**. H^+ is released by formation of HCO_3-catalyzed by the (Carb. Anh.) reaction. HCO_3-is subsequently assimilated by the Phosphoenolpyruvate-Carboxylase (PEPcase) synthesizing Oxaloacetate (OAA) from Phosphoenolpyruvate (PEP). Subsequently malate is formed by the NADPH-dependent Malate-Dehydrogenase (NADP-MDH), and malate passes through a yet unidentified transporter into the mitochondrial matrix. Subsequently, it can either be oxidized again to oxaloacetate by the NAD-dependent Malate-Dehydrogenase in the matrix (NAD-MDH), or it is decarboxylated to pyruvate by the NAD-dependent Malic Enzyme (NAD-ME) while binding a H^+. Thus, a pH gradient is built up across the membrane which is harnessed by F0F1 ATPase (complex V) to form ATP. For more details, see text.

volatile compounds to attract insects for pollination (Wagner et al. 2008). However, this specialized function does not explain the general presence of these enzymes in plant mitochondria, including root cells. Some authors speculated on a more widespread function of AOX in long-term temperature adjustment, though [summarized in Vanlerberghe (2013)]; (ii) It has been pointed out that part of the energy metabolism (and certainly glycolysis) has (at least) a dual function: Transforming the free energy stored in C-H and C-O bonds into a "universal currency," namely ATP (catabolic function), *and* providing building blocks for the synthesis of biomolecules such as peptides, fatty acids, and DNA [anabolic function; (Millenaar and Lambers, 2003; Vanlerberghe, 2013)]. The latter requires a sufficient throughput of enzymatic pathways, particularly the glycolysis and part of the TCA cycle, which, in turn, relies on a fast recovery of $NAD(P)^+$, the oxidized form of the nicotinamides. This is the

function of the electron transport chain in the inner mitochondrial membrane. Its potential blockage by low rates of ATP synthesis, e.g., due to low phosphate availability or low energy demand, may have a far-reaching systemic effect and feedback on the rates of biomolecule synthesis. According to this explanation, alternative oxidases have the function to guarantee a minimum NAD(P)H throughput in the mitochondria to keep the anabolic metabolism going, thus having a role in both redox balancing and carbon skeleton production. Vanlerberghe (2013) has re-evaluated this point, stating that AOX has a role in fine-tuning growth with nutrient efficiencies, particularly with respect to P_i. Phosphate deficiency tends to limit ATP synthesis. This could entail an energization of the inner mitochondrial membrane favoring the generation of reactive oxygen species (ROS) which threaten protein integrity (Wagner and Moore, 1997). Hence, a third major function of the AOX has been advocated, namely (iii) serving as a security valve for controlling the pH gradient and membrane potential across the mitochondrial inner membrane (both contributing to pmf) as well as the redox state (MP) of the electron transport chain, among other things for limiting ROS production. A large voltage drop of 220–250 mV (cytosol relative to matrix) was obtained by probing the MP, e.g., for mitochondria isolated from potato tubers, whereas the ΔpH was relatively small [0.2 units; Ducet et al. (1983)], and the membrane potential of individual mitochondria is controlled to minimize ROS production (Schwarzländer et al., 2012). Consistently, it was found that a low matrix pH activates AOX (Millenaar and Lambers, 2003), and external ROS have been shown to stimulate expression of AOX1. Usually matrix pH is at about 7.8.

The current state of discussion on the AOXs already highlights that there is no single answer to the question for its physiological function. However, some important findings are still left unconsidered or did not meet a satisfactory explanation yet. The most striking still unexplained finding is related to the AOX regulation under stress conditions. For conditions of drought stress (Costa et al., 2007) and salinity (Smith et al., 2009; Martí et al., 2011, Mhadhbi et al., 2013, Munns et al., 2020a) a significant *increase* in AOX activity has repeatedly been reported despite the fact that under these conditions additional energy is required to synthesize or accumulate osmotica and to detoxify the cytosol by dumping Na^+ in the vacuole or the apoplast, respectively. Hence, the efficiency of energy metabolism is expected to increase under stress conditions, apparently precluding any need for a non-functional energy *dissipation*. Focusing on salinity, a solution to this conundrum may come from the recent suggestion of Wegner and Shabala (2020) for an energization of membrane transport by direct coupling to energy metabolism, with no ATP hydrolysis directly involved. According to this "biochemical pH clamp" hypothesis already brought up in the Introduction (Figure 1), transport coupled to H^+ influx across the plasma membrane (such as antiport with Na^+) can be driven by biochemical reactions generating and capturing H^+ in the apoplast and in the cytosol, respectively. It is obvious that these active buffering processes must be tightly coupled to the metabolic carbon flow, and the AOX can adjust this flow according to need, de-coupling it from the actual rate of ATP hydrolysis. It is important to note that the ATP pool is always shared among various functions, the main ones being maintenance, growth, and membrane transport (Poorter et al., 1991; Amthor, 2000). Instead, the biochemical pH clamp exclusively fuels membrane transport, with no competition by the other consumers (Wegner and Shabala, 2020). This exclusiveness makes it particularly valuable for coping with stress conditions.

Previously, the biochemical pH clamp has been discussed as a mechanism for energizing membrane transport across the plasma membrane of root cells (Wegner and Shabala, 2020; Wegner et al., 2021), and this topic will be addressed in more detail in the following section. Here, I would like to suggest an additional role for this mechanism in ATP *synthesis* in mitochondria which has, to my knowledge, not been considered before. ATP synthesis *via* the F0F1 ATP synthase (complex V; Figures 2A,B) requires a sufficient chemiosmotic gradient across the inner mitochondrial membrane which is, according to a generally accepted dogma, exclusively generated by the electron transport chain (e.g., Vanlerberghe, 2013), translocating 3 H^+ per NADH molecule oxidized. It is an important corollary of this dogma, which I would like to challenge here, that no ATP can be synthesized at the inner mitochondrial membrane when the electron transport chain does not contribute to the pmf—as with the alternative ND and the AOX bypassing the "ordinary" transport chain. Under these conditions, H^+ transport for ATP synthesis could still be organized as a *linear* flux, though, purportedly organized in the following way: In the cytosol, malate is synthesized from phosphoenolpyruvate by the PEP carboxylase and the malate dehydrogenase, with oxaloacetate serving as an intermediate (Figure 2B). This involves the release of 1 H^+ per turnover. Malate subsequently enters the mitochondrial matrix by facilitated (electro) diffusion and is subsequently decarboxylated by the NADH-dependent malic enzyme, leading to the formation of pyruvate, at the expense of 1 H^+. Pyruvate is then fed into the TCA cycle. Note that this reaction sequence gives rise to a pH gradient across the inner mitochondrial membrane, which could be harnessed to drive a H^+ influx into the mitochondrial matrix and, in turn, ATP synthesis. For the stoichiometry of the F0F1 ATPase, a ratio of 4 H^+ per ATP has been determined (Steigmiller et al., 2008). The necessary molecular "infrastructure" for this reaction sequence has indeed been verified, and several experimental observations lend support to this scenario. When protocols for the isolation of viable mitochondria, e.g., from cauliflower buds and potato tubers, had been worked out in the 70s of the last century, it was soon observed that providing these mitochondrial preparations with external malate plus NAD^+ as substrates, respiratory activity was stimulated as monitored by O_2 consumption, providing evidence that malate readily diffuses into the matrix (Macrae and Moorhouse, 1970). Two enzymes were shown to compete for malate as a substrate (Figure 2B), namely the NADH-dependent malate dehydrogenase (NAD-MDH, directly catalyzing a step in

the TCA cycle) and malic enzyme (NAD-ME). Under most conditions, the contribution of the ME was marginalized by the MDH as determined by immediately measuring oxaloacetate vs. pyruvate levels (Rustin et al., 1980). Even when the MDH was blocked, the ME could only partly take over its role (Le et al., 2021a), and only a small fraction of ME-derived pyruvate was channeled into the TCA cycle (Le et al., 2021b). However, at high AOX activities, ME was the dominant enzyme. This even made researchers believe (erroneously) that AOX and the NADH-dependent malic enzyme were tightly associated and part of a separate redox pool (Rustin et al., 1980) but note recent data by Le et al. (2021b) suggesting that pyruvate imported *via* the pyruvate carrier (MPC) complex may not mix with that generated by the (NAD-ME). Interestingly, pyruvate, the product of the ME, directly activates the AOX when the dimer is in the reduced state (Day et al., 1994; Vanlerberghe, 2013). ME is also activated when the final electron acceptor O_2 becomes less available during hypoxia (Edwards et al., 1998). These experimental findings are in accordance with the hypothesis forwarded here. Another piece of evidence refers to malate flux which is supposed to carry negative charges for electrically balancing the H^+ transfer, thus avoiding any drift in membrane potential. Indeed, evidence for the existence of an electrogenic malate transporter not identical to or related with the MPC was obtained, even though its genetic basis still appears to be unidentified (Le et al., 2021a). A further critical corollary of the hypothesis is a *net* H^+ influx into mitochondria in the presence of malate—this should be accessible with the Microelectrode Ion Flux Estimation (MIFE) technique (Shabala et al., 2006).

Special aspects of mitochondrial function discussed above have highlighted the complexity of mitochondrial activity for plant metabolism, even beyond its key role in bioenergetics. Much progress has been made recently in understanding how mitochondria are "programmed" according to the actual status of the organism and its current requirements. An interesting aspect of this programming is the coordination of genetic information stored on the nucleus and on the mitochondrion. In recent years, the role of mitochondria in sensing stress and coordinating the cellular response by activating nuclear genes was gradually recognized, now known as the "mitochondrial retrograde response" (Wagner et al., 2018). A wide spectrum of nuclear genes, including those encoding for AOX1, is activated by inhibiting electron transport with Antimycin A, which acts on complex III and stimulates ROS production. The response to this chemical as well as other specific inhibitors like rotenone and oligomycin has been analyzed in quite detail, including transcription factors of the NAC family which coordinate the response. Interestingly, they originate from the ER and move into the nucleus after release into the cytosol in response to mitochondrial dysfunction. Inhibitors seem to mimic "natural" effects on electron transport by stress such as ozone or drought, and response to hypoxic conditions which also tend to block electron transport. Re-organization of energy metabolism induced by a lack of oxygen is a separate issue and will not be treated in more depth here. The reader is referred to recent review articles by Lee and Bailey-Serres (2021) and Loreti and Perata (2020).

Finally, recent findings on oxidative phosphorylation in arbuscular mycorrhiza will be treated briefly. Invasion of the fungus by endobacteria frequently adds a third partner to the symbiosis (Salvioli et al., 2016). Having a reduced genome and metabolism, these bacteria fully rely on their host, which itself depends on the supply of sugars by the plant upon root inoculation. As a model system, the fungus *Gigaspora margarita* was investigated which is infected by the bacterium Candidatus *Glomeribacter gigasporarum* (CaGg.; Salvioli et al., 2016; Vannini et al., 2016) Interestingly, the endobacterium stimulates, among other things, fungal ATP synthesis by activating enzymes of the inner mitochondrial membrane and activates pathways for ROS scavenging alternative to those operating in fungi cultures lacking endobacteria. The root infection process and antioxidant activities in the root were also affected (Venice et al., 2017).

The energetics of membrane transport

The previous section centered on the question how energy is provided and made accessible in the roots of higher plants, particularly dealing with processes in mitochondria. Efficient "management" of the ATP pool while, at the same time, minimizing hazards, e.g., by excessive ROS production turned out to be an important trade-off. Alternative mechanisms of energy conversion not involving the ATP pool were also mentioned, but so far rather *en passant*. In the following, the focus shifts to the way metabolic energy is "spent" on and allocated to basic root functions. The plasma membrane of cortical root cells and root hairs will receive most attention here, since they form the interface to soil solution and play a key role in nutrient and water acquisition. Furthermore, they are "in the first line of defense" against biotic and abiotic stresses. As a consequence, steep concentrations gradient for numerous solutes need to be established and maintained across the plasma membrane of these cells, either for accumulating them in the cytoplasm (as in the case of nutrients such as K^+) or to prevent their uptake, which applies to potentially harmful solutes such as Na^+ and Cl^-. In plant cells, membranes are generally energized by establishing a proton motive force across them, consisting of a pH gradient and an electrical membrane potential. For all other solutes, energetically uphill transport is coupled to the pmf, either to the pH gradient (as in the case of SOS1 catalyzing an electroneutral exchange of H^+ and Na^+), or to the membrane potential driving, e.g., K^+ into the cell *via* ion channels even against a concentration gradient, or to both. At the plasma membrane, P-type H^+ ATPases play a key role in pmf generation by pumping H^+ against its electrochemical gradient at the expense of splitting an energy-rich phosphate from ATP, ending up with ADP and P_i (Briskin et al., 1995; Falhof et al., 2016). The stoichiometry is generally 1 H^+ per ATP hydrolysis (Briskin and Reynolds-Niesman, 1991), but a value of 3 was

obtained under conditions of salinity stress (Janicka-Russak et al., 2013), indicating that the pump can also operate in a more efficient mode. P-type ATPases are encoded by the AHA gene family (for AUTOINHIBITED PLASMA MEMBRANE PROTON ATPases; Falhof et al., 2016; Hoffmann et al., 2019). In root cortical cells, AHA2 is expressed besides the constitutively present AHA1 and appears to be involved in nutrient acquisition. AHA7 is additionally expressed specifically in root hairs. AHA2 activity was maximal at a cytosolic pH of about 6.4 and strongly decreased when the pH was elevated to physiological values close above 7 (Hoffmann et al., 2019); still, it was clearly involved, e.g., in phosphate uptake in *Arabidopsis* roots and contributed to the acidification of the root surface in the elongation zone (Yuan et al., 2017). Similarly, in *Arabidopsis* roots it played a role in Fe acquisition (Santi and Schmidt, 2009). AHA7 differed from AHA2 with respect to its pH dependence: It showed full activity around cytosolic values around 7 (close to the physiological range), but was strongly inhibited at external pH values below ~pH 6.0; this is due to an extracellular autoinhibitory loop.

For a long time, P-type H^+ ATPases have been considered as the *exclusive* pmf source at the plasma membrane of plant cells, until experiments with the MIFE technique provided compelling evidence that this is not always the case. Under various experimental conditions summarized by Wegner and Shabala (2020), a *net* H^+ *influx* was measured into root cells for 2 h at least, indicated that H^+ flux by symporters and antiporters apparently *exceeded* active H^+ efflux mediated by the proton pump. Net influx was even recorded when fluxes were monitored at opposite sites of the same protoplast, with no cell wall potentially interfering with the measurement. Apparently, a pmf is maintained under these conditions despite the ongoing H^+ influx (Figure 1). As described in the Introduction, this is explained by active buffering which involves H^+ release and resorption in the apoplast and in the cytosol, respectively, by metabolism. Active buffering stabilizes the pH gradient during net H^+ influx (also denoted as the "biochemical pH clamp," see above). Note that H^+ influx is also associated with a positive charge transfer from the apoplast into the cytosol. Charge balance can either be achieved by simultaneous ion-channel mediated influx of anions (e.g., nitrate) and/or by K^+ efflux. The former will remain an exceptional case, and hence continuous K^+ release is likely to be a corollary of the biochemical pH clamp, unless the overall charge balance for all transport processes is neutral. Hence, the process will come to an end when the vacuolar K^+ pool is exhausted. This will take several hours (Wu et al., 2018). We have to conclude that the mechanism is not self-sustained, but requires an intermittent refilling of the cellular K^+ pool, possibly at night.

In the apoplast, a pH drift to values >~6 is prevented by the activity of an acid carbonic anhydrase. One H^+ is released when bicarbonate is formed from H_2O and CO_2, the latter being an end-product of respiration (see above). Moreover, the adjacent soil provides a huge H^+ reservoir whereas limited cell wall buffering only plays a minor role (the specific buffer capacity amounting to just about 10% of the cytosolic one; Felle (2001)) and can only transiently counteract a pH shift. All these mechanisms of pH control provide just for a rather loose clamp, and apoplastic pH can fluctuate to some extent, also allowing it to act as a second messenger e.g. under drought stress and hypoxia (Felle, 2001; Geilfus, 2017) and for growth regulation (Shao et al., 2021). Moreover, local pH gradients can prevail, e.g. perpendicular to the plasma membrane (Martinière et al., 2013) and between roots zones (Peters and Felle, 1999).

On the other hand, H^+ *scavenging* in the *cytosol* requires biochemical reactions involving a decarboxylation step. Two rather complex reaction schemes have been advanced by Wegner and Shabala involving the NADPH-dependent ME and the glutamate decarboxylase (GAD), respectively (Figures 3A,B). The first one closely follows the well-known Ben-Zioni Lips model of anion circulation in higher plants (Zioni et al., 1971). According to this model, nitrate taken up by the root is transported to the leaves for N assimilation *via* the transpiration stream. K^+, serving as a counterion, is subsequently cycled back to the root *via* the phloem. Charge balance in phloem transport is obtained by shoot-to-root transfer of malate, which is decarboxylated in the root, forming pyruvate (Figure 3A). The latter step involves binding of H^+ which enters the cytosol *via* various cotransporters. Note that malate derived from *glucose* is associated with the release of 4 H^+ and, hence, subsequent decarboxylation does not result in overall net H^+ consumption. However, when malate synthesis takes place in the leaves, alkalinization by photosynthetic nitrate assimilation is elegantly neutralized. Another metabolic pathway that is highly stimulated at various stress conditions, e.g., by salinity, and consuming H^+ is the so-called GABA shunt. GABA, or 4-aminobutyric acid, is a zwitterionic, non-protein amino acid that is found in almost all plants species and tissues. It is produced *via* an anaplerotic pathway branching from the TCA cycle that involves trans-amination of 2-oxoglutarate leading to the formation of glutamate, and subsequent decarboxylation (Figure 3B). The latter reaction is catalyzed by the Glutamate decarboxylase (GAD) and is associated with binding of one H^+ ion. GABA can be fed back into the TCA cycle by a two-step process yielding succinate. Alternatively, it is released into the apoplast—in fact, GABA has been identified as a signaling molecule for communication between individual plants (Ramesh et al., 2017). The pivotal role of the GABA shunt in preventing acidification of the cytosol is known since the pioneering work of Crawford (Crawford et al., 1994), but these authors did not consider the link with the energization of membrane transport processes. Interestingly, cytosolic acidification stimulates the GAD, and, in turn, GABA formation, e.g., in carrot suspension cells (Carroll et al., 1994; Crawford et al., 1994) originally derived from storage root tissue (Israel and Steward, 1967). For a review, the reader is referred to Shelp et al. (1999). GABA concentrations in the cytosol can be as high as 6–39 mM under stress conditions such as drought stress and salinity (Renault et al., 2010). Strong evidence supporting a role of the H^+ scavenging GABA shunt in salinity stress tolerance

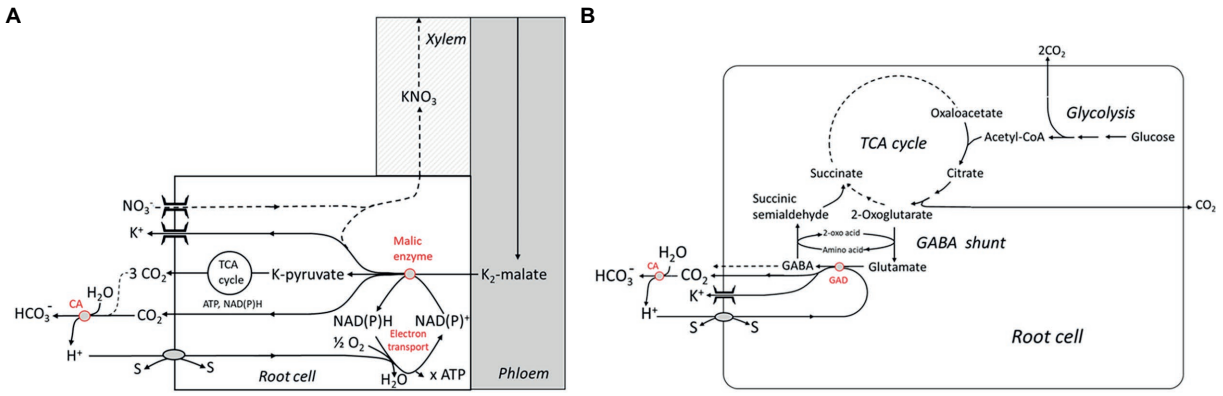

FIGURE 3
Metabolic schemes showing "active" buffering in the cytosol by malic enzyme and the electron transport chain **(A)** and the glutamate decarboxylase (GAD) which is part of the 4-Aminobutyric acid (GABA) shunt **(B)**. Both systems are capable of capturing H^+ imported by cotransport with or antiport against other substrates ("s"). Extracellular buffering is brought about by the carbonic anhydrase (CA). TCA, tricarbonic acid. Reproduced from Wegner and Shabala (2020), with permission.

was obtained by Nikolas Taylor and coworkers (Che-Othman et al., 2020). They reported on a complete re-organization of the TCA cycle with NaCl treatment in wheat leaves. Under these conditions, the GABA shunt was the preferred route, avoiding the 2-oxoglutarate dehydrogenase complex (OGDC) that was completely disintegrated when exposed to elevated Na^+ concentrations. This study was performed on leaf cells, but evidence for a similar mechanism operating in *Arabidopsis* roots had previously been presented (Renault et al., 2013). The observations are in line with a key role of the GAD in capturing H^+ entering the cytosol in exchange for Na^+. It should be noted that these biochemical pH stat mechanisms do not exert a tight control on cytosolic pH either; it can vary to some extent, allowing it to act as a second messenger (Felle, 2001), as described above for the apoplastic pH.

Thermodynamic aspects of the biochemical pH clamp hypothesis were discussed in detail by Wegner and Shabala (2020), estimating the metabolic free energy that needs to be invested into stabilizing the trans-membrane H^+ gradient for counteracting continuous H^+ influx. Among other things, it was pointed out that the decarboxylation step catalyzed by ME would even be slightly energetically uphill under standard conditions; hence, this reaction could only drive H^+ influx at a favorable ratio of products to educts. Since ME simultaneous decarboxylates *and* oxidizes malate, the reaction strongly depends on the redox state of the cell controlling the $NADP^+$/NADPH ratio. Hence, H^+ resorption is likely to depend on continuous oxidation of NADPH by the mitochondrial electron transport chain, possibly also involving the AOXs (see the previous section). Decarboxylation of glutamate catalyzed by GAD is slightly exergonic, the free energy balance being ~ −11 kJ/mol under standard conditions (calculated on the basis of data from Efe et al., 2008), and the whole GABA shunt is also associated with a release of free energy.

In addition to the plasma membrane, endomembranes are another relevant "energy sink," not only in roots. In the first place, this refers to vacuoles (Davies, 1997) which are used as intracellular storage sites for various solutes. Transport across the tonoplast is energized by V-type ATPases, which share many properties with their counterparts in the plasma membrane albeit with some remarkable exceptions such as their variable stoichiometry, and the Pyrophosphatases being specific for the tonoplast. Interestingly, cycling of Na^+ (and possibly of other solutes like K^+) is also likely to play a role at the tonoplast and may cause very high energetic costs at this membrane, too (Shabala et al., 2020).

The energetics of root growth

Transport and storage are important energy investments in the root, another very important one is growth (for recent reviews see Dupuy et al., 2018, Volkov et al., 2021). Root growth and building costs were already treated in the Introduction to motivate root bioenergetics as a timely issue. Exploring the heterogeneous soil for nutrient-rich sites relies on maintaining root growth at a high rate; this is of particular importance for getting access to resources of low mobility like phosphate (Lynch and Ho, 2005; Lynch, 2015, 2022), whereas mobile nutrients, e.g., N, can be mobilized more readily by the transpiration stream. In this context, building costs of root tissue per root length was identified as a key trait for optimizing the root growth rate. This can be expressed in terms of a carbon economy for soil exploration (Nielsen et al., 2001), which was indeed shown to be affected, e.g., by phosphate availability. Parameters like root diameter, cell size, and aerenchyma formation have been shown to be relevant. On the other hand, a detailed physiological comparison of slow and fast-growing grass species [which is a genetically encoded property, persisting at identical nutrient supply; Poorter et al. (1991)] revealed that metabolic energy spent on root growth normalized to dry weight was almost identical, e.g., in

fast-growing *Dactylus glomerata* and slow-growing *F. ovina*. However, *total* respiration did not scale with the growth rate, the fast-growing species being apparently more efficient [2.3 times faster growth at a factor of 1.2 for the specific respiration rate; Scheurwater et al. (1998)]. The difference was rather related to N uptake which consumed less energy in the fast-growing species than in the slow one due to a lower rate of N circulation across the plasma membrane of root cortical cells.

Anatomical and morphological traits leading to reduced specific building costs of roots have been well characterized, but their genetic basis is frequently still elusive, maybe with the exception of aerenchyma formation relying on programmed cell death (Evans, 2004). Only few genes have been identified so far which modify root system architecture in a clearly defined way (for reviews, see Wachsman et al., 2015; Uga, 2021). Among those is the gene DEEPER ROOTING 1 (DRO1) in rice encoding for a protein which has an impact on the angle at which the root growth relative to the gravitational field of the earth (and, hence, on the rooting depth) and PSTOL1, which speeds up lateral growth of rice roots in P-deficient soils. A more detailed evaluation of the genetic basis of root anatomical and morphological adaptation to the energy status as well as nutrient availability is expected in the years to come.

Final remarks

Numerous "construction sites" were identified in this short review on various aspects of root energetics which follow their own agenda. I do not want to be repetitive returning to these special topics, but raise a more fundamental issue instead. Traits leading to an efficient use of energy have been identified as highly beneficial from an evolutionary point of view, and crop breeding is being re-oriented toward that goal (De Block and Van Lijsebettens, 2011; Lynch, 2015; Munns et al., 2020b). A new twist was added to the field by introducing traits which had been undervalued so far such as an "energy-efficient" root architecture and anatomy (see Introduction). Another "mega-concept" is concerned with aspects of use efficiency of nutrient elements (N, S, and P) which also has bearing on the bioenergetics of plants (Lynch, 2019). Definitely, these approaches are promising and justified—still, I want to add a note of caution. Plants, as life in general, operate far from thermodynamic equilibrium and their existence relies on a constant flow of free energy (see the Introduction). Hence, they are not *per se* designed as "energy savers"—rather, they tend to gain biological function by "spending," or, rather, "investing" energy, in order to get some value in return with respect to fitness and viability. What at first sight appears as a waste of energy may in effect convey a hidden function. In fact, it may turn out as an important security valve proving its value at certain stress scenarios only. We have to be careful avoiding anthropomorphisms when judging plant "success" in "saving energy." The ongoing discussion on AOX and the other "energy spoilers" in mitochondrial electron transport (see section "Processes of energy conversion in mitochondria") provide a telling example. Apparently, plants have developed sophisticated mechanisms for—tightly regulated—energy *dissipation*, which is in obvious contrast to energy *efficiency* being, under all circumstances, a key trait for fitness. Another interesting case study refers to the breeding of salt-tolerant crops. The apparently "futile" cycling of Na^+ at the plasma membrane of root cortical cells has been identified as an important energy sink, and eliminating this trait has been defined as a goal in breeding salt-tolerant crops (Munns et al., 2020b). However, if this Na^+ cycling has a function in water acquisition as discussed by Munns et al. (2020a) loosing this trait will imply the loss of a potentially important function, with unforeseen costs and consequences for the entire organism. In fact, ionic cycling across the plasma membrane can be an investment into maintaining cellular homeostasis (Dreyer, 2021; see also the Introduction). We also have to keep in mind that under many environmental conditions, the availability of energy is not the rate-limiting factor for plant survival—rather, it is the availability of water, certain nutrients, or the avoidance of biotic or abiotic stressors. This is particularly true for (crop) plants growing in warm climates. Lynch has stressed the importance of searching for traits which allow for a resource-efficient agriculture, particularly in developing countries (Lynch, 2007b, 2015, 2022), but an efficient use of *energy* may not always be the major concern. At least this may not be a general concern, and hidden trade-offs need to be considered. For example, P deficiency tends to come with an energy deficit due to its effect on the adenylate availability, which will feed back on the respiration rate (see section "Processes of energy conversion in mitochondria"). In a recent broad meta-analysis, Han and Zhu (2021) investigated correlations between root morphological traits and root respiration and did not find a convincing relationship for traits like specific root length and root diameter, suggesting that interactions may be more complex and species-dependent. New approaches in quantitative modeling of plant performance with respect to certain parameters such as energy use efficiency will become available in the near future, such as those pioneered by Foster and Miklavcic (2020) and Arsova et al. (2020). Instead of just opting for "energy-efficient" plants, the task will rather be to find the best trade-off between energy efficiency and function, and to find algorithms reflecting this trade-off in the best way.

Author contributions

The author confirms being the sole contributor of this work and has approved it for publication.

Funding

This work was supported by a grant of the National Science Foundation of China to LW (grant no. 32070277).

Conflict of interest

The author declares that the research was conducted in the absence of any commercial or financial relationships that could be construed as a potential conflict of interest.

Publisher's note

References

Amthor, J. S. (2000). The McCree–de wit–penning de Vries–Thornley respiration paradigms: 30 years later. *Ann. Bot.* 86, 1–20. doi: 10.1006/anbo.2000.1175

Arsova, B., Foster, K. J., Shelden, M. C., Bramley, H., and Watt, M. (2020). Dynamics in plant roots and shoots minimize stress, save energy and maintain water and nutrient uptake. *New Phytol.* 225, 1111–1119. doi: 10.1111/nph.15955

Atkinson, C. J., and Farrar, J. F. (1983). Allocation of photosynthetically fixed carbon in *Festuca ovina* L. and *Nardus stricta* L. *New Phytol.* 95, 519–531. doi: 10.1111/j.1469-8137.1983.tb03517.x

Bendall, D. S., and Bonner, W. D. Jr. (1971). Cyanide-insensitive respiration in plant mitochondria. *Plant Physiol.* 47, 236–245. doi: 10.1104/pp.47.2.236

Bingham, I. J., and Stevenson, E. A. (1993). Control of root growth: effects of carbohydrates on the extension, branching and rate of respiration of different fractions of wheat roots. *Physiol. Plant.* 88, 149–158. doi: 10.1111/j.1399-3054.1993.tb01772.x

Bloom, A. J., Chapin, F. S. III, and Mooney, H. A. (1985). Resource limitation in plants-an economic analogy. *Annu. Rev. Ecol. Syst.* 16, 363–392. doi: 10.1146/annurev.es.16.110185.002051

Bouma, T. J., and De Visser, R. (1993). Energy requirements for maintenance of ion concentrations in roots. *Physiol. Plant.* 89, 133–142. doi: 10.1111/j.1399-3054.1993.tb01796.x

Bouma, T. J., De Visser, R., Janssen, J., De Kock, M. J., Van Leeuwen, P. H., and Lambers, H. (1994). Respiratory energy requirements and rate of protein turnover in vivo determined by the use of an inhibitor of protein synthesis and a probe to assess its effect. *Physiol. Plant.* 92, 585–594. doi: 10.1111/j.1399-3054.1994.tb03027.x

Briskin, D. P., Basu, S., and Assmann, S. M. (1995). Characterization of the red beet plasma membrane H^+-ATPase reconstituted in a planar bilayer system. *Plant Physiol.* 108, 393–398. doi: 10.1104/pp.108.1.393

Briskin, D. P., and Reynolds-Niesman, I. (1991). Determination of H—/ATP stoichiometry for the plasma membrane H^+-ATPase from red beet (*Beta vulgaris* L.) storage tissue. *Plant Physiol.* 95, 242–250. doi: 10.1104/pp.95.1.242

Carroll, A. D., Fox, G. G., Laurie, S., Phillips, R., Ratcliffe, R. G., and Stewart, G. R. (1994). Ammonium assimilation and the role of [gamma]-aminobutyric acid in pH homeostasis in carrot cell suspensions. *Plant Physiol.* 106, 513–520. doi: 10.1104/pp.106.2.513

Che-Othman, M. H., Jacoby, R. P., Millar, A. H., and Taylor, N. L. (2020). Wheat mitochondrial respiration shifts from the tricarboxylic acid cycle to the GABA shunt under salt stress. *New Phytol.* 225, 1166–1180. doi: 10.1111/nph.15713

Clifton, R., Lister, R., Parker, K. L., Sappl, P. G., Elhafez, D., Millar, A. H., et al. (2005). Stress-induced co-expression of alternative respiratory chain components in *Arabidopsis thaliana*. *Plant Mol. Biol.* 58:193. doi: 10.1007/s11103-005-5514-7

Clifton, R., Millar, A. H., and Whelan, J. (2006). Alternative oxidases in Arabidopsis: a comparative analysis of differential expression in the gene family provides new insights into function of non-phosphorylating bypasses. *Biochim. Biophys. Acta Bioenerg.* 1757, 730–741. doi: 10.1016/j.bbabio.2006.03.009

Colombi, T., Herrmann, A. M., Vallenback, P., and Keller, T. (2019). Cortical cell diameter is key to energy costs of root growth in wheat. *Plant Physiol.* 180, 2049–2060. doi: 10.1104/pp.19.00262

Costa, J. H., Jolivet, Y., Hasenfratz-Sauder, M.-P., Orellano, E. G., Lima, M. D. G. S., Dizengremel, P., et al. (2007). Alternative oxidase regulation in roots of *Vigna unguiculata* cultivars differing in drought/salt tolerance. *J. Plant Physiol.* 164, 718–727. doi: 10.1016/j.jplph.2006.04.001

Crawford, L. A., Bown, A. W., Breitkreuz, K. E., and Guinel, F. C. (1994). The synthesis of [gamma]-aminobutyric acid in response to treatments reducing cytosolic pH. *Plant Physiol.* 104, 865–871. doi: 10.1104/pp.104.3.865

Davies, J. M. (1997). Vacuolar energization: pumps, shunts and stress. *J. Exp. Bot.* 48, 633–641. doi: 10.1093/jxb/48.3.633

Day, D. A., Millar, A. H., Wiskich, J. T., and Whelan, J. (1994). Regulation of alternative oxidase activity by pyruvate in soybean mitochondria. *Plant Physiol.* 106, 1421–1427. doi: 10.1104/pp.106.4.1421

De Block, M., and Van Lijsebettens, M. (2011). Energy efficiency and energy homeostasis as genetic and epigenetic components of plant performance and crop productivity. *Curr. Opin. Plant Biol.* 14, 275–282. doi: 10.1016/j.pbi.2011.02.007

Demirel, Y., and Sandler, S. I. (2002). Thermodynamics and bioenergetics. *Biophys. Chem.* 97, 87–111. doi: 10.1016/S0301-4622(02)00069-8

Dreyer, I. (2021). Nutrient cycling is an important mechanism for homeostasis in plant cells. *Plant Physiol.* 187, 2246–2261. doi: 10.1093/plphys/kiab217

Ducet, G., Gidrol, X., and Richaud, P. (1983). Membrane potential changes in coupled potato mitochondria. *Physiol. Veg.* 21, 385–394.

Dupré, J. A., and Nicholson, D. (2018). "A manifesto for a processual philosophy of biology," in *Everything Flows: Towards a processual Philosophy of Biology*. eds. D. Nicholson and J. A. Dupré (Oxford, UK: Oxford University Press), 4–45.

Dupuy, L. X., Mimault, M., Patko, D., Ladmiral, V., Ameduri, B., MacDonald, M. P., et al. (2018). Micromechanics of root development in soil. *Curr. Opin. Genet. Dev.* 51, 18–25. doi: 10.1016/j.gde.2018.03.007

Edwards, S., Nguyen, B.-T., Do, B., and Roberts, J. K. (1998). Contribution of malic enzyme, pyruvate kinase, phosphoenol pyruvate carboxylase, and the Krebs cycle to respiration and biosynthesis and to intracellular pH regulation during hypoxia in maize root tips observed by nuclear magnetic resonance imaging and gas chromatography-mass spectrometry. *Plant Physiol.* 116, 1073–1081. doi: 10.1104/pp.116.3.1073

Efe, C., Straathof, A. J., and van der Wielen, L. A. (2008). Options for biochemical production of 4-hydroxybutyrate and its lactone as a substitute for petrochemical production. *Biotechnol. Bioeng.* 99, 1392–1406. doi: 10.1002/bit.21709

Evans, D. E. (2004). Aerenchyma formation. *New Phytol.* 161, 35–49. doi: 10.1046/j.1469-8137.2003.00907.x

Falhof, J., Pedersen, J. T., Fuglsang, A. T., and Palmgren, M. (2016). Plasma membrane H^+-ATPase regulation in the center of plant physiology. *Mol. Plant* 9, 323–337. doi: 10.1016/j.molp.2015.11.002

Fanello, D. D., Kelly, S. J., Bartoli, C. G., Cano, M. G., Alonso, S. M., and Guiamet, J. J. (2020). Plasticity of root growth and respiratory activity: root responses to above-ground senescence, fruit removal or partial root pruning in soybean. *Plant Sci.* 290:110296. doi: 10.1016/j.plantsci.2019.110296

Felle, H. H. (2001). pH: signal and messenger in plant cells. *Plant Biol.* 3, 577–591. doi: 10.1055/s-2001-19372

Fitter, A. H. (1991). Costs and benefits of mycorrhizas: implications for functioning under natural conditions. *Experientia* 47, 350–355. doi: 10.1007/BF01972076

Foster, K. J., and Miklavcic, S. J. (2020). A comprehensive biophysical model of ion and water transport in plant roots. III. Quantifying the energy costs of ion transport in salt-stressed roots of Arabidopsis. *Front. Plant Sci.* 11:865. doi: 10.3389/fpls.2020.00865

Geilfus, C.-M. (2017). The pH of the apoplast: dynamic factor with functional impact under stress. *Mol. Plant* 10, 1371–1386. doi: 10.1016/j.molp.2017.09.018

Graham, L. E., Cook, M. E., and Busse, J. S. (2000). The origin of plants: body plan changes contributing to a major evolutionary radiation. *Proc. Nat. Acad. Sci. U.S.A.* 97, 4535–4540. doi: 10.1073/pnas.97.9.4535

Groff, P. A., and Kaplan, D. R. (1988). The relation of root systems to shoot systems in vascular plants. *Bot. Rev.* 54, 387–422. doi: 10.1007/BF02858417

Han, M., Feng, J., Chen, Y., Sun, L., Fu, L., and Zhu, B. (2021). Mycorrhizal mycelial respiration: a substantial component of soil respired CO_2. *Soil Biol. Biochem.* 163:108454. doi: 10.1016/j.soilbio.2021.108454

Han, M., and Zhu, B. (2021). Linking root respiration to chemistry and morphology across species. *Glob. Chang. Biol.* 27, 190–201. doi: 10.1111/gcb.15391

Heinemeyer, A., Hartley, I. P., Evans, S. P., Carreira de La Fuente, J. A., and Ineson, P. (2007). Forest soil CO_2 flux: uncovering the contribution and environmental responses of ectomycorrhizas. *Glob. Chang. Biol.* 13, 1786–1797. doi: 10.1111/j.1365-2486.2007.01383.x

Herrmann, A. M., and Colombi, T. (2019). Energy use efficiency of root growth–a theoretical bioenergetics framework. *Plant Signal. Behav.* 14, 1685147. doi: 10.1080/15592324.2019.1685147

Hoffmann, R. D., Olsen, L. I., Ezike, C. V., Pedersen, J. T., Manstretta, R., López-Marqués, R. L., et al. (2019). Roles of plasma membrane proton ATPases AHA2 and AHA7 in normal growth of roots and root hairs in *Arabidopsis thaliana*. *Physiol. Plant.* 166, 848–861. doi: 10.1111/ppl.12842

Hopkins, F., Gonzalez-Meler, M. A., Flower, C. E., Lynch, D. J., Czimczik, C., Tang, J., et al. (2013). Ecosystem-level controls on root-rhizosphere respiration. *New Phytol.* 199, 339–351. doi: 10.1111/nph.12271

Hourton-Cabassa, C., Rita Matos, A., Zachowski, A., and Moreau, F. (2004). The plant uncoupling protein homologues: a new family of energy-dissipating proteins in plant mitochondria. *Plant Physiol. Biochem.* 42, 283–290. doi: 10.1016/j.plaphy.2004.01.007

Hughes, J. K., Hodge, A., Fitter, A. H., and Atkin, O. K. (2008). Mycorrhizal respiration: implications for global scaling relationships. *Trends Plant Sci.* 13, 583–588. doi: 10.1016/j.tplants.2008.08.010

Israel, H. W., and Steward, F. C. (1967). The fine structure and development of plastids in cultured cells of *Daucus carota*. *Ann. Bot.* 31, 1–18. doi: 10.1093/oxfordjournals.aob.a084118

Janicka-Russak, M., Kabała, K., Wdowikowska, A., and Kłobus, G. (2013). Modification of plasma membrane proton pumps in cucumber roots as an adaptation mechanism to salt stress. *J. Plant Physiol.* 170, 915–922. doi: 10.1016/j.jplph.2013.02.002

Jia, S., Wang, Z., Li, X., Zhang, X., and Mclaughlin, N. B. (2011). Effect of nitrogen fertilizer, root branch order and temperature on respiration and tissue N concentration of fine roots in Larix gmelinii and *Fraxinus mandshurica*. *Tree Physiol.* 31, 718–726. doi: 10.1093/treephys/tpr057

Lambers, H., Atkin, O. K., and Millenaar, F. F. (2002). "Respiratory patterns in roots in relation to their functioning," in *Plant Roots: The Hidden Half*. eds. Y. Waisel, A. Eshel, T. Beekman and U. Kafkafi (Boca Raton: CRC Press), 810–866.

Lambers, H., and Oliveira, R. S. (2019). "Photosynthesis, respiration, and long-distance transport: respiration," in *Plant Physiological Ecology*. eds. H. Lambers and R. S. Oliveira (Cham: Springer International Publishing), 115–172.

Le, X. H., Lee, C.-P., and Millar, A. H. (2021a). The mitochondrial pyruvate carrier (MPC) complex mediates one of three pyruvate-supplying pathways that sustain Arabidopsis respiratory metabolism. *Plant Cell* 33, 2776–2793. doi: 10.1093/plcell/koab148

Le, X. H., Lee, C.-P., Monachello, D., and Millar, A. H. (2021b). Metabolic evidence for distinct pyruvate pools inside plant mitochondria. bioRxiv [Preprint]. doi: 10.1038/s41477-022-01165-3

Lee, T. A., and Bailey-Serres, J. (2021). Conserved and nuanced hierarchy of gene regulatory response to hypoxia. *New Phytol.* 229, 71–78. doi: 10.1111/nph.16437

Loreti, E., and Perata, P. (2020). The many facets of hypoxia in plants. *Plan. Theory* 9, 745. doi: 10.3390/plants9060745

Luo, Y., and Zhou, X. (2006). *Soil Respiration and the Environment*. London: Academic Press.

Lynch, J. (1995). Root architecture and plant productivity. *Plant Physiol.* 109, 7–13. doi: 10.1104/pp.109.1.7

Lynch, J. P. (2007a). Rhizoeconomics: the roots of shoot growth limitations. *HortScience* 42, 1107–1109. doi: 10.21273/HORTSCI.42.5.1107

Lynch, J. P. (2007b). Roots of the second green revolution. *Aust. J. Bot.* 55, 493–512. doi: 10.1071/BT06118

Lynch, J. P. (2013). Steep, cheap and deep: an ideotype to optimize water and N acquisition by maize root systems. *Ann. Bot.* 112, 347–357. doi: 10.1093/aob/mcs293

Lynch, J. P. (2015). Root phenes that reduce the metabolic costs of soil exploration: opportunities for 21st century agriculture. *Plant Cell Environ.* 38, 1775–1784. doi: 10.1111/pce.12451

Lynch, J. P. (2019). Root phenotypes for improved nutrient capture: an underexploited opportunity for global agriculture. *New Phytol.* 223, 548–564. doi: 10.1111/nph.15738

Lynch, J. P. (2022). Harnessing root architecture to address global challenges. *Plant J.* 109, 415–431. doi: 10.1111/tpj.15560

Lynch, J. P., and Ho, M. D. (2005). Rhizoeconomics: carbon costs of phosphorus acquisition. *Plant Soil* 269, 45–56. doi: 10.1007/s11104-004-1096-4

Lynch, J. P., Strock, C. F., Schneider, H. M., Sidhu, J. S., Ajmera, I., Galindo-Castañeda, T., et al. (2021). Root anatomy and soil resource capture. *Plant Soil* 466, 21–63. doi: 10.1007/s11104-021-05010-y

Macrae, A. R., and Moorhouse, R. (1970). Oxidation of malate by mitochondria isolated from cauliflower buds. *Eur. J. Biochem.* 16, 96–102. doi: 10.1111/j.1432-1033.1970.tb01058.x

Makita, N., Fujimoto, R., and Tamura, A. (2021). The contribution of roots, mycorrhizal hyphae, and soil free-living microbes to soil respiration and its temperature sensitivity in a larch forest. *Forests* 12, 1410. doi: 10.3390/f12101410

Malagoli, P., Britto, D. T., Schulze, L. M., and Kronzucker, H. J. (2008). Futile Na^+ cycling at the root plasma membrane in rice (*Oryza sativa* L.): kinetics, energetics, and relationship to salinity tolerance. *J. Exp. Bot.* 59, 4109–4117. doi: 10.1093/jxb/ern249

Martí, C. M., Florez-Sarasa, I., Camejo, D., Ribas-Carbó, M., Lázaro, J. J., Sevilla, F., et al. (2011). Response of mitochondrial thioredoxin PsTrxo1, antioxidant enzymes, and respiration to salinity in pea (*Pisum sativum* L.) leaves. *J. Exp. Bot.* 62, 3863–3874. doi: 10.1093/jxb/err076

Martinière, A., Desbrosses, G., Sentenac, H., and Paris, N. (2013). Development and properties of genetically encoded pH sensors in plants. *Front. Plant Sci.* 4:523. doi: 10.3389/fpls.2013.00523

May, B., Young, L., and Moore, A. L. (2017). Structural insights into the alternative oxidases: are all oxidases made equal? *Biochem. Soc. Trans.* 45, 731–740. doi: 10.1042/BST20160178

Mhadhbi, H., Fotopoulos, V., Mylona, P. V., Jebara, M., Aouani, M. E., Alexios, N., et al. (2013). Alternative oxidase 1 (Aox1) gene expression in roots of *Medicago truncatula* is a genotype-specific component of salt stress tolerance. *J. Plant Physiol.* 170, 111–114. doi: 10.1016/j.jplph.2012.08.017

Millenaar, F. F., and Lambers, H. (2003). The alternative oxidase: in vivo regulation and function. *Plant Biol.* 5, 2–15. doi: 10.1055/s-2003-37974

Moore, A. L., and Rich, P. R. (1980). The bioenergetics of plant mitochondria. *Trends Biochem. Sci.* 5, 284–288. doi: 10.1016/0968-0004(80)90160-7

Moore, A. L., Shiba, T., Young, L., Harada, S., Kita, K., and Ito, K. (2013). Unraveling the heater: new insights into the structure of the alternative oxidase. *Annu. Rev. Plant Biol.* 64, 637–663. doi: 10.1146/annurev-arplant-042811-105432

Moyano, F. E., Kutsch, W. L., and Schulze, E.-D. (2007). Response of mycorrhizal, rhizosphere and soil basal respiration to temperature and photosynthesis in a barley field. *Soil Biol. Biochem.* 39, 843–853. doi: 10.1016/j.soilbio.2006.10.001

Munns, R., Day, D. A., Fricke, W., Watt, M., Arsova, B., Barkla, B. J., et al. (2020a). Energy costs of salt tolerance in crop plants. *New Phytol.* 225, 1072–1090. doi: 10.1111/nph.15864

Munns, R., Passioura, J. B., Colmer, T. D., and Byrt, C. S. (2020b). Osmotic adjustment and energy limitations to plant growth in saline soil. *New Phytol.* 225, 1091–1096. doi: 10.1111/nph.15862

Neumann, J., and Matzner, E. (2014). Contribution of newly grown extramatrical ectomycorrhizal mycelium and fine roots to soil respiration in a young Norway spruce site. *Plant Soil* 378, 73–82. doi: 10.1007/s11104-013-2018-0

Nicholls, D. G. (2013). *Bioenergetics. 4th Edn.* (Amsterdam: Elsevier).

Nielsen, K. L., Eshel, A., and Lynch, J. P. (2001). The effect of phosphorus availability on the carbon economy of contrasting common bean (*Phaseolus vulgaris* L.) genotypes. *J. Exp. Bot.* 52, 329–339. doi: 10.1093/jexbot/52.355.329

Peters, W. S., and Felle, H. H. (1999). The correlation of profiles of surface pH and elongation growth in maize roots. *Plant Physiol.* 121, 905–912. doi: 10.1104/pp.121.3.905

Peuke, A. D., Windt, C., and Van As, H. (2006). Effects of cold-girdling on flows in the transport phloem in *Ricinus communis*: is mass flow inhibited? *Plant Cell Environ.* 29, 15–25. doi: 10.1111/j.1365-3040.2005.01396.x

Poorter, H., der Werf, A. V., Atkin, O. K., and Lambers, H. (1991). Respiratory energy requirements of roots vary with the potential growth rate of a plant species. *Physiol. Plant.* 83, 469–475. doi: 10.1111/j.1399-3054.1991.tb00122.x

Ramesh, S. A., Tyerman, S. D., Gilliham, M., and Xu, B. (2017). γ-Aminobutyric acid (GABA) signalling in plants. *Cell. Mol. Life Sci.* 74, 1577–1603. doi: 10.1007/s00018-016-2415-7

Raven, J. A., and Edwards, D. (2001). Roots: evolutionary origins and biogeochemical significance. *J. Exp. Bot.* 52, 381–401. doi: 10.1093/jxb/52.suppl_1.381

Renault, H., El Amrani, A., Berger, A., Mouille, G., Soubigou-Taconnat, L., Bouchereau, A., et al. (2013). γ-Aminobutyric acid transaminase deficiency impairs central carbon metabolism and leads to cell wall defects during salt stress in Arabidopsis roots. *Plant Cell Environ.* 36, 1009–1018. doi: 10.1111/pce.12033

Renault, H., Roussel, V., El Amrani, A., Arzel, M., Renault, D., Bouchereau, A., et al. (2010). The Arabidopsis pop2-1mutant reveals the involvement of GABA transaminase in salt stress tolerance. *BMC Plant Biol.* 10, 20. doi: 10.1186/1471-2229-10-20

Rochette, P., and Hutchinson, G. (2005). Measurement of soil respiration in situ: chamber techniques. Publications from USDA-ARS/UNL Faculty. Available at: https://digitalcommons.unl.edu/usdaarsfacpub/1379

Ruehr, N. K., and Buchmann, N. (2010). Soil respiration fluxes in a temperate mixed forest: seasonality and temperature sensitivities differ among microbial and root–rhizosphere respiration. *Tree Physiol.* 30, 165–176. doi: 10.1093/treephys/tpp106

Rustin, P., Moreau, F., and Lance, C. (1980). Malate oxidation in plant mitochondria via malic enzyme and the cyanide-insensitive electron transport pathway. *Plant Physiol.* 66, 457–462. doi: 10.1104/pp.66.3.457

Salvioli di Fossalunga, A., and Novero, M. (2019). To trade in the field: the molecular determinants of arbuscular mycorrhiza nutrient exchange. *Chem. Biol. Technol. Agric.* 6, 1–12. doi: 10.1186/s40538-019-0150-7

Salvioli, A., Ghignone, S., Novero, M., Navazio, L., Venice, F., Bagnaresi, P., et al. (2016). Symbiosis with an endobacterium increases the fitness of a mycorrhizal fungus, raising its bioenergetic potential. *ISME J.* 10, 130–144. doi: 10.1038/ismej.2015.91

Santi, S., and Schmidt, W. (2009). Dissecting iron deficiency-induced proton extrusion in Arabidopsis roots. *New Phytol.* 183, 1072–1084. doi: 10.1111/j.1469-8137.2009.02908.x

Scheurwater, I., Cornelissen, C., Dictus, F., Welschen, R., and Lambers, H. (1998). Why do fast-and slow-growing grass species differ so little in their rate of root respiration, considering the large differences in rate of growth and ion uptake? *Plant Cell Environ.* 21, 995–1005. doi: 10.1046/j.1365-3040.1998.00341.x

Schwarzländer, M., Logan, D. C., Johnston, I. G., Jones, N. S., Meyer, A. J., Fricker, M. D., et al. (2012). Pulsing of membrane potential in individual mitochondria: a stress-induced mechanism to regulate respiratory bioenergetics in Arabidopsis. *Plant Cell* 24, 1188–1201. doi: 10.1105/tpc.112.096438

Shabala, S., Chen, G., Chen, Z.-H., and Pottosin, I. (2020). The energy cost of the tonoplast futile sodium leak. *New Phytol.* 225, 1105–1110. doi: 10.1111/nph.15758

Shabala, L., Ross, T., McMeekin, T., and Shabala, S. (2006). Non-invasive microelectrode ion flux measurements to study adaptive responses of microorganisms to the environment. *FEMS Microbiol. Rev.* 30, 472–486. doi: 10.1111/j.1574-6976.2006.00019.x

Shao, Y., Feng, X., Nakahara, H., Irshad, M., Eneji, A. E., Zheng, Y., et al. (2021). Apical-root apoplastic acidification affects cell wall extensibility in wheat under salinity stress. *Physiol. Plant.* 173, 1850–1861. doi: 10.1111/ppl.13527

Shelp, B. J., Bown, A. W., and McLean, M. D. (1999). Metabolism and functions of gamma-aminobutyric acid. *Trends Plant Sci.* 4, 446–452. doi: 10.1016/S1360-1385(99)01486-7

Smith, C. A., Melino, V. J., Sweetman, C., and Soole, K. L. (2009). Manipulation of alternative oxidase can influence salt tolerance in *Arabidopsis thaliana*. *Physiol. Plant.* 137, 459–472. doi: 10.1111/j.1399-3054.2009.01305.x

Steigmiller, S., Turina, P., and Gräber, P. (2008). The thermodynamic H^+/ATP ratios of the H^+-ATPsynthases from chloroplasts and *Escherichia coli*. Proceedings of the National Academy of Sciences of the USA 105, 3745–3750. doi: 10.1073/pnas.0708356105

Sweetman, C., Waterman, C. D., Rainbird, B. M., Smith, P. M. C., Jenkins, C. D., Day, D. A., et al. (2019). AtNDB2 Is the main external NADH dehydrogenase in mitochondria and Is important for tolerance to environmental stress. *Plant Physiol.* 181, 774–788. doi: 10.1104/pp.19.00877

Tomè, E., Ventura, M., Folegot, S., Zanotelli, D., Montagnani, L., Mimmo, T., et al. (2016). Mycorrhizal contribution to soil respiration in an apple orchard. *Appl. Soil Ecol.* 101, 165–173. doi: 10.1016/j.apsoil.2016.01.016

Uga, Y. (2021). Challenges to design-oriented breeding of root system architecture adapted to climate change. *Breed. Sci.* 71, 3–12. doi: 10.1270/jsbbs.20118

Vanlerberghe, G. C. (2013). Alternative oxidase: a mitochondrial respiratory pathway to maintain metabolic and signaling homeostasis during abiotic and biotic stress in plants. *Int. J. Mol. Sci.* 14, 6805–6847. doi: 10.3390/ijms14046805

Vanlerberghe, G. C., Dahal, K., Alber, N. A., and Chadee, A. (2020). Photosynthesis, respiration and growth: a carbon and energy balancing act for alternative oxidase. *Mitochondrion* 52, 197–211. doi: 10.1016/j.mito.2020.04.001

Vannini, C., Carpentieri, A., Salvioli, A., Novero, M., Marsoni, M., Testa, L., et al. (2016). An interdomain network: the endobacterium of a mycorrhizal fungus promotes antioxidative responses in both fungal and plant hosts. *New Phytol.* 211, 265–275. doi: 10.1111/nph.13895

Venice, F., de Pinto, M. C., Novero, M., Ghignone, S., Salvioli, A., and Bonfante, P. (2017). Gigaspora margarita with and without its endobacterium shows adaptive responses to oxidative stress. *Mycorrhiza* 27, 747–759. doi: 10.1007/s00572-017-0790-z

Volkov, V., Flowers, T. J., Zhukovskaya, N. V., and Ivanov, V. B. (2021). "Root growth and structure of growth zone in halophytes and glycophytes under salinity: role of ion transport," in *Handbook of Halophytes: From Molecules to Ecosystems Towards Biosaline Agriculture*. ed. M. N. Grigore (Cham: Springer), 1351–1393.

Wachsman, G., Sparks, E. E., and Benfey, P. N. (2015). Genes and networks regulating root anatomy and architecture. *New Phytol.* 208, 26–38. doi: 10.1111/nph.13469

Wagner, A. M., and Krab, K. (1995). The alternative respiration pathway in plants: role and regulation. *Physiol. Plant.* 95, 318–325. doi: 10.1111/j.1399-3054.1995.tb00844.x

Wagner, A. M., Krab, K., Wagner, M. J., and Moore, A. L. (2008). Regulation of thermogenesis in flowering Araceae: The role of the alternative oxidase. *Biochim. Biophys. Acta Bioenerg. BBA* 1777, 993–1000. doi: 10.1016/j.bbabio.2008.04.001

Wagner, A. M., and Moore, A. L. (1997). Structure and function of the plant alternative oxidase: its putative role in the oxygen defence mechanism. *Biosci. Rep.* 17, 319–333. doi: 10.1023/A:1027388729586

Wagner, S., Van Aken, O., Elsässer, M., and Schwarzländer, M. (2018). Mitochondrial energy signaling and its role in the low-oxygen stress response of plants. *Plant Physiol.* 176, 1156–1170. doi: 10.1104/pp.17.01387

Wang, W., and Fang, J. (2009). Soil respiration and human effects on global grasslands. *Glob. Planet. Chang.* 67, 20–28. doi: 10.1016/j.gloplacha.2008.12.011

Wegner, L. H. (2010). "Oxygen transport in waterlogged plants," in *Waterlogging Signalling and Tolerance in Plants*. eds. S. Mancuso and S. Shabala (Berlin, Heidelberg: Springer), 3–22.

Wegner, L. H. (2015). A thermodynamic analysis of the feasibility of water secretion into xylem vessels against a water potential gradient. *Funct. Plant Biol.* 42, 828–835. doi: 10.1071/FP15077

Wegner, L. H., Li, X., Zhang, J., Yu, M., Shabala, S., and Hao, Z. (2021). Biochemical and biophysical pH clamp controlling net H^+ efflux across the plasma membrane of plant cells. *New Phytol.* 230, 408–415. doi: 10.1111/nph.17176

Wegner, L. H., and Shabala, S. (2020). Biochemical pH clamp: the forgotten resource in membrane bioenergetics. *New Phytol.* 225, 37–47. doi: 10.1111/nph.16094

Windt, C. W., Vergeldt, F. J., De Jager, P. A., and Van As, H. (2006). MRI of long-distance water transport: a comparison of the phloem and xylem flow characteristics and dynamics in poplar, castor bean, tomato and tobacco. *Plant Cell Environ.* 29, 1715–1729. doi: 10.1111/j.1365-3040.2006.01544.x

Wu, H., Zhang, X., Giraldo, J. P., and Shabala, S. (2018). It is not all about sodium: revealing tissue specificity and signalling roles of potassium in plant responses to salt stress. *Plant Soil* 431, 1–17. doi: 10.1007/s11104-018-3770-y

Yuan, W., Zhang, D., Song, T., Xu, F., Lin, S., Xu, W., et al. (2017). Arabidopsis plasma membrane H^+-ATPase genes AHA2 and AHA7 have distinct and overlapping roles in the modulation of root tip H^+ efflux in response to low-phosphorus stress. *J. Exp. Bot.* 68, 1731–1741. doi: 10.1093/jxb/erx040

Zioni, A. B., Vaadia, Y., and Lips, S. H. (1971). Nitrate uptake by roots as regulated by nitrate reduction products of the shoot. *Physiol. Plant.* 24, 288–290. doi: 10.1111/j.1399-3054.1971.tb03493.x

frontiers | Frontiers in Plant Science

TYPE Original Research
PUBLISHED 24 October 2022
DOI 10.3389/fpls.2022.918397

OPEN ACCESS

EDITED BY
Lars Hendrik Wegner,
Foshan University, China

REVIEWED BY
Huakun Zhou,
Key Laboratory of Restoration Ecology in Cold Regions (CAS), China
Sabine Dagmar Zimmermann,
Délégation Languedoc Roussillon (CNRS), France

*CORRESPONDENCE
Baisha Weng
baishaweng@163.com

SPECIALTY SECTION
This article was submitted to Plant Biophysics and Modeling, a section of the journal Frontiers in Plant Science

RECEIVED 12 April 2022
ACCEPTED 27 September 2022
PUBLISHED 24 October 2022

CITATION
Deng B, Weng B, Yan D, Xiao S, Fang H, Li M and Wang H (2022) Construction of root tip density function and root water uptake characteristics in alpine meadows. *Front. Plant Sci.* 13:918397. doi: 10.3389/fpls.2022.918397

Construction of root tip density function and root water uptake characteristics in alpine meadows

Bin Deng[1,2], Baisha Weng[1,3]*, Denghua Yan[1], Shangbin Xiao[2], Haotian Fang[2], Meng Li[4] and Hao Wang[1]

[1]State Key Laboratory of Simulation and Regulation of Water Cycle in River Basin, China Institute of Water Resources and Hydropower Research, Beijing, China, [2]Engineering Research Center of Eco-Environment in TGR Region, Ministry of Education, College of Hydraulic and Environmental Engineering, China Three Gorges University, Yichang, China, [3]Yinshanbeilu National Field Research Station of Steppe Eco-Hydrological System, China Institute of Water Resources and Hydropower Research, Hohhot, China, [4]Department of Hydraulic Engineering, Tsinghua University, Beijing, China

Accurate calculation of root water uptake (RWU) is the key to improving vegetation water use efficiency and identifying water cycle evolution patterns, and root tips play an important role in RWU. However, most of the current RWU models in the alpine meadow are calculated based on the root length density (RLD) function. In this study, a large number of roots, soil hydraulic conductivity, and physicochemical property indices were obtained by continuous field prototype observation experiments for up to 2 years. It was found that the RLD and root tip density (RTD) in alpine meadows decrease by 16.2% and 14.6%, respectively, in the wilting stage compared to the regreening stage. The RTD distribution function of the alpine meadow was constructed, and the RWU model was established accordingly. The results show that the RTD function is more accurate than the RLD function to reflect the RWU pattern. Compared with RLD, the simulated RWU model constructed by using RTD as the root index that can effectively absorb water increased by 24.64% on average, and the simulated values were more consistent with the actual situation. It can be seen that there is an underestimation of RWU calculated based on the RLD function, which leads to an underestimation of the effect of climate warming on evapotranspiration. The simulation results of the RWU model based on RTD showed that the RWU rate in the regreening stage increased by 30.24% on average compared with that in the wilting stage. Meanwhile, the top 67% of the rhizosphere was responsible for 86.76% of the total RWU on average. This study contributes to the understanding of the alpine meadow water cycle system and provides theoretical support for the implementation of alpine meadow vegetation protection and restoration projects.

KEYWORDS

alpine meadow, root tip, root tip density equation, root water uptake model, regularity of root water uptake

1 Introduction

Alpine meadows are a type of vegetation ecosystem unique to the Qinghai-Tibet Plateau (QTP). In the context of climate warming, the climatic characteristics of the QTP have been significantly affected (Yuke, 2019). The alpine meadow also shows a clear trend of degradation (Ma et al., 2017) due to its extremely fragile ecosystem (Jin et al., 2019). The key to plant growth is the ability to utilize water, and an accurate grasp of the water uptake capacity of plants will help to protect and restore the alpine meadow ecosystem reasonably. Meanwhile, plants and their roots are also an important part of the water cycle (Wu et al., 1999). Plants directly influence the distribution of soil water through root uptake (Liao et al., 2018), and the vast majority of the absorbed water is released to the atmosphere in the form of canopy transpiration in addition to its growing consumption, connecting soil water to the atmospheric environment (Hupet et al., 2002). Therefore, an accurate calculation of the amount of water absorbed by roots is essential to improving the efficiency of plant water use and also to helping in the identification of the evolutionary pattern of the water cycle (Metselaar and Lier, 2011).

A common approach to quantifying the rate of RWU is to build an RWU model for simulation (Ojha et al., 2009; Barkaoui et al., 2016); usually, a one-dimensional macroscopic RWU model is used (Cowan, 1965; Janott et al., 2011). The external factors that affect water uptake by plants are soil moisture and meteorological conditions (Lai and Katul, 2000; Hodge et al., 2009), and as the soil acts on RWU (Jha et al., 2017), the water content of the soil near the root zone is likewise changing (Jia et al., 2016). Considering the factors affecting soil moisture changes, it is necessary to analyze the influence of the soil's water dynamic characteristics on RWU (Guo et al., 2019; Zhang and Huang, 2021). The role of soil hydraulic conductivity as a key index of the changes produced by soil water dynamics (Lebron et al., 2007) cannot be ignored. Therefore, the characteristics of RWU distribution described by the Selim–Iskandar model (Fred and Molz, 1981), which combines root indicators with soil hydraulic conductivity, may be more accurate. The plant's factor that affects its water uptake capacity is the density of the root index that can effectively absorb water. Driven by the growth and transpiration demand of plants (Peter et al., 2018), plants absorb soil water through the action of the roots, and the density of the root index that can effectively absorb water determines the water uptake efficiency of the roots. Therefore, an accurate grasp of the root index that can effectively absorb water is the key to the simulation process.

Nowadays, the methods for simulating the RWU rate that includes root parameters are based on RLD as the root index that can effectively absorb water (Molz and Remson, 1970). In the past, it was difficult to measure the root index that can effectively absorb water, so an exponential type of RWU model was established using the RLD distribution function, which is simpler to measure as the root index that can effectively absorb water (Li et al., 1999), which has greatly improved the progress of the study of RWU models. The models widely used today are based on this type of approach and have been used extensively in the study of field crops and trees (Faria et al., 2010; dos Santos et al., 2016; Su et al., 2017). However, these models may have some errors in the simulation process due to the inaccurate description of the root index that can effectively absorb water.

It has been shown that the main sites of water uptake in plants are the hairy roots and root tips of the roots (Gilroy and Jones, 2000; Luo et al., 2000; Huang et al., 2020). Different areas on the root segments have different water permeabilities (Nancy and Ian, 2012), with hairy roots and root tips exhibiting higher permeability. Their growth expands the root index that can effectively absorb water (Segal et al., 2008), ensuring that the roots can absorb sufficient water from the soil for their own growth needs and respiratory consumption. Therefore, root tips play an important role in RWU, and RTD determines the water uptake capacity of the roots. Thus, this paper accurately measured the RTD distribution characteristics by the minirhizotron technique and used it as the root index that can effectively absorb water to assess the water uptake characteristics of plants. The established model is more consistent with the actual physical laws, and its simulation performance may be improved to a certain extent compared with the traditional model.

This study aims to identify the RWU pattern of alpine meadows and solve the problem of estimating the water consumption capacity of alpine meadow vegetation and its RWU simulation method. The flow of the study is shown in Figure 1. The functional equation of root tip distribution of alpine meadows is constructed with the meadow roots as the research object, and the accuracy of the soil water change state reflected by the model is evaluated when the RTD function and RLD function are used as the root index that can effectively absorb water of the model based on Selim–Iskandar's RWU model. To eliminate the effects caused by experimental errors, the model was validated using measured soil water content data from Exp. 1~4 at four experimental sites a, b, c, and d on the QTP. The established RWU model was used to simulate and analyze the RWU patterns of alpine meadows at different phenological stages and altitudes. The improved simulation method in this study will help the development of the RWU model and the simulation results will provide theoretical support for the study of vegetation ecohydrological cycle in alpine meadows and the implementation of vegetation restoration projects.

2 Materials and methods

2.1 Experimental sites

The study area is located in the hinterland of QTP (30°54′ ~32°43′N, 91°12′~92°54′E), and the experimental sites are

shown in Figure 1 and Table 1. The climate type is a typical semiarid monsoon climate of the plateau subduction zone, which generally shows thin air, abundant sunshine, and strong radiation, with an annual average sunshine time of 2,723 h. The weather is cold and dry with a large temperature difference between day and night. The temperature decreases with the increase in altitude and latitude, with an annual average temperature of -0.6°C, a maximum temperature of 14.5°C, and a minimum temperature of -30°C. Rainfall is unevenly distributed during the year, with the warm and wet period from June to October being the peak period for rainfall, which accounts for 82.9% of the year (Lu, 2017; Gong, 2019). The entire QTP is rich in vegetation species, and the study area shows the most typical *Kobresia pygmaea*, covering more than 80% of the area. The vegetation is more fragile and degraded to some extent (Jiang et al., 2020; Duan et al., 2021). The study area contains a variety of soil types such as bog soils, alluvial soils, and felty soils, among which felty soils are the most abundant, accounting for 67.5% of the total area of the study area.

2.2 Selection of experimental sites and installation of experimental equipment

The study area has unique geographical and climatic conditions typical of alpine regions. In alpine regions, altitude, soil water content, and soil hydraulic conductivity are three important environmental factors affecting root growth and water uptake capacity, which are also important criteria for the selection of the experimental sites in this study. To ensure that the location of the selected experimental sites can accurately reflect the overall vegetation and eco-hydrological characteristics of alpine meadows but also facilitate the safety of field experiments, after a long field study, we established four typical experimental sites in August 2018 (Figure 2A).

Four experimental sample sites with more consistent vegetation and soil conditions were selected before deployment. According to the root distribution characteristics of the alpine meadow, we dug out a deep pit of nearly 50 cm and placed soil water potential and moisture sensors (instrument type 5TM) at 5, 10, 20, and 35 cm each and then buried the pit

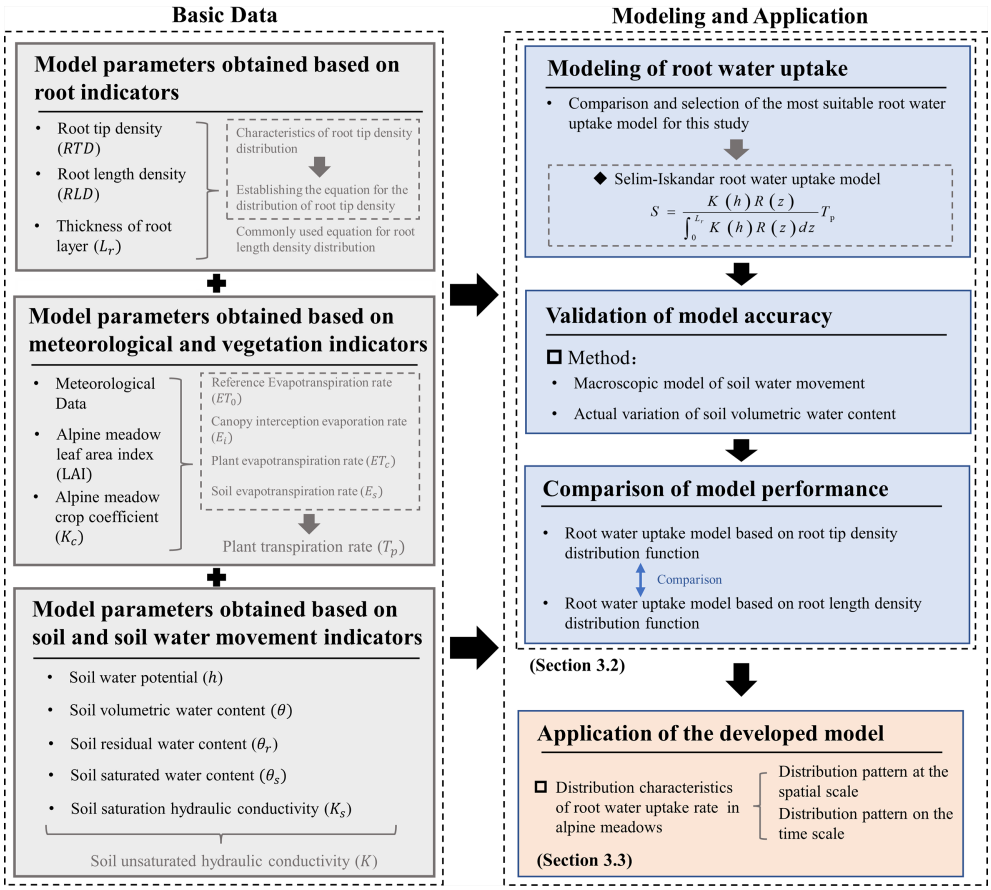

FIGURE 1
Research process.

TABLE 1 Measured experimental sites according to altitude (H), geographical location; soil type (ST) of experimental sites in the watershed obtained using remote sensing images; crop coefficients with mean values (k_{c1}) in the regreening stage and mean values (k_{c2}) in the wilting stage; the average leaf area index (LAI) for each location was obtained from the "National Tibetan Plateau Scientific Data Center" (http://data.Tpdc.ac.cn) (Zhang, 2021).

Sites	Longitude	Latitude	H (m)	ST	k_{c1}	k_{c2}	LAI
a	91°58′34″	31°25′4″	4460	Alpine meadow soil	0.68	0.42	1.44
b	91°41′34″	31°3′52″	4730	Alpine meadow soil	0.65	0.4	2.32
c	91°35′9″	32°16′47″	4760	Alpine meadow soil	0.55	0.33	1.29
d	91°49′26″	32°33′15″	5050	Alpine meadow soil	0.51	0.28	1.02

with the original soil to ensure that the soil could recover to its native state as quickly as possible (Figure 2D).

For root measurements using the minirhizotron technique (Figure 2D), minirhizotron tubes were laid out using the soil coring method at each experimental site in a circular hole dug at a depth of approximately 1 m and 30° in the vertical direction within four sample squares. A polyvinyl chloride transparent minirhizotron tube (1-m length, 6.4-cm inner diameter, 7-cm outer diameter) was inserted into the holes (Johnson et al., 2001); the mouth of the tube was covered with a cap and sealed with a void to prevent water infiltration, which could form water droplets on the inner wall and affect the subsequent minirhizotron window photography.

The installation of micro-root tubes can cut the plant roots and disturb the original state of the soil (Joslin and Wolfe, 1999), and the placement of soil sensors can also cause changes in soil temperature and humidity. Therefore, a 2-year recovery period for vegetation and soil ecology was given to each experimental site, while the experimental equipment was regularly checked and maintained, and the experimental monitoring was started in 2020.

2.3 Experimental design

2.3.1 Measurement of root indicators

Since this study focused on the RWU characteristics, the selection of the phenological stage was based on the phenological characteristics of the underground roots of alpine meadows. The

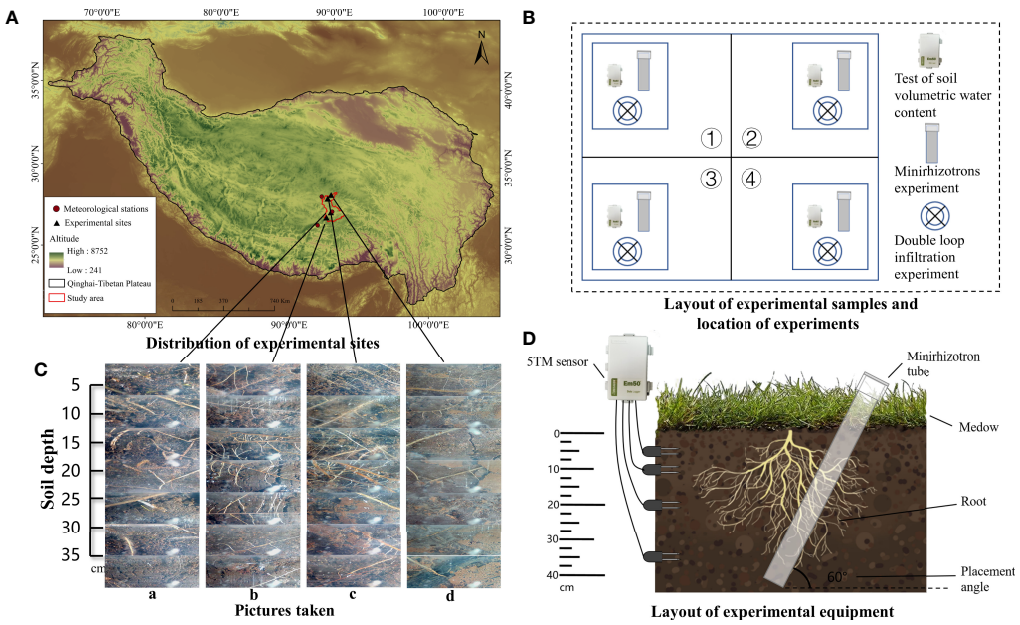

FIGURE 2
The distribution of experimental sites **(A)** and the meteorological stations selected for data are included, as well as the location of the study area and experimental sites. The layout of experimental samples and location of experiments **(B)** describes the distribution of the experimental sample at each experimental site, the location of each experiment. The pictures taken by the minirhizotron camera **(C)** and represent a set of photographs taken by the minirhizotron technique at sites a, b, c, and d at different soil depths, with significant variability in root density distribution at different experimental sites. The layout of experimental equipment **(D)** describes the method of deployment of the continuous soil water content and soil water potential testing instrument (5TM sensor) and minirhizotron tube.

beginning and end of the phenological period in the underground part of alpine meadows are the regreening and wilting stages. In the study area, the regreening stage is mainly concentrated in June and the wilting stage is concentrated in September each year. Considering this typical phenological feature, the experiment was conducted in June 2020 (Exp. 1), September 2020 (Exp. 2), June 2021 (Exp. 3), and September 2021 (Exp. 4).

The distribution of the experimental samples and the position of each experiment in the sample are shown in Figure 2B. We observed the morphological characteristics of plant roots through the minirhizotron technique [minirhizotron technique containing a minirhizotron tube, optical camera, calibration handle, controller, and computer (Ahrens and Reichstein, 2014)]. The camera was extended into the minirhizotron tube and moved down 5.8 cm at a time (about 5-cm vertical depth). The camera lens had a range of 2 cm × 2 cm and was rotated 45° after taking one photograph to ensure the integrity of the photograph. Eight consecutive photographs were taken and then moved down one layer until the roots could not be found in the lens. Based on this method, the minirhizotron tubes in the four sample squares of each experimental site were photographed (Figure 2C). It was found that almost no roots were found in the study area after 35 cm, so the thickness of the root layer was considered to be 35 cm (Table 2). The 896 root images taken were later processed by WinRHIZO TRON MF 2018b image analysis software to obtain root morphological data such as root tip number and root length. The RTD and RLD per unit soil volume were calculated by the formula:

$$D_{RT} = \frac{Tips}{A \,.\, DOF} \tag{1}$$

$$D_{RL} = \frac{L}{A \,.\, DOF} \tag{2}$$

where D_{RT} is the RTD per unit soil volume (tips.cm^{-3}); D_{RL} is the RLD per unit soil volume (cm.cm^{-3}); L is the total root length per layer observed by the minirhizotron camera (cm); *Tips* is the total number of root tips per soil layer observed by the minirhizotron camera; A is the area of the picture taken by the observation window (cm^2); and *DOF* is the distance from the minirhizotron camera to the surrounding photographed soil, which was taken as 0.3 cm (Wu et al., 2014).

2.3.2 Measurement of soil indicators and infiltration indicators

For the observation of root indicators, the water content and water potential values in the soil were obtained by reading the 5TM sensors in the sample cubes through the ECH2O Utility software, and the recording frequency was automatically recorded every 1 h. Soil water content (SWC) and soil water potential data for the regreening and wilting stages in 2020 and 2021 were used.

The double-ring infiltration experiments were conducted in four samples a, b, c, and d during the regreening and wilting stages in 2021 (Rnnqvist, 2018), and we obtained data on the saturated hydraulic conductivity of the soil at each experimental site in the study area during the regreening and wilting stages (Table 2). The experimental equipment was the DJ-IN12-W double-ring infiltrator, whose inner and outer ring diameters were 60 and 30 cm, respectively, to minimize the influence of soil spatial heterogeneity on the experiment (Li et al., 2019). The Mariotte tubes with volumes of 3 and 10 l were configured to supply water to the inner and outer rings, respectively.

Soil samples were collected at 5, 10, 20, and 35 cm using the soil coring method without destroying the minirhizotron tubes. Total organic matter, pH, total carbon, total nitrogen, total phosphorus, total salt, fast-acting potassium, saturated SWC, residual SWC, porosity, bulk weight, and agglomerate composition were measured in the laboratory according to international standards.

2.4 Construction and validation of a root water uptake model for alpine meadows

2.4.1 Construction of a root uptake model

In this paper, the Selim–Iskandar model (Fred and Molz, 1981) was selected to simulate the RWU by alpine meadows:

TABLE 2 The soil indicators and infiltration indexes for experimental sites a, b, c, and d which were measured in Exp. 1, Exp. 2, Exp. 3, and Exp. 4 are described, containing the thickness of the root layer (L_r); soil saturated hydraulic conductivity during the regreening and wilting stages (K_{s1} and K_{s2}); saturated soil water content (θ_s) and residual soil water content (θ_r); average soil water content in Exp. 1, Exp. 2, Exp. 3, and Exp. 4 (θ_1, θ_2, θ_3, θ_4); and L_1,L_2, and L_3 for soil depths of 0–10, 10–20, and 20–35 cm, respectively.

	L_r (cm)	K_{s1} (cm.min^{-1})	K_{s2} (cm.min^{-1})	θ_s (%)	θ_r (%)	θ_1 (%)			θ_2 (%)			θ_3 (%)			θ_4 (%)		
						L_1	L_2	L_3	L_1	L_2	L_3	L_1	L_2	L_3	L_1	L_2	L_3
a	35	0.012	0.013	38.62	12.17	27.51	28.24	22.38	21.72	14.14	17.05	24.3	28.5	27.3	22.45	26.09	20.48
b	35	0.099	0.17	32.64	7.43	14.82	14.03	12.94	11.85	12.66	11.32	17.92	27.66	9.78	19.03	15.74	12.39
c	35	0.095	0.076	40.41	15.87	21	23.19	27.64	17.01	20.48	23.11	20.72	20.37	23.92	20.79	20.3	24.75
d	35	0.068	0.057	28.27	7.41	14.96	22.31	21.75	16.03	10.4	10.83	20.64	24.38	22.53	16.41	24.06	22.29

$$S = \frac{K(h)R(z)}{\int_0^{L_r} K(h)R(z)dz} T_r \quad (3)$$

where S is the RWU rate (mm.day^{-1}); K (h) is the soil unsaturated hydraulic conductivity (cm.min^{-1}); $R(z)$ is the root density function that can effectively absorb water; L_r is the thickness of the root layer (cm); z is the depth from the ground surface (cm); and T_r is the plant transpiration rate (mm.day^{-1}).

The plant transpiration rates were simulated as follows (Belmans et al., 1983; Allen et al., 1998; Montero et al., 2001; Rouphael and Colla, 2004; Allen et al., 2006; Ojha et al., 2009; Fan, 2011; Genxu et al., 2012):

$$ET_c = K_c \times ET_0 \quad (4)$$

$$ET_0 = \frac{0.408\Delta(R_N - G) + \gamma \frac{900}{T+273} U_2(e_s - e_a)}{\Delta + \gamma(1 + 0.34U_2)} \quad (5)$$

$$E_i = 0.0025 \times F_c \times Ri^{0.34} \times T^{0.19} \quad (6)$$

$$E_s = ET_c \cdot f \cdot e^{-c \cdot LAI} \quad (7)$$

$$T_r = ET_c - E_s - E_i \quad (8)$$

where ET_c is the plant evapotranspiration rate (mm.day^{-1}); ET_0 is the vegetation reference evapotranspiration rate (mm.day^{-1}); k_c is the crop coefficient (Table 1); G is the sensible heat flux density from the surface to the soil (MJ.m^{-2}.d^{-1}); R_N is the net radiation (MJ.m^{-2}.d^{-1}) of vegetation; U_2 is the wind speed (m.s^{-1}) at the observed altitude; e_s is the saturation vapor pressure (kPa); e_a is the actual vapor pressure (kPa); Δ is the slope of the saturation vapor pressure versus temperature curve (kPa.°C^{-1}); γ is the humidity constant (kPa.°C^{-1}); T means the mean air temperature (°C) at the observed altitude; E_i is the canopy interception evaporation rate (mm.day^{-1}); F_c is the vegetation cover; R_i is the rainfall rate (mm.h^{-1}); E_s is the soil evapotranspiration rate; and f and c are regression coefficients. The plant transpiration rate at each experimental site is shown in Table 3.

The soil unsaturated hydraulic conductivity was simulated as follows (Mualem, 1976; van Genuchten, 1980):

$$S_e = \frac{\theta - \theta_r}{\theta_s - \theta_r} = [1 + (\eta h)^n]^{\frac{1}{n}-1} \quad (9)$$

$$K(h) = K_s S_e^{0.5} \left[1 - \left(1 - S_e^{\frac{1}{m}}\right)^m\right]^2 \quad (10)$$

where S_e is the effective soil saturation; θ is the measured soil water content (%) (Table 2); θ_s is the saturated soil water content (%);θ_r is the residual soil water content (%); h is the soil water potential (m); and n are empirical constants. Combined with the measured values, we obtained n and n for the individual experimental site by the inverse method.

The detailed calculation process and the acquisition method of each parameter are described in the Appendix.

2.4.2 Validation method of the root water uptake model

A macroscopic model of soil water movement considering RWU (Shao et al., 1986) can be tested for the RWU model, with the model equation:

$$\frac{\partial \theta}{\partial t} = \frac{\partial}{\partial z}\left[D(\theta)\frac{\partial \theta}{\partial z}\right] - \frac{\partial K(\theta)}{\partial z} - S(z,t) \quad (11)$$

where t is time; $D(\theta)$ is the soil water diffusion rate; $K(\theta)$ is the unsaturated soil hydraulic conductivity; and $S(z,t)$ is the RWU term. A discretization of the equation yields:

$$\frac{\theta_i^{j+1} - \theta_{i-1}^{j+1}}{\Delta t} = \frac{D_{i+\frac{1}{2}}^{j+1}(\theta_{i+1}^{j+1} - \theta_i^{j+1}) - D_{i-\frac{1}{2}}^{j+1}(\theta_i^{j+1} - \theta_{i-1}^{j+1})}{(\Delta z)^2} - \frac{(K_{i+1}^{j+1} + K_i^{j+1}) - (K_i^{j+1} + K_{i-1}^{j+1})}{2\Delta z} - S_i^{j+\frac{1}{2}} \quad (12)$$

The 35-cm soil layer is divided into seven layers equally, and the node number is defined as i. The spatial step Δz = 5 cm is set, the time step Δt = 1 day, and the node number is j. The initial conditions and boundaries are:

$$\begin{cases} \theta(z,0) = \theta_0(z) & 0 \le z \le L_r, t = 0 \\ -D(\theta)\frac{\partial \theta}{\partial z} + K(\theta) = -E_s & z = 0, t > 0 \\ \theta(L_r,t) = \theta_{L_r}(t) & z = L_r, t > 0 \end{cases} \quad (13)$$

TABLE 3 Plant transpiration rate at each experimental stage.

Sites	T_p (mm.day^{-1})			
	Exp. 1	Exp. 2	Exp. 3	Exp. 4
a	1.92	1.60	2.16	1.89
b	2.04	1.73	2.29	1.97
c	1.87	1.54	2.14	1.87
d	1.81	1.49	2.03	1.71

For the solution of the model, we calculate the soil water content on different soil layers based on the measured soil water content by equation recursion combined with numerical iterations.

In this paper, the root mean square error (RMSE) is used to assess the agreement between the simulation results of the model and the measured data:

$$RMSE = \sqrt{\frac{1}{n}\sum_{i=1}^{n}(S_i - M_i)^2} \quad (14)$$

where n is the number of measured data; S_i is the simulated value; and M_i is the measured value.

3 Results

3.1 Characteristics of alpine meadow root distribution and construction of distribution equation

3.1.1 Characteristics of root distribution in alpine meadows

The distribution of root indexes in alpine meadows is shown in Figure 3, and it shows a certain regularity in time and space. In terms of time, comparing the root density at the regreening stage and the wilting stage, we can find that the root density at the regreening stage of the alpine meadow is significantly greater than that at the wilting stage. Compared with the regreening stage, the RTD decreased by 14.6% and the RLD decreased by 16.2% on average in the wilting stage.

Spatially, from the lowest altitude a to the highest altitude d, both RTD and RLD showed a trend of increasing and then decreasing, and within the soil, there was a clear difference between the two root density indicators. At a, b, and c below the 5,000-m altitude, the maximum values of RTD were mainly concentrated in the middle layer of the rhizosphere, while the maximum values of RLD were mainly concentrated in the shallow layer of the rhizosphere. At d above 5,000 m, the distribution characteristics of RTD and RLD were very similar, both showing a trend of decreasing from shallow to deep.

3.1.2 Construction of root tip density equation and simulation of root distribution

There are obvious regularities in the distribution of RTD on the soil profile in alpine meadows. Therefore, in this paper, a generalized equation Eq 15 is constructed to fit the RTD distribution characteristics of alpine meadows, and the model equation is:

$$R(z) = \begin{cases} \left[1 + A_1 \ln\left(B_1 \frac{z}{Z}\right)\right] RTD_{\max} & z < z_{RTD_{\max}} \\ \frac{RTD^2_{\max}}{A_2 \cdot P} \times e^{-\frac{\overline{RTD} \cdot z}{B_2 \cdot Z}} & z \geq z_{RTD_{\max}} \end{cases} \quad (15)$$

where RTD_{max} is the maximum RTD (tips.cm^{-3}); z is the soil depth (cm); $z_{RTD_{max}}$ is the location of the maximum RTD (cm); Z is the thickness of the rhizosphere (cm); P is the proportion of part $z > z_{RTD_{max}}$ to the total rhizosphere; $\overline{RTD}$ is the average RTD (tips.cm^{-3}); and A_1, A_2, B_1, and B_2 are the coefficients related to the RTD (Table 4). Since the experimental site d was not measured at $z > z_{RTD_{max}}$, the parameters A_1 and B_1 were estimated by choosing the mean values of the remaining three positions, and the resulting fitted curves showed the same good performance.

We evaluated the simulation performance of the established root tip density distribution equation by R^2 and RMSE (**Eq 14**) (Table 4), and a large number of results showed that R^2 was larger and RMSE was less than 2. Therefore, we concluded that the equation could describe the distribution characteristics of RTD in alpine meadows more accurately.

For the description of the RLD, we adopted the more commonly used equation for the RLD distribution as the exponential equation (Feng et al., 2008). Moreover, in this paper, we set the expression of the equation as:

$$R(z) = C \cdot RLD_{\max} \cdot e^{-D\frac{z}{Z}} \quad (16)$$

where C and D are the coefficients related to RLD; RLD_{max} is the maximum RLD (cm.cm^{-3}). The equation of the RLD function at each location was obtained by fitting the RLD characteristics of the alpine meadow according to **Eq 16** with the fitted function graph (Figure 3). This equation can accurately reflect the distribution of RLD in most cases and also showed excellent performance in this study.

3.2 Validation and performance evaluation of the RWU model for alpine meadows

Based on Eqs. 3–10 and Eqs. 15–16, we constructed an alpine meadow RWU model with RTD distribution characteristics and RLD distribution characteristics as key RWU indicators, respectively. The accuracy of the RWU model is usually verified by using a soil water movement model that includes RWU (Eq. 11), simulating the changes in SWC, and comparing the differences between simulated and observed values of SWC.

Due to the variable climate and frequent atmospheric precipitation in the study area, the long time span will lead to significant effects of external factors on SWC, which will make great errors in the model validation process. Therefore, in this paper, we choose the short time span from September 1 to September 4, when the influence of external factors such as rainfall and snowfall in the study area is minimal and the weather conditions are normal and stable, as the starting and ending times for model validation.

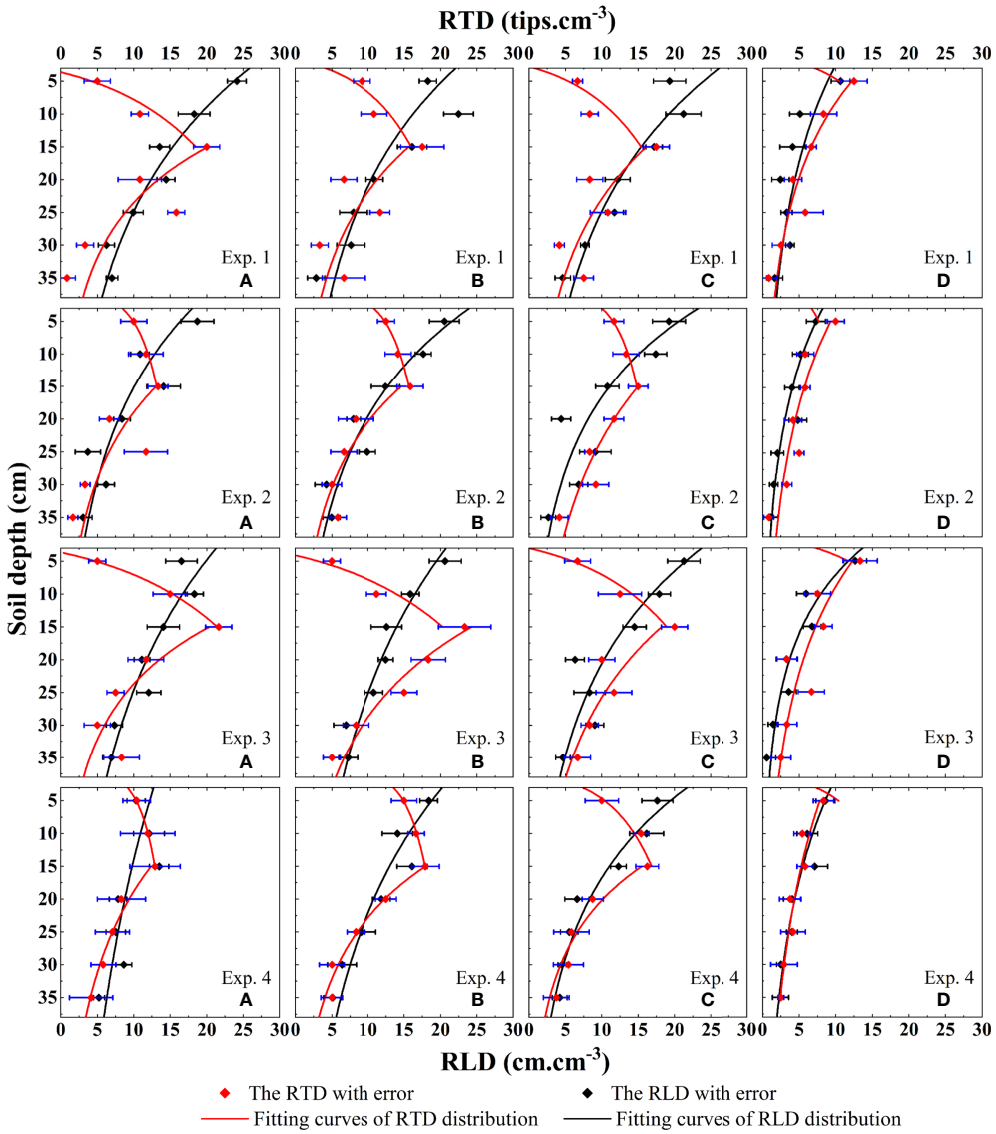

FIGURE 3
Based on the distribution characteristics of alpine meadow root indicators on soil profiles obtained from field experiments. The alpine meadow root length density index and root tip density index were included. The distribution equations of root tip density and root length density on the soil profile were fitted by Eq 15 and Eq 16 at the sites a, b, c, and d in Exp. 1 ~ 4.

Due to the variable climate and frequent atmospheric precipitation in the study area, a long time span will lead to a significant influence of external factors on SWC, which will lead to great errors in the model validation process. Therefore, in this paper, we choose the short time span from September 1 to September 4, when the influence of external factors such as rainfall and snowfall in the study area is minimal and the weather conditions are normal and stable, as the starting and ending times for model validation. At the same time, we use 16 sets of validation results to exclude errors due to chance.

The model validation results are shown in Figure 4. Relatively speaking, the model based on the RTD function simulates the SWC change more realistically. Integrating the simulated and actual values, we obtained the actual and simulated values of SWC change. It was found that both models underestimated the RWU capacity to some extent. Among them, the model based on RTD underestimated 14.93% on average and the model based on RLD underestimated 30.98% on average relative to the actual amount of SWC variation. Comparing the RWU simulated by the two models, we found that the RWU simulated by the model

based on RTD increased by 24.64% on average compared to the model based on RLD.

We compared the simulation performance of the two models by RMSE (Figure 5). It can be seen that the RMSE obtained from the model based on RTD is low, and it decreases by 40.56% on average compared to the model built on RLD.

Based on the above results, we concluded that the simulation performance of the established root uptake model with root tip density as the key root uptake parameter was high.

Based on the above results, we believe that the RWU model established with RTD as the key water uptake parameter has a high simulation performance.

3.3 Distribution characteristics of the RWU rate in alpine meadows

Since the simulation of the RWU model established by RTD is more accurate, this paper analyzes the RWU characteristics by simulating the RWU rate on the soil profile based on the above research method.

The daily average RWU rates at different locations at different experimental times are shown in Figure 6. It can be found that the characteristics of RWU in alpine meadows have obvious regularity in time and space. In the temporal scale, the RWU rate of the alpine meadow was larger in the regreening stage, and compared with the wilting stage, the RWU rate increased by 22.79%~45.8% in the regreening stage, with an average increase of 30.24%.

At the spatial scale, the intensity of RWU in the soil profile showed a maximum value in the middle rhizosphere, showing a ">" type change, which is increasing first and then decreasing. At the same time, the RWU rate in the soil profile showed a greater variation in the regreening stage and a flatter variation in the wilting stage. Among them, the top 67% of the roots in the rhizosphere bore an average of 86.76% of the total RWU.

4 Discussion

4.1 Analysis of the causes of root growth characteristics and root water uptake characteristics

There are obvious spatial and temporal distribution regularities in the root distribution characteristics and RWU distribution characteristics of alpine meadows. Based on the distribution of both the soil profile and different phenological stages, we analyzed the reasons for this regularity.

The pattern of alpine meadow RWU rate in time and space is consistent with the distribution pattern of meadow RTD, which indicates that the intensity of RWU is directly related to the density of the root index that can effectively absorb water. The alpine meadow exhibited a clear regreening stage in which both the root density index and the RWU rate were greater than that of the wilting stage, which is more consistent with the results of scholarly studies on alpine meadows (Wang et al. 2022). The reason for this phenomenon is attributed to the difference in water requirements of plants in different phenological stages.

Since there is a paucity of studies on RWU in alpine meadows, this paper is based on the study of root growth characteristics and water consumption capacity of maize and other (Yu et al., 2015; Zheng et al., 2022) crops as an analogy to alpine meadows. The results showed that the water consumption of plants differed in different phenological stages, with the maximum water consumption in the early stage of plant growth and decreasing in the maturity stage. The water consumption of alpine meadows showed a similar pattern. In the early stage of meadow growth, which is the most vigorous period of meadow growth, the larger growth water demand corresponds to the faster RWU rate. At the end of the meadow growth period, which is the wilting stage, the growth rate of the meadow is slower and the RWU rate is also slow. As a direct factor affecting RWU, the root density index tends to be larger when plant water consumption is higher.

4.2 Analysis of model validity based on soil physicochemical properties

In this paper, the accuracy of the RWU model was verified by using the soil water movement equation including RWU, and the simulation performance was compared when RTD and RLD were used as the root index that can effectively absorb water, respectively. The results showed that the simulation performance of the RWU model based on the RTD function was better and the simulated soil water distribution was more consistent with the actual situation. However, there are still some differences between the simulated results and the actual situation. Therefore, we analyzed the correlation between RWU rate, root density index, and soil physicochemical properties to further verify the validity of the model.

The correlation and cluster analysis plots for the four experimental sites are shown in Figure 7. All showed a significant correlation between RWU rate and RTD. The RWU will lead to certain changes in the water content of the soil profile, and the significant positive correlation between the rate of change in SWC and RTD further proves that RTD is the index of effective water-absorbing roots.

There is a clear correlation between RLD and soil physical properties, as the RLD index reflects the strength of root penetration ability (Liu et al., 2020). The higher the

10.3389/fpls.2022.918397

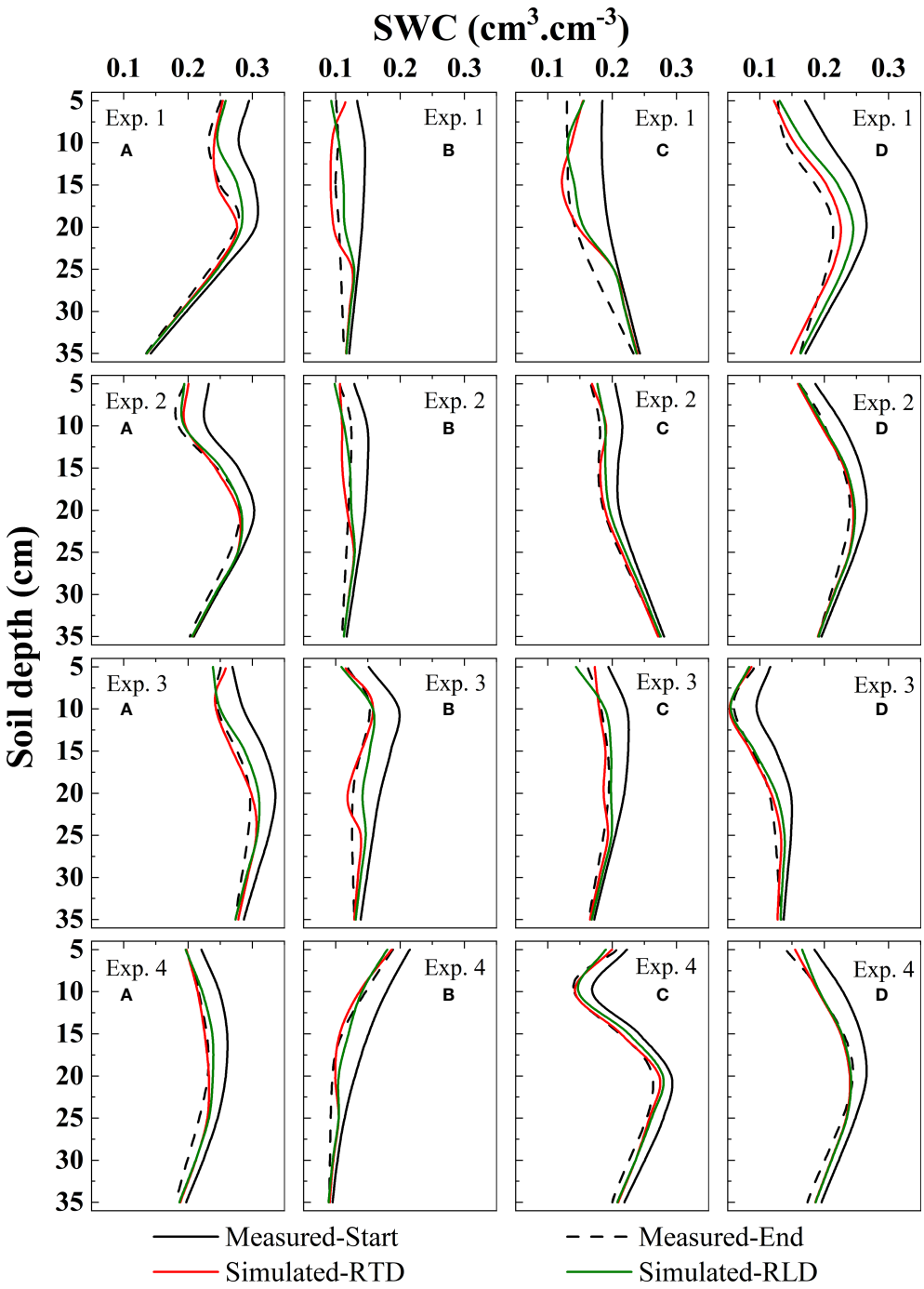

FIGURE 4
Based on the measured data, the accuracy of the root water uptake models of the sites a, b, c, and d inExp. 1 ~ 4 was verified. It contains soil water content distribution characteristics simulated by root tip density as root water uptake indicator (Simulated-RTD); soil water distribution characteristics simulated by root length density as root water uptake indicator (Simulated-RLD); measured soil water content starting and ending values (Measured-Start and Measured-End).

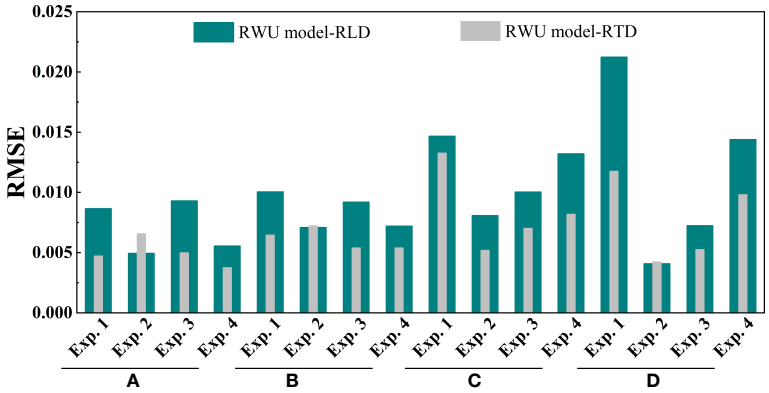

FIGURE 5
The model simulation performance was evaluated by the root mean square error (RMSE) (Eq. 14). In the process of model validation, we obtained the soil water content (SWC) changes simulated by the model built with root length density (RWU model-RLD) and root tip density (RWU model-RTD) at the sites a, b, c, and d in Exp. 1 ~ 4. Moreover, the simulated SWC distribution was analyzed and compared with the measured SWC distribution by RMSE.

porosity of the soil during root growth, the lower the resistance to root growth and the greater the RLD tends to be (Reichert et al., 2009). Also, a correlation was shown between RLD and soil chemical properties, probably because the greater the number of aging decayed roots in areas with higher RLD, the more nutrients from the root decay process are released into the soil, improving the content of many substances such as soil carbon, nitrogen, and phosphorus. However, the correlation between RLD and the rate of change in SWC and the rate of RWU was not significant, which also indicates that RLD is not a key root index affecting RWU and therefore has relatively poor performance in the simulation process.

4.3 Parameter selection and model limitations

The parameters of the RWU model, which are the main external factors affecting RWU, are mainly functional indexes such as soil water potential, soil water diffusion rate, and soil hydraulic conductivity. In this paper, SWC and soil depth are used as the independent variables of the model, which are more satisfied with the basic equations of soil hydraulics than the models with increasing time (Su et al., 2017; Liao et al., 2018) as the independent variables of the study, and the soil unsaturated hydraulic conductivity as the parameter of the model is more suitable for the selection of the research focus of this paper. In terms of the dimension of the model, considering that meadows cover the soil surface in the form of a surface, there is a clear difference from the study of individual plants, so this paper chooses to build a one-dimensional model about the soil depth to better represent the RWU of meadow vegetation.

This study also has some limitations in that some of the data calculated for the data were obtained through the literature, and the mean values in the study area did not take into account the variability with specific sites. More studies have utilized the improved Feddes model and thought that soil water potential is a key indicator of RWU rate. In addition, there is a certain interaction mechanism between soil water and solute movement and solute transformation and it has some influence on the accuracy of the mode (Zeng et al., 2018). There is a lack of basic RWU studies in alpine meadows on the QTP, and none of these factors were considered in the development of the RWU model applicable to alpine meadows in this paper. This may also be the reason for the large difference between model-simulated values and measured values in the deep region of the root layer.

5 Conclusion

The temporal regularity of root density in alpine meadows showed that the RLD and RTD decreased by 16.2% and 14.6%, respectively, during the wilting stage compared to the regreening stage. The spatial regularity was shown in that the RLD showed a gradual decrease from shallow to deep at each experimental site at different altitudes. The RTD increased and then decreased with

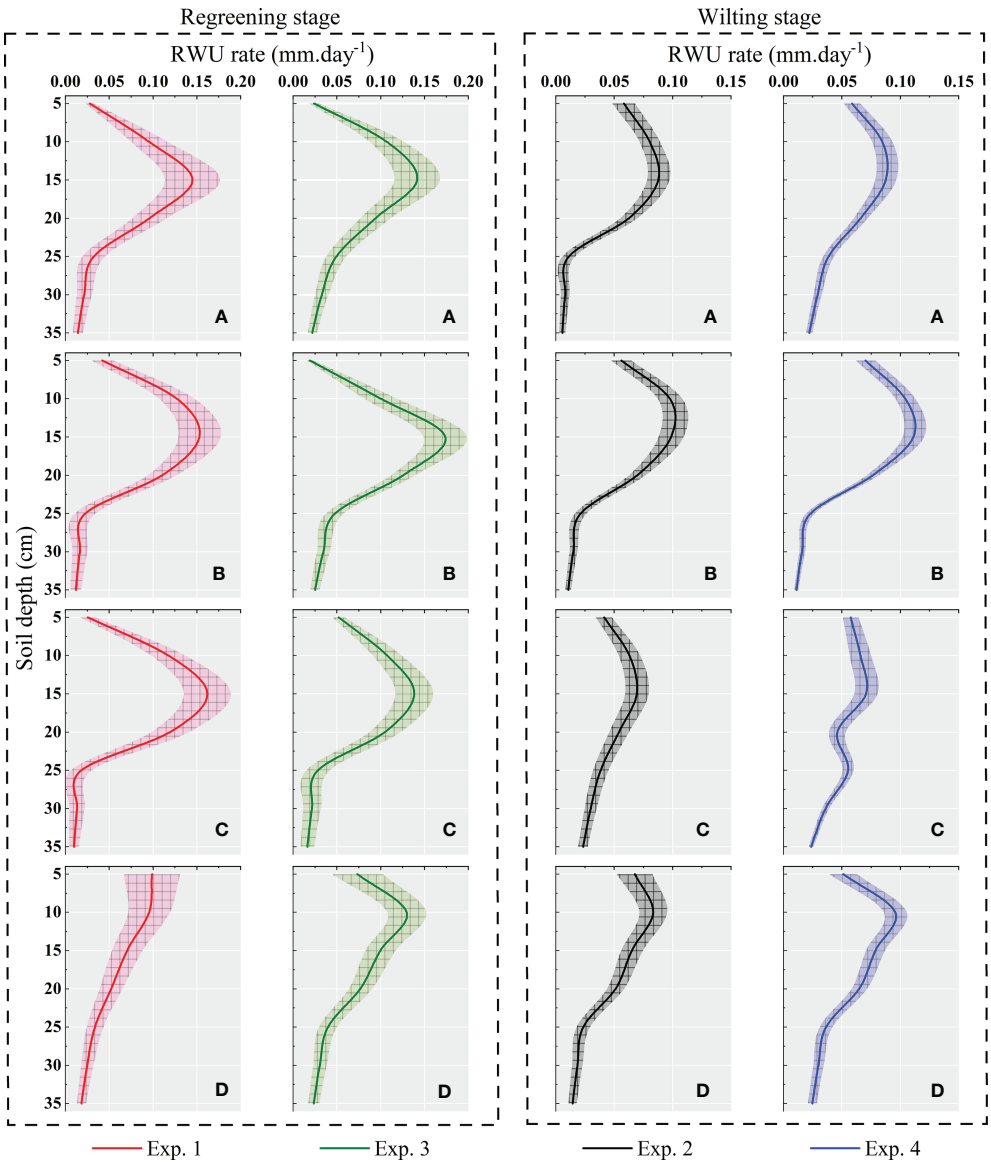

FIGURE 6
The distribution of root water uptake rate on the soil profile simulated by the root uptake model based on root tip density in Exp. 1 ~ 4 at the sites a, b, c, and d. The root water uptake characteristics at each experimental site during the rejuvenation and wilting stages were also compared.

increasing soil depth at lower altitude locations and was similar to the RLD distribution characteristics at higher altitude sites.

For the study of alpine meadow RWU, RTD was used as the index of root that can effectively absorb water, and its simulation performance was higher and more consistent with the actual situation.

The RWU characteristics of alpine meadows also showed obvious spatial and temporal regularity. Compared with the wilting stage, the RWU rate in the regreening stage increased by 30.24% on average. Meanwhile, the top 67% of the rhizosphere accounted for 86.76% of the total RWU on average.

Although the model has shown good performance in studying alpine meadows, further work is needed to demonstrate its applicability to other types of plants. There are still few studies on the alpine meadow RWU model, reference materials are scarce, and field experiments have more difficulties, so the indirect validation method of SWC variation has been used for model validation. However, the

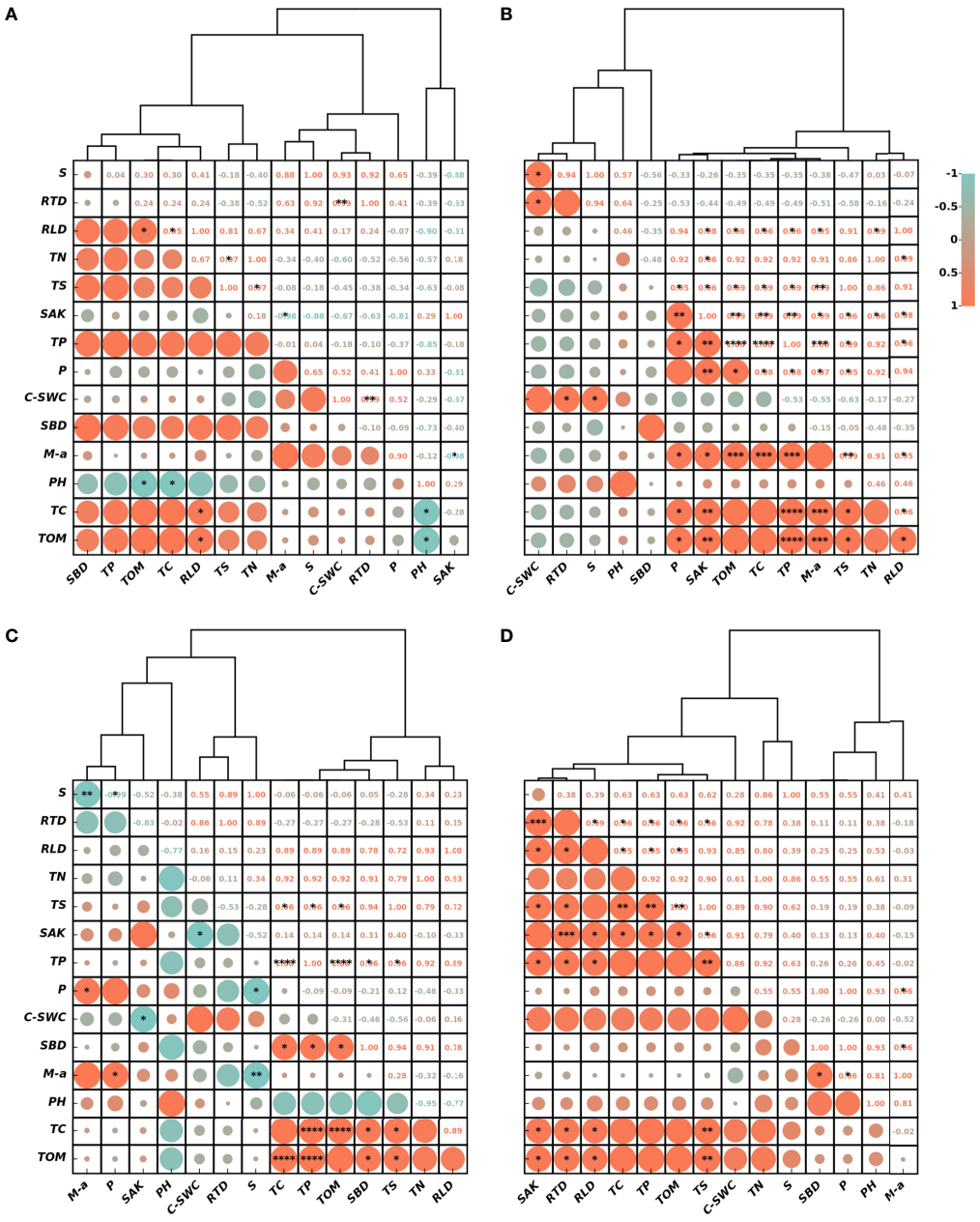

FIGURE 7
Cluster analysis profiles between root water uptake rate, root density indicators, and soil physicochemical properties in alpine meadows at the sites a, b, c and d **(A–D)**. It contains root water uptake rate (S), root tip density (RTD), root length density (RLD), total nitrogen (TN), total salt (TS), fast-acting potassium (SAK), total phosphorus (TP), porosity (P), soil water change rate (C-SWC), bulk weight (SBD), percentage of macroaggregates (M-a), acidity (PH), total carbon (TC), and total organic matter (TOM). (* means P<0.05, ** means P<0.01, *** means P<0.001, **** means significant level of P<0.0001. The figure was drawn on the https://www.chiplot.online/).

SWC may still be influenced by other unmeasured factors besides root water uptake and there are some errors. Therefore, there is still a need for improvement and innovation in the experimental method, especially in the direct measurement of RWU capacity, so that the RWU law can be directly verified. Since the model showed high susceptibility to the influence of external precipitation in the validation and reduced its simulation accuracy, and we collected root distribution characteristics for only two key phenological stages, the conclusions obtained were valid only

TABLE 4 Through the established Eq. 15, the RTD on soil profiles in Exp. 1~4 is fitted.

Sites		A_1	B_1	R^2	*RMSE*	A_2	B_2	R^2	*RMSE*
a	Exp. 1	0.65	2.08	0.92	1.69	10.11	3.3	0.73	1.68
	Exp. 2	0.22	2.2	0.98	0.20	8.6	3.5	0.64	1.43
	Exp. 3	0.7	2.3	0.99	0.25	11.9	3.71	0.84	1.32
	Exp. 4	0.18	2.32	0.99	0.05	10.21	4.45	0.96	0.66
b	Exp. 1	0.42	1.89	0.78	1.70	12.95	4.13	0.59	1.53
	Exp. 2	0.19	2.2	0.98	0.21	10.61	4.01	0.86	1.04
	Exp. 3	0.67	1.92	0.81	2.62	15	5.34	0.95	1.03
	Exp. 4	0.15	2.29	0.99	0.09	10.27	4.41	0.99	0.66
c	Exp. 1	0.52	1.85	0.74	2.41	13.38	4.26	0.8	1.37
	Exp. 2	0.2	2.2	0.98	0.20	12.44	5.99	0.9	0.93
	Exp. 3	0.59	2.13	0.95	1.20	16.66	5.54	0.81	1.22
	Exp. 4	0.36	2.56	0.94	0.69	8.43	3.15	0.95	0.87
d	Exp. 1	0.53	1.94			11.02	2.75	0.92	1.02
	Exp. 2	0.2	2.2			9.82	2.92	0.85	1.00
	Exp. 3	0.65	2.12			12.95	3.51	0.81	1.55
	Exp. 4	0.23	2.39			8.46	3.46	0.9	0.57

The parameters R^2 and root mean square error (RMSE) were obtained. Among them d due to the lack of shallower data, the average values of the other three locations are selected to estimate the values of their coefficients A_1 and B_1.

for these two stages. Therefore, in the follow-up study, we also need to take into account the ability of external precipitation to influence SWC and collect root distribution characteristics for longer time stages, to improve the model's understanding of plant transpiration in a long time span.

Data availability statement

The original contributions presented in the study are included in the article/Supplementary Material. Further inquiries can be directed to the corresponding author.

Author contributions

BW, DY, BD, and HF contributed to the conception and design of the study. BW, DY, and SX supervised the study activities. Acquisition of basic data was done by BD, HF, and ML. BD wrote the manuscript and performed the simulations. BD and HF built the model and applied it. BW, DY, and HW critically reviewed the manuscript. All authors contributed to this article and approved this version for submission.

Funding

This study was supported by the National Natural Science Foundation of China (Nos. 52022110, 51879276), the Second Tibetan Plateau Scientific Expedition and Research Program (STEP) (No. 2019QZKK0207), and the IWHR Research & Development Support Program (No. MK0145B022021).

Conflict of interest

The authors declare that the research was conducted in the absence of any commercial or financial relationships that could be construed as a potential conflict of interest.

Publisher's note

Supplementary material

The Supplementary Material for this article can be found online at: https://www.frontiersin.org/articles/10.3389/fpls.2022.918397/full#supplementary-material

References

Ahrens, B., and Reichstein, M. (2014). Reconciling 14C and minirhizotron-based estimates of fine-root turnover with survival functions. *J. Plant Nutr. Soil Sci.* 177, 287–296. doi: 10.1002/jpln.201300110

Allen, R. G., Pereira, L. S., Martin, S., and Smith, M. (1998). *Crop evapotranspiration: Guidelines for computing crop water requirements, FAO irrigation and drainage paper 56.* Vol. 300 (Rome: Fao), D05109.

Allen, R. G., Pruitt, W. O., Wright, J. L., Howell, T. A., Ventura, F., Snyder, R., et al. (2006). A recommendation on standardized surface resistance for hourly calculation of reference ETo by the FAO56 penman-monteith method. *Agric. Water Management.* 81, 1–22. doi: 10.1016/j.agwat.2005.03.007

Barkaoui, K., Roumet, C., and Volaire, F. (2016). Mean root trait more than root trait diversity determines drought resilience in native and cultivated Mediterranean grass mixtures. *Agriculture Ecosyst. Environment.* 231, 122–132. doi: 10.1016/j.agee.2016.06.035

Belmans, C., Wesseling, J. G., and Feddes, R. A. (1983). Simulation model of the water balance of a cropped soil: SWATRE. *J. Hydrol.* 63, 271–286. doi: 10.1016/0022-1694(83)90045-8

Cowan, I. R. (1965). Transport of water in the soil-Plant-Atmosphere system. *J. Appl. Ecol.* 2, 221–239. doi: 10.2307/2401706

dos Santos, M. A., van Lier, Q. J., van Dan, J. C., and Freire, A. H. (2016). Determination of empirical parameters for root water uptake models. *Hydrol Earth System Sci.* 21, 473–493. doi: 10.5194/hess-2016-59

Duan, H., Xue, X., Wang, T., Kang, W., Liao, J., and Liu, S. (2021). Spatial and temporal differences in alpine meadow, alpine steppe and all vegetation of the qinghai-Tibetan plateau and their responses to climate change. *Remote Sensing.* 13, 669. doi: 10.2307/2401706

Fan, X. M. (2011). *Influence of vegetation coverage on evapotranspiration process of alpine meadow in the head of the yangtza river, 19-52* (Lanzhou (Gansu: Lanzhou University).

Faria, L. N., Rocha, M., and Casaroli, L. D. (2010). A split-pot experiment with sorghum to test a root water uptake partitioning model. *Plant&Soil* 331, 299–311. doi: 10.1007/s11104-009-0254-0

Feng, Q., Si, J. H., and Li, J. L. (2008). Feature of root distribution of populus euphratica and its water uptake model in extreme arid region. *Adv. Earth Sci.* 23, 765–772. doi: 10.3321/j.issn:1001-8166.2008.07.016

Fred, J., and Molz, (1981). Models of water transport in the soil-plant system: A review. *Water Resour. Res.* 17, 1245–1260. doi: 10.1029/WR017i005p01245

Genxu, W., Guangsheng, L., and Chunjie, L. (2012). Effects of changes in alpine grassland vegetation cover on hillslope hydrological processes in a permafrost watershed. *J. Hydrol.* 444-445, 22–33. doi: 10.1016/j.jhydrol.2012.03.033

Gilroy, S., and Jones, D. L. (2000). Through form to function: root hair development and nutrient uptake. *Trends Plant Sci.* 5, 56–60. doi: 10.1016/S1360-1385(99)01551-4

Gong, B. Y. (2019). Geomorphic-centered analysis of water source in naqu river basin, qinghai-Tibetan plateau. (Beijing: China Institute of Water Resources and Hydropower Research).

Guo, X., Lei, T., Sun, X., Ma, J., and He, Q. (2019). Modelling soil water dynamics and root water uptake for apple trees under water storage pit irrigation. *Int. J. Agric. Biol. Eng.* 12, 126–134. doi: 10.25165/j.ijabe.20191205.4005

Hodge, A., Berta, G., Doussan, C., Merchan, F., and Crespi, M. (2009). Plant root growth, architecture and function. *Plant Soil.* 321, 153–187. doi: 10.1007/s11104-009-9929-9

Huang, F., Chen, Z., Du, D., Guan, P., Chai, L., Guo, W., et al. (2020). Genome-wide linkage mapping of QTL for root hair length in a Chinese common wheat population. *Crop J.* 8, 1049–1056. doi: 10.1016/j.cj.2020.02.007

Hupet, F., Lambot, S., and Javaux, M. (2002). On the identification of macroscopic root water uptake parameters from soil water content observations. *Water Resour. Res.* 38, 3601–3614. doi: 10.1029/2002WR001556

Janott, M., Gayler, S., Klier, C., and Priesack, E. (2011). A one-dimensional model of water flow in soil-plant systems. *Plant Soil.* 341, 233–256. doi: 10.1007/s11104-010-0639-0

Jha, S. K., Gao, Y., Liu, H., Huang, Z., Wang, G., Liang, Y., et al. (2017). Root development and water uptake in winter wheat under different irrigation methods and scheduling for north China. *Agric. Water Management.* 182, 139–150. doi: 10.1016/j.agwat.2016.12.015

Jiang, X., Zhu, X., Yuan, Z., Li, X., and Zakari, S. (2020). Lateral flow between bald and vegetation patches induces the degradation of alpine meadow in qinghai-Tibetan plateau. *Sci. Total Environment.* 751, 0048–9697. doi: 10.1016/j.scitotenv.2020.142338

Jia, X., Shao, M., Zhang, C., and Zhao, C. (2016). Variation and simulation of soil water content within different soil depths along the south-north transect of the loess plateau. *Adv. Water Sci.* 27, 520–528. doi: 10.14042/j.cnki.32.1309.2016.04.005

Jin, X., Jin, Y., and Mao, X. (2019). Ecological risk assessment of cities on the Tibetan plateau based on land use/land cover changes – case study of delingha city. *Ecol. Indicators.* 101, 185–191. doi: 10.1016/j.ecolind.2018.12.050

Johnson, M. G., Tingey, D. T., Phillips, D. L., and Storm, M. J. (2001). Advancing fine root research with minirhizotrons. *Environ. Exp. Botany.* 45, 263–289. doi: 10.1061/S0098-8472(01)00077-6

Joslin, J. D., and Wolfe, M. H. (1999). Disturbances during minirhizotron installation can affect root observation data. *Soil Sci. Soc. America J.* 63, 218–221. doi: 10.2136/sssaj1999.03615995006300010031x

Lai, C. T., and Katul, G. (2000). The dynamic role of root-water uptake in coupling potential to actual transpiration. *Adv. Water Resources.* 23, 427–439. doi: 10.1016/S0309-1708(99)00023-8

Lebron, I., Madsen, M., Chandler, D. G., Robinson, D. A., Wendroth, O., and Belnap, J. (2007). Ecohydrological controls on soil moisture and hydraulic conductivity within a pinyon-juniper woodland. *Water Resour. Res.* 43, 1073–1078. doi: 10.1029/2006WR005398

Liao, R., P., Y., Yu, H., Wu, W., and Ren, S. (2018). Establishing and validating a root water uptake model under the effects of superabsorbent polymers. *Land Degradation Dev.* 29, 1478–1488. doi: 10.1002/ldr.2907

Li, K. Y., Boisvert, J. B., and Jong, R. D. (1999). An exponential root-water-uptake model. *Can. J. Soil Sci.* 79, 333–343. doi: 10.4141/S98-032

Li, M., Liu, T., Duan, L., Luo, Y., and Chen, Z. (2019). The scale effect of double-ring infiltration and soil infiltration zoning in a semi-arid steppe. *Water* 11, 1457–1457. doi: 10.3390/w11071457

Liu, Y., Guo, L., Huang, Z., López-Vicente, M., and Wu, G.-L. (2020). Root morphological characteristics and soil water infiltration capacity in semi-arid artificial grassland soils. *Agric. Water Management.* 235, 106153. doi: 10.1016/j.agwat.2020.106153

Lu, Y.J. (2017). Interaction and Joint Regulation between Water and Soil Resources in the Alpine Region: A Case Study in the Naqu River Basin of Tibetan Plateau. (Beijing: China Institute of Water Resources and Hydropower Research).

Luo, Y., Yu, Q., OuYang, Z., Tang, D. Y., and Xie, X. Q. (2000). The evaluation of water uptake models by using precise field observation data. *J. Hydraulic Eng.* 4, 73–81. doi: 10.13243/j.cnki.slxb.2000.04.014

Ma, Z., Liu, H., Mi, Z., Zhang, Z., Wang, Y., Xu, W., et al. (2017). Climate warming reduces the temporal stability of plant community biomass production. *Nat. Commun.* 8, 15378. doi: 10.1038/ncomms15378

Metselaar, K., and Lier, Q. D. J. V. (2011). Scales in single root water uptake models: a review, analysis and synthesis. *Eur. J. Soil Sci.* 62, 657–665. doi: 10.1111/j.1365-2389.2011.01385.x

Molz, F. J., and Remson, I. (1970). Extraction term models of soil moisture use by transpiring plants. *Water Resour. Res.* 6, 1346–1356. doi: 10.1029/WR006i005p01346

Montero, J. I., Antón, A., Muñoz, P., and Lorenzo, P. (2001). Transpiration from geranium grown under high temperatures and low humidities in greenhouses. *Agric. For. Meteorol.* 107, 323–332. doi: 10.1016/S0168-1923(01)00215-5

Mualem, Y. (1976). A new model for predicting the hydraulic conductivity of unsaturated porous media. *Water Resour. Res.* 12, 513–522. doi: 10.1029/WR012i003p00513

Nancy, M., and Ian, M. (2012). Roots and root systems. *Handb. Plant Sci.* 2, 1–58. doi: 10.1002/9780470015902.a0002058.pub2

Ojha, C. S. P., Prasad, K. S. H., Shankar, V., and Madramootoo, C. A. (2009). Evaluation of a nonlinear root-water uptake model. *J. Irrigation Drainage Eng.* 135, 303–312. doi: 10.1061/(ASCE)IR.1943-4774.0000067

Peter, D. W., Marius, H., and Meine, V. N. (2018). Roots partially in contact with soil: Analytical solutions and approximation in models of nutrient and water uptake. *Vadose Zone J.* 17, 1–16. doi: 10.2136/vzj2017.03.0060

Reichert, J. M., Kaiser, D. R., Reinert, D. J., and Riquelme, U. F. B. (2009). Temporal variation of soil physical properties and root growth of black beans in four management systems. *Pesquisa Agropecuaria Brasileira.* 44, 310–319. doi: 10.1590/s0100-204x2009000300013

Rnnqvist, H. (2018). Double-ring infiltrometer for in-situ permeability determination of dam material. *Engineering* 10, 320–328. doi: 10.4236/eng.2018.106022

Rouphael, Y., and Colla, G. (2004). Modelling the transpiration of a greenhouse zucchini crop grown under a Mediterranean climate using the penman-monteith equation and its simplified version. *Aust. J. Agric. Res.* 55, 931–937. doi: 10.1071/AR03247

Segal, E., Kushnir, T., Mualem, Y., and Shani, U. (2008). Water uptake and hydraulics of the root hair rhizosphere. *Vadose Zone J.* 7, 1027–1034. doi: 10.2136/vzj2007.0122

Shao, M., Yang, W., and Li, Y. (1986). Mathematical model of soil moisture absorption by plant roots. *Acta Pedologica Sin.* 24, 295–305.

Su, L., Gulimire, H., and Liu, Q. (2017). Root water uptake model of populus euphratica in the lower reaches of tarim river. *Arid Land Geography*. 40, 102–107. doi: 10.13826/j.cnki.cn65-1103/x.2017.01.013

van Genuchten, M. T. (1980). A closed-form equation for predicting the hydraulic conductivity of unsaturated soils. *Soil Sci. Soc. America J.* 44, 892–898. doi: 10.2136/sssaj1980.03615995004400050002x

Wang, X., Zhou, B., Chen, Q., Fu, L. I., and Quan, C. (2022). Study on water consumption law of typical alpine meadow and alpine swamp wetland vegetation in qinghai-xizang plateau. *Plateau Meteorol.* 41, 338–348. doi: 10.7522/j.issn.1000-0534.2021.00079

Wu, Y., Che, R., Ma, S., Deng, Y., Zhu, M., and Cui, X. (2014). Estimation of root production and turnover in an apline meadow: comparison of three measurement methods. *Acta Ecologica Sinica.* 34, 3529–3537.

Wu, J., Zhang, R., and Gui, S. (1999). Modeling soil water movement with water uptake by roots. *Plant Soil.* 215, 7–17. doi: 10.1023/A:1004702807951

Yu, W., Ji, R., Feng, R., Zhao, X., and Zhang, Y. (2015). Response of water stress on photosynthetic characteristics and water use efficiency of maize leaves in different growth stage. *Acta Ecologica Sinica.* 35, 2902–2909. doi: 10.5846/stxb201306101632

Yuke, Z. (2019). Characterizing the spatio-temporal dynamics and variability in climate extremes over the Tibetan plateau during 1960–2012. *J. Resour. Ecol.* 10, 397–414. doi: 10.5814/j.issn.1674-764x.2019.04.007

Zeng, W., Lei, G., Zha, Y., Fang, Y., and Huang, J. (2018). Sensitivity and uncertainty analysis of the HYDRUS-1D model for root water uptake in saline soils. *Crop Pasture Sci.* 69, 163–173. doi: 10.1071/CP17020

Zhang, Z., and Huang, M. (2021). Effect of root-zone vertical soil moisture heterogeneity on water transport safety in soil-plant-atmosphere continuum in robinia pseudoacacia. *Agric. Water Management.* 246, 106702. doi: 10.1016/j.agwat.2020.106702

Zhang, Z. (2021). 30m resolution leaf area index products over the Tibetan Plateau (2010-2019). *National Tibetan Plateau Data Center*. doi: 10.11888/Ecolo.tpdc.271532

Zheng, X., Yu, Z., Shi, Y., and Liang, P. (2022). Differences in water consumption of wheat varieties are affected by root morphology characteristics and post-anthesis root senescence. *Front. Plant Sci.* 12, 814658. doi: 10.3389/fpls.2021.814658

Advantages of publishing in Frontiers

OPEN ACCESS
Articles are free to read for greatest visibility and readership

FAST PUBLICATION
Around 90 days from submission to decision

HIGH QUALITY PEER-REVIEW
Rigorous, collaborative, and constructive peer-review

TRANSPARENT PEER-REVIEW
Editors and reviewers acknowledged by name on published articles

Frontiers
Avenue du Tribunal-Fédéral 34
1005 Lausanne | Switzerland

Visit us: www.frontiersin.org
Contact us: frontiersin.org/about/contact

REPRODUCIBILITY OF RESEARCH
Support open data and methods to enhance research reproducibility

DIGITAL PUBLISHING
Articles designed for optimal readership across devices

FOLLOW US
@frontiersin

IMPACT METRICS
Advanced article metrics track visibility across digital media

EXTENSIVE PROMOTION
Marketing and promotion of impactful research

LOOP RESEARCH NETWORK
Our network increases your article's readership